Shear in reinforced concrete without transverse reinforcement: from refined experimental measurements to mechanical models

PAR

Francesco CAVAGNIS

EPFL

ÉCOLE POLYTECHNIQUE
FÉDÉRALE DE LAUSANNE

Suisse
2017

Foreword

Despite large research efforts performed in the past by the scientific community, there is still a lack of consensus on the mechanics leading to failure in structural concrete members without transverse reinforcement. Traditionally, simply supported beams have been tested under point loads and varying different geometrical parameters. This type of test is yet considered as "academic" (not representative of actual structures subjected to distributed loads and with redundant boundary conditions) and has been used mainly to determine the failure load without any detailed measurements on the phenomena leading to failure. On the basis of the measured strength, empirical formulae have been fitted in the past and are still found in many codes of practice. Also, several interpretations of the potential actions transferring shear have been proposed on the basis of the cracking pattern at failure, but without a direct proof of their development in actual members and yielding quite different (and even contradictory) explanations.

In order to advance knowledge in a consistent manner on this topic, a true understanding of the mechanisms leading to failure in shear and their connection with the potential shear-transfer actions is required. This is explored in the present thesis by Francesco Cavagnis presenting the results of an experimental programme on specimens tested under realistic loading and support conditions where innovative measurement techniques were implemented. The aim of these measurement techniques was to track in an accurate manner and at high frequencies the development of cracking and its progression to failure. The test results have provided a new view on the phenomenon of shear in structural concrete, showing with various potential modes of failure. Based on these results, Mr Cavagnis has performed detailed integrations of fundamental constitutive laws whose results provide a clear and undisputable view on the governing shear-carrying actions at failure, which may be very different depending on the specimen conditions.

As a result of the experimental programme and of the analyses of the test specimens, Mr Cavagnis investigates on a suitable physical approach to shear design of structural concrete. To that aim, a model has been developed allowing implementing realistic cracking patterns and their associated shear-transfer capacities. This work allows determining the amount of shear transferred by each potential action and the location and shape of the critical shear crack for any given load and boundary conditions. This analysis is eventually used to investigate on the suitability of the Critical Shear Crack Theory for shear design, where an improved failure criterion is proposed based on the previous results. The enhancement of the Critical Shear Crack Theory proposed by Mr Cavagnis is shown to be consistent and allows, in addition, to obtain closed-form solutions for the shear strength, with mechanically-based design expressions whose format is very simple and suited as code-like formulae.

Lausanne, November 2017   Prof. Dr Aurelio Muttoni

Funding

Acknowledgments

Abstract

Since the first applications of structural concrete, the shear behaviour of one-way slabs without transverse reinforcement has been largely investigated. The theoretical and experimental research efforts have allowed identifying the various shear-transfer actions carrying the load. Nevertheless, currently in the scientific community there is no general agreement on the mechanisms of shear failure, on the parameters governing the shear strength and on the predominant shear-transfer actions. Hence, several mechanical models, based on very different hypotheses, and empirical formulations, calibrated on the available experimental results, have been proposed in the last decades. In addition, these experimental results have been traditionally obtained from tests on simply supported beams subjected to point loading, whereas in most one-way slabs without transverse reinforcement in practice (foundations, retaining walls, slabs of cut-and-cover tunnels, silos) the support and loading conditions are typically different.

This thesis has therefore the objective to provide new experimental data on reinforced concrete members without transverse reinforcement subjected to different loading and support conditions, to increase the understanding on the mechanisms of shear failure and to develop a mechanical model based on the new experimental evidence.

In the first part of this thesis, the experimental results of 25 tests on 20 beams without transverse reinforcement subjected to different loading (concentrated and distributed load) and support conditions (simply supported beams, cantilevers and continuous beams) are presented. Refined measurement techniques allowed detailed tracking of the development of the crack pattern up to failure. The results show that the location, the inclination and the kinematics of the critical shear crack play a major role on the shear strength. Moreover, the amount of shear transferred by the various potential shear-transfer actions (inclination of the compression chord, arching action, residual tensile strength of concrete, dowelling action, aggregate interlock) has been estimated based on the experimental measurements and by using suitable mechanical models for each shear-transfer action. The analyses show that, for slender members, the shear-transfer actions contributing to the shear capacity are the inclination of the compression chord, the residual tensile strength of concrete, the dowelling action and the aggregate interlock, and the latter is the predominant one. For squat members or members in which the critical shear crack develops below the theoretical compression strut, differently, the arching action becomes governing.

In the second part of the thesis, a mechanical model, consistent with the main assumptions of the critical shear crack theory, is presented. The shear force that is transferred through the critical shear crack by the various shear-transfer actions is calculated by integration of simple constitutive laws and a failure criterion is obtained by summing the different contributions. The shear and deformation capacity and the location of the critical shear crack leading to failure can thus be calculated by intersection of the failure criterion with a load-deformation relationship. It is shown that the failure criteria obtained by integration of stresses at the crack surface can be approximated by power-law equations. Combining the power-law failure criteria with the load deformation relationship, a closed-form equation has been obtained. The closed-form equation provides almost identical results to the mechanical model and allows for direct design and assessment of existing structures. The mechanical model and the closed-form equation can be applied to members with different loading and support conditions. The accuracy of the two approaches has been checked against a large database of tests, showing a good agreement to the experimental results.

Key-words: reinforced concrete structures, shear strength, experimental programme, digital image correlation, shear transfer actions, mechanical model, critical shear crack theory, design equations

Résumé

Depuis les premières utilisations du béton structurel, le comportement à l'effort tranchant des dalles unidirectionnelles sans étriers a été largement étudié. Les investigations théoriques et expérimentales ont permis d'identifier les différentes modes de transmission de l'effort tranchant. Néanmoins, actuellement dans la communauté scientifique, il y a des désaccords sur les mécanismes de rupture à l'effort tranchant, sur les paramètres principaux influençant la résistance à l'effort tranchant et sur les modes de transmission prédominants. Par conséquent, plusieurs modèles mécaniques, basés sur des hypothèses très différentes, et des formulations empiriques, calibrées sur les résultats expérimentaux disponibles, ont été proposés durant ces dernières années. En outre, ces résultats expérimentaux ont été obtenus traditionnellement par des essais sur des poutres simplement appuyée soumise à une charge ponctuelle, alors que dans la plupart des dalles en pratique (fondations, murs de soutènement, dalles de tranchées couvertes, silos) les conditions aux limites et les types de chargement sont généralement différents.

Cette thèse a donc pour objectifs de fournir de nouvelles données expérimentales sur des éléments testés dans différents types de chargement et de conditions aux limites, afin d'améliorer la compréhension des mécanismes de rupture à l'effort tranchant et de développer un modèle mécanique basé sur des nouvelles preuves expérimentales.

Dans la première partie de cette thèse, les résultats expérimentaux de 25 tests sur 20 poutres sans armature d'effort tranchant avec des types de chargement (charge concentrée et répartie) et des conditions aux limites (poutres, porte-à-faux et poutres continues) différentes sont présentés. Les techniques de mesure raffinées ont permis de suivre en détail le développement des fissures jusqu'à la rupture. Les résultats montrent que l'emplacement, l'inclinaison et la cinématique de la fissure critique d'effort tranchant jouent un rôle principal sur la résistance à l'effort tranchant. En outre, la quantité d'effort tranchant transférée par les divers modes de transmission (inclinaison de la bielle dans la zone comprimée, appui direct de la bielle, résistance à la traction résiduelle du béton, effet goujon et engrènement) a été estimée sur la base des mesures expérimentales et en utilisant des modèles mécaniques appropriés pour chaque mode de transmission de l'effort tranchant. Les analyses montrent que, pour des éléments élancés, les modes contribuant à la transmission de l'effort tranchant sont l'inclinaison de la bielle dans la zone comprimée, la résistance à la traction résiduelle du béton, l'effet goujon et l'engrènement, ce dernier étant prédominant. Par contre, pour des éléments trapus ou des éléments dans lesquels la fissure critique d'effort tranchant se développe au-dessous de la bielle d'appui directe théorique, le mode de transmission par appui direct devient prédominant.

Dans la deuxième partie de la thèse, un modèle mécanique, conforme aux hypothèses principales de la théorie de la fissure critique, est présenté. L'effort tranchant pouvant être transféré à travers la fissure critique par les différents modes de transmission est calculé par intégration de lois constitutives simples et par la suite, un critère de rupture est obtenu en additionnant les différentes contributions. La résistance à l'effort tranchant, la capacité de déformation et la position de la fissure critique peuvent ainsi être calculées grâce à l'intersection du critère de rupture avec une loi charge-déformation. Les critères de rupture obtenus par l'intégration des contraintes à la surface de la fissure peuvent être approximés par des fonctions puissances. En combinant les fonction puissances avec la loi charge-déformation, une équation en forme fermée a été obtenue. L'équation en forme fermée donne des résultats presque identiques au modèle mécanique et permet le dimensionnement direct et la vérification des structures existantes. Le modèle mécanique et l'équation en forme fermée peuvent être appliqués aux éléments ayant des types de chargement et des conditions aux limites différentes. Les deux approches ont été vérifiée avec une grande base de données de campagnes d'essai, ce qui a permis de constater que les résultats obtenus ont une bonne concordance avec ceux expérimentaux.

Mots clés: structures en béton armé, résistance à l'effort tranchant, programme expérimental, vidéo corrélation, modes de transmission de l'effort tranchant, modèle mécanique, théorie de la fissure critique, équations de dimensionnement

Riassunto

Sin dalle prime applicazioni del calcestruzzo armato, il comportamento a taglio di travi senza armatura trasversale è stato oggetto di studi approfonditi. Le investigazioni sperimentali e teoriche hanno permesso di identificare i diversi meccanismi di trasmissione dello sforzo di taglio. Tuttavia ancora oggi nella comunità scientifica non c'è concordanza sulle cause che comportano la rottura, sui principali parametri che influenzano la resistenza a taglio e sui meccanismi di trasmissione predominanti. Pertanto negli ultimi anni sono stati proposti numerosi modelli meccanici basati su ipotesi molto diverse e formulazioni empiriche sviluppate calibrando i risultati sperimentali. Inoltre, questi risultati sperimentali sono stati ottenuti da test su travi semplicemente appoggiate soggette a carico puntuale, mentre nei casi reali (piastre di fondazione, muri di contenimento, piastre di trincee coperte, silos) le condizioni di vincolo e di carico sono spesso differenti.

Questa tesi ha quindi come obiettivo quello di fornire nuovi risultati sperimentali sotto condizioni di carico e di vincolo più varie, di migliorare la conoscenza dei meccanismi di rottura a taglio e di proporre un modello basato sulle nuove evidenze sperimentali.

Nella prima parte di questa tesi sono presentati i risultati sperimentali di 25 test su 20 travi senza armatura a taglio soggette a diverse condizioni di carico (concentrato e distribuito) e di vincolo (travi semplicemente appoggiate, mensole e travi continue). L'utilizzo di raffinati sistemi di misura ha permesso di seguire lo sviluppo di ciascuna fessura fino alla rottura. I risultati hanno messo in evidenza il ruolo chiave della posizione, dell'inclinazione e della cinematica della fessura critica sulla resistenza a taglio. Inoltre, è stato calcolato il contributo di ciascun meccanismo di trasmissione dello sforzo di taglio (inclinazione della biella nella zona compressa, trasmissione diretta o effetto arco, resistenza residua alla trazione, effetto spinotto, ingranamento) sulla base delle misure sperimentali e di modelli costitutivi adatti per ciascun meccanismo. I risultatati mostrano che per travi snelle la trasmissione dello sforzo di taglio avviene per compartecipazione dell'inclinazione della biella nella zona compressa, della resistenza residua alla trazione, dell'effetto spinotto e dell'ingranamento, ed è in particolare quest'ultimo il meccanismo predominante. Per travi tozze o travi in cui la fessura critica si sviluppa al di sotto della posizione teorica della biella a compressione, diversamente, la trasmissione per biella diretta diviene il meccanismo predominante.

Nella seconda parte della tesi è presentato un modello meccanico conforme con le principali ipotesi della teoria della fessura critica. La forza trasmessa tramite i diversi meccanismi di trasmissione dello sforzo di taglio attraverso la fessura critica è calcolata per integrazione di semplici leggi costitutive, e un criterio di rottura è ottenuto sommando i diversi contributi. La resistenza a taglio, la capacità di deformazione e la posizione della fessura critica possono quindi essere calcolate tramite intersezione del criterio di rottura con una legge carico-deformazione lineare. I criteri di rottura possono essere approssimati da equazioni di potenza. Combinando queste ultime con la legge carico-deformazione, è stato possibile ottenere una equazione in forma chiusa, più agevolmente utilizzabile per il dimensionamento e la verifica a taglio di strutture in calcestruzzo armato. Il modello meccanico e l'equazione in forma chiusa possono essere usati per elementi soggetti a diverse condizioni di carico e di vincolo. L'accuratezza dei due metodi è stata verificata utilizzando un vasto database di test, mostrando una buona correlazione con i risultati sperimentali.

Parole chiave: strutture in calcestruzzo armato, resistenza a taglio, programma sperimentale, digital image correlation, meccanismi di trasmissione dello sforzo di taglio, modello meccanico, teoria della fessura critica, equazioni di dimensionamento

Zusammenfassung

Seit den ersten Anwendungen von Stahlbeton im Ingenieurbau, ist das Verhalten von einachsig gelagerten Platten umfassend untersucht worden. Theoretische und experimentelle Forschungsarbeiten gestatteten mehrere die Last abtragende Schubübertagungsmechanismen zu identifizieren. Nichtsdestoweniger gibt es heutzutage in der wissenschaftlichen Gemeinschaft noch immer keine generelle Übereinstimmung, was die Mechanismen von Schubversagen, die die Schubfestigkeit bestimmenden Parameter und die dominierenden Schubtransfermechanismen angeht. Daher wurden in den letzten Jahrzehnten verschiedene auf unterschiedlichsten Annahmen basierende mechanische Modelle und mehrere mit verfügbaren Testergebnissen kalibrierte empirische Formulierungen vorgeschlagen. Darüber hinaus stammen jene Versuchsergebnisse üblicherweise von Tests an einfach gelagerten Balken mit Punktlasten, während bei einachsigen Platten in der Praxis (Fundamente, Stützmauern, Ausbauplatten im Tunnelbau, Silos) die Randbedingungen typischerweise andere sind.

Diese Arbeit hat sich deshalb zum Ziel gesetzt, neue Versuchsdaten von Balken unter verschiedenen Belastungen und Randbedingungen zur Verfügung zu stellen, um das Verständnis der Schubversagensmechanismen zu erhöhen und ein neues mechanisches Modell basierend auf den neuen Testergebnissen zu entwickeln.

Im ersten Teil werden die Ergebnisse von 25 Versuchen an 20 Balken ohne Schubbewehrung, die verschiedenen Lasten (Punktlasten und Gleichlasten) und Randbedingungen (einfach gelagerte Balken, Kragarme und Durchlaufträger) ausgesetzt wurden, vorgestellt. Verfeinerte Messmethoden erlaubten das detaillierte Verfolgen der Rissentwicklung bis zum Versagen. Die Ergebnisse zeigen, dass die Lage, die Neigung und die Kinematik des kritischen Schubrisses eine wichtige Rolle in der Schubfestigkeit spielen. Des Weiteren wurden, basierend auf den experimentellen Messungen und unter Anwendung geeigneter mechanische Modelle, für jeden Schubübertragungs-Mechanismus der Anteil der jeweiligen potentiellen Mechanismen (Neigung der Druckzone und Bogenwirkung, verbleibende Zugfestigkeit von Beton, Dübelwirkung, Verzahnung der Aggregate) abgeschätzt. Die Berechnungen zeigen, dass die zur Schubkapazität beitragenden Mechanismen für schlanke Bauteile die Neigung der Druckzone, die verbleibende Betonzugfestigkeit, die Dübelwirkung und die Aggregatverzahnung sind, wobei letztere dominiert. Für gedrungene Bauteile oder Bauteile in denen der kritische Schubriss sich unter der theoretischen Druckstrebe entwickelt, wird, im Gegensatz dazu, die Bogenwirkung maßgebend.

Im zweiten Teil dieser Arbeit, wird ein mechanisches Modell, das mit den Annahmen der Theorie des kritischen Schubrisses übereinstimmt, präsentiert. Die durch den kritischen Schubriss, mit Hilfe der verschiedenen Übertragungsmechanismen, weitergeleitete Schubkraft, wird durch die Integration von einfachen konstitutiven Gesetzen ermittelt und ein Versagenskriterium durch die Aufsummierung der unterschiedlichen Anteile gewonnen. Die Schub- und Verformungskapazität sowie die Lage des kritischen Schubrisses können daher durch Überschneidung des Versagenskriteriums mit der Last-Verformungsbeziehung bestimmt werden. Es wird gezeigt, dass die durch Integration der Spannungen auf der Rissoberfläche berechneten Versagenskriterien, durch Potenzfunktionen angenähert werden können. Die Kombination der Potenzfunktions-Versagenskriterien mit der Last-Verformungsbeziehung erlaubt die Herleitung einer geschlossenen Gleichung, die zu mit dem mechanischen Modell beinahe identischen Ergebnissen führt. Diese Gleichung kann direkt für die Bemessung von neuen sowie der Beurteilung der Tragfähigkeit von existierenden Strukturen herangezogen werden. Das mechanische Modell und die geschlossene Gleichung können auf Bauteile unter verschiedensten Lasten und Randbedingungen angewandt werden. Die Genauigkeit der beiden Ansätze wurde gegen eine große Versuchsdatenbasis geprüft und es zeigt sich eine gute Übereinstimmung mit den Testergebnissen.

Schlüsselworte: Stahlbetonbauteile, Schubfestigkeit, Versuchsreihe, Digitale Bildkorrelation, Schubübertragungsmechanismen, mechanisches Modell, Theorie des kritischen Schubrisses, Bemessungsgleichungen

Contents

Notations

Latin characters

lower case

a	shear span (for specimens subjected to point loads is the distance between the axis of the load and the axis of the support)
a_{cs}	M/V at the control section
$a_{cs,eff}$	effective control section shear span
a_{dir}	distance of direct support region
a_{eff}	effective shear span
a_x, a_y	projections of the contact areas in x and y directions
a_A	M/V at section A
a_F	M/V at section F
b	width of the beam
b_{ef}	effective width of concrete in tension
b_n	net width of the beam
c	depth of the compression zone
c_1, c_2, c_3, c_4	coefficients
c_b	concrete cover
c_m	distance from the top compression fibre to the centre of the inclined compression strut at the edge of the loading plate
c_n	distance from the top compression fibre to the axis where inclined force of the compression zone acts
c_t	depth of the tension zone
d	effective flexural depth
d'	distance from the compression reinforcement to the concrete surface
d_b	diameter of reinforcing bar
d_{dg}	d_g+16 [mm]
d_{fct}	location of fibre where tensile strength of concrete is attained (measured from the tension side)
d_g	maximum aggregate size
d_p	effective depth of the prestressed tendons in prestressed members
d_s	effective depth of the flexural reinforcement in prestressed members
d_B	vertical position of point B
d_F	vertical position of point F
e_p	eccentricity of tendons
f_c	concrete compressive strength measured in cylinder
f_{cc}	concrete compressive strength measured in cube
$f_{c,eff}$	effective concrete compressive strength
f_{ct}	concrete tensile strength
$f_{ct,ef}$	effective tensile strength of concrete
f_y	yielding strength flexural reinforcement
f_{yw}	yielding strength shear reinforcement
f_{ywo}	reference yielding strength of shear reinforcement
h	beam height
h_F	vertical distance from the top compression fibre to the tip of the shear crack
k	coefficient power-law failure criterion
k_a	coefficient of the closed-form equation that accounts for the influence of the inclination of the critical shear crack
k_b	reduction factor tensile strength of concrete
$k_{b,stirrups}$	reduction factor tensile strength of concrete for members with shear reinforcement
k_c	coefficient that that accounts for the influence of the compression zone
k_{c1}	coefficient compression zone

k_f	coefficient of the length l_F for SFRC beams
k_{lin}	coefficient of linearization in the closed-form equation for members with steel fibres or with low amount of shear reinforcement
k_S	coefficient of the length l_F for members with low amount of shear reinforcement
$k_{\rho w}$	coefficient dowelling action members with stirrups
l	span length
$l_1\ l_2\ l_3\ l_{F1}$	integration limits
l_d	length of the dowelling crack
l_{da}	length in which the longitudinal reinforcement is unbonded
l_{ef}	effective length
l_A	length of segment A-B of the critical shear crack
l_B	length of the region of the beam contributing to the opening of the critical crack
l_C	distance from the point of contraflexure to the axis of the fixed support in continuous members
l_F	length of segment B-F of the critical shear crack
l_{RS}	length along the crack where the residual tensile strength acts
l_{SS}	distance the axis of the end support to the point of contraflexure in continuous members
n	number of longitudinal bars
p_k	aggregate volume fraction
q	distributed load
r_A	distance from the axis of the load introduction to the onset of the shear crack
r_B	distance from the axis of the load introduction to the onset of the shear crack
r_F	distance from the axis of the load introduction to the tip of the shear crack
$r_{F,edge}$	distance from the edge of the loading plate to the tip of the shear crack
s	spacing between transversal bars
s_b	spacing between longitudinal bars
s_r	spacing between primary flexural cracks
t	time of the test
t_{max}	time at which maximum load is attained
u	opening of the crack measured along the horizontal direction
u_A	horizontal opening of the critical shear crack at point A
v	opening of the crack measured along the vertical direction
v_0, v_1	vertical displacements
$v_0{}', v_1{}'$	rotations
v_c	shear capacity per unit length
$v_{c,0}$	maximum shear strength per unit length
v_{distr}	normalized shear stress of members subjected to distributed load
v_{point}	normalized shear stress of members subjected to concentrated loads
v_A	vertical opening of the critical shear crack at point A
x_d	distance between two points located at the external regions of the dowelling crack used to calculate the vertical displacements and rotations
x_A	horizontal coordinate of the onset of the critical shear crack (point A)
x_B	horizontal coordinate of point B
x_F	horizontal coordinate of the tip of the critical shear crack (point F)
w	crack opening perpendicular to the crack surface
w_c	maximum crack width allowing tensile stresses transfer in concrete
w_A	opening perpendicular to the crack surface at point A
w_B	opening perpendicular to the crack surface at point B along segment A-B
w_F	G_F / f_{ct}
z	inner level arm

upper case

A_s	area of longitudinal bars
A_x, A_y	sum of the projections of the contact areas in x and y directions
E_c	modulus of elasticity of concrete
E_s	modulus of elasticity of steel
G_F	fracture energy of concrete
G_{F0}	base value of fracture energy (depending on the type of aggregate)
I	moment of inertia
K_f	orientation factor
M	bending moment
M_{cr}	cracking bending moment
M_{Right}	bending moment at the intermediate (right) support
M_A	bending moment at the section x_A
M_E	acting bending moment
M_F	bending moment at the section of the tip of the shear crack x_F
N	axial force ($N<0$ compression)
N_{Agg}	horizontal component of the aggregate interlock action
N_{Compr}	horizontal component of the inclined compression chord
N_{Res}	horizontal component of the residual tensile strength of concrete
P	prestressing force
Q	concentrated load
V	shear force
V_c	shear capacity of reinforced concrete members without transverse reinforcement
$V_{c,f}$	shear capacity of reinforced concrete members with steel fibres
$V_{c,S}$	shear capacity of reinforced concrete members with low amount of shear reinforcement
V_{exp}	measured shear force at failure
V_f	shear force carried by post-cracking tensile strength due to fibres
$V_{f,cl.form}$	shear force carried by post-cracking tensile strength due to fibres in the closed-form equation
V_{flex}	flexural strength
V_{left}	shear force at the end (left) support
V_{max}	shear force at failure (maximum value)
V_{right}	shear force at the intermediate (right) support
V_q	fraction of the distributed load carried by direct struts
V_A	acting shear force at the section x_A
$V_{A,F}$	shear force at which a crack type F propagates
V_F	acting shear force at the section of the tip of the shear crack x_F
V_{Agg}	shear force carried by aggregate interlock action
V_{Compr}	shear force carried by inclined compression chord
$V_{D,max}$	maximum dowelling action
$V_{D,tens}$	contribution of dowelling action of the tensile reinforcement
$V_{D,compr}$	contribution of dowelling action of the compression reinforcement
V_{Dowel}	shear force carried by dowelling action
$V_{Dowel,cl.form}$	enhanced contribution of dowelling action for members with low amount of shear reinforcement
V_E	acting shear force
V_{Res}	shear force carried by residual tensile strength of concrete
V_S	shear force carried by the shear reinforcement
$V_{S,cl.form}$	shear force carried by the shear reinforcement in the closed-form equation
$V_{Stirrups}$	shear force carried by the shear reinforcement and the enhanced dowelling action in the design equation

Greek characters

lower case

α_c	inclination of the compression chord
α_{cs}	shear slenderness ratio (a_{cs}/d)
α_f	aspect ratio fibres (l_f/d_f)
α_A	$M_A/(V_A \cdot d)$ in section A
β_l	angle of primary flexural crack between point A and the point along the crack at a vertical distance equal to $d/2$ from point A
β_{AB}	angle of segment A-B
β_{BF}	angle of segment B-F
γ	secant mixed mode angle
γ_T	tangent mixed mode angle
δ	crack sliding
δ_A	horizontal opening of the critical shear crack at point A
ε	strain
ε_l	principal tensile strains
ε_2	principal compressive strains
$\varepsilon_{2,min}$	minimum measured principal compressive strains
ε_{ct}	principal tensile strain leading to σ_l equal to f_{ct}
ε_s	steel strain
η	integration variable for the residual tensile stresses
η_c	reduction factor to account for the larger deformation at failure for members with fibres or with shear reinforcement
η_ε	reduction factor to account for the presence of transverse strains
κ	coefficient closed-form expression
μ	coefficient of friction
ξ	integration variable for the aggregate interlock stresses
ξ_B	location (distance) of point B from axis of load introduction
ρ	reinforcement ratio of tension flexural reinforcement
ρ'	reinforcement ratio of compression flexural reinforcement
ρ_f	volumetric fraction of fibres
ρ_p	reinforcement ratio of the prestressed tendons in prestressed members
ρ_s	reinforcement ratio of the flexural reinforcement in prestressed members
ρ_w	shear reinforcement ratio
$\rho_{w,min}$	minimum shear reinforcement ratio (assumed equal to 0.001)
σ	normal stresses
σ_l	principal tensile stress
σ_2	principal compressive stress
σ_{agg}	total aggregate interlock normal stress due to mixed mode response accounting for σ_{res} and $\sigma_{agg.0}$
$\sigma_{agg.0}$	aggregate interlock stress
σ_f	post-cracking tensile strength of fibres
σ_{pu}	compressive plastic strength of the cement matrix
σ_{res}	residual tensile stress
σ_s	stress in the tension reinforcement
σ_s'	stress in the compression reinforcement
τ	shear stress
τ_0	$0.2 \cdot f_{cc}$ (rough crack model)
τ_{agg}	aggregate interlock shear stress
τ_b	bond stress between fibres and concrete matrix
τ_{b0}	reference bond stress between fibres and concrete matrix

χ	curvature
ψ	rotation of the critical shear crack

upper case

Δx	length of loads on the tension face necessary to activate the full dowelling action
Δx_{tot}	length of loads that can be subtracted from the shear force at the control section
ΔN	horizontal shear force generated by bond in the reinforcement
ΔV	loads that can be subtracted from the shear force at the control section

Acronymes

CCDT	Critical Crack Development Type
COV	Coefficient of Variation
CSCT	Critical Shear Crack Theory
DIC	Digital Image Correlation
FT	Fibre type: H hooked, C crimped, P straight or plain
LED	Light Emitting Diode
LWC	Lightweight Concrete
SFRC	Steel Fibre Reinforced Concrete

Chapter 1   Introduction

1.1   Problem statement

Since the early developments of structural concrete, the shear strength of reinforced concrete one-way slabs and beams with and without transverse reinforcement has been the object of an extensive experimental and theoretical research. Several well-established theories based on equilibrium considerations (stress fields and strut-and-tie models) can be applied for members with transverse reinforcement. On the contrary, for one- way slabs and beams without transverse reinforcement there is still a large debate on suitable approaches for shear design, and the shear strength has been traditionally estimated by means of empirical models. Over the past years, several mechanical models have been proposed and successfully applied, leading to code provisions. Nevertheless, in the scientific community, there is still not yet an agreement on the phenomena and parameters governing the shear capacity of these members. A possible reason for this disagreement is that the mechanical models, which have been developed, are usually based on the interpretation of the crack pattern after (or well before) failure occurs. This is a consequence of conventional measurement techniques, which in many cases have not been capable of tracking the development of the critical shear crack during the process of failure. Recently, new measurement techniques, e.g. the digital image correlation (DIC) technique, have shown to be a consistent tool to investigate on shear failures, allowing tracking the development and kinematics of the critical shear crack and investigating the process of failure and the phenomena governing the shear strength.

Furthermore, the expressions of the mechanical models and codes of practice are usually based on tests on simply supported beams subjected to point load. However, most reinforced concrete members in practice are cantilevers or continuous one-way slabs without shear reinforcement subjected to distributed loading. This is for instance the case of cut-and-cover tunnels (Figure 1.1a), silos (Figure 1.1b), foundations (Figure 1.1c), retaining walls (Figure 1.1d) and bridges. Therefore, it is questionable whether the existing design formula can correctly describe the actual behaviour of such members.

(a)   (b)   (c)   (d)
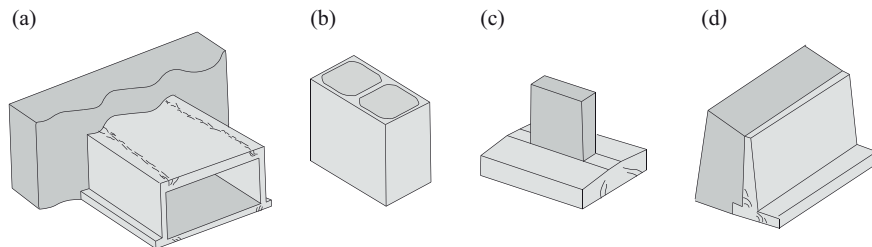
Figure 1.1 Examples of reinforced concrete one-way slabs and members without stirrups: (a) cut-and-cover tunnel; (b) silo; (c) foundation; (d) retaining wall

1.2   Objectives and scope of the study

Based on these abovementioned issues, the main objectives of this research are to:

- increase the number of available tests on reinforced concrete members without transverse reinforcement subjected to distributed loading;

- investigate by means of refined measurement techniques the development of the critical shear crack in members subjected to different loading and support conditions;

- provide experimental data on the shape and kinematics of the critical shear crack;

- increase the understanding of the mechanisms of shear failure;

- investigate on the role of the various shear-transfer actions carrying the shear force during loading and during the process of failure;

- study the influence on the shear resistance of distributed loads acting close to the support;

- develop a mechanical model based on the new experimental evidences that allows predicting the failure load, the deformation capacity and the theoretical location of the critical shear crack leading to failure;

- provide simplified design equations based on the mechanical model.

1.3 Organization of the thesis

This section provides a brief description of the topics covered in each chapters of the thesis:

- Chapter 2 provides a phenomenological description of the shear behaviour of reinforced concrete members without transverse reinforcement. First, the various shear-transfer actions involved in carrying the shear force are presented. Then, some selected experiments, which discuss the role of the shear-transfer actions and the influence of the location and shape of the critical shear crack, are reviewed. Finally, the main existing mechanical models and formulations for shear design are explained and discussed.

- Chapter 3 presents the experimental results of the first thirteen specimens of the experimental campaign. The cracking pattern and the development of the critical shear crack are tracked in detail and a number of typical cracks is identified and described. Furthermore, the experimental results are discussed and related to the various shear-transfer actions, demonstrating that there is not always a single shear-transfer action governing failure.

- In Chapter 4 the results of the entire experimental campaign are presented. The origin, development and role of each crack are further discussed in detail.

- Chapter 5 discusses, for the specimens tested, the role of the various shear-transfer actions during loading and at failure. The contribution of the shear-transfer actions is calculated on the basis of the measured shape and kinematics of the critical shear crack. The results show the influence of the shape and location of the critical shear crack on the activation of the shear-transfer actions and that different shear-transfer actions may govern the shear strength.

- In Chapter 6 a mechanical model for shear design of slender concrete members without shear reinforcement, based on the integration of the different shear-transfer actions and consistent with the main assumptions of the Critical Shear Crack Theory, is proposed and applied to simply supported members subjected to point loading. The main hypotheses and assumptions are validated through comparisons to detailed test measurements. Finally, the results of the mechanical model are checked against a large database.

- In Chapter 7, the mechanical model is applied to members subjected to different loading and support conditions (simply supported beams, continuous beams, cantilevers subjected to point load with and without axial forces and to distributed load) showing the ability of the approach to account in a consistent manner for the various shear-transfer actions and to predict rather accurately the failure load. Furthermore, a closed-form equation is derived from the mechanical model. Finally, the proposed mechanical model and the closed-form equation are checked against a large number of available experimental results.

- In Chapter 8, the mechanical model and the closed-form equation are extended and applied to lightweight reinforced concrete beams, reinforced concrete members with low amount of shear reinforcement and reinforced concrete members with steel fibres. Moreover, the closed-form equation derived in Chapter 7 is additionally simplified for design purposes.

Chapter 2   Shear in beams without transverse reinforcement: phenomenological considerations

This Chapter provides a phenomenological description of the shear behaviour of reinforced concrete members without transverse reinforcement. The various shear-transfer actions in a cracked concrete member are presented. A number of selected experiments are revised, providing evidence of the role of the shear-carrying mechanisms and their dependency on the location and shape of the critical shear crack. Finally, the available mechanical models and the shear formulations of some codes of practice are explained and discussed.

2.1   Shear-transfer actions

A reinforced concrete beam without transverse reinforcement subjected to point load, prior to crack development, can be analysed by means of the theory of elasticity. For increasing levels of load, several flexural cracks propagate from the tension side of the specimen. At this load stage, a number of shear-transfer actions [1] can develop allowing transferring the shear force from the load introduction plate to the end support.

Traditionally, the shear-transfer actions are classified into beam shear-transfer actions and arching action and the shear resistance in a reinforced concrete beam is almost always a combination of these two mechanisms. These mechanisms can be represented by strut and tie models [2] (refer to Figure 2.1). Beam shear-transfer actions allow varying the force in the flexural reinforcement and carrying shear keeping constant the level arm between the tension and compression chord. They are usually referred as cantilever action (or inclined compression chord, Figure 2.1a), aggregate interlock (Figure 2.1b), dowelling action (Figure 2.1c) and residual tensile strength of concrete (Figure 2.1d). On the contrary, the arching action (Figure 2.1e) allows carrying shear keeping constant the force in the flexural reinforcement.
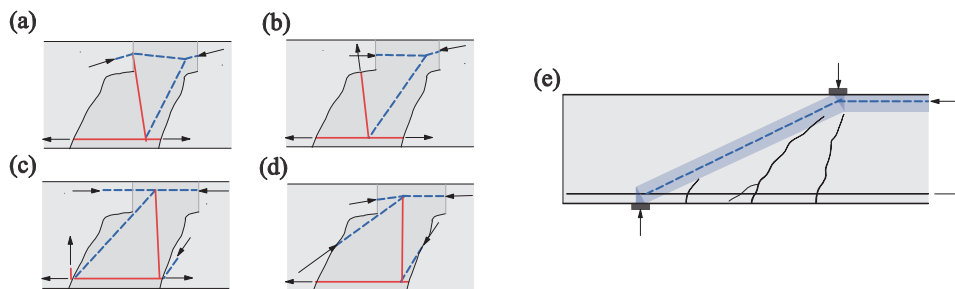
Figure 2.1 Shear-transfer actions (red: tensile forces, blue: compressive forces): (a) cantilever action (or inclined compression chord); (b) aggregate interlock; (c) dowelling action; (d) residual tensile strength of concrete; (e) arching action (adapted from Muttoni et al. [2])

2.1.1   Cantilever action

This mechanism was originally observed by Kani [3] as a fundamental shear-transfer action. According to Kani [3], the development of flexural cracks from the tension side of the member shapes the beam into a teeth-like structure (refer to Figure 2.2). The concrete elements between two consecutive flexural cracks can be visualized as cantilevers fixed in the upper compression zone. The concrete teeth are subjected to uneven tensile forces at the level of the longitudinal reinforcement, due to the varying acting bending moment in the longitudinal direction of the beam. Assuming that there is no load transferred through the cracks, these forces are equilibrated by an inclined compression chord and an inclined tension tie (refer respectively

to blue and red to Figure 2.1a). When the tensile strength of concrete is reached in the tension tie, the flexural crack propagates into a quasi-horizontal crack and the contribution of this action is reduced. The shear force carried by the cantilever action should not be misinterpreted as the vertical component of the arching action (which will be explained below).
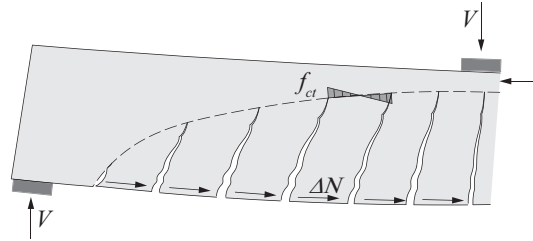
Figure 2.2 Kani's tooth-model [3]

2.1.2 Aggregate interlock

The ability to transfer shear through cracks is traditionally known as aggregate interlock or interface shear-transfer mechanism. This latter term indicates that this shear-transfer action depends on the surface conditions and it is not a characteristic of the type of concrete. On the contrary, the term aggregate interlock refers to the capacity to transfer shear force by contact between the aggregates protruding from one side of the crack surface with the matrix on the opposite side and it is specifically correct to describe the interface shear-transfer action for normal density concrete, where cracks develop normally between the aggregate particles and the concrete matrix. Although the term aggregate interlock is less appropriate to define this mechanism for all type of concretes, it will be used hereafter.

The aggregate interlock was first identified by Colley and Humphrey [4] and Nowlen [5] from experiments conducted on construction joints in concrete pavements. Following these investigations, several researchers developed direct shear test specimens to establish fundamental load-displacement relationships that describe this mechanism. Direct shear tests have been conducted by several authors: among all, by Fenwick et al. [6], Taylor [7], Houde et al. [8], Paulay et al. [9], Mattock et al. [10], Jimenez et al. [11], Hamadi et al. [12], Walraven [13] and Sagaseta et al. [14]. A variety of test specimens and setups has been employed to address the influence of the main parameters governing this shear-carrying mechanism: concrete strength, aggregate size, type of aggregate, initial crack width, normal restraining stiffness.

Fenwick et al. [6] performed a pioneering investigation, by testing the specimens shown in Figure 2.3a. The specimens were designed to study the effect of the crack width and the concrete strength on the shear stresses transferred through cracks. The specimens were cracked prior to testing by an external tensile force, and during testing the opening w was kept constant by means of an external force, normal to the crack plane. Although these members did not failed due to loss of aggregate interlock capacity at the preformed crack, but developed secondary flexural cracks (see Figure 2.3a), these experiments allowed investigating the aggregate interlock shear stresses for constant crack opening in the pre-peak phase. Typical results are shown in Figure 2.3b.

Taylor [7] was the first to observe that a crack in a reinforced concrete beam simultaneously opens and slides. Taylor performed laboratory tests with constant crack opening-to-shear displacement ratios. This ratio was introduced by means of a parallel ruler system. A schematic representation of the test setup is shown in Figure 2.4a. According to Taylor, the ratio between the aggregate strength and the matrix strength is the most important parameter, which influences the roughness and thus the shear stresses developing at the crack.

Paulay et al. [9] performed other tests with constant crack width, using an improved test setup and specimen (refer to Figure 2.4b). The tests series were designed to evaluate the effect of the aggregate size and the influence of the initial crack width on the ultimate shear stresses.

(a)

preformed crack
secondary cracks

100 mm

125 mm   100 mm

(b)

$w = 0.06$ mm

$w = 0.13$ mm

$w = 0.19$ mm

$w = 0.32$ mm
$w = 0.38$ mm

τ [MPa]

δ [mm]
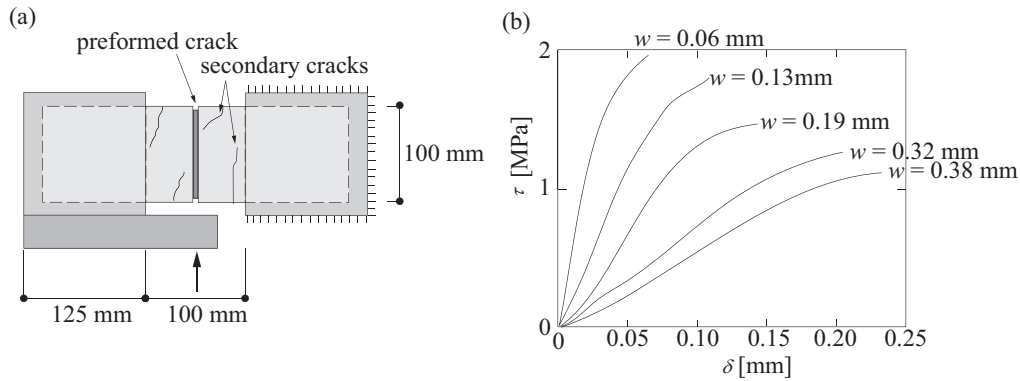
Figure 2.3 (a) Test setup used by Fenwick et al. [6]; (b) shear stress τ-shear sliding δ results as a function of the crack width w

(a)

355   140

127

890

(b)

300

190   470

119
114
152
19

(c)

400

150
300   600
150

150
120   150
15
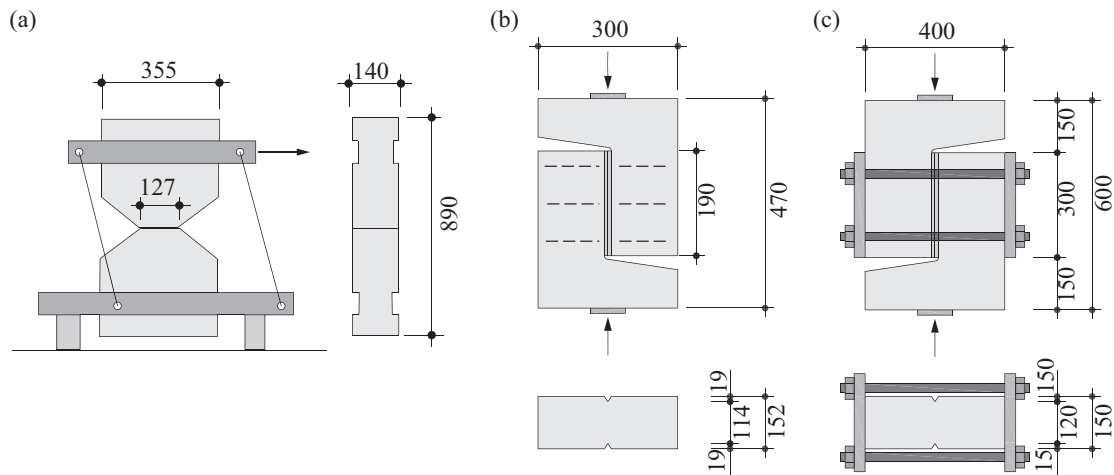
Figure 2.4 Test specimens used by: (a) Taylor [7]; (b) Paulay et al. [9]; (c) Walraven [13]

Mattock et al. [10] performed push-off experiments in order to study the influence of the aggregate type. These tests were carried out using either lightweight or normal gravel concretes. From the experimental results, Mattock concluded that the strength of normal gravel concrete was consistently higher than that of lightweight concrete and that the difference in the shear stresses can be attributed to the differences in roughness of the crack surfaces. Mattock observed that in normal concrete the strength between the matrix and the aggregate particles was lower than the tensile strength of the aggregate particles and the cracks generally propagated around the aggregate spheres. On the contrary, in lightweight concrete, the bond between the matrix and the aggregate was higher than the tensile strength of the aggregate particles and the cracks developed through the aggregates.

Walraven [13] performed tests on pre-cracked push-off specimens with external restraining bars (refer to Figure 2.4c) that allowed varying the crack width and shear displacement during loading. For these specimens the crack opening was restrained passively, so that the crack opened according to the internal equilibrium in the crack plane. The advantage of these tests was that shear stresses, normal stresses, crack opening and shear displacement were directly measured. The performed tests showed that the shear forces across cracks induce tangential and normal displacements between the crack faces and that these displacements generate normal and shear stresses. Therefore, Walraven concluded that crack width, crack slip, normal and shear stresses are all interrelated. The variables studied by the author where the concrete strength, the type of concrete, the grading of concrete, the aggregate size and the initial crack width.

More recently, biaxial test setups have been developed to characterize the behaviour of cracked concrete under mixed mode loading path (Nooru-Mohamed [15], Hassanzadeh [16], Østergaard et al. [17], and Jacobsen et al. [18]), which is more representative of the actual kinematics measured in cracks in reinforced concrete beams failing in shear [19]. Jacobsen et al. [18] performed tests on double notch concrete specimens to characterize the mixed mode behaviour. The tests were conducted in two steps: a pure mode I opening step, where an opening w_0 was initiated between notches, followed by a mixed mode-

opening step (combined opening and sliding). Jacobsen pointed out that there is a tendency that the shear and compression stresses raise for both decreasing mixed mode angle and decreasing initial opening.

On the basis of this experimental background, several empirical and theoretical formulations have been proposed to quantify the shear and normal stresses developing across cracks.

Walraven and Reinahrdt [20] proposed two simple equations based on linear regression analysis of the experimental results to evaluate shear stresses τ and normal stresses σ developing at the crack. According to the authors, the curves that fitted the experimental results with the greatest accuracy are:

$$\tau = -\frac{f_{cc}}{20} + \left[1.35 \cdot w^{-0.63} + \left(0.191 \cdot w^{-0.552} - 0.15\right) \cdot f_{cc}\right] \cdot \delta \tag{2.1}$$

and

$$\sigma = -\frac{f_{cc}}{30} + \left[1.8 \cdot w^{-0.80} + \left(0.234 \cdot w^{-0.707} - 0.20\right) \cdot f_{cc}\right] \cdot \delta \tag{2.2}$$

where w is the crack opening perpendicular to the crack surface, δ is the crack sliding and f_{cc} is the concrete cube compressive strength.

Bazant and Gambarova [21] developed the rough crack model by considering the crack surface as a regular array of trapezoidal asperities. This constitutive model was obtained by optimizing the test results by Paulay et al. [9]. An improvement to the rough crack model has been proposed by Gambarova and Karakoç [22]. The authors based their model on tests with constant confinement stress performed by Daschner and Kupfer [23] and introduced the dependency of the shear stresses on the maximum aggregate size. The equations proposed by the authors are:

$$\tau = \tau_0 \cdot \left(1 - \sqrt{\frac{2w}{d_g}}\right) \cdot r \cdot \frac{a_3 + a_4 \cdot |r|^3}{1 + a_4 \cdot r^3} \tag{2.3}$$

and

$$\sigma = -a_1 \cdot a_2 \cdot \sqrt{w} \cdot \frac{r}{\left(1 + r^2\right)^{0.25}} \cdot f_{ct} \tag{2.4}$$

where $r = \delta / w$, $a_1 \cdot a_2 = 0.62$, $a_3 = 2.45 / \tau_0$, $a_3 = 2.44 \cdot \left(1 - 4 / \tau_0\right)$, $\tau_0 = 0.2 \cdot f_{cc}$ and d_g is the maximum aggregate size

Other theoretical approaches to model the interface shear transfer mechanism are the two-phase model proposed by Walraven [13] and the contact density model developed by Li et al. [24].

The two-phase model [13] is a mechanical model based on statistical analyses of the crack surfaces and the associated contact areas as a function of the crack opening w, the shear displacement δ and the composition of the concrete mix. In the model, concrete is regarded as a two-phase material, with perfectly stiff spherical aggregate particles and a perfectly rigid plastic matrix and stresses are generated by contact of the aggregate particles on one side of the crack with the cement matrix on the opposite site. Cracks are assumed as being planar unless they encounter a spherical aggregate. In this case, the cracks go around the aggregate and then continue their globally planar path. The contact areas between the aggregate particles and the cement matrix are related to the crack kinematics by means of geometric relations and statistical considerations. The formulation of the model is given by the following equations:

$$\sigma = \sigma_{pu} \cdot \left(A_x - \mu \cdot A_y\right) \tag{2.5}$$

and

$$\tau = \sigma_{pu} \cdot \left(A_y + \mu \cdot A_x\right) \tag{2.6}$$

where σ_{pu} is the compressive plastic strength of the cement matrix, μ is a coefficient of friction and A_x and A_y are the sum of the projections (a_x and a_y) of the contact surfaces between the aggregate particles and the cement matrix. The projections a_x and a_y are derived as a function of displacements between the crack surfaces, accounting for the aggregate size d_g. A_x and A_y

are functions of the crack width w and the sliding δ, the maximum aggregate size d_g and the aggregate volume fraction p_k. The latter defines the probability that an arbitrary point in the concrete is located in an aggregate particle and it is equal to the ratio between the total volume of the aggregate particles and the concrete volume. With respect to the crack kinematics (Figure 2.5), Walraven assumed that the crack opening w develops prior to the sliding δ and identified three phases: phase of no contact (refer to Figure 2.5b, $0 < \delta < \delta_0$), phase of growing contact (refer to Figure 2.5c, $\delta_0 < \delta < \delta_b$) and phase of maximum contact (refer to Figure 2.5d, $\delta > \delta_b$).
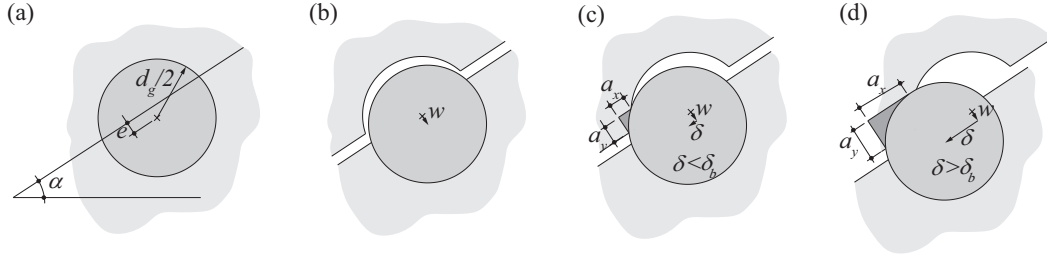
Figure 2.5 Crack kinematics proposed by Walraven [13]: (a) initial state before the development of the crack; (b) phase of no contact; (c) phase of growing contact; (d) phase of maximum contact

Ulaga [25] and Guidotti [26] applied the two-phase model developed by Walraven by using different history of crack kinematics (refer respectively to Figure 2.6 and Figure 2.7). Ulaga assumed that the crack opening w and the sliding δ develop simultaneously at a constant angle $\gamma = \arctan(w/\delta)$ and identified a phase of decreasing contact (refer to Figure 2.6b, $s < s_{sup}$), followed by a phase of separation (refer to Figure 2.6d, $s > s_{sup}$).
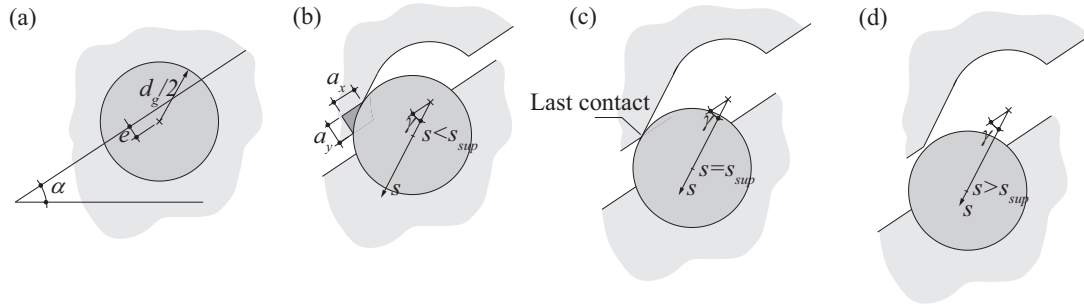
Figure 2.6 Crack kinematics proposed by Ulaga [25]: (a) initial state before the development of the crack; (b) phase of decreasing contact; (c) last point of contact; (d) phase of separation

Guidotti [26] further modified the history of crack kinematics (Figure 2.7) and assumed that a fraction of the total crack opening w_0 develops prior to the crack sliding δ, followed by an increase in both crack opening w and sliding δ at an angle γ_T. When this kinematics is considered, four phases can be observed: phase of no contact (refer to Figure 2.7b, $s < s_{lim}$), phase of growing contact (refer to Figure 2.7d, $s_{lim} < s < s_{max}$), phase of decreasing contact (refer to Figure 2.7f, $s_{max} < s < s_{sup}$) and phase of separation (refer to Figure 2.7h, $s > s_{sup}$). The characteristic points that define the transition from one phase to another (Figure 2.7c and e and g) and the projections of the contact surfaces can be determined geometrically as a function of crack displacements and the aggregate size d_g.
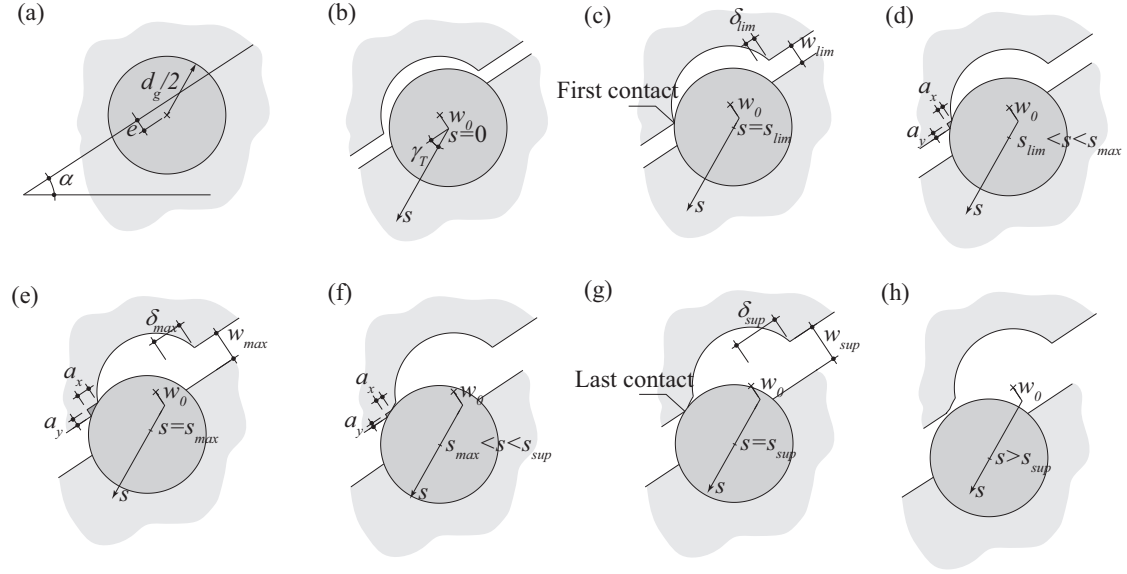
Figure 2.7 Crack kinematics proposed by Guidotti [26]: (a) initial state before the development of the crack; (b) initial opening of the crack; (c) first point of contact; (d) phase of growing contact; (e) phase of maximum contact; (f) phase of decreasing contact; (g) last point of contact; (h) phase of separation

The main differences between the original kinematics and the ones proposed by Ulaga and Guidotti can be identified in the phase of decreasing contact and the phase of separation. Indeed, in the original model the projections of the contact surfaces increase for increasing shear displacement up to a maximum value, resulting in a perfectly plastic behaviour, whereas according to Ulaga and Guidotti the projection of the contact surfaces decrease at a certain crack opening and sliding. A comparison of the computed stresses for the various kinematics as a function of the crack opening and sliding is shown in Figure 2.8. It can be observed, that the kinematics of Walraven represents an upper bound solution of the aggregate interlock stresses. The kinematics of Guidotti generates intermediate stress values that depend on the initial crack opening w_0. Finally, the aggregate interlock stresses calculated according to the kinematics of Ulaga represent a lower bound solution.

It shall be noted that some of the main assumptions of the two-phase model are limited to certain types of concrete and the model cannot thus be considered as a comprehensive mechanical description of this shear-transfer mechanism. For instance, the analysis of fracture surfaces have shown that even for normal strength concrete, cracks do not always develop around aggregates, but may partially pass through them [27]. Moreover, the model does not correctly assess the influence of the crack roughness (roughness at a macro-level) on the shear stresses developing at the crack surface for high-strength and lightweight concrete: these specimens are characterized by a certain level of roughness at the crack surface, although the aggregates are completely fractured.
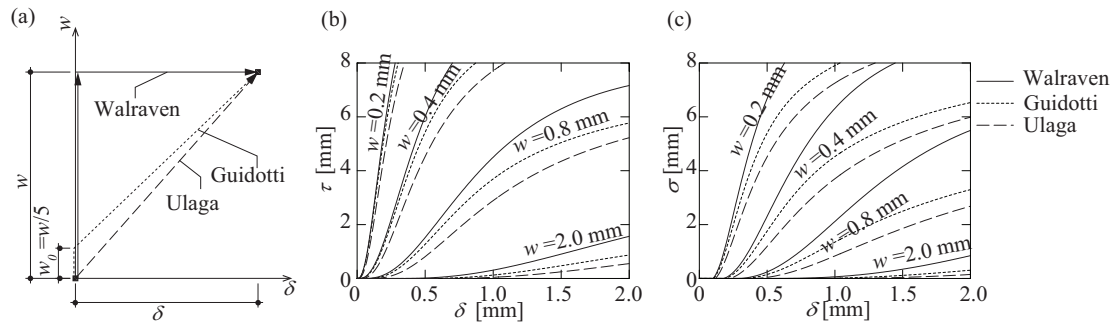
Figure 2.8 (a) Crack kinematics (opening and sliding); (b) shear and (c) normal aggregate interlock stresses according to the kinematics proposed by Walraven [13], Ulaga [25] and Guidotti [26] (adapted from Campana et al. [28])

Li et al. [24] developed the contact density model. The authors proposed an approach which involves considering the crack surface as an infinite number of small pieces defined as contact units (dA_θ, refer to Figure 2.9a). In the model each contact unit has an inclination θ which is a stochastic variable described by its density probability function $\Omega(\theta)$. By scanning several

fracture profiles and determining the inclination of each contact unit, it is possible to obtain the contact density function $\Omega(\theta)$ which is considered a material property, independent on the size and grading of the aggregates (Figure 2.9b). The mathematical formulation of the model is given by the following equations:

$$\tau = \int_{-\pi/2}^{\pi/2} \sigma_{con} \cdot K(\Delta w) \cdot A_t \cdot \Omega(\theta) \cdot \sin\theta \, d\theta \qquad (2.7)$$

and

$$\sigma = \int_{-\pi/2}^{\pi/2} \sigma_{con} \cdot K(\Delta w) \cdot A_t \cdot \Omega(\theta) \cdot \cos\theta \, d\theta \qquad (2.8)$$

where Ω is a trigonometric function, σ_{con} is the contact compressive stress (assumed to be governed only by the crack opening value and independent on the shear displacement component), K is the effective ratio of contact area (introduced to take into account the influence of the maximum aggregate size d_g on the aggregate interlock stresses) and A_t is the whole surface area per unit crack plane. Li et al. [24] proposed simplified equations based on the contact density model:

$$\frac{\tau}{m} = \frac{\varphi^2}{1+\varphi^2} \qquad (2.9)$$

and

$$\frac{\sigma}{m} = \left[\frac{\pi}{2} - \cot^{-1}\varphi - \frac{\varphi^2}{1+\varphi^2}\right] \qquad (2.10)$$

where $\varphi = \delta/w$, $m = 4.36 \cdot f_c^{1/3}$ and f_c is the compressive strength of concrete.
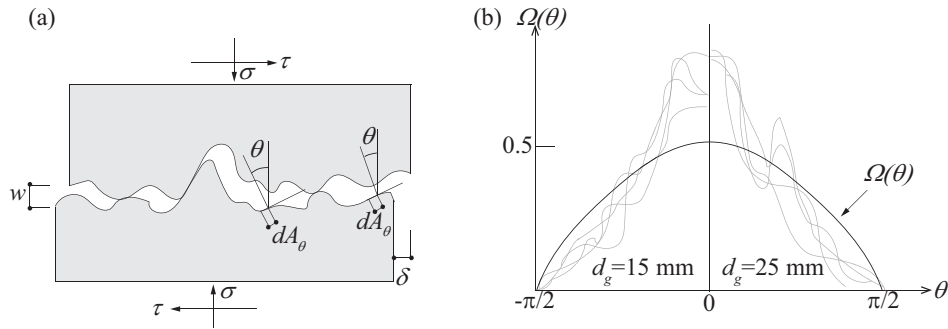
Figure 2.9 (a) Geometry of the crack and definition of contact unit and inclination; (b) smoothed histogram of measured inclination for specimens with different aggregate size and contact density function (adapted from Li et al. [24])

2.1.3 Dowelling action

The dowelling action can be defined as the capacity of the reinforcement bars to transfer forces perpendicular to their axis. This action has been studied by several researchers, employing different test setups and specimens, in order to develop fundamental load-displacement relationships that quantify the dowel capacity. Direct dowel setups (Figure 2.10a), divided beam tests (Figure 2.10b) and beam end tests (Figure 2.10c) have been used and have allowed understanding the main parameters governing the dowelling action. The first two types of tests enabled researchers to study the dowelling action with little or no axial tension forces in the reinforcement, whereas the beam end tests allowed characterizing the interaction between tensile forces and dowel forces on the ultimate capacity of the dowel [11].
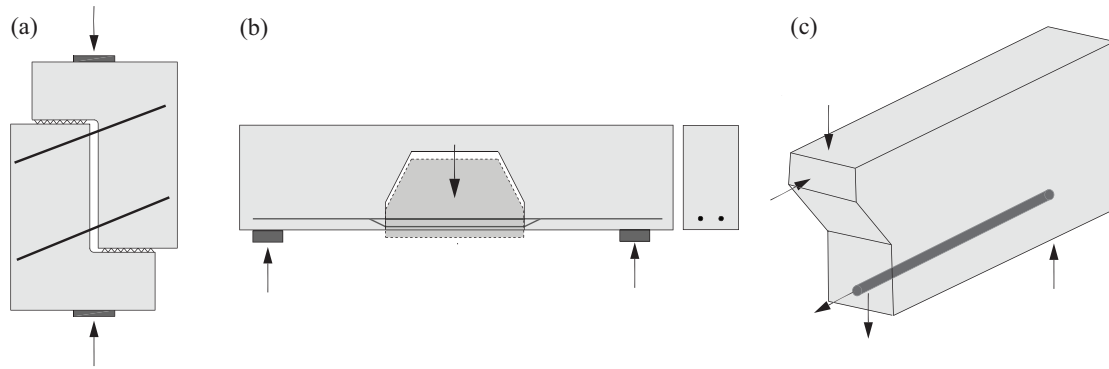
Figure 2.10 (a) Direct dowel tests; (b) divided beam tests; (c) beam end tests

Direct tests (Figure 2.10a) have generally reported two types of failures: splitting failure at the bottom for very small concrete cover, or at the side faces of the section (failure mode I, refer to Figure 2.11a), and crushing of concrete or yielding of the reinforcement (failure mode II, refer to Figure 2.11b). In particular, direct tests carried out by Fenwick et al. [6], Eleiott [29] and Paschen et al. [30] evidenced splitting cracks along the reinforcement bars (failure mode I), whereas those reported by Rasmussen [31], Hofbeck et al. [32], Dulaska [33], Dei Poli et al. [34] failed by crushing of the concrete or yielding of the reinforcement bar (failure mode II). The difference between the failure modes can be attributed to the concrete cover or the confinement provided by the transverse reinforcement. Vintzeleou et al. [35] reported that, for members without transverse reinforcement, when the concrete cover is greater than 6-7 times the diameter of the bar, crushing of concrete occurs (failure mode II). On the contrary, for smaller concrete cover, failure is governed by the development of splitting cracks (failure mode I).
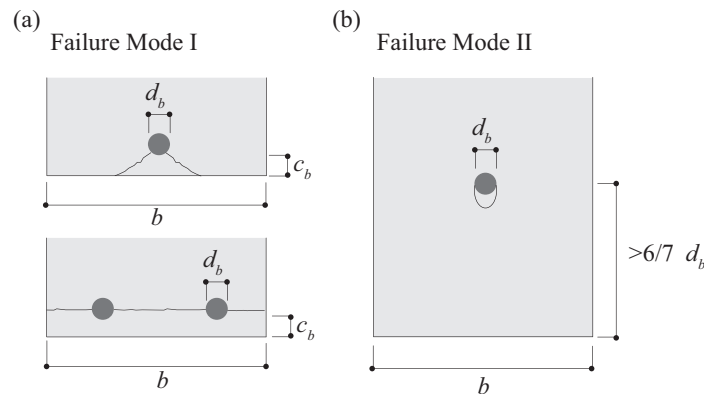
Figure 2.11 Failure mechanisms: (a) splitting cracks at the bottom or at the side; (b) crushing of concrete or yielding of the longitudinal bar

Direct tests have been complemented by investigations on divided beam specimens and beam-end specimens to study the propagation of splitting crack (failure mode I).

The divided beam setups (Figure 2.10b) have been employed by Krefeld and Thurston [36], Taylor [37] and Baumann and Rüsch [38]. Krefeld and Thurston [36] focused their investigation to study the effect of the bar diameter, the beam width and the distance of the crack to the end support. Taylor [37] and Baumann and Rüsch [38] tested specimens similar to those designed by Krefeld and Thurston and concluded that the dowel capacity increases with increasing tensile strength of concrete, beam net width and bar diameter. Typical results by Baumann and Rüsch [38] are shown in Figure 2.12a. It can be noted that the longitudinal bars were activated for low values of vertical displacement and that the dowelling action was roughly constant thereafter, yielding to the development of a splitting crack along the flexural bars.

Sharma [39] and Kemp et al. [40] used beam-end specimens (Figure 2.10c) to study the interaction between tensile forces and dowelling action. They observed a significant reduction in the dowel capacity for increasing axial tensile stresses in the dowel.

The influence of the reinforcement strains on the dowel capacity has been recently investigated by Plumey [41] who carried out experimental tests on arch-shaped members and showed that large strains in cracked concrete are associated to a reduction of the tensile strength of concrete and of the capacity to withstand dowelling forces. Figure 2.12b shows the reduction of the

tensile strength of concrete ($k=f_{ct,ef}/f_{ct}$) as a function of the strains in the flexural reinforcement bars (tests by Neuner et al. [42], Franz et al. [43], Intichar et al. [44] and Plumey [41]). Fernández Ruiz et al. [45] concluded that when failure develops prior to yielding of the reinforcement, the coefficient of reduction of the tensile strength of concrete k remains above 0.25, whereas for tests where failure develops after yielding of the longitudinal reinforcement, the factor k can be assumed equal to 1/6.
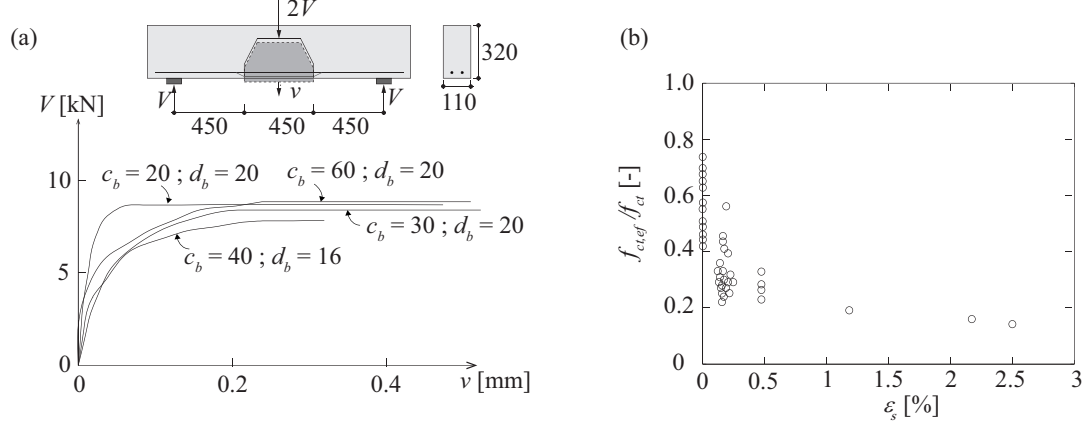
Figure 2.12 (a) Test results by Baumann and Rüsch [38]; (b) reduction of the tensile strength of concrete as a function of the longitudinal strains in the bar (experimental data according to Plumey [41])

The available experimental investigations have thus allowed identifying the main parameters governing the dowelling action: the bar diameter, the tensile strength of concrete, the concrete cover, the net width and the strains in the longitudinal reinforcement bars. However, several authors proposed additional parameters and there is no general agreement on the relative significance of each parameter on the dowel capacity. Several empirical formulae have been developed and a large discrepancy exists between the predicted dowel forces calculated by using the different available formulations. Three known approaches commonly used to calculate the dowelling action are listed below.

According to Baumann and Rüsch [38], the dowelling action is equal to:

$$V_{D,max} = 1.64 \cdot b_n \cdot d_b \cdot f_c^{1/3} \tag{2.11}$$

where b_n is the net width of the beam ($b_n = b - n \cdot d_b$), b is the width of the specimen, n is the number of bars, d_b is the bar diameter and f_c is the compressive strength of concrete.

Vintzeleou et al. [35] proposed two expressions to quantify the dowel capacity. One equation is valid when the concrete cover c_b is large enough in comparison with the net width of the beam b_n and side splitting cracks occur:

$$V_{D,max} = \xi \cdot b_n \cdot d_b \cdot f_{ct} \approx 2 \cdot b_n \cdot d_b \cdot f_{ct} \tag{2.12}$$

where f_{ct} is the tensile strength of concrete, b_n is the net width and d_b the bar diameter.

On the other hand, when the concrete cover c_b is small enough in comparison with the net width b_n and bottom splitting cracks occur, the dowelling capacity results:

$$V_{D,max} = n \cdot \psi \cdot c_b \cdot \frac{c_b}{0.66 c_b + d_b} \cdot d_b \cdot f_{ct} \approx n \cdot 5 \cdot c_b \cdot \frac{c_b}{0.66 c_b + d_b} \cdot d_b \cdot f_{ct} \tag{2.13}$$

Fernández Ruiz et al. [46] proposed the following equation:

$$V_{D,max} = n \cdot b_{ef} \cdot l_{ef} \cdot f_{ct} \tag{2.14}$$

where n refers to the number of bars, b_{ef} to the effective width per bar, l_{ef} to the concrete length in tension and f_{ct} to the tensile strength of concrete. According to Fernández Ruiz et al. [46], b_{ef} can be estimated as the minimum value between $s_b - d_b$ and $4 \cdot c_b$, where s_b is the spacing between bars, d_b is the bar diameter and c_b is the concrete cover of the bar and l_{ef} is estimated as $2 \cdot d_b$.

Among the three approaches, Eq. (2.14) provides the most accurate results when compared to the experimental results on direct dowel tests or divided beam tests with no axial tension forces in the reinforcement (average measured-to-calculated dowelling action for 110 tests (Taylor [37], Baumann et al. [38], Houde et al. [8], Neuner et al. [42], Paschen et al. [30]) is 0.84 and the coefficient of variation is 24.7%, refer to Figure 2.13). In Figure 2.13 the red markers refer to specimens where failure occurred at the bottom of the section, whereas the black markers represent failures at the side of the section.

It shall be noted that abovementioned expressions predict the maximum dowel capacity in the case of no strains in the reinforcement bars. However, most cases in practice correspond to members with longitudinal bars subjected to combined tensile strains and dowelling forces and a reduction of the tensile strength of concrete shall be considered to correctly predict the dowelling action for these members [41]. In a general manner, it has been shown that, for members without transverse reinforcement, the dowelling capacity decreases for increasing strains in the longitudinal reinforcement [47]. On the contrary, for members with stirrups or with lateral confinement generated by external loads [48], the dowelling action can be kept constant or eventually enhanced [38].
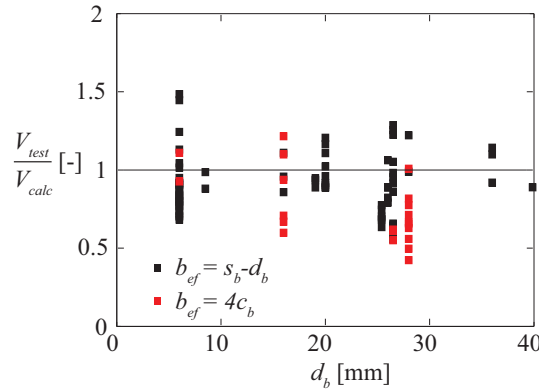
Figure 2.13 Ratio measured-to-predicted dowelling action according to Fernández Ruiz et al. [46] for 110 tests with no axial tension forces in the reinforcement bars (in red splitting failure at the bottom of the section, in black splitting failure at the side of the section)

2.1.4 Residual tensile strength of concrete

When concrete cracks, it exhibits a softening residual strength that allows stress transfer through the crack (Figure 2.14a). The softening behaviour of concrete in tension was firstly measured by Evans and Marathe [49]. The importance of the residual capacity to carry tensile stresses in structural concrete was recognized by Hillerborg [50], who developed the Fictitious Crack Model to study the behaviour of concrete in tension. This model, which is largely used in fracture mechanics, assumes that at peak load the strains start to localize within a narrow zone of micro-cracks (process zone, refer to point 1 in Figure 2.14). The micro-cracks allow stress decrease with increasing deformation (1-2, in Figure 2.14). When micro-cracks grow, a crack develops and stress transfer is still possible through the crack (2-3, in Figure 2.14). The concrete has no capacity to transfer any stress for crack openings larger than about 0.2 mm for normal strength concrete (3, in Figure 2.14b).
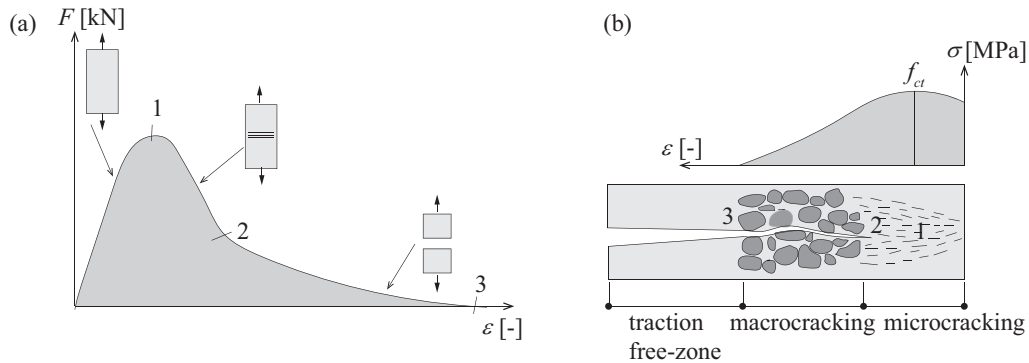
Figure 2.14 (a) Tensile load-deformation response of a concrete specimen; (b) illustration of the fracture process zone around the tip of the crack: micro-cracks (1-2), micro-cracks coalesce into a macro crack in the post-peak tensile softening region (2-3) [51]

The concrete softening behaviour can be described using several approaches. The most known stress-crack opening relationships are the one developed by Reinhardt [52], the one proposed by Hordijk [53] and the bilinear law defined in the Model Code 2010 [54].

Reinhardt [52] formulated the following non-linear tension softening equation:

$$\sigma_{res} = f_{ct} \cdot \left(1 - \left(\frac{w}{w_c}\right)^{0.31}\right)$$

(2.15)

where f_{ct} is the tensile strength of concrete, w is the crack opening, $w_c = 4.226 \cdot (G_F/f_{ct})$ represents the maximum crack width for stress transfer and G_F is the fracture energy of concrete and can be defined according to Model Code 2010 [54].

Hordijk [53] proposed the following exponential equation:

$$\sigma_{res} = f_{ct}\left[\left(1 + \left(c_1 \frac{w}{w_c}\right)^3\right)e^{-c_2(w/w_c)} - \frac{w}{w_c}\left(1 + c_1^3\right)e^{-c_2}\right]$$

(2.16)

where $w_c = 5.14 \cdot (G_F/f_{ct})$, $c_1 = 3$ and $c_2 = 6.93$.

Finally, according to Model Code 2010 [54], the stress-crack opening relationship can be estimated by the following bilinear law:

$$\sigma_{res} = f_{ct} \cdot \left(1 - 0.8 \cdot \frac{w}{w_1}\right) \qquad \text{for } w \leq w_1$$

(2.17)

and

$$\sigma_{res} = f_{ct} \cdot \left(0.25 - 0.05 \cdot \frac{w}{w_1}\right) \quad \text{for } w_1 < w \leq w_c$$

(2.18)

where $w_1 = G_F/f_{ct}$ when $\sigma_{res} = 0.2 \cdot f_{ct}$ and $w_c = 5 \cdot (G_F/f_{ct})$ when $\sigma_{res} = 0$.

2.1.5 Arching action

The arching action is an alternative shear-transfer mechanism that might develop in reinforced concrete beam due to the loss of bond between longitudinal bars and concrete [55]. This shear-carrying action, observed by Mörsch [56], and later confirmed by Drucker [57], corresponds to a plasticity-stress field in which the force in the flexural reinforcement remains constant and the load is carried directly by an inclined direct strut (refer to Figure 2.1e). In others words, the longitudinal reinforcement bars sustain the same strains throughout the length. The plasticity-based arching action is in agreement with experimental results for compact members where flexural cracks develop below the theoretical compression strut, but not for slender beams where inclined cracks may develop through the compression strut and limit its strength.

2.2 Role of shear-carrying mechanisms and development of the critical shear crack

In the following, the role of the various shear-transfer actions and the influence of the location of the critical shear crack on the shear strength are discussed on the basis of test series available in literature.

Kani [58] and Leonhardt et al. [59] observed that the amount of shear carried by the various shear-transfer actions is governed by the slenderness of the member and by the location of the critical shear crack with respect to the theoretical compression strut. The authors observed that four different possible regimes govern the shear failure:

- For very low shear spans, flexural cracks do no develop through the inclined compression strut and the shear strength is controlled by yielding of the longitudinal reinforcement and corresponds to the plastic strength of the member (specimen B2 in Figure 2.15a and b).

- For rather short-span beams (specimen B4 in Figure 2.15a), the arching action is still dominant. In this regime, flexural cracks propagate through the compression strut in a stable manner. Consequently, the plastic solution may overestimate the shear capacity of these members, as the strength of the inclined strut is reduced by the development of flexural cracks through it. For these members, the compression strut may eventually develop with an elbow-shaped form, as described by Muttoni et al. [2]. The load can be increased beyond the development of the critical shear crack and failure occurs due to crushing of concrete, which presents a reduced compressive strength caused by the crack propagation and transverse tensile strains. These members belong to the left-hand side region of the Kani's valley and can be studied with stress-fields approaches that account for a reduction of the compressive strength due to cracking in the compression field. However, it shall be noted that the position of the critical shear crack is governing for the shear strength and a large scatter in the experimental results has been reported for these members.

- For larger shear spans (specimen B6 in Figure 2.15a), the beam shear-transfer actions become dominant (a strut and tie model that combines the different beam shear-transfer actions is shown in Figure 2.15b). For these members, belonging to the right-hand side of the Kani's valley (Figure 2.15b), the critical shear crack develops through the compression strut carrying shear and failure occurs in a brittle manner and it is often named diagonal shear failure.

- For very slender beams (specimen B10/1 in Figure 2.15a), the shear strength is governed by yielding of the flexural reinforcement. For these members, the beam shear-transfer actions are capable of carrying loads larger than the one corresponding to the plastic strength and therefore flexural failure occurs (Figure 2.15b).
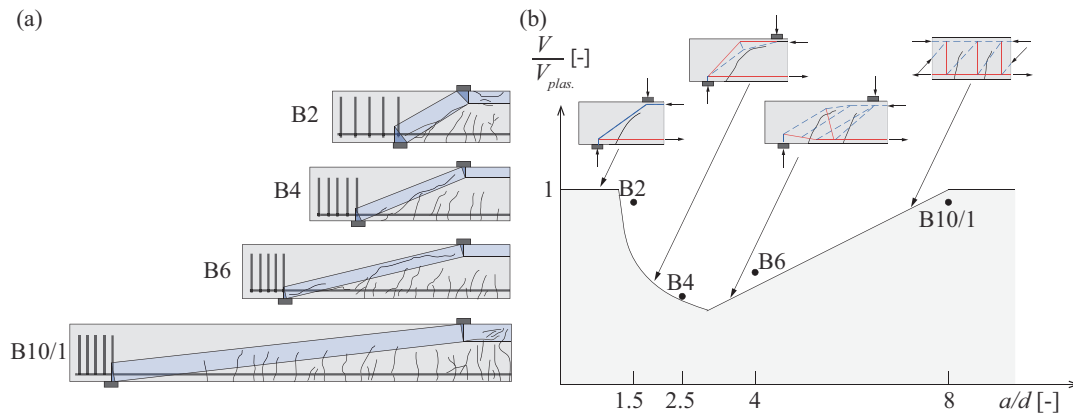
Figure 2.15 Influence of *a/d*: (a) tests B2, B4, B6, BP10/1 by Leonhardt and Walther [59], cracking pattern and theoretical strut position; (b) Kani's valley [58], comparing actual strength with failure load according to the theory of plasticity (adapted from Muttoni et al. [2])

The influence of the location of the critical shear crack was additionally investigated by Leonhardt et al. [59] on the basis of an experimental campaign aimed at studying the bond properties between the flexural reinforcement and the concrete matrix. Figure 2.16a shows the cracking pattern and the normalized shear strength of two geometrically identical specimens, but with different bond conditions. In beam EA1, deformed bars where used, whereas beam EB1 was cast with smooth bars. In specimen EA1, the critical shear crack developed through the theoretical compression strut and the failure load reached 50% of the plastic strength. On the contrary, for the beam EB1, as bond stresses were limited, only a few flexural cracks developed and the arching action could develop almost without any disturbance (the plastic strength was however not reached as the strut was partially affected by the development of the critical shear crack).

The influence of the location of the critical shear crack is also highlighted in Figure 2.16b, where the crack pattern and the normalized shear strength of two geometrically identical beams subjected to concentrated loading and different axial forces are compared (for a detailed description of the tests, see Madsen et al. [60]). Beam G1 was tested without axial compression forces, whereas beam F2 was subjected to large compression forces. For specimen G1, several cracks developed during loading and crossed the theoretical compression strut. On the contrary, for specimen F2 the critical shear crack disturbed only slightly the inclined strut carrying shear and its shear strength was significantly higher.

Further experimental evidences of the influence of cracks developing through the theoretical inclined compression strut were provided by Muttoni et al [19]. The authors tested two specimens with geometrical identical shear spans (refer to Figure 2.16c). Beam BP0 had only longitudinal reinforcement, whereas beam BP2 contained additionally a spiral reinforcement in the region close to the load introduction plate where the critical shear crack developed. Beam BP0 reached 50% of the plastic strength, whereas beam BP2 reached the full flexural strength: for this member the spiral reinforcement was effective in controlling the opening of the cracks within the inclined compression strut and thus the strength of the strut was not decreased [2].
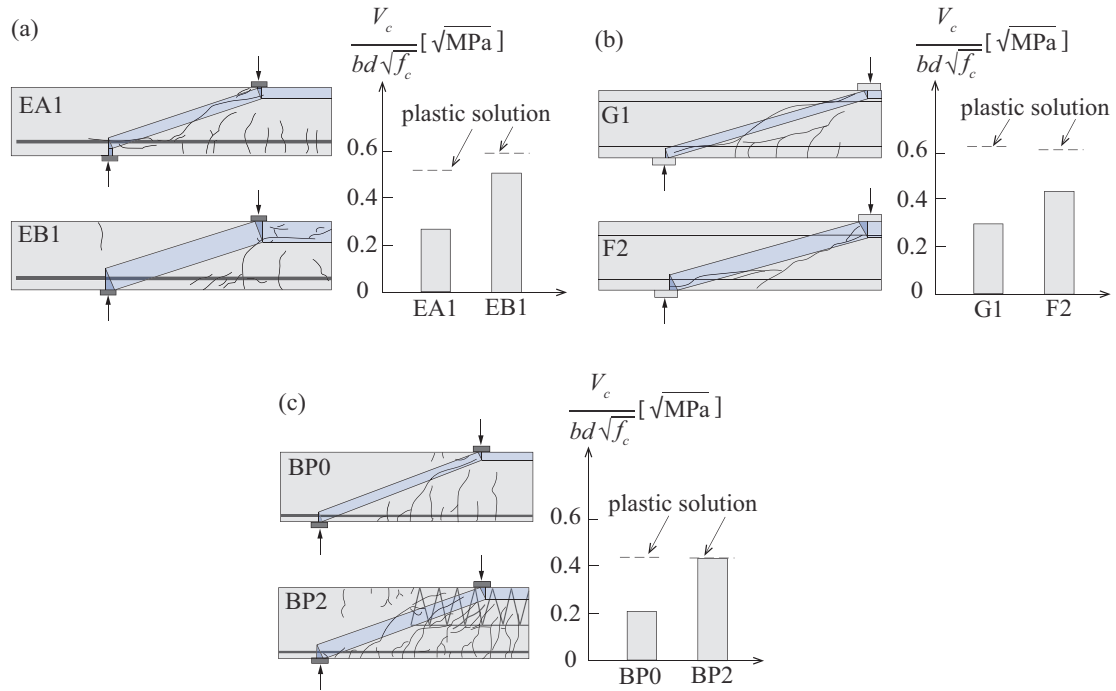
Figure 2.16 (a) Influence of bond on the shear strength and cracking pattern; (b) influence of axial normal force on the shear strength and cracking pattern; (c) influence of crack width on shear strength (adapted from Muttoni et al. [2])

On the basis of this available experimental background, it can be stated that the cases where the arching action is observed to be the dominant shear-transfer action correspond to [2]: (i) one-way slabs or beams with limited shear slenderness ($a/d < 2.5$); (ii) members with unbonded longitudinal reinforcement; (iii) prestressed members or members with large compressive normal forces.

On the contrary, beam shear-transfer actions are acknowledged to be governing in slender members without transverse reinforcement. However, in the scientific community there is not yet agreement on the predominant shear-transfer action and the phenomena governing the shear strength.

Taylor [7] was the first to calculate the contribution of the beam shear-transfer actions to the shear capacity of a slender cracked concrete member without shear reinforcement. Taylor observed that, as the critical shear crack develops, it is characterized by a combined opening and sliding and that the aggregate particles on one side of the crack enter in contact with the aggregates on the opposite side and activate aggregate interlock stresses. Taylor concluded that the contribution of the aggregate interlock is predominant (between 35% - 50% of the total shear force applied at the section), the contribution of the dowelling action varies between 15% and 25% and the compression zone carries between 20% and 40% of the total shear force. However, Taylor did not acknowledge the contribution of the residual tensile strength of concrete.

The role of the various shear-transfer actions in cracked reinforced concrete members without transverse reinforcement has been investigated more recently in more systematic testing programmes. For instance, Campana et al. [28] concluded that the activation of the various shear-transfer actions depends primarily on the shape, location and kinematics of the critical shear crack. Sherwood [61] showed that the primary mechanism of shear transfer is aggregate interlock, the uncracked compression zone carries up to 25% of the total shear force and failure is initiated by the breakdown of the aggregate interlock capacity. Huber et al. [62], on the basis of detailed analysis of the crack kinematics by means of photogrammetry techniques, showed that, in slender members without transverse reinforcement, the aggregate interlock is predominant, the contribution of the residual tensile stresses varies between 18% and 38% of the total shear force, the dowelling action is relatively small (10%-18%) and the contribution of the compression zone can be neglected. On the contrary, other researchers acknowledged that the shear resistance of a slender reinforced concrete beam is mainly provided by the uncracked compression zone and shear failure is triggered by the failure of the compression zone [63–65]. According to Zararis et al. [64], Kotsovos et al. [63, 66], Choi et al. [67, 68], the compression zone of intact concrete prevents shear-slip at the crack surfaces. Therefore, aggregate interlock and dowelling action do not contribute significantly to the shear strength of the beam and can be thus neglected.

2.3 Mechanical models

The investigations on the mechanisms of shear failure and on the role of the various shear-transfer actions allowed the development of mechanical models and non-linear finite element tools to design members without shear reinforcement.

An early attempt to give a physical explanation to shear failure of reinforced concrete beams without shear reinforcement was the Kani's tooth model [3, 69]. Kani assumed that flexural cracks shape the beam into a teeth-structure. The concrete between two adjacent flexural cracks is considered to behave as a cantilever fixed in the compression zone and loaded by the forces transferred by the longitudinal reinforcement (refer to Figure 2.2). According to Kani, the shear capacity of a cracked concrete beam can be expressed in term of the bending capacity of the teeth: when the bending moment at the fixed end of the cantilever attains a critical value, a horizontal crack propagates in the compression zone, causing the failure of the member.

Fenwick et al. [6] evaluated the Kani's model by comparisons with experiments and pointed out that the concrete teeth between two flexural cracks are limited from bending freely due to the friction between the crack faces and the dowelling action of the longitudinal reinforcement. The authors showed that aggregate interlock stresses, dowelling action and cantilever action are the main shear-transfer actions governing the shear strength. According to Fenwick et al. [6] when the moment at the fixed end of the cantilever reaches a critical value, cracks further propagate causing the collapse of the beam, unless the shear span-to-depth ratio is small enough to develop a compression strut above the critical shear crack.

Tooth models have been further developed by Hamadi et al. [12] and Reineck [70] and the mechanism of shear failure has evolved from the break of the tooth to the loss of aggregate interlock stresses between the crack surfaces. The main difference between the various tooth models are the spacing and inclination of the flexural cracks. Hamadi et al. [12] assumed that flexural cracks develop with a spacing s_r equal to one-half of the effective depth of the member, whereas Reineck [70] considered that cracks are inclined at 60° with respect to the beam axis with a spacing equal to $s_r=0.7 \cdot (d-c)$, where d is the effective depth and c is the depth of the compression zone. In addition, Reineck assumed that the depth of the compression zone c is constant along the beam and shear failure occurs at $1.5d$ from the load introduction plate. By defining a crack kinematics and a limiting value for the crack displacement and by considering the contribution of aggregate interlock, dowelling action and cantilever action, Reineck derived the following explicit equation for the ultimate shear strength:

$$V_c = \frac{0.4 \cdot b \cdot d \cdot f_{ct} + V_{du}}{1 + 0.16 \cdot \dfrac{f_{ct}}{f_c} \cdot \lambda \cdot \left(\dfrac{a}{d} - 1\right)}$$

(2.19)

where V_{du} is the dowelling action (refer to [70]), f_c and f_{ct} are the concrete compressive and tensile strength, b is the width, d is the effective depth, a is the shear span and λ is defined as:

$$\lambda = \frac{f_c \cdot d}{E_s \cdot \rho \cdot w_u}$$

(2.20)

where w_u is the limiting crack width (=0.09 mm), E_S is the elastic modulus of the steel bars and ρ is the reinforcement ratio.

The studies on the shear-transfer mechanisms evolved towards different approaches that consider a shear-transfer action as governing, disregarding the influence of the other shear-carrying mechanisms.

The Modified Compression Field Theory (MCFT) is a mechanical model based on the assumption that aggregate interlock is the governing shear-transfer action. The theory was originally developed by Mitchell and Collins [71] by observing the response of reinforced concrete elements loaded in pure shear or in shear combined with axial stresses and it was successively modified by Vecchio and Collins [72]. The MCFT consists of equilibrium, compatibility and stress-strain relationships and it is based on the main hypothesis which states that the direction of the average principle strains corresponds to the direction of the average principle stresses. The theory considers how the stresses are transmitted across the critical crack. The ability of the crack to transmit shear stresses is assumed to be influenced by the crack width w, the maximum aggregate size d_g and the concrete strength f_c. Based on the aggregate interlock experiments performed by Walraven [20], the shear stresses transferred through the crack are limited by the following equation:

$$\frac{V_c}{b \cdot d} \le \frac{0.18 \cdot \sqrt{f_c}}{0.31 + \dfrac{24 \cdot w}{d_g + 16}}$$

(2.21)

where the term d_g+16 characterizes the roughness of the crack.

Other approaches acknowledged the dowelling action as the governing shear-transfer action and associated the mechanism of shear failure with the loss of the dowelling force. According to Chana [73], the mechanism of shear failure is related to the development of a splitting crack along the longitudinal reinforcement. Kim and White [74] developed a physical model based on the calculation of the average shear stress developing in the region of the member slightly above the flexural reinforcement and adjacent to the critical crack. The authors related the initiation of the dowelling crack to the maximum bond stress between concrete and the flexural reinforcement in the vicinity of the critical shear crack and compared the bending moment with the development of the maximum bond stresses to derive the shear cracking load.

Alternatively, some approaches consider the uncracked compression zone as the most important parameter influencing the shear capacity. Zararis [75] showed that the critical diagonal crack is characterized by two branches which are formed at different time and due to different causes. The first branch is an inclined crack that develops up to the theoretical compression strut, whereas the second branch initiates from the tip of the first branch and propagates along the centre of the compression strut towards the loading point. The author suggested that failure is caused by the development of the second branch due to a type of splitting of concrete in the compression zone. Based on the theory of elasticity and equilibrium conditions, the author proposed the following equation to calculate the shear strength:

$$\frac{V_c}{b \cdot d} = \left(1.2 - 0.2 \cdot \frac{a}{d} \cdot d\right) \cdot \frac{c}{d} \cdot f_{ct} \tag{2.22}$$

where c is the depth of the compression zone, a is the shear span, f_{ct} is the tensile strength of concrete, b the width of specimen and d the effective depth. According to Zararis, the shear strength is purely carried by the uncracked compression zone, which essentially acts as a buffer preventing any contribution of shear along the crack surface.

Tureyen and Frosch [65] developed a model based on the assumption that the shear force is carried essentially by the uncracked compression zone. The authors proposed to evaluate the shear capacity by considering a parabolic distribution of the shear stresses and a linear distribution of the normal stresses in the compression zone and assumed that shear failure occurs when the principle tensile stresses reach the tensile strength of concrete. The following equation was proposed:

$$V_c = \frac{2}{3} \cdot b \cdot c \cdot \sqrt{f_{ct}^2 + f_{ct} \cdot \frac{\sigma_m}{2}} \tag{2.23}$$

where c is the depth of the compression zone, f_{ct} the tensile strength and σ_m the flexural stress at the extreme compression fibre.

Choi and Park [68, 76] proposed a strain-based model based on the failure of the compression zone. The authors developed a unified shear strength model for both deep and slender beams using the compression zone depth as the major design parameter and evaluated the shear strength by considering the interaction between normal and shear stresses in the compression zone and by using the Rankine's failure criteria. The authors showed that the compression zone may fail by compression crushing, in the case of deep beams, or by tensile cracking, in the case of slender beams.

Finally, other approaches account for all potential shear-transfer actions. This is for instance the approaches of Mari et al. [77], Yang [78], Tung et al. [79] and the Critical Shear Crack Theory [2, 47]. However, these approaches are not in agreement on the phenomena and mechanisms triggering shear failure. Mari et al. [77] acknowledged the contribution of all the various shear-transfer actions and assumed that failure occurs when the principle stresses in the compression zone reach the Kupfer's biaxial failure envelope. According to Yang [78], the propagation of a doweling crack along the longitudinal reinforcement causes the unstable propagation of the critical shear crack. The author proposed a simplified crack profile and kinematics and defined a critical shear displacement Δ_{cr} at the level of the longitudinal reinforcement as the criterion for the shear failure. Tung et al. [79] proposed a theoretical model that accounts for the component of the normal stress of concrete in the tension zone and is based on the assumption that the critical shear crack is initiated by the coalescence of micro cracks which are localized in a narrow band that connects the tips of existing flexural cracks. Muttoni et al. [2] developed the critical shear crack theory (CSCT) which is based on the assumption that the shear strength is governed by a flexural crack which develops diagonally (the critical shear crack) and disturbs the shear transfer actions.

The CSCT is a theory that was originally developed for punching shear design of slab-column connections without transverse reinforcement. The basic principles of the CSCT were introduced in the Draft Code Proposal of the Swiss Code for Structural Concrete in 1985 [80]. The theory was later extended to beams and one-way slabs without transverse reinforcement as well as two-way slabs with transverse reinforcement. The basis assumption of the CSCT states that the shear capacity depends on the member geometry (the width b and the effective depth d), the square root of the compressive strength of concrete f_c, the critical

shear crack opening w and its roughness (d_g+16 [72], where d_g is the maximum aggregate size). In the CSCT, the shear strength is checked at a control section (which depends on the load configuration) and the width is estimated to be proportional to a reference longitudinal strain times the effective depth of the member. The reference strain is evaluated in the control section at a depth of 0.6d from the compression face (see Figure 2.17a), assuming that plane sections remain plane and a linear elastic behaviour of concrete in compression, and it can be estimated as:

$$\varepsilon = \frac{M}{b \cdot d \cdot \rho \cdot E_s \cdot (d - c/3)} \frac{(0.6d - c)}{(d - c)} \tag{2.24}$$

where M is the bending moment at the control section, d is the effective depth, ρ is the reinforcement ratio, E_s is the elastic modulus of steel and c is the depth of the compression zone defined as:

$$c = d \cdot \rho \cdot \frac{E_s}{E_c} \cdot \left(\sqrt{1 + \frac{2E_c}{\rho E_s}} - 1 \right) \tag{2.25}$$

where E_c is the elastic modulus of concrete. Based on these assumptions, Muttoni et al. [2] proposed the following failure criterion to evaluate the shear strength (Figure 2.17b):

$$\frac{V_c}{b \cdot d \cdot \sqrt{f_c}} = \frac{1}{3 \cdot \left(1 + 120 \cdot \dfrac{\varepsilon \cdot d}{d_{g0} + d_g} \right)} \tag{2.26}$$

The shape of the hyperbolic failure criterion of the CSCT can be analytically derived by defining a crack shape and kinematics and some constitutive laws for the various shear-transfer actions. It can be demonstrated that the shear capacity, as well as the contribution of the shear-transfer actions, follows an hyperbolic decay for increasing opening of the critical crack (a qualitative comparison of the failure criterion of the CSCT and the contribution of the shear-transfer actions is shown in Figure 2.17c [47]).
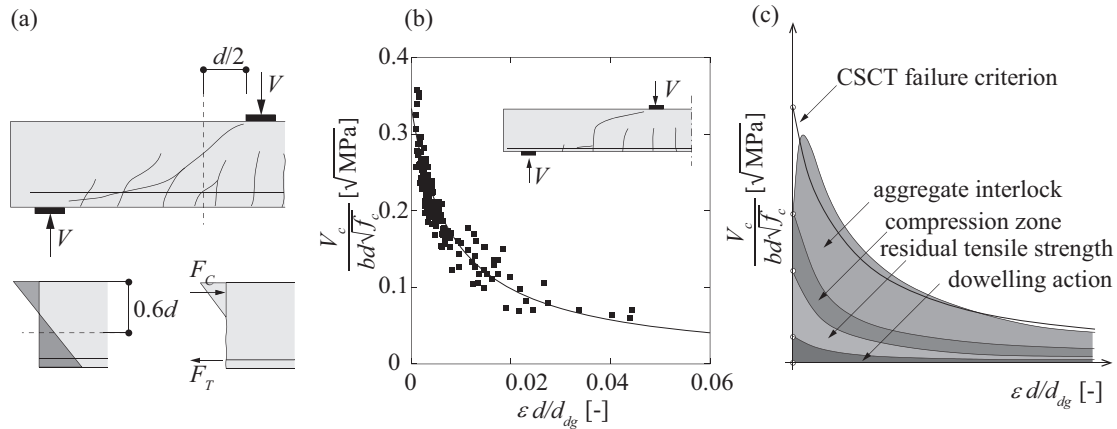
Figure 2.17 (a) Main assumptions of the critical shear crack theory (CSCT): control section and reference fibre; (b) hyperbolic failure criterion and comparison to test results [2]; (c) qualitative comparison of the shear-transfer actions and the failure criterion of the CSCT [47]

In addition to the previously described mechanical models based on the contributions of the different shear-transfer actions, numerous approaches based on the theory of plasticity have been successfully applied to determine the shear capacity of reinforced concrete beams without shear reinforcement. The applications of the theory of plasticity to members failing in shear was firstly investigated by Drucker [57], who proposed several stress fields in which the load is carried directly by inclined struts. Drucker developed both a lower and an upper bound solution and showed that the proposed lower and upper solutions provide the same failure load and correspond to the exact solution of the plastic analysis. However, the stress fields proposed by Drucker were found not suitable for slender reinforced concrete beams without shear reinforcement leading to unsafe design solutions and can be applied only for members with large amount of shear reinforcement or for squat members.

Some approaches have been derived on the basis of the lower bound theorem of plasticity. Collins et al [81] proposed a strut-and-tie model with a reduced compressive strength of the strut: for instance, for increasing slenderness, the strut becomes

flatter, the transverse tensile strain increases and the compressive strength of concrete is reduced. Braestrup [82] proposed an approach, where the compressive stresses are not related to the inclination of the strut, but the shear strength depends on the geometry of the nodal zone.

Some interesting approaches have also been developed based on the upper bound theorem of plasticity. For instance, the Contact Sliding Model is an upper bound plasticity approach that, contrary to the classic theory of plasticity, makes a distinction between yield lines formed in uncracked concrete and yield lines formed in cracked concrete. The model was initiated by Zhang [83] and was successively extended by Hoang for continuous beams and punching shear in slabs [84]. Contrary to the classic upper bound approach where the lowest upper bound solution is the diagonal crack developing from the end support to the load introduction plate, the inclination of the critical crack is determined by verifying the existence of the crack at failure, calculating the diagonal crack load P_{cr} by moment equilibrium of the rigid body shown in Figure 2.18a. Following the main principles of the plasticity approach, the total energy dissipated in a crack and the possible failure load P_u are calculated, accounting for a crack sliding reduction factor and an effectiveness compressive strength factor. Finally, the shear strength of the beam and the horizontal projection of the critical crack are determined by the intersection of the curves P_u and P_{cr}, as shown in Figure 2.18b.
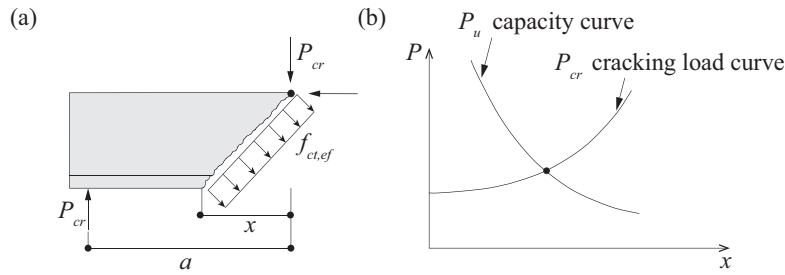
Figure 2.18 (a) Cracking mechanisms in a beam without shear reinforcement subjected to concentrated loading; (b) cracking load P_{cr} and shear capacity P_u curves as a function of the projection x of the critical shear crack [84]

Another mechanical model based on the upper bound principles of the theory of plasticity was developed by Fisker [85]. According to the author, the shear capacity is governed by a sliding failure mechanism, involving both sliding along an existing inclined flexural crack and sliding along a failure line within the uncracked compression zone developing from the tip of the flexural crack to the loading plate. In the model, both uncracked concrete and cracks are plastic materials, with the difference that the capacity of cracks is inversely proportional to the crack opening.

2.4   Code provisions

This section provides the shear formulations of some codes of practice for nonprestressed rectangular concrete members without shear reinforcement.

2.4.1   ACI 318

The shear strength formulation according to the ACI code [86] is:

$$V_c = \frac{1}{6} \cdot \sqrt{f_c} \cdot b_w \cdot d \qquad\qquad (2.27)$$

where V_c is the shear capacity (in [N]), b_w is the member width (in [mm]), d is the effective depth (in [mm]) and f_c is compressive strength of concrete (in [MPa]). For high-strength concrete members, the term $\sqrt{f_c}$ is limited to a value of 8.3 MPa. The shear strength is checked at a control section located at a distance d from the load introduction plate or the face of the support.

2.4.2   Eurocode 2

The shear strength formulation according to Eurocode 2 [87] is an empirical formulation, which was calibrated with experimental data through a statistical approach. The shear strength is given by:

$$V_c = 0.18 \cdot k \cdot \left(100 \cdot \rho \cdot f_c\right)^{1/3} \cdot b_w \cdot d \geq 0.035 \cdot k^{3/2} \cdot f_c^{1/2} \cdot b_w \cdot d \qquad\qquad (2.28)$$

where V_c is the shear capacity (in [N]), b_w is the member width (in [mm]), d is the effective depth (in [mm]), f_c is compressive strength of concrete (in [MPa]) and ρ is the longitudinal reinforcement ratio (that shall not be taken larger than 0.02). The parameter k can be determined as:

$$k = 1 + \sqrt{\frac{200}{d}} \leq 2 \quad d \text{ in [mm]} \tag{2.29}$$

The shear strength is verified at a control section located at a distance d from the plate of load introduction or the face of the support.

2.4.3   SIA 262:2013

The Swiss Code (SIA 262:2013 [88]) shear formulation is based on the Critical Shear Crack Theory [2]. The shear strength per unit length is given by:

$$v_c = k_d \cdot \tau_c \cdot d \tag{2.30}$$

with

$$\tau_c = 0.3 \cdot \sqrt{f_c} \tag{2.31}$$

$$k_d = \frac{1}{1 + \varepsilon_v \cdot d \cdot k_g} \tag{2.32}$$

and

$$k_g = \frac{48}{16 + d_g} \tag{2.33}$$

where v_c represents the shear strength per unit length (in [N/mm]), d is the effective depth (in [mm]), f_c is the compressive strength of concrete (in [MPa]), d_g is the maximum aggregate size (in [mm]). For concrete compressive strengths larger than 70 MPa (high-strength concrete) or for lightweight concrete, d_g shall be taken equal to zero in order to account for the loss of aggregate interlock capacity in the cracks due to the fracture of the aggregates. The shear resistance is calculated at a control section located at a distance $d/2$ from the plate of load introduction or the edge of the support.

If the main flexural reinforcement remains in the elastic domain, the deformation ε_v at the level of the longitudinal reinforcement can be estimated as:

$$\varepsilon_v = \frac{f_s}{E_s} \cdot \frac{m}{m_R} \tag{2.34}$$

where f_s is the yielding strength of the longitudinal reinforcement (in [MPa]), E_s is the modulus of elasticity of the reinforcement bars (in [MPa]), m is the acting bending moment per unit length at the control section (in [kNm/m]) and m_R is the yielding moment per unit length (in [kNm/m]). The flexural strength m_R can be estimated, assuming a plastic behaviour of the reinforcement after yielding, as:

$$m_R = \rho \cdot f_s \cdot b_w \cdot d^2 \cdot \left(1 - \frac{\rho \cdot f_s}{2 \cdot f_c}\right) \tag{2.35}$$

where ρ is the longitudinal reinforcement ratio and b_w is the width of the member (in [mm]).

If the reinforcement enters in the plastic domain, ε_v can be calculated as:

$$\varepsilon_v = 1.5 \cdot \frac{f_s}{E_s} \tag{2.36}$$

2.4.4 *fib*-Model Code 2010

The shear strength formulation according to the fib Model Code 2010 [54, 89] is based on the Modified Compression Field Theory [72]. The shear strength is given by:

$$V_c = k_v \cdot \sqrt{f_c} \cdot b_w \cdot z \tag{2.37}$$

where V_c is the shear capacity (in [N]), b_w is the member width (in [mm]), z is the inner level arm (in [mm]) that can be taken equal to $0.9d$ and f_c is the concrete compressive strength (in [MPa]). For high-strength concrete, the term $\sqrt{f_c}$ is limited to a maximum value of 8 MPa. The parameter k_v is determined as:

$$k_v = \frac{0.4}{1 + 1500 \cdot \varepsilon_x} \cdot \frac{1300}{1000 + k_{dg} \cdot z} \tag{2.38}$$

and k_{dg} as:

$$k_{dg} = \frac{32}{16 + d_g} \geq 0.75 \tag{2.39}$$

where d_g is the maximum aggregate size (in [mm]). For concrete compressive strengths larger than 70 MPa and lightweight concrete, d_g shall be taken equal to zero.

The shear resistance, and thus the term ε_x, is calculated at a control section located at a distance d from the plate of load introduction or the face of the support. If no axial force is applied, ε_x is given by:

$$\varepsilon_x = \frac{1}{2 \cdot E_s \cdot A_s} \cdot \left(\frac{M_E}{z} + V_E \right) \tag{2.40}$$

where E_s is the modulus of elasticity of the reinforcement bars (in [MPa]), A_s is the flexural reinforcement area (in [mm^2]), M_E and V_E are respectively the acting bending moment and shear force at the control section.

2.5   References

[1]   ACI-ASCE Committee 445. Recent Approaches to Shear Design of Structural Concrete. *Journal of Structural Engineering* 1998; 124 (12):1375–1417.

[2]   Muttoni A, Fernández Ruiz M. Shear strength of members without transverse reinforcement as function of critical shear crack width. *ACI Structural Journal* 2008; 105 (2):163–172.

[3]   Kani GNJ. The riddle of shear failure and its solution. *ACI Journal* 1964; 61 (4):441–467.

[4]   Coley BE, Humprey HA. Aggregate Interlock at Joints. In Concrete Pavements, Portland Cement Association Research & Development Laboratories, Bulletin D-124. 1967.

[5]   Nowlen WJ. Influence of Aggregate Properties on the Effectiveness of Interlock Joints. In Concrete Pavements, Portland Cement Association Research & Development Laboratories, Bullettin D-139. 1968.

[6]   Fenwick RC, Paulay T. Mechanisms of shear resistance of concrete beams. *Journal of the Structural Division ASCE* 1968; 94 (10):2325–2350.

[7]   Taylor HPJ. Investigation of the forces carried across cracks in reinforced concrete beams in shear by interlock of aggregate. Cement and Concrete Association, Technical Report No. 42.77, London (UK). 1970.

[8]   Houde J, Mirza MS. A finite element analysis of shear strength of reinforced concrete beams. *ACI Special Publication SP-42* 1974; 1:103–128.

[9]   Paulay T, Loeber PJ. Shear Transfer by Aggregate Interlock. *ACI Special Publication SP-42* 1974; 1:1–16.

[10]   Mattock AH, Li WK, Wang TC. Shear transfer in lightweight reinforced concrete. *PCI Journal* 1976; 21 (1):20–39.

[11]   Jimenez Perez R, Gergely P, White RN. Shear Transfer across Cracks. In Reinforced Concrete, Technical Report No. 78-4, Cornell University, NY, USA. 1978.

[12]   Hamadi YD, Regan PE. Behaviour in shear of beams with flexural cracks. *Magazine of Concrete Research* 1980; 32 (111):67–78.

[13]   Walraven JC. Fundamental analysis of aggregate interlock. *Journal of Structural Division* 1981; 107 (11):2245–2270.

[14]   Sagaseta J, Vollum R. Influence of aggregate fracture on shear transfer through cracks in reinforced concrete. *Magazine of Concrete Research* 2011; 63 (2):119–137.

[15]   Nooru-Mohamed M. Mixed-mode fracture of concrete: An experimental approach, Ph.D. Thesis, Delft, Netherlands: DTU. 1992:151.

[16]   Hassanzadeh M. Behaviour of fracture process zones in concrete influenced by simultaneously applied normal and shear displacements, Report TVBM 1010. 1992.

[17]   Østergaard L, Olesen JF, Poulsen PN. Biaxial testing machine for mixed mode cracking of concrete, Fracture mechanics of concrete and concrete structures: new trends in fracture mechanics of concretes. 2007.

[18]   Jacobsen JS, Poulsen PN, Olesen JF. Characterization of mixed mode crack opening in concrete. *Materials and Structures* 2012; 45 (1–2):107–122.

[19]   Muttoni A, Thürlimann B. Shear tests on beams and slabs without transverse reinforcement, Institut für Baustatik und Konstruktion, Zürich, Switzerland. 1986:12.

[20]   Walraven JC, Reinhardt HW. Theory and experiments on the mechanical behavior of cracks in plain and reinforced concrete subjected to shear loading. *Heron* 1981; 1a:5–68.

[21]   Bazant ZP, Gambarova PG. Rough Cracks in Reinforced Concrete, ASCE 15330 Proceeding. *Journal of Structural Division* 1980; 106:819–842.

[22]   Gambarova PG, Karakoc C. A new approach to the analysis of the confinement role in regularly cracked concrete elements. *Transactions of the 7. international conference on structural mechanics in reactor technology* 1983; H.

[23]   Daschner F, Kupfer H. Versuche zur Schubkraftubertragung in Rissen von Normalund Leichtbeton (in German). *Bauingenieur* 1982; 57 (2).

[24]   Li B, Maekawa K, Okamura H. Contact density model for stress transfer across cracks in concrete. *Journal of the Faculty of Engineering, University of Tokyo* 1989; 40 (1):9–52.

[25]   Ulaga T. Betonbauteile mit Stab- und Lamellenbewehrung: Verbund- und Zuggliedmodellierung. PhD Thesis. Thesis no. 15062 (in German). Zurich, Switzerland: ETHZ. 2003:160.

[26]   Guidotti R. Poinçonnement des planchers-dalles avec colonnes superposées fortement sollicitées. PhD Thesis. Thesis no. 4812 (in French). Lausanne, Switzerland: Ecole Polytechnique Fédérale de Lausanne. 2010:416.

[27]   Sagaseta J. The influence of aggregate fracture on the shear strength of reinforced concrete beams, PhD Thesis, London, UK: Imperial College. 2008:409.

[28]   Campana S, Anastasi A, Fernández Ruiz M, Muttoni A. Analysis of shear-transfer actions on one-way RC members based on measured cracking pattern and failure kinematics. *Magazine of Concrete Research* 2013; 65 (6):386–404.

[29]   Eleiott AF. An experimental investigation of shear transfer across cracks in reinforced concrete, Master of Science Thesis, Ithaca, NY,USA: Cornell University. 1974.

[30]   Paschen H, Schönhoff T. Untersuchungen übet in Beton eingelassene Scherbolzen aus Betonstahl, Heft 346. *Deutscher Ausschuss für Stahlbeton* 1983:105–149.

[31]   Rasmussen BH. Strength of transversely loaded bolts and dowels embedded in concrete, Meddelelse Laboratoriet for Bugningastatik, Denmark Technical University. 1962; 34 (2):39–55.

[32]   Hofbeck JA, Ibrahim IO, Mattock AH. Shear transfer in reinforced concrete. *ACI Journal Proceedings* 1969; 66 (2):119–128.

[33]   Dulacska H. Dowel action of reinforcement crossing cracks in concrete. *ACI Journal Proceedings* 1972; 69 (12):754–757.

[34]   Dei Poli S, Di Prisco M, Gambarova PG. Shear response, deformations, and subgrade stiffness of a dowel bar embedded in concrete. *ACI Structural Journal* 1992; 89 (6):665–675.

[35]   Vintzeleou EN, Tassios TP. Mathematical models for dowel action under monotonic and cyclic conditions. *Magazine of Concrete Research* 1986; 38:13–22.

[36]   Krefeld WJ, Thurston CW. Studies of the shear and diagonal tension strength of simply supported R/C-beams. *ACI Journal* 1966; 63 (4):451–476.

[37]   Taylor HPJ. Investigation of the dowel shear forces carried by tensile steel in reinforced concrete beams. Cement and Concrete Association, Technical Report no. TRA 431, London (UK). 1969.

[38]   Baumann T, Rüsch H. Versuche zum studium der Verdübelungswirkung der Biegezugbewehrung eines

Stahlbetonbalkens. *Deutscher Ausschuss für Stahlbeton* 1970; 210:42–83.

[39]   Sharma NK. Splitting Failures in Reinforced Concrete Members, PhD Thesis, Ithaca, N.Y., USA: Cornell University. 1969.

[40]   Kemp EL, Wilhelm WJ. An Investigation of the Parameters Influencing Bond Behaviour with a View Towards Establishing Deisgn Criteria, Report WVDOH 46-2, Dept. of Civil Engineering, West Virginia University, West Virginia. 1977.

[41]   Plumey S. Interaction sol-structure dans le domaine des tranchées couvertes. PhD Thesis. Thesis no. 3714 (in French). Lausanne (Switzerland): Ecole Polytechnique Fédérale de Lausanne. 2007:196.

[42]   Neuner J., Stöckl S. Versuche zur Aufnahme der Umlenkkräfte von gekrümmten Bewehrungsstäben durch Betondeckung und Bügel, Heft 322. *Deutscher Ausschuss für Stahlbeton* 1981:71–106.

[43]   Franz G, Fein HD. Tests on R/C Culvert and Tunnel Lining, 2nd test series (Betonversuche mit Baustahlgewebe-Bewehrungen für Rohre und Tunnelverkleidungen, Versuchsreihe 2), Baustahlgewebe Berichte aus Forschung und Technik, Heft 8, Düsseldorf-Oberkassel, Germany. 1971:52.

[44]   Intichar M, Ebner M, Sparowitz L. Deviation Forces in Curved Beams (Umlenkkräfte in gekrümmten Stahlbetonbalken),. *Österreichische Ingenieur-und Architekten-Zeitschrif* 2004; 149 (1):11–16.

[45]   Fernández Ruiz M, Plumey S, Muttoni A. Interaction between Bond and Deviation Forces in Spalling Failures of Arch-Shaped Members without Transverse Reinforcement. *ACI Structural Journal* 2010; 107 (3):346–354.

[46]   Fernández Ruiz M, Mirzaei Y, Muttoni A. Post-punching behavior of flat slabs. *ACI Structural Journal* 2013; 110 (5):801–812.

[47]   Fernández Ruiz M, Muttoni A, Sagaseta J. Shear strength of concrete members without transverse reinforcement: a mechanical approach to consistently account for size and strain effects. *Engineering Structures* 2015; 99:360–372.

[48]   Giurani E, Plizzari G, Schumm C. Role of Stirrups and Residual Tensile Strength of Cracked Concrete on Bond. *Journal of Structural Engineering* 1991; 117 (1):1–18.

[49]   Evans RH, Marathe MS. Microcracking and stress-strain curves for concrete in tension. *Materials and Structures* 1968; 1 (1):61–64.

[50]   Hillerborg A, Modéer M, Petersson PE. Analysis of crack formation and crack growth in concrete by means of fracture mechanics and finite elements. *Cement and concrete research* 1976; 6 (6):773–781.

[51]   Karihaloo BL. Fracture Mechanics and Structural Concrete, Longman Scientific and Technical, Harlow. 1995.

[52]   Reinhardt HW. Fracture Mechanics of an Elastic Softening Material like Concrete. *Heron* 1984; 29 (2):42.

[53]   Hordijk DA. Tensile and tensile fatigue behaviour of concrete; experiments, modelling and analysis. *Heron* 1992; 37 (1):3–79.

[54]   Fédération Internationale du Béton (fib), fib Model Code for Concrete Structures 2010, Ernst & Sohn. 2013:434.

[55]   Park P, Paulay T. Reinforced Concrete Structures, John Wiley & Sons, Inc., New York. 1975:769.

[56]   Mörsch E. Reinforced concrete construction, theory and application. 3rd ed. Verlag von Konrad Wittwer (Der Eisenbetonbau, seine theorie und anwendung, in German). 1908:376.

[57]   Drucker DC. *On Structural Concrete and the Theorems of Limit Analysis.* 1961.

[58]   Kani MW, Huggins MW, Wittkopp RR. Kani on shear in reinforced concrete. Deptartment of Civil Engineering, University of Toronto, Toronto, Canada. 1979.

[59]   Leonhardt F, Walther R. Schubversuche an einfeldrigen Stahlbetonbalken mit und ohne Schubbewehrung. DAfStb H.151, Berlin. 1962.

[60]   Madsen MB, Hansen S, Hoang LC, Maagard J. N-V Interaction in Reinforced Concrete Elements without Stirrups. The Twelth East Asia-Pacific Conference on Structural Engineering and Construction. *Procedia Engineering* 2011; 14:2511–2518.

[61]   Sherwood EG, Bentz EC, Collins MP. Effect of Aggregate Size on Beam-Shear Strength of Thick Slabs. *ACI Structural Journal* 2007; 104 (2):180–190.

[62]   Huber P, Huber T, Kollegger J. Investigation of the shear behaviour of RC beams on the basis of measured crack kinematics. *Engineering Structures* 2016; 113:41–58.

[63]   Kotsovos MD, Pavlovic MN. Ultimate Limit-State Design of Concrete Structures: A New Approach, Thomas Telford, London. 1998:208.

[64]   Zararis PD, Papadakis GC. Diagonal Shear Failure and Size Effect in RC Beams without Web Reinforcement. *Journal of Structural Engineering* 2001; 127 (733–742).

[65]   Tureyen AK, Frosch RJ. Concrete Shear Strength: Another Perspective. *ACI Structural Journal* 2003; 100 (5):609–615.

[66]   Kotsovos MD. Reinforced Concrete Shear Design: Shortcomings and Remedy. *ACI Structural Journal* 2017; 114 (4):1055–1066.

[67]   Choi K-K, Park H-G, Wight JK. Unified Shear Strength Model for Reinforced Concrete Beams—Part I: Development. *ACI Structural Journal* 2007; 104 (2):142–152.

[68]   Choi K-K, Kim J-C, Park H-G. Shear Strength Model of Concrete Beams Based on Compression Zone Failure Mechanism. *ACI Structural Journal* 2016; 113 (5):1095–1106.

[69]   Kani GNJ. How safe are our large reinforced concrete beams? *ACI Journal* 1967; 64 (3):128–141.

[70]   Reineck K-H. Ultimate shear force of structural concrete members without transverse reinforcement derived from a mchanical model. *ACI Structural Journal* 1991; 88 (5):592–602.

[71]   Mitchell D, Collins MP. Diagonal Compression Field Theory. *ACI Journal Proceedings* 1974; 71 (8):396–408.

[72]   Vecchio FJ, Collins MP. The modified compression field theory for reinforced concrete elements subjected to shear. *ACI Journal* 1986; 83 (2):219–231.

[73]   Chana PS. Investigation of the mechanism of shear failure of reinforced concrete beams. *Magazine of Concrete Research* 1987; 39 (141):196–204.

[74]   Kim W, White RN. Initiation of Shear Cracking in Reinforced Concrete Beams with No Web Reinforcement. *ACI Structural Journal* 1991; 88 (3):301–308.

[75]   Zararis PD. Shear strength and minimum shear reinforcement of reinforced concrete slender beams. *ACI Structural Journal* 2003; 100 (2):203–214.

[76]   Park H-G, Choi K-K, Wight JK. Strain-Based Shear Strength Model for Slender Beams without Web Reinforcement. *ACI Structural Journal* 2006; 103 (6):783–793.

[77]   Marí A, Bairán J, Cladera A, Oller E, Ribas C. Shear-flexural strength mechanical model for the design and assessment of reinforced concrete beams. *Structure and Infrastructure Engineering: Maintenance, Management, Life-Cycle Design and Performance* 2014; 8 (4):337–353.

[78]   Yang Y. Shear Behaviour of Reinforced Concrete Members without Shear Reinforcement A New Look at an Old Problem. PhD Thesis. Delft (Netherlands): Delft University of Technology. 2014:344.

[79]   Tung ND, Tue NV. A new approach to shear design of slender reinforced concrete members without transverse reinforcement. *Engineering Structures* 2016; 107:180–194.

[80]   Muttoni A. Punching shear – Draft code proposal, SIA 162, Working Group 5, Swiss Society of Engineers and Architects, Zürich. 1985:15.

[81]   Collins MP, Mitchell D. A Rational Approach to Shear Design - The 1984 Canadian Code Provisions. *ACI Journal* 1986; 83 (6):925–933.

[82]   Braestrup MW. Shear Strength Prediction-Plastic Method. In Reinforced Concrete Deep Beams, F. K. Kong, ed., Blackie and Son Ltd., Glasgow and London, and Van Nostrand Reinhold, N.Y. 1990:182–203.

[83]   Zhang J. Diagonal cracking and shear strength of reinforced concrete beams. *Magazine of Concrete Research* 1997; 49 (178):55–65.

[84]   Nielsen MP, Hoang LC. Limit analysis and concrete plasticity. CRC press. 2016.

[85]   Fisker J, Hagsten LG. Mechanical model for the shear capacity of R/C beams without stirrups: A proposal based on limit analysis. *Engineering Structures* 2016; 115:220–231.

[86]   ACI Committee 318. Building code requirements for structural concrete and commentary. Farmington Hills (USA): American Concrete Institute. 2011:503.

[87]   Eurocode 2. Design of concrete structures – general rules and rules for buildings. EN 1992-1-1. Brussels (Belgium): CEN European Committee for Standardization. 2004:225.

[88]   SIA. Code 262 for concrete structures. Zürich: Swiss Society of Engineers and Architects. 2013:102.

[89]   Sigrist V, Bentz EC, Fernández Ruiz M, Foster SJ, Muttoni A. Background to the Model Code 2010 Shear Provisions - Part I: Beams and Slabs. *Structural Concrete* 2013; 14 (2):157–167.

Chapter 3   Shear failures in reinforced concrete members without transverse reinforcement: an analysis of the critical shear crack development on the basis of test results

This Chapter presents the results of an experimental campaign of 13 beams tested under different loading conditions. The development of the critical shear crack and its kinematics are tracked in detail with the aim of providing useful materials for the development of a rational theory for shear design. This Chapter has been published in a scientific journal:

The first author carried out the experimental campaign, the analysis of test results under the guidance of the second and third author, who contributed to understanding, interpreting the experimental findings and writing the final draft of the paper.

3.1   Abstract

Shear in concrete members without transverse reinforcement can be carried by various potential shear-transfer actions, whose activation depends much on the actual cracking pattern and kinematics at failure. Failures can occur in a progressive manner (at the end of a stable propagation of a critical shear crack) or in a sudden manner (by an unstable progression or development of a new crack). In addition, the development and shape of the failure crack may also be very different from case to case. These differences influence which shear-transfer actions may be governing for a given member and loading situation. Despite the large number of specimens tested in shear, almost no information on the actual crack development during the process of failure is yet available. This paper presents the results of an experimental programme consisting of thirteen beams. The tests were designed to investigate different structural systems and loading conditions commonly found in practice (cantilevers with concentrated and distributed loading, single span beams with distributed loading and continuous beams). The cracking patterns and their associated kinematics were tracked in detail by using photogrammetric techniques at high frequencies during testing and particularly during the process of failure, providing data on the actual crack development leading to shear failure. The observations show that very different cracking patterns may be found and that they might be also developed in different manners. The results are interpreted with reference to the measured crack kinematics and related to the various potential shear-transfer actions, with the aim of providing a useful material towards the development of rational approaches for shear design.

Key-words: shear; concrete structures; experimental observations; photogrammetry.

3.2   Introduction

Shear design has attracted significant research efforts since the first constructions in reinforced concrete. Particularly, in the case of members without transverse reinforcement, shear is acknowledged as a failure mode potentially governing the design at ultimate limit state and being particularly critical due to its limited capacity of deformation and brittleness. Contrary to design of beams with transverse reinforcement, where consistent design methods based on equilibrium solutions were early developed [1–4], shear design of one-way slabs and beams without transverse reinforcement has mainly remained based on empirical equations in many codes of practice [5, 6].

Despite the lack of a generally-accepted mechanical approach, significant research efforts have been devoted in the last decades on the phenomenon of shear-transfer in reinforced concrete [7–15]. These investigations have allowed understanding the basic

shear-transfer actions in reinforced concrete members and have led to the development of mechanical models for shear design. These models have reached a certain level of maturity and are starting to be incorporated into design codes [16–18].

Nevertheless, it is interesting to observe that despite the fact that the different mechanical models predict similar shear strengths, they are not necessarily in agreement on the governing shear-transfer action carrying the load (or their relative significance). A potential reason for this disagreement is grounded on the fact that the mechanical models are usually based on the interpretation of a crack pattern after failure or based on a measured kinematics before it happens. This is the consequence of conventional measurement techniques that in many cases have not been capable of tracking the crack development during the process of failure. Thus, most times, the interpretation of the shear-transfer actions is performed on the basis of pictures taken prior failure or after it. This might nevertheless have consequences unless the analysis is performed on the basis of a picture taken right at failure (maximum load), as redistributions amongst the potential shear-transfer actions develop before or during the process of failure (sometimes allowing the member to withstand the applied actions in a stable manner, but sometimes not). In addition, the analysis of the kinematics and cracking pattern during the process of failure yields to a better understanding of the activation of the various shear-transfer actions and failure modes. In this situation, new measurements techniques are providing a significant breakthrough to obtain better interpretation of the experimental evidence [19]. In particular, digital measurement from high-resolution photography (photogrammetry) constitutes a consistent tool to obtain accurate measurements of strains and crack widths at high frequencies (even higher than 1 Hz). The use of this tool enables detailed investigation of the instants preceding the maximum load and right after it, allowing interpretation of the process during which failure occurs.

In this paper, the results of an experimental testing programme are presented. Other than conventional measurements, photogrammetric techniques were implemented and processed, allowing detailed observations of the actual mechanisms leading to failure. These results are thoroughly explained and related to the shear-transfer actions. It is observed that causes leading to failure are not necessarily the same for the tested members, partly justifying the points of view of different (even contradictory) approaches for mechanical modelling of shear. The experimental programme also investigates the differences that are found between classical laboratory testing (single span beams subjected to concentrated loads) with respect to conditions representative of actual members (continuous beams, distributed loading, compression reinforcement). On the basis of these observations, a critical review of the shear-transfer actions and their role is presented, as well as the agreement and disagreement with some selected mechanical models.

3.3 Classical definitions of shear-transfer actions and mechanical modelling in reinforced concrete members

The development of mechanical models in reinforced concrete beams without stirrups has been normally performed by accounting for the equilibrium of inner forces developing at a free-body (Figure 3.1a) or by considering the role of the potential shear-transfer actions (Figure 3.1b–f). Both approaches are in fact related to the principles of the upper- and lower-bound theorems of the theory of plasticity [20]. The former (forces acting on a free-body) investigates on the actions at the edges of the free-body related to the failure mechanism (without any further check inside the free bodies). The latter usually considers one or more shear-transfer actions as potentially governing, whose maximum strength is calculated on the basis of a licit stress field.

Developing a suitable approach should in fact incorporate both perspectives, accounting both for a suitable stress field and a compatible kinematics allowing activation of the shear-transfer actions. Conventionally, the shear-transfer actions are classified into beam shear-transfer actions (Figure 3.1c–f) and the arching action (Figure 3.1b). Beam shear-transfer actions require development of tensile stresses in concrete, and allow for the force in the tension chord to vary. They are usually referred as cantilever action (Figure 3.1c), residual tensile strength action (Figure 3.1d), dowel action (Figure 3.1e) and aggregate interlock (Figure 3.1f). With respect to full arching action (Figure 3.1b), no tensile strength is required in the concrete and the force in the reinforcement remains constant (according to limit analysis, all shear force can be carried without transverse reinforcement by an inclined direct strut [21]). In reality, arching action can also happen combined with the beam shear-transfer actions (Figure 3.1f). With respect to the beam shear-transfer actions:

- Cantilever action (Figure 3.1c) was acknowledged by Kani as a basic action for shear-transfer [10]. It consists on the development of inclined struts and ties in the concrete between two flexural cracks (Figure 3.1c). For a cross-section at the location of a bending crack, shear is carried by the inclination of the compression zone (component V_c in Figure 3.1a).

- Residual tensile stresses of concrete (Figure 3.1d, component V_t in Figure 3.1a). This action can be considered only significant for low cracks openings (or near the tip of the crack).

- Dowelling action (Figure 3.1e) requires developing tensile stresses in the concrete cover potentially leading to its delamination. Even after delamination, dowelling action is still possible [11, 22] (component V_d in Figure 3.1a). In members with compression reinforcement, significant dowelling action can develop provided that the reinforcement is intercepted by the failure crack [22].

- Aggregate interlock (Figure 3.1f) allows developing shear and compressive stresses through the cracks due to the roughness of cracked concrete [14, 23, 24] (component V_a in Figure 3.1a). It is an efficient shear-transfer action, yet quite sensitive to the opening of the cracks.
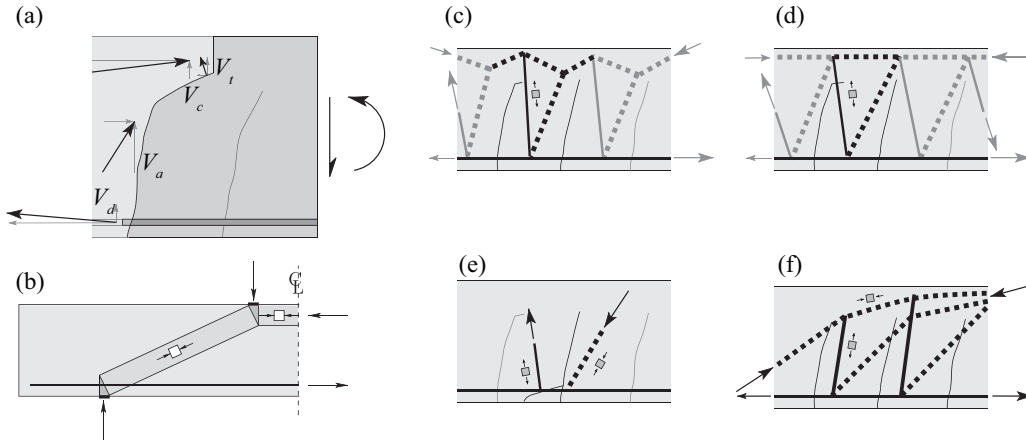
Figure 3.1 Analysis of shear-transfer actions: (a) free-body equilibrium and internal forces; (b) arching action; (c) cantilever action; (d) residual tensile strength of concrete; (e) dowelling action; and (f) aggregate interlock action

Most of the available design models for shear usually acknowledge one of the previous shear-carrying actions as governing. For instance, the Modified Compression Field Theory [12] can be considered as a theory accounting primarily for the role of aggregate interlock in case of members without transverse reinforcement. The role of the inclination of the compression chord (combined cantilever and arching action) is referred by Zararis [25] and Tureyen and Frosch [26]. The role of delamination and its influence in failures controlled by aggregate interlock has been recently explored by Yang [27]. There are also some approaches considering plasticity [28] and even modifying dissipation along the yield lines depending on the cracking state [29].

Other models for shear design, nevertheless, acknowledge also contribution of other actions and even allow calculating the contribution of each. A physical approach considering the contribution of all potential shear-transfer actions has recently been developed by Marí et al. [30] and also by Tue et al. [31]. The Critical Shear Crack Theory [32] has also acknowledged the role of the various shear-transfer actions, with cracking as an estimator of the decrease of the total shear strength.

3.4 Testing programme and refined measurements on kinematics at failure

In the following, the results of an experimental programme consisting of 13 beams (Figure 3.2 and Figure 3.3) tested at Ecole Polytechnique Fédérale de Lausanne (Switzerland) will be presented. The tests were performed with the aim of obtaining refined measurements on the crack development and kinematics during the process of failure. A total of 15 tests were performed on 13 specimens, as two of the specimens could be strengthened after failure on one side and then were reloaded until failure occurred on the other side (specimens SC51 and SC52). Some specimens were subjected to distributed loading whereas others were subjected to concentrated loads allowing for comparisons on their behaviour (completing a previous work of the authors and Pérez Caldentey et al. [33] on the shear capacity of cantilevers subjected to distributed – uniform or not – loading patterns). The present series was designed to investigate different structural systems and loading conditions commonly found in practice (cantilevers with concentrated and distributed loading, single span beams with distributed loading and continuous beams).
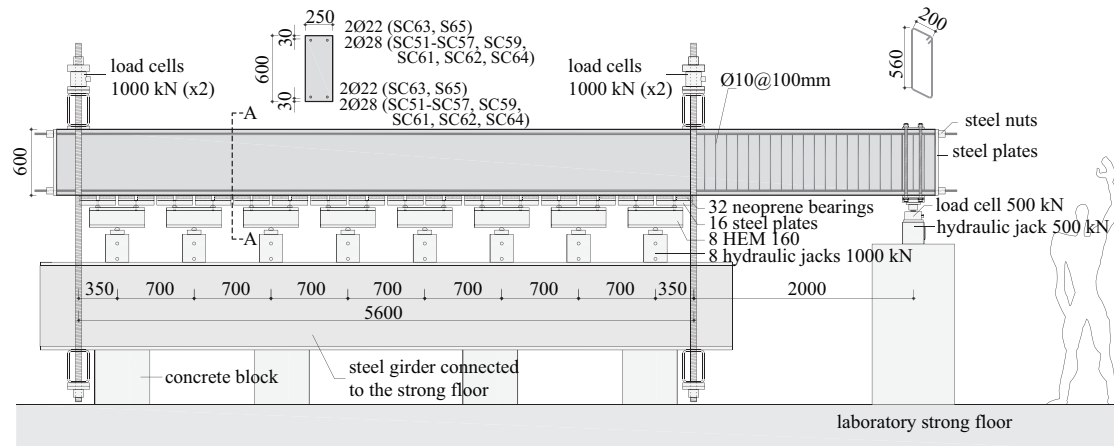
Figure 3.2 Test setup (dimensions in [mm])

3.4.1 Geometry

The specimens were rectangular beams of constant width (250 mm) and depth (600 mm), see Figure 3.2. Two amounts of flexural reinforcement ratio were used, corresponding to $\rho = 0.54\%$ (2 bars diameter 22 mm, effective flexural depth $d = 559$ mm,) and 0.89% (2 bars diameter 28 mm, effective flexural depth $d = 556$ mm). The same bars placed on the tension side were also arranged in the compression side (for casting, the top bars were hang from an external steel profile in order to keep a constant concrete cover). This was aimed at allowing the beams to be capable of bearing both positive and negative bending moments accounting for the test setup and to reproduce a situation commonly found in practice. The specimens have variable length in order to investigate on the influence of shear slenderness. The beams were tested as cantilevers, single span or continuous members under various loading conditions. For two-span members, only one span was investigated, whereas in the other span shear failures were avoided by arranging stirrups (diameter 10 spaced at 100 mm), refer to Figure 3.2. The loads were introduced by means of 200 x 150 mm neoprene pads (50 mm thick) spaced at 175 mm to simulate distributed loading conditions. At the supports, the reactions were applied by means of 250 x 200 mm steel plates with a thickness of 30 mm. The various hydraulic jacks reproducing a distributed load were connected to the same hydraulic system, ensuring same force at each actuator (neglecting differences in friction losses of the system).

3.4.2 Materials

Normal strength concrete with a maximum coarse aggregate size of 16 mm was used for all specimens. The compressive strength (f_c) at the time of testing ranged between 33.2 MPa and 36.8 MPa (measured in cylinders 160 mm-diameter and 320-mm height). Details on the compressive strength for each specimen are provided in Table 3.1. For the reinforcement, high-strength steel bars, with an average yield strength of 713 MPa was used (average tensile strength of the steel after strain hardening at 820 MPa). This reinforcement type was used in order to increase the bending resistance for the relatively moderate flexural reinforcement ratio to avoid flexural failures whenever possible. For the stirrups, ordinary reinforcement was used (with characteristic yield strength of 500 MPa).

3.4.3 Test setup

The test setup was designed to allow different loading conditions and shear slenderness. Details on each specimen are provided below and in Table 3.1 and Figure 3.3:

- Specimen SC51 is a simply supported member subjected to uniformly distributed loading. It was tested twice since it could be repaired after first failure (by means of external plates fixed together with prestressed bolts);

- Specimens SC52-55 are continuous beams subjected to uniform loading and with different negative bending moment (refer to Figure 3.3 for details on the point of contraflexure of bending moments and zero shear force). Specimen SC52 could also be tested twice, as it was strengthened after first failure;

- Specimens SC56-57, SC59 and SC62-63 are cantilevers subjected to uniformly distributed loading, with varying slenderness except for specimens SC59 and SC63, where the slenderness was the same, but the reinforcement ratio was varied ($\rho = 0.54\%$ for specimen SC63 and 0.89% for specimens SC59);

28

- Specimens SC61 and SC64-65 were tested as cantilevers subjected to a concentrated load at their tip. The concentrated load was applied by means of four neoprene pads for consistency with the load introduction system used for the other specimens. These members were also designed in order to provide equivalent shear slenderness as those of specimens SC57 and SC59-63 respectively. The reinforcement ratio was 0.89% for all specimens except for SC65, where it was 0.54%.

Test	l [mm]	a [mm]	$M/V{\cdot}d$ [-]	f_c [MPa]	ρ [%]	q [kN/m]	V_{left} [kN]	V_{right} [kN]	Remarks	CCDT
SC51a	5'600		0	33.6	0.886%	60.4	169	(169)	1st failure near left support	(4)
SC51b	5'600		0	33.6	0.886%	57.8	(162)	162	2nd failure near right support	(2)
SC52	5'600		1.68	36.8	0.886%	59.5	(133)	200	Diagonal cracking near right support	(1)
SC52a	5'600		1.68	36.8	0.886%	77.1	173	(259)	1st failure near left support	(2)
SC52b	5'600		1.68	36.8	0.886%	85.0	(190)	286	2nd failure in the central part	(4)
SC53	5'600		2.88	33.2	0.886%	40.2	(68)	158	Maximum load followed by failure	(2)
SC54	5'600		3.78	36.5	0.886%	40.6	(46)	182	Maximum load followed by failure	(4)
SC55	5'600		4.48	33.7	0.886%	33.4	(19)	168	Diagonal cracking near right support	(3)
	5'600		4.48	33.7	0.886%	38.5	(22)	194	Failure near right support after reloading	(2-1)
SC56	5'600		5.04	35.3	0.886%	28.2	(-)	158	Maximum load followed by failure	(3)
SC57	4'900		4.41	33.2	0.886%	30.0	(-)	147	Maximum load followed by failure	(2)
SC59	3'500		3.15	35.5	0.886%	52.3	(-)	183	Maximum load followed by failure	(2)
SC62	2'800		2.52	35.8	0.886%	62.1	(-)	174	Maximum load followed by failure	(4)
SC63	3'500		3.13	33.6	0.544%	60.8	(-)	213	Yielding of longitudinal reinforcement	(-)
SC61		2'450	4.41	35.3	0.886%		103	103	Maximum load followed by failure	(4)
SC64		1'750	3.15	35.6	0.886%		108	108	Diagonal cracking (maximum load)	(3)
		1'750	3.15	35.6	0.886%		108	105	Failure after reloading	(2-1)
SC65		1'750	3.13	35.5	0.544%		102	102	Maximum load followed by failure	(3)

Table 3.1 Properties of the tested specimens and failure loads (V_{left}: shear force at the left support; V_{right}: shear force at the right support; values in brackets (-) indicating that failure did not develop at that side; parameter $M/(V{\cdot}d)$ refers to internal forces at support; CCDT refers to the Critical Crack Development Type).

29
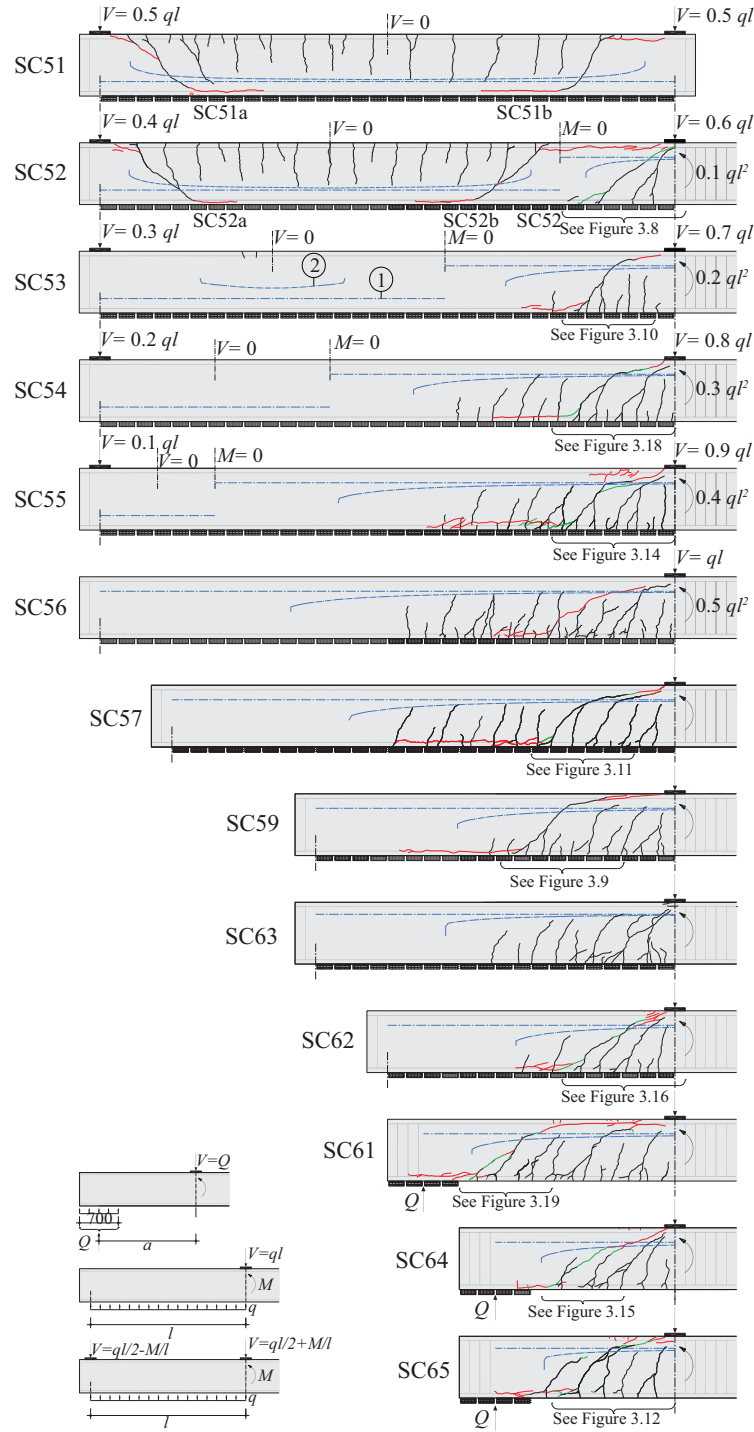
Figure 3.3 Testing programme: loading conditions and observed cracking patterns: dashed blue horizontal line (refer to curve (1) in specimen SC53): location of neutral axis according to a bending analysis assuming no tensile strength (calculated according to Appendix B of this paper); curved blue horizontal line (refer to curve (2) in specimen SC53): location of fibre at which the tensile strength is reached (assuming cracked analysis with a maximum tensile strength of concrete equal to f_{ct}). Cracks in black for increasing load until maximum load; Cracks in green for decreasing load after maximum load (before unstable crack growth); Cracks in red after unstable crack growth leading to failure. (For interpretation of the references to colour in this figure legend, the reader is referred to the web version of this article)

3.4.4   Observed cracking patterns

Cracking patterns were recorded and photographed during loading and until the test were stopped after failure. Pictures were taken normally at 1 Hz frequency, although for some cases, the frequency was lower (0.5 Hz) depending on the number of channels where data was acquired. Photogrammetry was performed with two cameras Nikon D800 (36.3 megapixels), whose images were analysed using the VIC3D software [34]. These pictures were also used by digital post-processing of the images to compute the strains at the concrete surface.

A random pattern with small, rounded, not overlapping speckles of constant size was applied on the beam surface. It was generated by using specific software provided by VIC3D for this purpose. The pattern was laser cut into cardboard, glued on the specimen and sprayed in black. Special attention was paid to the influence of the size of the speckles on the measurement accuracy. Depending on the size of the investigated zone, the speckles varied between 3 and 5 pixels and each pixel had a physical dimension of approximately 0.35 mm (with an upper extreme of 0.6 mm in the case of large areas of interest). A good calibration allowed obtaining accurate displacement measurements with an error of 1/50 of a pixel.

In addition, LED targets were also glued at the surface of some specimens. The LED targets blink at a selected frequency (about 2 Hz) allowing also detailed measurements on the strains of the system. The results of the two techniques (photogrammetry and LED targets) were compared and in general, fine agreement was found. Yet, the photogrammetry measurements were found more suitable to provide detailed tracking of the displacement field. They will thus be preferably presented hereafter.

The observed cracking patterns differed much amongst the different specimens (Figure 3.3). Yet, a number of typical cracks could be identified due to their shape and origin. The following definitions of crack types will be used later to interpret and to describe the tests (Figure 3.4):
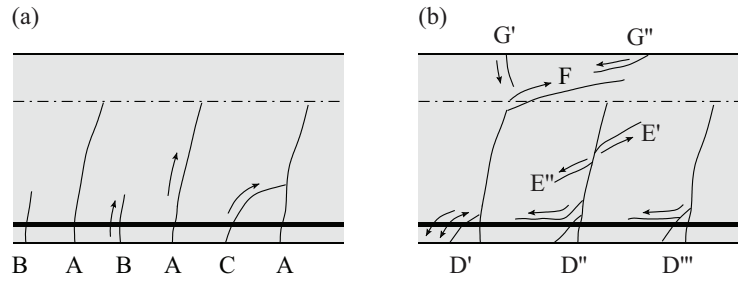
Figure 3.4 Crack types: (a) primary and secondary flexural cracks; and (b) cracks originated by the shear-transfer actions

- Type A (Figure 3.4a): Primary flexural cracks. These cracks have a bending origin. They are early developed and typically present a rather steep slope (yet they are normally inclined in the shear span). The cracks develop normally up to the theoretical location of the fibre where the longitudinal stress reaches the tensile strength of concrete according to a cracked sectional analysis (d_{fct} in Figure 3.5a) but, in all cases, the crack extends at least up to one-half of the effective depth of the member. This fact can be observed in Figure 3.3 and Figure 3.5b where d_{fct} is calculated according to Appendix B of this paper. The angle of the primary flexural cracks (β) is variable, becoming flatter when the acting bending moment reduces for a given level of shear force, refer to Figure 3.5c. This trend shows some scatter, yet it can be reasonably approximated by the following analytical expression:

$$\beta = \mathrm{atan}\left(1 + 1.25 \frac{M(x)}{V(x) \cdot d}\right) \tag{3.1}$$

where β (Figure 3.5a) is calculated as the angle of a line passing through point A (Figure 3.5a, at the flexural reinforcement level) and the point of the actual crack at a vertical distance equal to $d/2$ from point A. A comparison of this expression and the test results is shown in Figure 3.5c (average of measured-to-predicted values equal to 0.99 with a Coefficient of Variation of 10%). Figure 3.5f plots additionally the distribution of measured distance between flexural cracks type A. It can be observed that this distance normally varies between 0.4 and 0.8 times d, for all the investigated slenderness, loading types and reinforcement ratios, in accordance to previous experimental observations of [35]. The average value is 0.56d with a standard deviation of 0.16d.

- Type B (Figure 3.4a): Secondary flexural cracks. These cracks are located in between two primary flexural cracks or near the supports of the specimen. They develop for advanced loading stages and usually their height is lower than those of type A (below one-half of the effective depth of the member as assumed here). The spacing between primary

and secondary flexural cracks is governed at the level of the reinforcement by bond conditions and the amount of reinforcement.

- Type C (Figure 3.4a): Secondary or primary flexural cracks merging with another primary flexural crack. This case develops when a crack type A or B develops at such an angle and distance that it eventually becomes connected to another crack type A.

- Type D (Figure 3.4b): Delamination (dowelling) crack developing at the level of the flexural reinforcement. Three different possibilities could be observed for this crack type (Figure 3.4b):

  • Type D' with an inclined crack developing from the surface of the specimen to a primary flexural crack (type A). These cracks developed systematically as soon as the cracks type A started to develop in an inclined manner (after appearance of a quasi-vertical branch, refer to Figure 3.4b, or if they were inclined from the beginning). These cracks can be originated at the level of the reinforcement (specimens SC59 and SC64, propagating both upwards and downwards) or at the specimen surface. They appear normally at low load levels, clearly below the failure load (for vertical relative displacements at the level of the reinforcement lower than 0.15 mm).

  • Type D'' with the delamination crack developing above an inclined crack.

  • Type D''' with the delamination crack developing from a secondary inclined crack.

  Cracks type D'' or D''' were usually observed to develop (according to photogrammetric measurements) after the maximum load was reached, but not at maximum load or before it.

- Type E (Figure 3.4b): Aggregate-interlock induced cracks. These cracks can develop at both sides of an existing crack (refer to types E' and E'') and usually originate from a primary or secondary flexural cracks transferring shear by aggregate interlock. The development and origin of such cracks has been recently traced by Jacobsen et al. [36]. According to refined photogrammetric measurements on notched specimens (refer to Figure 3.6, adapted from [36]), when an existing pure tension crack (mode I) is subsequently subjected to shear displacements (mixed mode I and II), inclined cracks develop due to the local aggregate interlock forces. These inclined interlock cracks develop according to the geometry of the original tension crack and potentially at both sides of the crack (Figure 3.6e). Similar crack developments and shape have been observed in the beams presented in this paper. According to the literature, the capacity of cracked concrete to transfer shear and normal forces through aggregate interlocking is strongly influenced by the opening and roughness of the crack. Figure 3.7 presents for instance the calculated interface stresses according to the approaches of various authors [14, 23, 24]. That will be used later in this paper. In spite of some differences, all models yield a similar trend, with decreasing interlock stresses for increasing crack opening and/or decreasing sliding.

- Type F (Figure 3.4b): Propagation of a primary flexural crack within the compression chord. This usually happens with a rather flat crack originating from a primary flexural crack. The length of cracks type F at maximum load was relatively variable (generally varying between $0.05d$ and $0.8d$, refer to Figure 3.5e) as well as its angle with respect to the axis of the member (generally varying between 5° and 50°, and in between 5° and 30° in cases when crack types F became critical). Despite the scatter, some trends can however be observed. For instance, as Figure 3.5e shows, when the cracks are close to the load introduction region ($\xi_B < 0.5d$ in Figure 3.5e), the length of the crack type F is limited by its distance to the load ($\xi_B \approx l_F$ in Figure 3.5e). When the cracks are located at larger distances ($0.5d < \xi_B < 2d$ in Figure 3.5e), there exists a correlation between the length of the crack F and its distance to the load (with increasing length of the crack for larger distances, refer to Figure 3.5e). Finally, for relatively large distances of the crack to the load ($\xi_B > 2d$ in Figure 3.5e) the length of the crack type F drastically reduces to values around 0.2 times d (Figure 3.5e). The level of load at which propagation of a crack type F started was dependent on the acting moment-to-shear ratio. This is shown in Figure 3.5d, where the ratio amongst the load for beginning of this crack with respect to the failure load is plotted against the acting moment-to-shear ratio at the section where crack A crosses the reinforcement. It can be observed that cracks type F propagated at load levels close to failure for low values of the acting moments (crack near support or point of moment inflection) whereas it developed already for relatively low levels of load when the acting bending moment was significant. More details on this topic will be provided in next section.
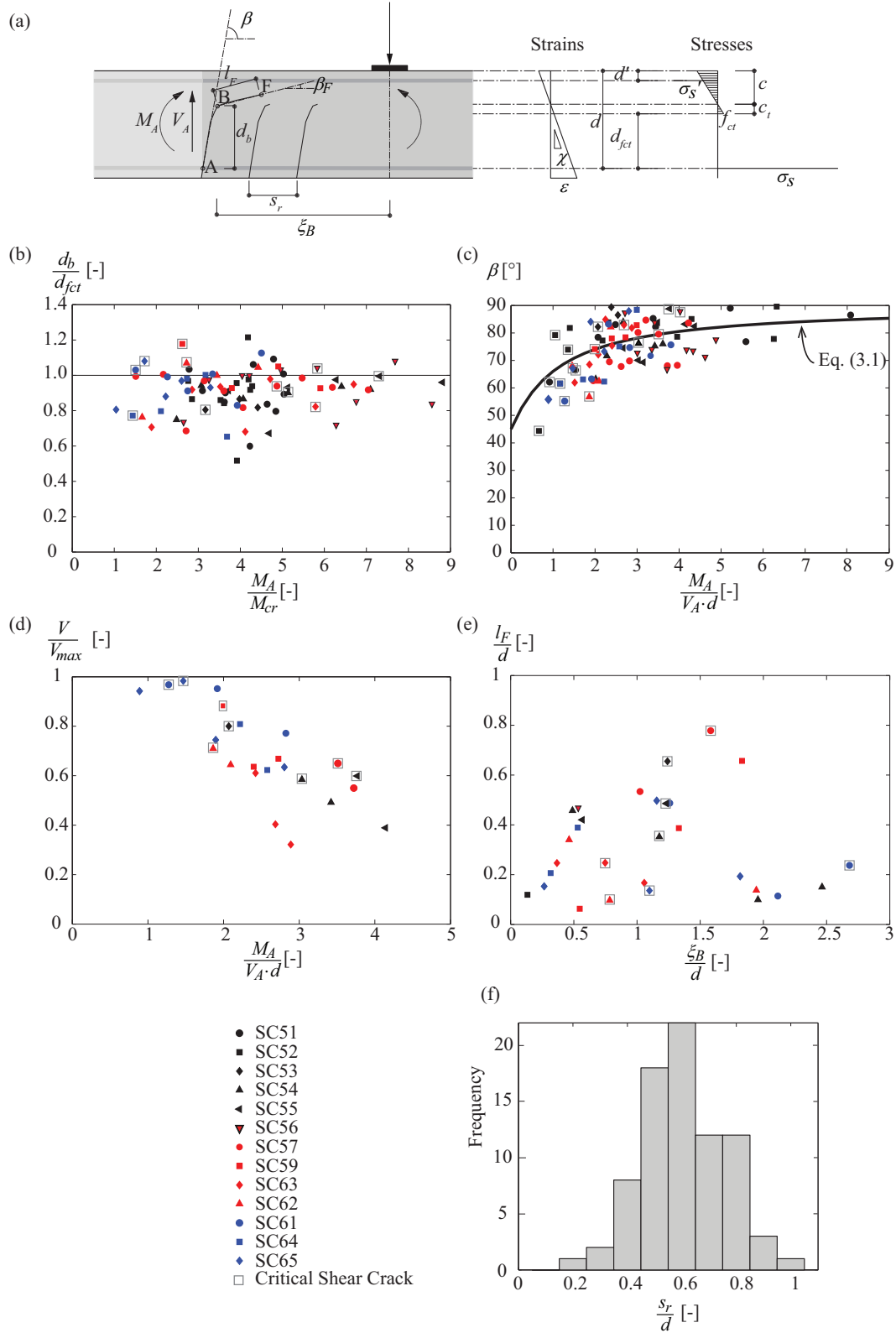
Figure 3.5 Crack development: (a) geometry, parameters investigated, stresses and strains profiles; (b) height of cracks type A with respect to the theoretical location of the fibre where tensile strength is reached; (c) angle of cracks type A with respect to the beam axis; (d) level of load at which cracks type F starts to develop (V_F); (e) length of cracks type F at failure; and (f) measured distance between cracks type A (parameter $M/(V \cdot d)$ refers to internal forces at a cross section where the crack intercepts the longitudinal reinforcement)

- Type G (Figure 3.4b): Development of a crack within the compression chord but not originating from a primary flexural crack. These cracks usually develop perpendicular to the edge of the slab (G', due to local bending of the compression chord as explained in [32]) or at flat angles near the load introduction region (G'', due to the large shear forces in the compression chord and/or crushing of the compression chord).
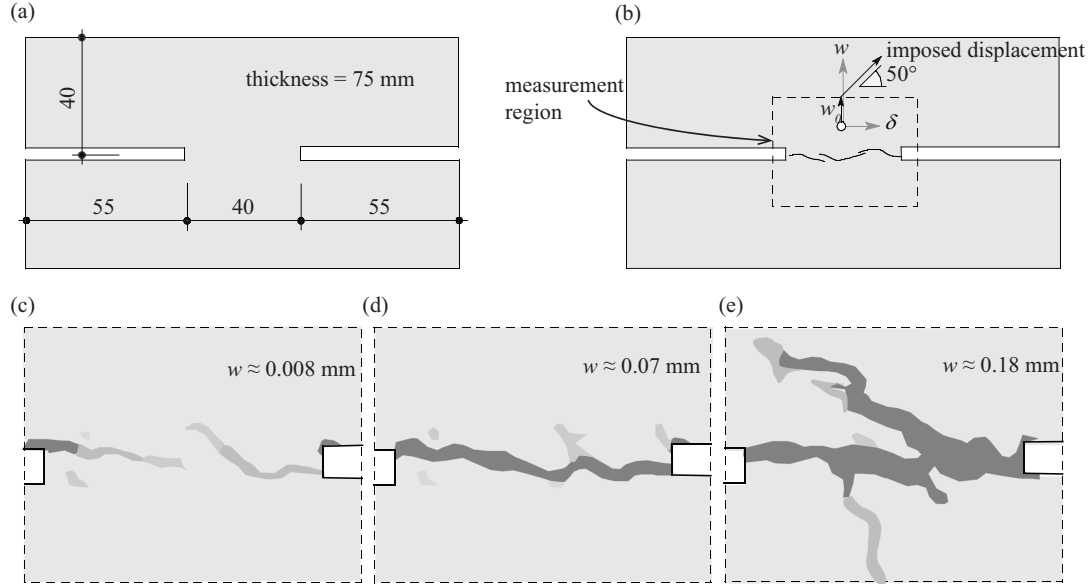
Figure 3.6 Experimental investigation on the development of cracking originated by aggregate interlock (adapted from [36]): (a) test specimen (dimensions in [mm]); (b) specimen precracked in tension ($w_0 = 0.025$ mm; $\delta_0 = 0$ mm) and with imposed displacements thereafter ($\Delta w = \Delta \delta \tan 50°$); (c) cracking pattern during loading in tension ($w = 0.008$ mm; $\delta = 0$ mm); (d) cracking with increasing opening and sliding ($w = 0.07$ mm; $\delta = 0.037$ mm); and (e) cracking at maximum load ($w = 0.18$ mm; $\delta = 0.13$ mm)
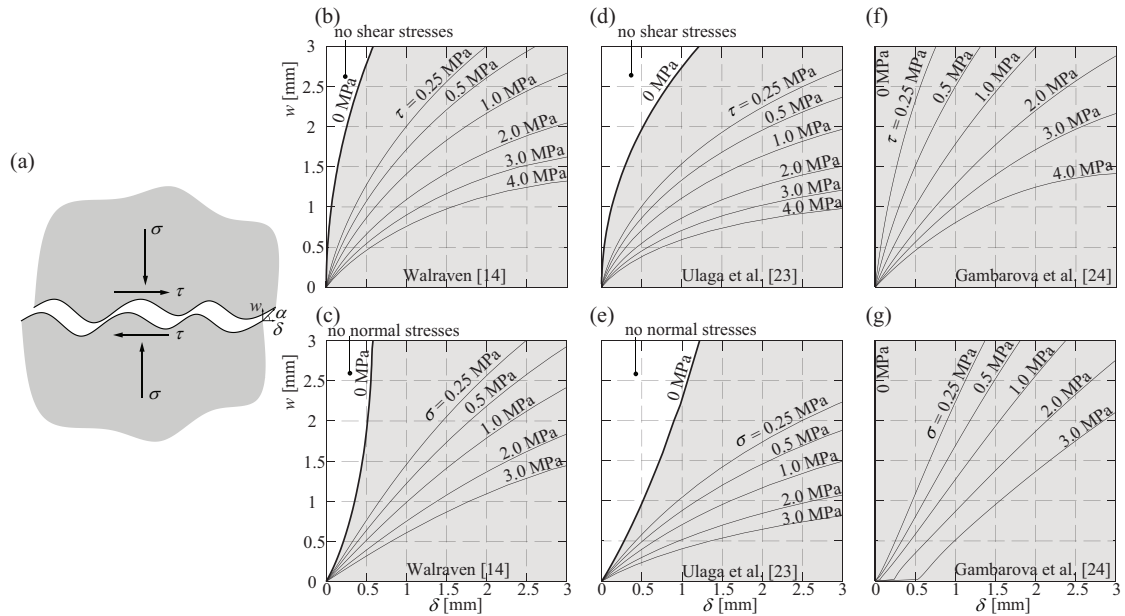
Figure 3.7 Analysis of aggregate interlock stresses (calculated for a concrete $f_c = 28$ MPa, $d_g = 16$ mm): (a) displacements and interface stresses; shear and normal aggregate interlock stresses according to (b and c) Walraven [14]; (d and e) Ulaga [23]; and (f and g) Gambarova et al. [24]

3.5 Measured crack development and kinematics at failure

By means of the photogrammetry measurements, the development of cracks could be accurately tracked before failure and, particularly, in the seconds before and after reaching the maximum load. Several evolutions of the cracking patterns have been observed. These patterns are not consistent amongst them and even present large differences. It was observed in all cases the development of a critical shear crack progressing to failure, yet in different manners. The critical shear crack refers to an existing crack (usually type A–E or A–F) whose opening leads eventually to the failure of the specimen. It can be noted that the final failure surface is not always identical to the critical shear crack (as it can be intercepted or merged to other cracks during the process of failure), but it is at least partly coincident with it. This failure surface will be referred as the failure crack in order to distinguish it from the critical shear crack.

3.5.1 Potential critical shear crack allowing direct strut action to develop (Critical Crack Development Type (1))

Whenever a direct strut action (Figure 3.1b) can develop without being disturbed by the presence of a shear crack, the plastic solution to shear strength [21] can develop [32]. This case was for instance observed in specimen SC52 near the right support, Figure 3.8. The beam developed a diagonal crack (A_1 in Figure 3.8) at the positive bending moment region for a load $q = 59.5$ kN/m, leading to a small drop in the applied load (about 4%). This crack however did not become critical, as the specimen could be reloaded and failure cracks developed at other places for higher levels of load ($q = 77.1$ kN/m and $q = 85$ kN/m, refer to Table 3.1 and Figure 3.3). The reason for the shear crack not to become critical can be found in the possibility of developing a direct strut action in the uncracked region above the crack (the point of contraflexure of bending moments was located at approximately $2d$ from the edge of the intermediate support). It is interesting to note from the crack relative displacements that hardly any aggregate interlock stresses developed in this crack as there was almost no crack sliding (refer to Figure 3.7).

A similar case occurred also for specimen SC64 and SC55. After a first failure triggered by the propagation of an aggregate interlock originated crack, the specimens could be reloaded up to 97% of the failure load for specimen SC64 and up to 115% for specimen SC55.

Similar cases have been reported elsewhere [32], for beams with cracks developing at locations such that the inclined struts of the arching action can develop undisturbed. This behaviour clearly shows the significant dependence of the shear strength on the crack location and shape.
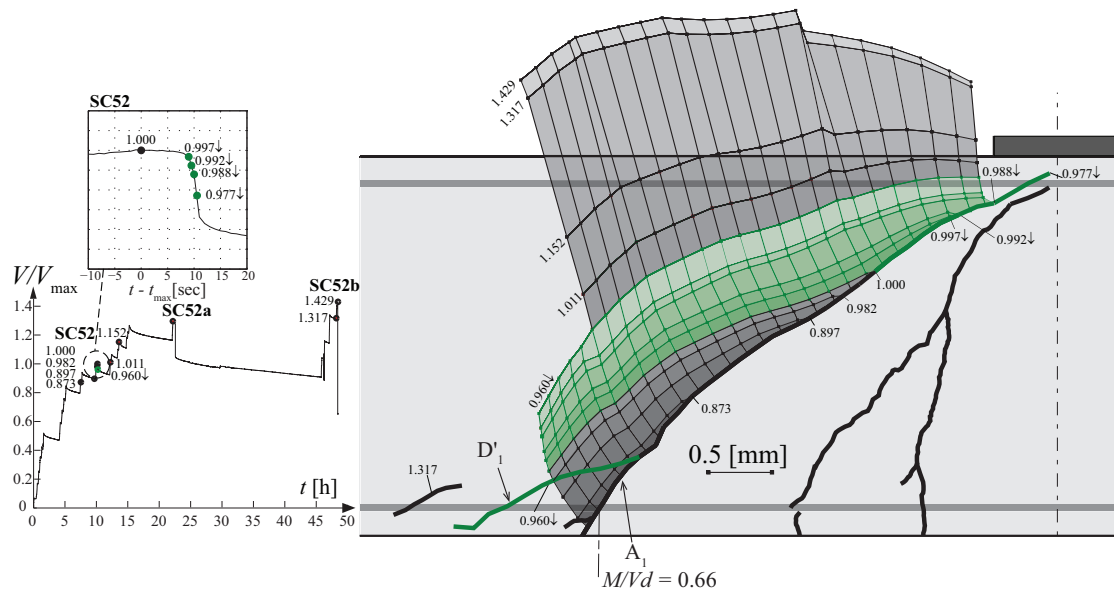
Figure 3.8 Specimen SC52 (diagonal cracking near the right support): Development of cracking and relative crack displacements at selected load steps ($V_{max} = 200$ [kN], see Table 3.1; crack colours – black, green – defined in Figure 3.3; Cracks in black over $V/V_{max} = 1$ refer to stable crack growth for increasing load). (For interpretation of the references to colour in this figure legend, the reader is referred to the web version of this article)

3.5.2 Failures following a stable propagation of a critical shear crack (Critical Crack Development Type (2))

Specimen SC59, Figure 3.9, failed in shear after a crack type F propagated in a stable manner from the critical shear crack. This crack originated from a primary flexural crack (crack A_1 in Figure 3.9) who merged a crack type C at approximately 82% of the failure load (refer to crack C_1 in Figure 3.9). Then, the primary flexural crack develops at a flatter angle as a crack type F (F_1 in Figure 3.9) until failure. At that moment, also a delamination crack appeared (crack D_1''' in Figure 3.9). Measurements on the crack relative displacements indicate that aggregate interlock stresses were potentially developing along the steeper part of the crack A_1 since large crack sliding occurred (Figure 3.7). It is also interesting to note that the critical shear crack eventually reached the location of the compression reinforcement, and it could potentially also develop some dowelling action of the top reinforcement prior to failure (refer to the delamination cracks in the top part of Figure 3.9).
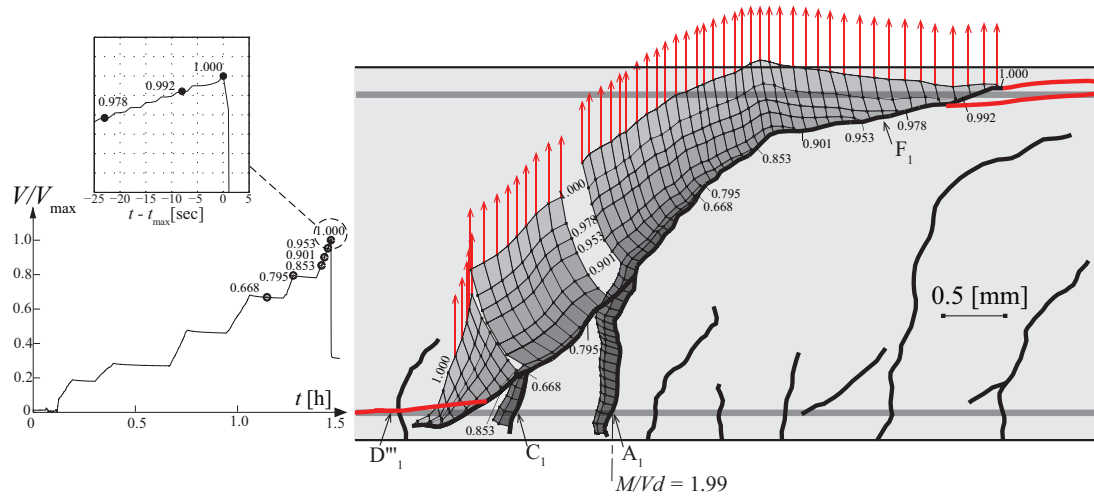
Figure 3.9 Specimen SC59: Development of cracking and relative crack displacements at selected load steps (the numbers in the figure indicate the level V/V_{max}; crack colours – black, red – defined in Figure 3.3; red vertical displacement vectors refer to unstable failure process). (For interpretation of the references to colour in this figure legend, the reader is referred to the web version of this article)

Other specimens exhibiting the stable propagation of the critical shear crack were tests SC51b and SC52a. In addition, such stable crack propagation was also observed for specimens SC53 (Figure 3.10) and SC57 (Figure 3.11). Particularly for specimen SC53, aggregate interlock stresses could be mobilized at the critical shear crack accounting for its relative displacements. Failure was for this specimen followed by the development of a delamination crack D_1''' along the top reinforcement (Figure 3.10).
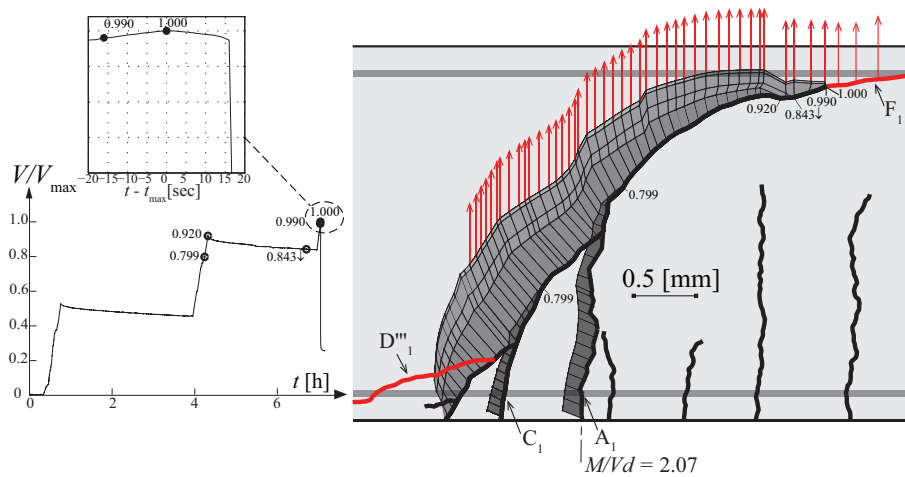
Figure 3.10 Specimen SC53: Development of cracking and relative crack displacements at selected load steps (the numbers in the figure indicate the level V/V_{max}; crack colours – black, red – defined in Figure 3.3; red vertical displacement vectors refer to unstable failure process). (For interpretation of the references to colour in this figure legend, the reader is referred to the web version of this article)
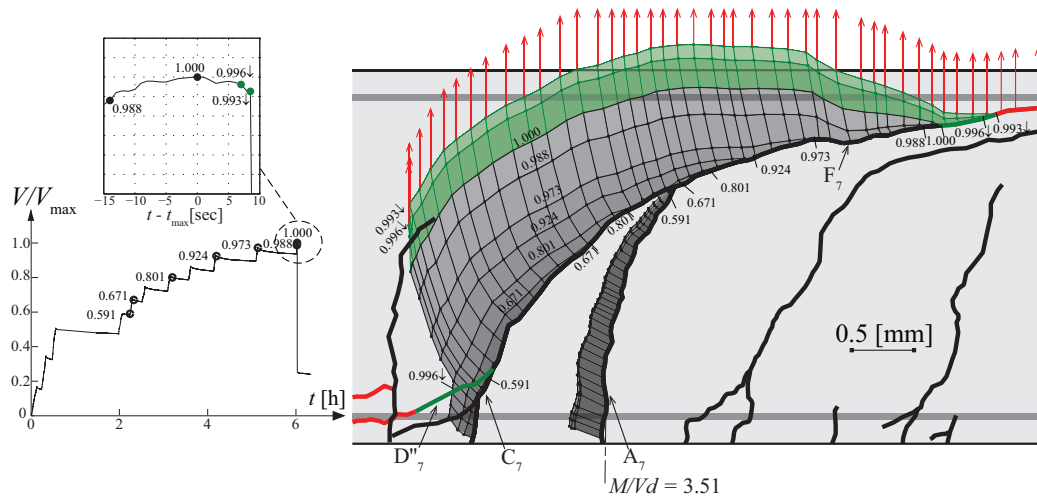
Figure 3.11 Specimen SC57: Development of cracking and relative crack displacements at selected load steps (the numbers in the figure indicate the level V/V_{max}; crack colours – black, green, red – defined in Figure 3.3; red vertical displacement vectors refer to unstable failure process). (For interpretation of the references to colour in this figure legend, the reader is referred to the web version of this article)

3.5.3 Failures driven by loss of aggregate interlock capacity due to development of an interlock crack (Critical Crack Development Type (3))

In some regions of the critical shear cracks, large interlock stresses could be mobilized. For some specimens, the concentrations of aggregate-interlock stresses led to the propagation of a new crack, eventually leading to the failure of the specimens. These cracks (inclined cracks developing from a crack originated in bending) are in fact in agreement to the inclined cracks observed to develop from the first (tension-induced) crack as shown in Figure 3.6e by Jacobsen et al. [36].

This can for instance be observed in specimen SC65. As Figure 3.12 shows, a well-defined critical shear crack was already formed and stable (crack A_2 with a small delamination crack type D_2'). The measurement of relative displacements of the crack faces of the critical shear crack indicated also large potential aggregate interlock stresses being activated (crack sliding under low crack openings in Figure 3.7). As a result, a new crack developed suddenly in this region (E_2'', drawn in blue in Figure 3.12) at approximately 99% of the failure load. This can be clearly observed in the detailed photogrammetric measurements of Figure 3.13. As a consequence, the interlock stresses dropped and failure was triggered by a progression of the critical shear crack into the compression chord (crack F_2 in Figure 3.12). At that moment (after maximum load), a new delamination crack (type D_2''') also formed on the bottom reinforcement (above D_2'), as well as on the top reinforcement.
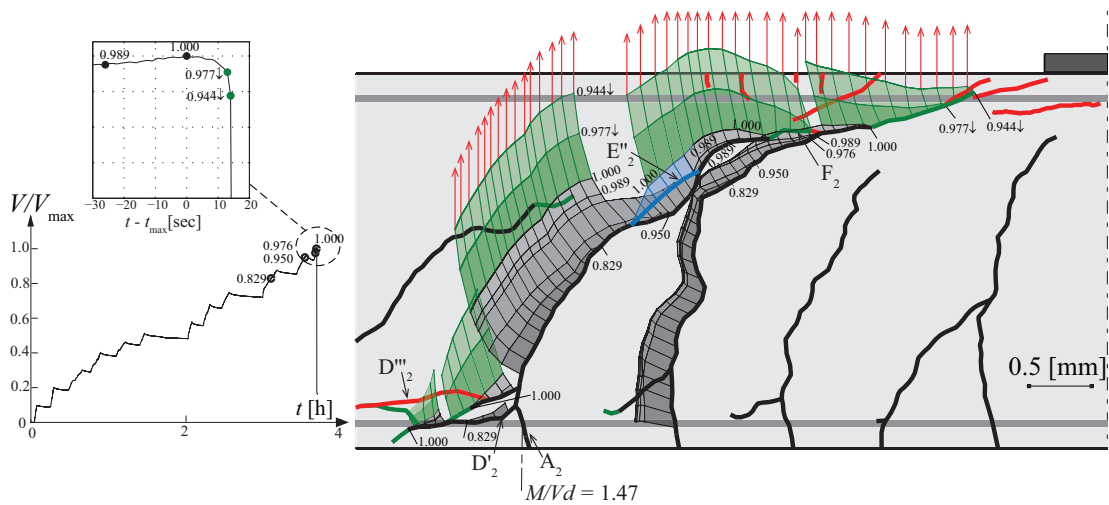
Figure 3.12 Specimen SC65: Development of cracking and relative crack displacements at selected load steps (the numbers in the figure indicate the level V/V_{max}; crack colours – black, green, red – defined in Figure 3.3; red vertical displacement vectors refer to unstable failure process). (For interpretation of the references to colour in this figure legend, the reader is referred to the web version of this article)
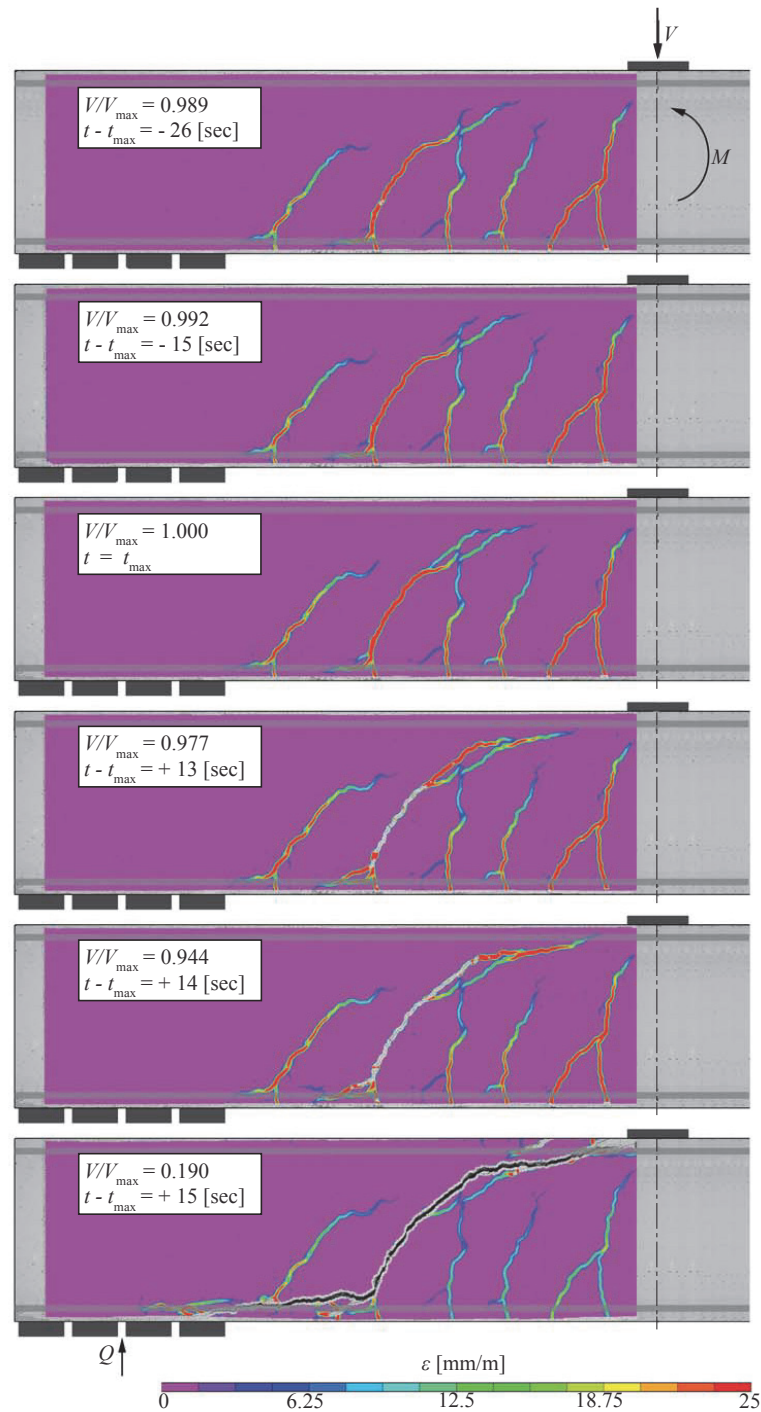
Figure 3.13 Specimen SC65: Detailed development of cracking on the basis of photogrammetric analysis at selected load steps (ε refers to calculated principal tensile strain from photogrammetric measurements)

The same development of cracking due to loss of aggregate interlock was also observed for specimens SC56 and SC63 (yielding of the longitudinal reinforcement was however governing for the strength of the latter). Specimen SC64 also presented a similar failure mode (Figure 3.15). Yet, in this case, the diagonal crack type E (crack E_1' in Figure 3.15) was originated from a flexural crack (A_1) which was less developed (as the acting bending moment was lower at the location of that crack). After the diagonal

crack E₁' developed and a drop of the load occurred, the specimen could be reloaded (Figure 3.15) but the load could not be increased above the previous one.

It can be noted that also the diagonal crack (first failure) of specimens SC55 (crack E₅' Figure 3.14) was also due to the development of an aggregate-interlock crack. This specimen could however be reloaded to a higher level due to the critical shear crack shape (refer to Critical Crack Development Type (1)).
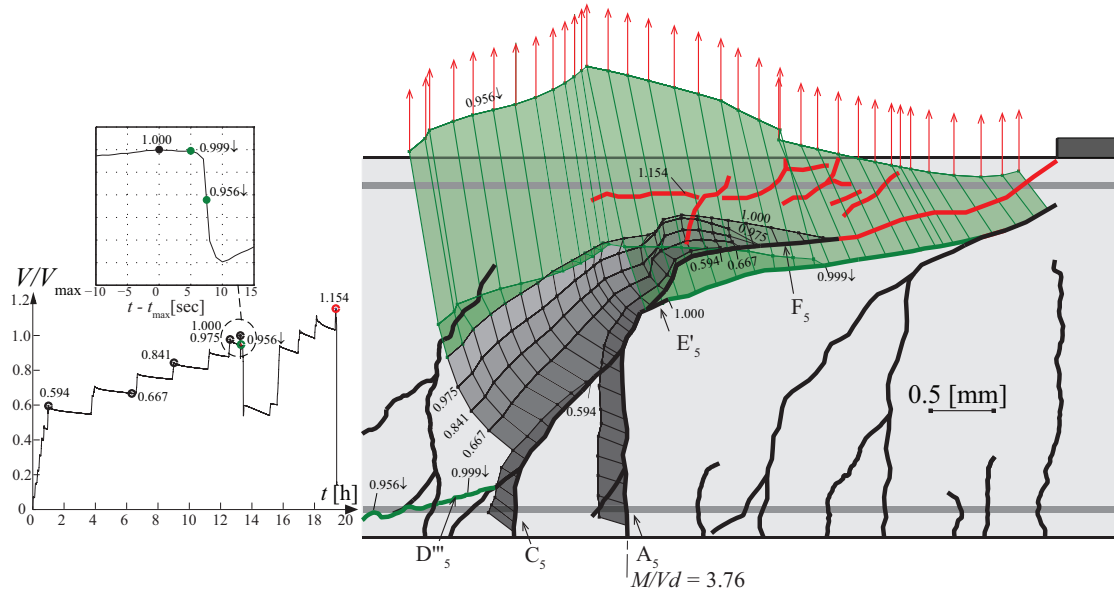
Figure 3.14 Specimen SC55: Development of cracking and relative crack displacements at selected load steps (V_{max} = 168 [kN], see Table 3.1; crack colours – black, green, red – defined in Figure 3.3; red vertical displacement vectors refer to unstable failure process). (For interpretation of the references to colour in this figure legend, the reader is referred to the web version of this article)
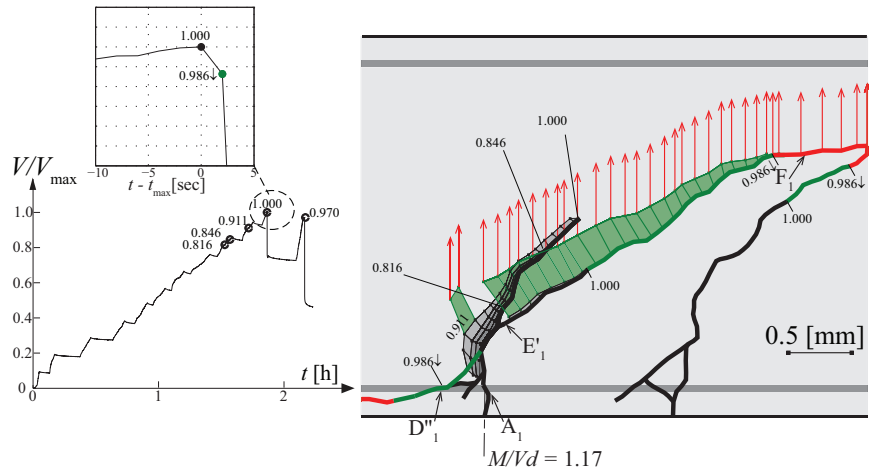
Figure 3.15 Specimen SC64: Development of cracking and relative crack displacements at selected load steps (the numbers in the figure indicate the level V/V_{max}; crack colours – black, green, red – defined in Figure 3.3; red vertical displacement vectors refer to unstable failure process). (For interpretation of the references to colour in this figure legend, the reader is referred to the web version of this article)

3.5.4 Failures driven by merging of flexural cracks type A and C (Critical Crack Development Type (4))

This failure type has been observed for specimens SC61, SC62, SC51a, SC52b and SC54. A representative case is that of specimen SC62 shown in Figure 3.16. In this specimen, a primary flexural crack (crack A_2, Figure 3.16) was clearly developed at already 80% of the failure load. Aggregate-interlock stresses could be activated (sliding of the crack lips) but only in the vertical parts of the crack due to its kinematics (corresponding to a location of the instantaneous centre of rotations at the tip of the crack). At this load level, a secondary flexural crack started to progress in an inclined manner. Eventually, this crack merged the primary flexural crack becoming thus a crack type C (crack C_2 in Figure 3.16). When both cracks merged, a significant portion of crack A_2, whose geometry and kinematics allowed to carry shear forces by aggregate interlock (quasi-vertical part below the merging point), was deactivated. Merging of both cracks occurred at maximum load. At that moment, the opening of crack A_2 increased abruptly, and even a new interlock-type crack (E_2') developed aligned with the crack C_2 deactivating another vertical portion of crack A_2 where shear forces were carried. Both phenomena (increase of crack opening and new crack development) led to a loss of the aggregate interlock capacity. In addition, a delamination crack (type D_2'') originated and progressed after maximum load was reached. During failure, a number of cracks type G'' (Figure 3.16) also developed in the compression zone. The process of failure, with merging of the cracks C_2 and A_2, as well as the development of crack E_2', can clearly be appreciated on the sequence of pictures shown in Figure 3.17 on the basis of the photogrammetric measurements.

For specimen SC54 (Figure 3.18) failure occurred also when the crack type C merged with the crack type A. This increased the opening of the critical shear crack and led to failure (yet no aggregate-interlock crack (type E) developed).

A similar case was also found for specimen SC61, refer to Figure 3.19. In that specimen, a primary flexural crack A_1 developed and progressed in a stable manner as a crack type F (F_1 in Figure 3.19). Aggregate interlock stresses could be mobilized according to the crack kinematics at the steeper branch, where significant sliding with low crack openings occurred (particularly near the inflexion point) (refer to Figure 3.7). Also, residual tensile stresses of concrete were potentially possible between the tip of the crack and the inflexion point accounting for such low crack openings (stresses in pure tension, mode I). However, at a certain moment, a new crack (crack C_1 in Figure 3.19) appeared and progressed in an inclined manner. The origin of this crack could be possibly a combination of bending and dowelling forces. It progressed rapidly and eventually merged the primary flexural crack (becoming thus a crack type C) leading to failure with a sudden increase of the opening of the critical shear crack (and thus a total loss of aggregate-interlock capacity).
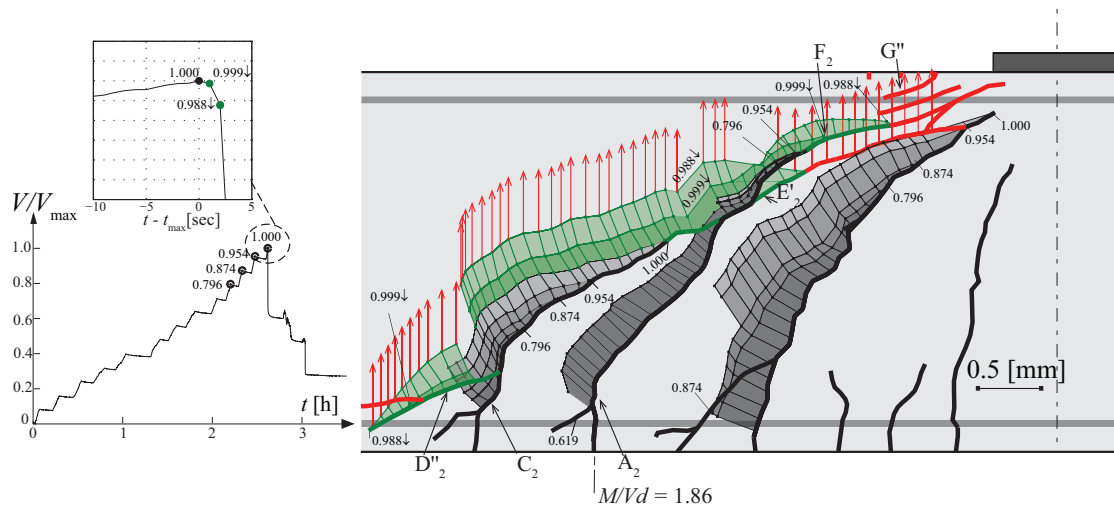
Figure 3.16 Specimen SC62: Development of cracking and relative crack displacements at selected load steps (the numbers in the figure indicate the level V/V_{max}; crack colours – black, green, red – defined in Figure 3.3; red vertical displacement vectors refer to unstable failure process). (For interpretation of the references to colour in this figure legend, the reader is referred to the web version of this article)
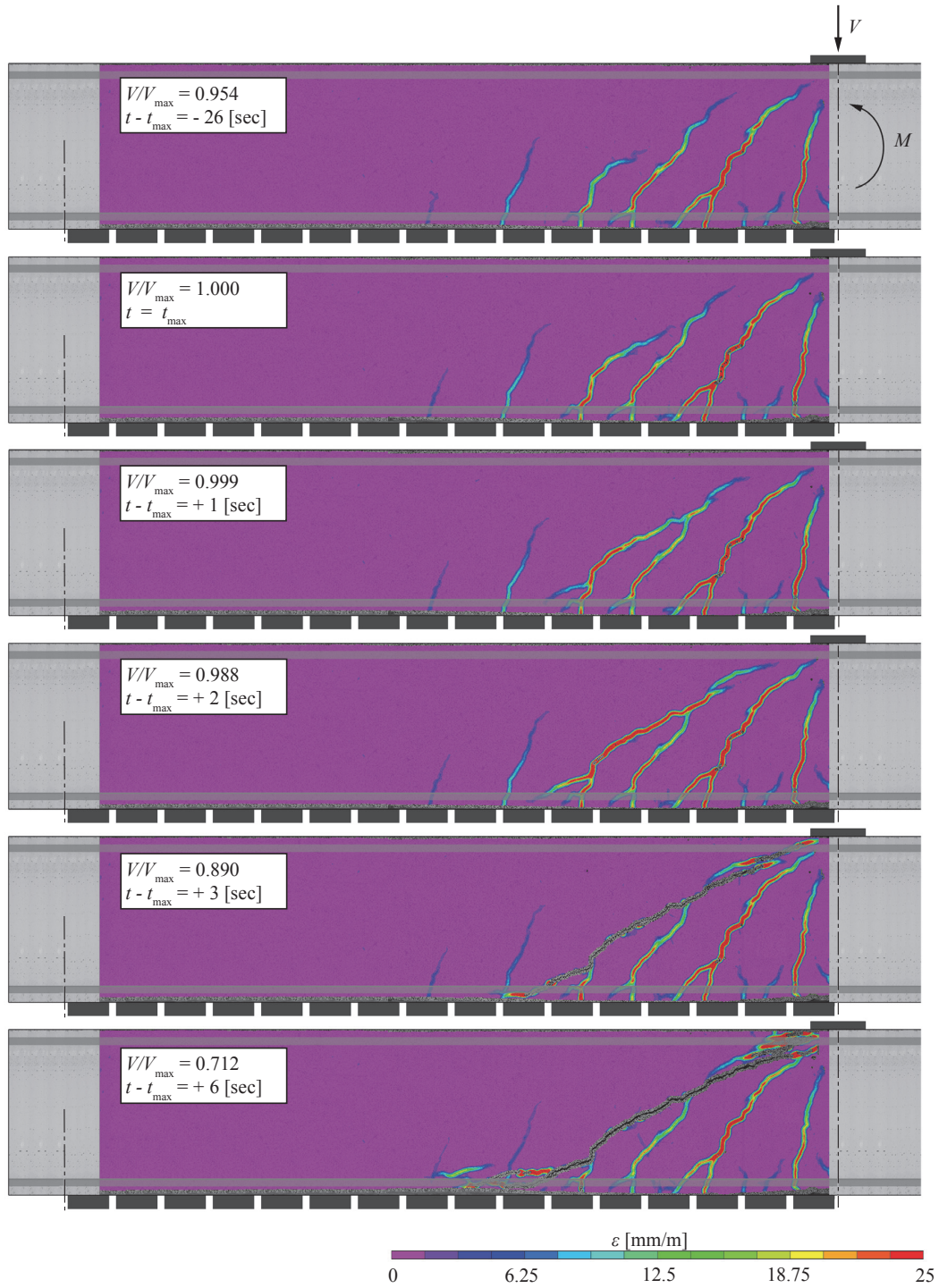
Figure 3.17 Specimen SC62: Detailed development of cracking on the basis of photogrammetric analysis at selected load steps (ε refers to calculated principal tensile strain from photogrammetric measurements)
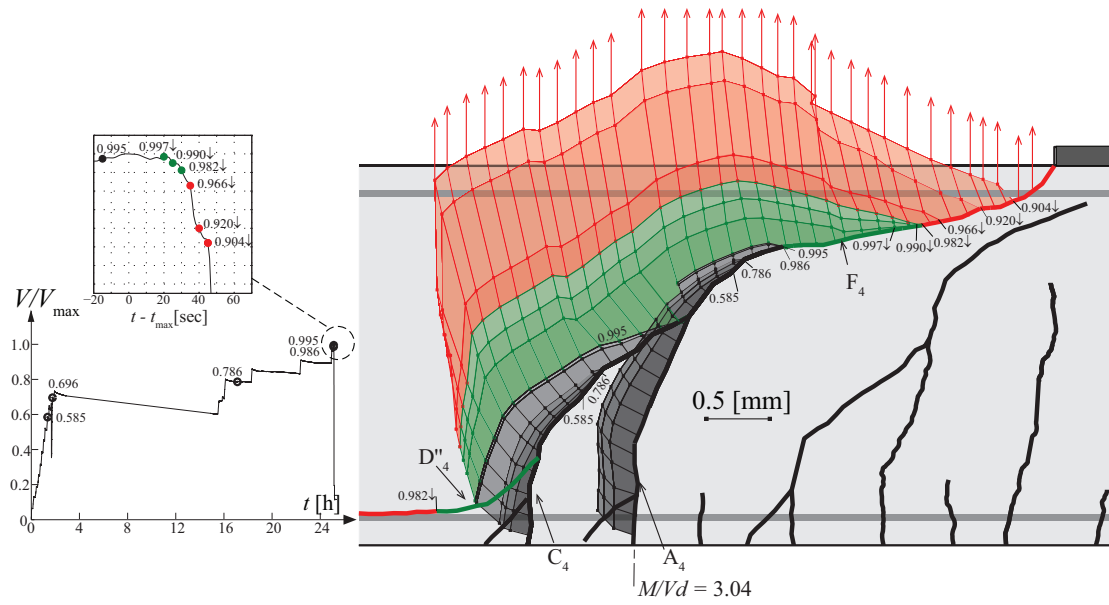
Figure 3.18 Specimen SC54: Development of cracking and relative crack displacements at selected load steps (the numbers in the figure indicate the level V/V_{max}; crack colours – black, green, red – defined in Figure 3.3; red vertical displacement vectors refer to unstable failure process). (For interpretation of the references to colour in this figure legend, the reader is referred to the web version of this article)
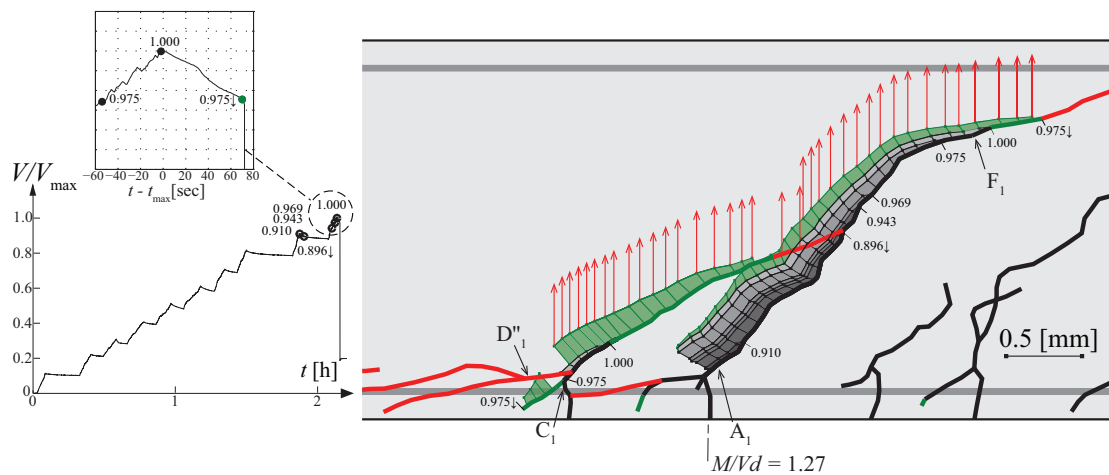
Figure 3.19 Specimen SC61: Development of cracking and relative crack displacements at selected load steps (the numbers in the figure indicate the level V/V_{max}; crack colours – black, green, red – defined in Figure 3.3; red vertical displacement vectors refer to unstable failure process). (For interpretation of the references to colour in this figure legend, the reader is referred to the web version of this article)

3.6 Critical analysis on the role of shear-transfer actions and mechanical modelling based on test observations

On the basis of the previous observations, it can be stated that different kinematics may govern at failure. In addition, it cannot be excluded that cracking patterns and kinematics at failure different to those previously described could have potentially been observed for beams tested with other parameters (size, slenderness, tensile and compression reinforcement ratio, aggregate size, cross section, bond behaviour between rebars and concrete…). This implies that different potential shear-transfer actions may be more or less active on the shear strength of a member depending on the actual cracking pattern and its associated kinematics.

It is also noticeable that the strength provided by different failure modes and even different shear-transfer actions may lead to similar strengths. That was for instance observed for specimen SC64, where first failure (propagation of an aggregate interlock crack) and reloading, with a completely different crack geometry and kinematics, provided a similar strength, with only 3%

42

difference. Yet, the load configuration and support conditions significantly influence the level of shear at which failure occurs for the same cross-section and flexural reinforcement (Table 3.1), contrary to many code formulas for shear design [5, 6].

With respect to the suitability of the shear-transfer actions (and the associated modelling approaches), a critical comparison shows that they account reasonably for some cases yet they fail in explaining others:

- Aggregate interlock seems very reasonable to explain shear-transfer for Critical Crack Development Types (2) and (3) as well as some cases of Type (4). This fact is supported by the observed crack pattern and kinematics. Also, Figure 3.20 compares the calculated contribution of aggregate interlock to the total measured shear resistance for some selected specimens. The analyses are performed following the methodology presented in Campana et al. [37] and for different aggregate-interlock models [14, 23, 24] (refer to Figure 3.7). As Figure 3.20 shows, the contribution of aggregate interlock is variable, more significant for some specimens than for others. In some cases, almost all shear force could be explained by this shear-carrying action, although for others this contribution was relatively moderate. These results are in agreement to those presented in [37], although it can be noted that the models overestimate the contribution of aggregate interlock (in some specimens, according to Walraven's and Gambarova's models, the calculated contribution is larger than the acting shear force).

- When a secondary flexural crack merges with a primary one (Critical Crack Development Type (4)), the additional opening of the critical shear crack as well as its change of shape (to a more straight one) limit the possibility of developing the aggregate-interlock stresses, deactivating portions of crack type A where significant shear forces could be carried, and potentially triggers failure (in agreement to [27]).

- The contribution of the compression chord can be observed as very active particularly when the critical shear crack develops such that a direct strut action is possible. This refers to Critical Crack Development Type (1).

- The role of dowelling action of the tensile reinforcement seems potentially notable for short-span beams when the failure crack is close to the supported area (refer for instance to specimens SC65, SC64 and SC63). A significant influence of cracks related to dowelling action (type D) seems in fact that it increases the opening of the critical shear crack (due to the unbonded length over the delaminated zone), weakening other shear-transfer actions as aggregate interlock. Cracks type D'' or D''' however have been observed in most tests to develop after reaching of the maximum load. Also, some contribution can be expected for dowelling of the compression reinforcement when the failure crack reaches its level.

These findings from the present experimental programme explain why different mechanical approaches might lead to similar results in terms of strength. This is consistent with the analyses performed by Campana et al. [37] which showed that the governing shear-transfer actions may be rather different even for identical specimens depending on the cracking pattern and associated kinematics.
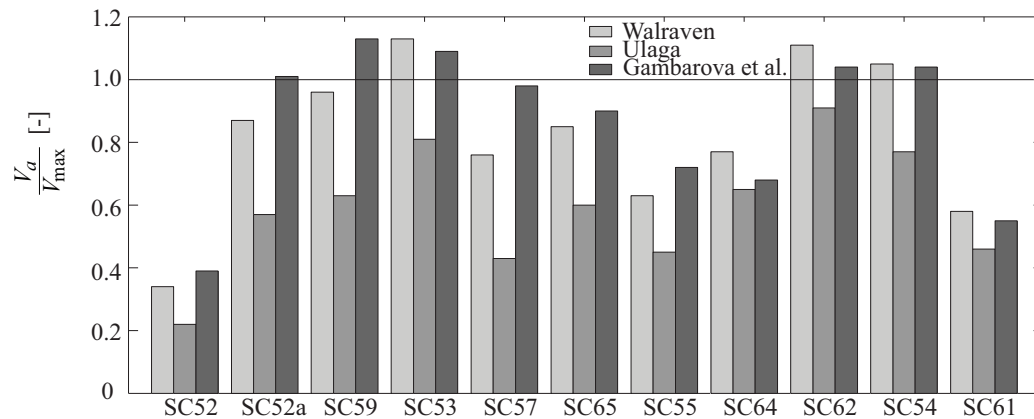
Figure 3.20 Calculated contribution of aggregate interlock at maximum load (V_a) with respect to the total acting shear in the critical shear crack section at maximum load (V_{max}). Analyses performed using the methodology of Campana et al. [37] for the measured crack pattern and kinematics and for the aggregate interlock models of Walraven [14], Ulaga [23] and Gambarova and Karakoç [24] (refer to Figure 3.7)

3.7 Conclusions

This paper presents detailed measurements on the crack development and kinematics of beams during the process of failure. The measurements allow identifying different governing failure modes and their potentially governing shear-transfer actions. The main conclusions of this investigation are listed below:

1. Detailed investigation on the role of the shear-transfer actions and the suitability of mechanical models should be based not only on the cracking pattern after failure, but should account for the development of cracking (geometry and kinematics) right before and during the process of failure.

2. Photogrammetry is a very suitable tool for that purpose, allowing detailed tracking of cracks and analysis of the crack kinematics.

3. The experimental measurements show that failure may occur in different manners. Even, some specimens, reloaded after a first failure, are capable of developing alternative shear-transfer actions with a strength comparable in some cases to the one leading to first failure. This is particularly significant with respect to the capacity of the compression and tension chords (combined arching and dowelling actions).

4. Cracking due to bending (location, inclination and crack opening) plays a major role on the shear strength. The angle of the bending cracks is influenced by the level of shear forces.

5. Aggregate interlock depends mainly on the crack geometry and its kinematics (with the vertical upper parts of the crack carrying more shear forces). This shear transfer action can be limited by development of new cracks starting from an existing one.

6. It cannot be identified a unique shear-transfer action governing shear strength based on the performed tests. This makes in fact all actions to influence the failure strength and mode. Nevertheless, an analysis based on existing aggregate-interlock models and accounting for the actual cracking pattern and kinematics at failure shows that aggregate interlock may play a significant role in many of the investigated specimens.

7. On the basis of the test results, consistent modelling of shear strength should in principle account for all potential shear-transfer actions as well as for their dependence on the cracking state, pattern and development.

3.8 Acknowledgments

3.9 Appendixes

3.9.1 Appendix A. Notation

a	Shear span (defined for specimens subjected to concentrated loads as the distance between the centre of the load and the centre of the support)
b	Beam width
c	Depth of compression zone
c_t	Depth of tension zone
d	Effective flexural depth
d_{fct}	Location of fibre where tensile strength of concrete is attained (measured from tension side)
d_g	Maximum aggregate size
d'	Distance from the compression reinforcement to the concrete surface
f_c	Concrete compressive strength measured in cylinder
f_{cc}	Concrete compressive strength measured in cube
f_{ct}	Concrete tensile strength
h	Beam height
q	Distributed load

l	Span length
t	Time of test
t_{max}	Time at which maximum load is attained
w	Crack width
E_c	Modulus of elasticity of concrete
E_s	Modulus of elasticity of steel
M	Acting bending moment
N	Normal force
Q	Concentrated load
V	Acting shear force
V_{left}	Shear force at the left support
V_{max}	Shear force at failure (maximum value)
V_{right}	Shear force at the right support
V_a	Contribution of aggregate-interlock stresses to shear resistance
V_c	Contribution of inclined compression chord to shear resistance
V_d	Contribution of dowelling action to shear resistance
V_F	Level of shear at which crack type F develops
V_t	Contribution of residual tensile stresses to shear resistance
β	Angle of flexural cracks with respect to the beam axis
χ	Curvature
δ	Relative crack sliding
ρ	Reinforcement ratio of tension reinforcement
ρ'	Reinforcement ratio of compression reinforcement
σ	Normal component of aggregate-interlock stresses
σ_s	Stress in the tension reinforcement
σ_s'	Stress in the compression reinforcement
τ	Shear component of aggregate-interlock stresses
ξ_B	Location (distance) of point B

3.9.2 Appendix B. Location of the fibre where the tensile strength of concrete is reached in bending

In this Appendix, the theoretical location of the fibre where concrete reaches its tensile strength following a pure bending analysis is presented. The following hypotheses are accepted (Figure 3.5a):

- Concrete has a linear-elastic behaviour in compression (characterized by its modulus of elasticity E_c). In tension, the behaviour of concrete is linear until the tensile strength (f_{ct}) is reached. Thereafter, the concrete exhibits no residual tensile strength.

- Plane sections before cracking remain plane after cracking.

- Tension-stiffening effects are neglected.

According to compatibility conditions, plane sections remain plane, the following condition can be established:

$$f_{ct} = \chi \cdot c_t \cdot E_c \tag{3.2}$$

The equilibrium of moments and normal forces yield additionally:

$$N = 0 = -\frac{c^2}{2} b \cdot \chi \cdot E_c + \frac{f_{ct}^2 \cdot b}{2\chi \cdot E_c} + \chi \cdot b \cdot d \cdot E_s \left(\rho \cdot (d - c) + \rho' \cdot (d' - c) \right) \tag{3.3}$$

$$M = \frac{c^3}{3} b \cdot \chi \cdot E_c + \frac{f_{ct}^3 \cdot b}{3\chi^2 \cdot E_c^2} + \chi \cdot b \cdot d \cdot E_s \left(\rho \cdot (d - c)^2 + \rho' \cdot (d' - c)^2 \right) \tag{3.4}$$

where c and c_t can be calculated by solving numerically Eqs. (3.3) and (3.4) for a given acting moment M. From those values the location of d_{fct} (location of fibre where f_{ct} is attained) results: $d_{fct} = d - c - c_t$.

If f_{ct} is neglected (c_t=0), a closed-form solution exists for c:

$$c = d \cdot (\rho + \rho') \cdot \frac{E_s}{E_c} \cdot \sqrt{1 + 2 \frac{\rho + \rho' \cdot d'/d}{E_s / E_c \cdot (\rho + \rho')^2}} - 1 \tag{3.5}$$

leading to $d_{fct} = d - c$.

3.10 References

[1]   Ritter W. The Hennebique construction method. Schweizerische Bauzeitung, XXXIII, No. 7 (Die Bauweise Hennebique, in German). 1899:41–61.

[2]   Mörsch E. Reinforced concrete construction, theory and application. 3rd ed. Verlag von Konrad Wittwer (Der Eisenbetonbau, seine theorie und anwendung, in German). 1908:376.

[3]   Nielsen MP, Braestrup MW, Bach F. Rational analysis of shear in reinforced concrete beams. In IABSE colloquium proceedings P-15, vol. 2, Bergamo, Italy. 1978:16.

[4]   Thürlimann B. Plastic analysis of reinforced concrete beams. In IABSE colloquium – plasticity in reinforced concrete, reports of the working commissions, vol. 28, Copenhagen, Denmark. 1979:71–90.

[5]   Eurocode 2. Design of concrete structures – general rules and rules for buildings. EN 1992-1-1. Brussels (Belgium): CEN European Committee for Standardization. 2004:225.

[6]   ACI Committee 318. Building code requirements for structural concrete and commentary. Farmington Hills (USA): American Concrete Institute. 2011:503.

[7]   Chana PS. Investigation of the mechanism of shear failure of reinforced concrete beams. *Magazine of Concrete Research* 1987; 39 (141):196–204.

[8]   Fenwick RC, Paulay T. Mechanisms of shear resistance of concrete beams. *Journal of the Structural Division ASCE* 1968; 94 (10):2325–2350.

[9]   Paulay T, Loeber PJ. Shear Transfer by Aggregate Interlock. *ACI Special Publication SP-42* 1974; 1:1–16.

[10]   Kani GNJ. The riddle of shear failure and its solution. *ACI Journal* 1964; 61 (4):441–467.

[11]   Taylor HPJ. Investigation of the dowel shear forces carried by the tensile steel in reinforced concrete beams. London, Cement and Concrete Association, Technical Report 431. 1969:24.

[12]   Vecchio FJ, Collins MP. The modified compression field theory for reinforced concrete elements subjected to shear. *ACI Journal* 1986; 83 (2):219–231.

[13]   Taylor HPJ. Investigation of the forces carried across cracks in reinforced concrete beams in shear by interlock of aggregate. Cement and Concrete Association, Technical Report No. 42.77, London (UK). 1970.

[14]   Walraven JC. Aggregate interlock: a theoretical and experimental investigation. PhD thesis. Delft (Netherlands): Delft University of Technology. 1980:197.

[15]   Bazant ZP, Kim J-K. Size effect in shear failure of longitudinally reinforced beams. *ACI Structural Journal* 1984; 81 (6):456–468.

[16]   Fédération Internationale du Béton (Fib). Model code 2010 – final draft, volume 1, Bulletins 65. 2012:350.

[17]   SIA. Code 262 for concrete structures. Zürich: Swiss Society of Engineers and Architects. 2013:102.

[18]   CSA Committee A23.3. Design of concrete structures (CSA A23.3-04): Canadian Standards Association, Mississauga, ON, Canada. 2004:214.

[19] Benning W, Lange J, Schwermann R, Effkemann C, Görtz S. Monitoring crack origin and evolution at concrete elements using photogrammetry. In Proceedings of the ISPRS conference, international society for photogrammetry and remote sensing, vol. B, Istanbul, Turkey. 2004:678–683.

[20] Muttoni A, Fernández Ruiz M, Niketic F. Design versus assessment of concrete structures using stress fields and strut-and-tie models. *ACI Structural Journal* 2015; 112 (5):605–615.

[21] Drucker DC. On structural concrete and the theorems of limit analysis. *International Association for Bridge and Structural Engineering* 1961; 21:49–59.

[22] Fernández Ruiz M, Mirzaei Y, Muttoni A. Post-punching behavior of flat slabs. *ACI Structural Journal* 2013; 110 (5):801–812.

[23] Ulaga T. Betonbauteile mit Stab- und Lamellenbewehrung: Verbund- und Zuggliedmodellierung. PhD Thesis. Thesis no. 15062 (in German). Zurich, Switzerland: ETHZ. 2003:160.

[24] Gambarova PG, Karakoc C. A new approach to the analysis of the confinement role in regularly cracked concrete elements. *Transactions of the 7. international conference on structural mechanics in reactor technology* 1983; H.

[25] Zararis PD. Shear strength and minimum shear reinforcement of reinforced concrete slender beams. *ACI Structural Journal* 2003; 100 (2):203–214.

[26] Tureyen AK, Frosch RJ. Concrete Shear Strength: Another Perspective. *ACI Structural Journal* 2003; 100 (5):609–615.

[27] Yang Y. Shear Behaviour of Reinforced Concrete Members without Shear Reinforcement A New Look at an Old Problem. PhD Thesis. Delft (Netherlands): Delft University of Technology. 2014:344.

[28] Nielsen MP, Hoang LC. Limit analysis and concrete plasticity. CRC press. 2016.

[29] Fisker J. Shear capacity of reinforced concrete beams without shear reinforcement. PhD thesis. Aarhus (Denmark): Aarhus University. 2014:155.

[30] Marí A, Bairán J, Cladera A, Oller E, Ribas C. Shear-flexural strength mechanical model for the design and assessment of reinforced concrete beams. *Structure and Infrastructure Engineering: Maintenance, Management, Life-Cycle Design and Performance* 2014; 8 (4):337–353.

[31] Tue N, Theiler W, Tung N. Shear behaviour of bended members without transverse reinforcement (Schubverhalten von Biegebauteilen ohne Querkraftbewehrung, in German). *Beton- und Stahlbetonbau* 2014; 109 (10):666–677.

[32] Muttoni A, Fernández Ruiz M. Shear strength of members without transverse reinforcement as function of critical shear crack width. *ACI Structural Journal* 2008; 105 (2):163–172.

[33] Pérez Caldentey A, Padilla P, Muttoni A, Fernández Ruiz M. Effect of load distribution and variable depth on shear resistance of slender beams without stirrups. *ACI Structural Journal* 2012; 109 (5):595–603.

[34] Correlated Solutions. VIC 3D Software, Reference Manual. 2010.

[35] Collins MP, Mitchell D, Adebar P, Vecchio F. A general shear design method. *ACI Structural Journal* 1996; 93 (5):36–45.

[36] Jacobsen JS, Poulsen PN, Olesen JF. Characterization of mixed mode crack opening in concrete. *Materials and Structures* 2012; 45 (1–2):107–122.

[37] Campana S, Anastasi A, Fernández Ruiz M, Muttoni A. Analysis of shear-transfer actions on one-way RC members based on measured cracking pattern and failure kinematics. *Magazine of Concrete Research* 2013; 65 (6):386–404.

Chapter 4 Refined experimental measurements on the development of the critical shear crack and implications for developing mechanical models

This Chapter reviews the results of the entire experimental campaign of 20 reinforced concrete beams without shear reinforcement, tested under different loading and support conditions, investigated by means of refined measurement techniques. The cracking patterns were tracked in detail at high frequencies, allowing to identify the different crack types and their progress up to failure. Finally, the origin, shape and role of each observed crack is discussed, with the aim of providing consistent and objective data for development of mechanical models for shear design.

4.1 Experimental programme

The development of the critical shear crack leading to failure in reinforced concrete one-way slabs and beams without transverse reinforcement is the basic input for a consistent understanding of the shear behaviour. Due to the brittle nature of shear failures in such members, accurate and detailed measurements during the process of failure have always been challenging to obtain. Conventional measurement techniques, in most cases, have not been capable of providing a continuous tracking of the crack development during testing, particularly close to failure. These difficulties are currently being overcome with the use of the digital image correlation (DIC) technique, which provides very accurate and detailed information of the full displacement field and the cracking pattern during loading at high-acquisition frequencies.

Table 4.1 Loading conditions, material properties and failure loads (V_{left}: shear force at the end (left) support; V_{right}: shear force at the intermediate (right) support (refer to Figure 4.1a for loading conditions); values in brackets (*) indicate that failure did not develop at that side); $M/(V \cdot d)$ refers to the moment-to-shear ratio at the right support, see loading and support conditions in Figure 4.1).

	Test	l [mm]	a [mm]	$M/V \cdot d$ [-]	f_c [MPa]	ρ [%]	q [kN/m]	V_{left} [kN]	V_{right} [kN]	Remarks
Simply supported beams	SC51a	5'600		(-)	33.6	0.886	60.4	169	(169)	Shear failure at the left support
subjected to uniform load	SC51b	5'600		(-)	33.6	0.886	57.8	(162)	162	Shear failure at the right support
	SC52	5'600		1.68	36.8	0.886	59.5	(133)	200	Diagonal cracking right support[r]
	SC52a	5'600		1.68	36.8	0.886	77.1	173	(259)	Shear failure at the left support
	SC52b	5'600		1.68	36.8	0.886	85.0	(190)	(286)	Shear failure in the central part
Continuous beams	SC53	5'600		2.88	33.2	0.886	40.2	(68)	158	Maximum load
subjected to uniform load	SC54	5'600		3.78	36.5	0.886	40.6	(46)	182	Maximum load
	SC55	5'600		4.48	33.7	0.886	33.4	(19)	168	Diagonal cracking[r]
	SC55a	5'600		4.48	33.7	0.886	38.5	(22)	194	Maximum load
	SC56	5'600		5.04	35.3	0.886	28.2	(-)	158	Maximum load
	SC57	4'900		4.41	33.2	0.886	30.0	(-)	147	Maximum load
	SC58	4'200		3.78	36.1	0.886	50.6	(-)	213	Maximum load; yielding
Cantilevers	SC59	3'500		3.15	35.5	0.886	52.3	(-)	183	Maximum load
subjected to uniform load	SC62	2'800		2.52	35.8	0.886	62.1	(-)	174	Maximum load
	SC66	2'100		1.89	31.2	0.886	91.4	(-)	192	Maximum load
	SC63	3'500		3.13	33.6	0.544	60.8	(-)	213	Maximum load; yielding
	SC60	2'800		2.50	36.9	0.544	58.9	(-)	165	Maximum load
	SC70		3'850	6.92	33.3	0.886		114	114	Maximum load
	SC69		3'150	5.67	32.9	0.886		107	107	Maximum load
	SC61		2'450	4.41	35.3	0.886		103	103	Maximum load
Cantilevers	SC64		1'750	3.15	35.6	0.886		108	108	Maximum load
subjected to point load	SC68		1'400	2.52	32.6	0.886		124	124	Maximum load
	SC67		1'050	1.89	32.0	0.886		393	393	Diagonal cracking[r]
	SC67a		1'050	1.89	32.0	0.886		429	429	Maximum load
	SC65		1'750	3.13	35.5	0.544		102	102	Maximum load

[r] reloading of the specimen after diagonal cracking (drop in the applied load of 5-10%)

In this Chapter, the results of 7 reinforced concrete beams without transverse reinforcement, completing a previous experimental campaign on 13 beams, are presented. A detailed description of crack pattern of the first 13 beams tested and the test setup is available in Cavagnis et al. [1].

The material properties and main results of the entire testing programme are summarized in Table 4.1. In particular, specimen SC67 developed a diagonal crack near the right support, leading to a small drop in the applied load of about 8%. The specimen, however, could be reloaded and failed due to crushing of concrete between the support and the loading plate.
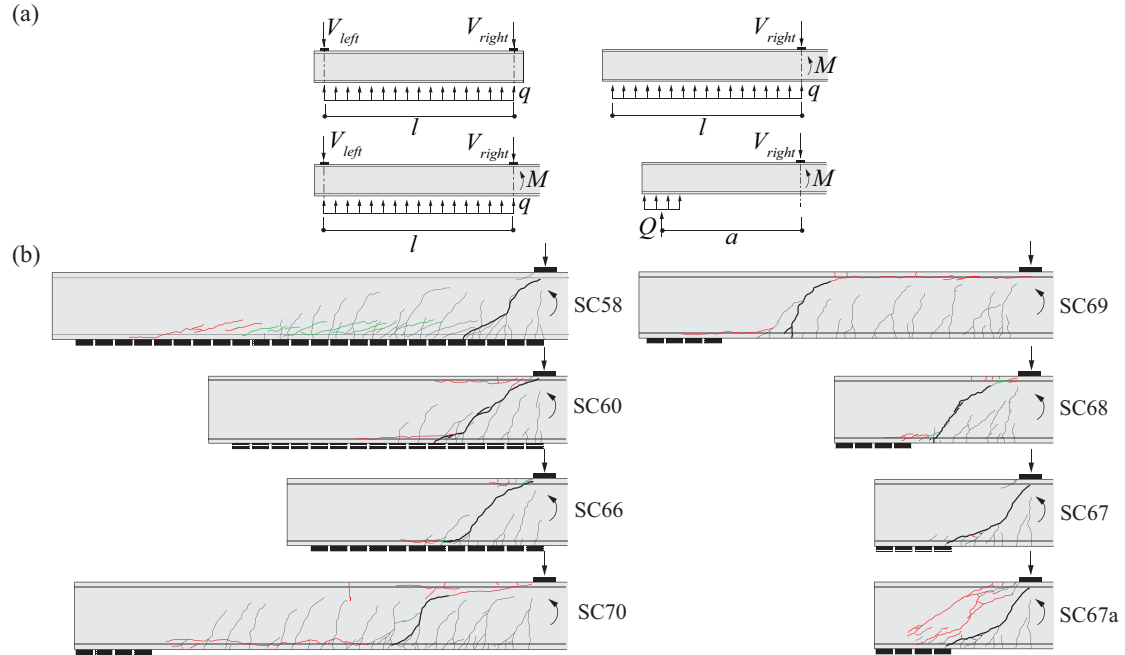
Figure 4.1 Experimental programme: (a) loading conditions and (b) observed cracking pattern of some selected specimens (cracks in black for increasing load until maximum load; cracks in green for decreasing load after maximum load during stable crack propagation; cracks in red after unstable crack growth)
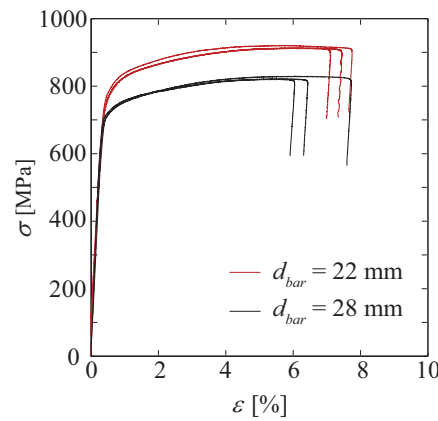
Figure 4.2 Measured stress-strain relationship of reinforcement bars

The overall experimental programme was primarily aimed at investigating the shear behaviour of members subjected to different loading conditions (point or uniform load) and support conditions (simply supported beams, continuous beams and cantilevers, see Table 4.1 and Figure 4.1a), by means of refined measurement techniques. The aim of the tests was to investigate the shear strength under realistic loading conditions, commonly found in practice. The specimens had a rectangular cross-section of 250 mm x 600 mm. Two reinforcement layout were used: 2 bars diameter 22 mm (ρ=0.54%) or 2 bars diameter 28 mm (ρ=0.89%). Concrete cover was 30 mm for all specimens and the effective depth d was equal to 559 mm for members with ρ=0.54% and 556 mm for members with ρ=0.89%. The top and bottom reinforcement were identical. Normal strength

concrete was used for all specimens. The concrete strength (measured on cylinders 320 mm height-160 mm diameter, at the age of testing) ranged between 31.2 MPa and 36.9 MPa and the maximum aggregate size d_g was equal to 16 mm. One cubic meter of concrete was composed of 164 kg of water, 306 kg of Portland cement, 844 kg of sand, 402 kg of gravel ranging from 4 to 8 mm and 696 kg of gravel ranging from 8 to 16 mm. Tensile and compression reinforcement consisted of high-strength bars (see Figure 4.2) with average yielding strength of 713 MPa (bar diameter 28 mm) and 760 MPa (bar diameter 22 mm), and with average ultimate tensile strength after hardening of 820 MPa (bar diameter 28 mm) and 920 MPa (bar diameter 22 mm).

In this Chapter, some detailed measurements of selected tests are presented in detail with the aim to investigate the process of crack development and failure.

4.2 Cracking pattern

Cracking pattern and displacement field were tracked by using the digital image correlation (DIC) technique. The DIC approach involved applying a stochastic pattern with small, rounded speckles on the entire surface of the specimens (see Figure 4.3a). Alternatively, when the size of the pixel was smaller than 0.30-035 mm, the pattern was sprayed uniformly on the area of interest, as shown in Figure 4.3b. Then, the area of interest was photographed by a pair of cameras Nikon D800 (36.3 Megapixels) at high frequencies (1-2 Hz). In addition, a pair of Manta (5 Megapixels) was used in order to investigate the compression zone on the opposite face of the member in the vicinity of the intermediate support. In this case, the pattern was sprayed uniformly, as shown in Figure 4.3b.
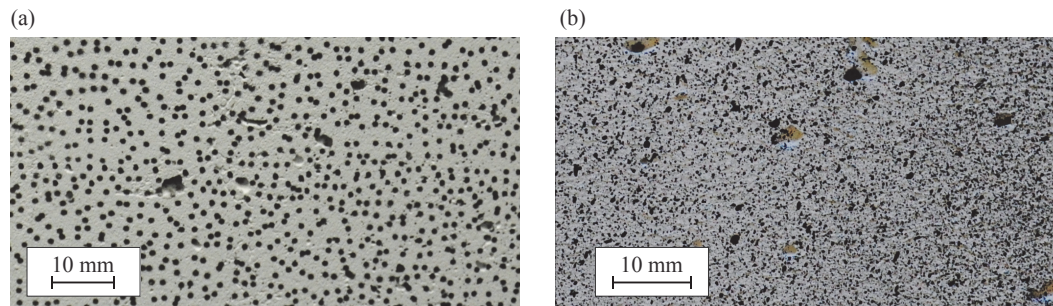
Figure 4.3 Pattern used for the DIC measurement system (a) pattern with rounded speckles, (b) sprayed pattern.

The photos were post-processed using VIC3D [2], which, comparing each pair of images with the reference ones (taken prior to testing), computes the full displacement field of the area of interest. The post-processing of the images provides displacement measurements with a maximum error of 1/50 of a pixel, obtained by comparing the 2D coordinates of the investigated area of several images taken before the beginning of the test. The physical dimensions of a pixel varied between 0.2 mm x 0.2 mm to 0.6 mm x 0.6 mm.

On the basis of the DIC measurements, a number of cracks has been identified and named (refer to Figure 4.4a for sketches and to Figure 4.4b-c for cracks in actual specimens), according to the notation presented in [1]:

- Type A: primary flexural crack;

- Type B and C: secondary flexural crack;

- Type D: delamination (or dowelling) crack;

- Type E: aggregate-interlock induced crack;

- Type F: propagation of a primary flexural crack within the compression zone;

- Type G: crack within the compression zone not developing from a primary flexural crack.

In particular, the critical shear crack is a crack type A-F (or crack A-E), whose development lead to the failure of the specimen [1]. It shall be noted that the eventual failure crack is not always completely coincident with the critical one, but it is initiated by it or it is at least partially correspondent.

In the following, the different types of cracks, their origin and shape will be investigated in detail.
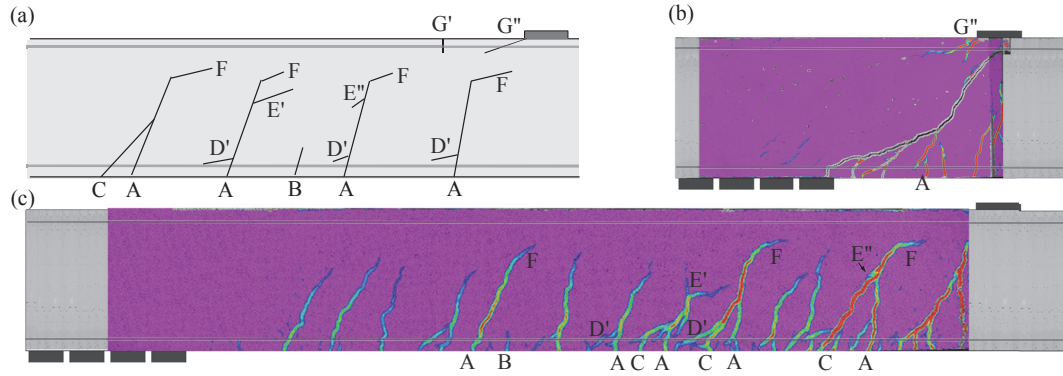
Figure 4.4 (a) Definition of crack type (refer to [1]); (b-c) observed crack types in specimens SC67 and SC70 at maximum load

4.2.1 Observations on primary flexural cracks (crack type A)

Primary flexural cracks (crack type A, refer to Figure 4.4) develop on the tension side of the beam as soon as the bending moment reaches the cracking moment and develop up to the theoretical location of the fibre where the longitudinal stress reaches the tensile strength of concrete [1]. It has been observed that the distance between two cracks of this type (s_r) at mid-height varies between $0.4d$ and $0.8d$ (with an average value $0.56d$, in agreement to [3–5]). This distance (s_r) is significantly larger than the cracking distance at the level of the longitudinal bars (governed by bond), as only some flexural cracks fully develop up to one-half of the effective depth. This phenomenon, shown in Figure 4.5 (specimen SC59), yields to the fact that the maximum opening of the critical shear crack occurs at approximately mid-height of the specimens (where secondary flexural cracks of type B or C do not progress), decreasing towards the tip of the crack (centre of rotation) and towards the level of the longitudinal reinforcement (where various secondary cracks of type B or C develop and reduce the opening of the primary flexural crack). Yet, when the opening of all secondary cracks between two primary flexural cracks ($0.4d$-$0.8d$) is summed (Figure 4.5a-b), the total opening respects an almost linear profile (sum of the horizontal crack opening u linearly increasing for linearly increasing distance from the crack tip). The length l_B, shown in Figure 4.5a-b, represents the region that contributes to the total opening of the primary flexural crack and it is comparable to the distance s_r between two flexural cracks, but not exactly coincident with it. Yet, this length will be discussed later in the Chapter.
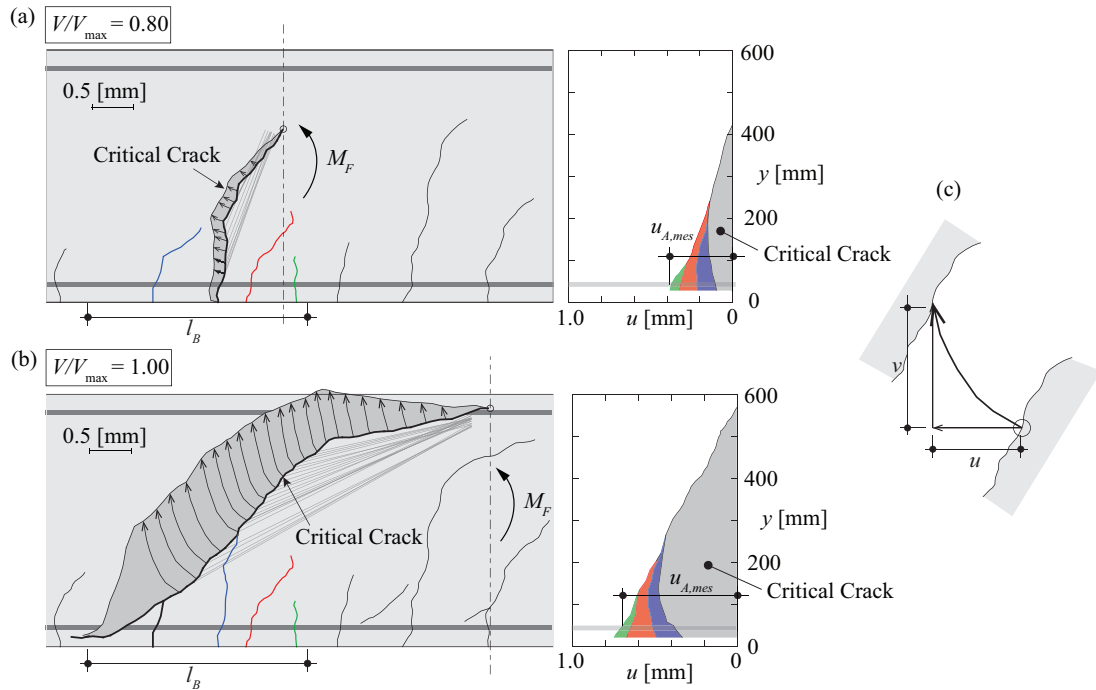
Figure 4.5 Crack kinematics, centre of rotation and horizontal opening u for Specimen SC59 (a) before and (b) after the development of cracks of type F and C; (c) definition of horizontal component of crack opening u and vertical component v

With respect to the angle of the primary flexural crack (refer to β_1 in Figure 4.6a), calculated between point A located at the level of the reinforcement and the point along the crack at a vertical distance equal to $d/2$ from point A, it has been observed that it is related to the ratio $M_{A(x)}/V_{A(x)} \cdot d$ (in agreement to [6]) and it can be approximated by the following equation (previously used in [1], see Figure 4.6b):

$$\tan(\beta_1) = 1 + 1.25 \frac{M_A(x)}{V_A(x) \cdot d} = 1 + 1.25 \cdot \alpha_A \tag{4.1}$$

where M_A and V_A are the acting bending moment and the shear force at the point where the flexural crack intercepts the flexural reinforcement and $\alpha_A = M_{A(x)}/V_{A(x)} \cdot d$. The average measured-to-predicted values, for approximately 130 flexural cracks developing in the specimens listed in Table 4.1 is 0.98 and the Coefficient of Variation is 10%.

In addition to the previous findings [1], the test results of the experimental programme have shown that the inclination of a crack type A is not constant along its height. Generally, at mid-height, the crack tends to slightly reduce its inclination with respect to the beam axis (refer to angle β_2 in Figure 4.6a). When only critical shear cracks are considered (squares in the figure), the average inclination of the primary flexural cracks from the level of the longitudinal reinforcement up to the neutral axis (or up to the location where the stress reaches the tensile strength of concrete if the crack propagates below the neutral axis, e.g. specimen SC61, refer to angle β_{AB} in Figure 4.6a) follows nevertheless a trend that can be approximated by the following relation:

$$\beta_{AB} = \frac{\pi}{4} + \frac{\pi}{12} \cdot \alpha_A^{1/3} < \frac{\pi}{2} \tag{4.2}$$

A comparison of β_{AB} calculated according to this expression and the measured angle β_{AB} of the critical shear crack of the investigated specimens is shown in Figure 4.6c (the average measured-to-predicted values for the critical shear cracks of the investigated specimens in Figure 4.6c is 1.02 and the Coefficient of Variation is 10%).
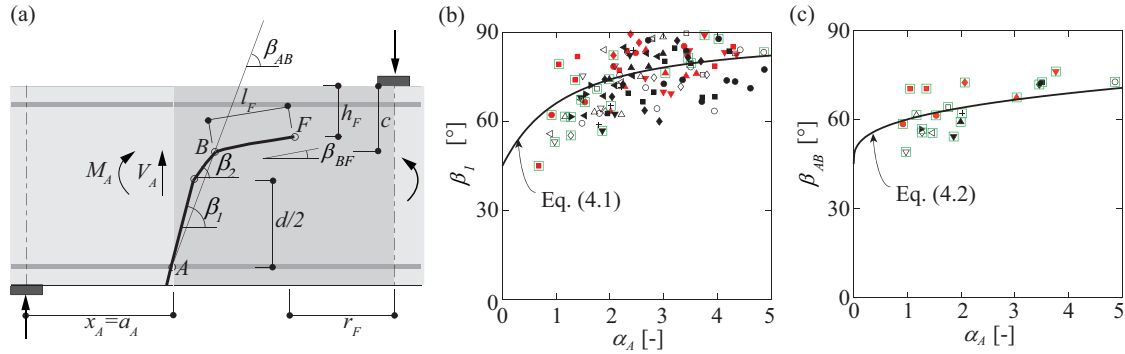
Figure 4.6 (a) Geometry and definition of parameters investigated; (b) angle β_1 of cracks of type A with respect to the beams axis; (c) angle β_{AB} of cracks of type A with respect to the beams axis (squares represent critical shear cracks, other symbols represent other cracks, see legend in Figure 4.7)

4.2.2 Cracks developing in the compression zone (crack type F)

According to the definition of Figure 4.4, a crack type F is a propagation of a primary flexural crack within the compression zone (quasi-horizontal branch of the crack). In Figure 4.7a, the normalized acting shear force when a crack type F starts developing ($V_{A,F}$) is plotted versus the moment-to-shear ratio α_A for specimens with reinforcement ratio $\rho = 0.89\%$. It can be noted that these cracks propagate at higher shear forces for low values of moment-to-shear ratio α_A (crack near end support or point of contraflexure).

It has already been observed in [1] that for very low values of α_A, a crack type F develops at a load level close to failure. On the contrary, for cracks at a larger distance from the point of contraflexure (large values of α_A), the development of a crack type F is not directly associated to failure, and in some cases the load can still be increased significantly. This observation has been confirmed by the additional tests described in this Chapter. In Figure 4.7b, it can be observed that the quasi-horizontal branch of the critical shear crack may develop, for large values of α_A, below 50% of the maximum load (e.g. specimen SC70, refer to Figure 4.8 and Figure 4.9a). In Figure 4.7b, the magenta circles represent the shear force at the onset of the crack type F ($V_{A,F}$) and the green squares represent the maximum shear force ($V_{A,max}$).

The shear force at which a crack type F propagates ($V_{A,F}$) can be calculated, in accordance to the Kani's tooth model [7], in terms of the bending capacity of a vertical cantilever developing between two primary flexural cracks. The procedure to calculate $V_{A,F}$ will be presented in detail in the following section.
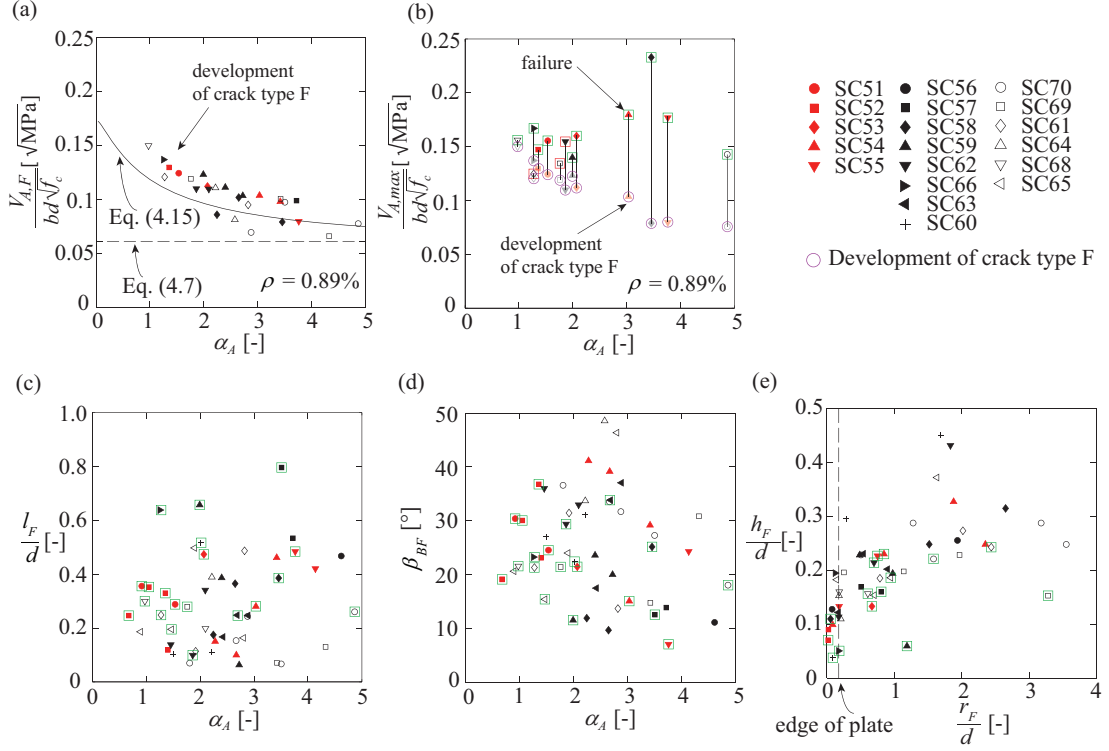
Figure 4.7 (a) Normalized shear force in section A when a crack type F starts propagating as a function of the moment-to-shear ratio α_A for $\rho = 0.89\%$ and comparison with calculated value; (b) increase of the shear force in A after the development of a crack type F up to the maximum load; (c) length of cracks of type F; (f) angle of cracks of type F; (g) location of the tip of cracks of type F at the peak load (squares represent critical shear cracks, other symbols represent other cracks)
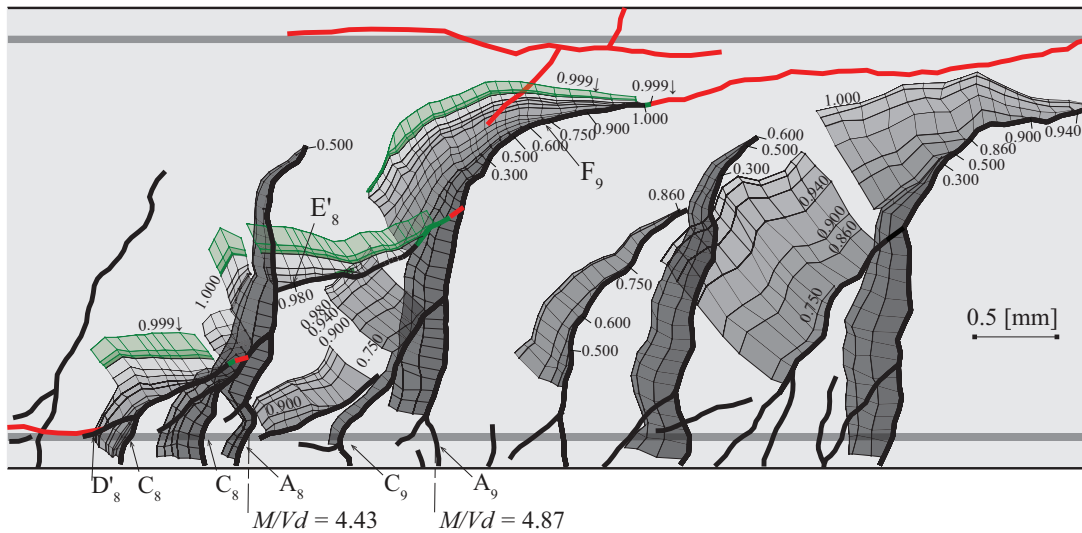
Figure 4.8 Specimen SC70: development of cracking and relative crack displacements at selected load steps (colour black-green-red defined in legend of Figure 4.1)
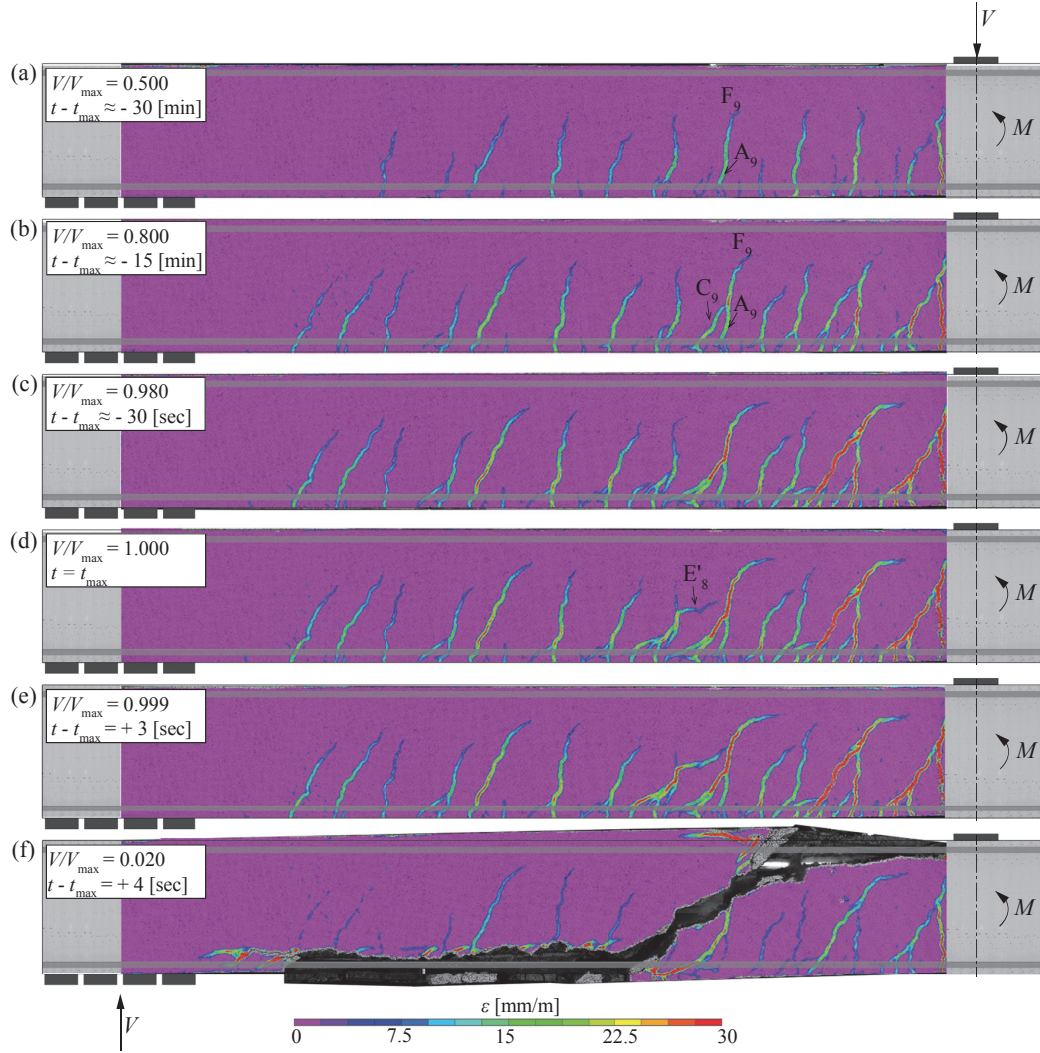
Figure 4.9 Specimen SC70: detailed development of cracking on the basis of DIC analyses at selected load steps; V/V_{max}: (a) 0.500; (b) 0.800; (c) 0.980; (d) 1.000; (e) 0.999; (f) 0.020 (ε refers to principle tensile strains from DIC measurements)

With respect to the length of cracks of type F (l_F, measured from point B to the tip of the crack A-F at peak load, refer to Figure 4.7c), it can be observed that its value is relatively variable ($0.05d$-$0.8d$). However, it can be noted that when a crack type C merges during loading with a primary flexural crack, the length l_F at maximum load is usually longer than $0.25d$, whereas when the critical shear crack corresponds to a crack type A-F with no additional secondary cracks connected, the length l_F at peak load varies between $0.05d$ and $0.3d$ (e.g. specimens SC61, SC62, SC69).

Furthermore, a very large scatter can be observed with respect to the angle β_{BF} between the crack type F and the longitudinal axis of the beam (calculated as the angle of a line passing through point B and point F, which corresponds to the tip of crack type F, Figure 4.6a). For the presented tests (Figure 4.7d), it varies between 8° and 35°, with an average value of 22°.

Finally, it can be noted that the distance of the tip of a crack type F at peak load from the axis of right support plate (r_F in Figure 4.6a) varies between 0 and $3d$ in the case of cantilever beams subjected to concentrated loading and between 0 a d for cantilever and continuous beams subjected to distributed loading (Figure 4.7e).

Following the observations of the present testing programme, a clear dependency can be observed between the total horizontal opening $u_{A,mes}$ at the level of the longitudinal reinforcement and the acting bending moment (M_F) at the section corresponding to the tip of the crack, whose position varies during loading. It has to be mentioned that the total horizontal opening shown in

Figure 4.10a refers to the sum of the openings of the primary flexural crack and secondary cracks at the level of the longitudinal reinforcement along a length l_B, which represents the region that contributes to the opening of the primary flexural crack (refer to Figure 4.5). The indicated points in Figure 4.10a represent the value of u_A at peak load.

Assuming that the crack opening $u_{A,mes}$ is proportional to the product of the strain at the level of the longitudinal reinforcement times a length l_B (the tributary length to the crack opening [8]):

$$u_{A,mes} = \varepsilon_s \cdot l_B = \frac{M_F}{A_s \cdot E_s \cdot z} \cdot l_B \tag{4.3}$$

the ratio l_B/z can be calculated as a function of the measured crack opening $u_{A,mes}$:

$$\frac{l_B}{z} = \frac{u_{A,mes}}{\dfrac{M_F}{A_s \cdot E_s}} \tag{4.4}$$

The values of l_B/z, calculated according to Eq. (4.4), are plotted in Figure 4.10b as a function of the acting bending moment at the section corresponding to the tip of the crack (M_F), whose position varies as the crack progresses for increasing values of the applied load (refer to Figure 4.8 and Figure 4.9). The magenta circles represent the value of l_B/z at the onset of the crack type F. It can be observed that the value of l_B/z when a crack type F starts developing varies between 0.5 and 0.8 (the average value is 0.67 and the Coefficient of Variation is 10%). At the peak load (squares in the diagram), l_B/z reaches an average value equal to 0.83 with a Coefficient of Variation of only 6%. The fairly constant value of l_B/z at failure is in agreement with the almost linear correlation between the crack opening and the acting bending moment at failure (symbols in Figure 4.10a).

It is important to note that the linear relationship between the crack opening and the acting bending moment M_F is no longer valid at peak load for (i) squat members (e.g. specimen SC67), or for (ii) slender members characterized by a critical shear crack developing such that the arching action is still possible (e.g. specimens SC58 and SC63, see Figure 4.1b and Chapter 3) or for (iii) slender members characterized by a critical shear crack progressing such that the compressive reinforcement acts as an integrity reinforcement [9] (e.g. specimen SC60). For these members, the fairly constant value of l_B/z can be measured before the activation of the direct strut or the dowelling action of the compressive reinforcement (that allow a further increase in the applied load), in the instant in which the sum of the contribution of the beam shear-transfer actions reaches its maximum value. Further analyses on the various shear-transfer actions during loading and at failure are presented in Chapter 5.

Assuming $z=d-c/3$, the value of l_B can be generalized, for members with different longitudinal reinforcement ratios ρ, to be approximately equal to $d-c$, where c is the depth of the compression zone (calculated by assuming a linear response of concrete in compression and neglecting concrete in tension). The average of measured-to-calculated values for 12 specimens (10 with ρ=0.89% and 2 with ρ=0.54%) is equal to 1.01 and the Coefficient of Variation is 6%. Consistent results have also been obtained for 3 slender members with a reinforcement ratio equal to 1.32% [10]. It is interesting to observe that the length l_B at maximum load is considerably larger than the spacing between primary flexural cracks s_r: after the development of the quasi-horizontal branch, the ratio l_B/z increases, leading to a localization of strains in the critical shear crack.
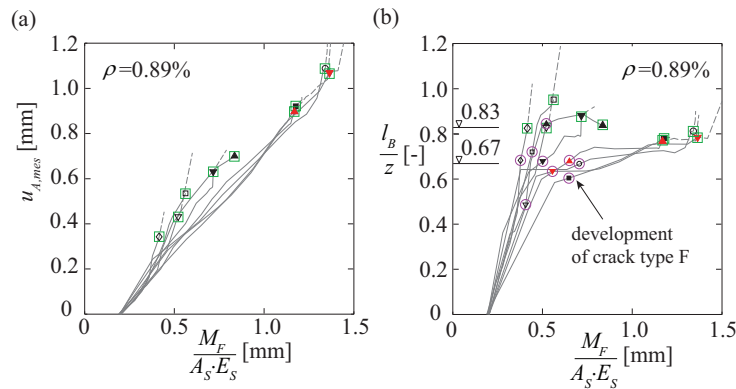
Figure 4.10 (a) Measured crack opening at the longitudinal reinforcement level $u_{A,mes}$ as a function of the moment at the section corresponding to the tip of the critical crack M_F (squares in the diagram refer to peak load, see legend in Figure 4.7); (b) l_B/z as a function of M_F (continuous lines refer to pre-peak, dashed lines refer to post-peak)

4.2.3 Conditions for the development of cracks of type F

As shown in Figure 4.7b, the shear force at which a crack type F propagates ($V_{A,F}$) does not correspond to the ultimate shear strength, as, in most cases, a significant strength increase has been obtained after its development (e.g. specimen SC70, refer to crack F_9 in Figure 4.8 and Figure 4.9a).

The shear force that causes the development of a crack type F can be calculated, in accordance with the simple Kani's tooth model [7], in terms of the bending capacity of a tooth, assuming a vertical cantilever developing between two flexural cracks of type A: when the bending moment at the clamping of the cantilever attains a critical value such that the stresses at the tip of the crack reach the tensile strength of concrete f_{ct}, a crack type F propagates within the beam's compression zone. The procedure to calculate the theoretical shear force at the initiation of a crack type F is based on the following assumptions:

– Flexural cracks develop from the tension side of the member up to the neutral axis and shape the beam into a teeth-like structure, as considered by Kani (1964) (Figure 4.11a);

– The cracks are assumed to be straight segments;

– The concrete teeth are assumed to be cantilevers clamped in the compression zone of the beam and loaded by the horizontal shear force ΔN generated by bond in the reinforcement;

– The depth of the compression zone c is calculated neglecting the tensile stress of concrete in the flexural crack;

– The level arm of the longitudinal forces is assumed to be constant and equal to $z=d-c/3$;

– The spacing between the flexural cracks is assumed equal to $s_r = 0.56d$ [1];

– A crack type F originates from a primary flexural crack when the stresses due to the bending moment at the fixed end of the tooth reach the tensile strength of concrete f_{ct}.
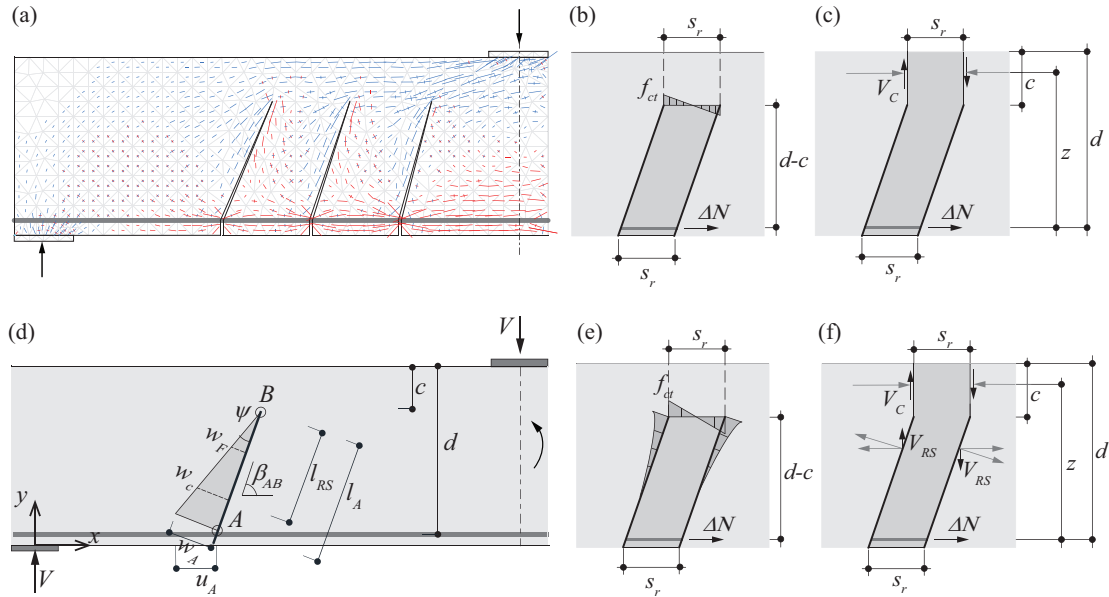
Figure 4.11 (a) Concrete stress field obtained from a linear elastic finite element analysis of the Kani's tooth model [7]; scheme of a single tooth, treated as cantilever, used to determine the shear force that causes the propagation of the crack into the compression zone accounting for the contribution of the compression zone: (b) stresses distribution and (c) forces; (d) assumed kinematics of a crack type A before the development of a crack type F; scheme of a single tooth accounting for the contribution of the compression zone and the residual tensile strength of concrete: (e) stresses distribution and (f) forces

In the following, two different approaches that account for different contributions of the shear-transfer actions are presented. The first one is consistent with Kani's assumption that only the cantilever action (V_C) is responsible for carrying the total shear force before the propagation of a crack type F. In this case, the cantilever action requires the compression chord to be inclined, as it can be observed in Figure 4.11a, where the stress field obtained from a linear elastic finite element analysis of the Kani's

tooth model is shown (the finite element analysis is performed assuming a varying angle of the flexural cracks according to Eq. (4.2) and neglecting all stresses developing across the cracks).

Using Kani's schematization, the maximum moment at the fixed end of the tooth is governed by the maximum tensile stress of concrete (refer to Figure 4.11b, $f_{ct} = 0.3 \cdot f_c^{\ 2/3}$):

$$\frac{f_{ct} \cdot b \cdot s_r^{\ 2}}{6} = \Delta N \cdot (d-c) \tag{4.5}$$

Examining the free-body diagram of the tooth presented in Figure 4.11c, the moment equilibrium gives the following relation:

$$\Delta N \cdot z = V \cdot s_r \tag{4.6}$$

By substituting Eq. (4.6) into Eq. (4.5), the shear force that determines the breaking of the concrete tooth can be determined as:

$$V = \frac{f_{ct} \cdot b \cdot s_r \cdot z}{6 \cdot (d-c)} \tag{4.7}$$

It can be noted that an additional flexural strength of the cantilever could be attained due to a non-linear distribution of the stresses represented in Figure 4.11b. Nevertheless, this additional strength is activated after the development of the critical shear crack in a quasi-horizontal direction.

In the second approach, both the cantilever action (V_C) and the residual tensile strength of the concrete (V_{RS}) in the flexural crack type A are considered (see Figure 4.11e-f). The contribution of the residual tensile strength of concrete is calculated taking into account the inclination of the flexural crack β_{AB} defined as in Eq. (4.2), assuming a linear distribution of the horizontal opening u along the crack (see Figure 4.11d), where u_A is expressed according to Eq. (4.4) and l_B/z is assumed equal to 0.67, in accordance with the experimental measurements at the initiation of crack type F (refer to Section 4.2.2).

Following the same procedure as the one adopted in the first approach, the maximum moment at the fixed end of the tooth and the equilibrium of the free-body are calculated (refer to Figure 4.11e and f):

$$\frac{f_{ct} \cdot b \cdot s_r^{\ 2}}{6} = \Delta N \cdot (d-c) - V_{RS} \cdot s_r \tag{4.8}$$

and

$$\Delta N \cdot z = V_C \cdot s_r + V_{RS} \cdot s_r \tag{4.9}$$

The contribution of the cantilever action becomes:

$$V_C = \frac{z}{(d-c)} \left(V_{RS} + \frac{f_{ct} \cdot b \cdot s_r}{6} \right) - V_{RS} \tag{4.10}$$

Thus, the shear force at the initiation of a crack type F results as the sum of cantilever action and the residual tensile strength of concrete:

$$V = V_C + V_{RS} = \frac{z}{(d-c)} \left(V_{RS} + \frac{f_{ct} \cdot b \cdot s_r}{6} \right) \tag{4.11}$$

The length l_{RS} where the residual strength acts is (refer to Figure 4.11d):

$$l_{RS} = l_A \cdot \frac{w_c}{w_A} = (d-c) \cdot \frac{w_c}{u_A} \tag{4.12}$$

and u_A is defined as (see Eq. (4.4)):

$$u_A = \frac{M_B}{b \cdot d \cdot \rho \cdot E_s} \cdot \frac{l_B}{z} = \frac{V \cdot a_B}{b \cdot d \cdot \rho \cdot E_s} \cdot \frac{l_B}{z} \tag{4.13}$$

where $a_B = a_A + (d - c) \cdot \cot\beta_{AB}$.

The contribution of the residual tensile strength of concrete can be calculated as:

$$V_{RS} = b \cdot l_{RS} \cdot \frac{G_F}{w_c} \cdot \cos\beta_{AB} = b \cdot (d-c) \frac{G_F}{u_A} \cdot \cos\beta_{AB} = b \cdot f_{ct} \cdot (d-c) \cdot \frac{w_F}{u_A} \cdot \cos\beta_{AB} \tag{4.14}$$

where G_F is the fracture energy of concrete and $w_F = G_F/f_{ct}$. It can be noted that if $w_A > w_c$, the result does not depend on the distribution of the residual stresses, but only on its integral which is a function of the fracture energy G_F.

By assuming $w_A > w_c$ and substituting Eq. (4.13) and Eq. (4.14) in Eq. (4.11), the shear force at the onset of a crack type F can be expressed in a closed-form equation:

$$V = \frac{f_{ct} \cdot b \cdot s_r \cdot z}{6 \cdot (d-c)} \cdot \left[\frac{1}{2} + \sqrt{\frac{1}{4} + 36 \cdot \frac{w_F}{d} \frac{\rho \cdot E_s \cdot \left(1 - \frac{c}{d}\right)^2}{f_{ct} \cdot \frac{a_B}{d} \frac{l_b}{z} \cdot \frac{z}{d} \cdot \left(\frac{s_r}{d}\right)^2} \cdot \cos\beta_{AB}} \right] \tag{4.15}$$

where the first part of this equation is equivalent to Eq. (4.7) and β_{AB} is defined as in Eq. (4.2).

The shear capacity of the tooth accounting for the contribution of cantilever action and residual tensile strength of concrete (Eq. (4.15)) gives a consistent prediction of the experimental results (the average measured-to-predicted values is 1.10 and the Coefficient of Variation is 14.4% for 28 cracks in Figure 4.7b). The ratio 1.10 shows that Eq. (4.15) generally underestimates the shear force corresponding to the initiation of a crack type F. This is particularly the case for small values of moment-to-shear ratio ($M/(V \cdot d) < 3$). A reasonable explanation to this can be grounded on the fact that the dowelling action, whose contribution can play a role for cracks with a flatter inclination with respect to the beam axis, is neglected. However, for high values of moment-to-shear ratio, Eq. (4.15) provides a good estimate of $V_{A,F}$ since flexural cracks are generally steeper and the dowelling action is very limited or negligible (e.g. specimen SC70, refer to crack A_9 in Figure 4.9a).

4.2.4 Secondary flexural cracks: crack type C

A crack type C is a secondary flexural crack that can develop between two primary flexural cracks (Figure 4.4a) and its development is governed by the amount of flexural reinforcement and by bond conditions. A crack type C propagates with an angle flatter than the one of a primary flexural crack, and becomes connected to a primary flexural crack generally below one-half of the effective depth of the member.

It has been experimentally observed that a crack type C propagates and merges with a crack type A, after the propagation from the primary flexural crack of the quasi-horizontal branch within the compression zone (cracks A_9-F_9 in specimen SC70 at 80% of the maximum load, refer to Figure 4.9b).

When a crack type C and a primary flexural crack merge, a portion of the critical shear crack below the merging point is deactivated. At this stage two possible scenarios can occur: (i) when the primary flexural crack is sufficiently steep (cracks C_9 and A_9 of Figure 4.8 and Figure 4.9b), measurements of the crack kinematics (Figure 4.8) show that some aggregate interlock stresses can be still mobilized in the upper parts of the crack type A and the load could be further increased; (ii) when the primary flexural crack is rather flat (generally for α_A smaller than 2, e.g. specimens SC61 and SC69), the merging of both cracks cause an abrupt increase of the opening of the critical shear crack, triggering loss of aggregate interlock capacity and failure.

4.2.5 Dowelling cracks: crack type D'

As defined in [1], a crack type D' is an inclined crack that develops from a flexural crack or in its vicinity at the level of the longitudinal reinforcement or just above it (typically between c_b and $3c_b$ from the tension side of the specimen, where c_b refers to the concrete cover). Cracks of type D' appear for vertical relative displacements of the primary flexural crack at the level of the longitudinal reinforcement (v_A in Figure 4.12a), lower than 0.15 mm (Figure 4.12c). The described tests have shown that a crack type D' can either develop before the development of crack type F for very inclined primary flexural cracks or

immediately after the propagation of crack type F for rather steep primary flexural cracks. In some cases, if a crack type C (see Figure 4.4) originates in the vicinity of a crack type A, it leads to a loss of bond along the longitudinal reinforcement and cracks of type D' due to dowelling do not necessarily appear (e.g. potential critical shear crack in specimen SC69 in Figure 4.1b).

As the shear force increases, the crack type D' (or crack type C) may eventually propagate along the longitudinal bars in a stable manner. However, it can be noted that horizontal cracking along the longitudinal reinforcement is not a sufficient condition for shear failure. In fact, a crack characterized by an extensive horizontal cracking does not necessarily become critical if the crack type A-F is still capable of developing aggregate interlock forces in the steeper part of the crack or alternative shear-transfer actions develop (e.g. potential critical crack in specimen SC61 in [1]).
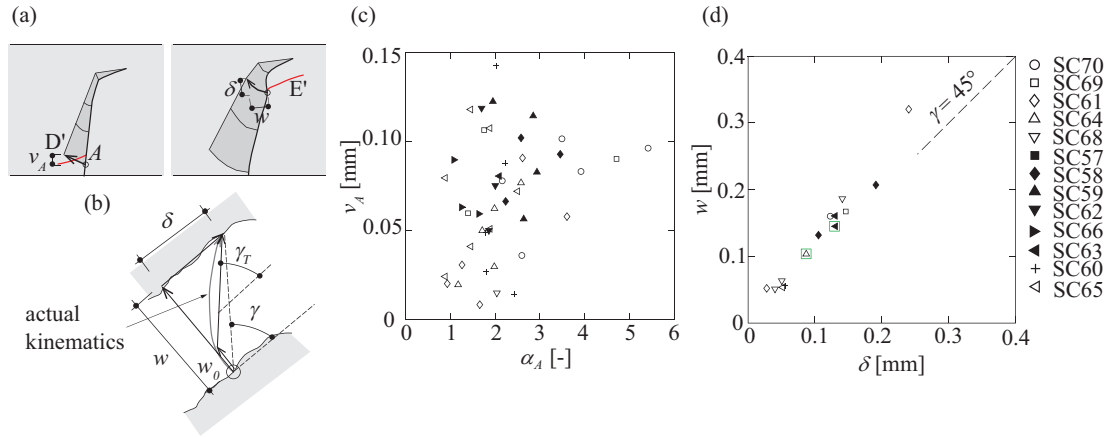
Figure 4.12 (a) Cracks of type D' and E'; (b) Definition of crack opening w, sliding δ, mixed mode angle γ and γ_T (c) vertical displacement v_A at the level of the longitudinal reinforcement when a crack type D' starts developing; (c) crack opening w and sliding δ of the point along a crack type A when a crack type E' starts propagating (squares represent critical shear cracks, other symbols represent other cracks)

4.2.6   Aggregate interlock induced cracks: crack type E'

With respect to a crack type E' (see Figure 4.4), its development has been investigated by Jacobsen et al. [11] and can be explained by high aggregate interlock forces [1].

It can be observed that a crack type E' propagates where a primary flexural crack is particularly steep and generally above mid-height of the primary flexural crack. As described in [1], in some cases, a crack type E' can develop almost parallel and near to a crack type F (E'$_8$ in Figure 4.8 and Figure 4.9d). This observation shows that such a crack cannot be induced by other tensile forces and the only explanation is a concentration of aggregate interlock forces at crack type A. On the basis of the DIC measurements, it can be observed that a crack type E' propagates for an initial opening w_0 (refer to Figure 4.12b) generally lower than 0.05 mm (when aggregate interlock stresses can be potentially very high). Moreover, the secant mixed mode angle γ between the crack opening w and crack sliding δ at the instant in which a crack type E' starts developing (refer to Figure 4.12b) is approximately equal to 45° (Figure 4.12d). These results confirm the observations pointed out by Jacobsen et al. [11].

The propagation of a crack type E' can be followed either by the development of a stable crack A-E transferring shear by aggregate interlock or by other shear-transfer mechanisms (e.g. direct strut action, specimen SC63) or can be followed by failure (e.g. specimens SC64 and SC56 in Cavagnis et al. [1]).

4.2.7   Cracks within the compression chord: crack type G' and G''

As defined in [1], crack types G' and G'' develops within the compression zone but not originating from a crack type A-F. Such cracks may propagate only when the critical shear crack develops below the right support region (or in its vicinity) or below the theoretical compression strut, allowing a direct strut to develop. The latter may develop without any disturbance (e.g. specimen SC67, Figure 4.1b) or may be partially affected by the development of the critical shear crack (e.g. specimen SC60, Figure 4.1b).

On the contrary, when the critical shear crack develops far from the right support region, fully disturbing the theoretical compression strut (e.g. specimens SC59, SC61, SC64, SC69, SC70 in Figure 4.1b and [1]), detailed measurements of the longitudinal strains along the compression face of the beam show that no bending or shear cracks occur within the compression chord before failure.

A crack type G'' develops at flat angles near the right support plate at a load lower than the maximum load (e.g. for specimens SC67 at 75% of the peak load). At peak load, a crack type G'' can eventually merge with the critical shear crack (e.g. specimen SC60) or propagate within the theoretical compression strut (e.g. specimen SC67), leading to the collapse of the member.

4.3 Conclusions

This Chapter reviews detailed DIC measurements of the cracking patterns of 20 beams without shear reinforcement. The main conclusions are listed below:

1. The development of quasi-horizontal cracking within the compression zone from a bending crack is suitably explained and predicted by the Kani's model (refinements are possible accounting for the fracture properties of concrete). Such crack development does not necessarily correspond to the ultimate shear strength, as, in most cases, a significant strength increase has been obtained after the propagation of the quasi-horizontal crack.

2. It has been experimentally measured that the maximum crack opening develops approximately at mid-height of the specimen. Crack spacing at this location is approximately $0.4d$-$0.8d$ and it is not governed by bond of the flexural reinforcement. When the contribution of the secondary cracks, developing at the level of the longitudinal reinforcement, is accounted for, the total crack opening follows a linear distribution over the height of the critical shear crack.

3. At peak load, the length contributing to the opening of the critical crack l_B is roughly constant for the tested specimens and it can be approximated by d-c. The horizontal opening of the critical shear crack at the level of the longitudinal reinforcement can be assumed to be equal to the product between the longitudinal strain (calculated according to a cracked sectional analysis) and the length l_B. With this assumption, the opening of the critical crack can be easily calculated as it is proportional to the acting bending moment at the section corresponding to the tip of the crack.

4. It has been experimentally observed that, after the development from a flexural crack of a quasi-horizontal crack within the compression zone, combined crack opening and sliding may cause large concentration of aggregate interlock forces in the steeper part of the flexural crack and failure may be associated to the development of an aggregate interlock induced crack.

4.4 Appendix A

In this Appendix the development of critical shear crack and the relative crack displacements at selected load steps are shown for the tests where DIC technique was employed that have not be included in Cavagnis et al. [1] or in other Chapters.
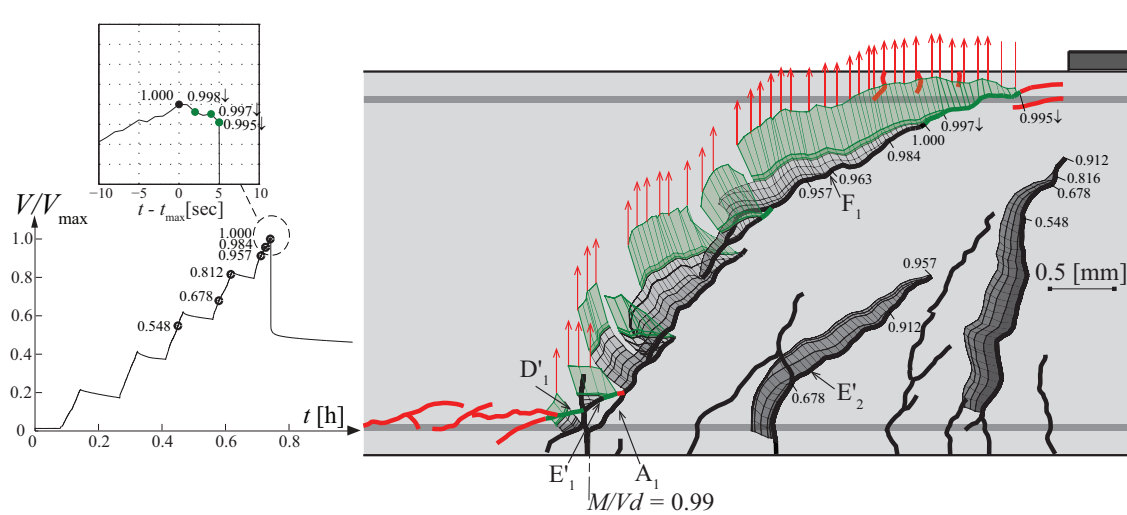
Figure 4.13 Specimen SC68: development of cracking and relative crack displacements (colour black-green-red defined in Figure 4.1)
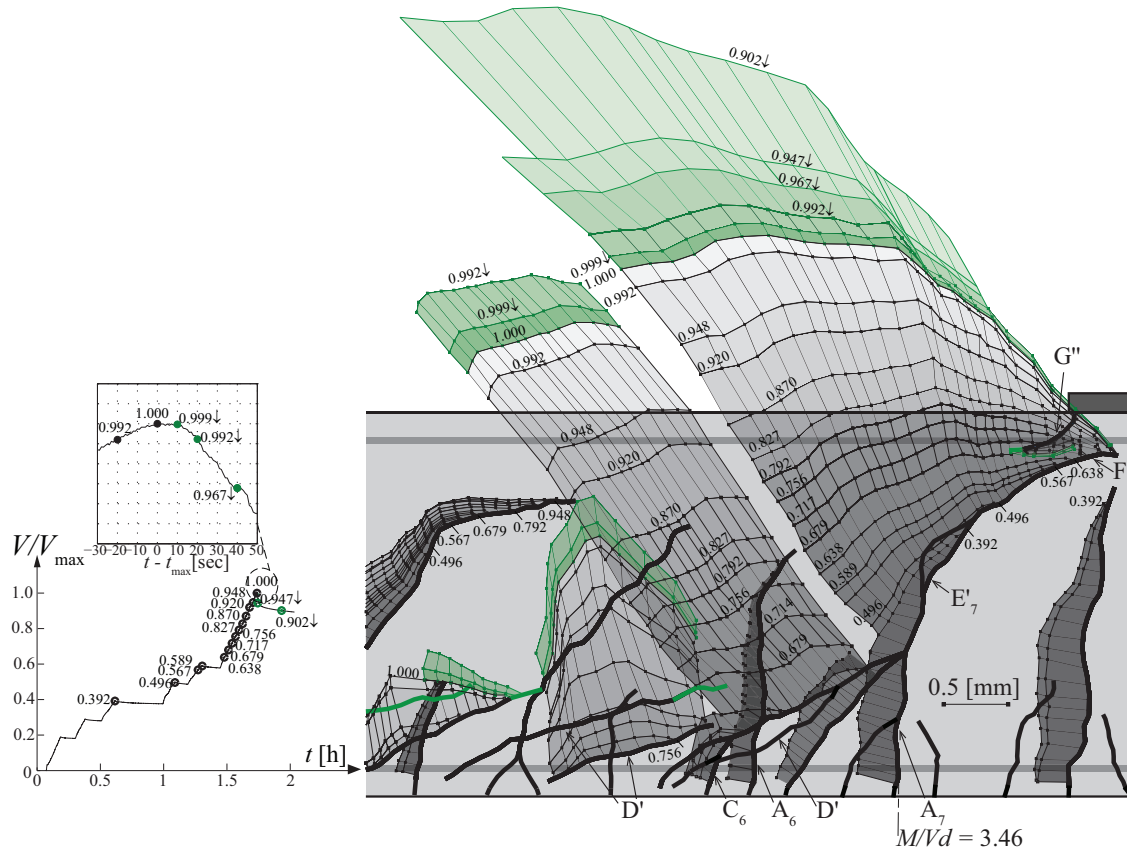
Figure 4.14 Specimen SC58: development of cracking and relative crack displacements (colour black-green defined in Figure 4.1)
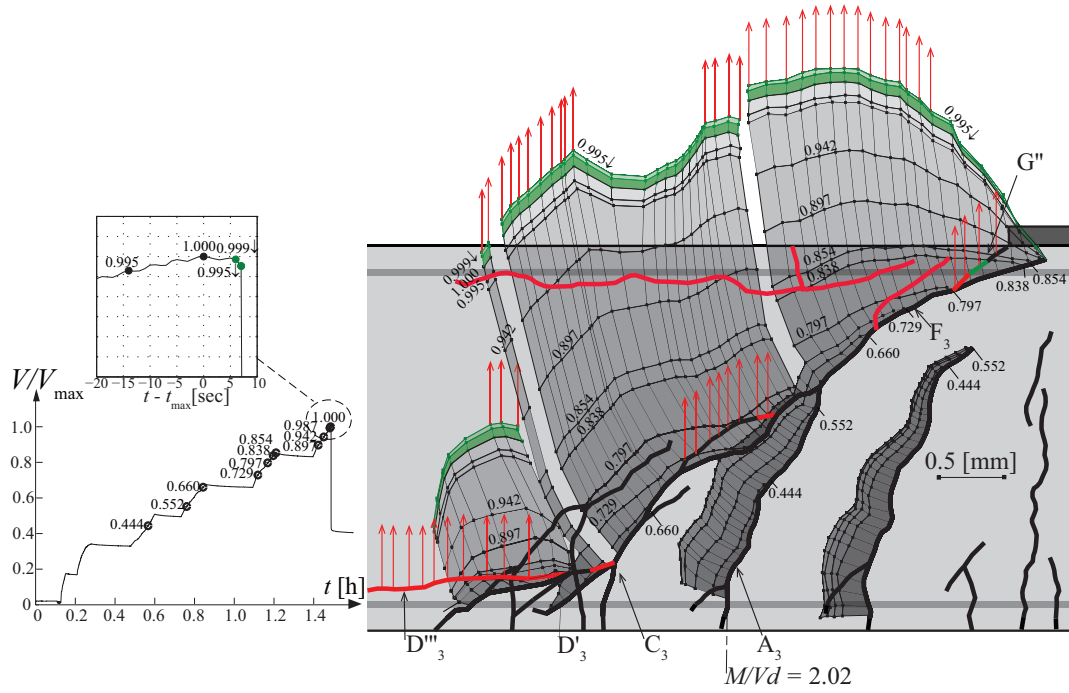
Figure 4.15 Specimen SC60: development of cracking and relative crack displacements (colour black-green-red defined in Figure 4.1)
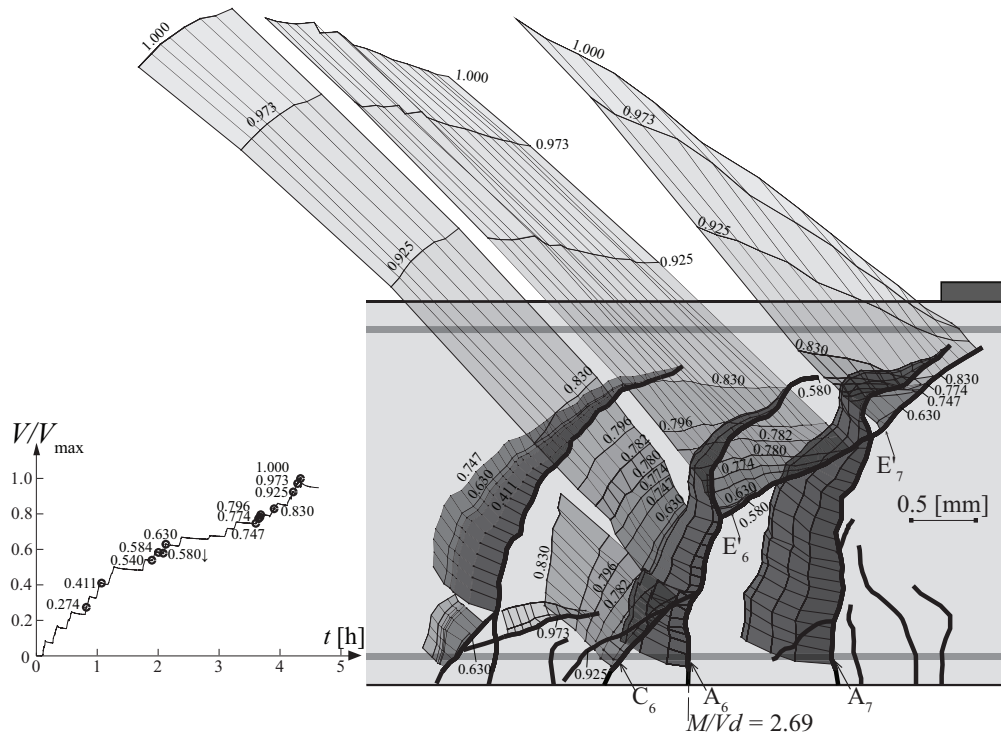
Figure 4.16 Specimen SC63: development of cracking and relative crack displacements (colour black defined in Figure 4.1)
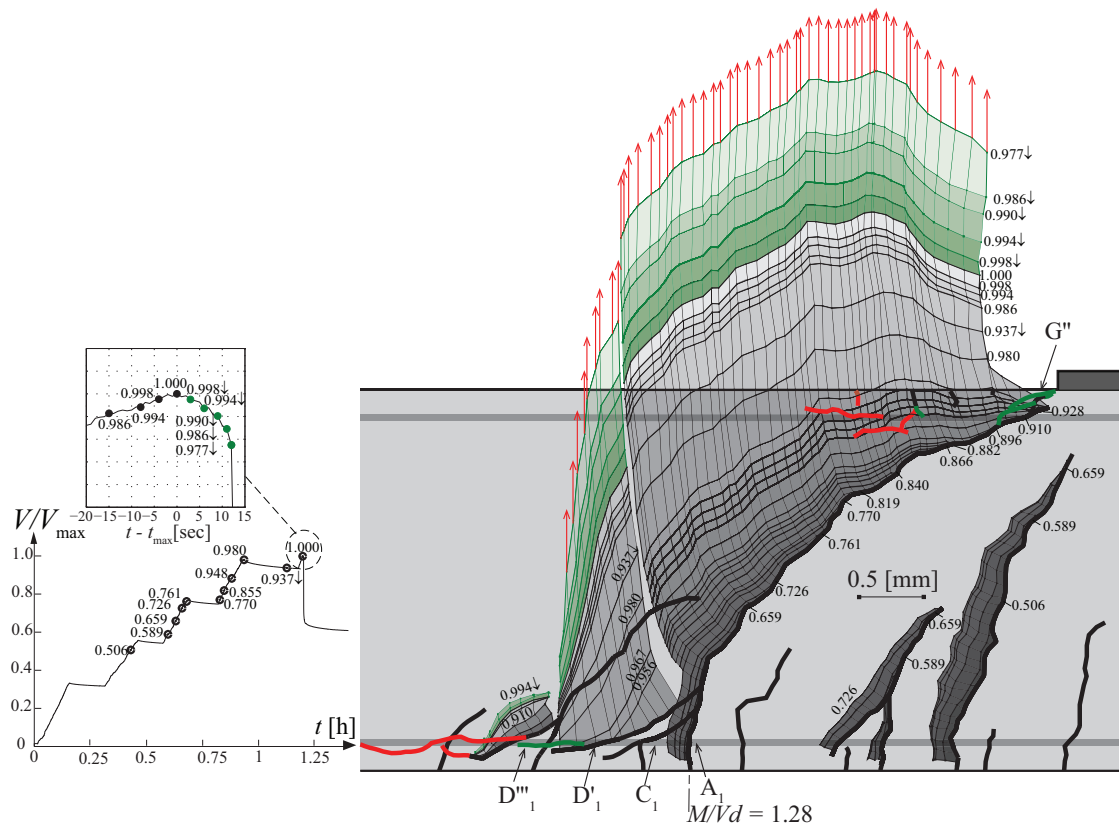
Figure 4.17 Specimen SC66: development of cracking and relative crack displacements (colour black-green-red defined in Figure 4.1)

63
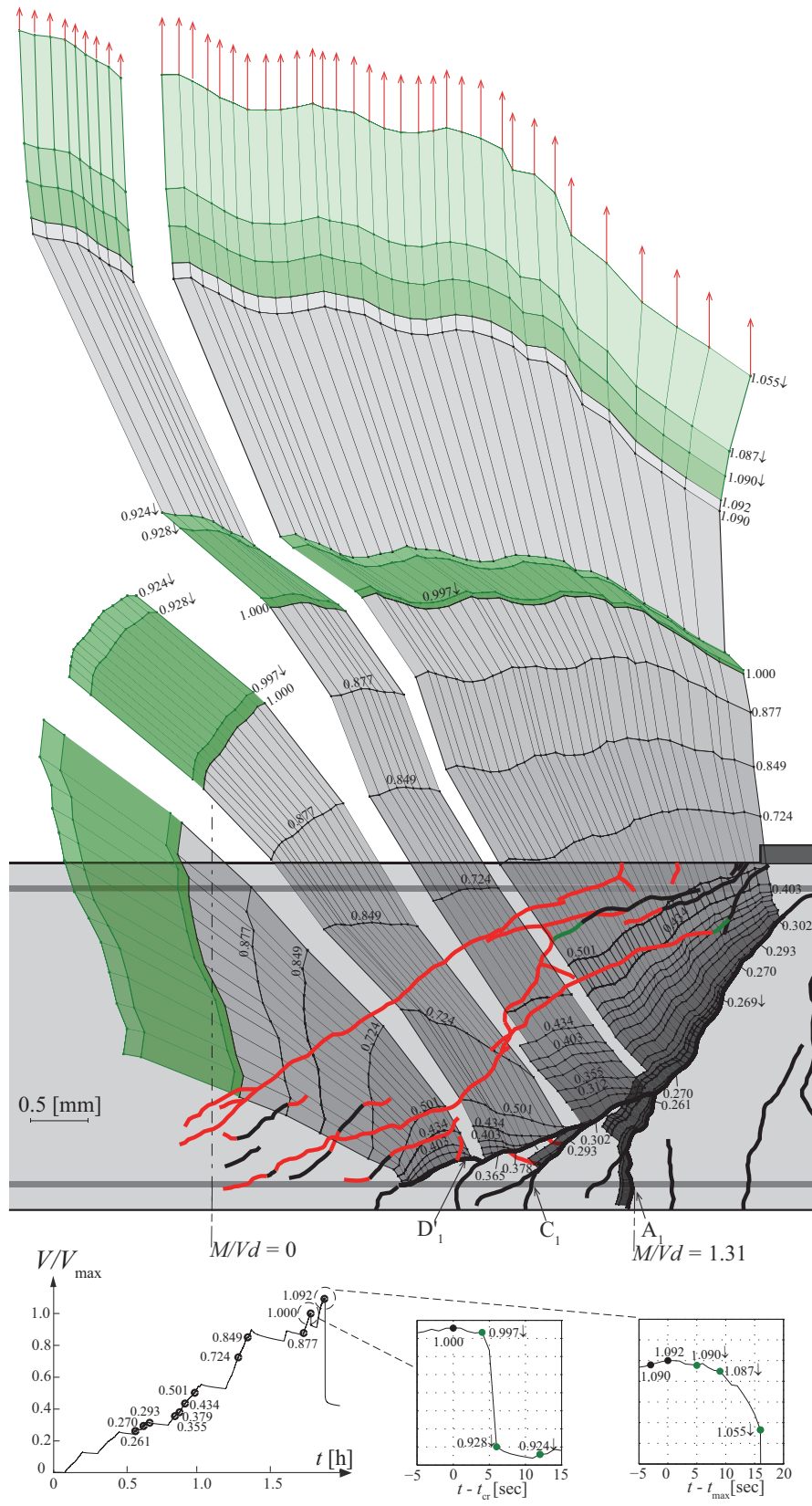
Figure 4.18 Specimen SC67: development of cracking and relative crack displacements (colour black-green-red defined in Figure 4.1)
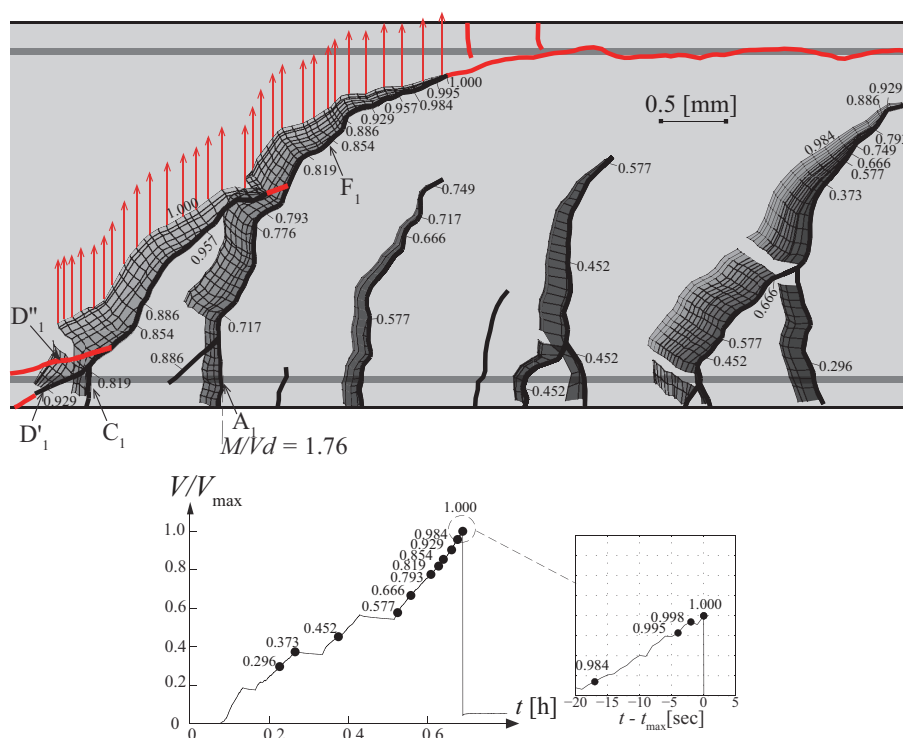
Figure 4.19 Specimen SC69: development of cracking and relative crack displacements (colour black -red defined in Figure 4.1)

4.5 References

[1] Cavagnis F, Fernández Ruiz M, Muttoni A. Shear failures in reinforced concrete members without transverse reinforcement: An analysis of the critical shear crack development on the basis of test results. *Engineering Structures* 2015; 103:157–173.

[2] Correlated Solutions. VIC 3D Software, Reference Manual. 2010.

[3] Reineck K-H. Ultimate shear force of structural concrete members without transverse reinforcement derived from a mchanical model. *ACI Structural Journal* 1991; 88 (5):592–602.

[4] Shioya T. Shear Properties of Large Reinforced Concrete, Special Report (in Japanese), Institute of Technology, Shimizu Corp., No. 25. 1989.

[5] Khaja MN, Sherwood EG. Does the shear strength of reinforced concrete beams and slabs depend upon the flexural reinforcement ratio or the reinforcement strain? *Canadian Journal of Civil Engineering* 2013; 40 (11):1068–1081.

[6] Yang Y, Walraven J, den Uijl J. Shear Behavior of Reinforced Concrete Beams without Transverse Reinforcement Based on Critical Shear Displacement. *Journal of Structural Engineering* 2016; 143 (1):4016146.

[7] Kani GNJ. The riddle of shear failure and its solution. *ACI Journal* 1964; 61 (4):441–467.

[8] Fernández Ruiz M, Muttoni A, Sagaseta J. Shear strength of concrete members without transverse reinforcement: a mechanical approach to consistently account for size and strain effects. *Engineering Structures* 2015; 99:360–372.

[9] Fernández Ruiz M, Mirzaei Y, Muttoni A. Post-punching behavior of flat slabs. *ACI Structural Journal* 2013; 110 (5):801–812.

[10] Tasevski D, Muttoni A. Shear tests under varying strain rate, Internal report IBETON, EPFL. 2017.

[11] Jacobsen JS, Poulsen PN, Olesen JF. Characterization of mixed mode crack opening in concrete. *Materials and Structures* 2012; 45 (1–2):107–122.

Chapter 5 — An analysis of the shear transfer actions in reinforced concrete members without transverse reinforcement

In this Chapter, a complete analysis of the shear-transfer actions of 20 beams without shear reinforcement is performed during loading and the process of failure. The amount of shear carried by the various shear-transfer is estimated by using detailed measurements on the shape and kinematics of the critical shear crack and suitable mechanical models. The results show good predictions in term of the shear strength of the members and allow identifying the shear-transfer actions governing for the shear capacity. This Chapter has been accepted for publication in a scientific journal:

The first author carried out the experimental campaign, the analysis of the experimental measurements and the quantification of the shear-transfer actions under the guidance of the second and third author.

This Chapter comprises an additional section (Section 5.11), in which further results are shown, that have not been included in the paper submitted due to word/character limit constraints.

5.1 Abstract

A traditional difficulty in the understanding of the role of the various shear transfer actions in members without transverse reinforcement has been a lack of detailed measurements on the development of shear cracking and their associated kinematics during the process of failure. In this paper, this issue is addressed on the basis of an experimental programme on 20 beams investigated by means of digital image correlation. The measurements are shown to allow a clear understanding of the mechanisms leading to shear failure and their evolution (transfer of forces between the various potential shear-carrying actions) during the loading process. The amount of shear carried by the various potential shear transfer actions is estimated for varying levels of load accounting for the cracking pattern and actual kinematics on the basis of fundamental constitutive laws for concrete and steel. The results are shown to be consistent and to provide a rational basis for the understanding of the phenomenon of shear transfer in reinforced concrete members without transverse reinforcement.

Key-words: shear, experimental programme, digital image correlation (DIC), shear-transfer actions, mechanisms of shear failure

5.2 Introduction

Shear design of one-way slabs and beams without shear reinforcement has attracted significant research efforts in the last decades. These studies have allowed recognizing the different shear-transfer actions that contribute to the shear strength of reinforced concrete members without transverse reinforcement [1, 2]. Traditionally, the shear-transfer actions are classified [3] into beam shear transfer actions (where the force in the tension chord varies and transverse tensile stresses develop) and the arching action (where the force in the tension chord is constant and no transverse tensile stresses are necessary for carrying shear). With respect to the beam shear-transfer actions [3], shear can be carried by the so called cantilever action [4], the residual tensile strength, the dowelling action or the aggregate interlock.

Various approaches for shear design have been developed in the past considering one of these actions as governing (compression zone [5–7], aggregate interlock [8]) or combining them [9–12]).

Despite these research efforts, there is still no general consensus on the main parameters governing the shear resistance and the mechanisms triggering the shear failure. In this context, detailed measurements of the failure process are probably the most consistent manner to advance on this issue. With this respect, digital image correlation (DIC) is a very suitable tool that allows tracking the displacement field and investigating the redistribution between the different load-carrying actions and the process of failure [13].

In this paper, the results of 7 beams are presented, completing a previous experimental campaign on 13 beams without transverse reinforcement reproducing various loading and support conditions [13]. Detailed DIC measurements were recorded and used to track the crack shape and kinematics. On that basis, a complete analysis of the various potential shear-transfer actions is performed during loading as well as in the instants before and after reaching the maximum load. This analysis is performed by accounting for the measured kinematics and by using fundamental mechanical models. As a result, this paper aims at clarifying the role of the shear-transfer actions in the failure process and to identify the mechanisms triggering the shear failure.

5.3   Experimental programme

In Cavagnis et al. [13], 17 tests on 13 beams without shear reinforcement tested under different loading conditions were presented (SC51-SC57, SC59, SC61-SC65). That experimental programme is completed in this manuscript with 8 additional tests on 7 beams (SC58, SC60, SC66-SC70, refer to Table 5.1). The test setup was maintained (a detailed description of the test setup is provided in Cavagnis et al. [13], Figure 5.1a) allowing to reproduce various loading and support conditions: simply supported beams (Figure 5.1b), continuous beams (Figure 5.1c) and cantilevers (Figure 5.1d) subjected to distributed loading and cantilevers subjected to point loading, where the load is concentrated at the end of the cantilever (acting on a distance of 700 mm, Figure 5.1e).

The investigated specimens had a rectangular cross-section of 250 x 600 mm [13]. Two amounts of longitudinal reinforcement ratio were used: ρ=0.54% (corresponding to 2 bars diameter 22 mm, effective depth d = 559 mm) and ρ=0.89% (corresponding to 2 bars diameter 28 mm, effective depth d = 556 mm). The top and bottom reinforcement were identical.
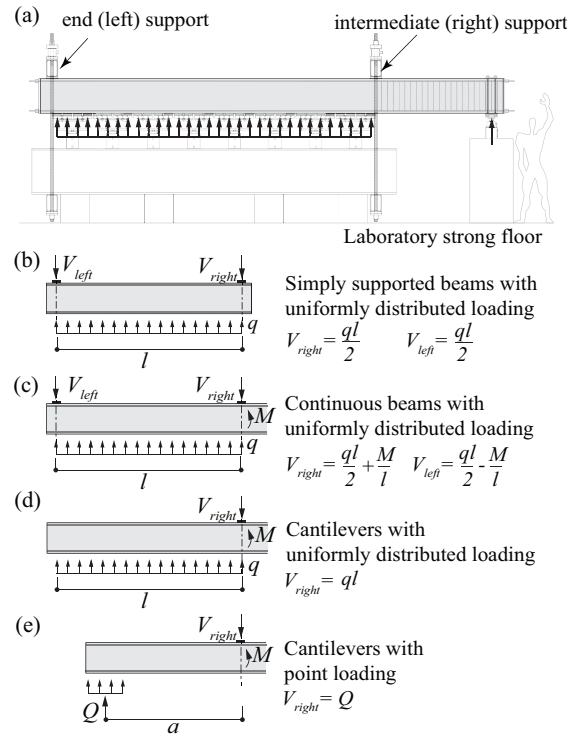
Figure 5.1 Experimental programme: (a) scheme of the test setup and loading conditions: (b) simply supported beams, (c) continuous beams and (d) cantilevers subjected to uniformly distributed loading, (e) cantilevers subjected to point loading (for more detailed description of the test setup, see Cavagnis et al. [13])

Table 5.1 Geometrical and material properties of the tested specimens and failure loads (V_{left}: shear force at the end (left) support; V_{right}: shear force at the intermediate (right) support; $M/(V \cdot d)$ refers to internal forces at the right support; CCDT refers to the Critical Crack Development Type)

	Test	l [mm]	a [mm]	$M/V \cdot d$ [-]	f_c [Mpa]	ρ [%]	q [kN/m]	V_{left} [kN]	V_{right} [kN]	$\frac{V_{exp}}{b \cdot d \cdot \sqrt{f_c}}$ [$\sqrt{\text{Mpa}}$]	CCDT	Remarks
Figure 5.1b	SC51a	5'600		(-)	33.6	0.886	60.4	169	(169)	0.210	(4)	Shear failure at the left support
	SC51b	5'600		(-)	33.6	0.886	57.8	(162)	162	0.201	(2)	Shear failure at the right support
Figure 5.1c	SC52	5'600		1.68	36.8	0.886	59.5	(133)	200	0.237	(1)	Diagonal cracking right support [1]
	SC52a	5'600		1.68	36.8	0.886	77.1	173	(259)	0.205	(2)	Shear failure at the left support
	SC52b	5'600		1.68	36.8	0.886	85.0	(190)	(286)	0.226	(4)	Shear failure in the central part
	SC53	5'600		2.88	33.2	0.886	40.2	(68)	158	0.197	(2)	Maximum load followed by failure
	SC54	5'600		3.78	36.5	0.886	40.6	(46)	182	0.217	(4)	Maximum load followed by failure
	SC55	5'600		4.48	33.7	0.886	33.4	(19)	168	0.208	(3)	Diagonal cracking [1]
	SC55a	5'600		4.48	33.7	0.886	38.5	(22)	194	0.240	(2-1)	Maximum load followed by failure
Figure 5.1d	SC56	5'600		5.04	35.3	0.886	28.2	(-)	158	0.191	(3)	Diagonal cracking (maximum load)
	SC57	4'900		4.41	33.2	0.886	30.0	(-)	147	0.184	(2)	Maximum load followed by failure
	SC58	4'200		3.78	36.1	0.886	50.6	(-)	213	0.254	(2-1)	Maximum load ; yielding
	SC59	3'500		3.15	35.5	0.886	52.3	(-)	183	0.221	(2)	Maximum load followed by failure
	SC62	2'800		2.52	35.8	0.886	62.1	(-)	174	0.209	(4)	Maximum load followed by failure
	SC66	2'100		1.89	31.2	0.886	91.4	(-)	192	0.247	(2)	Maximum load followed by failure
	SC63	3'500		3.13	33.6	0.544	60.8	(-)	213	0.263	(3-1)	Maximum load ; yielding
	SC60	2'800		2.50	36.9	0.544	58.9	(-)	165	0.194	(2-1)	Maximum load followed by failure
Figure 5.1e	SC70		3'850	6.92	33.3	0.886		114	114	0.142	(3-4)	Maximum load followed by failure
	SC69		3'150	5.67	32.9	0.886		107	107	0.134	(4)	Maximum load followed by failure
	SC61		2'450	4.41	35.3	0.886		103	103	0.125	(4)	Maximum load followed by failure
	SC64		1'750	3.15	35.6	0.886		108	108	0.131	(3)	Diagonal cracking maximum load
	SC68		1'400	2.52	32.6	0.886		124	124	0.156	(2)	Maximum load followed by failure
	SC67		1'050	1.89	32.0	0.886		393	393	0.500	(1)	Diagonal cracking [1]
	SC67a		1'050	1.89	32.0	0.886		429	429	0.546	(1)	Maximum load followed by failure
	SC65		1'750	3.13	35.5	0.544		102	102	0.123	(3)	Maximum load followed by failure

[1] diagonal cracking followed by a drop in the applied load of 5-10%; the specimen could be reloaded to larger shear strengths

All beams were cast with normal strength concrete with maximum aggregate size d_g of 16 mm. At the time of testing, the measured cylinder compressive strength f_c varied between 31.2 Mpa and 36.9 Mpa. Tensile reinforcement consisted in high-strength deformed steel bars with average yield stress of 713 Mpa (bar diameter 28 mm) and 760 Mpa (bar diameter 22 mm). The average ultimate tensile strength after strain hardening was 820 Mpa (bar diameter 28 mm) and 920 Mpa (bar diameter 22 mm).

The test setup allowed varying the loading conditions and the shear slenderness. All details concerning the properties of the specimens (material properties, geometry and test results) are summarised in Table 5.1. All beams failed in shear (in tests SC58, SC63 and SC67a after yielding of the flexural reinforcement) and presented different cracking patterns at failure (refer to Figure 5.2). In particular, specimen SC67 developed a diagonal crack close to the right support, leading to a drop in the applied load (about 8%). The specimen however could be reloaded and failure occurred due to concrete crushing.
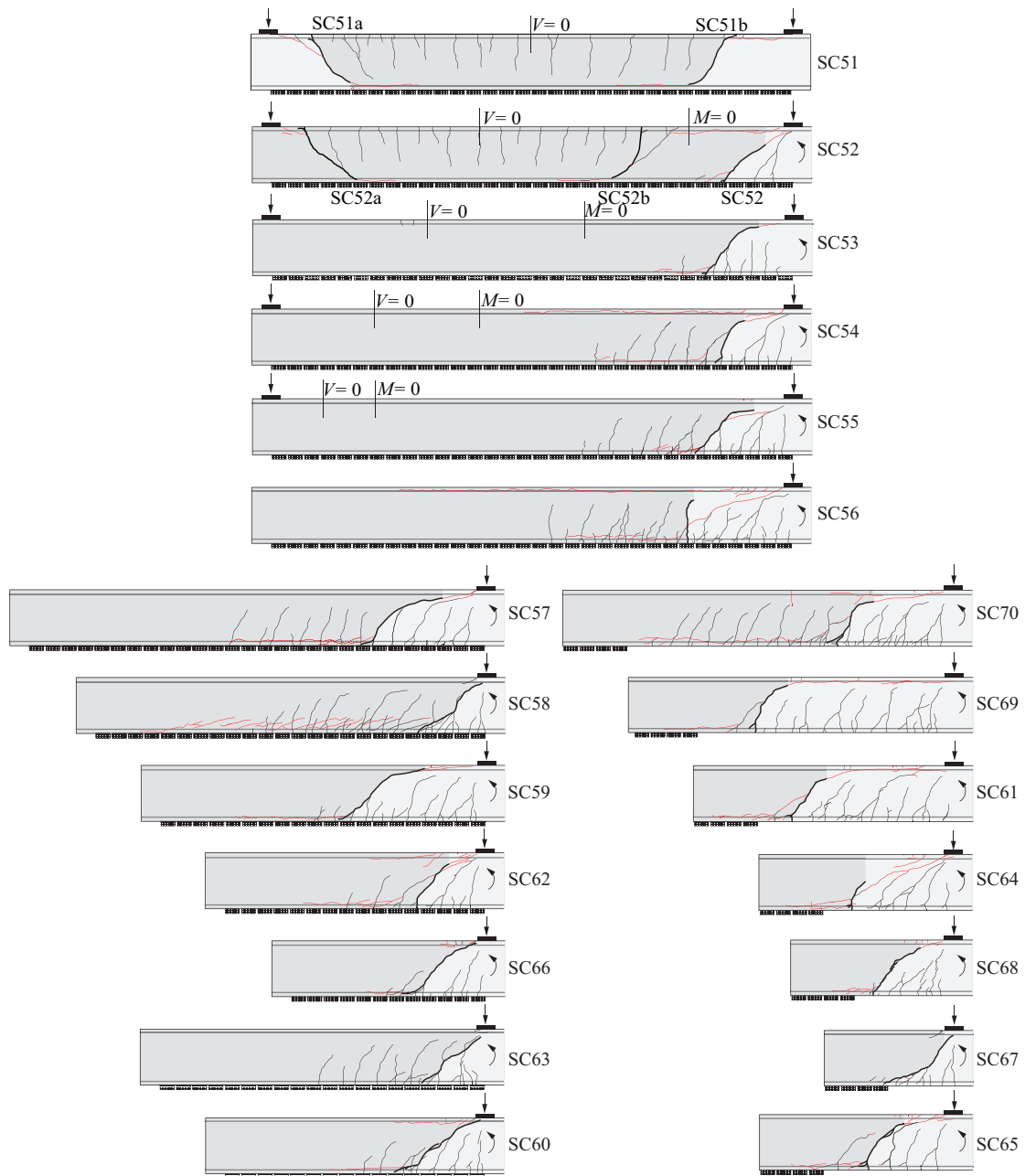
Figure 5.2 Observed cracking patterns and considered rigid bodies for the calculation of the shear-transfer actions (cracks in black for increasing load until maximum load, cracks in red after maximum load)

5.3.1 Measurement of crack kinematics

In addition to conventional measurement techniques, three-dimensional digital image correlation (DIC) has been used to track the cracking pattern and the displacement field of the specimens. The DIC required painting the surface of the specimens with a speckle pattern. Photogrammetry was performed on the entire surface of the beams with two digital cameras Nikon D800 (36.3 Megapixels). The pattern applied to the entire surface consisted of rounded speckles of constant size and not overlapping. Speckles varied between 1 and 2 mm as a function of the size of the investigated specimen, and the dimension of each pixel was averagely 0.35 mm (with an upper value of 0.6 mm for the large specimens). In addition, two cameras Manta (5 Megapixels) were installed on the opposite side of the beam in order to monitor the compression zone close to the intermediate support (right support in Figure 5.1). In this area, the pattern was sprayed uniformly on the surface and the images had a

resolution of 0.2 mm/pixel. The image acquisition rate of the cameras varied during the test and was increased up to 1 Hz (in some tests up to 2 Hz) prior to failure.

The main challenge of using the DIC technique was to obtain a good accuracy in measuring displacements and strains. Images were analysed using the VIC3D software [14]. Each image was divided into a grid of facets which were used to track the displacements between images. Within the facets, displacements were computed at specific points, with a maximum error of 1/50 of a pixel. Strains were computed directly from the measured displacement points. Principal strains have been observed to be influenced by the dimension of the area used for the calculation. In this paper, the value of the strains in the compression zone have been computed from the images taken by the cameras Manta, assuming an area of approximately 50 mm x 50 mm, which was reduced if the thickness of the compression zone was smaller than the assumed area.

5.3.2   Main results

The measured shear strengths are presented in Table 5.1 and Figure 5.3. With respect to the influence of the shear slenderness ratio a/d on the shear strength of cantilevers subjected to concentrated load, it can be observed that the shear stress at failure was significantly larger for specimen SC67 ($a/d < 2.5$) than for the other specimens ($a/d > 2.5$) (Figure 5.3). The development of the critical crack (refer to Figure 5.2) and its influence on the shear strength of the member shows a strong dependency on the shear slenderness ratio, as already noted by Kani [4]. For specimen SC67, the critical crack did not develop through the theoretical inclined compression strut and thus the flexural strength could almost be reached (at failure, the tensile reinforcement was at the beginning of the yielding process). For specimens with larger values of a/d, the critical cracks developed through the theoretical compression strut between loading and support [3], decreasing consequently the shear strength. For specimen SC70 ($a/d \approx 7$), the flexural strength could again almost be reached (Figure 5.3b).

The influence of the shear slenderness can also be observed for cantilevers subjected to distributed loading (refer to Figure 5.3c): the shear strength at the intermediate support decreases for increasing value of the length-to-span ratio (l/d).
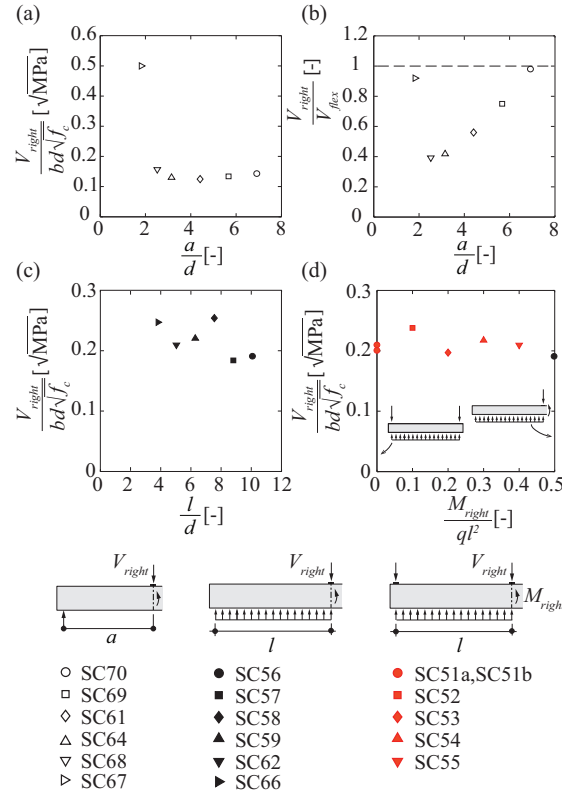
Figure 5.3 (a) Influence of the shear slenderness ratio (a/d) on the shear strength of cantilevers subjected to point loading; (b) comparisons of the experimental results with the flexural strength for cantilevers subjected to point loading; (c) influence of the shear slenderness on the shear strength of cantilevers subjected to distributed loading; (d) influence of the moment at the intermediate support on the shear strength for continuous beams subjected to distributed loading (only tests with ρ=0.89% are considered)

The effect of the location of the point of contraflexure in continuous beams (due to the different acting moment at the intermediate support, M_{right}) is depicted in Figure 5.3d. It can be observed that in general, this parameter does not appear to have a notable influence on the shear strength at the intermediate support (V_{right}).

With respect to the influence of the direct strut action of the distributed loads near supports, it was recently investigated by Pérez Caldentey et al. [15], who showed that the loads applied near the support do not need to be transferred through the critical shear crack, but can directly be strutted to the support. In reference [15] it was concluded that these direct struts justify the increase on the shear force observed for members subjected to distributed loading compared to members subjected to point loading. The tests presented in this manuscript and in reference [13] confirm that for slender members, the shear resistance effectively increases when uniformly distributed load is applied (refer to Table 5.2). For non-slender members, however, this influence depends on the location and shape of the critical shear crack. For instance, within the present testing programme, for specimen SC66 (distributed load) developing the full-arching action was not possible since the theoretical direct compression strut was intercepted by the critical crack, whereas for specimen SC67 (point load) the critical crack did not penetrate within the theoretical strut [3] and the plastic strength could almost be reached.

Table 5.2 Shear force at failure at the right support for cantilevers subjected to point and distributed load

Test with distributed load / Test with point load	$\dfrac{M}{V \cdot d}$ [-]	$\dfrac{V_{right,distr.}}{b \cdot d \cdot \sqrt{f_c}}$ [√MPa]	$\dfrac{V_{right,point}}{b \cdot d \cdot \sqrt{f_c}}$ [√MPa]	$\dfrac{v_{right,distr.}}{v_{right,point}}$ [-]
SC57 / SC61	4.41	0.184	0.125	1.48
SC59 / SC64	3.15	0.221	0.131	1.69
SC63 / SC65	3.13	0.263	0.123	2.14
SC62 / SC68	2.52	0.209	0.156	1.34
SC66 / SC67	1.89	0.247	0.500	0.49

5.4 Cracking pattern

5.4.1 Critical Shear Crack and Failure Crack

By means of the DIC technique, the cracking pattern could be tracked in a very detailed manner. A number of typical cracks has been identified and named, according to the notation presented in Cavagnis et al. [13] (refer to Figure 5.4 for the definition of crack types). The critical shear crack will be referred to an existing crack (type A-F or type A-E, Figure 5.4b), whose development and opening lead to the failure of the specimen. The final failure surface, which develops after reaching the maximum load, may however not be completely coincident with the critical shear crack and will be named hereafter as the failure crack [13].
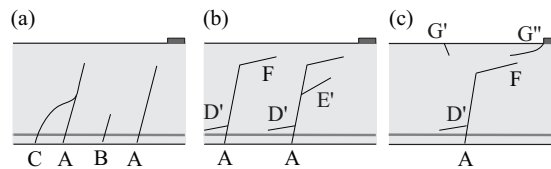
Figure 5.4 (a-c) Definition of crack types (refer to Cavagnis et al. [13])

Four different developments of failure crack have been previously identified ([13], see also Figure 5.5) and are confirmed with the new experiments:

- Critical shear crack allowing full arching action to develop (Critical Crack Development Type 1, CCDT 1). This crack development has been observed for specimens with crack propagating at locations such that a direct compression strut can develop without being disturbed by the development of the critical shear crack (Figure 5.5a, e.g. specimen SC67).

- Failures following a stable propagation of the critical shear crack (CCDT 2). This failure type is characterized by the development within the compression zone of a quasi-horizontal crack (crack type F) from a primary flexural crack (crack type A) in a stable manner up to failure (crack A-F, Figure 5.5b, e.g. specimen SC68). A secondary flexural crack (crack type C) may merge with a primary flexural crack at low load level followed by a stable development of a crack type F (Figure 5.5c, e.g. specimen SC57).

- Failure triggered by local loss of aggregate interlock capacity due to the propagation of an internal crack (CCDT 3). This failure type is determined by the development of a diagonal aggregate-interlock crack (crack type E') from a primary flexural crack, due to large aggregate-interlock forces [13], leading to failure of the specimen (Figure 5.5d, e.g. specimens SC64 or SC56).

- Failure triggered by the merging of a secondary flexural crack (crack type C) with a primary flexural crack (crack type A) (CCDT 4). This failure type has been observed to be due to the merging of a crack type C with a crack type A-F, leading to an increase of the opening of the critical shear crack and a loss of shear-carrying capacity, triggering failure (Figure 5.5e, e.g. specimen SC69).

The observed critical crack development types (CCDTs) are given for every tests in Table 5.1. It is important to note that different failure modes may lead to similar shear capacity and that similar members may develop rather different failure cracks.
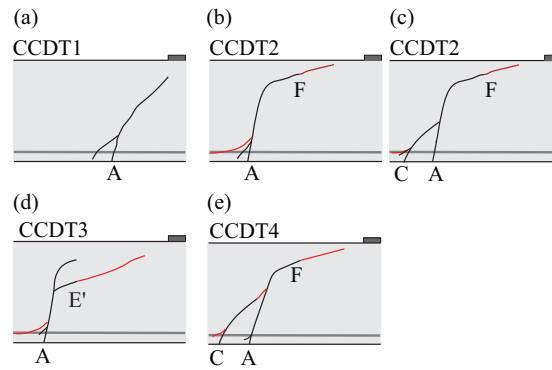
Figure 5.5 (a-e) Critical Shear Crack Development Types (CCDT, refer to Cavagnis et al. [13], cracks in black for increasing load until maximum load, cracks in red after maximum load)

5.5 Analysis of the shear-transfer actions

A methodology to evaluate the amount of force carried by each shear-transfer action on the basis of the crack kinematics was presented by Campana et al. [16] for members with low amount of transverse reinforcement. Similar calculations have been presented recently by Huber et al. [17] using a consistent approach confirming its validity. The results of these studies showed that the governing shear-transfer actions depends mainly on the kinematics and on the shape of the critical crack and may significantly vary even for similar specimens. However, little information is available on the phenomena governing the shear strength during failure (in particular before and after reaching the peak load).

In the following, the investigation of the shear-transfer actions is performed by considering the cracks and rigid bodies highlighted in Figure 5.2. The forces potentially acting on them are illustrated in Figure 5.6. The total shear force at the right support can be considered equal to the sum of the vertical component of the shear-transfer actions that are transferred through the critical shear crack (V_{Agg}: aggregate interlock; V_{RS}: residual tensile strength of concrete; $V_{D,tens}$: dowelling action of the tensile reinforcement; $V_{D,compr}$: dowelling action of the compression reinforcement, when the critical shear crack intercepts the compression reinforcement; V_C: inclined compression chord or arching action) and, in the case of members subjected to distributed loading, the amount of load which is directly strutted to the support V_q without crossing the critical shear crack (refer to Figure 5.6b).

The amount of shear transferred by the various shear-transfer actions is estimated on the basis of the measured crack kinematics and by using different constitutive models, which are explained below. For the calculation of the shear-transfer actions, the shape of the crack is approximated by a polyline whose points are spaced at a maximal distance equal to the aggregate size d_g (=16 mm) and the crack kinematics is calculated on the basis of the DIC measurements in a similar manner as described in Campana et al. [16].
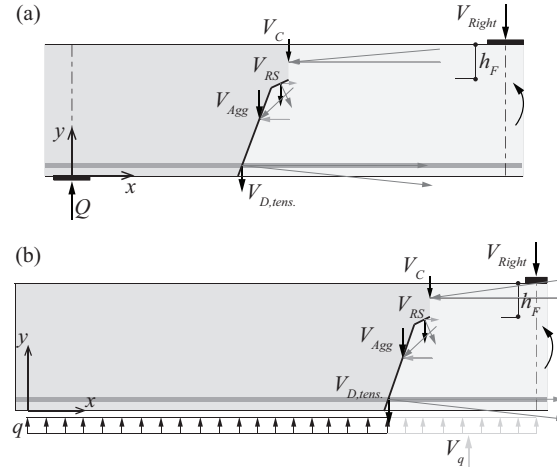
Figure 5.6 Analysis of shear transfer actions: free-body equilibrium and internal forces: (a) cantilever subjected to point load; (b) cantilever subjected to distributed load

5.5.1   Aggregate interlock contribution

Aggregate interlock was early acknowledged as an important mode of transfer shear across cracks [1]. This action develops through contact in the rough cracks, developing normal and tangential stresses and allowing thus to transfer shear forces.

In the literature, several models have been proposed to calculate aggregate interlock stresses [18–20]. In this paper, the two-phase model proposed by Walraven [18] will be used due to its physical basis. The two-phase model is a mechanical approach based on statistical and geometrical considerations of the crack surfaces and the associated contact areas between the aggregate particles and the cement matrix. The model allows calculating the interface stresses by means of the following equations:

$$\sigma = \sigma_{pu} \cdot \left(A_x - \mu \cdot A_y \right)$$ (5.1)

and

$$\tau = \sigma_{pu} \cdot \left(A_y + \mu \cdot A_x \right)$$ (5.2)

where σ_{pu} is the compressive plastic strength of the cement matrix, μ is a coefficient of friction and A_x and A_y are respectively the sum of the projections a_x and a_y of the contact surfaces between the aggregate particles and the cement matrix (see Figure 5.7a). The projections a_x and a_y are derived as a function of the crack opening w and sliding δ and the maximum aggregate size d_g.

With respect to the crack kinematics, Walraven [18] assumed that the crack opening w develops prior to crack sliding δ (refer to Figure 5.7b). Ulaga [21] applied the same model by using a different crack kinematics, assuming that the crack opening w and the sliding δ develop simultaneously at a constant angle γ (refer to Figure 5.7c). The main difference between the original kinematics and the one proposed by Ulaga can be identified in the different projections a_x and a_y of the contact surfaces between the aggregates and the cement matrix (Figure 5.7b and c respectively). A detailed analysis of the two-phase model and the calculated shear and normal stresses as a function of the different crack kinematics can be found elsewhere [13, 16, 22].

In Figure 5.7e-f the shear stresses measured by Jacobsen et al. [23] (black lines in the figure) for some double notch concrete specimens tested under different kinematics (first a mode I, where an initial crack opening w_0 is created between notches, followed by a mixed mode kinematics, with combined opening and sliding at an angle γ_r, refer to Figure 5.7d) are compared to the shear stresses calculated according to the model of Walraven and using the crack kinematics proposed by Walraven (green lines) and Ulaga (red lines). It shall be noted that the crack kinematics imposed by Jacobsen et al. [23] is representative of the kinematics experimentally measured in the upper and steeper parts of the critical shear crack of slender members, where the largest aggregate interlock stresses are activated (initial opening $w_0 < 0.05$ mm and mixed mode angle $\gamma > 45°$, refer to [13]).

In Figure 5.7e-f, it can be observed that the pre- and post-peak response is overestimated when the crack kinematics proposed by Walraven is adopted. On the contrary, the kinematics of Ulaga leads to solutions that slightly underestimate the peak stresses and overestimate the stresses for sliding larger than 0.25 mm.
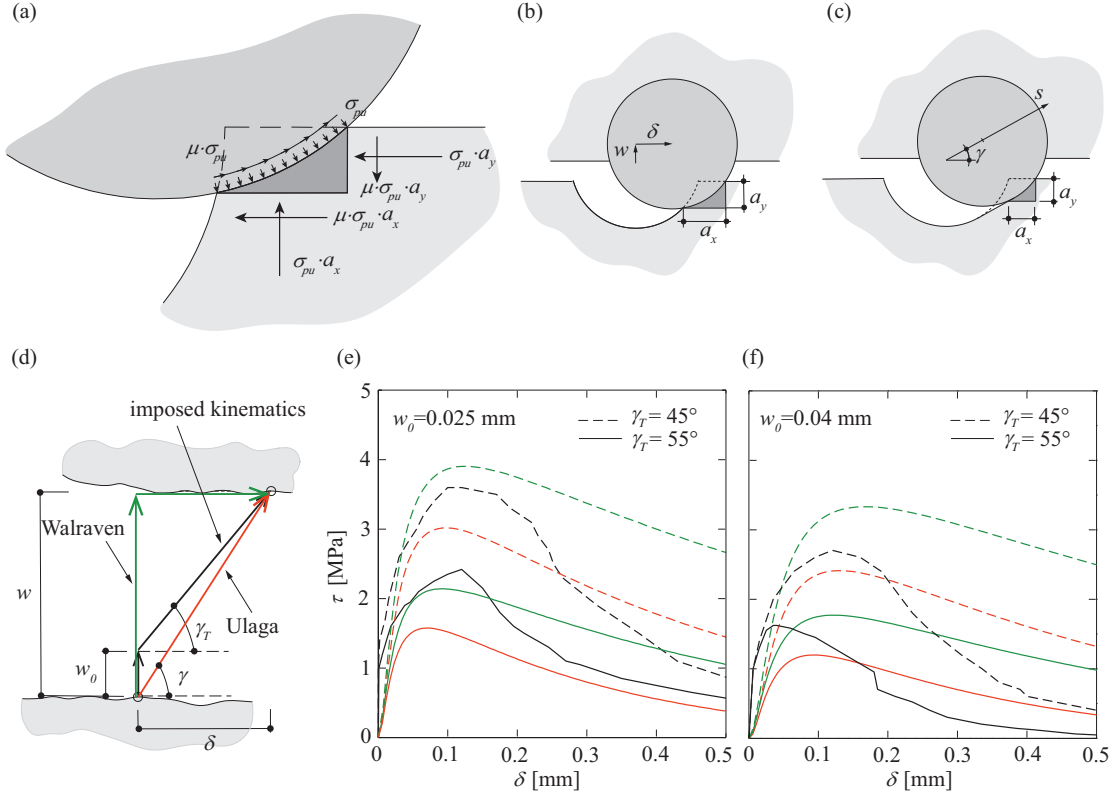
Figure 5.7 Aggregate interlock contribution: (a) contact zone between aggregate and cement matrix and aggregate interlock stresses; (b-c) projections areas according to the kinematics proposed by Walraven [18] and Ulaga [21]; (d) crack kinematics proposed by Walraven and Ulaga and kinematics of mixed mode tests performed by Jacobsen et al. [23], (e-f) comparison of shear stresses experimentally measured by Jacobsen et al. ([23], black lines) and calculated according to the model of Walraven and the crack kinematics of Walraven ([18], green lines) and Ulaga ([21], red lines)

On that basis, the transferred normal and shear interface stresses are estimated using the crack kinematics proposed by Ulaga [21], which better reproduces the kinematics experimentally measured in comparison to the one assumed by Walraven and represents a lower bound solution of the aggregate interlock stresses.

Finally, by integration of the stresses along the crack in the vertical direction, the shear force $V_{Agg.}$ Is obtained (Figure 5.6).

5.5.2 Concrete residual strength contribution

The residual tensile strength of concrete consists on the capacity to transfer tensile stresses through the fracture process zone of a crack [24]. As experimentally observed [13], the top part of the critical shear crack (quasi-horizontal part) is characterized by a pure mode I opening response and is thus governed by the residual tensile strength of concrete [9].

In this paper, the relation proposed by Hordijk [25] for the concrete residual strength is used (see Figure 5.8a):

$$\sigma_{res} = f_{ct}\left[\left(1+\left(c_1\frac{w}{w_c}\right)^3\right)e^{-c_2(w/w_c)} - \frac{w}{w_c}\left(1+c_1^3\right)e^{-c_2}\right] \tag{5.3}$$

where $w_c = 5.14 \cdot (G_F/f_{ct})$ represents the maximum crack width for stress transfer, $c_1 = 3$ and $c_2 = 6.93$ are constants, G_F is defined according to fib Model Code 2010 [26] equal to:

$$G_F = 73 \cdot f_c^{0.18} \quad \left(\frac{N}{m}, MPa\right) \tag{5.4}$$

and the tensile strength of concrete f_{ct} is assumed equal to $f_{ct}=0.3 \cdot f_c^{2/3}$ (for $f_c< 50$ MPa, [26]). Only openings w larger than 0.02 mm (accounting for DIC reliability) have been considered for the calculation of the residual tensile stresses, as the position of the crack tip has been assumed where the relative displacements reach that value.

Due to the crack inclination, the normal stresses in the crack lead to a component in the vertical direction, named V_{RS} (Figure 5.6).
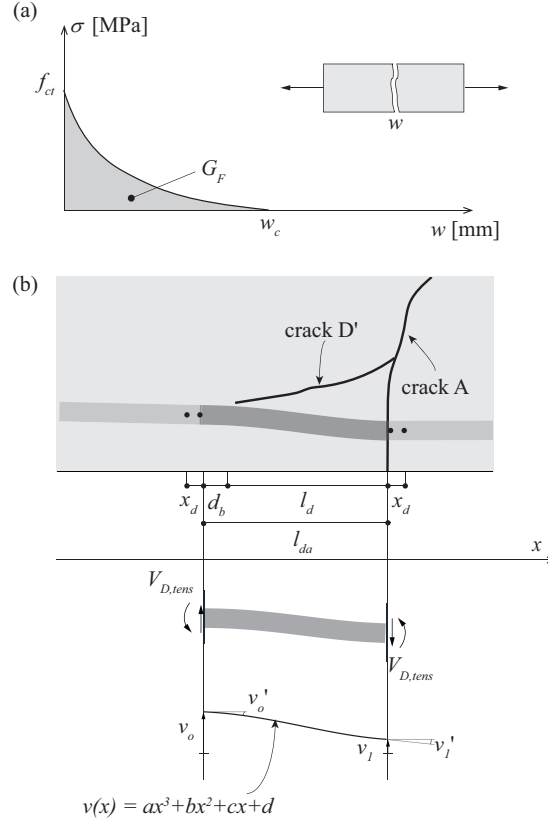
Figure 5.8 (a) Tension softening of concrete under pure tensile stresses; (b) dowelling action: deflection of the flexural reinforcement in the proximity of the dowelling crack (crack type D')

5.5.3 Dowelling action

The dowelling action refers to the capacity of flexural reinforcement bars to transfer shear forces across the crack, which can be activated when the longitudinal reinforcement follows a transversal displacement. In the analyses presented in this paper, the dowelling contribution of the tensile reinforcement $V_{D,tens}$ is obtained from the measured displacements of the concrete surface in the vicinity of the critical shear crack. It is assumed that the bar is unbonded in a length $l_{da}=l_d + d_b$, where l_d is the horizontal length affected by the dowelling crack and d_b is the diameter of the bar. The deflection is approximated to a third order polynomial on the basis of the vertical displacements and rotations at the extremities of l_{da} (v_0, v_0' and v_1, v_1'), which are derived through the measurements of two points located in each external region at a distance $x_d = d_b/2$ (refer to Figure 5.8b). Assuming a linear-elastic behaviour of the bar and differentiating three times the deflection with respect to x-coordinate, the shear carried by the dowelling action can be obtained:

$$V_{D,tens} = n \cdot E_S \cdot I \cdot \frac{d^3 v(x)}{dx^3} = \frac{6 \cdot n \cdot E_S \cdot I}{l_{da}^3} \cdot \left[v_0 - v_1 + \frac{l_{da}}{2}(v_0' + v_1') \right] \qquad (5.5)$$

where n is the number of bars and I the moment of inertia of a longitudinal bar. It can be noted that if the reinforcement partially yields (only for specimens SC58, SC63, SC67a), the dowelling capacity of the rebars is reduced [27]. For the only specimens where this situation happened, the contribution of dowelling to the overall shear strength was null or very limited and this phenomenon is thus neglected.

With respect to the dowelling action of the compression reinforcement ($V_{D,compr}$), it can be activated only when the critical crack intercepts the compression reinforcement (only specimens SC59, SC60 and SC66 at peak load). In these cases, the correspondent shear force contribution can be calculated with Eq. (5.5).

5.5.4 Compression chord and arching action

The contribution of the inclined compression chord and the arching action (V_C in Figure 5.6) is calculated in the section located at the tip of the investigated critical shear crack (vertical section between the tip of the crack and the extreme compression fibre of the specimen, refer to the height h_F in Figure 5.6). This is performed on the basis of the measured principal strains along this length and adopting the constitutive law for concrete explained below. When the critical shear crack propagates up to the region below the intermediate support (e.g. specimens SC58, SC63, SC60 and SC67), the investigated section corresponds to the one at the edge of the reaction plate consistently with the rest of the analyses (refer to Figure 5.2).

In this work, the strains have been computed from the DIC measurements in a number of points located at an average vertical distance of 6 mm in the portion investigated. For specimens SC52, SC54 and SC57, the DIC technique could not be used (readings at the investigated section were not available), but LED targets were used [13], allowing also refined measurements of the principal strains in the compression zone. The principal strains could not be computed for specimens SC53 and SC55, due to the lack of any instrumentation in the critical region of the compression zone.

In this paper, the principal stress directions are assumed to be parallel to the principal strain directions and the principal stresses are directly computed from the principal strains. To that purpose, principal tensile stresses are calculated assuming a linear-elastic behaviour of concrete before reaching its tensile strength ($\sigma_1 = E_c \cdot \varepsilon_1$ and $\sigma_1 = 0$ (if $E_c \cdot \varepsilon_1 > f_{ct}$) refer to Figure 5.9, where E_c is taken equal to $E_c = 10'000 \cdot f_c^{1/3}$ in [MPa]). Principal compressive stresses are computed according to a stress-strain relationship accounting for the pre- and post-peak behaviour (refer to Figure 5.9a and [28]):

$$\sigma_2 = \frac{E_c \cdot \varepsilon_2}{1 + \left(\dfrac{\varepsilon_2}{\varepsilon_0}\right)^\alpha} \tag{5.6}$$

with:

$$\varepsilon_0 == \frac{\alpha \cdot f_{c,eff}}{E_c \cdot (\alpha-1)^{\left(1-\frac{1}{\alpha}\right)}} \tag{5.7}$$

and

$$\alpha = 0.5 + \frac{f_{c,eff}}{20} + \frac{f_{c,eff}^2}{1500} \tag{5.8}$$

where ε_2 refers to the measured principal compressive strain and $f_{c,eff}$ is the effective compressive strength expressed in [MPa]. It can be noted that according to the measured strains, the post-peak part of the curve was not governing for most specimens, and only limited post-peak deformations were attained in a few tests (SC60, SC63, SC67 and SC67a).

For uncracked concrete, $f_{c,eff}$ is derived on the basis of the biaxial failure criterion accounting for the interaction between tension and compression stresses [29]. The concrete failure surface in the combined tension-compression regime (left upper and right lower quadrant) is simplified by a bilinear law (Figure 5.9b), whose slope is determined by that of the Mohr-Coulomb failure envelope, using a friction angle $\varphi = 37°$ [30]. Both the contribution of the inclined tension and compression stresses were accounted for in the calculation of the shear force V_C with the pertinent surfaces and angles.

For specimens SC58, SC60, SC67 and SC63, smeared cracking (refer to Figure 5.2 and to cracks type G'' in Figure 5.4c) was observed within the compression zone (these cracks were not connected to the critical shear crack). For these cases (closer to the behaviour of a cracked panel with smeared cracking), the tensile strength of concrete is neglected and the effective compressive strength is reduced on the basis of the compression-softening law proposed by Vecchio and Collins [31]:

$$f_{c,eff} = f_c \cdot \frac{1}{0.8 + 170 \cdot \varepsilon_1} \leq f_c \tag{5.9}$$
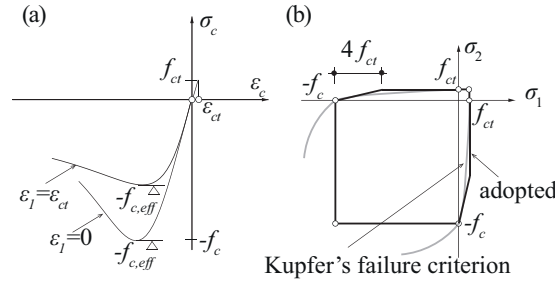
Figure 5.9 (a) Adopted stress-strain diagram for concrete [28]; (b) Kupfer's failure surface [29] and adopted one [30]

The shear stresses are then computed from the principal strains and principal stress directions. Finally, by integration of the shear stresses along the length h_F, the shear force V_C is obtained.

5.5.5 Distributed load not carried by the critical shear crack

In reinforced concrete members subjected to distributed load, a fraction of the load near the support is carried directly to the support without crossing the critical shear crack [15]. The load directly strutted V_q has been computed as the integration of the load applied between the intermediate support (right support) and the position at which the critical shear crack (crack type A) intercepts the flexural reinforcement (e.g. specimen SC62, Figure 5.2). When a secondary flexural crack (crack type C) becomes connected during loading with a primary flexural crack and the crack propagation remains stable, (e.g. specimen SC59, Figure 5.2), the interception between the secondary flexural crack and the longitudinal reinforcement is considered.

5.5.6 Calculated shear-transfer actions on the basis of the measured kinematics

The main analysis of the contribution of the various shear-transfer actions is plotted in Figure 5.10, which depicts the amount of shear carried by each action for each specimen at the maximum load (tests SC51a, SC51b, SC52a, SC52b, SC55a, SC56 and SC67a are not considered due to lack of reliable measurements of the crack kinematics at peak load).
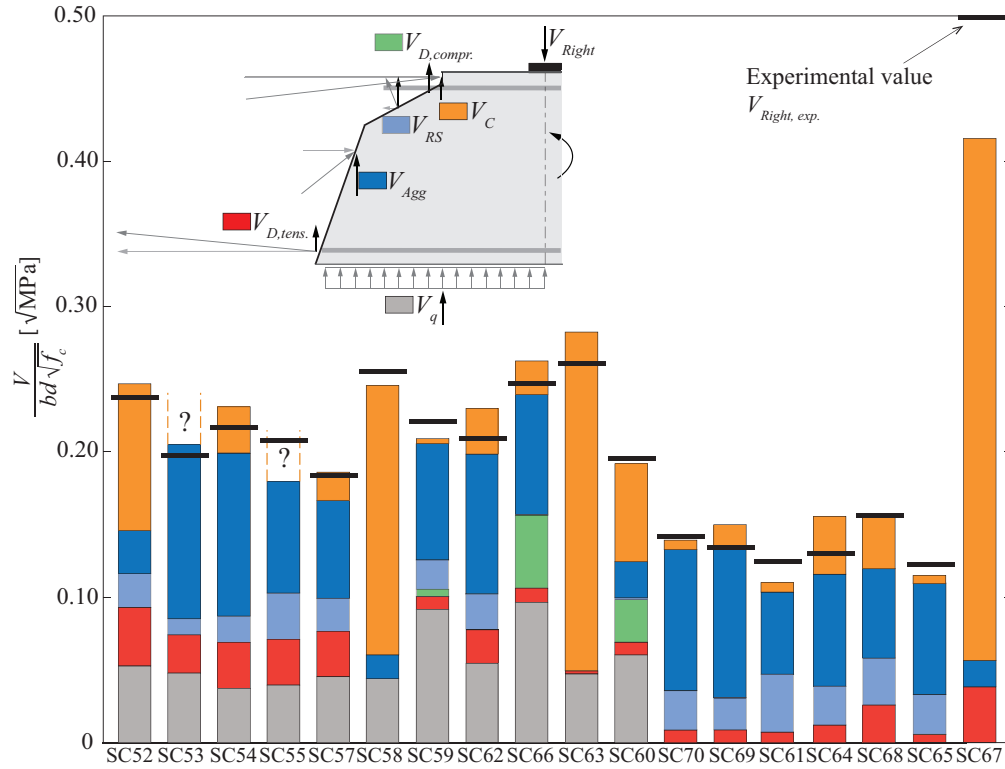
Figure 5.10 (a) Amount of calculated shear carried by each shear-transfer action at peak load compared to the experimental shear strength $V_{Right,exp.}$ (all shear forces are with respect to the intermediate support)

(a)

(b)
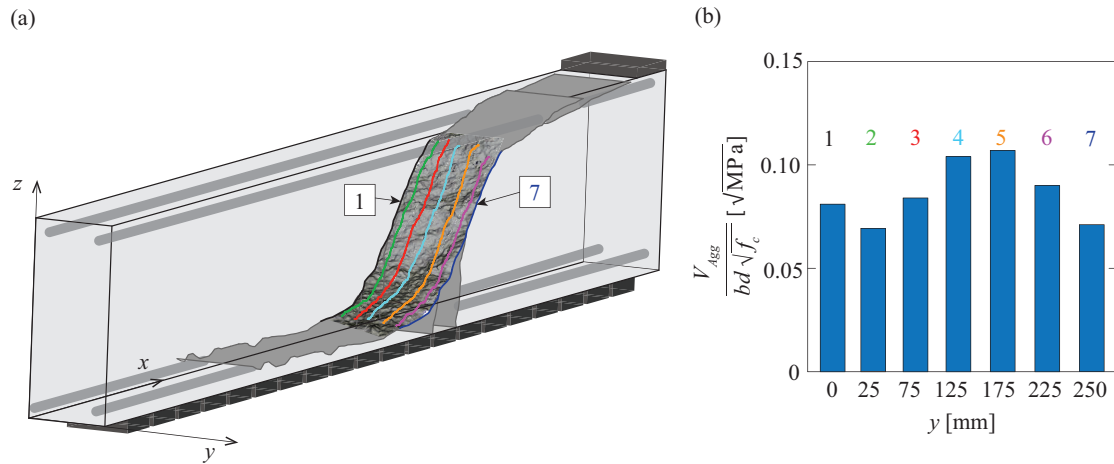
Figure 5.11 (a) Scan of the crack surface of specimen SC59 and geometry of the different sections through the width of the specimen used to calculate the aggregate interlock contribution; (b) aggregate interlock stresses computed at 7 different sections (at different values of y through the width of the specimen), accounting for the measured crack geometry and kinematics extrapolated from the measurements on the surface (y=0 mm)

The comparison between the sum of the estimated contributions and the acting shear force at the right support shows a good agreement (average ratio experimental-to-sum of estimated contributions equal to 1.01 with a Coefficient of Variation of 9% for 16 specimens in Figure 5.10, disregarding specimens SC53 and SC55 due to lack of detailed measurements of the principal strains in the compression zone).

The analyses have been performed on the basis of the DIC measurements obtained at one side of the specimen. It shall nevertheless be noted that the profile of the crack is not uniform through the width of the member (Figure 5.11a). This leads potentially to differences in the calculated contributions of the shear transfer actions. As an instance, Figure 5.11b depicts the calculated shear force transferred by aggregate interlocking for seven crack profiles through the width of the member, where the crack displacement have been extrapolated from the measurements on the surface (average normalized aggregate interlock stress $V_A/(b \cdot d \cdot \sqrt{f_c})$ equal to 0.081 and COV 17%). Although some level of variability exists due to the considered profile, it remains nevertheless within the scatter of the fundamental constitutive laws adopted [13, 17].

It can be noted that, at the maximum load, the amount of shear carried by each shear-transfer actions is variable. For specimens SC52, SC58, SC63, SC60 and SC67, the shear strength was governed (particularly for specimens SC58, SC63 and SC67) by the arching action, whereas for all the other specimens, the amount of shear carried by aggregate interlock is generally governing and the measured maximum shear force can be almost fully explained by the calculated contribution of the beam shear-transfer actions (aggregate interlock, dowelling action, residual tensile strength of concrete and inclined compression chord) and the distributed load directly strutted. It is notable that for specimens SC59, SC60 and SC66, the critical shear cracks reached the compression reinforcement and activated the dowelling action of the compression reinforcement before failure.

In the following, the differences between cases governed by the arching action and by beam shear-transfer actions will be presented and discussed on the basis of some selected specimens.

5.5.7 Behaviour of specimens governed by arching action

Whenever a direct strut can develop (CCDT1, Figure 5.5a), the contribution of the inclined compression strut can be observed to be governing. This was for instance the case of specimen SC58, where the contribution of the beam shear-carrying actions only explains a limited amount of the total shear force (Figure 5.12a). For this specimen, in fact, the shear crack originated near the intermediate support region (refer to Fig. 4.14). It developed in a stable manner and almost did not penetrate within the theoretical compression strut. After full development of the critical crack, at about 70% of the maximum load, even if the beam shear-transfer actions decayed (Figure 5.12a), the load could still be increased, as the arching action became dominant. Eventually, the flexural strength of the member was reached. A close look to the inclination of the principal compressive strains at the maximum load (Figure 5.12b) shows that the contribution of the direct strut was clearly governing.

A similar case was observed also for specimen SC67 (Figure 5.12c), where most of the shear force was transferred to the support through a direct compression strut. In this case, failure occurred due to crushing of the compression zone, with the

appearance of a crack (crack type G'', Figure 5.4c) that was originated not from the flexural crack but from the intermediate support (right support) and that developed at a flat angle (first crack from the top side of the specimen, in Figure 5.2).
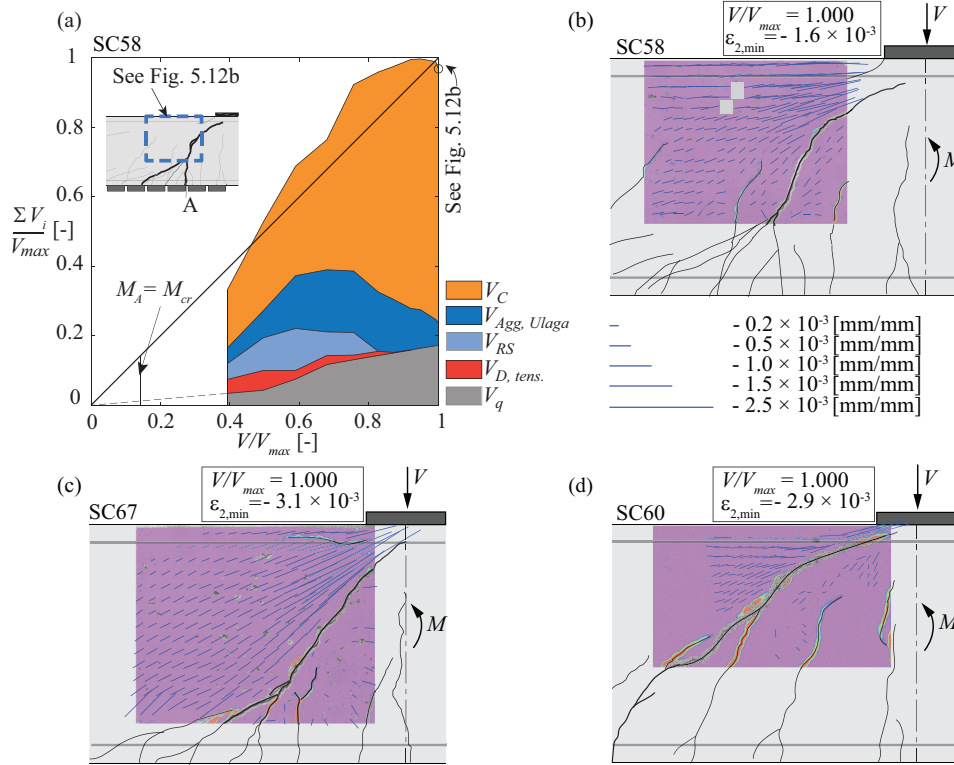
Figure 5.12 (a) Shear-transfer actions for specimen SC58. Direction and magnitude of the experimentally measured principal compressive strains at V/V_{max} =1.000: (b) for specimens SC58, (c) SC67 and (d) SC60

The arching action plays a role also for specimen SC60 (refer to Figure 5.10), even if the critical crack penetrated within the theoretical compression strut (Figure 5.12d). In fact, a close look to the cracking patterns and to the detailed measurements of the inclination of the principal compressive strains at the maximum load (Figure 5.12d) shows that a direct strut developed above the critical shear crack, which propagated in a stable manner up to the support.

5.5.8 Behaviour of specimens governed by beam shear-transfer actions

When the critical crack does not develop close to the intermediate support, the contribution of the compression zone after the propagation of a crack type F from the primary flexural crack is rather limited. Representative cases are specimens SC51, SC53, SC54, SC55, SC56, SC57, SC59, SC62, SC70, SC69, SC61, SC64, SC68 and SC65 (refer to Figure 5.10). These tests correspond mostly to slender members.

In Figure 5.13a, the contribution of the different shear-transfer actions during loading are shown for specimen SC70 (refer to Fig. 4.8 for crack kinematics). It can be observed that, before the development of the quasi-horizontal branch that initiated at about 40% of the maximum load, shear was carried by the compression chord, by aggregate interlock stresses, which are activated locally in the steeper parts of the crack, and by the residual tensile strength of concrete. After the propagation of the crack type F, the contribution of aggregate interlock became dominant, whereas the contribution of the compression chord progressively decreased. At maximum load, the contribution of the compression chord is almost negligible (the direction of the principal compressive strains is practically horizontal, refer to Figure 5.13b) and the contribution of aggregate interlock is governing. Figure 5.13c-e show the normal and shear stresses and the forces computed along the crack surface on the basis the measured crack kinematics. With respect to the interface tangential stress τ (Figure 5.13c), it can be observed that it reaches a maximum value of 3.1 MPa in the steeper part of the crack and it decreases for larger openings towards the tensile longitudinal reinforcement. The shear stresses become eventually null in the quasi-horizontal branch of the crack. From Figure 5.13e, it can be observed that aggregate interlock forces developed in the steeper parts of the critical crack, whereas the forces due to residual tensile strength of concrete developed in the quasi-horizontal part of the critical crack (crack type F). It can be thus noted that both tension and compression normal forces can be developed at the critical shear crack (as observed in [23, 32]).
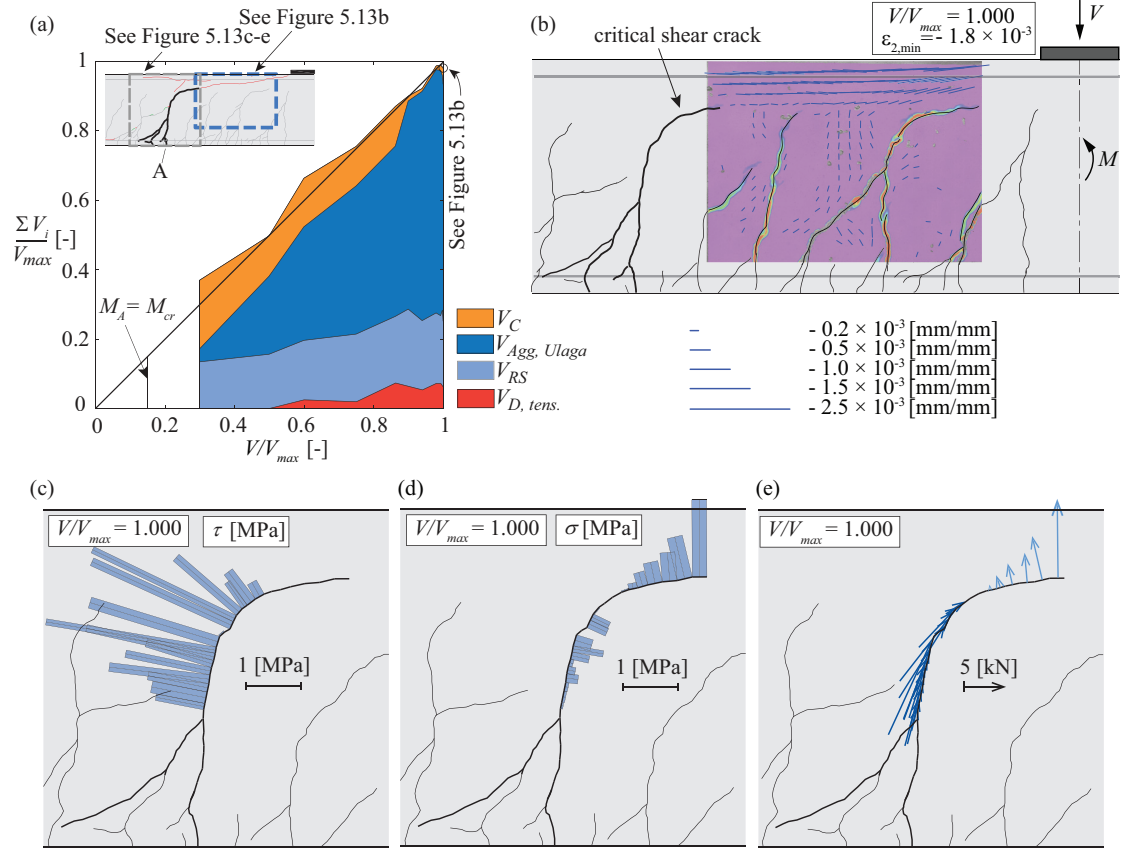
Figure 5.13 (a) Shear-transfer actions for specimen SC70; (b) direction and magnitude of the experimentally measured principal compressive strains at V/V_{max} =1.000; (c) shear and (d) normal stresses developing along the crack surfaces and (e) aggregate interlock and residual tensile forces at V/V_{max} =1.000

It is notable that for this specimen, another potential critical crack developed near the intermediate support. However, as the tip of the crack was located only at about 0.2 d from the intermediate support, the compression zone was able to carry a fraction of the shear force (inclined compressive strains above the tip of this crack in Figure 5.13b) and this crack did not become critical.

5.6 Discussions of results

On the basis of the previous findings, it can be stated that the amount of shear force carried by the various shear-transfer actions during loading and at the maximum load depends on the location, geometry and kinematics of the critical shear crack. Interesting results can be obtained by analysing the contributions of the various shear-carrying mechanisms in a cross section located at representative cracks:

- The cantilever action, where the shear force at the cross section corresponding to a flexural crack is carried by the inclination of the compression chord, plays a significant role before the propagation of the critical crack in a quasi-horizontal manner (crack type F). This has been observed to develop at a load level which may be significantly lower than the maximum load [13].

- For slender members, characterized by a critical shear crack developing far from the intermediate support region, the contribution of the inclined compression chord at the maximum load is rather limited (less than 30%), and, in some cases, almost negligible.

- The contribution of the arching action can be observed to be dominant only if the critical crack propagates near the intermediate support region and develops in a stable manner below the intermediate support plate (e.g. specimens SC52, SC58, SC63, SC60 and SC67).

- The contribution of aggregate interlock depends on the geometry, on the location and on the kinematics of the critical crack. Aggregate interlock stresses are mobilized when both opening and sliding develop and are activated in particular in the steeper and upper parts of the crack. For cracks developing below or in the vicinity of the intermediate support, hardly any aggregate interlock develops, since almost no crack sliding occurs (e.g. specimen SC52 in [13]). On the contrary, if the critical crack is sufficiently far from the intermediate support, aggregate interlock contributes for a significant percentage to the shear resistance (up to 80% of the total applied load).

- Residual tensile strength of concrete at the maximum load depends mainly on the opening and on the length and inclination of the quasi-horizontal branch of the critical crack (crack type F). The contribution of the residual tensile strength (up to 32% of the total applied shear force) is of particular relevance for cracks type F with an extended length and a very limited crack opening (e.g. specimens SC68, SC61).

- The capacity of the dowelling action of the tensile reinforcement to transfer shear for specimens under a single point load depends mainly on the location of the critical crack and is very limited when the crack develops far from the end support (e.g. specimen SC70, Figure 5.13a), whereas it is more notable (up to 20% of the applied shear force) if the critical crack is located close to it (e.g. specimen SC68). In the case of continuous beams or cantilevers subjected to distributed loading, the contribution of the longitudinal reinforcement is generally more significant (see Figure 5.10).

- When the critical crack develops in a stable manner through the compression reinforcement, dowelling action of the compression reinforcement can develop and it can become efficient when the critical crack intercepts the reinforcement in the proximity of the intermediate support region. The compression reinforcement has been observed to contribute significantly in the post-peak shear strength (e.g. specimens SC64, SC68). In these cases, the compression reinforcement acts in a similar manner as the integrity reinforcement in slabs after punching in the column region [33].

- With respect to continuous beams and cantilevers subjected to distributed loading, the load applied between the intermediate support region and the critical shear crack is assumed to be carried directly to the support by direct struts. On the basis of the current experimental results, the distance at which the critical crack intercepts the longitudinal reinforcement varies between d and $2.6d$ (refer to Figure 5.2 and [13]), lower values than those reported in [15].

5.7 Conclusions

In this paper, the results of 7 reinforced concrete beams without shear reinforcement that complete an extensive experimental campaign with detailed measurements of 13 specimens described in Cavagnis et al. [13], are presented. In addition, the role of the shear-transfer actions and the mechanisms of shear failure are investigated in detail. The main conclusions are listed below:

1. The relative significance of the various potential shear-transfer actions varies with the cracking shape and position. During the process of loading, as cracks progress, some shear-transfer actions become predominant while others reduce their significance.

2. On the basis of refined kinematical measurements and by using suitable mechanical models, the contribution of each shear-transfer actions can be calculated:

   - For slender specimens, the shear force is carried by a combination of aggregate interlock, dowelling action, residual tensile strength of concrete and inclined compression chord, with aggregate interlock being the dominant shear-transfer action.

   - The arching action becomes the governing shear-transfer action only when the critical shear crack develops below the intermediate support and below the theoretical direct strut carrying shear. This is mostly the case of squat members.

3. These findings are confirmed by a close look to the principal compressive strains, which are almost horizontal when the contribution of the compression zone is rather limited, or almost negligible, while they are clearly inclined when a direct strut develops.

4. When the critical shear crack develops below the intermediate support and is approximately straight, aggregate interlocking is practically negligible.

5. Although a crack presents a variation on its geometry through the width of the member, analyses of the sum of the contributions of the shear-transfer actions do not reflect high sensitivity to this issue.

5.8   Acknowledgements

5.9   Appendix A. Notation

a	shear span (defined for specimens subjected to concentrated loads as the distance between the axis of the load and the axis of the right support)
a_x, a_y	projected contact areas in x and y directions
b	width of the beam
c_1, c_2	constants
d	effective flexural depth
d_b	diameter of reinforcing bar
d_g	maximum aggregate size
f_c	concrete compressive strength measured in cylinder
$f_{c,eff}$	effective compressive strength of concrete
f_{ct}	concrete tensile strength
h	beam height
h_F	distance from the top compression fibre to the tip of crack type F
l	span length
l_d	length of the dowelling crack
l_{da}	length in which the longitudinal reinforcement is unbonded
n	number of bars
q	distributed load
v_0, v_1	vertical displacements
v_0', v_1'	rotations
$v_{distr.}$	normalized shear stress of members subjected to distributed loading
v_{point}	normalized shear stress of members subjected to point loading
w	crack width
w_c	maximum crack width allowing tensile stresses transfer in concrete
x_d	distance between two points located at the external regions of the dowelling crack
A_x, A_y	sum of the projected contact areas in x and y directions
CSCT	critical shear crack theory
DIC	digital image correlation
E_c	modulus of elasticity of concrete
E_s	modulus of elasticity of steel
G_F	fracture energy
I	moment of inertia
M	bending moment
M_{cr}	cracking bending moment
M_{right}	bending moment at the intermediate (right) support
M_A	Bending moment at point A
Q	concentrated load
V	acting shear force
V_{exp}	measured shear force

V_{flex}	flexural strength	
V_{left}	shear force at the end (left) support	
V_{max}	shear force at failure (maximum value)	
V_{right}	shear force at the intermediate (right) support	
V_{Agg}	contribution of aggregate interlock to shear resistance	
V_C	contribution of inclined compression chord or arching action to shear resistance	
V_D	contribution of dowelling action to shear resistance	
$V_{D,tens}$	contribution of dowelling action of the tensile reinforcement	
$V_{D,compr}$	contribution of dowelling action of the compression reinforcement	
V_{RS}	contribution of residual tensile stresses to shear resistance	
V_q	fraction of the distributed load carried by direct struts	
α	brittleness factor	
γ	mixed mode angle	
γ_T	tangent mixed mode angle	
δ	relative crack sliding	
ε_{ct}	principal tensile strain leading to σ_1 equal to f_{ct}	
ε_0	reference strain in the compression stress-strain relationship	
ε_1	principal tensile strains	
ε_2	principal compressive strains	
$\varepsilon_{2,min}$	minimum measured principal compressive strains at peak load in the investigated area	
μ	coefficient of friction	
ρ	reinforcement ratio of tension reinforcement	
σ	normal stress	
σ_1	principal tensile stresses	
σ_2	principal compressive stresses	
σ_{pu}	compressive plastic strength of cement matrix	
σ_{res}	residual tensile strength of concrete	
τ	shear stress	

5.10 References

[1] Fenwick RC, Paulay T. Mechanisms of shear resistance of concrete beams. *Journal of the Structural Division ASCE* 1968; 94 (10):2325–2350.

[2] ACI-ASCE Committee 445. Recent Approaches to Shear Design of Structural Concrete. *Journal of Structural Engineering* 1998; 124 (12):1375–1417.

[3] Muttoni A, Fernández Ruiz M. Shear strength of members without transverse reinforcement as function of critical shear crack width. *ACI Structural Journal* 2008; 105 (2):163–172.

[4] Kani GNJ. The riddle of shear failure and its solution. *ACI Journal* 1964; 61 (4):441–467.

[5] Zararis PD. Shear strength and minimum shear reinforcement of reinforced concrete slender beams. *ACI Structural Journal* 2003; 100 (2):203–214.

[6] Tureyen AK, Frosch RJ. Concrete Shear Strength: Another Perspective. *ACI Structural Journal* 2003; 100 (5):609–615.

[7] Choi K-K, Kim J-C, Park H-G. Shear Strength Model of Concrete Beams Based on Compression Zone Failure Mechanism. *ACI Structural Journal* 2016; 113 (5):1095–1106.

[8] Collins MP, Mitchell D, Adebar P, Vecchio F. A general shear design method. *ACI Structural Journal* 1996; 93 (5):36–45.

[9] Fernández Ruiz M, Muttoni A, Sagaseta J. Shear strength of concrete members without transverse reinforcement: a mechanical approach to consistently account for size and strain effects. *Engineering Structures* 2015; 99:360–372.

[10] Yang Y, Walraven J, den Uijl J. Shear Behavior of Reinforced Concrete Beams without Transverse Reinforcement Based on Critical Shear Displacement. *Journal of Structural Engineering* 2016; 143 (1):4016146.

[11] Tung ND, Tue NV. A new approach to shear design of slender reinforced concrete members without transverse reinforcement. *Engineering Structures* 2016; 107:180–194.

[12] Fisker J, Hagsten LG. Mechanical model for the shear capacity of R/C beams without stirrups: A proposal based on limit analysis. *Engineering Structures* 2016; 115:220–231.

[13] Cavagnis F, Fernández Ruiz M, Muttoni A. Shear failures in reinforced concrete members without transverse reinforcement: An analysis of the critical shear crack development on the basis of test results. *Engineering Structures* 2015; 103:157–173.

[14] Correlated Solutions. VIC 3D Software, Reference Manual. 2010.

[15] Pérez Caldentey A, Padilla P, Muttoni A, Fernández Ruiz M. Effect of load distribution and variable depth on shear resistance of slender beams without stirrups. *ACI Structural Journal* 2012; 109 (5):595–603.

[16] Campana S, Anastasi A, Fernández Ruiz M, Muttoni A. Analysis of shear-transfer actions on one-way RC members based on measured cracking pattern and failure kinematics. *Magazine of Concrete Research* 2013; 65 (6):386–404.

[17] Huber P, Huber T, Kollegger J. Investigation of the shear behaviour of RC beams on the basis of measured crack kinematics. *Engineering Structures* 2016; 113:41–58.

[18] Walraven JC. Fundamental analysis of aggregate interlock. *Journal of Structural Division* 1981; 107 (11):2245–2270.

[19] Gambarova PG, Karakoc C. A new approach to the analysis of the confinement role in regularly cracked concrete elements. *Transactions of the 7. international conference on structural mechanics in reactor technology* 1983; H.

[20] Li B, Maekawa K, Okamura H. Contact density model for stress transfer across cracks in concrete. *Journal of the Faculty of Engineering, University of Tokyo* 1989; 40 (1):9–52.

[21] Ulaga T. Betonbauteile mit Stab- und Lamellenbewehrung: Verbund- und Zuggliedmodellierung. PhD Thesis. Thesis no. 15062 (in German). Zurich, Switzerland: ETHZ. 2003:160.

[22] Guidotti R. Poinçonnement des planchers-dalles avec colonnes superposées fortement sollicitées. PhD Thesis. Thesis no. 4812 (in French). Lausanne, Switzerland: Ecole Polytechnique Fédérale de Lausanne. 2010:416.

[23] Jacobsen JS, Poulsen PN, Olesen JF. Characterization of mixed mode crack opening in concrete. *Materials and Structures* 2012; 45 (1–2):107–122.

[24] Hillerborg A, Modéer M, Petersson PE. Analysis of crack formation and crack growth in concrete by means of fracture mechanics and finite elements. *Cement and concrete research* 1976; 6 (6):773–781.

[25] Hordijk DA. Tensile and tensile fatigue behaviour of concrete; experiments, modelling and analysis. *Heron* 1992; 37 (1):3–79.

[26] Fédération Internationale du Béton (fib), fib Model Code for Concrete Structures 2010, Ernst & Sohn. 2013:434.

[27] Hars E, Niketić F, Fernández Ruiz M. Response of RC panels accounting for crack development and its interaction with rebars. *Magazine of Concrete Research* 2017:in press.

[28] Fernández Ruiz M, Muttoni A, Gambarova PG. Relationship between nonlinear creep and cracking of concrete under uniaxial compression. *Journal of Advanced Concrete Technology* 2007; 5 (3):383–393.

[29] Kupfer H, Hilsdorf HK, Rusch H. Behavior of Concrete Under Biaxial Stresses. *ACI Journal Proceedings* 1969; 66 (8):656–666.

[30] Nielsen MP, Hoang LC. Limit analysis and concrete plasticity. CRC press. 2016.

[31] Vecchio FJ, Collins MP. The modified compression field theory for reinforced concrete elements subjected to shear. *ACI Journal* 1986; 83 (2):219–231.

[32] Calvi PM, Bentz EC, Collins MP. Reversed Cyclic Experiments on Shear Stress Transfer across Cracks in Reinforced Concrete Elements. *ACI Structural Journal* 2016; 113 (4):851–859.

[33] Fernández Ruiz M, Mirzaei Y, Muttoni A. Post-punching behavior of flat slabs. *ACI Structural Journal* 2013; 110 (5):801–812.

5.11 Further analyses on the role of the shear-transfer actions

In this section, the role of the various shear-transfer actions is reviewed with reference to additional tests. Moreover, the analysis of the shear-carrying actions in the post-peak regime and the mechanisms of shear failure are discussed for some cases.

As shown in the Section 5.5, the arching action plays a significant role for tests SC52, SC55a, SC58, SC63, SC67 and SC67a. For these members a clear direct strut forms and its contribution is predominant (CCDT1, refer to Figure 5.5a). In some cases, a direct strut developed even if the critical crack penetrated within the theoretical compression strut. This is for instance the case of specimen SC60. For this specimen, it can be observed that the contributions of the residual tensile strength and of the aggregate interlock at the critical shear crack decreased after the full development of the critical crack (at 75% of peak load, refer to Figure 5.14). These reductions were compensated by the activation of the dowelling action of the compression reinforcement and the arching action, allowing a further increase of the applied load. This redistribution of internal forces was possible due to the location and shape of the critical shear crack. A close look to the cracking patterns and to the inclination of the principal compressive strains at the maximum load shows that a direct strut developed above the critical shear crack (see Figure 5.12d). Failure occurred due to crushing of the compression zone: a crack of type G'' developed within the compression zone originating from the load introduction plate and merged with the critical shear crack, triggering failure.
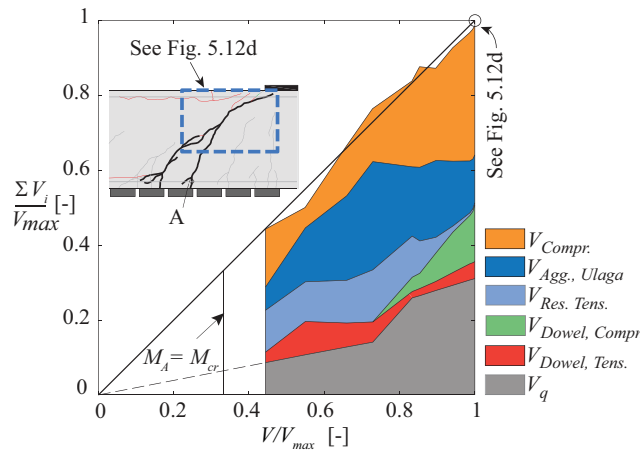
Figure 5.14 Shear-transfer actions for specimen SC60

When the critical shear crack does not develop close to the intermediate support (slender beams), the contribution of the inclined compression chord, after the propagation of the quasi-horizontal branch from the primary flexural crack, is rather limited (between 0 and 26% for the investigated specimens, but normally less than 15% of the total shear force). Representative cases are, for instance, tests SC51a, SC51b, SC52a, SC52b, SC53, SC54, SC55, SC56, SC57, SC59, SC61, SC62, SC64, SC65, SC8, SC69 and SC70.

Specimen SC69 is investigated in Figure 5.15and two potential critical shear cracks are considered: the one highlighted in Figure 5.15a is the critical shear crack, whereas the one shown in Figure 5.15b is a potential shear crack that did not become critical. It can be observed that, for both cracks, the contribution of aggregate interlock is governing at peak load, whereas the contribution of the inclined compression chord is rather limited. A close look to the shear-carrying mechanisms of the crack, highlighted in Figure 5.15b, shows that, before the development of the quasi-horizontal branch of the crack within the compression zone (V/V_{max}=0.373, refer to Figure 5.15c), the shear force is carried by the inclined compression chord (cantilever action), whereas the contributions of dowelling action, aggregate interlock and residual tensile strength are almost negligible due to the vertical development of the flexural crack. At peak load, after the full development of the crack type F (V/V_{max}=1.000, refer to Figure 5.15d), however, the contribution of aggregate interlock becomes predominant, and the aggregate interlock stresses are activated especially in the steeper and upper part of the crack. With respect to the critical shear crack (Figure 5.15a), it can be observed that the maximum value of the dowelling action is reached before the development of a dowelling crack (crack type D') along the longitudinal reinforcement (at approximately 80% of the maximum load). At peak load, aggregate interlock is still predominant (70% of the sum of the various shear-transfer actions), whereas the compression chord carries approximately 10% of the total shear force. The crack in Figure 5.15b did not become critical due to its steeper thus more favourable inclination, which was eventually capable of developing additional aggregate interlock stresses for potential larger values of the applied load.
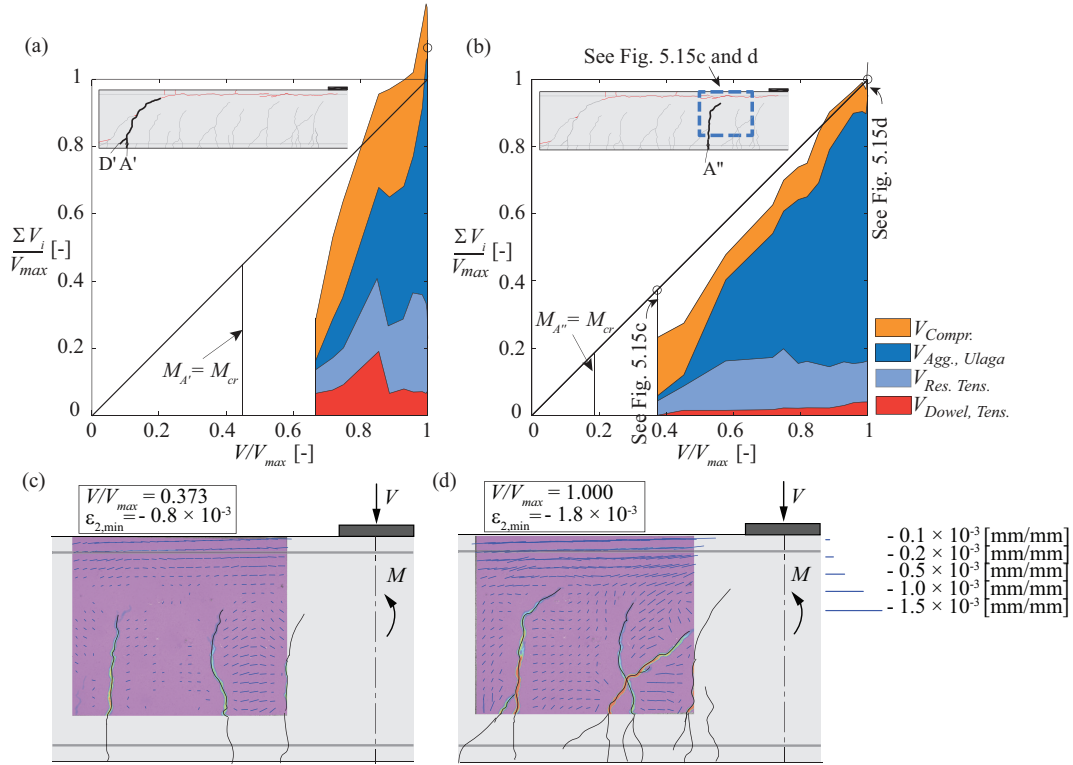
Figure 5.15 (a) Specimen SC69: shear transfer actions activated (a) along the critical crack and (b) a potential critical crack; (c) and (d) direction and magnitude of the experimentally measured principal compressive strains at V/V_{max} = 0.373 and at V/V_{max} =1.000

As shown in Section 5.4.1, when the critical shear crack does not develop in the vicinity of the intermediate support, three different potential developments of the critical shear crack have been identified and named (CCDT2, CCDT3 and CCDT4, refer to Figure 5.5b-e). Based on the analyses of the shear-transfer actions, it has been observed that the primary mechanism of shear-transfer for these members at peak load is aggregate interlock. The shape and development of the critical shear crack influence the post-peak response and how the mechanisms of shear resistance vary in the post-peak regime. For some cases, failure is directly associated to the loss of the aggregate interlock capacity at the critical crack. This is noticeable for members characterized by a critical shear crack of type 3 (crack type A-E'. CCDT3, refer to Figure 5.5d), where an aggregate interlock induced crack (crack type E') develops from the primary flexural crack leading to a drop in the applied load or failure (e.g. specimen SC55, SC56, SC64). Moreover, this is also notable for members characterized by a critical crack of type 4 (CCDT4, refer to Figure 5.5e), where a secondary flexural crack merges with the primary flexural crack, disabling aggregate interlock stresses at the critical shear crack below the merging point and triggers failure (specimens SC61, SC69). For specimens of CCDT2 (refer to Figure 5.5b-c), the role of the various shear-transfer actions in the post-peak regime varies as function of the shape and location of the critical shear crack. A particular case is represented for instance by specimen SC68. For this specimen, it can be observed that at 95.5% of the maximum load, the critical crack had not yet developed within the compression zone (refer to Figure 5.16a and b) and the whole shear force was transferred by means of the cantilever action, the dowelling action of the longitudinal reinforcement and the contribution of the residual tensile stresses. At the maximum load, however, aggregate interlock can be observed as the main shear-transfer mechanism (40% of the total applied load, Figure 5.16a). Moreover, for this specimen both dowelling action (about 17%) and residual tensile strength of concrete (about 21%) play a role and the amount of load which is transferred through the compression zone is also not negligible (about 23% at failure), due to the location and geometry of the critical crack and to the height h_F of the compression zone above the tip of the crack (refer to Figure 5.16c). It is interesting to note that after reaching the peak load, the critical crack developed in a stable manner for approximately 5 seconds for decreasing values of the applied load. During this stable crack propagation, the sum of the contribution of the various shear-transfer action decreases. In particular, the contribution of the compression zone, the dowelling action and the residual tensile strength decrease, whereas the aggregate interlock contribution increases. In addition, some dowelling action of the compression reinforcement develops. This stable crack propagation beyond the peak load (to 0.995↓) was followed by an unstable crack growth and a drop in the applied load (of about 45%). At that moment, the test was stopped and it can be observed that the compression reinforcement was capable of developing a significant strength (66% of the post-peak strength), acting as integrity reinforcement (Figure 5.16a). Its activation, however, is significantly dependent on the position and shape of the critical crack, which intercepted the top reinforcement in the proximity of the intermediate support.
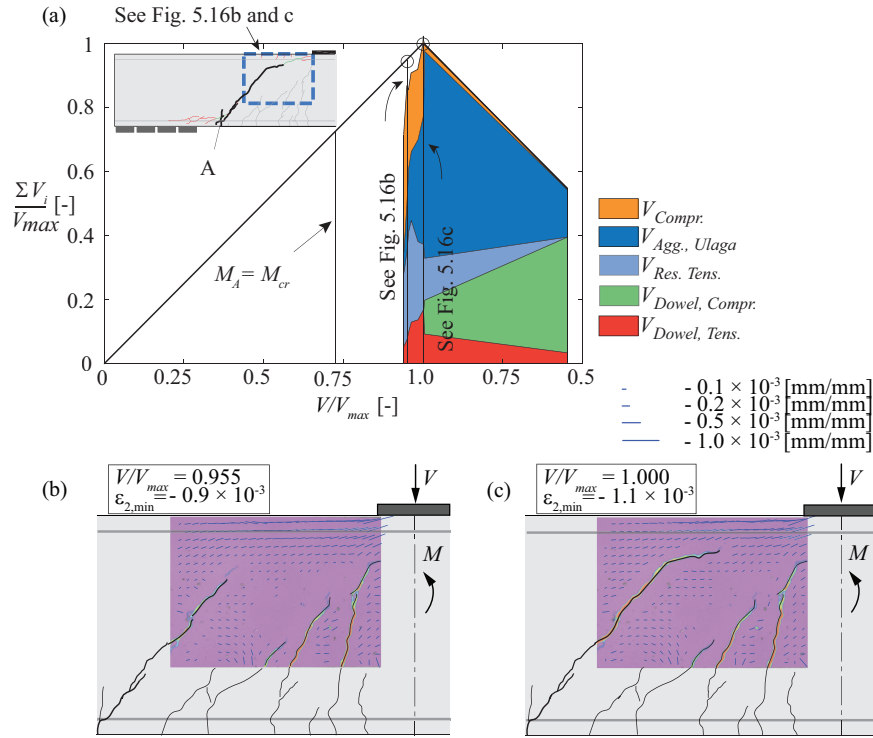
Figure 5.16 (a) Shear-transfer actions for specimen SC68; (b) and (c) direction and magnitude of the experimentally measured principal compressive strains at $V/V_{max} = 0.955$ and at $V/V_{max} = 1.000$

The mechanisms of shear failure and the role of aggregate interlock can be further investigated on the basis of the measured kinematics at the crack. In Figure 5.17a, the measured kinematics of the points along the critical shear cracks of some selected specimens (SC57, SC59, SC68, SC69 and SC70), where the largest aggregate interlock stresses develop, is shown. These points are located in the steeper parts of the critical shear cracks. In Figure 5.17b, the normal and shear stresses have been calculated, using the model of Walraven [18] generalized by Guidotti [22], that accounts for the measured kinematics shown in Figure 5.17a. As already investigated in [13], the kinematics of quasi-vertical branch of the critical shear crack is characterized by an initial opening w_0 perpendicular to the crack plane, followed, after the initiation of a crack type F, by an increase of both opening w and sliding δ. This observation is confirmed in Figure 5.17a: it can be noted that, in the part of the crack where the largest aggregate interlock stresses develop, the initial openings w_0 are in general very small ($w_0 < 0.1$ mm) and at peak load (markers in Figure 5.17a) the mixed mode angle γ remains larger than 45° (for definition of crack opening, sliding, mixed mode angle, see Figure 5.7d). Note that the mixed mode angle γ may eventually reach values lower than 45° at peak load only for (i) squat members (e.g. specimen SC67, see Figure 4.18), for (ii) slender members characterized by a critical shear crack developing below the theoretical compression strut, such that the arching action is still possible (e.g. SC58, see Figure 4.14) or for (iii) slender members characterized by a critical shear crack progressing in a stable manner in the vicinity of the loading plate, such that the compressive reinforcement acts as an integrity reinforcement (e.g. specimens SC60 and SC66 see Figure 4.15 and 4.17).

In Figure 5.17a it can be observed that for specimens SC57, SC59, SC68 and SC70, during loading, the tangent mixed mode angle γ_T decreases. The propagation of the critical shear crack within the compression zone determines a progressive reduction of the tangent mixed mode angle for increasing values of opening and sliding and allows developing aggregate interlock stresses at the crack. For specimens SC57, SC59 and SC70, it can be noted that at peak load (markers in Figure 5.17) the largest aggregate interlock stresses are developed. For specimen SC57, during the post-peak response (green curves in Figure 5.17a and b), the quasi-horizontal brunch further propagated causing a reduction of the angle γ_T. However, the significant width of the critical crack did not allow activating sufficient aggregate interlock forces for decreasing value of γ_T. Failure is thus triggered by the breakdown of the aggregate interlock capacity: when the aggregate interlock stresses start decreasing and no alternative shear-transfer mechanisms with a comparable strength develop, the member fails.

However, as previously observed, the maximum aggregate interlock forces do not always develop at peak load. A close look to the measured kinematics of specimen SC68 shows that, beyond peak load, the angle γ_T decreases progressively to almost 40°, allowing an increase of the aggregate interlock stresses that compensates the reduction of the contributions of the inclined

compression chord, the dowelling action and the residual tensile strength of concrete. Beyond the maximum load, at 0.995↓ of the peak load, the crack reached the compression reinforcement close to the load introduction region, and in order to sustain or increase the applied load, either the activation of alternative shear-transfer actions or the reduction of the mixed model angle γ_T was required. However, the shape and location of the critical shear crack did not allow these situations to occur, triggering an unstable crack growth.

Concerning specimen SC69, it can be observed that during loading the tangent mixed mode angle remains larger than 50° (Figure 5.17a) and, at peak load (marker in Figure 5.17), the aggregate interlock shear stress reaches its maximum value. Moreover, the merging of the crack type C with the crack type A-F leads to a sudden increase of the opening of the critical shear crack and the deactivation of some aggregate interlock forces below the merging point (almost 45% of the total shear force). The failure crack (crack type C combined with crack type A-F), is thus characterized by a flat inclination and only the development of alternative shear-transfer actions may eventually avoid failure. Failure is thus initiated by the loss of the aggregate interlock capacity.
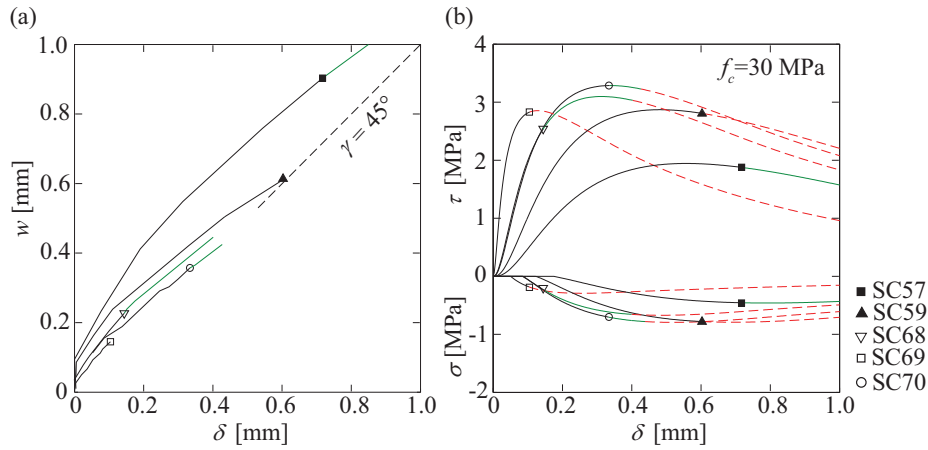
Figure 5.17 (a) Kinematics (crack opening w vs. crack sliding δ) of the investigated points along the critical shear crack cracks of specimens SC57, SC59, SC68, SC69, SC70, (b) normal and shear stresses calculated according to the model of Walraven [18], generalized by Guidotti [22], accounting for the measured kinematics of Figure 5.17a (f_c=30 MPa, d_g= 16 mm, markers represents values of kinematics and stresses at peak load, curves in black refer to increasing load up to peak load, curves in green refer to decreasing load after maximum load (stable crack propagation), curves in red represent unstable crack growth triggering failure)

On the basis of the previous observations, it can be concluded that, for slender members when the critical shear crack does not develop in the vicinity of the intermediate support: (i) during the process of loading, the quasi-horizontal branch develops within the compression zone and allows activating aggregate interlock stresses at the critical shear crack; (ii) at peak load, aggregate interlock is the predominant shear-transfer mechanism; (iii) the mechanism of shear failure is initiated by the loss of the beam-shear transfer actions capacity; (iv) during the stable propagation of the critical shear crack for decreasing load beyond the peak load, the role of the various shear-transfer actions varies as a function of the critical shear crack shape and its associated kinematics; however, aggregate interlock remains the primary mechanism of shear-transfer; (v) when the critical crack is no more capable of developing shear stresses across the crack or in the uncracked compression zone, unstable crack growth occurs.

Chapter 6   A mechanical model for failures in shear of members without transverse reinforcement based on development of a critical shear crack

This Chapter presents a mechanical model for shear design of slender reinforced concrete members without transverse reinforcement consistent with the main assumptions of the Critical Shear Crack Theory. The calculation of the shear strength is performed by intersecting a failure criterion (obtained by integration of the various shear-transfer actions) with a load deformation relationship. The model allows predicting the shear and deformation capacity and the location of the critical shear crack leading to failure. It is shown that the failure criteria obtained by integration of the shear-transfer actions can be approximated by a power-law equation. This Chapter has been accepted for publication in a scientific journal:

Cavagnis, F., Fernández Ruiz M., and Muttoni, A. (2017). A mechanical model for failures in shear of members without transverse reinforcement based on development of a critical shear crack. Engineering Structures.

The first author developed the mechanical model consistently with the main ideas of previous works of the second and third author. The mechanical model presented in this Chapter is a quantitative investigation of the various shear-transfer actions and it is based on the qualitative analytical considerations presented in a previous paper of the second and third author:

Fernández Ruiz M., Muttoni, A., and Sagaseta J. (2015). Shear strength of concrete members without transverse reinforcement: A mechanical approach to consistently account for size and strain effects. Engineering Structures, 99, 360-372.

6.1   Abstract

In this paper, a mechanical model consistent with the main assumptions of the Critical Shear Crack Theory (CSCT) is proposed for shear design of slender concrete members without shear reinforcement. To that aim, the shear force that can be transferred through the critical shear crack by aggregate interlock, residual tensile strength and dowelling action as well as due to the inclination of the compression chord are calculated by integration of fundamental constitutive laws accounting for the critical shear crack opening and kinematics at failure. The pertinence of the assumptions is validated through comparisons to detailed test measurements to assess their validity. The model allows predicting the failure load, the deformation capacity and the location of the critical shear crack leading to failure. The results are checked against large datasets and the model is finally used to discuss on the influence of the various parameters on the governing shear-transfer actions. The results are eventually used to propose improvements on the CSCT failure criterion for shear, relating the shear strength and its associated deformation capacity.

Key-words: concrete structures, shear strength, critical shear crack theory, shear-transfer actions

6.2   Introduction

The shear strength of reinforced concrete beams without transverse reinforcement has been extensively investigated in the past and many mechanical approaches have been proposed to address this issue [1–7]. Yet, these models present significant discrepancies on the mechanical parameters and shear-transfer actions governing failure and this is still a topic of controversy and open discussion. As established since long, there are various potential shear-carrying actions that allow transferring shear forces in cracked concrete members. They are usually classified as beam shear-transfer actions (where the force in tension

chord varies)—cantilever action (Figure 6.1a), residual tensile strength of concrete (Figure 6.1b), dowelling action (Figure 6.1c) aggregate interlock (Figure 6.1d), which may also be combined (Figure 6.1e)—and the arching action (where the force in the tension tie remains constant, Figure 6.1f). A complete description of each of them can be found elsewhere [8].

One mechanical approach which considers the contribution of all potential shear-carrying actions is the Critical Shear Crack Theory (CSCT) proposed by Muttoni et al. [3]. This theory is based on the assumption that the shear strength of slender members without stirrups is governed by the development of a critical shear crack that limits the strength of the theoretical inclined compression strut carrying shear. According to this theory, both the shear strength and the deformation capacity of a member are related through a failure criterion (Figure 6.1g), with lower strengths associated to larger deformation capacities (and thus larger crack widths).

A detailed description of the CSCT and of the development of the critical shear crack can be found elsewhere [9–11]. These investigations have shown that rather different crack patterns may develop for similar reinforced concrete members and that the contribution of each-shear transfer action may significantly vary during loading (being this strongly dependent on the shape, location and kinematics of the critical shear crack).
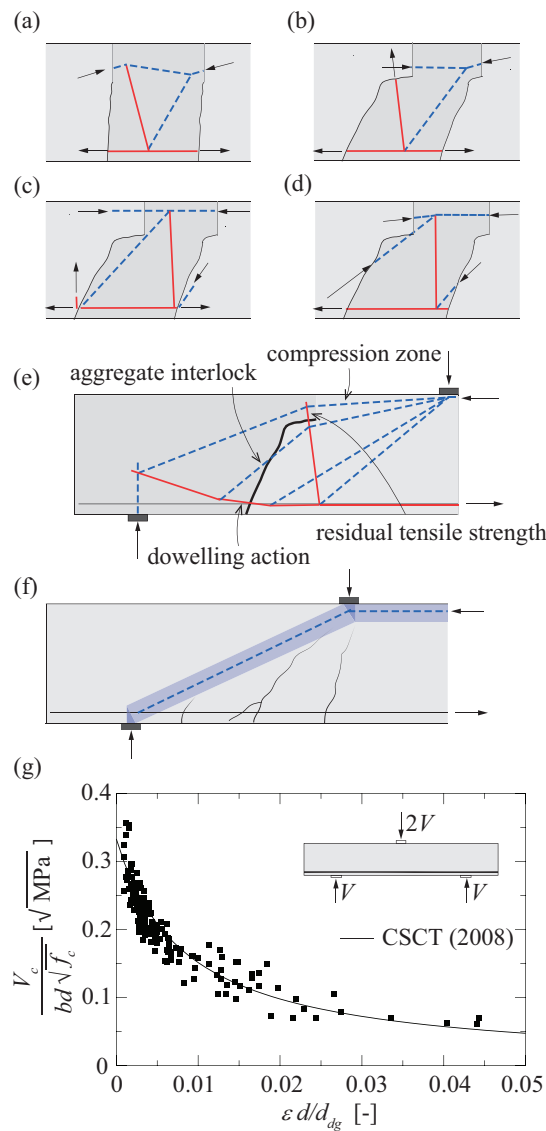
Figure 6.1 Shear-transfer actions described with strut and tie models (tensile forces in red and compressive forces in blue): (a) cantilever action; (b) residual tensile strength of concrete; (c) dowelling action; (d) aggregate interlock; (e) combined shear-transfer actions; (f) arching action; (g) failure criterion of the Critical Shear Crack Theory (CSCT) (adapted from Muttoni et al. [3])

A theoretical description of the main physical parameters governing the shear capacity can be found in Fernández Ruiz et al. [8]. This work shows, by means of an analytical approach based on simple constitutive laws that all shear-transfer actions depend eventually on the same mechanical parameters (concrete compressive strength, effective depth, maximum aggregate size and crack width). These results confirmed the validity of the failure criterion of the CSCT relating the shear strength and the deformation capacity at failure (Figure 6.1g) in terms of its shape and governing parameters. Since that work [8], a number of detailed testing programmes using digital image correlation (DIC) have been performed [10–12]. These programmes provide very detailed information on the development of the critical shear crack and on the associated capacity of each shear-transfer action. In this paper, this new experimental data is used in combination with refined constitutive laws to perform detailed calculations on the contribution of the various potential shear-transfer actions during the process of loading and at failure. As a result, predictions can be made not only on the strength and deformation capacity, but also on the shape and location of the critical shear crack as well as on the amount of the shear carried by each shear-transfer action. The results are compared to actual tests to show the consistency of the approach and to discuss on the role and significance of the various shear-transfer actions. On that basis, improvements on the CSCT failure criterion will be presented and discussed.

6.3   Load-critical shear crack opening relationship

One of the main assumptions of the CSCT, according to Muttoni et al. [3], is that the width w of the critical shear crack can be assumed to be proportional to the product of the longitudinal strain in a control section times the effective depth of the member ($w \propto \varepsilon \cdot d$, where the strain ε can be calculated according to a cracked sectional analysis). The validity of this assumption has been confirmed again by recent experimental investigations [11] on the basis of DIC measurements. According to these measurements, although cracks at narrow spacing may develop at the level of the longitudinal reinforcement, they merge thereafter and the sum of all cracks tributary to the critical shear crack yields an approximately linear horizontal opening profile (refer to Figure 6.2). This tributary length l_B has been experimentally observed to be fairly constant at peak load [11] and can be approximated by the expression:

$$l_B = d - c \tag{6.1}$$

(average of measured-to-calculated values equal to 1.01 with a Coefficient of Variation of 7% for 11 specimens presented in [11]), where c is the depth of the compression zone, calculated by assuming a linear response of concrete in compression and neglecting concrete in tension:

$$c = d \cdot \rho \cdot \frac{E_s}{E_c}\left(\sqrt{1 + \frac{2 \cdot E_c}{\rho \cdot E_s}} - 1 \right) \tag{6.2}$$

with E_c taken as $E_c = 10'000 f_c^{1/3}$ in MPa.

Thus, considering that the reinforcement strains can be calculated as (linear profile of compression stresses):

$$\varepsilon_s = \frac{M_F}{A_s \cdot E_s \cdot z} = \frac{M_F}{A_s \cdot E_s \cdot \left(d - c/3\right)} \tag{6.3}$$

and assuming that the horizontal crack opening at the level of the reinforcement is proportional to the product of the tributary length l_B times the strain at the level of the longitudinal reinforcement $u_A = \varepsilon_s \cdot l_B$, it results:

$$u_A = \frac{M_F}{A_s \cdot E_s} \cdot \frac{d - c}{d - c/3} \tag{6.4}$$

In simply supported elements subjected to point load, for instance, $M_F = V_F \cdot a_F$ and thus Eq. (6.4) yields:

$$u_A = \frac{V_F \cdot a_F}{A_s \cdot E_s} \cdot \frac{d - c}{d - c/3} \tag{6.5}$$

where a_F refers the moment-to-shear ratio of the investigated section, corresponding to the distance x_F of the section to the support in this case (the so called shear span, see Figure 6.3a).
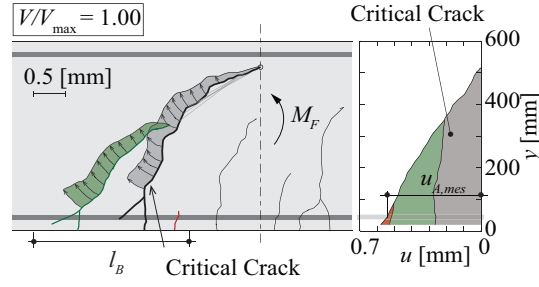
Figure 6.2 Crack kinematics, centre of rotation and horizontal opening u of the cracks tributary to the opening of the critical shear crack in a region of length l_B (specimen SC69 [11])

It has to be noted that Eq. (6.3) is an approximation as the contribution of the internal forces acting on the critical shear crack (refer to Figure 6.3d) to the moment M_F at a section located at crack tip are neglected (in accordance to the numerical results of detailed calculations accounting for all potential forces in the critical shear crack [11]).

6.4 Contribution of the shear-transfer actions

In the following, the contribution of the various shear-transfer actions to the shear resistance will be investigated by integration of fundamental constitutive laws. This will be done with reference to a potential critical shear crack characterized by a given shape and kinematics (crack opening and sliding). The location of the potential critical shear crack will then be varied in order to find the governing location leading to the minimum shear strength.

6.4.1 Crack shape and kinematics

The shape of the critical shear crack for slender members failing in shear has been investigated in detail and described by Cavagnis et al. [10]. The critical crack at failure can be approximated by a bi-linear shape comprising a quasi-vertical part (segment A-B in Figure 6.3a, whose inclination is related to the moment-to-shear ratio [10]) and a quasi-horizontal part (segment B-F in Figure 6.3a).

A trend for the inclination of the quasi-vertical segment A-B with respect to the moment-to-shear ratio α_A was experimentally investigated in [10] and it can approximated by the following expression:

$$\beta_{AB} = \frac{\pi}{4} \cdot \left(1 + \frac{\alpha_A^{1/3}}{3}\right) \tag{6.6}$$

where α_A is the shear slenderness ratio defined as $\alpha_A = M_A(x)/V_A(x) \cdot d$, with M_A and V_A corresponding to the acting bending moment and shear force at the section where the investigated crack intercepts the flexural reinforcement.

The length l_A of the segment A-B of the crack can be calculated assuming that it propagates up to the neutral axis [10]:

$$l_A = \frac{d-c}{\sin\beta_{AB}} \tag{6.7}$$

With respect to the quasi-horizontal part of the crack, it was observed that its origin is related to the (quasi-vertical) tensile stresses developing at the tip of the crack, due to the cantilever action between the flexural cracks (Kani's tooth model, Figure 6.1a, [3, 11]) and that it propagates at a load level which can be significantly lower than the failure load. Although the length l_F and the angle β_{BF} of the segment B-F were observed to have some level of scatter [3], in the following, l_F is assumed to be equal to $d/6$ and β_{BF} equal to $\pi/8$ in agreement to experimental measurements [10, 11].
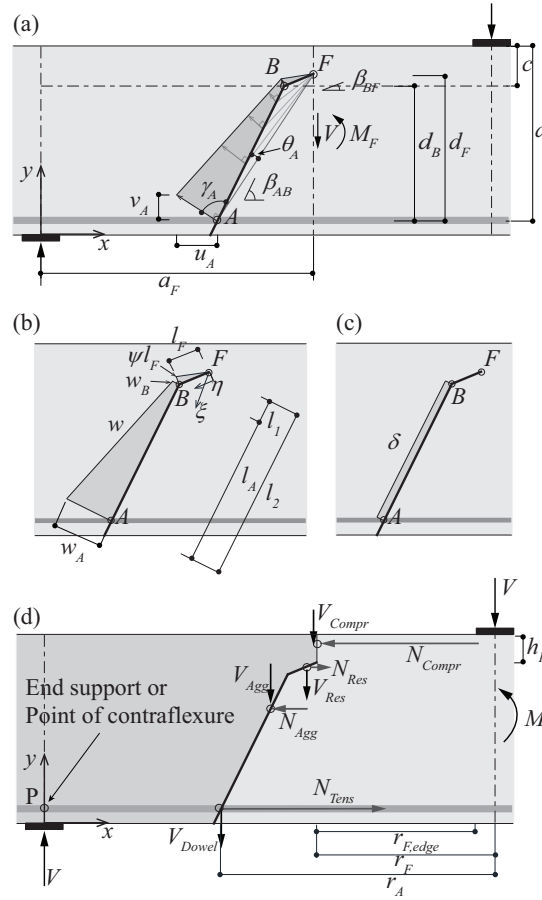
Figure 6.3 (a) Kinematics and displacements of the crack lips according to the adopted crack shape; (b) crack opening w perpendicular to the crack surface and (c) sliding δ; (d) equilibrium of the rigid-body and internal forces

The kinematics of such crack is presented in Figure 6.3b and c. According to [8] and to the measurements of [11], it can be assumed that the centre of rotation is approximately located at the tip of the crack. The rotation of the crack can thus be calculated as a function of the reinforcement strain:

$$\psi = \frac{u_A}{d_F} = \frac{\varepsilon_s \cdot l_B}{d_F} \tag{6.8}$$

where u_A and ε_s are respectively the horizontal opening of the crack and the strain at the level of the longitudinal reinforcement, l_B is the length contributing to the opening of the critical crack according to Eq. (6.1) (see Figure 6.2) and $d_F = d - c + l_F \cdot \sin\beta_{BF}$ defines the vertical distance from the tip of the crack to the flexural reinforcement (Figure 6.3b and c).

The associated relative movements are depicted in Figure 6.3a. The shape and kinematics allow defining the opening and sliding at each point of the critical crack (opening in Figure 6.3b and sliding in Figure 6.3c). It can be noted that the top part of the crack is characterized by pure opening (mode I), whereas the quasi-vertical part of the crack by a combined crack opening and sliding (mixed mode I-II).

6.4.2   Residual tensile strength contribution

Cracked concrete has a residual capacity to transfer tensile stresses for low crack openings. The softening behaviour can be modelled using several approaches. In this work, the proposal by Reinhardt [13] characterized by a simple power law equation will be used:

$$\sigma_{res} = f_{ct} \cdot \left(1 - \left(\frac{w}{w_c}\right)^{c_1}\right) \geq 0 \tag{6.9}$$

where $c_1 = 0.31$ and $w_c = G_F / f_{ct} \cdot (1 + c_1) / c_1$ represents the maximum crack width for stress transfer. The fracture energy of ordinary normal weight concrete G_F can be calculated according to *fib* Model Code 2010 [14] as $G_F = 0.073 \cdot f_c^{0.18}$ (N/mm, MPa) and the tensile strength of concrete is assumed equal to $f_{ct} = 0.3 \cdot f_c^{2/3}$ for $f_c < 50$ MPa [14] and $f_{ct} = 0.3 \cdot (50 \cdot f_c)^{1/3}$ for $f_c \geq 50$ MPa (approximating [14]). It shall be noted that the *fib* Model Code 2010 does not explicitly account for the size of the aggregates on the value of the fracture energy. Nevertheless, this dependence is acknowledged by the code in its commentary and also considered in previous versions of the *fib* Model Code (as that of 1990 [15]), implying that the shear transfer capacity of the residual tensile strength depends eventually upon the aggregate size [8].

It is important to note that only the top part of the critical shear crack (segment B-F) is characterized by a response in mode I and it is then governed by residual tensile strength of concrete. The quasi-vertical part (segment A-B) is characterized by a mixed mode response so that the residual concrete tensile strength in that part is considered together with the aggregate interlock contribution (see following subsection). By integration of the stresses along segment B-F, the shear force can be determined as:

$$V_{Res} = \int_0^{l_{F1}} \sigma_{res} \cdot b \cdot \cos\beta_{BF} \cdot d\eta \tag{6.10}$$

where η is the integration variable, l_{F1} is the integration limit, b is the width of the member, σ_{res} refers to the residual stress normal to the crack and β_{BF} is the angle of segment B-F.

The resulting shear force carried by the residual tensile strength of concrete according to Eq. (6.10) thus results:

$$
\begin{aligned}
V_{Res} &= f_{ct} \cdot b \cdot \cos\beta_{BF} \int_0^{l_{F1}} \left(1 - \left(\frac{\psi \cdot \eta}{w_c}\right)^{c_1}\right) \cdot d\eta = \\
&= f_{ct} \cdot b \cdot \cos\beta_{BF} \cdot l_{F1} \cdot \left(1 - \frac{1}{1 + c_1} \cdot \left(\frac{u_A \cdot l_{F1}}{d_F \cdot w_c}\right)^{c_1}\right)
\end{aligned}
\tag{6.11}
$$

and the associated normal force is:

$$N_{Res} = V_{Res} \cdot \tan\beta_{BF} \tag{6.12}$$

The integration of stresses leads to two possible regimes: (i) cases where the normal stresses develop along the whole length of segment B-F ($\psi \cdot l_F < w_c$) so that $l_{F1} = l_F$ and (ii) cases where the normal stresses develop only close to the tip of the crack ($\psi \cdot l_F \geq w_c$), with l_{F1} equal to:

$$l_{F1} = \frac{w_c}{\psi \cdot l_F} \cdot l_F = \frac{w_c}{u_A} \cdot d_F \tag{6.13}$$

It is interesting to note that for the latter case, Eq. (6.11) and (6.13) give a simple expression:

$$V_{Res} = \frac{G_F \cdot b \cdot \cos\beta_{BF} \cdot d_F}{u_A} \tag{6.14}$$

where the residual strength contribution depends on the fracture energy of concrete G_F and not on the distribution of the tensile stresses (Eq. (6.9)). In addition, Eq. (6.14) clearly shows the hyperbolic decay of the contribution V_{Res} with increasing crack opening u_A (in agreement to [8]).

6.4.3 Aggregate interlock contribution

Many approaches based on the opening and sliding between the rough surfaces of the crack have been proposed in the literature to calculate the aggregate interlock stresses [16–18]. A consistent approach to this issue was developed by Walraven [16], as a two-phase model, whose application has been generalized by Ulaga [19] and Guidotti [20] accounting for different kinematical paths. A detail description of them can be found in [9, 20]. However, the integration of Walraven's equations requires numerical procedures and it cannot be solved in a closed-form manner. In order to avoid the use of numerical procedures in this work, two analytical equations have been calibrated by the authors of this paper on the basis of the Walraven's model for aggregate interlock, but considering the kinematics of Guidotti which is more representative of the actual case (see Figure 6.2). These assumptions allow calculating the transferred shear stresses (τ) for a given opening (w) and sliding (δ) as:

$$\tau_{agg} = \tau_{agg,0} = \sqrt{f_c} \cdot \frac{c_3 \cdot \overline{\delta}^{4/3}}{\left(c_2 \overline{w}\right)^{1.8 + c_2 \cdot \overline{\delta}}} \tag{6.15}$$

as well as the normal stresses (σ):

$$\tau_{agg} = \tau_{agg,0} = \sqrt{f_c} \cdot \frac{c_3 \cdot \overline{\delta}^{4/3}}{\left(c_2 \overline{w}\right)^{1.8 + c_2 \cdot \overline{\delta}}} \tag{6.16}$$

where σ_{res} is defined according to Eq. (6.9), $c_2=40$, $c_3=35$ and $c_4=400$ are constants; $\overline{\delta} = \delta/d_{dg}$ and $\overline{w} = w/d_{dg}$ are the normalized crack sliding and crack opening and d_{dg} is an average roughness whose value can be calculated as follows:

$$d_{dg} = \min\left(40\,\text{mm}, 16 + d_g\right) \qquad \text{for } f_c \leq 60 \text{ MPa}$$

$$d_{dg} = \min\left(40\,\text{mm}, 16 + d_g \cdot \left(60/f_c\right)^2\right) \qquad \text{for } f_c > 60 \text{ MPa}$$

$$\tag{6.17}$$

where d_g refers to the maximum aggregate size. Justification of Eq. (6.17) is provided later in this section.
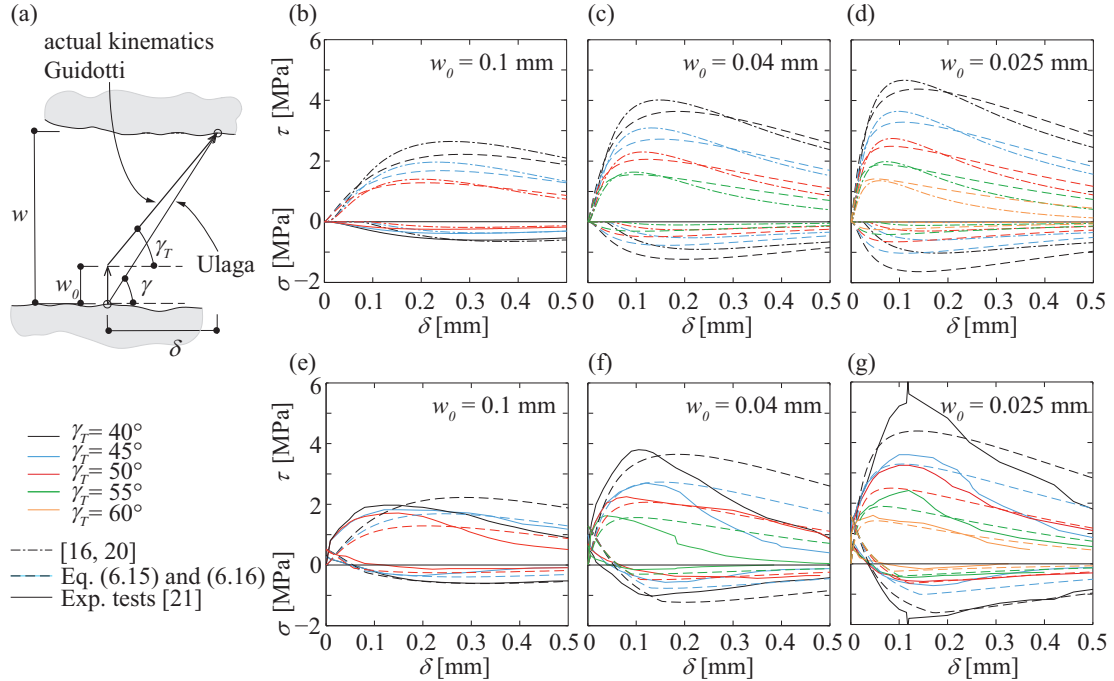
Figure 6.4 (a) Kinematics of mixed mode tests performed by Jacobsen et al. (f_c =41 MPa, d_g =8 mm) [21]; (b-d) comparisons of aggregate interlock stresses according to the model of Walraven [16] for kinematics analogue to that of Guidotti [20] and the aggregate interlock stresses calculated according to Eqs. (6.15) and (6.16) but neglecting the term σ_{res}; (e-g) comparison of mixed mode test results [21] with shear and normal stresses calculated according to Eqs. (6.15) and (6.16)
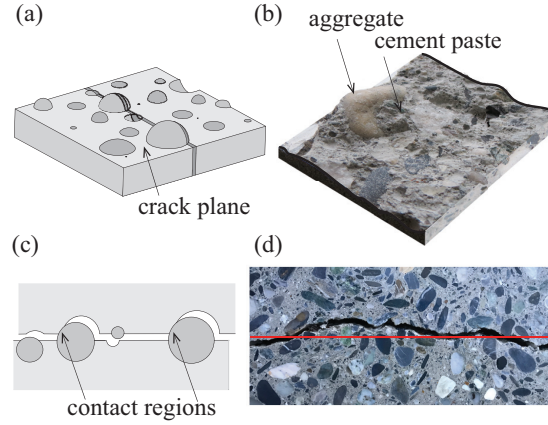
Figure 6.5 (a) Idealized crack plane according to the model of Walraven [16] and (b) actual crack plane; crack surface near the aggregates: (c) idealized, according to the Walraven [16] and (d) actual

Figure 6.4b-d show comparisons between the aggregate interlock stresses calculated according to the model of Walraven [16] for a kinematics analogue to that of Guidotti [20] (initial opening w_0 followed by a combined opening and sliding, Figure 6.4a) and the normal and shear stresses calculated according to Eqs. (6.15) and (6.16), but neglecting the term σ_{res} which is not accounted for in the theoretical model of Walraven. The same comparisons are shown in Figure 6.4e-g to aggregate interlock stresses measured by Jacobsen et al. [21] for specimens tested with the same kinematics, but accounting for the term σ_{res} (which is actually present in the tests). It can be noted that the peak value of the calculated shear and normal stresses is in good agreement with the theoretical and experimental ones, as well as the stiffness and softening properties. In addition, the simple superposition of the residual tensile stresses (σ_{res}) and aggregate interlock stresses ($\sigma_{agg,0}$) gives reasonable results compared to the test measurements (Figure 6.4e-g): it can be observed that the normal stresses vary from tension to compression during the combined opening w and sliding δ, but remain in tension for low values of δ.

It is important to mention that Eqs. (6.15) and (6.16) have been calibrated to be applied to calculate the aggregate interlock stresses for mixed mode crack openings, with initial openings w_0 and secant mixed mode angle γ which are typical of critical shear cracks of slender members (w_0 between 0.025-0.25 mm and mixed mode angle $\gamma > 45°$, [10]). With respect to the average roughness (d_{dg}), this term accounts for two issues:

– The first is that concrete cracks present an undulated (rough) surface (Figure 6.5b and d), contrary to Walraven's approach which assumes cracks as perfect planar surfaces with protruding aggregates (Figure 6.5a and c). This roughness, ensuring the transfer of shear forces by interlocking, is referred to as meso-roughness [8]. The value of the meso-roughness depends on the surface properties after crack development, but can be assumed as 16 mm [3] for normal cases (refer to Eq. (6.17)).

– The second is that, as observed by Sherwood et al. [22], the increase of the interlock capacity is limited for large aggregates. In addition, for high-strength concrete ($f_c > 60$ MPa), a reduction of the aggregate size shall be considered [3], since cracks develop through the aggregates, resulting in crack surfaces that are relatively smooth [23].

As shown in Figure 6.3a, only the quasi-vertical branch of the critical shear crack (segment A-B) is characterized by a mixed mode I and II behaviour. On the basis of the aggregate interlock laws and the relative displacements between the lips of the crack, the aggregate interlock forces at the critical crack can be determined as:

$$V_{Agg} = b \cdot \left(\int_{l_1}^{l_2} \tau_{agg,0} \cdot \sin\beta_{AB} d\xi - \int_{l_1}^{l_2} \sigma_{agg,0} \cdot \cos\beta_{AB} d\xi \right) + b \cdot \int_{l_1}^{l_3} \sigma_{res} \cdot \cos\beta_{AB} d\xi = V_{Agg,0} + V_{Agg,res} \tag{6.18}$$

$$N_{Agg} = b \cdot \left(\int_{l_1}^{l_2} \tau_{agg,0} \cdot \cos\beta_{AB} d\xi + \int_{l_1}^{l_2} \sigma_{agg,0} \cdot \sin\beta_{AB} d\xi \right) - b \cdot \int_{l_1}^{l_3} \sigma_{res} \cdot \sin\beta_{AB} d\xi = N_{Agg,0} + N_{Agg,res} \tag{6.19}$$

where ξ is the integration variable, l_1, l_2 and l_3 are the integration limit, b is the width of the member, $\tau_{agg,0}$, $\sigma_{agg,0}$ and σ_{res} are defined in Eqs. (6.15) and (6.16) and β_{AB} refers to the inclination of segment A-B. Note that the integration of $\tau_{agg,0}$ and $\sigma_{agg,0}$ leads to $V_{Agg,0}$ and $N_{Agg,0}$, whereas the integration of σ_{res} leads to $V_{Agg,res}$ and $N_{Agg,res}$.

In a general manner, the resulting shear force that can be transferred by aggregate interlock can be written as:

$$\frac{V_{Agg}}{\sqrt{f_c} \cdot b} = \int_{l_1}^{l_2} \frac{\sin\beta_{AB} \cdot c_3 \cdot \overline{\delta_A}^{4/3}}{\left(c_2 \cdot \psi \cdot \dfrac{\xi}{d_{dg}}\right)^{1.8+c_2 \cdot \overline{\delta A}}} - \frac{\cos\beta_{AB} \cdot c_4 \cdot \overline{\delta_A}^{7/3}}{\left(c_2 \cdot \psi \cdot \dfrac{\xi}{d_{dg}}\right)^{3+c_2 \cdot \overline{\delta A}}} d\xi + \int_{l_1}^{l_3} \cos\beta_{AB} \cdot \left(1 - \left(\frac{\psi \cdot \xi}{w_c}\right)^{c_1}\right) d\xi =$$

$$= \sin\beta_{AB} \cdot \frac{c_3 \cdot \overline{\delta_A}^{4/3}}{\left(c_2 \overline{\delta_A} + 0.8\right) \cdot \left(\dfrac{u_A}{d_F} \cdot \dfrac{c_2}{d_{dg}}\right)^{1.8+c_2 \overline{\delta_A}}} \cdot \frac{l_2^{0.8+c_2 \overline{\delta_A}} - l_1^{0.8+c_2 \overline{\delta_A}}}{\left(l_2 \cdot l_1\right)^{0.8+c_2 \overline{\delta_A}}} +$$

$$\hspace{8cm} (6.20)$$

$$- \cos\beta_{AB} \cdot \frac{c_4 \cdot \overline{\delta_A}^{7/3}}{\left(c_2 \overline{\delta_A} + 2\right) \cdot \left(\dfrac{u_A}{d_F} \cdot \dfrac{c_2}{d_{dg}}\right)^{3+c_2 \overline{\delta_A}}} \cdot \frac{l_2^{2+c_2 \overline{\delta_A}} - l_1^{2+c_2 \overline{\delta_A}}}{\left(l_2 \cdot l_1\right)^{2+c_2 \overline{\delta_A}}} +$$

$$+ \cos\beta_{AB} \cdot \left[l_3 \cdot \left(1 - \frac{1}{1+c_1} \cdot \left(\frac{u_A \cdot l_3}{d_F \cdot w_c}\right)^{c_1}\right) - l_1 \cdot \left(1 - \frac{1}{1+c_1} \cdot \left(\frac{u_A \cdot l_1}{d_F \cdot w_c}\right)^{c_1}\right) \right] \cdot \frac{f_{ct}}{\sqrt{f_c}}$$

where $\overline{\delta}_A = \dfrac{\delta_A}{d_{dg}} = \dfrac{\sqrt{u_A{}^2 + v_A{}^2} \cdot \sin\theta_A}{d_{dg}}$, $v_A = \dfrac{u_A}{d_F} \cdot \left(l_F \cdot \cos\beta_{BF} + l_A \cdot \cos\beta_{AB}\right)$ and $\theta_A = \beta_{AB} - \text{atan}\dfrac{d_F}{l_F \cdot \cos\beta_{BF} + l_A \cdot \cos\beta_{AB}}$
(refer to Figure 6.3a).

The integration limits l_1 and l_2 can be calculated on the basis of the geometry of the crack (refer to Figure 6.3b): $l_1 = l_F \cdot \cos\left(\beta_{AB} - \beta_{BF}\right)$ and $l_2 = l_1 + l_A$. With respect to l_3, the integration of aggregate interlock stresses leads to three potential regimes:

(i) cases where the residual stresses σ_{res} develop through the whole length of segment A-B ($w_A < w_c$ corresponding to low crack openings), hence l_3 is equal to l_2; (ii) cases where the residual stresses develop only on the top region of the segment A-B ($w_B < w_c < w_A$) so that l_3 results:

$$l_3 = \frac{w_c}{w_A} \cdot l_2 \hspace{7cm} (6.21)$$

and (iii) cases where no residual tensile stresses develop through the quasi-vertical branch of the crack since the opening of the crack along the whole segment A-B exceeds w_c (corresponding to large crack openings), hence l_3 is equal to l_1 and $V_{Agg,res}$ and $N_{Agg,res}$ are equal to zero.

6.4.4   Dowelling action

Dowelling forces can be activated due to relative vertical displacement between the crack surfaces at the level of the longitudinal reinforcement [9]. The capacity of dowelling action to transfer shear is governed by the effective area of the concrete in tension near the bars and by its effective tensile strength [24]:

$$V_{Dowel} = n \cdot f_{ct,ef} \cdot b_{ef} \cdot l_{ef} \hspace{6cm} (6.22)$$

where n is the number of bars activated, $f_{ct,ef}$ is the effective tensile strength, b_{ef} and l_{ef} are the effective width and length in which the tensile strength develops (Figure 6.6a and b). The effective length is estimated as $l_{ef} = 2d_b$ [24] (where d_b is the diameter of the reinforcing bars, Figure 6.6a) and the effective width b_{ef} (Figure 6.6b) can be calculated as [24]:

$$b_{ef} = \min\left[b/n - d_b, 4 \cdot c_b\right] \hspace{6cm} (6.23)$$

where b is the width of the member and c_b is the concrete cover.
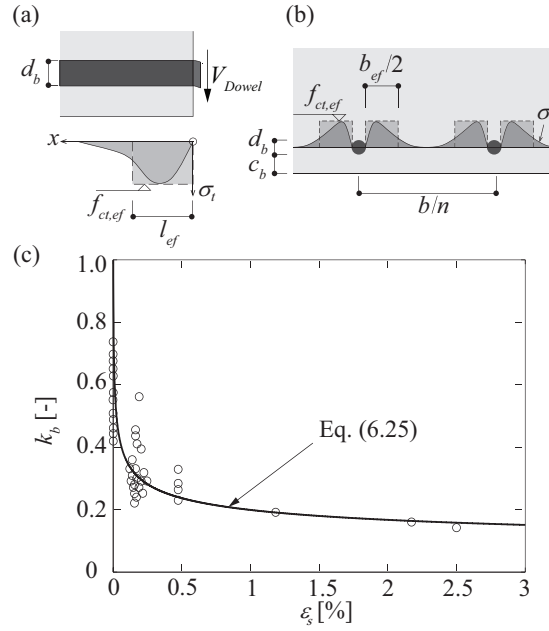
Figure 6.6 (a) Development of transverse stresses at the cover region along the bar and definition of effective length l_{ef}; (b) distribution of transverse tensile stresses (perpendicular to the bar) and definition of effective width b_{ef} (adapted from [24]); (c) reduction of the effective tensile strength as a function of the longitudinal strains in the bar (experimental data from [25])

With respect to the effective tensile strength of concrete ($f_{ct,ef}$), it should be noted that its value is strongly influenced by the state of strains in the flexural reinforcement (due to its interaction with bond [24]). This effect can be estimated as [25]:

$$f_{ct,ef} = k_b \cdot f_{ct} \tag{6.24}$$

where k_b is a strength reduction factor and it follows a decay for increasing strains in the flexural reinforcement (Figure 6.6c). When the reinforcement is not strained, k_b can be assumed equal to 1. In the following, the reduction factor for increasing value of strains in the longitudinal reinforcement is calibrated by fitting the experimental data presented in [25] as (refer to Figure 6.6c):

$$k_b = 0.063 \cdot \varepsilon_s^{-1/4} \leq 1 \tag{6.25}$$

By replacing the steel strain ε_s with the value $\varepsilon_s = u_A / l_B$, the coefficient k_b becomes:

$$k_b = 0.063 \cdot \left(\frac{l_B}{u_A}\right)^{1/4} = 0.063 \cdot \left(\frac{d-c}{u_A}\right)^{1/4} \leq 1 \tag{6.26}$$

The shear resistance due to dowelling action of one-ways slabs with one layer of reinforcement bars is thus:

$$V_{Dowel} = k_b \cdot f_{ct} \cdot n \cdot (b/n - d_b) \cdot 2 \cdot d_b \tag{6.27}$$

For comparison with test data, when no information is available on the bar spacing or for multiple layers, a value of $3d_b$ will be assumed as bar spacing. With this assumption, the last part of Eq. (6.27) becomes $4n \cdot d_b^2$ which can be expressed as a function of the reinforcement ratio ($16\rho \cdot b \cdot d / \pi$), so that the shear strength due to the dowel contribution can be approximated by:

$$V_{Dowel} \approx 5 \cdot k_b \cdot f_{ct} \cdot \rho \cdot b \cdot d \tag{6.28}$$

6.4.5   Contribution of the compression zone

Shear can also be transferred by means of the inclination of the compression chord [8]. For slender beams, this action is significant mostly before the propagation of the segment B-F of the critical crack within the compression zone and then it decreases progressively as the inclination of the compression chord is rather flat (Figure 6.1e and Figure 6.7a) [11]. For short-span beams (associated to low slenderness), with cracks developing without disturbing the theoretical direct strut (typically cracks whose tip is located close to the acting load), the arching action can develop almost undisturbed and the shear strength is mostly controlled by this action (refer to Figure 6.1f and Figure 6.7b).

A realistic assumption for the inclination of the compression zone is derived based on the detailed observations of the principal strain directions shown in Figure 6.7a and b and in [11] (assuming that the inclination of principal strains and stresses is parallel). According to these measurements, it can be assumed that the resultant of the forces of the compression zone at the section corresponding to point F acts at a distance $c_n = 1/3\ h_F$ from the top compressive fibre, where h_F is the thickness of the compression zone above the tip of the crack ($h_F = d - d_F$). In addition, at the edge of the loading plate, a stress block of thickness $2c_m$ with compressive stresses equal to the full compressive strength f_c can be assumed (refer to Figure 6.7c). This can be presumed to be a lower-bound of the actual contribution, as the tensile stresses perpendicular to the strut are neglected. The horizontal and vertical component acting in the compression zone can thus be calculated iteratively by moment equilibrium of the rigid body with respect to point of contraflexure (point P, in Figure 6.3d). The iterative procedure involves assuming an initial distance c_m between the top compressive fibre and the centre of the theoretical strut at the edge of the loading plate, which allows defining the inclination α_c of the compression zone:

$$\tan\alpha_c = \frac{c_n - c_m}{r_{F,edge}} \tag{6.29}$$

where $r_{F,edge}$ is the distance between the tip of the crack and the edge of the loading plate (Figure 6.7c).

Varying the value of c_m, the iterative procedure ends when σ reaches the compressive strength of concrete f_c and the vertical component results:

$$V_{Compr} = N_{Compr} \cdot \frac{c_n - c_m}{r_{F,edge}} = f_c \cdot b \cdot 2 \cdot c_m \cdot \frac{c_n - c_m}{r_{F,edge}} \tag{6.30}$$

Since the location of the critical shear crack is unknown a priori, the iterative procedure that allows calculating the contribution of the compression zone shall be performed for any potential shear crack in the span of the member. It can be noted that an increase of the moment-to-shear ratio of the critical shear crack leads to an increase of the normal force in the compression zone and thus to an increase also of the contribution of the compression chord [7]. In Figure 6.7d, the contribution of the compression zone is calculated for 629 slender beams included in the database by Reineck et al. [26] assuming $x_A = 0.5a$ for all tests (in agreement with [26]). It can be observed that the percentage of the total shear carried by the compression zone depends significantly on the ratio r_F/h_F, where r_F is the distance between the tip of the crack and the axis where the load is applied. As the contribution of the compression zone shown in Figure 6.7d is relatively low for slender beams compared to other shear-transfer actions, a simplified expression can be used despite the non-negligible scatter:

$$\frac{V_{Compr}}{V_c} = \frac{k_{c1} \cdot h_F}{r_F} < 1 \tag{6.31}$$

where V_c is the total shear capacity ($V_c = V_{Res} + V_{Agg} + V_{Dowel} + V_{Compr}$) and k_{c1} is a constant obtained by fitting of the calculated contribution of the compression zone and that can be assumed equal to 0.5. It is important to mention that when a direct strut can develop, this approach is no longer valid since the theoretical strut carries almost the total shear force (refer to Figure 6.7b). This is for instance the case of members with low shear-to-span ratios ($a/d < 2.5$), with high pre-stressing forces (associated to low effective slenderness [27]), or with no or limited bond strength [3].

The shear carried by the inclination of the compression chord yields thus from Eq. (6.31):

$$V_{Compr} = \frac{k_{c1} \cdot h_F / r_F}{1 - k_{c1} \cdot h_F / r_F} \cdot \left(V_{Res} + V_{Agg} + V_{Dowel}\right) \tag{6.32}$$

It can be noted that according to this approach, the contribution of the compression zone is determined by the geometry and the location of the critical shear crack and it is governed by the same mechanical parameters as the other shear-transfer actions.
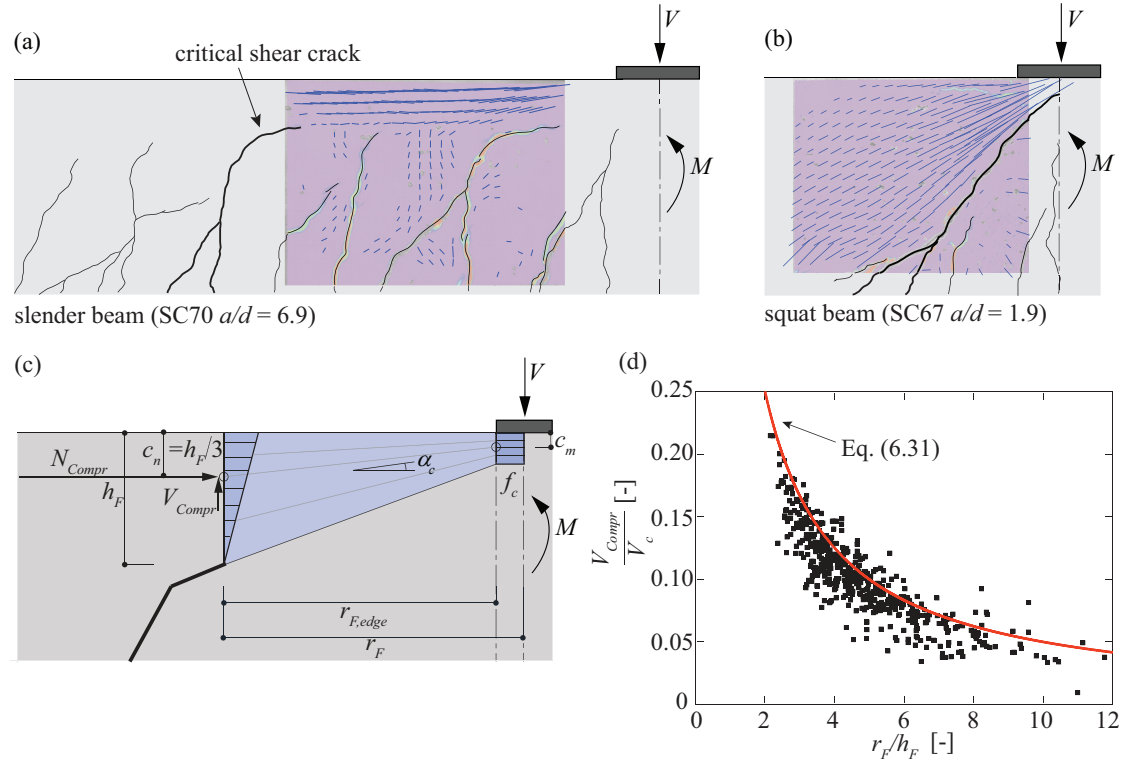
Figure 6.7 Crack pattern and principal compressive strains at failure load for (a) a slender beam (specimen SC70) and (b) a squat beam (specimen SC67) (adapted from Cavagnis et al. [11]); (c) hypothesis of a stress field used to determine the contribution to the shear strength of the compression zone; (d) calculated contribution of the compression zone with respect to the total shear capacity as a function of the distance between the tip of the crack and the axis where the load is applied (tests included in the database from Reineck et al. [26], assuming $x_A=0.5a$)

6.5 Evaluation of the shear capacity

The total shear strength V_c can be calculated by summing the contribution of the various shear-transfer actions:

$$V_c = V_{Res} + V_{Agg} + V_{Dowel} + V_{Compr} = \frac{V_{Res} + V_{Agg} + V_{Dowel}}{1 - k_{c1} \cdot h_F / r_F} \qquad (6.33)$$

The three components V_{Res}, V_{Agg} and V_{Dowel} contained in Eq. (6.33) are strain-dependent, which means that they can be expressed as a function of the crack opening u_A (see Eq. (6.11), (6.20) and (6.22)). The crack opening u_A can be calculated using Eq. (6.4) which means that an iteration is required (as the crack opening depends on the shear force V). Calculating the shear strength requires thus assuming a location of the critical crack and then iteratively increasing the crack opening and checking that the acting shear force V is equal to the shear capacity V_c. The solution $V=V_c$ is the intersection between the load-deformation relationship of Eq. (6.4) and the failure criterion of Eq. (6.33) as shown in Figure 6.8a. The governing location of the critical shear crack can therefore be calculated as the one leading to the minimum strength of all potential locations.

The iterative procedure for calculation of the strength can be summarized in the following steps:

1. Choose a location of the critical shear crack x_A.

2. Calculate the angle β_{AB} as a function of $\alpha_A = M_A/(V_A \cdot d)$ according to Eq. (6.6) (refer to Figure 6.3a).

3. Assume an initial crack opening u_{Ai} (as a first step $u_{A0} = 0.001$ mm can be assumed).

4. Calculate, as a function of the shape of the crack and its kinematics, the residual tensile strength force (V_{Res}, Eq. (6.11) in Section 6.4.2), the aggregate interlock force (V_{Agg}, Eq. (6.20) in Section 6.4.3), the dowelling action (V_{Dowel}, Eq. (6.22) in Section 6.4.4), the contribution of the compression zone (V_{Compr}, Eq. (6.32) in Section 6.4.5) and the shear capacity as the sum of these contributions (V_c, Eq. (6.33)).

5. Calculate the crack opening u_A as a function of the acting bending moment at the section corresponding to the tip of the crack (M_F), (refer to Eq. (6.4) in Section 6.3), where M_F is proportional to the shear force (V).

6. Iterate the crack opening u_{Ai} at step 3 and repeat from step 3 to 6, until u_A is equal to u_{Ai}.

One of the main advantages of this approach is that it can be applied to general or more complex cases and to different loading conditions. This can be done by accounting for the influence of the main governing mechanical parameters (moment-to-shear ratio a_F, crack opening, reinforcement ratio, aggregate size, compressive strength) and evaluating the contribution of the different load-carrying actions at the peak load.

Figure 6.8a shows an instance of the contribution of the different shear-transfer actions to the shear strength as a function of the strains at the level of the longitudinal reinforcement. The example refers to a simply supported beam without transverse reinforcement subjected to point loading. The failure criterion in Figure 6.8a is expressed as a function of the parameter $\varepsilon_s \cdot d/d_{dg}$, where the product $\varepsilon_s \cdot d$ is assumed to be proportional to the crack opening. Such normalization is consistent to that used by the CSCT [3] (Figure 6.1g) and allows for a direct comparison. It can be observed that in this example the aggregate interlock is the governing shear-transfer action and that the contribution of the concrete in tension is significant for low openings of the critical shear crack. On the contrary, the contribution of the compression zone and the longitudinal bars (dowelling action) to the shear strength are very limited in this case. Moreover, it can be noted that the strength of each shear-transfer action decreases for increasing opening of the critical crack and that their decay follows a similar trend (in agreement to [8]). The reason for this strength decay with increasing crack opening u_A is illustrated in Figure 6.8b and c, where the residual tensile stresses (σ_{res}) and the aggregate interlock stresses (σ_{agg} and τ_{agg}) are shown for three different values of the opening of the shear crack ($\varepsilon_s \cdot d/d_{dg}$=0.01, 0.03 and 0.05). It can be noted that the normal stress σ_{agg} is in tension in a part of segment A-B for low openings of the critical shear crack ($\varepsilon_s \cdot d/d_{dg}$=0.01), whereas for larger openings it is always in compression. With respect to the shear stress τ_{agg}, it reaches a maximum value of 5 MPa in the upper part of the segment A-B and it decreases for increasing openings of the critical shear crack.
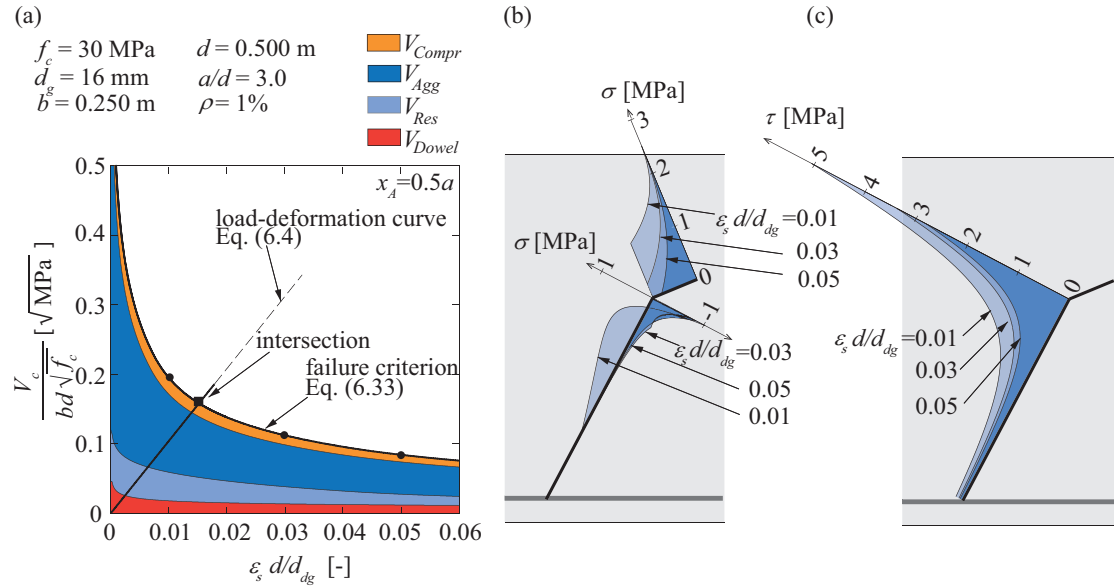
Figure 6.8 (a) Failure criterion and load-deformation curve; shear-transfer actions: aggregate interlock, residual tensile strength of concrete, dowelling action and contribution of the compression zone; (b) normal and (c) shear stresses developing along the critical shear crack for three different values of $\varepsilon_s \cdot d/d_{dg}$ (0.01, 0.03 and 0.05)

6.6 Discussion on the significance of shear-transfer actions for members subjected to point load

In Figure 6.9 the location of the critical crack and the associated capacities of the shear-transfer actions are investigated with reference to an actual test (specimen SC61, presented in detail in [10]). The specimen corresponds to a simply supported beam tested under concentrated load (a/d = 4.41, d = 556 mm, ρ = 0.89%, f_c = 35.3 MPa, d_g = 16 mm). Three different potential positions of the critical shear crack ($x_A = d$, $x_A = 0.5a$ and $x_A = a - d$) are investigated. Their inclinations β_{AB} are calculated

according to Eq. (6.6) and correspond well with the observed cracks (Figure 6.9a). From Figure 6.9b-d it can be noted that the strains at the level of the longitudinal reinforcement and the contribution of the different shear-transfer actions vary as a function of the location of the critical shear crack. It can be observed that the contribution of aggregate interlock is dominant in this case for all investigated positions of the critical shear crack. Moreover, when the crack is located close to the end support (in a general case, the point of contraflexure with zero bending moment), the contribution of the compression zone is very limited and the tensile strength of concrete plays a role, whereas when the critical crack develops closer to the load introduction plate (section of maximum bending moment), the contribution of the compression zone increases and the shear carried by the tensile strength of concrete decreases. In a general manner, the governing theoretical position of the critical crack is defined as the location where the sum of the contributions of the different shear-transfer actions reaches its minimum value. In Figure 6.9b-d, it can be observed that the shear capacity (sum of all shear-transfer actions, intersection between the load-deformation relationship and the failure criterion) does not significantly vary between the investigated sections x_A and that the location of the critical crack has thus a limited influence on the shear strength of the member. This explains why for this type of members, the experimentally observed position of the failure crack can present a large scatter and different shear-transfer actions may eventually be governing [8, 11].

The governing location of the critical crack is also investigated in Figure 6.10 for different values of slenderness ratio (a/d), reinforcement ratio (ρ) and effective depth (d). In Figure 6.10a, the contribution of the different shear-transfer actions to the shear capacity is shown for each position x_A of the critical shear crack. It can be observed that for cracks developing within a region between 0.4a and 0.6a, the total shear capacity is almost constant but the amount of shear carried by each shear-transfer action shows some levels of variation. In Figure 6.10b and c it can be observed that an increase of the slenderness ratio leads to a variation of the governing position of the critical crack, with the governing crack closer to mid-span for less slender members. In Figure 6.10d it can be noted that the distance r_F between the tip of the critical shear crack and the axis where the load is applied varies between d and 2d. A similar trend, concerning the location of the governing critical shear crack has been experimentally observed in the tests performed by Leonhardt and Walther [28]. The influence of the reinforcement ratio is illustrated in Figure 6.10e. An increase in the reinforcement ratio leads to an increase of the height of the compression zone, which therefore plays a more significant contribution in carrying the shear. Consequently, for increasing values of the reinforcement ratio, the governing location of the critical crack shifts towards mid-span. It can be shown that almost all other parameters have low influence on the governing position of the critical shear crack (for instance, effective depth d in Figure 6.10f).
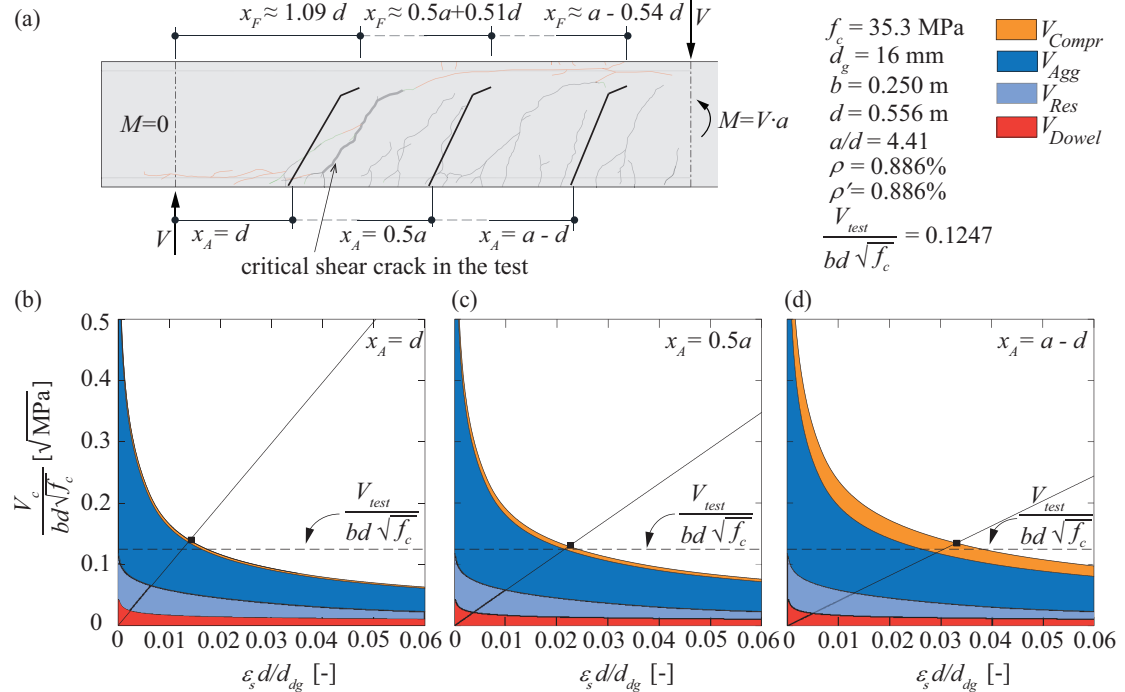
Figure 6.9 (a) Specimen SC61 [10]: crack pattern at maximum load and selected potential location of the critical shear crack x_A; (b-c-d) contribution of the various shear-transfer actions at the different locations of the critical shear crack ($x_A = d$, $x_A = 0.5a$ and $x_A = a - d$) and intersection of the load-deformation relationship with the failure criterion
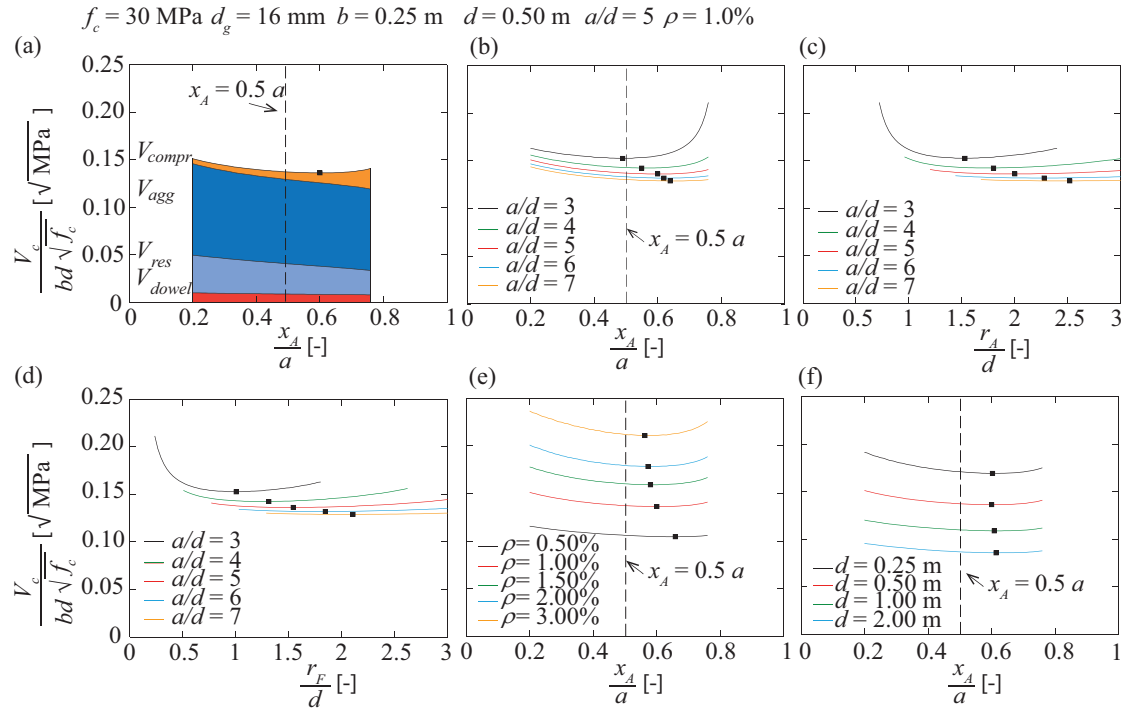
Figure 6.10 Normalized shear strength as a function of the location of the critical crack (points in black refer to the location with the minimum shear strength): (a) contribution of the different shear-transfer actions at different critical crack locations x_A; (b-d) influence on the location of the critical shear crack of the slenderness ratio a/d, (e) of the longitudinal reinforcement ratio ρ and (f) of the effective depth d

An interesting fact to be noted is that the curves representing the shear capacity are very flat around the minimum (at a distance between $1.5d$ and $2.25d$ from the load introduction plate and between $0.4a$ and $0.6a$). For these cases, adopting a fixed control section within this region is even sufficient for calculating the shear strength (although the relative significance of the shear-transfer actions may not be accurately assessed). To that aim, for instance, a value $x_A=0.5a$ in agreement with the considerations of Reineck et al. [26] is reasonable.

In Figure 6.11, the calculated shear capacity of 635 rectangular concrete beams without shear reinforcement (data from Reineck et al. [26] completed with the tests by Cavagnis et al. [11]) is plotted against the normalized crack width parameters. The plot is normalized to account for the effective depth, the width, the compressive strength and the aggregate size of the member [8]. The black points in Figure 6.11 represent the intersection between the failure criteria calculated according to Eq. (6.33) at the control section $x_A = 0.5a$ and the load-deformation relationship (refer to Eq. (6.5)). In addition, the direction of the failure envelopes in the vicinity of the intersection is plotted (grey lines in Figure 6.11). It is interesting to note that failures occur actually in a narrow band despite the large range of cases considered (effective depth d ranging 50-2000 mm, flexural reinforcement ratio ρ ranging 0.4-7%, concrete strength f_c ranging 10-110 MPa, aggregate size d_g ranging 0-32 mm, shear span a ranging $2.5d$ - $8.5d$).

For design purposes, instead of calculating the failure criteria by integration of the stresses along the critical shear crack, Muttoni et al. [3] proposed a simple hyperbolic failure criterion (Figure 6.1g) that approximates the failure band. Although the CSCT failure criterion provides a reasonable estimate of the shear capacity, Figure 6.11 shows that its accuracy can be enhanced for low values of the term $\varepsilon_s \cdot d/d_{dg}$ with a power law-expression (red line in Figure 6.11) where the exponent of the term $\varepsilon_s \cdot d/d_{dg}$ is -1/2:

$$v_c = \frac{V_c}{b} = \frac{k \cdot d \cdot \sqrt{f_c}}{\sqrt{\varepsilon_s \cdot d/d_{dg}}} \leq v_{c0} \tag{6.34}$$

where v_c is the shear capacity per unit length, k is a constant that can be obtained by fitting of the calculated shear strengths ($k = 0.019$ in Figure 6.11) and v_{c0} refers to the maximum shear strength per unit length (not investigated in this study).
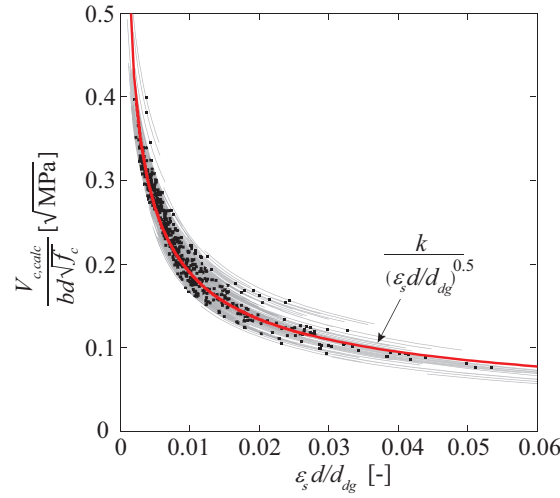
Figure 6.11 Calculated shear strengths of 635 rectangular beams failing in shear ($a/d \geq 2.5$) (data from Reineck et al. [26] completed with the tests by Cavagnis et al. [11]) as a function of the reinforcement strains at the critical section ($x_A = 0.5a$)

6.7 Validation of the approach with test results and improvement of the CSCT

Figure 6.12 shows the comparison between the shear strengths calculated according to the general procedure (Eq. (6.5) + Eq. (6.33)), the simplified approach (Eq. (6.3) + Eq. (6.34)) and the original procedure of the CSCT [3] with some selected experimental test series. The main parameters governing the shear strength are investigated: the shear-to-span ratio a/d, the longitudinal reinforcement ratio ρ, the effective depth d, the compressive strength f_c, the aggregate size d_g and the elastic modulus of the longitudinal bars E_s. The comparison shows that the calculated shear strengths are in very good agreement when compared with experimental results and the three approaches follow similar trends.

Figure 6.13 presents a systematic comparison of the shear strengths calculated solving the set of Eqs. (6.5) and (6.33) against 635 tests on simply supported beams or cantilevers subjected to point loading (see also Appendix B). The database used is that of Reineck et al. [26] completed with the tests by Cavagnis et al. [11], where only rectangular beams with $a/d \geq 2.5$ have been considered. It can be observed that there are no clear trends for the main mechanical and geometrical parameters. The average measured-to-calculated shear strength is 1.01 and the Coefficient of Variation is 13.6% (Appendix B and Table 6.1).

The accuracy of the model is comparable to that obtained using the original formulation of the CSCT [3] (average measured-to-calculated shear strength 1.02, CoV 15.6%, refer to Table 6.1). Based on the observations of the present study and recent experimental investigations [22], the CSCT [3] can be improved accounting for d_{dg} defined according to Eq. (6.17) (the ratio between measured-to-calculated shear strength results equal to 1.01 with a CoV of 14.5%, refer to Table 6.1)

Moreover, as shown in Section 6.6, the accuracy of the hyperbolic failure criterion of the CSCT can be enhanced assuming a power law failure criterion (refer to Figure 6.11). The shear capacity can thus be calculated in a simple manner by combining the load-deformation relationship of Eq. (6.3) and the simplified power law failure criterion of Eq. (6.34), assuming the control section at $x_A = 0.5a$. For this simplified approach, a good agreement is also found between the measured shear strength in the tests and the calculated one, with an average ratio of 1.03 and with a value of CoV of 14.2% (Table 6.1).
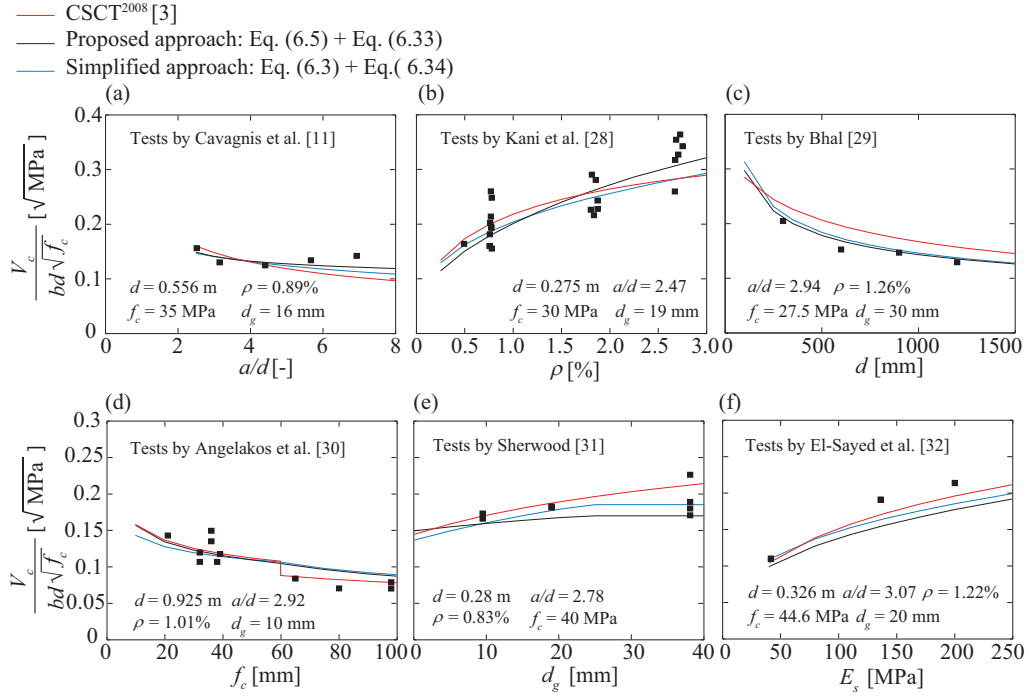
Figure 6.12 Comparison of the proposed approaches and the CSCT [3] to test series investigating: (a) the slenderness ratio a/d [11], (b) the reinforcement ratio ρ [29], (c) the effective depth d [30], (d) the compressive strength f_c [31], (e) the aggregate size d_g [32] and (f) the reinforcement elastic modulus E_s (steel and non-metallic reinforcements) [33]
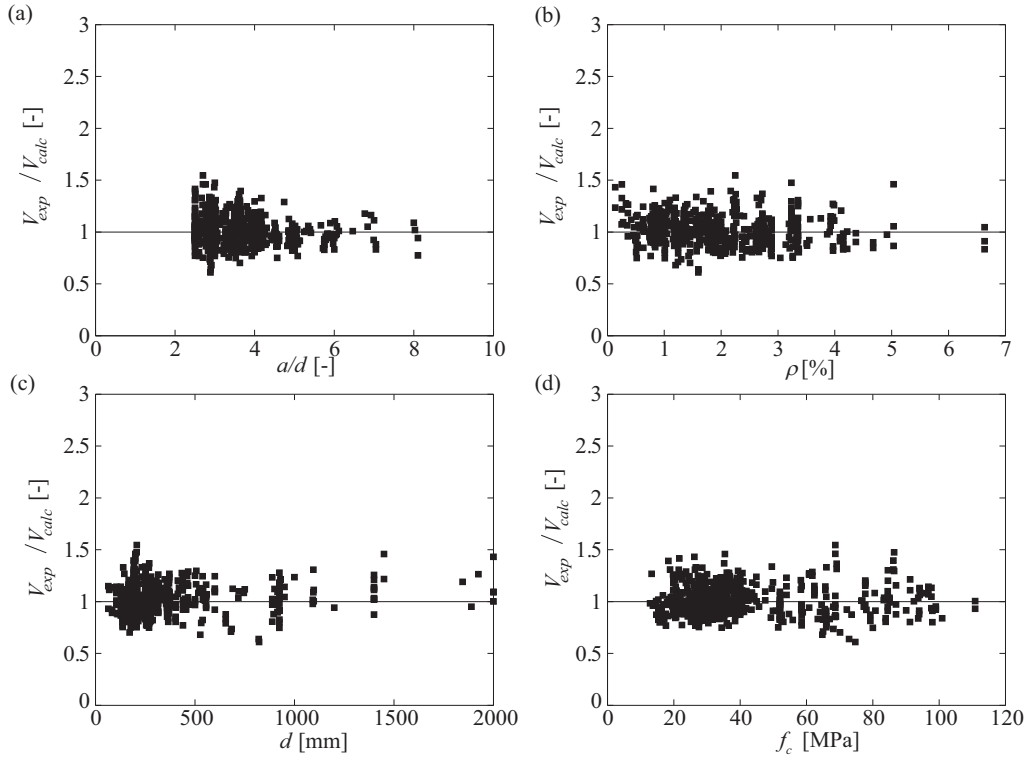
Figure 6.13 Ratio V_{exp}/V_{calc} (V_{calc} calculated according to the presented procedure: Eqs. (6.5) and (6.33), assuming $x_A=0.5a$) as a function of the different mechanical and geometrical parameters for the cases of simply supported and cantilever slender beams subjected to concentrated load (data from Reineck et al. [26] completed with the tests by Cavagnis et al. [11]): (a) shear span-to-effective depth ratio a/d; (b) longitudinal reinforcement ratio ρ; (c) effective depth d and (d) compressive strength f_c

	V_{exp} / V_{calc} [-]	CoV [-]
CSCT[2008] [3], x_{cr}=a-d/2	1.02	0.156
Proposed approach Eq. (6.5) + Eq. (6.33), assuming x_A =0.5a	1.01	0.136
Improvement of the CSCT[2008] [3] assuming d_{dg} according to Eq. (6.17)	1.01	0.145
Simplified power law failure criterion Eq. (6.3) + Eq. (6.34), assuming x_A =0.5a	1.03	0.142

Table 6.1 Comparison of calculated and experimental shear strengths: average value V_{exp} / V_{calc} and coefficient of variation (CoV)

6.8 Conclusions

This paper presents an overview of the shear-transfer actions and their contribution to the shear strength of slender reinforced concrete members without transverse reinforcement. The contribution of the various shear-transfer actions is quantified on the basis of fundamental constitutive laws and accounting for a realistic crack shape and kinematics (based on detailed measurements on tests). The main conclusions are listed below:

1. Shear can be carried by a number of potential shear transfer actions. In a general manner, there is not a governing shear transfer action, and the amount of shear force carried by each action depends on the location of the critical shear crack, its kinematics (opening and sliding) and the crack roughness properties.

2. The cantilever action (as described in the Kani's tooth model) is governing for load levels which are generally lower than the actual failure load. This shear-carrying action is disabled by the development of a horizontal branch of the critical shear crack generated by the tensile stresses near the crack tip. The load can further be increased above the capacity of the cantilever action as other shear-carrying actions develop.

3. For slender members, the failure load is eventually governed by beam shear-transfer actions (aggregate interlock, residual tensile strength and dowelling action):

   – For low crack widths in slender members, both aggregate interlock and tensile strength of concrete play an important role. For large crack widths, aggregate interlock becomes more dominant.

   – The dowelling action of the longitudinal reinforcement exhibits a more limited contribution than the other beam shear-carrying actions. Yet, its contribution is not necessarily negligible.

   – The contribution of the inclined compression chord for slender members depends significantly on the location of the tip of the critical shear crack. For critical shear cracks located at a certain distance from the load introduction, its contribution is rather low.

   For squat members, arching action is governing.

4. Despite the fact that the relative amount of each shear-transfer action may differ depending on the location and shape of the critical shear crack, the total shear capacity (sum of the various contributions) is relatively constant independently of the location of the critical shear crack. This explains why the location of the failure crack may vary significantly even for similar specimens.

5. The force transferred by the different shear-transfer actions decay for increasing openings of the critical shear crack and they are governed by the same mechanical parameters. Accounting for this fact and for the relatively constant sum of the various shear-transfer actions, shear failures can be described by a single failure criterion.

6. The main assumptions of the Critical Shear Crack Theory are in agreement to the previous conclusions and allow describing shear failures in a general manner. The shape of its failure criterion can be derived by analytical and numerical considerations, allowing relating the shear strength to the deformation capacity at failure, and can be enhanced by a power-law equation.

6.9 Acknowledgments

6.10 Appendixes

6.10.1 Appendix A. Notation

a	shear span (defined for specimens subjected to concentrated loads as the distance between the centre of the load and the centre of the support)
a_A	M/V at section A
a_F	M/V at section F
b	width of the beam
b_{ef}	effective width of concrete in tension
c	depth of the compression zone
c_1, c_2, c_3, c_4	constants of the model
c_b	concrete cover
c_m	distance from the top compression fibre to the centre of the inclined compression strut at the edge of the loading plate
c_n	distance from the top compression fibre to the axis where inclined force of the compression zone acts
d	effective flexural depth
d_b	diameter of reinforcing bar
d_{dg}	d_g+16 [mm]
d_F	vertical position of the tip of the crack
d_g	maximum aggregate size
f_c	concrete compressive strength measured in cylinder
f_{ct}	concrete tensile strength
$f_{ct,ef}$	effective tensile strength of concrete
h	beam height
h_F	distance from the top compression fibre to the tip of the shear crack
k	coefficient power-law failure criterion
k_b	reduction factor tensile strength of concrete
k_{c1}	coefficient compression zone
l	span length
$l_1\ l_2\ l_3\ l_{F1}$	integration limits
l_{ef}	effective length
l_A	length of segment A-B of the critical shear crack
l_B	length of the region of the beam contributing to the opening of the critical crack
l_F	length of segment B-F of the critical shear crack
n	number of longitudinal bars
r_A	distance from the axis of the load introduction to the onset of the critical shear crack
r_F	distance from the axis of the load introduction to the tip of the critical shear crack
$r_{F,edge}$	distance from the edge of the loading plate to the tip of the critical shear crack
u	opening of the crack measured along the horizontal direction
u_A	horizontal opening of the critical shear crack at point A
v	opening of the crack measured along the vertical direction
v_A	horizontal opening of the critical shear crack at point A
v_c	shear capacity per unit length
$v_{c,0}$	maximum shear strength per unit length
w	crack width perpendicular to the crack surface
$\overline{w}$	normalized crack opening w / d_{dg}
w_A	opening perpendicular to the crack surface at point A
w_B	opening perpendicular to the crack surface at point B along segment A-B

w_c	maximum crack width allowing tensile stresses transfer in concrete
x_A	distance from point A to the support
x_F	distance from point F to the support
z	inner level arm
A_s	area of longitudinal bars
E_c	modulus of elasticity of concrete
E_s	modulus of elasticity of steel
G_F	fracture energy
M	bending moment
M_F	bending moment at the section corresponding to the tip of the critical shear crack
N_{Agg}	horizontal component of the aggregate interlock action
N_{Compr}	horizontal component of the inclined compression chord
N_{Res}	horizontal component of the residual tensile strength of concrete
V	acting shear force
V_c	shear capacity
V_{max}	shear force at failure (maximum value)
V_{Agg}	shear force carried by aggregate interlock action
V_{Compr}	shear force carried by inclined compression chord
V_{Dowel}	shear force carried by dowelling action
V_{Res}	shear force carried by residual tensile strength of concrete
α_c	inclination of the compression chord
α_A	$M_A/(V_A \cdot d)$ in section A
β_{AB}	angle of flexural cracks
β_{BF}	angle of crack type F
γ	secant mixed mode angle
γ_T	tangent mixed mode angle
δ	crack sliding
δ_A	horizontal opening of the critical shear crack at point A
$\bar{\delta}$	normalized crack sliding δ / d_{dg}
ε_s	steel strain
η	integration variable for the residual tensile stresses
ξ	integration variable for the aggregate interlock stresses
ρ	reinforcement ratio of tension reinforcement
σ_{agg}	aggregate interlock normal stress
σ_{res}	residual tensile stress
τ_{agg}	aggregate interlock shear stress
ψ	rotation of the critical shear crack

6.10.2 Appendix B. Database

Test series considered in this study and comparison with the proposed expressions: Eq. (6.5)+ Eq. (6.33).

Researchers	No. of specimens	f_c [MPa]	b [mm]	d [mm]	a/d [-]	ρ [%]	V_{exp}/V_{calc} (COV)
Adebar et al. [34]	5	49.3 to 58.9	290 to 360	178 to 278	2.92 to 4.56	0.99 to 3.04	0.84 (0.068)
Ahmad et al. [35]	17	63.4 to 68.7	127	184 to 208	2.70 to 4.00	1.77 to 6.64	1.03 (0.210)
Ahmad et al. [36]	3	43.6 to 80.8	102	178	3.70	1.40	0.95 (0.070)
Angelakos et al. [31]	7	21 to 80	300	895 to 925	2.88 to 2.97	0.50 to 2.09	0.96 (0.146)
Aster et al. [37]	5	24.6 to 30.4	1000	250 to 750	3.65 to 3.68	0.42 to 0.91	1.01 (0.072)
Lubell et al. [38]	11	37.1 to 64.6	250 to 3005	306 to 916	2.87 to 3.27	0.76 to 0.93	1.12 (0.089)
Bernander [39]	6	27.6 to 29.1	100	168	4.17	0.97 to 1.17	1.07 (0.062)

Bhal [30]	8	23.2 to 29.6	240	300 to 1200	2.94	0.63 to 1.26	1.03 (0.114)
Bresler et al. [40]	3	22.6 to 37.6	305 to 310	461 to 466	3.80 to 6.77	1.81 to 2.73	1.24 (0.046)
Cladera et al. [41]	6	49.9 to 87	200	360	2.90	2.23	1.00 (0.135)
Cao [42]	2	27.5 to 30.1	300	1845 to 1925	2.77 to 2.89	0.36 to 1.52	1.23 (0.042)
Cederwall et al. [43]	1	29.3	135	234	3.42	1.07	1.24 (-)
Chana [44]	23	20.8 to 38.9	60 to 203	106 to 356	3.00	1.74 to 1.78	1.02 (0.073)
Chang et al. [45]	15	17.7 to 38.6	102	137	2.60 to 4.09	1.86 to 2.89	0.91 (0.115)
Collins et al. [23]	7	36 to 98	300	925	2.88	1.01	1.07 (0.156)
Diaz de Cossio et al. [46]	5	19.5 to 31.5	152	254	3.30 to 5.30	0.98 to 3.33	0.99 (0.061)
Thorenfeldt et al. [47]	14	54 to 97.7	150 to 300	207 to 442	3.00 to 4.00	1.82 to 3.24	1.15 (0.119)
Elzanaty et al. [48]	11	20.7 to 79.3	177.8	267 to 273	4.00 to 6.00	0.93 to 3.21	0.88 (0.060)
Feldman et al. [49]	8	21.5 to 36.7	152	252	2.87 to 6.04	3.35	1.11 (0.141)
Ferguson [50]	1	29.3	101	189	3.23	2.08	0.82 (-)
Ghannoum [51]	22	34.2 to 58.6	400	65 to 889	2.50	1.15 to 2.00	0.98 (0.110)
Grimm [52]	11	90.1 to 110.9	300	146 to 746	3.53 to 3.90	0.83 to 4.22	1.00 (0.130)
Hallgreen [53]	23	31.1 to 92.4	150 to 337	191 to 211	2.61 to 3.66	0.57 to 4.11	1.21 (0.084)
Hamadi [54]	4	21.0 to 30.4	100	370 to 372	3.37 to 5.90	1.08 to 1.79	1.17 (0.082)
Hanson [55]	4	20.9 to 31.0	152	267	4.95	1.25 to 3.50	0.97 (0.073)
Hedman et al. [56]	4	19.9 to 29.5	152	267	4.95	1.25 to 2.22	1.03 (0.051)
Islam et al. [57]	5	26.6 to 83.3	150	203 to 207	3.86 to 3.94	2.03 to 3.22	1.02 (0.105)
Johnson et al. [58]	1	55.9	305	539	3.10	2.49	0.82 (-)
Kani [59]	37	24.8 to 30.8	150 to 612	132 to 1097	2.50 to 8.03	2.59 to 2.87	1.02 (0.106)
Kani et al. [29]	52	15.4 to 36.7	149 to 157	264 to 287	2.50 to 5.97	0.49 to 2.83	0.95 (0.108)
Kawano et al. [60]	8	20.6 to 27.3	105 to 600	300 to 2000	3.00	1.18 to 1.37	1.06 (0.099)
Kim et al. [61]	18	52	170 to 300	142 to 915	3.00 to 6.00	1.01 to 4.68	0.94 (0.087)
Krefeld et al. [62]	50	12.9 to 39.0	152 to 254	238 to 483	2.67 to 8.10	0.80 to 4.92	0.95 (0.092)
Küng [63]	7	18.4 to 21.7	140	200	2.50	0.36 to 1.82	1.20 (0.154)
Kuhlmann et al. [64]	2	49.6	402	250	2.86 to 4.86	1.56	1.23 (0.121)
Kuhlmann et al. [65]	4	43.4 to 47.6	400	250	2.86 to 4.86	1.57 to 1.92	1.05 (0.033)
Kulkarni et al. [66]	4	40.6 to 43.6	102	152	3.50 to 5.00	1.38	1.04 (0.053)
Laupa et al. [67]	6	14.8 to 32.3	152	262 to 269	4.82 to 4.95	1.91 to 3.97	0.89 (0.062)
Leonhardt et al. [28]	26	13.3 to 38.3	50 to 500	70 to 600	2.78 to 5.91	1.33 to 2.40	1.01 (0.113)
Marti et al. [68]	2	29.3 to 29.5	400	167	3.83	1.38 to 1.84	1.18 (0.029)
Mathey et al. [69]	9	23.5 to 30.6	203	403	2.84 to 3.78	0.47 to 2.54	0.93 (0.085)
Moody et al. [70]	23	15.4 to 41.2	152 to 178	262 to 272	2.85 to 3.41	1.60 to 2.37	0.95 (0.078)
Morrow et al. [71]	12	14.7 to 45.7	305 to 308	356 to 375	3.00 to 8.10	1.27 to 3.91	1.00 (0.045)
Mphonde et al. [72]	9	21.3 to 96.1	152.4	298	3.49	2.33 to 3.34	1.07 (0.043)
Niwa et al. [73]	3	24.6 to 27.1	300 to 600	1000 to 2000	2.98	0.14 to 0.28	1.25 (0.135)
Podgomiak [74]	8	37 to 99	300	225 to 925	2.88 to 2.97	0.51 to 3.14	0.98 (0.101)
Rajagopalan et al. [75]	10	23.7 to 36.6	151 to 154	259 to 268	3.83 to 4.27	0.25 to 1.73	0.99 (0.170)
Regan [76]	5	24.5 to 29.9	152	272	3.27	1.46	1.06 (0.076)
Rehm et al. [77]	1	23.7	900	313	3.19	1.21	1.18 (-)
Reineck et al. [78]	3	24.6 to 25.8	500	225 to 226	2.50 to 3.50	0.79 to 1.39	1.02 (0.032)
Remmel [79]	4	84.5 to 85.1	150	160 to 165	3.06 to 4.00	1.87 to 4.09	0.97 (0.053)
Rüsch et al. [80]	3	23 to 24.2	90 to 180	111 to 262	3.60 zo 3.62	2.64 to 2.65	0.87 (0.014)
Salandra et al. [81]	4	53 to 70.1	102	171	2.59 to 3.63	1.45	0.83 (0.127)
Scholz [82]	7	80.6 to 96.8	200	362 to 372	3.00 to 4.00	0.81 to 3.36	1.01 (0.132)
Taylor [83]	6	27.8 to 33.2	203	370	3.02 to 3.50	1.03 to 1.55	1.09 (0.104)
Taylor [84]	5	22 to 28.7	200 to 400	465 to 930	3.01	1.35	1.12 (0.090)
Walraven [85]	3	24.1 to 24.4	200	125 to 720	3.00	0.74 to 0.83	1.07 (0.077)
Xie et al. [86]	2	38.5 to 100.9	127	216	2.93	2.08	0.83 (0.022)
Yoon et al. [87]	3	36 to 87	375	655	3.23	2.88	0.83 (0.052)
Yoshida [88]	1	33.6	300	1890	2.82	0.74	0.95 (-)
Lubell [89]	7	36.9 to 41	249 to 1170	287 to 538	2.91 to 3.57	0.33 to 1.73	1.19 (0.079)
Sherwood [32]	21	28.1 to 77.3	122 to 300	280 to 1450	2.77 to 2.87	0.25 to 0.83	1.11 (0.111)
Thiele [90]	5	24.6 to 42.5	400	167 to 297	3.47 to 4.97	0.93 to 2.41	1.05 (0.092)
Winkler [91]	5	35.1	150 to 450	200 to 900	3.91 to 3.94	1.18 to 1.20	1.09 (0.067)
Rosenbusch [92]	2	43.4	200	260	3.37	0.65 to 3.55	0.98 (0.077)
Tureyen et al. [93]	3	40.9 to 43.7	457	360	3.38	0.36 to 1.92	1.07 (0.121)
Bentz et al. [94]	9	34.3 to 36.1	101 to 106	84 to 333	2.80 to 2.94	1.55 to 1.63	1.05 (0.091)
Sneed et al. [95]	8	64.8 to 74.8	203 to 613	233 to 822	2.87 to 2.92	1.20 to 1.60	0.79 (0.290)
Cavagnis et al. [11]	6	32.6 to 35.6	250	556 to 559	2.52 to 6.92	0.54 to 0.89	1.04 (0.078)
	635						**1.01 (0.136)**

6.11 References

[1]   Collins MP, Mitchell D, Adebar P, Vecchio F. A general shear design method. *ACI Structural Journal* 1996; 93 (5):36–45.

[2]   Park H-G, Choi K-K, Wight JK. Strain-Based Shear Strength Model for Slender Beams without Web Reinforcement.

ACI Structural Journal 2006; 103 (6):783–793.

[3] Muttoni A, Fernández Ruiz M. Shear strength of members without transverse reinforcement as function of critical shear crack width. *ACI Structural Journal* 2008; 105 (2):163–172.

[4] Yang Y, Walraven J, den Uijl J. Shear Behavior of Reinforced Concrete Beams without Transverse Reinforcement Based on Critical Shear Displacement. *Journal of Structural Engineering* 2016; 143 (1):4016146.

[5] Tung ND, Tue NV. A new approach to shear design of slender reinforced concrete members without transverse reinforcement. *Engineering Structures* 2016; 107:180–194.

[6] Fisker J, Hagsten LG. Mechanical model for the shear capacity of R/C beams without stirrups: A proposal based on limit analysis. *Engineering Structures* 2016; 115:220–231.

[7] Marí A, Bairán J, Cladera A, Oller E, Ribas C. Shear-flexural strength mechanical model for the design and assessment of reinforced concrete beams. *Structure and Infrastructure Engineering: Maintenance, Management, Life-Cycle Design and Performance* 2014; 8 (4):337–353.

[8] Fernández Ruiz M, Muttoni A, Sagaseta J. Shear strength of concrete members without transverse reinforcement: a mechanical approach to consistently account for size and strain effects. *Engineering Structures* 2015; 99:360–372.

[9] Campana S, Anastasi A, Fernández Ruiz M, Muttoni A. Analysis of shear-transfer actions on one-way RC members based on measured cracking pattern and failure kinematics. *Magazine of Concrete Research* 2013; 65 (6):386–404.

[10] Cavagnis F, Fernández Ruiz M, Muttoni A. Shear failures in reinforced concrete members without transverse reinforcement: An analysis of the critical shear crack development on the basis of test results. *Engineering Structures* 2015; 103:157–173.

[11] Cavagnis F, Fernández Ruiz M, Muttoni A. An analysis of the shear transfer actions in reinforced concrete members without transverse reinforcement, accepted for publication in Structural Concrete. 2017.

[12] Huber P, Huber T, Kollegger J. Investigation of the shear behaviour of RC beams on the basis of measured crack kinematics. *Engineering Structures* 2016; 113:41–58.

[13] Reinhardt HW. Fracture Mechanics of an Elastic Softening Material like Concrete. *Heron* 1984; 29 (2):42.

[14] Fédération Internationale du Béton (fib), fib Model Code for Concrete Structures 2010, Ernst & Sohn. 2013:434.

[15] CEB-FIP Model Code 1990: Design Code, Thomas Telford, London. 1993.

[16] Walraven JC. Fundamental analysis of aggregate interlock. *Journal of Structural Division* 1981; 107 (11):2245–2270.

[17] Gambarova PG, Karakoc C. A new approach to the analysis of the confinement role in regularly cracked concrete elements. *Transactions of the 7. international conference on structural mechanics in reactor technology* 1983; H.

[18] Li B. Contact density model for stress transfer across cracks in concrete. *Journal of the Faculty of Engineering, the University of Tokyo* 1989; 1:9–52.

[19] Ulaga T. Betonbauteile mit Stab- und Lamellenbewehrung: Verbund- und Zuggliedmodellierung. PhD Thesis. Thesis no. 15062 (in German). Zurich, Switzerland: ETHZ. 2003:160.

[20] Guidotti R. Poinçonnement des planchers-dalles avec colonnes superposées fortement sollicitées. PhD Thesis. Thesis no. 4812 (in French). Lausanne, Switzerland: Ecole Polytechnique Fédérale de Lausanne. 2010:416.

[21] Jacobsen JS, Poulsen PN, Olesen JF. Characterization of mixed mode crack opening in concrete. *Materials and Structures* 2012; 45 (1–2):107–122.

[22] Sherwood EG, Bentz EC, Collins MP. Effect of Aggregate Size on Beam-Shear Strength of Thick Slabs. *ACI Structural Journal* 2007; 104 (2):180–190.

[23] Collins MP, Kuchma D. How safe are our large, lightly reinforced concrete beams, slabs, and footings? *ACI Structural Journal* 1999; 96 (4):482–490.

[24] Fernández Ruiz M, Mirzaei Y, Muttoni A. Post-punching behavior of flat slabs. *ACI Structural Journal* 2013; 110 (5):801–812.

[25] Fernández Ruiz M, Plumey S, Muttoni A. Interaction between Bond and Deviation Forces in Spalling Failures of Arch-Shaped Members without Transverse Reinforcement. *ACI Structural Journal* 2010; 107 (3):346–354.

[26] Reineck K, Bentz EC, Fitik B, Kuchma DA, Bayrak O. ACI-DAfStb Database of Shear Tests on Slender Reinforced Concrete Beams without Stirrups. *ACI Structural Journal* 2013; 110 (5):867–876.

[27] Fernández Ruiz M, Campana S, Muttoni A. Discussion of paper "Influence of Flexural Reinforcement on Shear Strength of Prestressed Concrete Beams" by E. I. Saquan and R. J. Frosch. *ACI Structural Journal* 2009; 106 (6):907–908.

[28]   Leonhardt F, Walther R. Schubversuche an einfeldrigen Stahlbetonbalken mit und ohne Schubbewehrung. DAfStb H.151, Berlin. 1962.

[29]   Kani MW, Huggins MW, Wittkopp RR. Kani on shear in reinforced concrete. Deptartment of Civil Engineering, University of Toronto, Toronto, Canada. 1979.

[30]   Bhal NS. Über den Einfluß der Balkenhöhe auf die Schubtragfähigkeit von einfeldrigen Stahlbetonbalken mit und ohne Schubbewehrung. Otto-Graf-Institut, H.35, Stuttgart. 1968.

[31]   Angelakos D, Bentz EC, Collins MP. Effect of Concrete Strength and Minimum Stirrups on Shear Strength of Large Members. *ACI Structural Journal* 2001; 98 (3):290–300.

[32]   Sherwood EG. One-way shear behaviour of large, lightly-reinforced concrete beams and slabs. PhD Thesis, Toronto, Canada: University of Toronto. 2008:547.

[33]   El-Sayed AK, El-Salakawy EF, Benmokrane B. Shear Strength of FRP-Reinforced Concrete Beams without Transverse Reinforcement. *ACI Structural Journal* 2006; 103 (2):235–243.

[34]   Adebar P, Collins MP. Shear Strength of members without transverse reinforcement. *Canadian Journal of Civil Engineering* 1996; 23 (1):30–41.

[35]   Ahmad SH, Khaloo AR, Poveda A. Shear Capacity of Reinforced High-Strength Concrete Beams. *ACI Structural Journal* 1986; 83:297–305.

[36]   Ahmad SH, Park F, El-Dash K. Web reinforcement effects on shear capacity of reinforced highstrength concrete beams. *Magazine of Concrete Research* 1995; 47 (172):227–233.

[37]   Aster H, Koch R. Schubtragfähigkeit dicker Stahlbetonplatten. *Beton- und Stahlbetonbau* 1974; 69 (11):266–270.

[38]   Lubell A, Sherwood T, Bentz E, Collins M. Safe Shear Design of Large Wide Beams. *Concrete International* 2004; 26 (1):62–78.

[39]   Bernander KG. An investigation of the shear strength of concrete beams without stirrups or diagonal bars, reinforced with high tensile steel with various rib patterns. In Proc., RILEM Symposium on Bond and Crack Formation in Reinforced Concrete. 1957:211–214.

[40]   Bresler B, Scordelis AC. Shear strength of reinforced concrete beams. *ACI Journal* 1963; 60 (1):51–74.

[41]   Cladera A, Marí A. Experimental study on high-strength concrete beams failing in shear. *Engineering Structures* 2005; 27 (10):1519–1527.

[42]   Cao S. Size Effect and the Influence of Longitudinal Reinforcement on the Shear Response of Large Reinforcement Concrete Members. PhD Thesis, Toronto, Canada: Univerisity of Toronto. 2001.

[43]   Cederwall K, Hedman O, Losberg A. Shear strength of partially prestressed beams with pretensioned reinforcement of high grade deformed bars. *Special Publication* 1974; 42:215–230.

[44]   Chana PS. Some aspects of modelling the behaviour of reinforced concrete under shear loading, Technical Report 43. *Cement and Concrete Association* 1981:22.

[45]   Chang TS, Kesler CE. Static and fatigue strength in shear of beams with tensile reinforcement. *ACI Journal* 1958; 54 (6):1033–1057.

[46]   Diaz de Cossio R, Siess CP. Behavior and strength in shear of beams and frames without web reinforcement. *ACI Journal* 1960; 31 (8):695–735.

[47]   Thorenfeldt, E., Drangsholt G. Shear capacity of reinforced high-strength concrete beams. *ACI Special Publications* 1990; 121:129–154.

[48]   Elzanaty AH, Nilson A., Slate FO. Shear capacity of reinforced concrete beams using high-strength concrete. *ACI Journal* 1986; 83 (2):290–296.

[49]   Feldman A, Siess CP. Effect of Moment Shear Ratio on Diagonal Tension Cracking and Strength in Shear of Reinforced Concrete Beams. Univ. of Illinois Civil Eng. Studies, Struct. Research Series No. 107. 1955.

[50]   Ferguson PM. Some implications of recent diagonal tension tests. *ACI Journal Proceedings* 1956; 53 (8):157–172.

[51]   Ghannoum WM. Size Effect on Shear Strength of Reinforced Concrete Beams. Department of Civil Engineering and Applied Mechanics, McGill University Montréal, Canada. 1995.

[52]   Grimm R. Einfluß bruchmechanischer Kenngrößen auf das Biege-und Schubtragverhalten hochfester Betone. *Deutscher Ausschuss fuer Stahlbeton* 1997; 477.

[53]   Hallgren M. Shear tests on reinforced high and normal strength concrete beams without stirrups, Dept. of Structural Engineering, Royal Institute of Technology, Stockholm, Sweden. 1994.

[54] Hamadi YD. Force transfer across cracks in concrete structures, PhD Thesis, London, UK: Polytechnic of Central London. 1976.

[55] Hanson JA. Tensile strength and diagonal tension resistance of structural lightweight concrete. *ACI Journal* 1961; 58 (7):1–40.

[56] Hedman O, Losberg A. Design of concrete structures with regard to shear forces. CEB Bulletin D'Information No. 126. 1978.

[57] Islam MS, Pam HJ, Kwan AKH. Shear capacity of high-strength concrete beams with their point of inflection within the shear span. *Proceedings of the Institution of Civil Engineers: Structures and Buildings.* 1998; 128:91–99.

[58] Johnson MK, Ramirez JA. Minimum Shear Reinforcement in Beams with Higher Strength Concrete. *ACI Structural Journal* 1989; 86 (4):376–382.

[59] Kani GNJ. How safe are our large reinforced concrete beams? *ACI Journal* 1967; 64 (3):128–141.

[60] Kawano H, Watanabe H. Shear strength of reinforced concrete columns – Effect of specimen size and load reversal. *Proceedings of the Second Italy-Japan Workshop on Seismic Design and Retrofit of Bridges* 1997:141–154.

[61] Kim J-K, Park Y-D. Shear strength of reinforced high strength concrete beam without web reinforcement. *1Magazine of Concrete Research* 1994; 46 (166):7–16.

[62] Krefeld WJ, Thurston CW. Studies of the shear and diagonal tension strength of simply supported R/C-beams. *ACI Journal* 1966; 63 (4):451–476.

[63] Küng R. Ein Beitrag zur Schubsicherung im Stahlbetonbau. Betonstahl in Entwicklung, H.33. Luxemburg: TOR-ISTEG Steel Corp. 1985:8–25.

[64] Kuhlmann U, Ehmann J. Versuche zur Ermittlung der Querkrafttragfähigkeit von Verbundplatten unter Längszug ohne Schubbewehrung. *Versuchsbericht, Mitteilung* 2001; 6X.

[65] Kuhlmann U, Zilch K, Ehmann J, Jähring A, Spitra F. Querkraftabtragung in Verbundträgern mit schlaff bewehrter und aus Zugbeanspruchung gerissener Stahlbetonplatte ohne Schubbewehrung- Mitteilungen. Institut für Konstruktion und Entwurf Stahl-, Holz-, und Verbundbau, Universität Stuttgart, Germany. 2002:109.

[66] Kulkarni SM, Shah SP. Response of reinforced concrete beams at high strain rates. *ACI Structural Journal* 1998; 95 (6):705–714.

[67] Laupa A, Siess CP, Newmark NM. The shear strength of simple-span reinforced concrete beams without web reinforcement. Research Series No. 52, University of Illinois at Urbana-Champaign, USA. 1953.

[68] Marti P, Pralong J, Thürlimann B. Schubversuche an Stahlbeton-Platten. IBK-Bericht No. 7305-2, ETH Zürich, Zürich, Switzerland. 1977.

[69] Mathey RG, Watstein D. Shear strength of beams without web reinforcement containing deformed bars of different yield strengths. *ACI Journal* 1963; 60 (2):183–207.

[70] Moody KG, Viest IM, Elstner RC, Hognestad E. Shear Strength of R.C. beams: Part 1 – Tests of Simple Beams. *ACI Journal* 1954; 26 (4):317–332.

[71] Morrow J, Viest IM. Shear Strength of Reinforced Concrete Frame Members Without Web Reinforcement. *ACI Journal* 1957; 53 (3):833–869.

[72] Mphonde AG, Frantz GC. Shear tests of high- and low- strength concrete beams without stirrups. *ACI Journal* 1984; 81:350–357.

[73] Niwa J, Yamada K, Yokozawa K, Okamura M. Revaluation of the equation for shear strength of R.C.-beams without web reinforcement. Proceedings JSCE No. 372/V-5 1986-8 Translation in: Concrete Library of JSCE, No. 9. 1987.

[74] Podgorniak-Stanik BA. he influence of concrete strength, distribution of longitudinal reinforcement, amount of transverse reinforcement and member size on shear strength of reinforced concrete members. PhD Thesis, Toronto, Canada: University of Toronto. 1998.

[75] Rajagopalan KS, Ferguson PM. Exploratory shear tests emphasizing percentage of longitudinal reinforcement. *ACI Journal* 1968; 65 (8):634–638.

[76] Regan PE. Shear in Reinforced Concrete – an experimental study. CIRIA-Report, a report to the Construction Research and Information Association. Imperial College of Science and Technology, Dep. of Civil Engineering, Concrete Section. 1971.

[77] Rehm G, Eligehausen R, Neubert B. Rationalisierung der Bewehrungstechnik im Stahlbetonbau. *Betonwerk + Fertigteil-Technik* 1978; 44:222–227.

[78] Reineck K-H, Koch R, Schlaich J. Shear tests on reinforced concrete beams with axial compression for offshore

structures. Institut für Massivbau, Universität Stuttgart, Stuttgart, Germany. 1978.

[79]   Remmel G. Zum Zugtragverhalten hochfester Betone und seinem Einfluß auf die Querkrafttragfähigkeit von schlanken Bauteilen ohne Schubbewehrung. PhD Thesis, Darmstadt, Germany: TH Darmstadt. 1991.

[80]   Rüsch H, Haugli FR, Mayer H. Schubversuche an Stahlbeton Rechteckbalken mit Gleichmassig Verteilter Belastung, Deutscher Ausschuss fur Stahlbeton, Heft 145, W. Ernst und Sohn, West Berlin. 1962.

[81]   Salandra MA, Ahmad SH. Shear Capacity of reinforced Lightweight High-Strength Concrete Beams. *ACI Structural Journal* 1989; 86 (6):697–704.

[82]   Scholz H. Ein Querkrafttragmodell für Bauteile ohne Schubbewehrung im Bruchzustand aus normalfestem und hochfestem Beton. Berichte aus dem Konstruktiven Ingenieurbau Heft 21, Technische Universität Berlin, Berlin, Germany. 1994.

[83]   Taylor HPJ. Shear stress in reinforced concrete beams without shear reinforcement. Cement and Concrete Ass., Techn. Rep. No.407. 1968.

[84]   Taylor HPJ. Shear strength of large beams. *ASCE Journal of Structural Division* 1972; 98:2473–2490.

[85]   Walraven JC. The influence of depth on the shear strength of lightweight concrete beams without shear reinforcement. Report S-78-4, Stevin Lab., Delft University, Delft, Netherlands. 1978.

[86]   Xie Y, Ahmad SH, Yu T, Hino S, Chung W. Shear Ductility of reinforced Concrete Beams of normal and high-strength concrete. *ACI Structural Journal* 1994; 91 (2):140–149.

[87]   Yoon Y-S, Cook WD, Mitchell D. Minimum Shear Reinforcement in Normal, Medium and High- Strength Concrete Beams. *ACI Structural Journal* 1996; 93 (5):576–584.

[88]   Yoshida Y. Shear Reinforcement for Large Lightly Reinforced Concrete Members. PhD Thesis, Toronto, Canada: University of Toronto. 2000.

[89]   Lubell A. Shear in wide reinforced concrete beams. PhD Thesis, Toronto, Canada: University of Toronto. 2006:455.

[90]   Thiele C. Zum Tragverhalten von Stahlbetonplatten ohne Querkraftbewehrung mit integrierten Leitungsführungen. PhD Thesis, Kaiserslautern, Germany: TU Kaiserslautern. 2010.

[91]   Winkler K. Querkraftversuche an maßstäblich skalierten, schubunbewehrten Stahlbetonbalken. Versuchsbericht 2011-1. Lehrstuhl für Massivbau, Ruhr Universität Bochum, Bochum, Germany. 2011:105.

[92]   Rosenbusch J. Zur Querkrafttragfähigkeit von Balken aus stahlfaserverstärktem Stahlbeton, TU Braunschweig, Braunschweig, Germany. 2003:199.

[93]   Tureyen AK, Frosch RJ. Shear tests of FRP-reinforced concrete beams without stirrups. *ACI Structural Journal* 2002; 99 (4):427–434.

[94]   Bentz EC, Buckley S. Repeating a classic set of experiments on size effect in shear of members without stirrups. *ACI Structural Journal* 2005; 102 (6):832–838.

[95]   Sneed LH, Ramirez JA. Influence of effective depth on shear strength of concrete beams - experimental study. *ACI Structural Journal* 2010; 107 (5):554–562.

Chapter 7   A closed-form equation for shear design of slender beams without transverse reinforcement

In this Chapter, the main assumptions of the refined theoretical approach presented in Chapter 6 are revised. Then, the mechanical model is extended and applied to members subjected to different boundary conditions. By applying the mechanical model to slender members subjected to different loading and support conditions, it can be observed that the failure criteria obtained by integration of stresses at the crack surface can be approximated by power-law equations. These power law failure criteria, in combination with the load-deformation relationship, allow deriving a closed-form equation. The latter is validated against available test data.

The derivation of a closed-form equation, on the basis of an improved failure criterion of the Critical Shear Crack Theory (proposed according to the results of Chapter 6), has been recently published in a paper for a new *fib* bulletin:

> Muttoni, A., Fernández Ruiz M., and Cavagnis F. (2016). Shear in members without transverse reinforcement: from detailed test observations to a mechanical model and simple expressions for codes of practice, *fib* International Workshop on Beam Shear, Zurich, Switzerland.

This closed-form equation has been proposed by Professor A. Muttoni and Dr. M. Fernández Ruiz for the new generation of Eurocode 2.

The closed-form equation derived in this Chapter presents some differences with respect to the closed-form equation of the proposal for the new Eurocode 2 and it is a more general formulation, being based on the mechanical model presented in this thesis.

7.1 Introduction

As shown in Chapter 2, shear design of one-way slabs and beams without shear reinforcement can be performed using different approaches. One physical model that accounts for all the shear-transfer actions is the Critical Shear Crack Theory (CSCT) [1, 2]. The CSCT is based on the assumption that the shear strength in members without transverse reinforcement is governed by the opening and roughness of the critical shear crack [1]. For the calculation of the shear strength of beams and one-way slabs without transverse reinforcement, Muttoni et al. [1] proposed a single hyperbolic failure criterion (see Figure 7.1):

$$\frac{V_c}{b \cdot d \cdot \sqrt{f_c}} = \frac{1/3}{1 + 120 \cdot \dfrac{\varepsilon \cdot d}{d_{dg}}} \tag{7.1}$$

where f_c is the cylinder compressive strength of concrete, d is the effective depth, d_{dg} refers to the roughness of the critical shear crack (for normal strength concrete, it is equal to d_g+16 mm, where d_g is the maximum aggregate size) and ε is a reference strain. Fernández Ruiz et al. [2], by means of an analytical integration of stresses at the critical crack surface, showed that the failure criterion of the CSCT reproduces the shape and parameters observed for the activation of all shear-transfer actions, thus validating the main hypotheses of the CSCT.
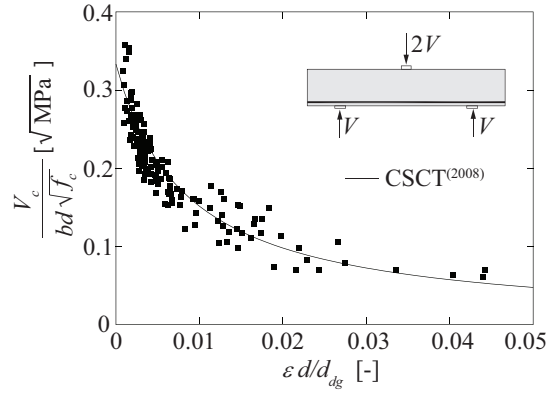
Figure 7.1 Failure criterion of the Critical Shear Crack Theory (CSCT) (refer to Muttoni et al. [1])

Following a similar approach to that of Fernández Ruiz et al. [2], assuming a realistic shape and kinematics of the critical shear crack (based on test measurements) and by integrating fundamental constitutive laws for cracked concrete in Mode I (residual tensile strength of concrete) and Mode I-II (aggregate interlock), for uncracked concrete (compression zone) and for the dowelling action, the contributions of the various shear-carrying mechanisms have been quantified and a shear strength criterion has been obtained summing the various contributions (refer to [3]). The calculation of the shear capacity can be thus performed iteratively, by intersecting the shear strength criterion and a load-deformation relationship. However, for practical purposes, the calculation of the failure criterion by means of integration of stresses at the crack surface is not convenient. Therefore, the possibility to derive a closed-form equation, on the basis of the results of the refined procedure, is shown.

In this Chapter, first the main assumptions of the mechanical model based on the integration of stresses along the critical shear crack are reviewed, illustrating the ability of the mechanical approach to account in a constituent manner the phenomena governing the shear capacity (Section 7.2). Then, on the basis of the mechanical model, a closed-form equation is derived (Section 7.3). The latter is shown to be simple, but capable of describing the role of the main mechanical parameters governing the shear strength (Section 7.4). Then, the mechanical model and the closed-form expression are validated for simply supported beams subjected to point loading without and with axial forces (Sections 7.4 and 7.5.1), simply supported beams subjected to distributed loading (Section 7.5.2), cantilevers and continuous beams subjected to distributed loading (Sections 7.5.3 and 7.5.4). Finally, the results of the mechanical model and the closed-form equation are compared to actual tests, showing the accuracy of the presented approaches (Sections 7.6 and 7.7).

7.2 Review of the mechanical model based on the development of the critical shear crack

In the following, the main assumptions and equations of the mechanical model originally introduced in [3], are briefly revised.

7.2.1 Failure criterion

Experimental evidences have shown that the critical shear crack originates from a quasi-vertical bending crack, which extends up to the neutral axis, followed by the development of a quasi-horizontal branch within the compression zone (Figure 7.2a, [4]). The critical shear crack can thus be idealized by a bilinear segment (segment A-B and segment B-F, refer to Figure 7.2b) representing the previous parts experimentally observed. The angle of segment A-B has been measured to be related to the moment-to-shear ratio a_A and it can be approximated by the following analytical equation (according to [5]):

$$\beta_{AB} = \frac{\pi}{4} \cdot \left(1 + \frac{\alpha_A^{1/3}}{3} \right) \tag{7.2}$$

where $\alpha_A = M_A / (V_A \cdot d)$, M_A and V_A refer respectively to the acting bending moment and shear force at the section at which the crack intercepts the longitudinal reinforcement and d is the effective depth of the member.
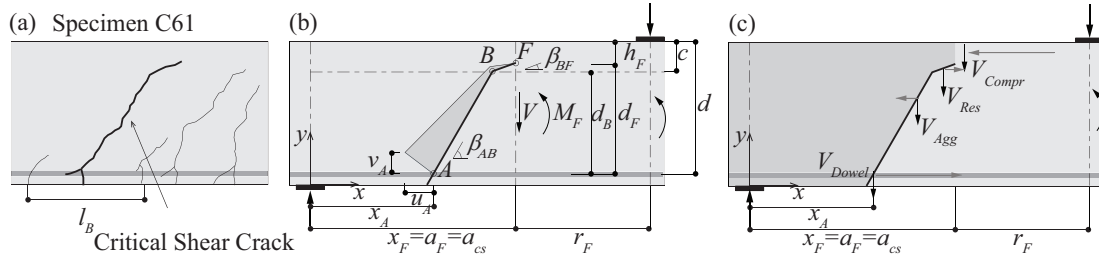
Figure 7.2 (a) Critical crack shape experimentally measured at peak load (specimen SC61, [4]); (b) kinematics and shape of the adopted critical shear crack; (c) equilibrium of the rigid body and internal forces

Segment A-B can be assumed to develop up to the neutral axis ($d_B=d-c$), in agreement with the experimental observations (Figure 7.2a), where c is the depth of the compression zone, calculated assuming a linear response of concrete in compression and neglecting concrete in tension. Segment B-F was observed to develop at a load level lower than the peak load. Its angle β_{BF} and its length l_F can be respectively assumed to be equal to $\pi/8$ and to $1/6d$, although a non-negligible scatter in the experimental tests has been observed [4]. With respect to the crack kinematics, detailed measurements allowed determining the sliding δ and the opening w between the lips of the crack at each point along the crack surface [4] and the location of the centre of rotation (which can be reasonably assumed to correspond to the tip of the critical shear crack, in agreement with [2]).

On the basis of the assumed shape and kinematics, using some suitable constitutive models for uncracked and cracked concrete and steel, the contribution of the various shear transfer actions can be calculated by integration of stresses throughout the crack surface and in the compression zone above the tip of the critical shear crack. A detailed description of the constitutive laws adopted for the various shear-transfer action can be found in [3]. Finally, the total shear strength can be obtained by vertical equilibrium of the rigid-body shown in Figure 7.2c [3]:

$$V_c = V_{Res} + V_{Agg} + V_{Dowel} + V_{Compr} = \frac{V_{Res} + V_{Agg} + V_{Dowel}}{1 - 0.5 \cdot h_F/r_F} \qquad (7.3)$$

where V_{Res}, V_{Agg}, V_{Dowel} and V_{Compr} are respectively the contribution of the residual tensile strength of concrete, the aggregate interlock, the dowelling action and the compression zone, h_F is the thickness of the compression zone above the tip of the critical shear crack ($h_F = d - d_F$) and r_F is the horizontal distance between the tip of the critical shear crack and the axis of load introduction (refer to Figure 7.2b).

7.2.2   Load-deformation relationship

As previously stated, the calculation of the shear strength requires defining a law that describes the load-deformation (load-crack crack opening) relationship during loading and at failure load. According to Muttoni et al. [1] a linear relationship between the acting bending moment and the strain at the level of the longitudinal reinforcement can be assumed:

$$\varepsilon_s = \frac{M_E}{A_s \cdot E_s \cdot z} \qquad (7.4)$$

where M_E refers to the bending moment at the control section, A_s to the reinforcement area, E_s to its elastic modulus and z to the inner level arm.

Following the experimental observations presented in [4, 5], it can be stated that the reinforcement strains ε_s are proportional to the acting bending moment at the section corresponding to the tip of the critical shear crack x_F (M_F), yielding $M_E=M_F$ (x_F will be referred hereafter as control section). For instance, for simply supported members subjected to point load, $M_F=V_F \cdot a_F$, where V_F ($=V_E$) is the acting shear force and a_F ($=a_{cs}$) is the moment-to-shear ratio (or shear span) at the control section x_F (see Figure 7.2b). Eq. (7.4) thus results:

$$\varepsilon_s = \frac{M_F}{A_s \cdot E_s \cdot z} = \frac{V_F \cdot x_F}{A_s \cdot E_s \cdot z} = \frac{V_F \cdot a_F}{A_s \cdot E_s \cdot z} = \frac{V_E \cdot a_{cs}}{A_s \cdot E_s \cdot z} \qquad (7.5)$$

Experimental measurements have shown that all cracks developing within a region of length l_B (Figure 7.2a) contribute to the opening of the critical shear crack and the sum of all cracks within this tributary length yields an almost linear horizontal profile

[5]. This tributary length has been observed to vary during loading and to be fairly constant at peak load and it can be approximated by:

$$l_B = d - c \tag{7.6}$$

According to the experimental measurements, the horizontal crack opening at the level of the reinforcement bars is proportional to the acting bending moment at section x_F and can therefore be assumed equal to the product of the tributary length l_B times the strains at the reinforcement level:

$$u_A = \varepsilon_s \cdot (d - c) = \frac{M_F}{A_s \cdot E_s} \cdot \frac{d-c}{d - c/3} \tag{7.7}$$

7.2.3 Evaluation of the shear capacity

Calculating the shear strength requires an iterative procedure that can be summarized in the following steps: (i) choose a location of the critical shear crack x_A; (ii) assume an initial horizontal opening u_A; (iii) calculate the contribution of the various shear-transfer actions and the shear strength as the sum of the shear carried by the various shear-carrying mechanisms (Eq. (7.3)); (iv) check that the shear force (defined in the load-deformation relationship) is equal or smaller than the shear capacity.

This approach is qualitatively shown in Figure 7.3a: when the shear force (defined by the load-deformation relationship) equals the shear capacity (defined by the failure criterion), failure occurs (intersection between Eq. (7.3) and Eq. (7.7)). In Figure 7.3a the failure criterion and the load-crack opening relationship are normalized to account for the width b, the effective depth d, the compressive strength f_c and are expressed in terms of $\varepsilon_s \cdot d/d_g$. This iterative procedure can be applied for any possible location of the critical shear crack and it allows determining the shear capacity, the deformation capacity, the role of the various shear-transfer actions and the theoretical governing location of the critical shear crack (the location where the shear capacity reaches its minimum value).
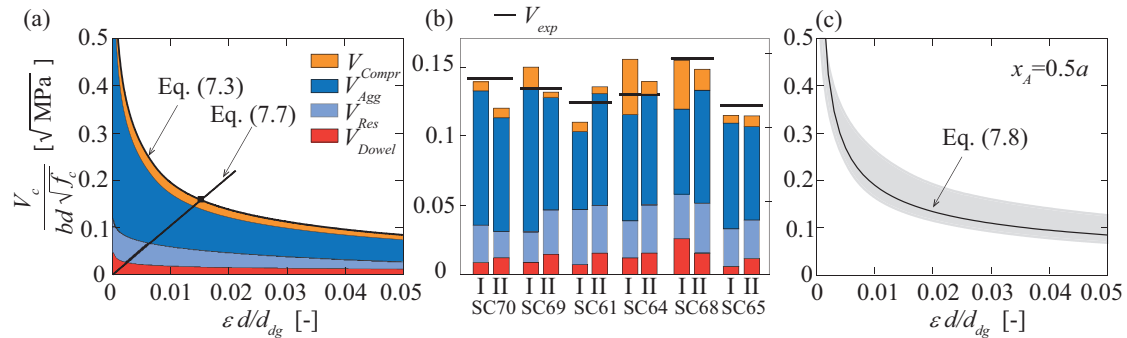
Figure 7.3 (a) Failure criterion and load-deformation relationship; (b) comparison of the shear-transfer actions calculated according to the mechanical model (II) with the ones calculated accounting for the shape and kinematics experimentally measured (I); (c) failure envelopes (Eq. (7.3)) for reinforced concrete beams subjected to point loading as a function of the reinforcement strains (results for specimens with compressive strength f_c 20-100 MPa, aggregate size d_g 8-32 mm, flexural reinforcement ratio ρ 0.5-3%, effective depth d 200-2000 mm, shear slenderness ratio a/d 3-8, assuming x_A=0.5a) and power-law failure criterion (Eq. (7.8))

Table 7.1 Comparison of calculated and experimental shear strengths and crack opening

Test	f_c [MPa]	a [mm]	d [mm]	ρ [%]	α_A [-]	$u_{A,mes}$ [mm]	$u_{A,calc}$ [mm]	$u_{A,mes}/u_{A,calc}$ [-]	$\frac{V_{exp}}{b \cdot d \cdot \sqrt{f_c}}$ [√MPa]	$\frac{V_{calc,xA}}{b \cdot d \cdot \sqrt{f_c}}$ [√MPa]	$V_{exp}/V_{calc,xA}$ [-]
SC70	33.3	3'850	556	0.886	4.87	1.09	0.94	1.16	0.142	0.120	1.18
SC69	32.9	3'150	556	0.886	1.76	0.53	0.45	1.18	0.134	0.132	1.01
SC61	35.3	2'450	556	0.886	1.30	0.34	0.39	0.87	0.125	0.136	0.92
SC64	35.6	1'750	556	0.886	1.17	(0.16)[I]	0.37	0.43	0.131	0.140	0.93
SC68	32.6	1'400	556	0.886	1.00	0.43	0.35	1.23	0.156	0.148	1.05
SC65	35.5	1'750	559	0.544	1.47	0.70	0.61	1.15	0.123	0.114	1.08

[I] Failure driven by the development of a localized aggregate interlocking crack (crack type E', refer to [5])

In Figure 7.3b the shear capacity and the contribution of the various shear transfer actions at failure load obtained by applying Eq. (7.3) and Eq. (7.7) (II in Figure 7.3b) are compared to the ones calculated using the kinematics and shape of the critical shear crack experimentally measured (I in Figure 7.3b, refer to Chapter 5). For these cases, the refined procedure is applied at

the experimentally measured location of the critical shear crack (x_A). In Figure 7.3b and in Table 7.1, it can be observed that the refined approach allows estimating the relative significance of the various shear-transfer actions, the shear resistance and the horizontal crack opening at failure load. However, it can be noted that, for some cases, although the shear capacity is correctly predicted, the calculated crack opening is slightly lower than the measured one: this result is due to the assumed length of the quasi-horizontal branch ($l_F=d/6$), which represents a lower-bound value of the length l_F experimentally measured [4].

With respect to the theoretical governing location of the critical shear crack, parametric analyses have shown that the shear capacity is almost constant for values of x_A within the region $0.4a$ - $0.6a$ and at a distance between $1.5d$ and $2.25d$ from the axis of load introduction [3]. Assuming that the critical shear crack develops at $x_A=0.5a$, it can be observed that shear failures occur in a narrow band (see Figure 7.3c) when extreme values of the various mechanical and geometrical parameters are assumed (aggregate size d_g ranging 8 - 32 mm, compressive strength f_c ranging 20 - 100 MPa, flexural reinforcement ratio ρ ranging from 0.5 - 3%, shear slenderness ratio a/d ranging 2.5 - 8 and effective depth d ranging from 200 to 2000 mm). Therefore, the failure band can be described by a failure criterion, whose shape can be approximated by a power-law expression:

$$\frac{V_c}{b \cdot d \cdot \sqrt{f_c}} = k \cdot \left(\frac{d_{dg}}{\varepsilon_s \cdot d} \right)^{1/2} \tag{7.8}$$

where d is the effective depth, f_c is the compressive strength of concrete, ε_s is the reinforcement strain (refer to Eq. (7.5)), and $d_{dg} = 16 + d_g$ accounts for the average roughness of the critical shear crack (with d_g equal to the maximum aggregate size). A correction on the aggregate size equal to $d_g \cdot (60/f_c)^2$ is introduced for high-strength concrete (in agreement to Collins et al. [6]) and d_{dg} is limited to 40 mm (in agreement to Sherwood et al. [7]). According to the analyses in Figure 7.3c, a decay of the shear strength is observed for increasing openings of the critical shear crack, in agreement to the fundamental hypothesis of the CSCT. In addition, Figure 7.3c shows that different analytical expressions approximating the failure band can be selected and that, although a hyperbolic failure criterion reproduce the shape of the failure region, its accuracy can be enhanced with a power-law expression for low values of crack openings.

The coefficient k depends on the main mechanical and geometrical parameters (reinforcement ratio ρ, slenderness ratio a/d, compressive f_c, effective depth d and shear slenderness ratio α_A). However, as shown in Figure 6.11, when the critical shear crack is assumed to develop at mid-span ($x_A=0.5a$), its value may be eventually assumed constant and equal to 0.019 for 635 beams (data from Reineck et al. [8] completed with the tests by Cavagnis et al. [5]).

The power-law failure criterion, in combination the load-deformation relationship, allows a direct calculation of the shear strength without the need of performing a full integration of the various shear-transfer actions throughout the critical shear crack surface: this can be done iteratively by intersecting the load-deformation relationship (Eq. (7.5)) and the power law failure criterion (Eq. (7.8)).

7.3 Development of a closed-form equation based on the mechanical model

Although the use of Eq. (7.5) and Eq. (7.8) is quite straightforward and simple, the calculation of the shear capacity requires still an iterative procedure.

In the following, it is shown that combining the power-law failure criterion with the load-deformation relationship, a closed-form equation can be obtained. By introducing the value of the reinforcement strain of Eq. (7.5) into Eq. (7.8), and assuming that at failure the acting shear force is equal to the shear capacity ($V_E=V_c$), the shear strength results:

$$V_c = k \cdot b \cdot d \cdot \left(\frac{f_c \cdot d_{dg}}{\varepsilon_s \cdot d} \right)^{1/2} = k \cdot b \cdot d \cdot \left(\frac{b \cdot \rho \cdot E_s \cdot z}{V_c \cdot a_{cs}} \cdot f_c \cdot d_{dg} \right)^{1/2} \tag{7.9}$$

which leads to:

$$V_c = k^{2/3} \cdot b \cdot d \cdot \left(\frac{\rho \cdot E_s \cdot z}{a_{cs} \cdot d} \cdot f_c \cdot d_{dg} \right)^{1/3} \tag{7.10}$$

where a_{cs} is the moment-to-shear ratio M_E/V_E at the control section, which for simply supported members corresponds to the distance x_F from the end support (refer to Figure 7.2b). This expression can be written for steel reinforcement bars ($E_s = 200'000$ MPa), assuming $z=0.9d$, in the following manner:

$$V_c = \kappa \cdot \left(100\rho \cdot f_c \cdot \frac{d_{dg}}{a_{cs}}\right)^{1/3} \cdot b \cdot d \tag{7.11}$$

where $\kappa = k^{2/3} \cdot (0.9 \cdot 2000)^{1/3}$. According to Eq. (7.11), the shear strength depends on the control section shear span a_{cs}, the concrete type (aggregate size d_g), the concrete strength f_c, the flexural reinforcement ratio ρ and the coefficient κ. The coefficient κ can be directly obtained from the mechanical model by equating Eq. (7.11) and Eq. (7.3):

$$\kappa = \frac{1}{1 - 0.5 \cdot h_F / r_F} \cdot \frac{V_{Res} + V_{Agg} + V_{Dowel}}{\left(100 \cdot \rho \cdot f_c \cdot \frac{d_{dg}}{a_{cs}}\right)^{1/3} \cdot b \cdot d} = k_c \cdot k_a \tag{7.12}$$

where $k_c = \dfrac{1}{1 - 0.5 \cdot h_F / r_F}$ and $k_a = \dfrac{V_{Res} + V_{Agg} + V_{Dowel}}{\left(100 \cdot \rho \cdot f_c \cdot \frac{d_{dg}}{a_{cs}}\right)^{1/3} \cdot b \cdot d}$.

With respect to k_c, r_F is the distance between the control section and the axis of load introduction (for simply supported beams subjected to point loading $r_F = a - x_F$, where a is the shear span of the member), and h_F is the vertical distance between the tip of the critical shear crack and the top compression fibre (refer to Figure 7.2b). On the basis of the refined approach, h_F varies between $0.2d$ (for reinforcement ratio ρ lower than 1%) and $0.4d$ (for reinforcement ratio ρ larger than 3%) and it can be reasonably assumed, in the following, equal to $0.3d$.

The coefficient k_a (see Figure 7.4) can be calculated according to Eq. (7.12) for each possible critical shear crack developing within the shear span a. In particular, the contribution of residual tensile strength of concrete (V_{Res}) and aggregate interlock (V_{Agg}) can be obtained by integration of stresses at the crack surface, adopting the constitutive laws presented in [3]. With respect to the dowelling action (V_{Dowel}), its contribution can be expressed in a general manner as [9]:

$$V_{Dowel} = k_b \cdot f_{ct} \cdot n \cdot (b/n - d_b) \cdot 2d_b \tag{7.13}$$

where k_b is a strength reduction factor, b is the width of the section, n is the number of bars and d_b is the diameter of the reinforcing bars. In the following analyses in order to facilitate comparisons between specimens with different geometrical and mechanical properties, the bar spacing will be assumed equal to $3d_b$. Based on this assumption, the dowel capacity results:

$$V_{Dowel} = 5 \cdot k_b \cdot f_{ct} \cdot \rho \cdot b \cdot d \tag{7.14}$$

where k_b is defined as in [3]:

$$k_b = 0.063 \cdot \left(\frac{1}{\varepsilon_s}\right)^{1/4} = 0.063 \cdot \left(\frac{d - c}{u_A}\right)^{1/4} \tag{7.15}$$

It shall be noted that Eq. (7.14) provides a lower bound solution for the dowelling action, since the spacing between flexural bars is normally higher ($\approx 5d_b$).

The value of k_a is shown in Figure 7.4a-d for each possible control section shear span a_{cs} for some simply supported beams subjected to point load, varying the main mechanical (compressive strength of concrete f_c (Figure 7.4a) and flexural reinforcement ratio ρ (Figure 7.4b)) and geometrical parameters (effective depth d (Figure 7.4c) and shear slenderness ratio a/d (Figure 7.4d)). It can be noted that an increase of the control section shear span a_{cs} leads to an increase of k_a, and almost all the other geometrical and mechanical parameters have a negligible influence on its value. k_a can be thus approximated by the following analytical equation:

$$k_a = 0.5 + 0.2 \cdot \alpha_{cs}^{1/3} \tag{7.16}$$

where α_{cs} ($= a_{cs}/d$) is the shear slenderness ratio at the control section x_F. Note that Eq. (7.16) slightly overestimates the calculated value of k_a for a_{cs}/d lower than 1.5 and underestimates its value of a_{cs}/d larger than 5 (see Figure 7.4a). However, with the purpose of describing k_a in a simple way, Eq. (7.16) is assumed in the following.

f_c = 30 MPa d_g = 16 mm b = 0.25 m d = 0.50 m a/d = 5 ρ = 1.0%
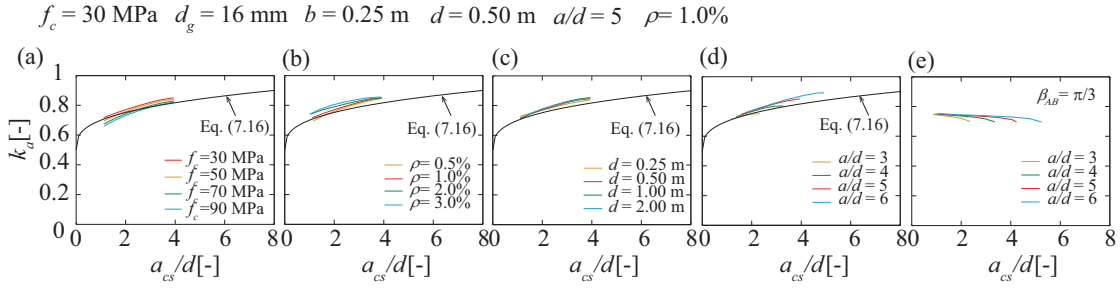
Figure 7.4 Coefficient k_a: (a) influence of the compressive strength f_c; (b) reinforcement ratio ρ; (c) effective depth d; (d) slenderness ratio a/d. (e) k_a calculated assuming a fixed angle β_{AB} (for instance equal to $\pi/3$) for each possible location of the critical shear crack

It shall be noted that in the analyses shown in Figure 7.4a-d, the various shear-transfer actions (V_{Res}, V_{Agg} and V_{Dowel}), and thus the values of k_a, are calculated for each possible location of the critical shear crack x_A, following the main steps of the mechanical model presented in [3], thus assuming the angle β_{AB} as defined in Eq. (7.2). In Figure 7.4e, the same analyses are performed for members with different shear span-to-effective depth ratio a/d, assuming a constant angle β_{AB} (for instance equal to $\pi/3$ for each possible location of the critical shear crack): it can be noted that whether the angle β_{AB} is assumed constant, the trend of k_a with respect to the control section shear span a_{cs} cannot be observed. On this basis, it can be stated that the coefficient k_a accounts for the influence of the angle β_{AB} of the critical shear crack on the contribution of the various shear-transfer actions. By substituting Eq. (7.16) into Eq. (7.12) and assuming h_F equal to 0.3d, as previously stated, the value of κ results:

$$\kappa = k_c \cdot k_a = \left(\frac{1}{1 - 0.15 \cdot d/r_F} \right) \cdot \left(0.5 + 0.2 \cdot \alpha_{cs}^{1/3} \right) \tag{7.17}$$

It can be noted that, if the critical shear crack is assumed to develop at x_A=0.5a (in agreement to Cavagnis et al. [3]), its tip is located approximately at $x_F \approx x_A + 0.5d$, leading to $a_{cs} \approx 0.5a + 0.5d$. The calculated value of κ according to Eq. (7.17) for 635 rectangular concrete beams without shear reinforcement (database from Reineck et al.[8], completed with the tests by Cavagnis et al. [5]), assuming a_{cs}=0.5a+0.5d is on average equal to 0.87. The almost constant value of κ is consistent with the previous observations on the coefficient k in the power-law failure criterion (Eq. (7.8)), which can be assumed constant for simply supported beams subjected to point load, despite the scattered values of the main mechanical and geometrical parameters in the database.

Finally, by introducing Eq. (7.17) into Eq. (7.11), the closed-form equation can be written in the following manner:

$$V_c = k_c \cdot k_a \cdot \left(100 \cdot \rho \cdot f_c \cdot \frac{d_{dg}}{a_{cs}} \right)^{1/3} \cdot b \cdot d \tag{7.18}$$

where V_c is the shear capacity at the control section x_F, a_{cs} is the moment-to-shear ratio at the control section x_F and k_c and k_a are defined in Eq. (7.17). Eq. (7.18) is a general formulation that allows evaluating the shear capacity in a compact manner without the need of an iterative procedure. In addition, it accounts intrinsically, through the coefficient κ, for the different failure criteria obtained by integration of the shear-transfer actions at the different potential location of the critical shear crack.

7.4 Discussion on the closed-form equation for simply supported member subjected to point loading

Figure 7.5 illustrates a comparison between the shear capacity calculated according to the general procedure (Eq. (7.3) + Eq. (7.7), continuous lines) and according to the closed-form equation (Eq. (7.18), dashed lines) for different simply supported members subjected to point loading, varying the slenderness ratio a/d, the reinforcement ratio ρ, the effective depth d and the compressive strength of concrete f_c. Figure 7.5a shows the shear capacity and the contribution of the different shear-transfer actions, for each potential control section x_F, for a selected simply supported beam subjected to point loading (a/d=5, d=500 mm, ρ=1.00%, f_c=30 MPa, d_g=16 mm). It is interesting to note that the closed-form equation provides almost identical results to the more refined calculation based on the integration of stresses along the critical shear crack surface (Eq. (7.3) + Eq. (7.7)), and it is able to capture in a simple manner the role of the various shear-transfer actions.
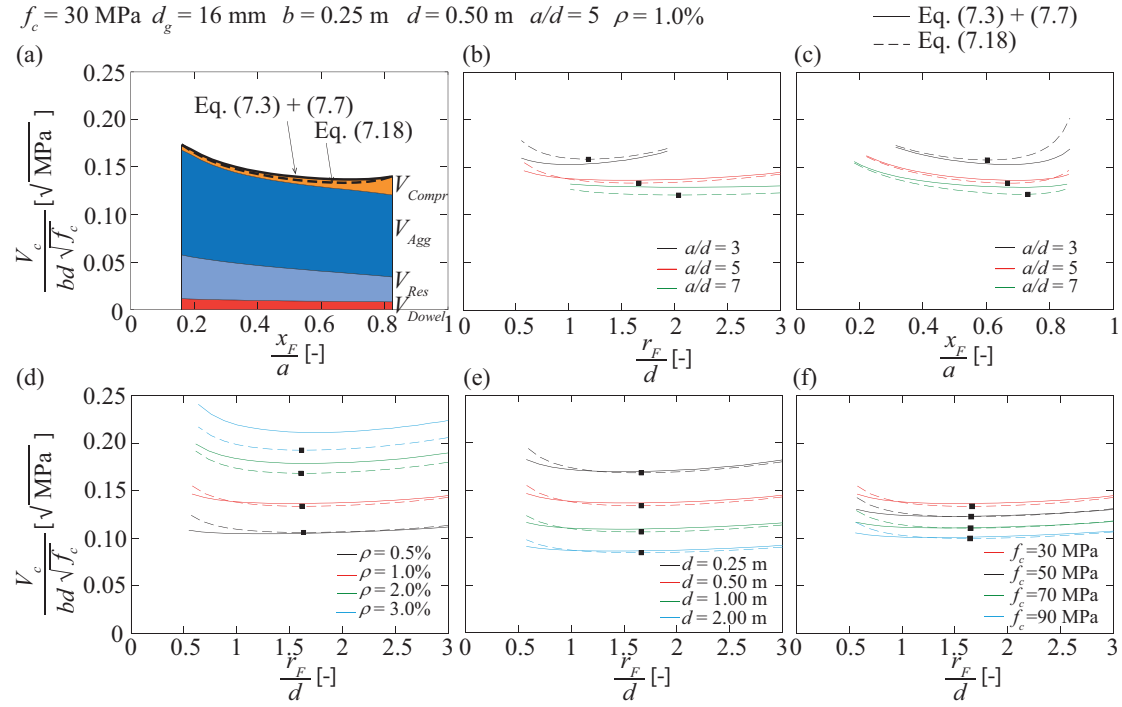
Figure 7.5 Normalized shear strength as a function of the position of the critical shear crack: (a) contribution of the shear-transfer actions for different section x_F; (b-c) influence of the slenderness ratio a/d, (d) the reinforcement ratio ρ, (e) the effective depth d and (f) the compressive strength f_c on the theoretical governing location of the critical shear crack: comparison between the mechanical model (Eq. (7.3) + Eq. (7.7)) and the closed-form expression (Eq. (7.18))

Concerning the influence of the investigated parameters (Figure 7.5b-f), it can be observed that the closed-form equation slightly overestimates the shear capacity, compared to the one calculated using the refined approach (Eq. (7.3) and Eq. (7.7)), for beams with a shear-slenderness ratio a/d lower than 3 (refer to Figure 7.5b and Figure 7.5c). On the contrary, it underestimates the shear strength for members with a shear span larger than $7d$ and with a reinforcement ratio ρ larger than 2% (refer to Figure 7.5b-d). These trends are a consequence of the previous assumptions (i) on the thickness of the compression zone h_F (which is assumed constant and equal to $0.3d$ for all members, although its value shows a dependency on the depth of the compression zone c and on the reinforcement ratio ρ) and (ii) on the analytical equation that defines the coefficient k_a (for $a/d>6$, Eq. (7.16) slightly underestimates the value of k_a obtained by integration of the different shear-transfer actions, refer to Eq. (7.12) and Figure 7.4d).

Eq. (7.18) allows also investigating the theoretical governing location of the critical shear crack. In Figure 7.5b-f it can be noted that the curves representing the shear strength are very flat around the minimum (black markers), which corresponds to values of r_F between d and $2d$ from the axis of load introduction (Figure 7.5b) and of x_F within the interval $0.5a$ and $0.75a$ (Figure 7.5c). Adopting a fixed control section within this region is thus sufficient for calculating the shear strength. For design purposes, it is convenient to define the control section at a fixed distance from a static or geometric discontinuity, and therefore in agreement with the previous observations (refer to Figure 7.5), it is proposed to calculate the shear strength at a control section located at a distance d from the axis of load introduction ($r_F=d$ and $x_F=a-d$).

In Figure 7.6, the shear strengths calculated according to the original formulation of the CSCT assuming the control section at $a-d/2$ (red lines), the refined approach (Eq. (7.3) + Eq. (7.7)) assuming the critical shear crack developing at $x_A=0.5a$ (in agreement to [3], black lines), and the closed-form equation (Eq. (7.18)) assuming the control section $x_F=a-d$ (black dashed lines) are compared to the tests results of different experimental campaigns that investigate the influence of the shear span-to-effective depth ratio a/d, the longitudinal reinforcement ρ, the effective depth d, the compressive strength f_c and the aggregate size d_g. The comparison shows that the three approaches have similar trends and that the closed-form equation, despite its simplicity, yields good estimates of the shear capacity.
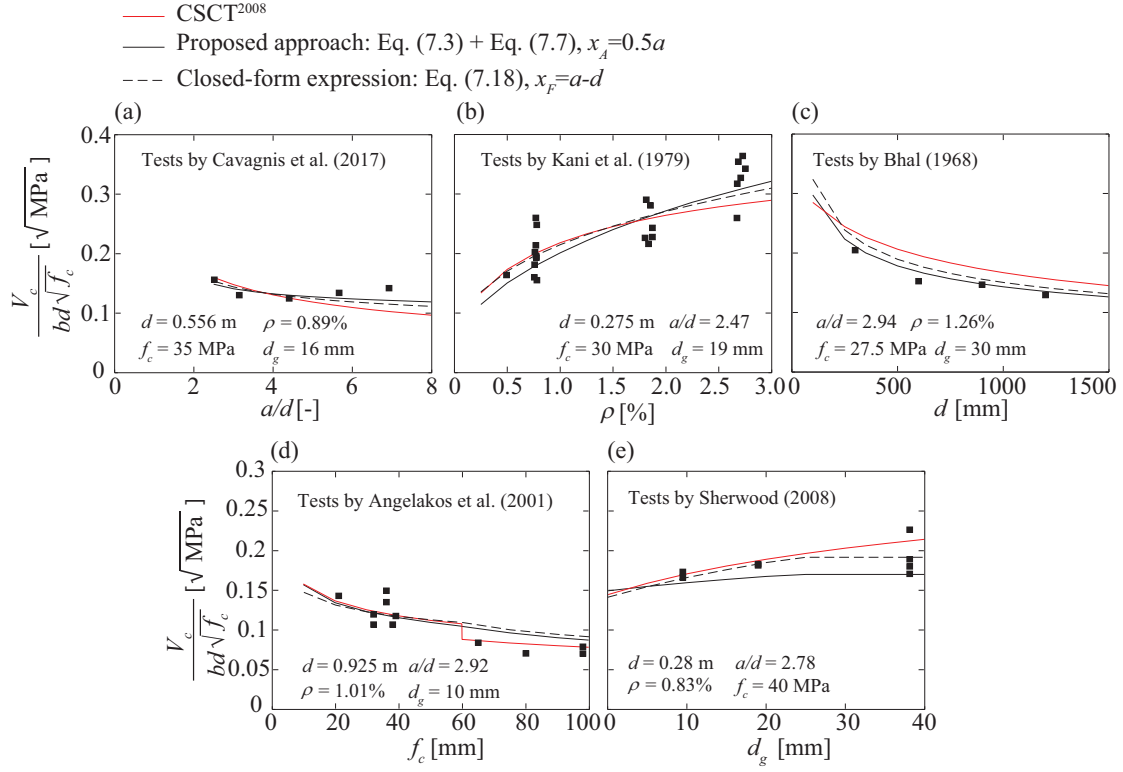
Figure 7.6 Comparison of CSCT [1], Eq. (7.3) + Eq. (7.7) and Eq. (7.18) for various test series varying the main mechanical and geometrical parameters: (a) tests by Cavagnis et al. [5]; (b) tests by Kani et al. [10]; (c) tests by Bhal [11]; (d) tests by Angelakos et al. [12]; (e) tests by Sherwood [13]

7.5 Applications of the mechanical model and the closed-form equation to members subjected to different loading conditions

The refined approach (Eq. (7.3) + Eq. (7.7)) and the closed-form equation (Eq. (7.18)) can be easily extended to general or more complex cases and different loading conditions, by accounting for the influence of the main mechanical parameters (e.g. control section shear span, reinforcement activation…) on the shear strength.

In the following, applications to simply supported members subjected to axial forces, simply supported beams subjected to distributed loading, cantilever and continuous beams subjected to distributed loading will be presented.

7.5.1 Applications to simply supported members subjected to point loading and axial forces

It is generally recognized that the shear strength of reinforced concrete members without transverse reinforcement can be enhanced by the presence of axial compression forces. The presence of compressive normal forces has been experimentally observed to influence the crack pattern and the development of the critical shear crack, which propagates at a higher load level and at a lower angle than in similar members without axial compression [14]. On the contrary, when axial tension is applied, the shear strength is reduced. A typical crack pattern for members subjected to axial tension is characterized by very steep flexural cracks followed by the development of a quasi-horizontal branch [15].
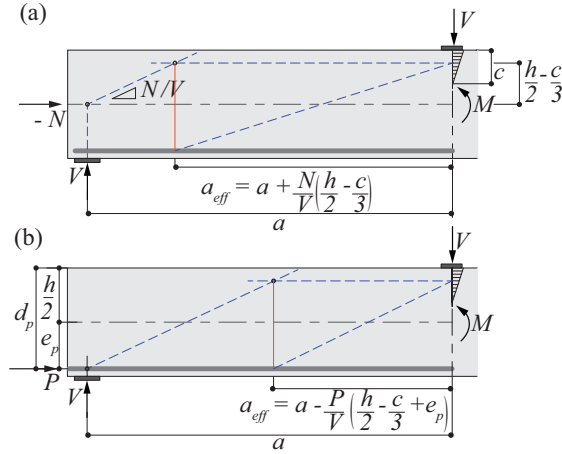
Figure 7.7 Equilibrium of internal forces and definition of a_{eff} for a reinforced concrete beam without shear reinforcement subjected to axial compression forces or prestressing (compressive forces in blue and tensile forces in red)

Fernández Ruiz et al. [16] observed that, in members subjected to axial compression, the amount and layout of axial compression may significantly shorten the effective shear span a_{eff}, which is necessarily smaller than the geometric one. The physical meaning of the effective shear span a_{eff} is described in Figure 7.7. The effective shear span for members subjected to axial compression (Figure 7.7a) shall be evaluated as follows:

$$a_{eff} = a + \frac{N}{V} \cdot \left(\frac{h}{2} - \frac{c}{3} \right) \approx a + \frac{N}{V} \cdot \frac{d}{3} \tag{7.19}$$

where N is the normal force ($N < 0$ for compression), h is the height of the beam and c is the depth of the compression zone.

For members subjected to axial tension, the amount of axial tension may increase the effective shear span a_{eff}, which is proposed to be evaluated in agreement with [1] as:

$$a_{eff} = a + \frac{N}{V} \cdot \left(\frac{h}{2} - d' \right) \approx a + \frac{N}{V} \cdot \frac{d}{3} \tag{7.20}$$

where N is the normal force ($N > 0$ for tension).

When effects of prestressing are considered as an external action (Figure 7.7b), Eq. (7.19) shall be replaced by:

$$a_{eff} = a - \frac{P}{V} \cdot \left(\frac{h}{2} - \frac{c}{3} + e_p \right) \approx a - \frac{P}{V} \cdot \left(\frac{d}{3} + e_p \right) \tag{7.21}$$

where P refers to the prestressing force after losses ($P > 0$) and e_p refers to the eccentricity of the tendons to the centroid of the cross-section (positive on the tension side). For prestressed members with tendons, the effective depth d and the reinforcement ratio ρ shall be calculated as follows:

$$d = \frac{d_s^2 \cdot A_s + d_p^2 \cdot A_p}{d_s \cdot A_s + d_p \cdot A_p} \tag{7.22}$$

and

$$\rho = \frac{d_s^2 \cdot \rho_s + d_p^2 \cdot \rho_p}{d^2} \tag{7.23}$$

It is important to mention that only members with $a_{eff}/d \geq 2.5$ behave as slender beams and can be satisfactorily estimated by the theoretical approach presented in this study [1]. In Eq. (7.19), Eq. (7.20) and Eq. (7.21), $h/2-c/3$ and $h/2-d'$ can be eventually approximated to be equal to $d/3$.

In a general manner, it can be noted that when axial compression forces are applied, both a_{eff}/d and β_{AB} decrease (β_{AB} is calculated according to Eq. (7.2), where a_A is defined assuming the shear span equal to the effective shear span a_{eff}): although a lower angle β_{AB} yields a reduction of the shear capacity, the latter increases since the decrease of a_{eff}/d determines an increase of the shear strength which prevails on the global response. On the contrary, when axial tension forces are applied, both the effective shear span-to-effective depth ratio a_{eff}/d and the angle β_{AB} increase (in agreement with the cracking patterns experimentally observed [15]) and the shear capacity decreases: despite a larger β_{AB} causes an increase of the shear capacity, the combined increase of a_{eff}/d and β_{AB} determines a reduction of the shear strength.

The closed-form equation can be applied to members subjected to axial compression or tension forces, by suitably evaluating the effective control section shear span $a_{cs,eff}$, which is directly derived from Eq. (7.19), Eq. (7.20) and Eq. (7.21). In the presence of normal forces the effective control section shear span $a_{cs,eff}$ can be approximated to:

$$a_{cs,eff} = a_{cs} + \frac{N}{|V|} \cdot \frac{d}{3} = \frac{M}{V} + \frac{N}{|V|} \cdot \frac{d}{3} \tag{7.24}$$

where $N>0$ refers to tension forces and a_{cs} is the moment-to-shear ratio at the control section x_F. The control section x_F can be assumed to be located at a distance d from the point of load introduction (in agreement with the case of simply supported beams subjected to point loading without axial forces, refer to Section 7.4), yielding $a_{cs,eff}=a_{eff}-d$.

When prestressing is considered as an internal action, Eq. (7.24) shall be replaced by:

$$a_{cs,eff} = a_{cs} - \frac{P}{|V|} \cdot \left(e_p + \frac{d}{3}\right) = \frac{M}{V} - \frac{P}{|V|} \cdot \left(e_p + \frac{d}{3}\right) \tag{7.25}$$

It can be mentioned that when axial compression forces are applied, both $a_{cs,eff}$ and k_a (calculated according to Eq. (7.16), with $\alpha_{cs}=\alpha_{cs,eff}$) decrease and the shear capacity increases: although a smaller k_a is associated to a decrease of the shear strength, the reduction of the effective control section shear span $a_{cs,eff}$ yields an increase of the shear strength. On the contrary, when axial tension forces are applied, both $a_{cs,eff}$ and k_a increase and despite a higher k_a yields an increase of the shear capacity, the latter decreases since the influence of $a_{cs,eff}$ is predominant on the global response.

Figure 7.8a and b illustrate a comparison of the calculated shear strength according to the original formulation of the CSCT (red lines), the refined approach (Eq. (7.3) + Eq. (7.7)) assuming the critical shear crack developing at $x_A=0.5a_{eff}$ (in agreement to [3], black lines) and Eq. (7.18) (black dashed lines) assuming the control section located at $x_F=a_{eff}-d$ against the test results by Madsen et al. [17] and Jørgensen et al. [15]. It can be observed that the three approaches have similar trends and correctly describe the influence of compressive and tensile stresses on the shear capacity.
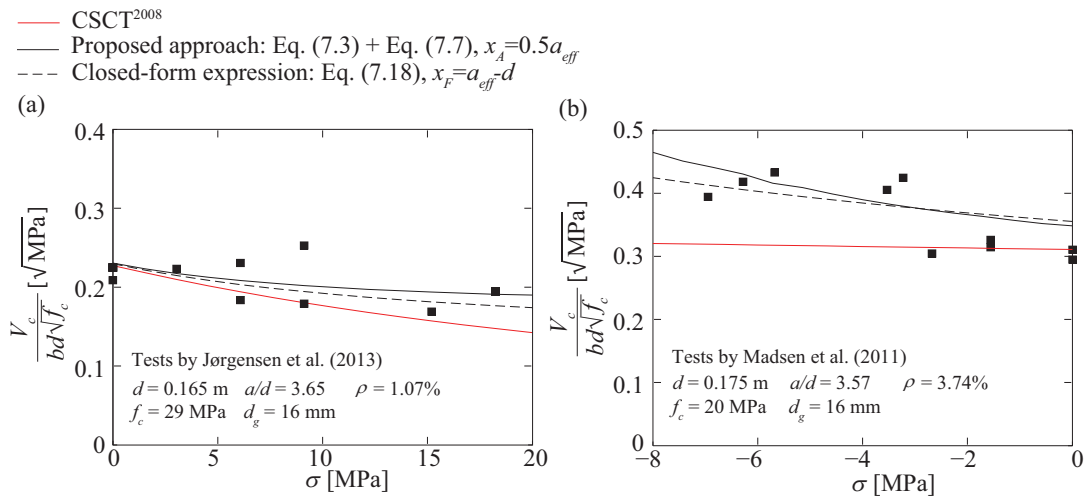
Figure 7.8 Comparison of shear strength according to the CSCT [1], Eq. (7.3) + Eq. (7.7) and Eq. (7.18), assuming $a=a_{eff}$ and $a_{cs}=a_{c,seff}$: (a) tests by Jørgensen et al. [15] ($\sigma>0$ tension) and (b) tests by Madsen et al. [17] ($\sigma<0$ compression)

7.5.2   Applications to simply supported members subjected to distributed loading

The shear behaviour of reinforced concrete beams without shear reinforcement subjected to uniformly distributed load has been investigated in several studies [18–20]. Experimental evidences have shown that the behaviour of beams with $l/d > 10$, whose failure is driven by the loss of the beam-shear transfer actions capacity, is different from that of beams with $l/d < 10$, whose failure occurs due to crushing of uncracked concrete above the tip of the critical crack [21]. Therefore, only members with $l/d > 10$ are considered in the present study.

Following the same procedure described for simply supported beams subjected to point loading, the various shear-transfer actions can be calculated in order to satisfy the equilibrium of the rigid body shown in Figure 7.9: it can be noted that the bending moment and the shear force are both calculated at the section corresponding to the tip of the critical shear crack (x_F).
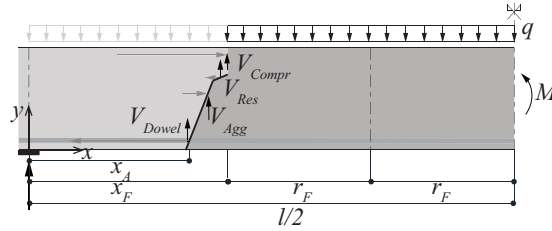
Figure 7.9 Simply supported beam subjected to distributed loading: free-body equilibrium, internal forces and definition of r_F

With respect to the crack shape, the angle β_{AB} of segment A-B of the critical shear crack is defined according to Eq. (7.2), where α_A is equal to:

$$\alpha_A = \frac{M_A}{V_A \cdot d} = \frac{x_A}{d} \cdot \frac{l - x_A}{l - 2 \cdot x_A} \tag{7.26}$$

and r_F can be assumed (refer to Figure 7.9):

$$r_F = \frac{\left(l/2 - x_F\right)}{2} \tag{7.27}$$

The load-crack opening relationship shall be calculated as in Eq. (7.7), where:

$$M_F = q \cdot \left(\frac{l}{2} \cdot x_F - \frac{x_F^2}{2} \right) \tag{7.28}$$

and the failure load q by equilibrium of the rigid body is:

$$q = \frac{V_{Res} + V_{Agg} + V_{Dowel} + V_{Compr}}{l/2 - x_F} \tag{7.29}$$

The location of the theoretical governing critical shear crack can be determined as the section where the shear capacity equals the value of the shear force. For these members, close to the support, the shear force is high and the bending moment is low, whereas close to the mid-span, the bending moment is maximal and the shear force is minimal. Therefore, the moment-to-shear ratio increases more rapidly than in the case of simply supported beams subjected to concentrated load. This fact indicates that the critical shear crack shall develop closer to the end support than in the case of beams subjected to point loading [1].

In Figure 7.10a, the contribution of the various shear-transfer actions are shown for a typical case (l/d =15, ρ =1.00%, f_c=30 MPa, d=500 mm, b=250 mm) at each possible location of the critical shear crack x_F. The analyses show that the contribution of aggregate interlock is governing, whereas the contribution of the compression zone is almost negligible. It can be also observed that for cracks developing close to the support (low values of x_F) the contribution of the residual tensile strength of concrete plays a more significant role than for cracks developing close to mid-span, where its contribution is reduced.

The influence of the location of the critical section on the load capacity q is investigated in Figure 7.10b and c for members with different slenderness ratio l/d. It can be noted that the governing control section x_F is located where the shear strength is tangent to the shear force, and it is approximately located at $0.1l$ from the support (Figure 7.10b). Moreover, the onset of the

critical crack x_A can be observed to vary between $0.5d$ (for $l/d<12$) and $1.5d$ (for $l/d>18$), and the curves representing the load capacity are very flat around the minimum (black markers in Figure 7.10c). For these cases, adopting a fixed control section x_A within this interval is sufficient for calculating the shear strength. To that aim, a value of $x_A=d$ is a reasonable assumption.

$f_c = 30$ MPa $d_g = 16$ mm $b = 0.25$ m $d = 0.50$ m $l/d = 15$ $\rho = 1.0\%$
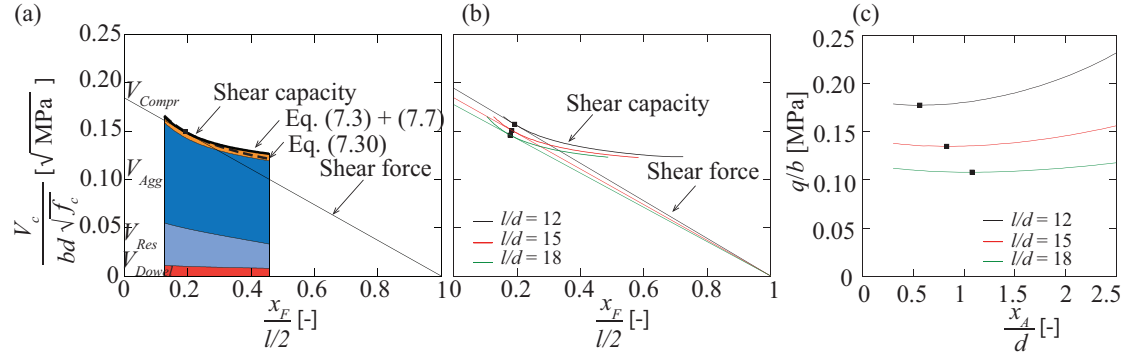
Figure 7.10 Simply supported beams subjected to distributed loading: (a) contribution of the shear-transfer actions for different section x_F; (b-c) influence of the shear slenderness ratio l/d on the control section x_F and on the onset of the critical shear crack x_A according to the mechanical model (Eq. (7.3) + Eq. (7.7))
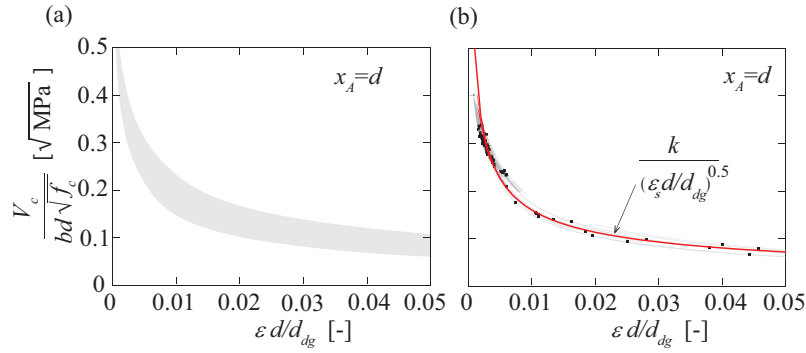
Figure 7.11 (a) Failure envelopes for simply supported reinforced concrete beams subjected to distributed loading as a function of the reinforcement strains (results for specimens with compressive strength f_c 20-100 MPa, aggregate size d_g 8-32 mm, flexural reinforcement ratio ρ 0.5-3%, effective depth d 200-2000 mm, shear slenderness ratio l/d 10-25, assuming $x_A=d$) (b) calculated shear strengths (black points) of 63 rectangular simply supported beams subjected to distributed loading ($l/d \geq 10$, see Appendix A) as a function of the reinforcement strains at the critical shear crack ($x_A=d$) and power-law failure criterion (Eq. (7.8))

Assuming that the critical shear crack develops at $x_A=d$, the failure criteria can be calculated by integration of stresses at the crack surface: it can be observed that shear failures occur in a narrow band (see Figure 7.11a) when extreme values of the various mechanical and geometrical parameters are assumed (aggregate size d_g ranging 8-32 mm, compressive strength f_c ranging 20-100 MPa, flexural reinforcement ratio ρ ranging 0.5-3%, shear slenderness ratio l/d ranging 10-25 and effective depth d ranging 200-2000 mm). By comparing Figure 7.3c and Figure 7.11a, it can be observed that the failure bands obtained for simply supported beams subjected to point and distributed loading are very similar but do not precisely coincide. Moreover, it can be noted that, for the same value of reinforcement strain ($\varepsilon_s \cdot d/d_{dg}$), the calculated shear capacity of simply supported beams subjected to distributed loading is lower than the calculated shear strength of simply supported beams subjected to point loading. These differences are due to the shape, to the theoretical governing location of the critical shear crack and to the different role of the various shear-transfer actions at failure: in particular, the critical values of a_{cs} and β_{AB} and the contribution of the compression zone are generally lower for simply supported beams subjected to distributed loading than for members subjected to point loading.

In Figure 7.11b, the calculated shear capacity at the control section of 63 rectangular concrete beams subjected to distributed loading (see database in Table 7.6) is plotted against the normalized crack width parameters. The black points in Figure 7.11b represent the intersection between the failure criteria calculated according to Eq. (7.3), assuming the critical shear crack developing at $x_A=d$, and the load–deformation relationship (Eq. (7.5)). In addition, the direction of the failure envelopes in the vicinity of the intersection is plotted (grey lines in Figure 7.11b). It is interesting to observe that shear failures occur in a narrow band, that can be approximated by a power law failure criterion (refer to Figure 7.3c). The coefficient k in the power-law

equation that fits the calculated shear strengths with the greatest accuracy is approximately equal to 0.016. Note that the coefficient k, obtained by fitting of the calculated shear strengths for simply supported beams subjected to point load, was equal to 0.019, underlining that shear failures cannot be described by a single failure criterion.

The closed-form equation (Eq. (7.18)) can be also extended to calculate the shear capacity of simply supported members subjected to distributed loading, by defining r_F according to Eq. (7.27). The shear capacity at the section x_F results:

$$V_c = \kappa \cdot \left(100 \cdot \rho \cdot f_c \cdot \frac{d_{dg}}{a_{cs}}\right)^{1/3} \cdot b \cdot d = \left(\frac{1}{1 - 0.6 \cdot d/(l - 2x_F)}\right) \cdot k_a \cdot \left(100 \cdot \rho \cdot f_c \cdot \frac{d_{dg}}{a_{cs}}\right)^{1/3} \cdot b \cdot d \qquad (7.30)$$

where a_{cs} is the moment-to-shear ratio at the control section x_F: $a_{cs} = \dfrac{M_F}{V_F} = x_F \cdot \dfrac{l - x_F}{l - 2 \cdot x_F}$.

Figure 7.12 shows a comparison of the load capacities q/b calculated by full integration of the shear-transfer actions at the crack surface (Eq. (7.28), Eq. (7.29) and Eq. (7.7), continuous lines) and by the closed-form equation (Eq. (7.30), dashed lines), as a function of the parameter x_F/d. The influence of the slenderness ratio l/d (Figure 7.12a), the flexural reinforcement ratio ρ (Figure 7.12b) and the effective depth d (Figure 7.12c) has been investigated. For these cases, a good agreement between the mechanical model and the closed-form equation can be observed. The closed-form equation allows investigating the theoretical governing location of the critical shear crack: in Figure 7.12 it can be noted that the curves representing the load capacity q/b are very flat around the minimum (black markers), which corresponds to values of x_F between d and $1.75d$.
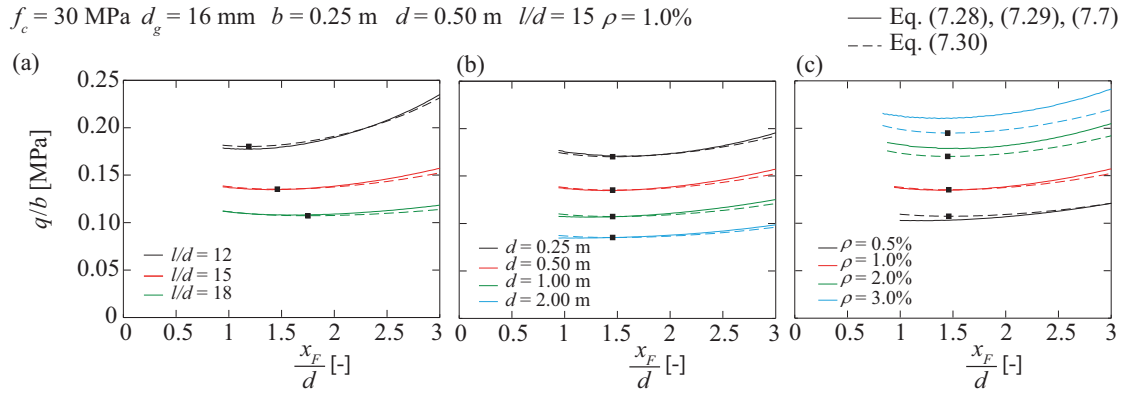
Figure 7.12 Comparison between the calculated load capacities according to the mechanical model (Eq. (7.28), Eq. (7.29)+ Eq.(7.7), continuous lines) and the closed-form expression (Eq.(7.30), dashed lines) for each possible control section x_F varying: (a) shear slenderness ratio l/d, (b) effective depth d and (c) reinforcement ratio ρ

The control section x_F shall be assumed at a distance of approximately $1.5d$ from the end support, to be consistent with the mechanical model (as shown in [3], $x_F \approx x_A + 0.5d$ leading to $x_F = 1.5d$). Assuming $x_F = 1.5d$, the calculated value of κ for 63 rectangular concrete beams listed in Table 7.6, varies between 0.76 and 0.81 with an average value for the investigated specimens of 0.79. Note that this value is lower than the one calculated for investigated beams subjected to point loading ($\kappa = 0.87$, refer to Section 7.3). These results are consistent with the calculated values of k in the power law failure criteria (respectively 0.016 for simply supported beams subjected to distributed loading (Figure 7.11b) and 0.019 for simply supported beams subjected to point loading [3]). Based on these observations, it can be stated that the closed-form equation is a very general formulation that can be applied to members subjected to different loading conditions. In particular, the coefficient κ allows considering the role of the various shear-transfer actions and different governing shear-failure criteria in a very simple manner.

With the purpose of maintaining the control section at the same fixed distance from a static or geometric discontinuity (consistently to the case of simply supported beams subjected to point loading), the control section x_F in the closed-form approach can be eventually assumed to be located at a distance d from the end support (Figure 7.12 confirms the validity of this assumption for these cases, since the load capacity is almost constant for any control section x_F within the interval d-$1.75d$). Figure 7.13 shows a comparison between the failure load calculated according to the original formulation of the CSCT (evaluating the shear capacity at $d/2$ and $l/6$ from the support and taking the failure load q as the minimum of the two calculated values, red lines), the refined approach Eq. (7.28), Eq. (7.29) and Eq. (7.7) (assuming that the critical shear crack develops at $x_A = d$, black lines), and the closed-form equation Eq. (7.30) (assuming the control section $x_F = d$, dashed lines) against the

experimental results of some test series. Within these experimental campaigns, the influence of slenderness ratio l/d, reinforcement ratio ρ and effective depth d was investigated. Figure 7.13 shows the ability of the refined approach and the closed-form formulation to correctly describe the effects of the above-mentioned parameters. The same trends are also captured by the CSCT, although the effect of the reinforcement ratio ρ is less pronounced and a lower increase of the load capacity in comparison with the experimental results is predicted (Figure 7.13b).
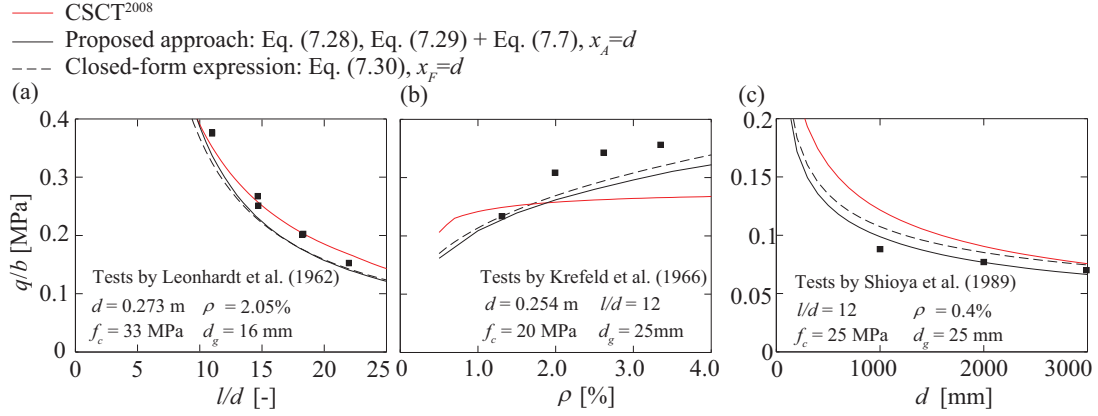
Figure 7.13 Comparison of the load strengths according to the CSCT [1], Eq. (7.28), Eq. (7.29) + Eq.(7.7) and Eq. (7.30) for various test series that investigate the following parameters: (a) slenderness ratio l/d (tests by Leonhardt et al. [18]), (b) reinforcement ratio ρ (tests by Krefeld et al. [19]) and (b) effective depth d (tests by Shioya et al. [22])

7.5.3 Applications to cantilevers subjected to distributed loading

The behaviour of cantilevers subjected to distributed loading has been recently described by Pérez Caldentey et al. [23], who showed that the loads acting on the tension face in the vicinity of the reaction plate are directly strutted to the support, leading to an increase of the shear strength of these members with respect to cantilevers subjected to concentrated loading. According to Pérez Caldentey et al. [23], all loads between the support and the distance at which the critical shear crack intercepts the flexural reinforcement do not concur to the shear force that has to be carried by the critical shear crack, and can be thus neglected. A recent experimental investigation [4] showed that this distance can vary between d and $2.6d$ from the support but, despite a certain scatter, its value is larger for higher values of moment-to-shear ratio at the fixed support.

The shear strength of these members can be calculated by integration of stresses at the crack surface, following the same procedure described for simply supported beams subjected to point load (Eq. (7.3) + Eq. (7.7)). The load capacity under this assumption is obtained by equilibrium of the rigid body shown in Figure 7.14a: it can be noted that the bending moment (M_F in Eq. (7.7)) and the shear strength (V_c in Eq. (7.3)) are calculated respectively at the section corresponding to the tip (x_F) and to the onset (x_A) of the critical shear crack.
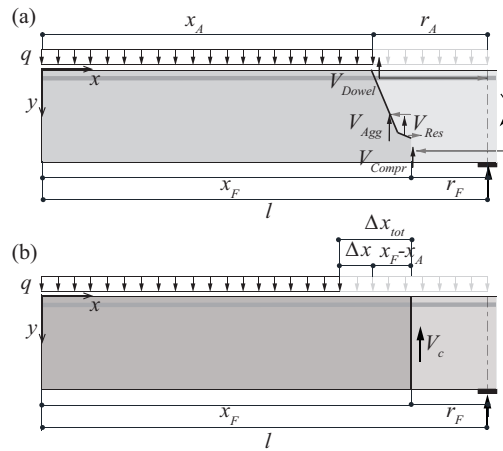
Figure 7.14 Cantilever subjected to distributed loading: (a) rigid body equilibrium and internal forces; (b) definition of Δx_{tot}

The shape and kinematics of the critical shear crack are defined in Section 7.2. The angle β_{AB} is defined according to Eq. (7.2), where α_A for a cantilever subjected to distributed load is equal to:

$$\alpha_A = \frac{0.5 \cdot x_A}{d} \tag{7.31}$$

The load-crack opening relationship shall be calculated according to Eq. (7.7), where:

$$M_F = q \cdot \left(\frac{x_F^{\,2}}{2}\right) \tag{7.32}$$

and the distributed load q shall be determined by equilibrium of the rigid body shown in Figure 7.14a:

$$q = \frac{V_{Res} + V_{Agg} + V_{Dowel} + V_{Compr}}{x_A} \tag{7.33}$$

It shall be noted that Eq. (7.32) is an approximation, as the contributions of all forces acting at the critical shear crack to the moment M_F at a section located at the crack tip are neglected (in accordance to the case of simply supported beams subjected to point load). Moreover, the loads acting between the onset and the tip of the critical shear crack are accounted for in Eq. (7.32), although they are neglected in the equilibrium of the free-body shown in Figure 7.14a. Note that for slender cantilevers, detailed calculation accounting for all forces acting on the rigid body provides values of bending moment M_F up to 5% lower.

The presented procedure, however, underestimates the shear capacity of these members, since it does not take into account an increase of the dowel capacity, due to the confining action generated by the external loads applied on the tension side of the member (as observed in Chapter 5, the dowelling action in cantilevers subjected to distributed loading is larger than in members subjected to point loading). The distributed load q shall thus be calculated by equilibrium of the rigid body shown in Figure 7.14a accounting for the maximum dowelling capacity (k_b=1 in Eq. (7.14)). Note that the assumption of k_b equal to 1 in Eq. (7.14) means that the explicit strain-dependency of the dowelling action is neglected for these cases.

The theoretical governing location of the critical shear crack x_A can be determined as the section where the shear capacity equals the value of the shear force. In Figure 7.15a, the shear capacity and the contribution of the various shear-transfer actions are shown for a typical case (l/d=7.5, d=500 mm, ρ=1.00%, f_c=30 MPa, d_g=16 mm). It can be noted that the theoretical governing location of the critical shear crack x_A is located where the shear strength curve is tangent to the shear force line. In Figure 7.15b and c the load capacity is plotted versus r_A/d, showing that the theoretical governing critical shear crack develops at a distance between d and $1.5d$ from the support. In Figure 7.15b and c it can be noted that, for increasing values of the slenderness ratio l/d and the reinforcement ratio ρ, the theoretical governing location shifts further from the fixed support. It can also be shown that all other mechanical parameters (effective depth d, compressive strength f_c) have almost no influence on the theoretical governing position x_A of the critical shear crack. Therefore, for these cases adopting a fixed critical shear crack developing at x_A=l-d is a reasonable assumption. This approach allows quantifying the loads that do not cross the critical shear crack and do not concur to the shear force that has to be carried by the critical shear crack (which are equal to $q \cdot r_A$).

$f_c = 30$ MPa $\quad d_g = 16$ mm $\quad b = 0.25$ m $\quad d = 0.50$ m $\quad l/d = 7.5 \quad \rho = 1.0\%$
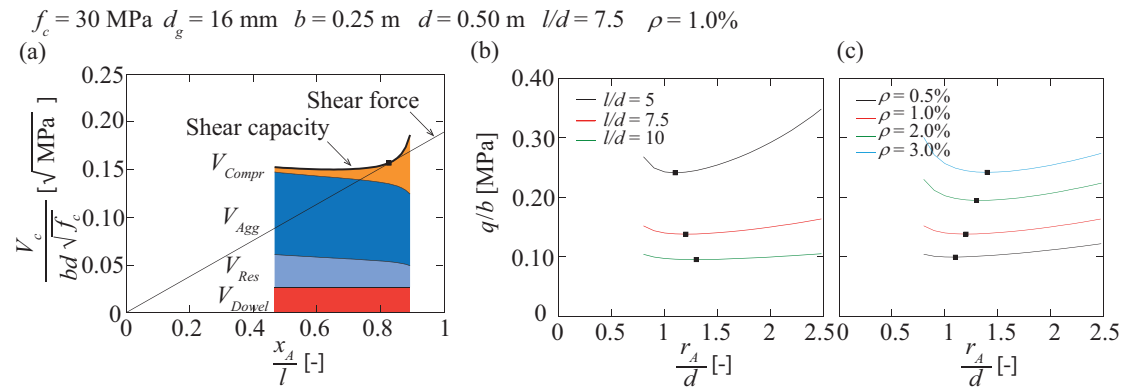
Figure 7.15 Cantilevers subjected to distributed loading (a) contribution of the shear-transfer actions for different section x_A according to the mechanical model (Eq. (7.32), Eq. (7.33) + Eq.(7.7)); (b) influence of the slenderness ratio l/d and (c) of the reinforcement ratio ρ on the distance between the onset of the critical shear crack and the axis of the reaction plate (r_A) according to the mechanical model

The closed-form expression (Eq. (7.18)) can also be applied to cantilevers subjected to distributed load. However, an important clarification is required. Although the moment to shear ratio a_{cs} is calculated at a control section x_F, the calculated shear capacity refers to the strength at the section $x_F - \Delta x_{tot} = x_A - \Delta x$ (refer to Figure 7.14b). This can be physically justified by the following considerations: (i) although the control section shear span a_{cs} is calculated as the moment-to-shear ratio at the control section x_F, the equilibrium of the rigid body shown in Figure 7.14a implies that the calculated shear capacity refers to the shear force at the section x_A, and not at the control section x_F. In fact, the critical shear crack intercepts the longitudinal reinforcement at x_A and the load that equilibrates the vertical components of the various shear-transfer actions is equal to $q \cdot x_A$. (ii) Moreover, it has to be underlined that Eq. (7.18) has been derived for simply supported members subjected to point or distributed load, in which the dowelling action follows a decay for increasing strains in the reinforcement bars ($k_b<1$ in Eq. (7.14)). This is not the case for cantilevers subjected to distributed loading, where the loads acting on the tension side allow activating the full dowelling action ($k_b=1$). Therefore, Eq. (7.18) shall be applied accounting for an additional reduction $q \cdot \Delta x$ (Figure 7.14b).

The value of $q \cdot \Delta x$ (and thus of $\Delta x_{tot}=x_F-x_A+\Delta x$ (refer to Figure 7.14b)) is unknown a priori and it can be calculated as the load that allows activating the full dowelling action, compensating the reduction of the effective tensile strength of concrete that would occur in the case of no distributed loads acting on the tension side. By defining k_b as in Eq. (7.15), Δx results:

$$\Delta x = \frac{V_{Dowel(k_b=1)} - V_{Dowel(k_b=f(u_A))}}{q} = \frac{5 \cdot (1 - k_b) \cdot f_{ct} \cdot \rho \cdot b \cdot d}{q} \tag{7.34}$$

where q is the distributed load calculated applying the refined procedure (Eq. (7.32), Eq. (7.33) and Eq. (7.7)). In Figure 7.16a-d, the calculated values of $\Delta x_{tot}/x_F = (x_F-x_A+\Delta x)/ x_F$ are plotted as a function of r_F/d for some cantilevers varying the main mechanical parameters. It can be observed that the compressive strength of concrete f_c, the effective depth d, the reinforcement ratio ρ, the slenderness ratio l/d and the position of the control section x_F influence the ratio $\Delta x_{tot}/x_F$, which varies between 1/6 and 1/4. The calculated values of $\Delta x_{tot}/x_F$, shown in Figure 7.16a-d, may represent lower-bound solutions, for the following reasons: (i) Δx is calculated according to Eq. (7.14), which provides a lower-bound estimate of the dowelling action, due to the assumption of a spacing between the longitudinal bars equal to $3d_b$; (ii) the rigid-body in Figure 7.14a does not account for a possible secondary flexural crack (crack type C, refer to [4]) that may merge with the primary flexural crack during loading, yielding a redistribution of the load-transfer mechanisms and an increase of the loads that are directly strutted to the support. A crack type C, in fact, generally develops at a distance from the critical shear crack equal to one-half the spacing between two primary flexural cracks and may lead to an increase of Δx_{tot} of approximately $0.28d$ [4].
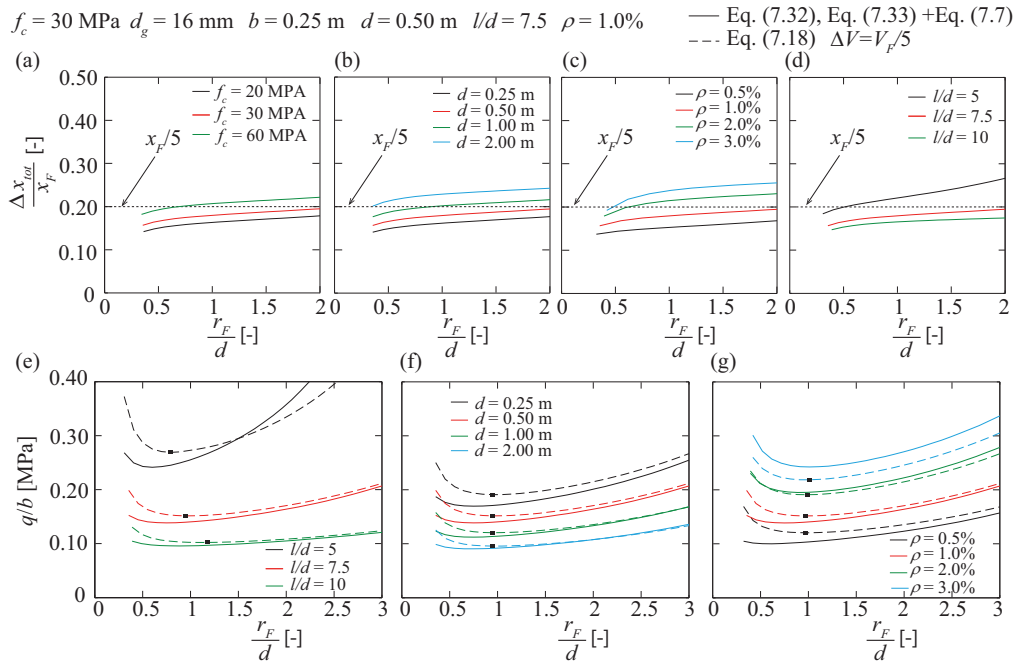
Figure 7.16 (a-d) $\Delta x_{tot}/x_F$ as a function of the main mechanical and geometrical parameters (compressive strength f_c, effective depth d, reinforcement ratio ρ, shear slenderness ratio l/d). Comparison between the calculated load capacities according to the mechanical model (Eq. (7.32), Eq. (7.33) + Eq.(7.7), continuous lines) and the closed-form expression (Eq.(7.18) with $\Delta V=V_F/5$, dashed lines) for each potential control section x_F varying: (e) slenderness ratio l/d, (f) effective depth d and (g) reinforcement ratio ρ

Based on Figure 7.16a-d, $\Delta x_{tot}/x_F$ can be assumed, without great loss of accuracy on the calculated shear strength, equal to 1/5 for all cases. Therefore, it can be concluded that at failure the shear capacity V_c, calculated at the control section x_F by using Eq. (7.18), refers to the shear force at the section x_F-Δx_{tot} (Figure 7.14b). In other words, at failure, the calculated shear capacity at the control section x_F is equal to the shear force V_F-ΔV:

$$V_c = V_F - \Delta V = \frac{4}{5} \cdot V_F \qquad\qquad (7.35)$$

where ΔV (= $V_F/5$) represents the loads that are not transferred through the critical shear crack, due to its shape, and has to be subtracted from the shear force at the control section. In other words, the calculated load capacity at the control section x_F can be enhanced by 25%. In the following, for comparisons with test results or with the solutions of the refined approach, the load capacity will be calculated at the control section x_F and it will be multiplied time 5/4 in agreement with Eq. (7.35).

Figure 7.16e-g show, for some selected cantilevers, the load capacities q/b calculated by full integration of the various shear-transfer actions at the failure surfaces (Eq. (7.32), Eq. (7.33) and Eq. (7.7), with k_b=1, continuous lines) and by the closed-form equation with the assumption of ΔV=$V_F/5$ (Eq. (7.18), dashed lines), for each possible control section x_F. The comparisons highlight that the two approaches provide consistent results. Nonetheless, the closed-form equation (with the assumption of a constant Δx_{tot} equal to $x_F/5$) estimates higher load capacities than the refined approach for low values of reinforcement ratio ρ, shear slenderness ratio l/d and effective depth d. Moreover, it can be noted that the minimum load capacity is attained, for almost all cantilevers, at values of r_F equal to d, allowing defining a fixed control section located at x_F=l-d for these cases.

In Figure 7.17 the failure load of some tests detailed in Cavagnis et al. [5] (cantilevers subjected to distributed loading with different values of l/d) is compared to the load capacity calculated according to the original formulation of the CSCT (red line), to the refined mechanical model (Eq. (7.32), Eq. (7.33) and Eq. (7.7) adopting x_A=l-d) and to the proposed closed-form equation (Eq. (7.18) with x_F=l-d) with ΔV=0 (black dotted line) and ΔV=$V_F/5$ (black dashed line). It can be observed that the approaches have similar trends and capture an increase in the load capacity for lower values of the shear slenderness ratio l/d. Moreover, it can be noted the closed-form equation, with the assumption of ΔV=$V_F/5$, and the refined approach give consistently good results. In addition, it can be observed that the CSCT is more conservative, since all loads acting at a distance larger than $0.5d$ from the fixed support participate without any reduction to the shear force carried by the critical shear crack. A particular case in Figure 7.17 is represented by specimen SC58 ($l/d \approx 8$, [5]): for this specimen, the closed-form equation with ΔV=$V_F/5$ and the refined approach provide a safe estimate of the load capacity. This can be explained by considering the crack pattern experimentally observed for this member: during loading, the critical shear crack developed in a stable manner close to the fixed support and it allowed activating the arching action and the plastic strength of the member was eventually reached. The additional load capacity of this member with respect to the calculated one is due to the shape and location of the critical shear crack experimentally observed, which is rather different from the one assumed in the mechanical model, and due to the development of a clear direct strut. Therefore, based on these observations, it can be stated that the closed-form expression with ΔV=$V_F/5$ and the refined approach allow a correct estimate of the load capacity for members whose critical shear crack is located such that an inclined direct strut, which may lead to an increase on the shear capacity of the member, does not develop.

——— CSCT^{2008}
——— Proposed approach: Eq. (7.32), Eq. (7.33) + Eq. (7.7), x_A=l-d
········ Closed-form expression: Eq. (7.18), x_F=l-d, ΔV=0
– – – Closed-form expression: Eq. (7.18), x_F=l-d, ΔV=$V_F/5$
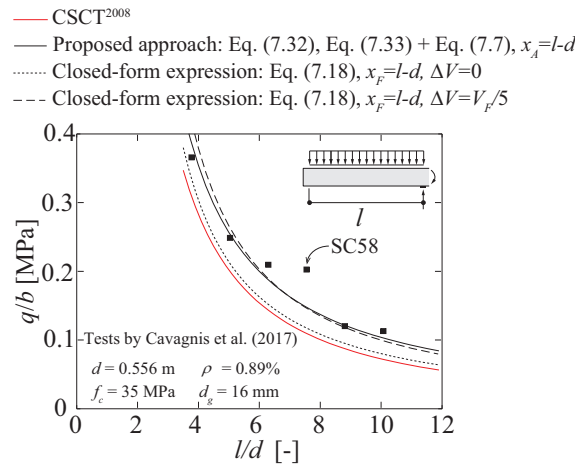
Figure 7.17 Comparison of the load strengths according to the CSCT [1] (red continuous line), Eq. (7.32), Eq. (7.33) + Eq.(7.7) (black continuous line) and Eq. (7.18) with ΔV=0 (black dotted line) and ΔV=$V_F/5$ (black dashed line) and the experimental results of cantilevers subjected to distributed (tests by Cavagnis et al. [5])

7.5.4   Applications to continuous beams to distributed loading

A continuous beam is characterized by a static system in which the bending moment varies its sign along the length of the member, therefore the critical crack can develop either within the region of negative or positive bending moment (see Figure 7.18a and b). In the first case, the critical crack propagates from the side where the loads are applied (the top face of the beam in Figure 7.18a), and the failure mechanism resembles the one of a cantilever subjected to distributed load. Differently, in the second case, the critical crack progresses from the opposite side of the applied loads (the bottom face of the beam in Figure 7.18b), reproducing the behaviour of a simply supported beam subjected to distributed loading. Whether failure occurs in one region or the other depends on the location of the point of contraflexure, therefore, a priori, both regions of positive and negative bending moment should be investigated.

In Figure 7.18, the contribution of the various shear-transfer actions and the shear capacity of a continuous beam (l/d=10, d=500 mm, ρ=1.00%, f_c=30 MPa, d_g=16 mm, M_{right}/ql^2=0.1) are calculated for each possible position of the critical shear crack. The region with negative bending moment (Figure 7.18a) is analysed following the procedure described for cantilevers (k_b=1 in Eq. (7.14)), whereas the region with positive bending moment is studied as a simply supported beam of length l_{SS} subjected to distributed loading (Figure 7.18b).

The theoretical governing location of the critical crack corresponds to the section where the shear capacity equals the value of the shear force (squared markers in Figure 7.18c and d). The acting shear force at failure is defined by the tangent to the shear capacity at the control section. In Figure 7.18c and d it can be noted that at the right support a lower shear force (V_{right}), and therefore a lower load capacity, is obtained for the potential critical shear crack developing within the region of the negative bending moment. Therefore, for the selected specimen the critical shear crack is expected to develop within this region.

$f_c = 30$ MPa $d_g = 16$ mm $b = 0.25$ m $d = 0.50$ m $\rho = 1.0\%$ $M_{right}/ql^2 = 0.1$
$l/d = 10$ $l_{SS}/d = 8$ $l_0/d = 6$
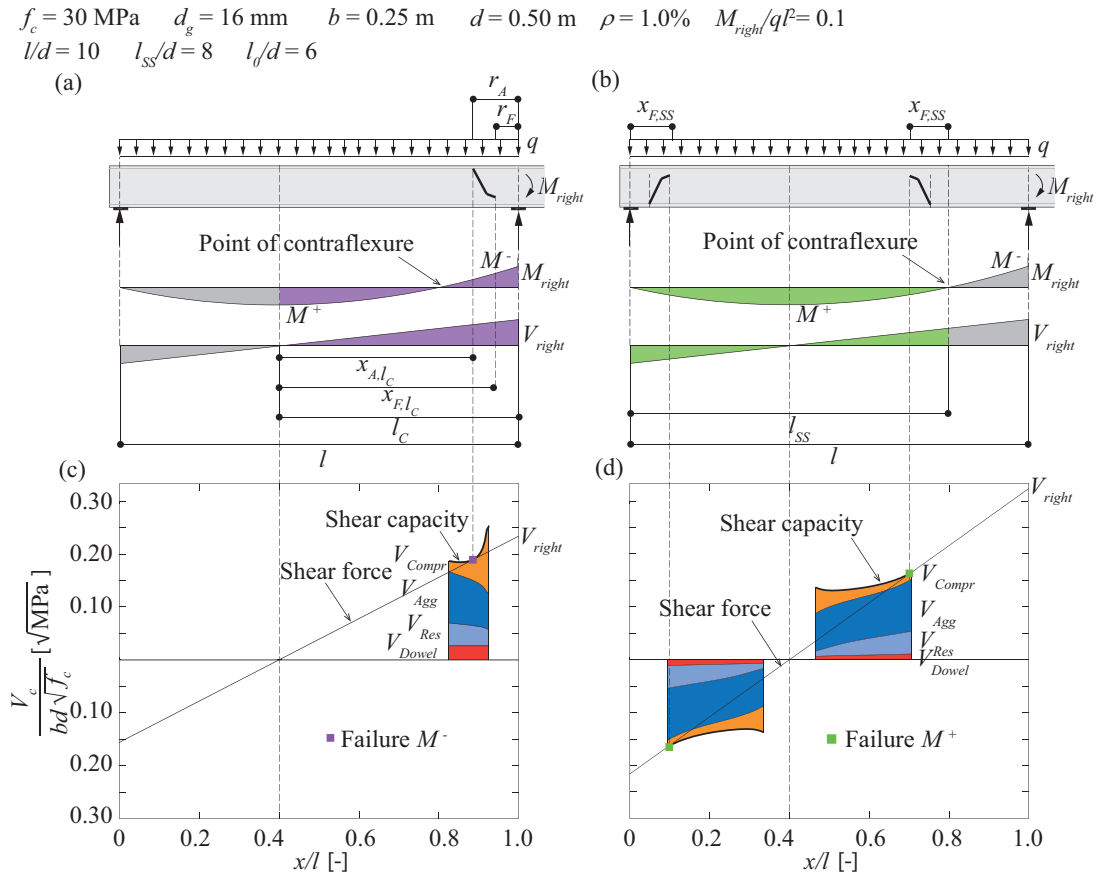
Figure 7.18 (a-b) Continuous beam subjected to distributed loading: moment and shear force diagrams, definition of l_C and l_{SS}. Shear capacity and contribution of the various shear-transfer actions, obtained by using Eq. (7.3) + Eq. (7.7)), within the region of (c) negative and (d) positive bending moment
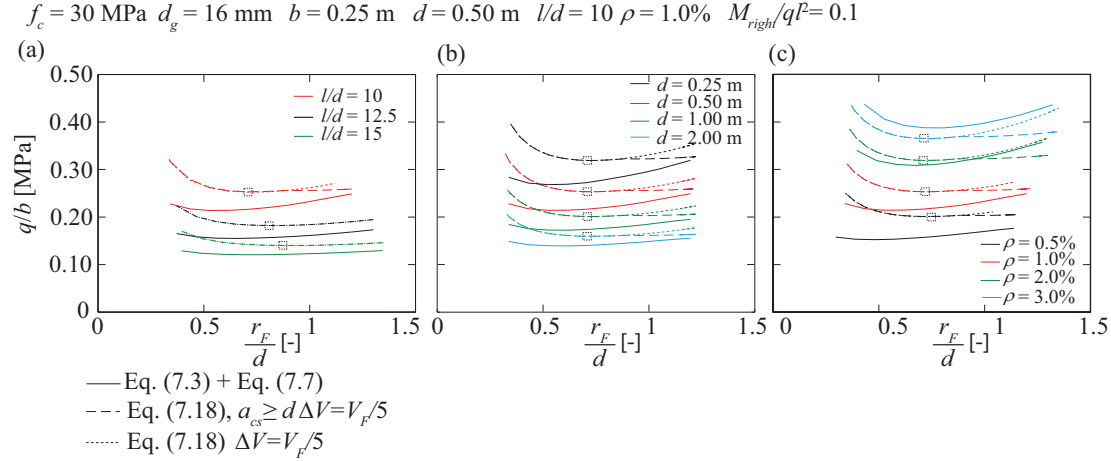
Figure 7.19 Load capacity and theoretical governing location of the critical shear crack varying (a) the ratio l/d, (b) the effective depth d and (c) the reinforcement ratio ρ: refined approach (continuous lines), closed-form equation with $\Delta V = V_F/5$ without any limit on the control section shear span a_{cs} (dotted lines) and closed-form equation with $\Delta V = V_F/5$ and with $a_{cs} \geq d$ (dashed lines)

The load capacities calculated according to the refined approach (continuous lines) and the closed-form equation (Eq. (7.18) with $\Delta V = V_F/5$, dotted lines) for different continuous beams with M_{right}/ql^2 equal to 0.1, failing within the region of negative bending moment are shown in Figure 7.19. It can be noted that the agreement between the two approaches is less accurate than in the previous cases considered (cantilevers and simply supported beams). The reason of this disagreement lies on: (i) Eq. (7.16), which, as observed in Section 7.3, slightly overestimates the value of k_a for low values of a_{cs}/d, and thus for low values of M_{right}/ql^2 at the intermediate support; (ii) the assumption of ΔV equal to $V_F/5$, which shall be lower for values of reinforcement ratio lower than 2% (Figure 7.16c). However, as shown in Figure 7.19c, for reinforcement ratio larger than 2%, the two approaches provide almost identical results. With respect to the solutions of the closed-form equation, it can be observed that the minimum load capacity (represented by dotted square markers) is obtained at a control section located between $0.5d$ and $0.75d$ from the right support. With the purpose of maintaining the control section at a distance d from the support ($r_F=d$), to be consistent with the case of cantilevers subjected to point and distributed loading, a limit on $a_{cs} \geq d$ shall be introduced in the closed-form equation. The results of the closed-form equation Eq. (7.18) with $a_{cs} \geq d$ are shown in Figure 7.19 (dashed lines): it can be noted that the load capacity is almost constant for r_F larger than $0.75d$, justifying the assumption of a fixed control section at a distance d from the right support ($x_F=l-d$).

The influence of the bending moment at the right support (M_{right}/ql^2) is investigated in Figure 7.20a, where the experimental results of some beams presented in this thesis, failing within the region of positive or negative bending moments (green and purple markers respectively), are shown. In Figure 7.20a it can be noted that, when the static system is more similar to the one of a cantilever ($M_{right}/ql^2=0.5$), the maximum load capacity is lower than when its behaviour is closer to the one of a simply supported beam ($M_{right}/ql^2=0$). Moreover, it is evident that when M_{right} is lower than $0.05ql^2$ the critical shear crack will develop within the region of positive bending moment, whereas when M_{right} is larger than approximately $0.1ql^2$ failure will occur within the region of negative bending moment. The three markers at $M_{right}/ql^2=0.1$ refer to the three shear failures of specimen SC52 (see Figure 3.3). In the latter, a diagonal crack developed close to the right support (purple marker, SC52), leading to a small drop in the applied load (about 5%). However, this diagonal crack did not lead to the failure of the specimen, as the arching action developed, and the load could be further increased. Failure occurred then within the region of positive bending moment close to the left support (green marker, SC52a), and successively, after the specimen was repaired by means of external plates fixed together with prestressed bolts, a second failure was attained close of point of contraflexure (green marker, SC52b).

Figure 7.20a shows the capability of both the refined approach (black continuous lines) and the closed-form equation (dashed lines) to correctly describe the effect of the maximum bending moment at the right support and to give consistently good results for both failures within the region of positive (green dashed line) and negative (purple dashed line) bending moment. In particular, the full integration of stresses at the crack surface is performed at a crack developing at $x_A=0.5d$ within the region of positive bending moment (in agreement with the theoretical governing location of the critical shear crack for simply supported members subjected to distributed load with $l/d=l_{SS}/d <10$, refer to Figure 7.10) and at a crack $x_A=l-d$ within the region of negative bending moment (in agreement with the theoretical governing location of the critical shear crack for cantilevers subjected to distributed load, refer to Figure 7.15). In Figure 7.20a it can be noted that the CSCT (red lines) underestimates the load capacities of continuous beams failing within the region of negative bending moment, since no reduction of the loads acting at a distance larger than $0.5d$ from the fixed support is accounted for (as already observed in Section 7.5.3).
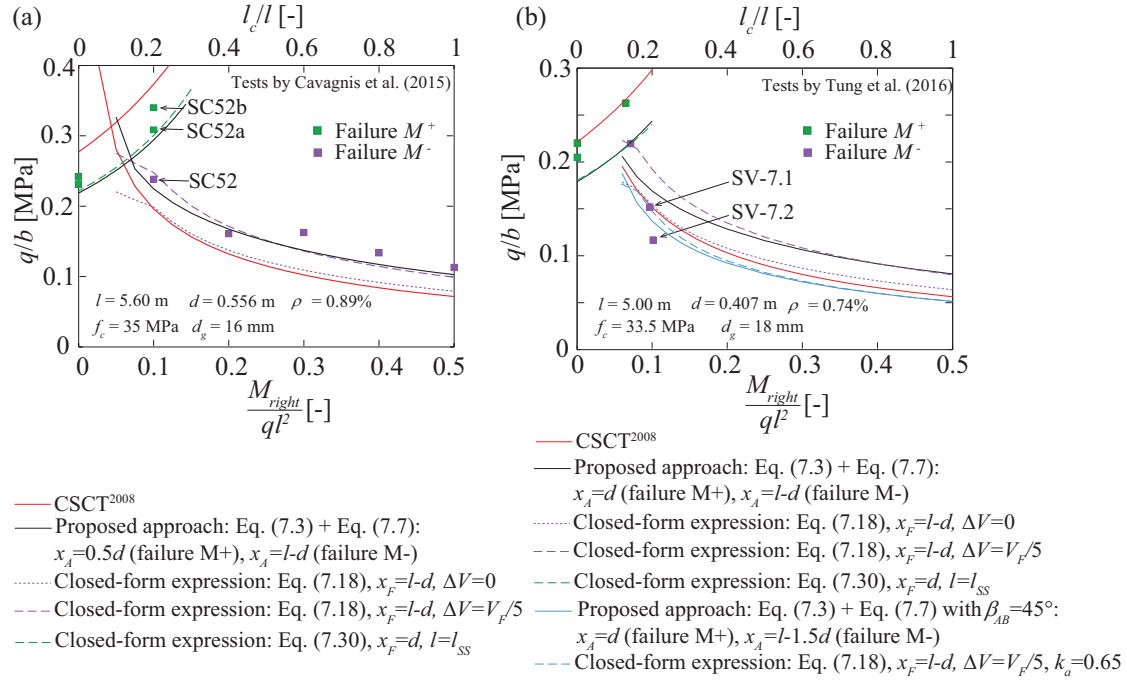
Figure 7.20 Comparison of the load strengths according to the CSCT [1], Eq. (7.3) + Eq. (7.7) and Eq. (7.18) and the experimental results of test series varying the maximum negative bending moment at the right support and the position of the point of contraflexure: (a) tests by Cavagnis et al. [4] and (b) test by Tung et al. [24]

Another interesting experimental investigation on continuous members subjected to distributed loading has been recently carried out by Tung et al. [24]. Figure 7.20b shows a comparison between the experimental results and the calculated load capacities according to the original formulation of the CSCT [1], the refined approach and the closed-form equation. It can be observed that the three approaches provide unsafe design solutions for specimens SV-7.1 and SV-7.2, whereas they estimate more accurately the shear capacity of the other specimens. Moreover, it shall be noted that, for specimens SV-7.1 and SV-7.2, the original formulation of the CSCT (red line) and the closed-form equation with $\Delta V=0$ (purple dotted line) provide the most accurate results.

The unsafe solutions of the theoretical models presented in this Chapter can be explained by considering the static scheme of these tests, which was varied during loading: close to peak load, the distance of the point of contraflexure from the axis of the fixed support ($l-l_{SS}$, in Figure 7.18) was expanded to 2.5d, from an initial value of approximately 1.5d. At failure, the authors observed that the critical shear crack propagated from an existing flexural crack [24]. Therefore, the critical crack developed at an angle β_{AB} lower than the one that would have occurred in the case the position of the point of contraflexure would have been kept constant and equal to 2.5d during the entire test. This imply an influence of the loading history and the variable load combinations on the shape of the critical shear crack.

Therefore, in order to predict correctly the shear capacity of these members, the refined approach shall be applied by assuming a more realistic shape of the critical shear crack: the inclination of the critical crack (β_{AB}) shall be calculated as a function of the moment-to-shear ratio at the control section prior to the loading adjustment ($l-l_{SS}$ equal to approximately 1.5d). On the contrary, the bending moment in the load-crack opening relationship (Eq. (7.7)) shall be determined on the basis of the static scheme at failure ($l-l_{SS}$ equal to approximately 2.5d). Note that, assuming a lower angle β_{AB}, the theoretical governing location of the critical shear crack shifts further from the fixed support. The onset of the critical shear crack can thus be assumed equal to $l-1.5d$, which leads to an angle β_{AB} equal to 45° (refer to light blue continuous line in Figure 7.20b).

The closed-form equation can also be applied for these tests by assuming a coefficient k_a=0.65 (due to a lower a_{cs} at the control section prior to the loading adjustment), in agreement with the flatter angle β_{AB} previously assumed in the refined approach. In the right part of Eq. (7.18), differently, a_{cs} is assumed equal to the moment-to-shear ratio obtained from static scheme at failure (refer to light blue dashed line in Figure 7.20b).

In Figure 7.20b it can be observed that assuming a more realistic shape of the critical shear crack, the refined approach (blue continuous line) and the closed-form equation (blue dashed line) provide a good estimate of the load capacity of these members.

137

Based on the previous observations it can be concluded that in the case of variable loads the following recommendations shall be implemented: (i) the bending moment and shear force diagrams shall be calculated from the different load combinations; (ii) in each section the minimum and maximum moment-to-shear ratio shall be determined. In the refined approach, the shear capacity shall be checked at any possible location of the critical shear crack x_A within the investigated span. The inclination of the critical shear crack β_{AB} at each section x_A shall be calculated according to Eq. (7.2), where a_{cs} is the lowest moment-to-shear ratio obtained at each investigated section from the analyses of the different load combinations. Moreover, if the distributed loading is not applied on the entire tension side of the member, the dowelling action shall be determined accounting for its strain-dependency (k_b defined according to Eq. (7.15)). In the closed-form equation, the shear capacity shall be checked at the control section located at a distance d from a static or geometric discontinuity. In Eq. (7.18), k_a shall be calculated according to Eq. (7.16), where a_{cs} is the minimum moment-to-shear ratio at the control section obtained from the different load combinations. Differently, in the right part of Eq. (7.18), a_{cs} shall be assumed equal to maximum moment-to-shear ratio at the control section obtained from the different load combinations. Moreover, ΔV could be reduced and eventually assumed equal to zero, if the distributed loading is not applied on the entire tension side of the member in the proximity of the critical shear crack.

The significance of this topic in structural applications encourages further experimental and theoretical investigations, in order to provide more insights on the dowel capacity and on the influence of variable loads on the shape of the critical shear crack.

7.6 Examples of application

7.6.1 Verification of a thick slab without transverse reinforcement

In the following, an example of a very thick one-way slab, tested at the University of Toronto [25], is investigated. The dimensions, properties and acting shear forces V_E at failure are given in Figure 7.21. For this specimen f_{ct} is assumed equal to 3 MPa [26]. The self-weight of a thick slab cannot be neglected and thus the acting shear force (green line) is calculated accounting for a distributed load due to the weight of the specimen (q=25 kN/m). Figure 7.21b shows the shear capacity calculated according to the refined approach and the closed-form equation for each possible location of the critical shear crack x_F. The refined approach is applied at any possible location of the critical shear crack x_A and β_{AB} is calculated according to Eq. (7.2), where a_A is the moment-to-shear ratio derived from the experimental failure load. Theoretically, an iteration on β_{AB} would be needed. However, it was observed that β_{AB} calculated iteratively (where a_A changes at each iteration due the different calculated failure load) is practically identical to β_{AB} calculated from the measured failure load. It is then assumed that the calculated shear capacity corresponds to the one at the control section x_F, in agreement with the equilibrium of the rigid body shown in Figure 7.9.

In Figure 7.21b, it can be observed that the closed-form equation slightly overestimates the shear capacity, compared to the one calculated according to the refined approach (Eq. (7.3) + Eq. (7.7)). Moreover, the theoretical governing control section x_F is located closer to the end support (right support in Figure 7.21a), in comparison to smaller specimens where the self-weight is neglected (refer to Figure 7.5).

Two potential control section x_F located respectively (i) at a distance d from the axis of load introduction and (ii) at a distance $1.75d$ from the axis of the right support (corresponding to the control section x_F of a shear crack developing at $x_A \approx 1.2d$) are investigated in Figure 7.21b. Section (ii) corresponds to the section where the bending moment reaches the cracking moment, assuming f_{ct}=3 MPa [26].

For the control section (i) $V_{E(i)}$=:286 kN.

$$V_{c(i)} = \frac{1}{1-0.15} \cdot \left(0.5 + 0.2 \left(\frac{11070}{3840} \right)^{1/3} \right) \cdot \left(0.656 \cdot 40 \cdot \frac{30}{11070} \right)^{1/3} \cdot 350 \cdot 3840 = 367 \text{kN} \tag{7.36}$$

For the control section (ii) $V_{E(ii)}$=:322 kN and

$$V_{c(ii)} = \frac{1}{1-0.15 \cdot \dfrac{3840}{5280}} \cdot \left(0.5 + 0.2 \left(\frac{8473}{3840} \right)^{1/3} \right) \cdot \left(0.656 \cdot 40 \cdot \frac{30}{8473} \right)^{1/3} \cdot 350 \cdot 3840 = 371 \text{kN} \tag{7.37}$$
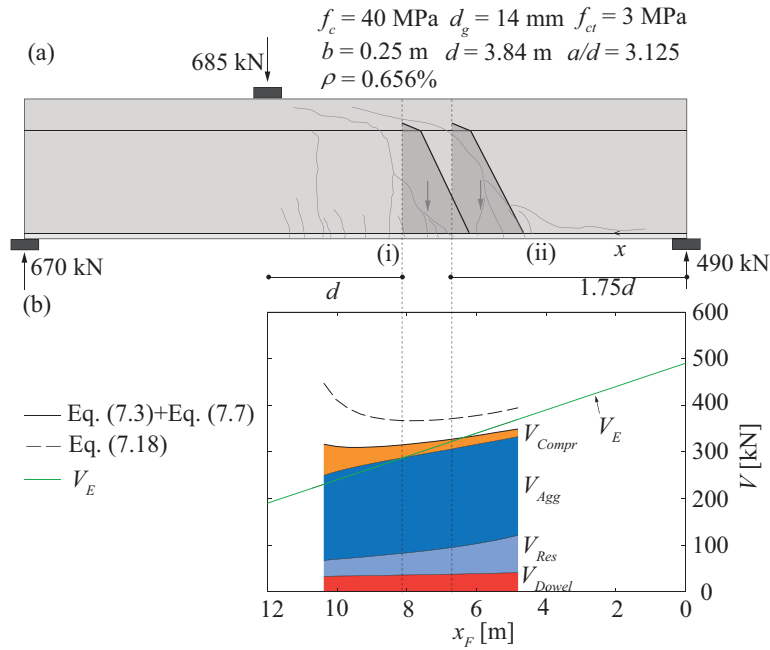
Figure 7.21 (a) Details of the specimen [25]: dimension, properties, observed crack pattern and investigated cracks; (b) calculated shear capacity according to the refined approach (dark continuous line) and the closed-form equation (dark dashed line) and acting shear force V_E at failure (green continuous line)

According to Section 7.5.2, the distributed loads which are not transferred through the critical shear crack are not accounted for in the shear force at the control section x_F (refer to rigid body in Figure 7.9). Nonetheless, the self-weight is not applied as a uniformly distributed load acting on the compression side of the specimen. Therefore, the portion of self-weight acting below the critical shear crack has to be added to the acting shear V_E at the control section x_F (see darker grey in Figure 7.21a). A shown in Chapter 6, the horizontal projection of critical shear crack depends on the inclination of the segment AB of the critical shear crack, but it can be estimated for these cases to be equal to approximately $0.56d$. On this basis, the portion of the load ΔV that has to be added to the acting shear force results: $\Delta V = q \cdot 0.56 \cdot d/2 = 27$ kN, and thus $V_{E(i)} = 286$kN$+\Delta V = 313$ kN and $V_{E(ii)} = 322 + \Delta V = 349$ kN. It can be concluded that the theoretical governing location is located at $1.75d$ from the right support and the closed-form equation slightly underestimates the shear capacity for this case ($V_{E(ii)} / V_{calc,closed-form(ii)} = 0.94$). Better results are obtained applying the refined approach for the critical shear crack developing at $x_A = 1.2d$ ($V_{E(ii)} / V_{calc,refined(ii)} = 1.06$).

7.6.2 Design of deck slab of a cut-and-cover tunnel

The following example is taken from Sigrist et al. [27]. A deck slab of a cut-and-cover tunnel is analysed (refer to Figure 7.22). The deck slab is a part of a frame structure and consists of two spans of 10.55 m between axes. The thickness of the slab h is 0.8 m. The concrete is C30/37 (f_{ck}=30 MPa, γ_c=1.5), with a maximum aggregate size of 32 mm. The reinforcement class is B500S (f_{yk} =500 Mpa, γ_s =1.15). The top longitudinal reinforcement is equal to 2945 mm^2/m (ρ=0.398%) and the effective depth d is equal to 0.74 m. Only one load arrangement of q_d=80kN/m^2 has been considered, which is in equilibrium with a reaction in the middle of the internal column of 950 KN/m.

The maximum internal forces at the edge of the internal column are: m_{Ed}= -869 kNm/m and v_{Ed}= 455 kN/m. The control section is taken at a distance d from the axis of the intermediate support and the corresponding sectional forces are: m_{Ed}= -599 kNm/m and v_{Ed}= 416 kN/m. The control section shear span a_{cs} is thus equal to m_{Ed}/v_{Ed} = 1440 mm. The shear resistance is determined using Eq. (7.18):

$$v_c = \frac{1}{\gamma_c} \frac{1}{1-0.15} \cdot \left(0.5 + 0.2\left(\frac{1440}{740}\right)^{1/3}\right) \cdot \left(0.398 \cdot 30 \cdot \frac{40}{1440}\right)^{1/3} \cdot 740 = 302 \, \text{kN/m} \tag{7.38}$$

The distributed loads acting near to the control section which can be subtracted are $\Delta v = v_{Ed}/5 = 83$ kN/m. The shear capacity is thus insufficient as v_c=302 kN/m < 416 kN/m – 83 kN/m = 333 kN/m (v_{Ed} - Δv).
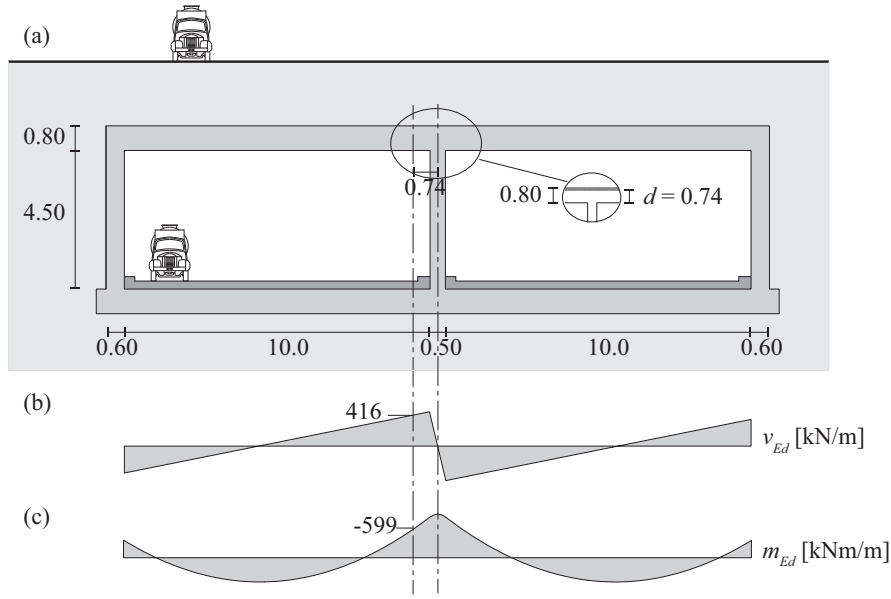
Figure 7.22 (a) Geometry and cross-sectional dimensions of the tunnel [27] (dimensions in m); (b) shear force and (c) moment diagrams (adapted from Sigrist et al. [27])

As the shear resistance is not sufficient, one of the following measures may be chosen: (i) using a concrete with higher strength; (ii) providing transversal reinforcement; (iii) increasing the slab thickness; (iv) increasing the flexural reinforcement; (v) prestressing the deck slab.

In the following, the same slab is prestressed and the slab thickness h is reduced to 0.7 m (to enable comparison the load q_d is kept constant and equal to 80 kN/m). The prestressing comprises of 5 strands per metre (a_p=750 mm²/m) with a nominal yielding strength of $f_{p,yk}$=1500 MPa. The maximum eccentricity at the intermediate support is 0.27 m and the radius of curvature of the tendons is 5.18 m over a length of 1.80 m. Assuming a stress of 1275 MPa in the strands at tensioning, after friction losses and assuming shrinkage, creep and relaxation losses of 22%, the final prestressing force is 745 kN/m, which is assumed constant on the entire slab and equal to the normal force n_{Pd}. In addition, a moment due to static indeterminacy of 15 kNm/m is accounted for. In addition to tendons, conventional steel reinforcement of a_s=1340 mm²/m with an effective depth d_s of 0.64 m is adopted. At the cross section located at a distance d_s from the axis of the intermediate support, the effective depth of prestressing is d_p =0.70/2+0.27-(0.64)²/(2·5.18)=0.580 m. The effective depth d, according to Eq. (7.22) is:

$$d = \frac{d_s^2 \cdot a_s + d_p^2 \cdot a_p}{d_s \cdot a_s + d_p \cdot a_p} = 0.620 \text{ m} \qquad (7.39)$$

The average reinforcement ratio ρ is (refer to Eq. (7.23)):

$$\rho = \frac{d_s^2 \cdot \rho_s + d_p^2 \cdot \rho_p}{d^2} = 0.336\% \qquad (7.40)$$

The control section is thus located at a distance d from the axis of the intermediate support (an iteration is needed, but it can be omitted since d is practically unchanged). The internal forces at the control section thus results: n_{Pd} = -745 kN/m, v_{Ed} = 336 kN/m and m_{Ed} = -463 kNm/m.

The effective control section shear span $a_{cs,eff}$ can be calculated according to Eq. (7.24):

$$a_{cs,eff} = \frac{|m_{Ed}|}{|v_{Ed}|} + \frac{n_{Pd}}{|v_{Ed}|} \cdot \frac{d}{3} = 918 \text{mm} \qquad (7.41)$$

and the shear resistance (Eq. (7.18)) results:

$$v_c = \frac{1}{\gamma_c} \frac{1}{1-0.15} \cdot \left(0.5 + 0.2\left(\frac{918}{620}\right)^{1/3}\right) \cdot \left(0.336 \cdot 30 \cdot \frac{40}{918}\right)^{1/3} \cdot 620 = 269.2\,\text{kN/m} \tag{7.42}$$
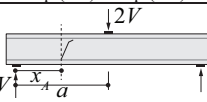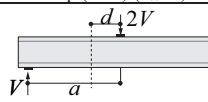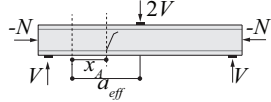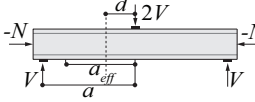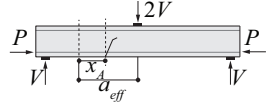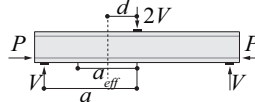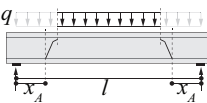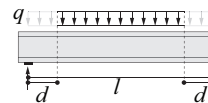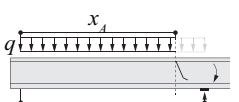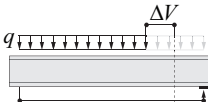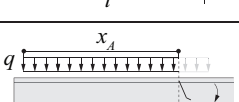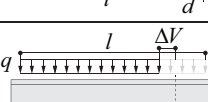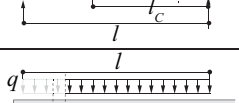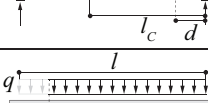
The distributed loads acting near to the control section which can be subtracted from the acting shear force at the control section are $\Delta v = v_{Ed}/5 = 67$ kN/m. The shear capacity is thus sufficient for this case as $v_c = 269.2$ kN/m > 336 kN/m $- 67$ kN/m $= 269$ kN/m ($v_{Ed} - \Delta v$).

7.7 Validation and comparison to experimental results

The closed-form equation (Eq. (7.18)) has shown to provide almost identical results to the mechanical model (Eq. (7.3) + Eq. (7.7)) (refer to Figure 7.5, Figure 7.10d-f and Figure 7.16e-g). The closed-form equation is grounded on a refined approach (Eq. (7.3) + Eq. (7.7)), which allows estimating the shear strength taking into account the contribution of all potential shear-transfer actions. In addition, the influence of the shape (k_a) and location of the critical shear crack with respect to the point of load introduction (k_c) are explicitly considered. As shown in the previous sections, the closed-form equation can be applied checking the shear strength at each potential control section located at a distance d, either from a static discontinuity (concentrated load or intermediate support) or from a section with zero acting bending moment (end support or points of contraflexure in continuous beams). Furthermore, the control section shear span a_{cs} is limited by the condition $a_{cs} \geq d$ (following the observations of Section 7.5.4).

The main assumptions of the refined approach and the closed-form equation are summarized in Table 7.2. Table 7.3 shows a detailed comparison of the results of the original formulation of the CSCT [1], the refined approach (Eq. (7.3) + Eq. (7.7)) and the closed-form equation (Eq. (7.18)), with $a_{cs} \geq d$ against the experimental results of simply supported, cantilevers and continuous beams subjected to concentrated and distributed loading with and without axial forces (refer to sketched in the tables for definition of loading and support conditions).

Table 7.2 Summary of the location of the control section for the refined approach and the closed-form equation
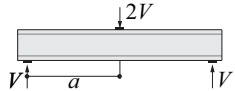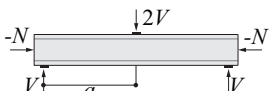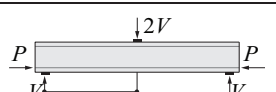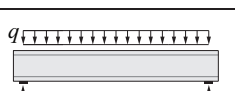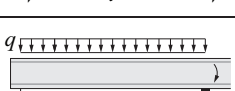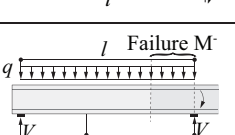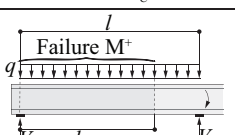
Refined approach: Eq. (7.3) + Eq. (7.7)	x_A	k_b	Closed-form: Eq. (7.18) ($a_{cs} \geq 1$)	x_F	r_F	ΔV
	$0.5a$	Eq. (7.15)		$a-d$	d	(-)
	$0.5a_{eff}$	Eq. (7.15)		$a_{eff}-d$	d	(-)
	$0.5a_{eff}$	Eq. (7.15)		$a_{eff}-d$	d	(-)
	d	Eq. (7.15)		d	$(l/2-d)/2$	(-)
	$l-d$	1		$l-d$	d	$V_F/5$
	$l-d$	1		$l-d$	d	$V_F/5$
	$0.5d$ ($l/d<10$) d ($l-d\geq10$)	Eq. (7.15)		d	$(l_{SS}/2-d)/2$	(-)

It shall be noted that only slender members failing in shear are considered in this study: simply supported beams subjected to concentrated loading with a/d (or a_{eff}/d for prestressed members) ≥ 2.5, simply supported beams subjected to distributed loading with $l/d \geq 10$ or cantilevers and continuous beams subjected to distributed loading with l/d (or l_C/d) ≥ 3.5. With respect to continuous beams failing within the region of positive bending moment, also members with $l_{SS}/d < 10$ are assumed to behave as slender members, due to lack of a reaction plate close to the point of contraflexure, and are therefore included in the database. For simply supported beams subjected to point loading, the database of Reineck et al. [8] (where only rectangular beams with $a/d \geq 2.5$ have been considered), completed with the tests by Cavagnis et al. [5], is used (see [3]). Section 7.9 provides the databases used for members with different loading and support conditions: simply supported beams subjected to point load and axial forces (Table 7.4), prestressed beams (Table 7.5), simply supported beams (Table 7.6), cantilevers (Table 7.7) and continuous beams subjected to distributed loading (Table 7.8 and Table 7.9). Appendix 2 provides the main mechanical and geometrical properties and the failure loads of all specimens used to validate the theoretical approaches presented in this thesis. For all specimens, the eventual compression reinforcement was not accounted for in the evaluation of the shear strength. The tests performed with variable the static scheme during loading [24] have not been used for comparison.

As shown in Table 7.3, the CSCT shows a good agreement with test results for simply supported beams subjected to point loading and provides a reasonable estimate of the shear capacity for simply supported members subjected to distributed loading. As already point out in [3], the accuracy of the CSCT could be enhanced for low crack openings (large reinforcement content) by modifying the hyperbolic failure criterion with a power-law failure criterion (refer to Eq. (7.8)). Moreover, the CSCT can be improved accounting for d_{dg} defined according to Eq. (6.17). In addition, it can be noted that the CSCT underestimates the shear capacity of cantilevers and continuous beams subjected to distributed loading (failure M⁻ in Table 7.3). A physical meaning of this issue has been outlined in the previous sections and in the work by Perez Caldentey et al. [23]: according to the CSCT, all loads acting at a distance larger than $0.5d$ from the fixed support participate without any reduction to the shear force at the control section, leading to safe design solutions.

Table 7.3 Summary of ratio of experimental results to calculated shear strengths according to the models investigated in this study

		N. tests	CSCT [1]		Refined approach: Eq. (7.3)+ Eq. (7.7)		Closed-form: Eq. (7.18) ($a_{cs}\geq 1$)	
			Mean Value	COV	Mean Value	COV	Mean Value	COV
[3]		635	1.02	0.156	1.01	0.136	1.00	0.141
Table 7.4		95	1.04	0.160	1.02	0.126	1.02	0.132
Table 7.5		27	1.21	0.123	1.21	0.123	1.21	0.127
Table 7.6		63	1.03	0.176	1.05	0.119	1.02	0.132
Table 7.7		20	1.44	0.144	1.12	0.109	1.12	0.119
Table 7.8		26	1.64	0.195	1.18	0.129	1.13	0.122
Table 7.9		16	1.18	0.186	1.03	0.105	1.02	0.102
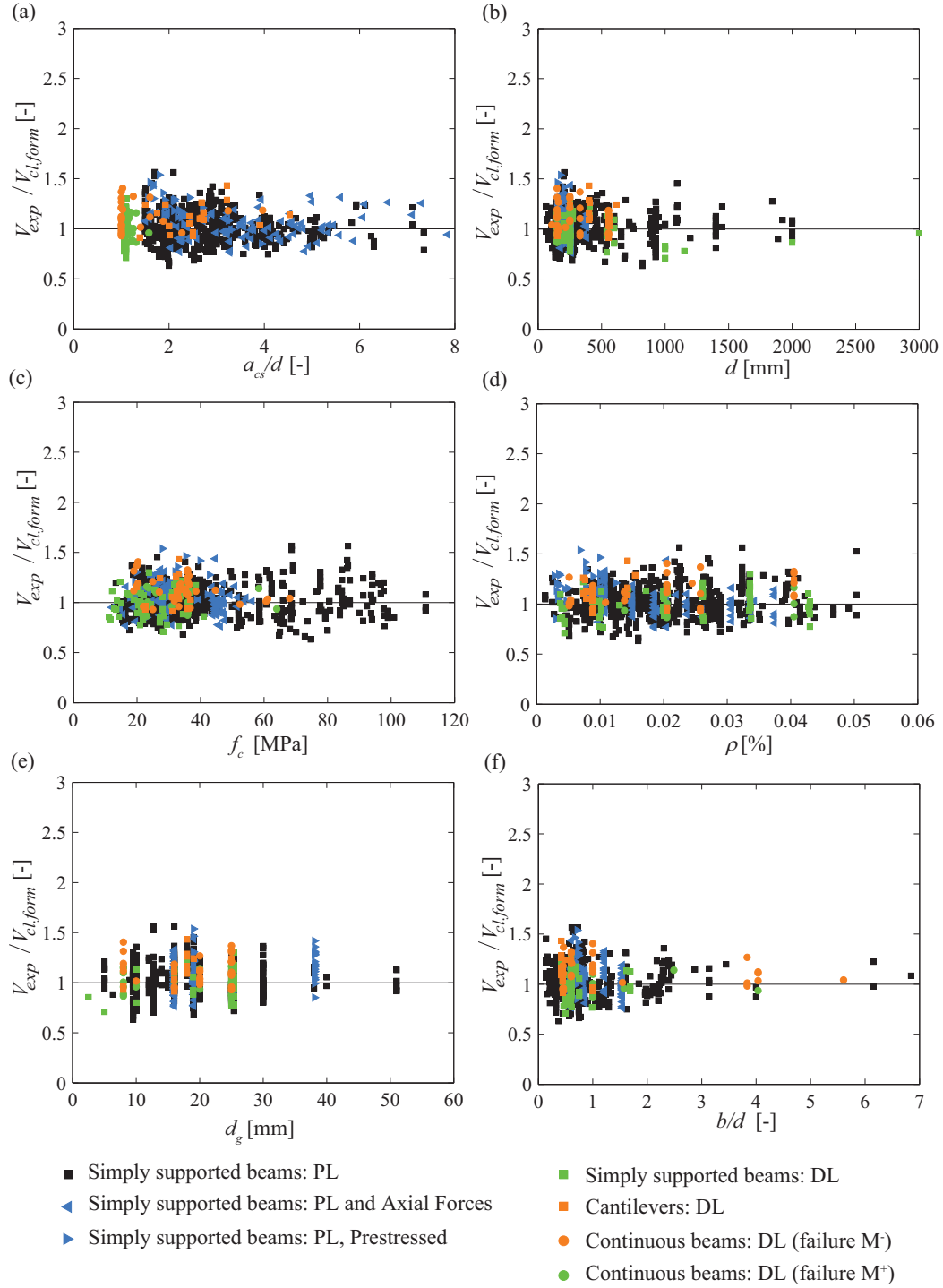
Figure 7.23 Ratio V_{test}/V_{calc} as a function of different mechanical and geometrical parameters for the cases of simply supported beams, cantilevers and continuous beams without transverse reinforcement subjected to point and distributed loading, with and without axial forces

The refined approach (Eq. (7.3) + Eq. (7.7)) and the closed-form equation (Eq. (7.18)) provide good predictions of the experimental results of slender members subjected to various loading conditions (refer to Table 7.3). A good agreement with no noticeable trends for the main mechanical and geometrical parameters can be observed when comparing the closed-form solutions to the available test results: control section shear span a_{cs}/d (Figure 7.23a), effective depth d (Figure 7.23b), compressive strength f_c (Figure 7.23c), reinforcement ratio ρ (Figure 7.23d), maximum aggregate size d_g (Figure 7.23e) and width-to-depth ratio b/d (Figure 7.23f). It is interesting to observe that, although there is still disagreement within the research

community on the influence of the width-to-effective depth ratio on the shear stress at failure, the comparison between the available experimental results and the predicted shear strengths do not show a clear trend with respect to this parameter (as observed in [28–30]).

However, it shall be noted the refined approach (Eq. (7.3) + Eq. (7.7)) and the closed-form equation (Eq. (7.18)) slightly underestimate the shear capacity of cantilevers and continuous beams subjected to distributed loading (refer to Table 7.7 and Table 7.8). As observed in the previous sections, this may be due to one the following reasons: (i) the assumed shape of the critical shear crack does not consider that a possible secondary flexural crack (crack type C, refer to [4]) may merge with the primary flexural crack (crack type A, refer to [4]) during loading, leading to a reduction of the loads transferred through the critical shear crack (see Section 7.5.3) and a redistribution of the shear-transfer actions; (ii) for some cases, when no information is available on the reinforcement layout or for multiple layers, a value of $3d_b$ has been assumed as bar spacing: this may lead to a safe estimate of the contribution of the dowelling action and thus of the shear strength of the member (see [3] and Section 7.2.3); (iii) in the closed-form equation, the assumption of a $\Delta V = V_F/5$ may be too conservative for cantilevers with large reinforcement content (refer to Figure 7.16a-d).

7.8 Conclusions

This Chapter presents an overview on the shear design of slender beams and one-way slabs without transverse reinforcement subjected to different loading and support conditions. The main conclusions are summarized below:

1. The contribution of the various shear-transfer actions can be calculated for simply supported beams, cantilevers and continuous beams subjected to concentrated and distributed loading, by assuming a realistic shape and kinematics of the critical shear crack and by integration of stresses at the crack surface.

2. The shear strength is shown to be significantly dependent on the location and shape of the critical shear crack. Different shear failure criteria are governing for different loading and support conditions.

3. By selecting a power-law equation that approximates the failure criteria obtained by integration of stresses along the crack surfaces, a simple closed-form equation can be derived. This equation is shown to be simple to be used and to allow calculating the shear capacity and understanding the role of the main mechanical parameters governing the shear strength (flexural reinforcement ratio ρ, compressive strength f_c, aggregate size d_g, moment-to-shear ratio at the control section a_{cs}).

4. It is shown that for each possible location of the control section, the closed-form expression provides almost identical results to the refined approach that accounts for the contribution of the various shear-transfer actions.

5. The shear capacity can be estimated by using the closed-form equation. The shear strength has to be checked at any potential control section located at a distance d from a static discontinuity (intermediate support, end support, point of contraflexure or concentrated load) or geometric discontinuity (change of cross-section geometry or reinforcement). In the presence of distributed loads acting on the tension face of the member in the proximity of the intermediate supports in continuous beams or fixed supports in cantilevers, a fraction of the load ΔV shall be subtracted from the shear force acting at the control section.

6. In the case of different load combinations applied, the angle β_{AB} and the coefficient k_a shall be calculated assuming at the investigated section the minimum experienced moment-to-shear ratio due to the different load combinations. On the contrary, ε_s in the load-deformation relationship and a_{cs} in the right part of the closed-form equation shall be calculated assuming the less favourable load combination (lowest shear capacity).

7.9 Appendix A

Table 7.4 Simply supported beams or cantilevers subjected to point load and axial forces

Researchers	No. of specimens	f_c [MPa]	σ [MPa]	d [mm]	a/d [-]	ρ [%]	$V_{exp}/V_{closed-eq.}$ (COV)
Jøregensen et al. [15]	19	24.8 to 30.2	2.94 to 18.2	164	2.74 to 3.34	1.07	1.14 (0.121)
Khulmann et al. [31]	32	27.1 to 51.5	1.44 to 7.69	260	2.88 to 4.81	0.97 to 2.60	0.97 (0.107)
Morrow et al. [14]	11	12.1 to 44.6	-1.81 to -0.84	349 to 387	3.67 to 5.71	0.96 to 3.43	1.03 (0.082)
Madsen et al. [17]	6	19.5 to 23.6	-5.67 to-1.56	175	3.57	3.74	0.98 (0.142)
Diaz de Cossio et al. [32]	7	26.3 to 29.3	-2.32	252	3.63 to 6.65	1.01 to 3.37	1.02 (0.113)
Mattock et al. [33]	20	15.5 to 56.2	-3.37 to 2.11	254	3.00 to 5.40	1.02 to 3.07	1.01 (0.148)
	95						1.02 (0.132)

Table 7.5 Prestressed simply supported beams or cantilevers subjected to point loading

Researchers	No. of specimens	f_c [MPa]	σ [MPa]	d [mm]	a/d [-]	ρ [%]	$V_{exp}/V_{closed-eq.}$ (COV)
Kar [34]	7	28 to 35.9	-1.52 to -4.00	152 to 178	4.00 to 5.00	0.45 to 1.25	1.31 (0.107)
Sozen et al. [35]	20	17.8 to 42.9	-0.17 to -4.89	204 to 238	3.84 to 6.48	0.28 to 0.96	1.17 (0.121)
	27						1.21 (0.127)

Table 7.6 Simply supported beams subjected to distributed load

Researchers	No. of specimens	f_c [MPa]	b [mm]	d [mm]	l/d [-]	ρ [%]	$V_{exp}/V_{closed-eq.}$ (COV)
Acevedo et al. [36]	1	32.4	332	205	13	1.72	1.13 (-)
Cavagnis et al. [4]	2	33.6	250	556	10.1	0.89	1.08 (0.031)
Dassaw [37]	3	24.3 to 28.1	914	541	10.1	1.02	1.01 (0.100)
Diaz de Cossio et al. [32]	2	19 to 41	152	252	11.1	0.99	0.95 (0.124)
Feldman et al. [38]	4	23.8 to 38.6	152	252	11.1	3.36	1.15 (0.101)
Klein [39]	2	29.4 to 33.1	533	541 to 1151	12	0.98 to 1.05	0.77 (0.013)
Krefeld et al. [19]	29	11.2 to 36.8	152	250 to 256	11.9 to 19.5	1.31 to 4.30	1.01 (0.114)
Leonhardt et al. [18]	7	31.1 to 33.6	189 to 190	272 to 274	11 to 22	2.05 to 2.06	1.15 (0.030)
Shioya et al. [20]	8	21.1 to 28.5	300 to 1500	600 to 3000	12	0.38 to 0.44	0.89 (0.138)
Smith [40]	3	28 to 36.2	150	200	12.2 to 18.3	2.01	0.95 (0.095)
Tung et al. [24]	2	33.8	170	407	12.3	0.74	1.11 (0.050)
	63						1.02 (0.132)

Table 7.7 Cantilevers subjected to distributed load

Researchers	No. of specimens	f_c [MPa]	b [mm]	d [mm]	l/d [-]	ρ [%]	$V_{exp}/V_{closed-eq.}$ (COV)
Cavagnis et al. [5]	6	31.2 to 36.9	250	556 zo 559	3.78 to 10.07	0.54 to 0.89	1.02 (0.087)
Pérez Caldentey et al. [23]	2	31.1 to 33.6	250	562	5.87	0.79	1.09 (0.046)
Tung et al. [24]	6	32.4 to 33.2	170	403 to 407	6.14 to 7.20	0.74 to 1.55	1.22 (0.105)
Uzel et al. [41]	1	27.3	300	617	4.86	0.76	1.24 (-)
Aoyagi et al. [42]	1	36	150	250	4	4.05	1.24 (-)
TNO (d_g = 8 mm) [43]	4	19.8 to 22.7	150	150	4.50 to 6.00	2.05	1.05 (0.116)
	20						1.12 (0.119)

Table 7.8 Continuous beams subjected to distributed load (failure within the region of negative bending moment)

Researchers	No. of specimens	f_c [MPa]	d [mm]	l_c/d [-]	M_{right}/ql^2 [-]	ρ [%]	$V_{exp}/V_{closed-eq.}$ (COV)
Cavagnis et al. [4]	4	33.2 to 36.8	556	6.04 to 9.06	0.100 to 0.400	0.89	1.07 (0.125)
Klaus [44]	7	36.4 to 68.1	109 to 159	6.38 to 7.00	0.056 to 0.062	0.51 to 1.39	1.08 (0.089)
Acevedo et al. [36]	1	31.8	216	6.62	0.125	1.09	1.02 (-)
Bryant et al. [45]	5	20 to 27	330	4.91	0.125	2.45 to 2.58	1.11 (0.163)
Aoyagi et al. [42]	5	36	250	4.00 to 6.00	0.115 to 0.206	4.05	1.20 (0.098)
TNO (d_g = 8 mm) [43]	4	19 to 20.3	150	4.50 to 6.00	0.167	2.05	1.26 (0.101)
	26						1.13 (0.122)

Table 7.9 Continuous beams subjected to distributed load (failure within the region of positive bending moment)

Researchers	No. of specimens	f_c [MPa]	d [mm]	l_{SS}/d [-]	M_{right}/ql^2 [-]	ρ [%]	$V_{exp}/V_{closed-eq.}$ (COV)
Cavagnis et al. [4]	2	36.8	556	8.06	0.100	0.089	1.06 (0.070)
Acevedo et al. [36]	1	30.9	211	3.73	0.125	0.44	0.96 (-)
Klaus [44]	2	58.4 to 64	151 to 245	10.73 to 11.24	0.025 to 0.056	1.39 to 1.44	1.04 (0.140)
Aoyagi et al. [42]	3	36	250	6.00 to 7.00	0.033 to 0.071	4.05	1.01 (0.144)
TNO (d_g = 8 mm) [43]	8	22.2 to 26.0	150	5.20 to 10.39	0.036 to 0.086	2.05	1.01 (0.109)
	16						1.02 (0.102)

7.10 References

[1]   Muttoni A, Fernández Ruiz M. Shear strength of members without transverse reinforcement as function of critical shear crack width. *ACI Structural Journal* 2008; 105 (2):163–172.

[2]   Fernández Ruiz M, Muttoni A, Sagaseta J. Shear strength of concrete members without transverse reinforcement: a mechanical approach to consistently account for size and strain effects. *Engineering Structures* 2015; 99:360–372.

[3]   Cavagnis F, Fernández Ruiz M, Muttoni A. A mechanical model for failures in shear of members without transverse reinforcement based on development of a critical shear crack, submitted for publication in Engineering Structures. 2017.

[4]   Cavagnis F, Fernández Ruiz M, Muttoni A. Shear failures in reinforced concrete members without transverse reinforcement: An analysis of the critical shear crack development on the basis of test results. *Engineering Structures* 2015; 103:157–173.

[5]   Cavagnis F, Fernández Ruiz M, Muttoni A. An analysis of the shear transfer actions in reinforced concrete members without transverse reinforcement, accepted for publication in Structural Concrete. 2017.

[6]   Collins MP, Kuchma D. How safe are our large, lightly reinforced concrete beams, slabs, and footings? *ACI Structural Journal* 1999; 96 (4):482–490.

[7]   Sherwood EG, Bentz EC, Collins MP. Effect of Aggregate Size on Beam-Shear Strength of Thick Slabs. *ACI Structural Journal* 2007; 104 (2):180–190.

[8]   Reineck K, Bentz EC, Fitik B, Kuchma DA, Bayrak O. ACI-DAfStb Database of Shear Tests on Slender Reinforced Concrete Beams without Stirrups. *ACI Structural Journal* 2013; 110 (5):867–876.

[9]   Fernández Ruiz M, Mirzaei Y, Muttoni A. Post-punching behavior of flat slabs. *ACI Structural Journal* 2013; 110 (5):801–812.

[10]   Kani MW, Huggins MW, Wittkopp RR. Kani on shear in reinforced concrete. Deptartment of Civil Engineering, University of Toronto, Toronto, Canada. 1979.

[11]   Bhal NS. Über den Einfluß der Balkenhöhe auf die Schubtragfähigkeit von einfeldrigen Stahlbetonbalken mit und ohne Schubbewehrung. Otto-Graf-Institut, H.35, Stuttgart. 1968.

[12]   Angelakos D, Bentz EC, Collins MP. Effect of Concrete Strength and Minimum Stirrups on Shear Strength of Large Members. *ACI Structural Journal* 2001; 98 (3):290–300.

[13]   Sherwood EG. One-way shear behaviour of large, lightly-reinforced concrete beams and slabs. PhD Thesis, Toronto, Canada: University of Toronto. 2008:547.

[14]   Morrow J, Viest IM. Shear Strength of Reinforced Concrete Frame Members Without Web Reinforcement. *ACI Journal* 1957; 53 (3):833–869.

[15]   Joergensen HB, Hoang LC, Fabrin LS, Malgaard J. Influence of High Axial Tension on the Shear Strength of non-shear RC Beams Influence of High Axial Tension on the Shear Strength of non-shear RC Beams, Proceedings of the International IABSE conference: Assessment, Upgrading, Refurbishment of Infrastruct. 2013:7.

[16]   Fernández Ruiz M, Campana S, Muttoni A. Discussion of paper "Influence of Flexural Reinforcement on Shear Strength of Prestressed Concrete Beams" by E. I. Saquan and R. J. Frosch. *ACI Structural Journal* 2009; 106 (6):907–908.

[17]   Madsen MB, Hansen S, Hoang LC, Maagard J. N-V Interaction in Reinforced Concrete Elements without Stirrups. The Twelth East Asia-Pacific Conference on Structural Engineering and Construction. *Procedia Engineering* 2011; 14:2511–2518.

[18]   Leonhardt F, Walther R. Schubversuche an einfeldrigen Stahlbetonbalken mit und ohne Schubbewehrung. DAfStb H.151, Berlin. 1962.

[19]   Krefeld WJ, Thurston CW. Studies of the shear and diagonal tension strength of simply supported R/C-beams. *ACI Journal* 1966; 63 (4):451–476.

[20]   Shioya T, Iguro M, Nojiri Y, Akiayma H, Okada T. Shear Strength of Large Reinforced Concrete Beams. *Special Publication* 1989; 118:259–280.

[21]   Zararis PD, Zararis IP. Shear Strength of Reinforced Concrete Beams under Uniformly Distributed Loads. *ACI Structural Journal* 2008; 105 (6):711–719.

[22]   Shioya T. Shear Properties of Large Reinforced Concrete, Special Report (in Japanese), Institute of Technology, Shimizu Corp., No. 25. 1989.

[23]   Pérez Caldentey A, Padilla P, Muttoni A, Fernández Ruiz M. Effect of load distribution and variable depth on shear resistance of slender beams without stirrups. *ACI Structural Journal* 2012; 109 (5):595–603.

[24]   Tung ND, Tue NV. Effect of support condition and load arrangement on the shear response of reinforced concrete beams without transverse reinforcement. *Engineering Structures* 2016; 111:370–382.

[25] Collins MP, Bentz EC, Quach PT, Proestos GT. The challenge of predicting the shear strength of very thick slabs. *Concrete International* 2015; 37 (11):29–37.

[26] Červenka V, Červenka J, Sajdlová T, Pukl R. Uncertainty of Predicting Shear Strength. *Solid State Phenomena. Trans Tech Publications* 2017; 259:244–248.

[27] Sigrist V, Bentz EC, Fernández Ruiz M, Foster SJ, Muttoni A. Background to the Model Code 2010 Shear Provisions - Part I: Beams and Slabs. *Structural Concrete* 2013; 14 (2):157–167.

[28] Kani GNJ. How safe are our large reinforced concrete beams? *ACI Journal* 1967; 64 (3):128–141.

[29] Regan PE. Tests of the Wide-beam Shear Resistance of Concrete Slabs, Structures Research Group, Polytechnic of Central London, London, UK. 1982.

[30] Lubell A, Sherwood T, Bentz E, Collins M. Safe Shear Design of Large Wide Beams. *Concrete International* 2004; 26 (1):62–78.

[31] Kuhlmann U, Zilch K, Ehmann J, Jähring A, Spitra F. Querkraftabtragung in Verbundträgern mit schlaff bewehrter und aus Zugbeanspruchung gerissener Stahlbetonplatte ohne Schubbewehrung- Mitteilungen. Institut für Konstruktion und Entwurf Stahl-, Holz-, und Verbundbau, Universität Stuttgart, Germany. 2002:109.

[32] Diaz de Cossio R, Siess CP. Behavior and strength in shear of beams and frames without web reinforcement. *ACI Journal* 1960; 31 (8):695–735.

[33] Mattock AH. Diagonal tension cracking in concrete beams with axial forces. *Journal of Structural Division* 1969; 95 (9):1887–1900.

[34] Kar JN. Diagonal cracking in prestressed concrete beams. *Journal of Structural Division* 1968; 94 (1):83–110.

[35] Sozen MA, Zwoyer EM, Siess CP. Investigation of Prestressed Concrete for Highway Bridges, Part I, Strength in Shear of Beams without Web Reinforcement, Engineering Experiment Station Bulletin No.452, University of Illinois, Urbana, USA. 1959:68.

[36] Acevedo AB, Bentz EC, Collins MP. Influence of Clamping Stresses on the Shear Strength of Concrete Slabs under Uniform Loads, Research Report No. ROSE-2008/0.5, Rose School, Pavia, Italy. 2008:227.

[37] Dassow NA. Effect of Uniform Load on the Shear Strength of Slender Beams without Shear Reinforcement, Master of Science Thesis, University of Texas at Austin, USA. 2014:117.

[38] Feldman A, Siess CP. Effect of Moment Shear Ratio on Diagonal Tension Cracking and Strength in Shear of Reinforced Concrete Beams. Univ. of Illinois Civil Eng. Studies, Struct. Research Series No. 107. 1955.

[39] Klein JR. Behavior of Slender Beams without Stirrups: Effects of Load Distribution and Member Depth, Master of Science Thesis, University of Texas at Austin, USA. 2015:164.

[40] Smith RBL. Shear Reinforcement of Reinforced Concrete Beams Subjected to Distributed Loading. *Magazine of Concrete Research* 1970; 22 (70):17–24.

[41] Uzel A, Podgorniak B, Bentz EC, Collins MP. Design of Large Footings for One-Way Shear. *ACI Structural Journal* 2011; 108 (2):131–138.

[42] Aoyagi Y, Endo T. Ultimate Shear Capacity of Continuous RC Beams Subjected to Distributed Loading, Proceedings, Fourth East Asia-Pacific Conference on Structural Engineering and Construction, Seoul, South Korea. 1993:727–732.

[43] van den Beukel A, Monnier T. Dwarskracht, Rapport B-84-522/62.5.0804 IBBC TNO Delft, Netherlands. 1985:48.

[44] Klaus T. Shear Behaviour of Reinforced Concrete Box Culverts, Master of Science Thesis, Univesity of Toronto, Canada. 2007:197.

[45] Bryant RH, Bianchini AC, Rodriguez JJ, Kesler CE. Shear Strength of Two-Span Continuous Reinforced Concrete Beams with Multiple Point Loading. *ACI Structural Journal* 1962; 59 (9):1143–1177.

Chapter 8 Further applications of the mechanical model and the closed-form equation

This Chapter presents how the mechanical model and the closed-form equation can be extended and applied to lightweight reinforced concrete beams, to reinforced concrete members with low amount of shear reinforcement (in percentage less than 0.2% - 0.3%), and to reinforced concrete members with steel fibres (in proportion of less than 2% in volume). Moreover, the closed-form equation (Eq. (7.18)) derived in Chapter 7 is simplified for design purposes.

8.1 Extension of the mechanical model and the closed-form equation

8.1.1 Applications to lightweight reinforced concrete beams

The basic principles of the mechanical model based on the integration of the shear-transfer actions at the critical shear crack surface were introduced in Cavagnis et al. [1] for normal and high-strength reinforced concrete beams without transverse reinforcement. The mechanical model and the closed-form equation can be extended to lightweight reinforced concrete (LWC) members, introducing some modifications in order to account for the different behaviour of these members, due to the replacement of normal weight aggregates with lightweight aggregates.

It has been experimentally observed that the crack surface of normal strength concrete beams is generally formed through the concrete matrix and around the aggregate particles, whereas that of lightweight concrete members mainly passes through the aggregate particles [2]. Therefore, the aggregate interlock contribution for LWC members is expected to be lower than for normal-strength concrete members. In addition, experimental investigations have shown that the softening behaviour in tension of LWC is steeper than in normal weight concrete and the fracture energy is reduced [3]. This different behaviour can be explained on the basis of the smaller strength of lightweight aggregates and the reduced capacity of the aggregates to control the crack opening.

Therefore, on the basis of the previous observations, the refined approach can be applied to LWC members introducing the following modifications: (i) the aggregate size is assumed equal to 0, in agreement with the CSCT [4]; (ii) the fracture energy G_F is calculated according to *fib* Model Code 2010 [5], as $G_F=G_{F0}+1.6 \cdot f_{ct}$ (expressed in N/m), where G_{F0} is assumed equal to 24 N/m for lightweight concrete with normal weight sand and equal to 0 for lightweight concrete with lightweight sand.

The closed-form equation (Eq. (7.18)) can also be applied to lightweight reinforced concrete beams, assuming d_{dg}=16 mm, in agreement with the previous observations and with the assumptions of the CSCT [4].

In order to validate the proposed approaches, a total of 50 lightweight reinforced concrete beams with normal weight sand subjected to point load have been collected from literature and compared with both the refined approach and the closed-form equation. Table 8.1 shows that the presented approaches provide consistent and accurate results. However, the knowledge of the fracture properties and the aggregate interlock capacity of LWC is still insufficient and further investigations are needed to determine the softening behaviour and the influence of the aggregate size in lightweight concrete members.

	V_{exp} / V_{calc} [-]	CoV [-]
Refined approach Eq. (6.5).+ Eq. (6.33), assuming x_A =0.5a	1.04	0.110
Closed-form equation (Eq. (7.18)), assuming x_F =a-d	1.05	0.104

Table 8.1 Comparison of calculated and experimental shear strengths of LWC simply supported beams subjected to point load: average value V_{exp} / V_{calc} and coefficient of variation (CoV)

8.1.2 Applications to reinforced concrete beams with low amount of transverse reinforcement

Members with low amount of transverse reinforcement fail by localization of strains in the critical shear crack [6]. Therefore, the shear design of these members shall be based on strain-based models [4]. On the contrary, in members with large amount of transverse reinforcement (generally above 0.3%), cracks are distributed over the height of the specimens and avoid strain localization and failure is related to crushing of concrete. Such members shall thus be designed on the basis of equilibrium-based approaches such as stress fields [7] or strut-and-ties models.

An attempt to describe the kinematics of the critical shear crack and the contribution of the various shear-transfer actions of beams with low amount of transverse reinforcement has been recently presented by Campana et al. [8] and Huber et al. [9]. By analysing the various shear-transfer actions, the authors agreed that the shear reinforcement provides a significant contribution to the shear strength, important dowel forces occur in the longitudinal bars when the critical crack develops in the vicinity of a vertical stirrup and the height of the uncracked concrete above the tip of the critical crack is reduced with respect to members without transverse reinforcement. From [8] and [9], the critical shear crack can be idealized by a bilinear shape (segment A-B and segment B-F) and it can be observed that its kinematics is characterized by a centre of rotation located near the tip of the crack (in agreement to the available experimental measurements on members without shear reinforcement, refer to Chapter 3 and 4). Segment A-B can be assumed to develop up to the neutral axis $d_B = d-c$ and its angle can be approximated by Eq. (6.6). With respect to segment B-F, it has been experimentally observed [8, 9] that it propagates in a stable manner within the compression zone for a longer length l_F ($l_F > 0.5d$ [8]) than the one measured in members without transverse reinforcement [10]. This difference is due to the fact that the transversal reinforcement controls the opening of the critical shear crack and allows a stable propagation of the critical shear crack for a longer length than the one experimentally measured in members without shear reinforcement. Therefore, the length l_F of the segment B-F can be assumed, in agreement with these experimental evidences [8, 9], to vary as a function of the spacing between stirrups (s) and the amount of transverse reinforcement ($f_{yw} \cdot \rho_w$), according to the following analytical expression:

$$l_F = d \cdot \left(\frac{1}{6} + k_S \cdot \frac{x_B - x_A}{s} \cdot \frac{f_{yw} \cdot \rho_w}{f_{yw0}} \right) \leq \frac{1}{2} d \qquad (8.1)$$

where $x_B - x_A$ is the horizontal projection of the quasi-vertical branch of the critical shear crack (refer to Figure 8.1), f_{yw0} is a reference yielding strength of the stirrups assumed equal to 500 MPa and k_S is a constant of the model, which can be estimated equal to 200. It can be noted that in Eq. (8.1), l_F is limited by an upper value of $0.5d$, to guarantee that the critical shear crack develops within the height of the specimen. The associated angle β_{BF} of segment B-F can be taken equal to $\pi/8$ in agreement with the one assumed for members without shear reinforcement.

The shear capacity of simply supported beams with shear reinforcement can be thus calculated, by vertical equilibrium of the rigid body shown in Figure 8.1, as follows:

$$V_{c,S} = V_{Res} + V_{Agg} + V_{Dowel} + V_{Compr} + V_S = \frac{V_{Res} + V_{Agg} + V_{Dowel} + V_S}{1 - 0.5 \cdot h_F / r_F} \qquad (8.2)$$

where V_{Res}, V_{Agg}, V_{Dowel}, V_{Compr} and V_S are respectively the contribution of the residual tensile strength of concrete, aggregate interlock, dowelling action, compression zone and shear reinforcement, h_F is the thickness of the uncracked concrete above the tip of the critical shear crack ($h_F = d - d_F$) and r_F is the horizontal distance between the tip of the critical shear crack and the axis of load introduction (refer to Figure 8.1).
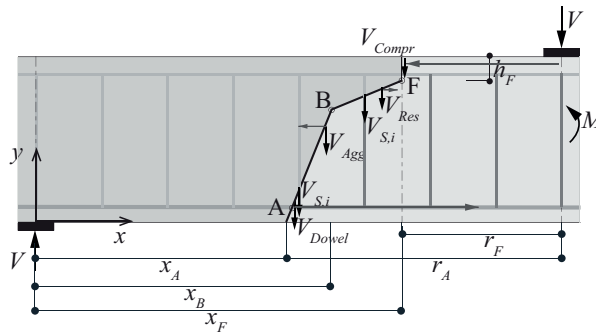
Figure 8.1 Simply supported beam with shear reinforcement subjected to point loading: rigid body equilibrium and internal forces

Based on the experimental measurements, it is reasonable to consider that all stirrups intersected by the critical crack profile are fully activated at peak load: as observed by Campana et al. [8], a very small vertical opening of the critical crack is sufficient to yield the bars (vertical opening $v = 0.3$ mm) and with the assumption of an upper limit of the length l_F equal to 0.5d, which represents a lower-bound value of the length l_F experimentally measured, it is reasonable to assume that all stirrups intercepted by the critical crack are yielded. Therefore, V_s can be defined as:

$$V_S = \rho_w \cdot f_{yw} \cdot b \cdot (x_F - x_A)$$

(8.3)

where $\rho_w = A_{sw}/(b \cdot s)$ is the ratio of transverse reinforcement, A_{sw} is the area of the stirrups, s is the spacing of the stirrups, f_{yw} is the yield strength of the stirrups, x_A and x_F are respectively the horizontal coordinates of the onset and the tip of the critical shear crack.

With respect to the dowelling action (V_{Dowel}), Yoon et al. [6] observed that an appropriate amount of transverse reinforcement helps controlling bond splitting cracks along the longitudinal reinforcement and allows increasing the dowel capacity of the flexural bars. Campana et al. [8] developed a numerical model to investigate the influence of the shear reinforcement on this action and showed that the maximum dowelling action is reached closed to the end support (left support in Figure 8.2a). Moreover, the authors noted that the dowel capacity increases in the vicinity of a stirrup and its value remains almost constant for a length L_{dow} along the longitudinal reinforcing bars (dashed black curve in Figure 8.2b). The authors also showed that the dowelling action is reduced if the critical crack intercepts the longitudinal reinforcement at a distance larger than L_{dow} from the closest intercepted stirrup, but its contribution remains more significant than the one calculated for members without transverse reinforcement (continuous black curve in Figure 8.2b). Since the location of the critical shear crack with respect to the position of the stirrups is a priori unknown, it is proposed to define a coefficient $k_{b,stirrups}$, which provides an average value of the dowelling action within the spacing between two stirrups. Based on the numerical results [8], the coefficient $k_{b,stirrups}$ can be assumed to increase for larger transverse reinforcement ratios (ρ_w), flexural strength of the stirrup (f_{yw}) and diameter of the longitudinal bars (d_{bar}). On the contrary, its value decreases for increasing values of the spacing between stirrups (s). Moreover, $k_{b,stirrups}$ shall always be larger than k_b (k_b is the reduction factor for members without transverse reinforcement (Eq. (6.25)). In addition, an upper limit of $k_{b,stirrups}$ equal to 1 is proposed (continuous red curved in Figure 8.2b), although the dowel action may eventually be larger for larger values of shear reinforcement [11].

The dowelling action (Eq. (6.27)) thus results (dashed red curve in Figure 8.2b):

$$V_{Dowel} = k_{bstirrups} \cdot f_{ct} \cdot n \cdot (b/n - d_b) \cdot 2d_b$$

(8.4)

and $k_{b,stirrups}$ can be defined, on the basis of the numerical results, as:

$$k_{b,stirrups} = \max \left(k_{\rho w} \frac{f_{yw} \cdot \rho_w}{f_{yw0} \cdot \rho_{wmin}} \cdot \frac{d_b}{s}, k_b \right) = \max \left(10 \cdot f_{yw} \cdot \rho_w \cdot \frac{d_b}{s}, k_b \right) \le 1$$

(8.5)

where $\rho_{w,min}$ and $k_{\rho w}$ are assumed constant and equal respectively to 0.001 and to 5, and k_b is defined as in Eq. (6.25).
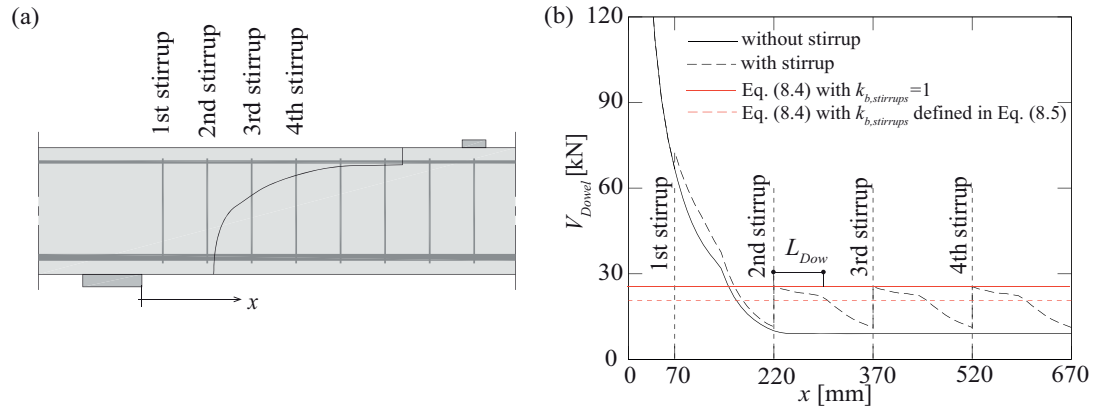
Figure 8.2 (a) Scheme of the investigated beam; (b) dowelling action as a function of the distance of the critical shear crack to the edge of the end support (analyses performed by Campana et al. [8] for two beams with and without shear reinforcement) and definition of $k_{b,stirrups}$
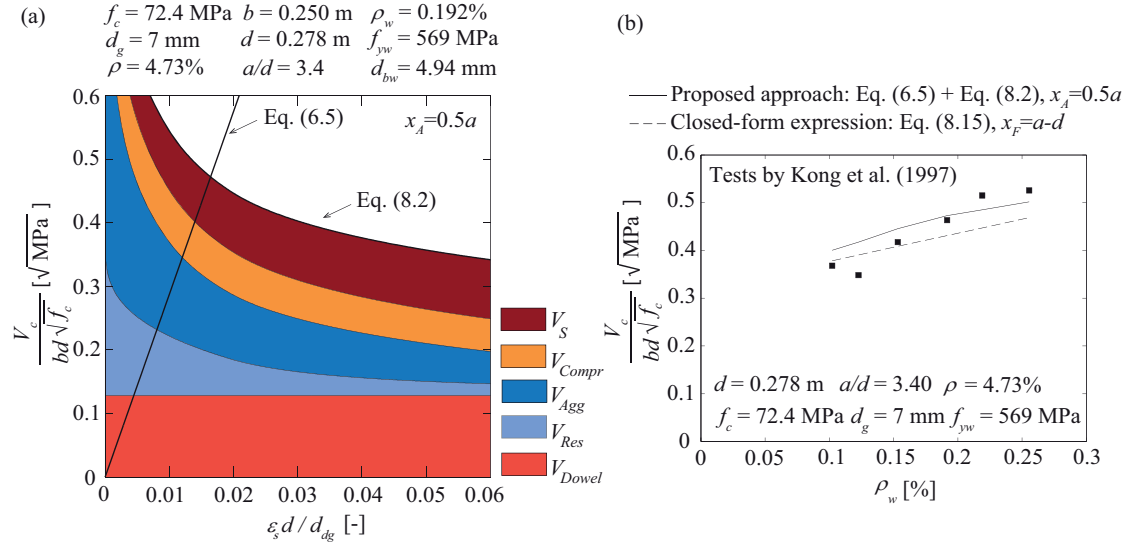
Figure 8.3 (a) Failure criterion and load-deformation relationship and contribution of the shear-transfer actions for a simply supported beam with shear reinforcement subjected to point loading; (b) comparison of the solutions of the refined approach and the closed-form equation with the experimental results of a test campaign investigating the influence of the shear reinforcement ratio ρ_w [12]

Figure 8.3a shows an instance of the contribution of the different shear-transfer actions to the shear strength as a function of the strains at the level of the longitudinal reinforcement for a simply supported beam with transverse reinforcement subjected to point loading. When the shear force (defined by the load-deformation relationship) equals the shear capacity (defined by the failure criterion), failure occurs (intersection between Eq. (6.5) and Eq. (8.2)). It can be observed that the contribution of the dowelling action is dominant for this case (about 27% of the total shear force), whereas the shear reinforcement and the aggregate interlock carry respectively 20% and 23% of the total shear force. However, it shall be noted that for a member with the same geometrical and mechanical parameters but with a reinforcement ratio ρ equal to 1%, the shear reinforcement becomes governing (43% of the total shear force) and the contribution of the dowelling action is reduced (11%).

The closed-form expression (Eq. (7.18)) can also be applied to reinforced concrete beams with low amount of transverse reinforcement. However, Eq. (7.18) shall be modified, in order to account for the contribution of the shear reinforcement and for the enhanced dowel capacity compared to members without shear reinforcement (refer to [8] and Eq. (8.4)) .

The contribution of the stirrups to the shear strength can be calculated using Eq. (8.3), which can be simplified introducing an average value of the horizontal projection of the critical shear crack: x_F-x_A can be assumed for the closed-form equation equal to·d. The contribution of the transverse reinforcement to be accounted for in the closed-form equation results:

$$V_{S,cl.form} = \rho_w \cdot f_{yw} \cdot b \cdot \left(x_F - x_A\right) \approx \rho_w \cdot f_{yw} \cdot b \cdot d \tag{8.6}$$

With respect to the dowelling action, it has been experimentally and numerically observed [8] that its contribution to the shear strength is more significant than in members without shear reinforcement. Therefore, Eq. (7.18) should be adapted taking into account this additional dowel capacity. It shall be noted that a fraction of the total dowelling action is accounted for in the closed-form equation. Eq, (7.18) has been derived from the mechanical model, where the contribution of the dowelling action is calculated according to Eq. (6.27). Based on these observations, assuming an average spacing between longitudinal bars equal to $3d_b$, the additional dowel capacity results:

$$V_{Dowel,cl.form} = k_{b,stirrups} \cdot f_{ct} \cdot 5 \cdot \rho \cdot b \cdot d - k_b \cdot f_{ct} \cdot 5 \cdot \rho \cdot b \cdot d \tag{8.7}$$

where k_b is the reduction factor that accounts for the state of strains in the flexural reinforcement (refer to Eq. (6.25)). For shear design, k_b can be estimated, in agreement with Fernandez et al. [13], equal to 0.25 (the beams investigated in this paper are members that failed prior to the development of plastic strains in the longitudinal reinforcement and the assumption of k_b=0.25 is a safe estimate for design [13]). Eq. (8.7) can thus be simplified:

$$V_{Dowel,cl.form} = \left(k_{b,stirrups} - 0.25\right) \cdot f_{ct} \cdot 5 \cdot \rho \cdot b \cdot d \geq 0 \tag{8.8}$$

By introducing Eq. (8.6) and Eq. (8.8) in Eq. (8.2), the shear capacity results:

$$V_{c,S} = V_c + \frac{V_{S,cl.form} + V_{Dowel,cl.form}}{1 - 0.5 \cdot h_F / r_F} = V_c + \frac{V_{S+D}}{1 - 0.5 \cdot h_F / r_F} \tag{8.9}$$

where V_c corresponds to the contribution of concrete and steel to the shear strength of the same member designed without transverse reinforcement (calculated according to Eq. (7.3)) and V_{S+D} is the sum of the contribution of the transverse reinforcement (Eq. (8.6)) and the enhanced dowel capacity (Eq. (8.8)). Eq. (8.9) can also be written as (see Figure 8.4a):

$$V_{c,S} = V_c(\varepsilon_E) + k_c \cdot V_{S+D} = \eta_c \cdot V_c + k_c \cdot V_{S+D} \tag{8.10}$$

where $V_c(\varepsilon_E)$ represents the contribution to the shear strength obtained from the failure criterion of a member designed without shear reinforcement, ε_E is the deformation at failure, η_c is a reduction factor and k_c can defined according to Eq. (7.17). The factor η_c can be calculated, based on Figure 8.4a, using the power-law failure criterion (Eq. (7.8)) and the linear load-deformation relationship (Eq. (7.3)):

$$\eta_c = \frac{V_c(\varepsilon_E)}{V_c} = \frac{\left(\frac{k}{\varepsilon_E}\right)^{1/2}}{\left(\frac{k}{\varepsilon_c}\right)^{1/2}} = \left(\frac{\varepsilon_c}{\varepsilon_E}\right)^{1/2} = \left(\frac{V_c}{V_E}\right)^{1/2} \tag{8.11}$$

By replacing Eq. (8.11) in Eq. (8.10), the shear strength is given by:

$$V_{c,S} = \left(\frac{V_c}{V_E}\right)^{1/2} \cdot V_c + k_c \cdot V_{S+D} \tag{8.12}$$

Assuming that at failure the acting shear force is equal to the shear capacity ($V_E = V_{c,S}$), Eq. (8.12) results:

$$\frac{V_{c,S}}{V_c} = \left(\frac{V_c}{V_{c,S}}\right)^{1/2} + \frac{k_c \cdot V_{S+D}}{V_c} \tag{8.13}$$

Eq. (8.13) can be used to calculate the shear strength, even though it required an iterative procedure. Although Eq. (8.13) converges in a fast manner, it can be approximated by a linear equation (refer to Figure 8.4b):

$$\frac{V_{c,S}}{V_c} \approx 1 + k_{lin} \cdot \frac{k_c \cdot V_{S+D}}{V_c} \tag{8.14}$$

where the value of k_{lin} that provides the most accurate approximation of Eq. (8.13) is equal to 0.75.

By introducing Eq. (7.18) in Eq. (8.14), the closed-form equation for reinforced concrete members with low amount of shear reinforcement can be written in the following manner:

$$V_{c,S} = k_c \cdot \left[k_a \cdot \left(100 \cdot \rho \cdot f_c \cdot \frac{d_{dg}}{a_{cs}} \right)^{1/3} \cdot b \cdot d + k_{lin} \cdot \left(V_{Dowel,cl.form} + V_{S,cl.form} \right) \right] \tag{8.15}$$

where k_c and k_a are defined according to Eq. (7.17), ρ is the reinforcement ratio, f_c it the compressive strength of concrete, d_{dg} is the crack roughness (refer to Eq. (6.17)), a_{cs} is the moment-to-shear ratio at the investigated section, k_{lin} is equal to 0.75, and $V_{Dowel,cl.form}$ and $V_{S,cl.form}$ are respectively defined in Eq. (8.6) and Eq. (8.8).

Figure 8.4 (a) Definition of contributions of concrete and steel for members without transverse reinforcement and contribution of shear reinforcement and enhanced dowel capacity; (b) iterative equation and its linearization

In Figure 8.3b, the shear strengths calculated according to the refined approach (continuous black curve, Eq. (6.5) and Eq.(8.2) assuming x_A=0.5a, in agreement with simply supported beams without shear reinforcement subjected to point load) and the closed-form equation (dashed black curve, Eq. (8.15) assuming x_F=a-d) are compared to the test results of an experimental campaign investigating the influence of the transversal reinforcement ratio on the shear capacity. The comparison shows that both approaches have similar trends and provide a rather good estimate of the shear strength for these members.

In order to verify the proposed approaches (the refined approach Eq. (6.5) + Eq. (8.2) and the closed-form equation Eq. (8.15)), 105 rectangular reinforced concrete beams with transverse reinforcement subjected to point loading failing in shear have been collected from literature (rectangular beams with $a/d \geq$2.5 and low amount of shear reinforcement ρ_w<0.35%, see Section 8.4). Figure 8.5 and Table 8.2 show a comparison of the solutions of the refined approach and the closed-form equation against the experimental results: both approaches provide good results with a rather low coefficient of variation (respectively 12.7% and 13.7%).

Figure 8.5 Ratio V_{exp}/V_{calc} as a function of transverse reinforcement ratio ρ_w: (a) V_{calc} calculated according to the refined approach (Eq. (6.5) and Eq. (8.2)); (b) V_{calc} calculated according to the closed-form equation (Eq. (8.15))

	V_{exp}/V_{calc} [-]	CoV [-]
Refined approach Eq. (6.5).+ Eq. (8.2), assuming x_A =0.5a	1.08	0.127
Closed-form equation (Eq. (8.15)), assuming x_F =a-d	1.09	0.137
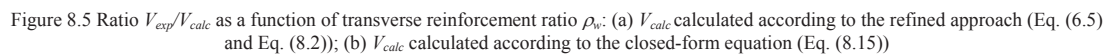
Table 8.2 Comparison of calculated and experimental shear strengths of simply supported beams with low amount of shear reinforcement subjected to point load: average value V_{exp}/V_{calc} and coefficient of variation (CoV)

8.1.3   Applications to steel fibre reinforced concrete beams

The shear strength of steel fibre reinforced concrete (SFRC) beams have been largely investigated in the last decades [14–17]. It has been widely recognized that the addition of steel fibres to the concrete matrix significantly enhances the shear capacity of members without transverse reinforcement and, if a sufficient volume of fibres is added, the brittle shear failure can be replaced in favour of a more ductile behaviour.

In this study, only members made of steel micro-fibres in proportion of less than 2% in volume are considered, in which typically multiple inclined cracks may progress during loading and one critical shear crack develops localizing strains [18]. The approach presented herein is not suitable for members that develop a clear direct strut above the critical shear crack and fail by concrete crushing. In general, this failure mechanism occurs in members with large fibres content, or squat members. However, it has been experimentally observed that the fibre bridging effect delays the propagation of flexural cracks, keeping the compression zone depth larger also for rather slender members ($a/d \approx 3.5$ [19]), and for these cases a theoretical direct strut may develop above the critical shear yielding larger shear capacities. Moreover, the crack pattern experimentally observed in SFRC beams may differ quite significantly from the one of RC members: the former are often characterized by primary flexural cracks with an average spacing s_r at mid-height of the specimen equal to $0.4d$ [20], which is lower than the one experimentally measured in RC members.

Despite these differences the critical shear crack can still be idealized by a quasi-vertical branch (segment A-B) and a quasi-horizontal branch (segment B-F). Segment A-B can be assumed to develop up to the neutral axis and its angle can be approximated by Eq. (6.6), in agreement with members with and without transverse reinforcement. With respect to segment B-F, it can be assumed that its length l_F is related to the parameters that control the opening of the critical shear crack: the volumetric fraction of fibres ρ_f, the aspect ratio of the fibre $\alpha_f = l_f/d_f$ and the bond stress between fibres and concrete matrix τ_b. This assumption is consistent with the one made for reinforced concrete beams with low amount of shear reinforcement, where l_F is assumed to be proportional to the yielding strength of the shear reinforcement f_{yw} and to the transversal reinforcement ratio ρ_w (a large amount of fibres or stirrups helps controlling the opening of the critical shear crack and allows a stable propagation of the crack within the compression zone). Therefore, the length of the quasi-horizontal part of the critical crack can be expressed by the following equation:

$$l_F = d \cdot \left(\frac{1}{6} + k_f \cdot \frac{\alpha_f \cdot \rho_f \cdot \tau_b}{\tau_{b0}} \right) \leq \frac{1}{2} d \tag{8.16}$$

where τ_{b0} is the reference bond stress between the fibres and the matrix, assumed equal to 5 MPa, and k_f is a constant of the model equal to 1/5.

The shear capacity of a SFRC beam can be defined, by vertical equilibrium of the rigid body shown in Figure 8.6, as:

$$V_{c,f} = V_{Res} + V_{Agg} + V_{Dowel} + V_{Compr} + V_f = \frac{V_{Res} + V_{Agg} + V_{Dowel} + V_f}{1 - 0.5 \cdot h_F / r_F} \tag{8.17}$$

where V_{Res}, V_{Agg}, V_{Dowel}, V_{Compr} and V_f are respectively the contribution of the residual tensile strength of concrete, aggregate interlock, dowelling action, compression zone and post-cracking tensile strength due to the bridging action of the fibres after cracking of the concrete matrix. The residual tensile strength of concrete and the post-cracking tensile strength due to fibres are considered separately, although both contributions describe the capacity of cracked concrete to transfer stresses in mode I and may eventually be described by a single contribution.
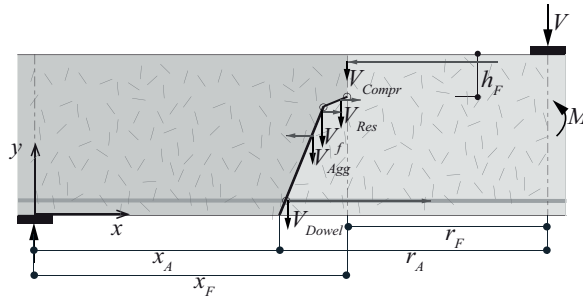
Figure 8.6 Simply supported beam with steel fibre subjected to point loading: rigid body equilibrium and internal forces

The contribution of the various shear-transfer actions is calculated by using the constitutive models presented in Chapter 6. The contribution of the post-cracking tensile strength is calculated on the basis of the constitutive law explained below.

Extensive experimental investigations and analytical studies have shown that adding steel fibres to the concrete matrix significantly increases the post-cracking tensile strength, the post-cracking toughness and the ductility of concrete [21, 22]. The post-cracking tensile strength provided by the fibres over a plane of unit area can be defined according to [23]:

$$\sigma_f = K_f \cdot \alpha_f \cdot \rho_f \cdot \tau_b \tag{8.18}$$

where $\alpha_f = l_f/d_f$ is the aspect ratio of the fibre, ρ_f is the volumetric fraction of the fibres, K_f is the orientation factor and τ_b is the bond stress between the fibres and the concrete matrix.

Various formulae for the determination of K_f have been proposed in literature. Voo and Foster [24] defined the global orientation factor in 3-D condition as a function of the crack opening w. Other authors proposed different and constant values of K_f. Among all, Rajagopalan et al. [25] and Parimi et al. [26] suggested K_f to be equal to 0.637 in 2-D condition, Swamy et al. [27] and Casanova et al. [28] assumed K_f, equal to 0.41 in 3-D condition.

With respect to the bond stress τ between the fibres and the concrete matrix, Lim et al. [29] suggested a value of 6.8 MPa, on the basis of test results. Naaman et al. [22] demonstrated that there is an increase in the bond stress for increasing values of the compressive strength of concrete and suggested a typical value of τ as two times the tensile strength of concrete. Finally, Sharma [30] suggested that the interfacial bond stress can be taken proportional to $\sqrt{fc}$.

In this study, the orientation factor K_f is assumed constant and equal to 0.5, accounting for the fact that in beams, the effects of vibration cause a re-orientation of the fibres inside the concrete and encourage a tendency towards a 2-D distribution (in agreement to [26]). Moreover, the fibre-matrix interfacial bond stress is estimated, in agreement to [31], as $\tau_{bond} = k_{bond} \cdot \sqrt{fc}$, where k_{bond} is equal to 0.8 for end hooked fibres, 0.6 for crimped fibres and 0.4 for straight fibres.

An instance of the adopted post-cracking tensile stresses-crack opening relationship is shown in Figure 8.7a: after cracking, the bridging action of the fibres allows enhancing the deformation capacity and the tensile stresses are kept equal to σ_f for openings larger than w_c (maximum crack width for stress transfer in plain concrete, [32]). Note that, assuming a constant value of K_f, the fibre bridging stresses are assumed constant at the crack surface. By doing so the total fibre contribution can thus be calculated by multiplying the post-cracking stresses times the area of the crack surface. In other words, V_f can be thus calculated by integrating the post-cracking stresses along the crack and projecting them vertically. This leads to:

$$V_f = \sigma_f \cdot b \cdot (x_F - x_A) = K_f \cdot \alpha_f \cdot \rho_f \cdot \tau_b \cdot b \cdot (x_F - x_A) \tag{8.19}$$

Calculating the shear strength can thus be performed iteratively by using Eq. (6.5) and Eq. (8.17), with V_f defined in Eq. (8.19). Figure 8.7b shows an instance of the contributions of the different shear-transfer actions to the shear strength as a function of the strains at the level of the longitudinal reinforcement for a simply supported SFRC beams subjected to point loading. When the shear force (defined by the load-deformation relationship) equals the shear capacity (defined by the failure criterion), failure occurs (intersection between Eq. (6.5) and Eq. (8.17) in Figure 8.7b). It can be observed that, for this case, at failure, the three primary contributions carrying the shear force are the aggregate interlock (almost 50%), the residual tensile strength of concrete (about 20%) and the post-cracking tensile strength provided by the fibres (15%). However, it shall be noted that for larger volume of fibres, the shear force at failure is mainly carried by the post-cracking tensile strength of the fibres, whereas the contribution of aggregate interlock can be significantly reduced (for instance for a member with the same mechanical and geometrical properties but with a volume of fibre of 1.5%, the aggregate interlock contributes for less than 20% of the total shear strength).

As stated previously, in the analysis shown in Figure 8.7b, the dowel capacity is calculated according to Eq. (6.22) defined in Section 6.4.4. However, as observed by Zarrinpour et al. [19], after the initiation of a dowelling crack, steel fibres hold the longitudinal bars by bridging, allowing them to develop some dowelling action and to contribute to the shear strength more significantly than in plain concrete. Moreover, the load-deformation relationship is defined according to Eq. (6.5), where the length l_B contributing to the opening of the critical shear crack is assumed equal to $d-c$ in agreement with reinforced concrete beams without transverse reinforcement. However, this assumption is questionable, since the lower spacing between the adjacent primary flexural cracks in SFRC members (0.4d instead of 0.56d) may influence the length l_B contributing to the opening of the critical shear crack at failure. Further investigations on the critical shear crack shape, on the dowel capacity and on the load-deformation relationship in SFRC beams are thus necessary.
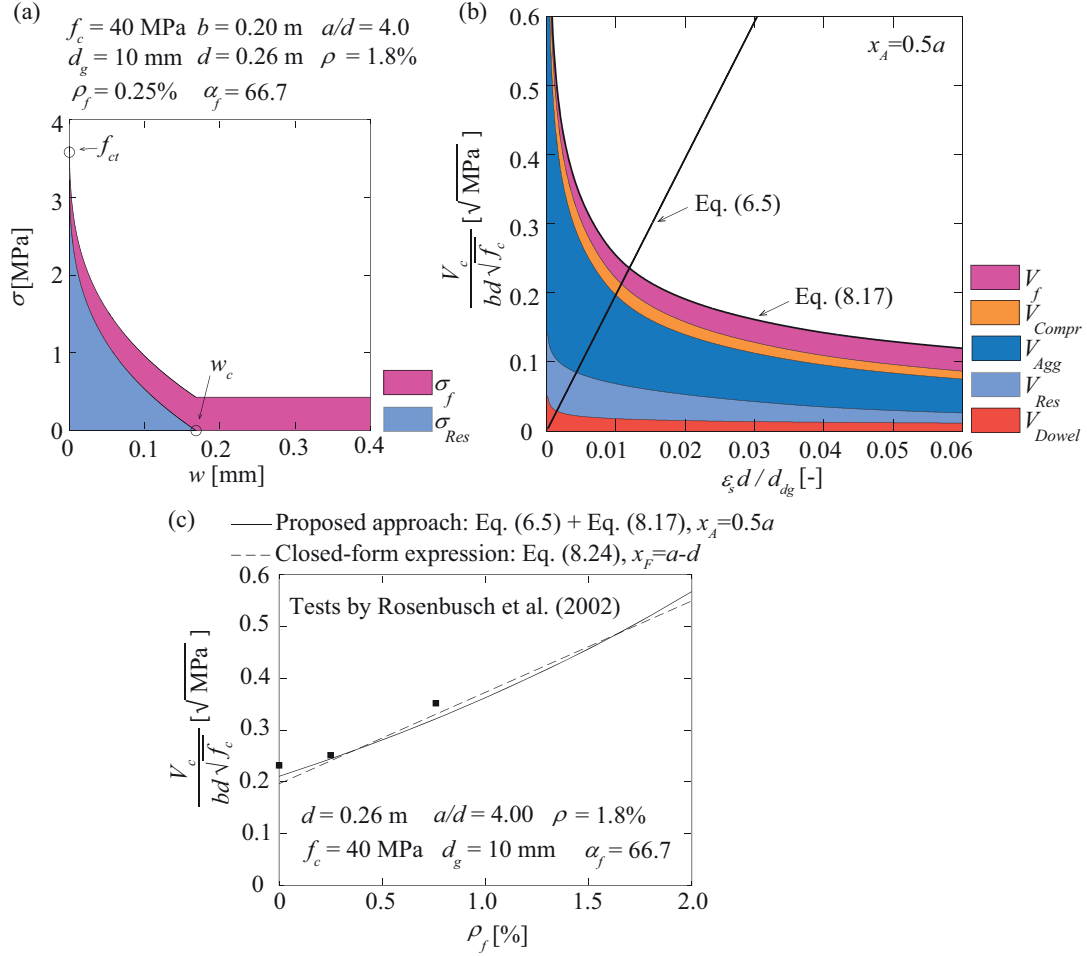
Figure 8.7 (a) Post-cracking behaviour of steel fibre reinforced concrete; (b) failure criterion and load-deformation relationship and contribution of the shear-transfer actions for a simply supported beam with steel fibre subjected to point load; (c) comparison of the refined approach and the closed-form equation with the experimental results of a campaign investigating the influence of the volume of steel fibres

The closed-form equation can also be applied to SFRC beams, by modifying Eq. (7.18) in order to take into account the post-cracking tensile strength due to the presence fibres in the concrete matrix. The contribution to the shear strength induced by the fibres can be calculated by using Eq. (8.19), which can be simplified introducing an average value of the horizontal projection of the critical shear crack: x_F-x_A can be assumed in the closed-form equation equal to 0.75 d. Eq. (8.19) thus results:

$$V_{f,cl.form} = K_f \cdot \alpha_f \cdot \rho_f \cdot \tau_b \cdot b \cdot (x_F - x_A) \approx 0.5 \cdot \alpha_f \cdot \rho_f \cdot \tau_b \cdot b \cdot 0.75 \cdot d \tag{8.20}$$

The closed-form equation for SFRC members can be analytically derived following the main ideas described for members with low amount of shear reinforcement. By introducing Eq. (8.20) in Eq. (8.17), the shear capacity can be written:

$$V_{c,f} = V_c + \frac{V_{f,cl.form}}{1 - 0.5 \cdot h_F / r_F} \tag{8.21}$$

where V_c corresponds to the contribution of concrete and steel to the shear strength of the same member designed without transverse reinforcement (calculated according to Eq. (7.3)) and V_f is the additional residual tensile strength due to fibres. Eq. (8.21) can also be reformulated (by replacing V_{S+D} with $V_{f,cl.form}$ in Figure 8.4a):

$$V_{c,f} = V_c(\varepsilon_E) + k_c \cdot V_{f,cl.form} = \eta_c \cdot V_c + k_c \cdot V_{f,cl.form} \tag{8.22}$$

where $V_c(\varepsilon_E)$ represents the contribution to the shear strength obtained from the failure criterion of a member designed without shear reinforcement, ε_E is the deformation at failure, η_c is a reduction factor (refer to Eq. (8.11)) and k_c is defined in Eq. (7.17).

Assuming that at failure the acting shear force is equal to the shear capacity ($V_E = V_{c,f}$) and dividing Eq. (8.22) by V_c, Eq. (8.22) results:

$$\frac{V_{c,f}}{V_c} = \left(\frac{V_c}{V_{c,f}}\right)^{1/2} + \frac{k_c \cdot V_{f,cl.form}}{V_c} \tag{8.23}$$

Eq. (8.23) can be approximated by a linear relationship as shown in Figure 8.4b for reinforced concrete beams with low amount of shear reinforcement. The closed-form equation for SFRC beams can thus be written in the following manner:

$$V_{c,f} = k_c \cdot \left[k_a \cdot \left(100 \cdot \rho \cdot f_c \cdot \frac{d_{dg}}{a_{cs}}\right)^{1/3} \cdot b \cdot d + k_{lin} \cdot V_{f,cl.form} \right] \tag{8.24}$$

where k_{lin} is equal to 0.75 (refer to Figure 8.4b).

Figure 8.7c illustrates a comparison of the calculated shear strength according to both the refined approach (Eq. (6.5) and Eq. (8.17), assuming $x_A = 0.5a$) and the closed-form equation (Eq. (8.24), assuming $x_F = a-d$) against some test results by Rosenbusch et al. [33]. It can be observed that the two approaches have similar trends and can describe the influence of the volumetric fraction of the fibres on the shear capacity.

In order to verify the proposed approaches, 142 rectangular slender SFRC beams failing in shear have been collected from literature and used for comparison (see Section 8.4). Table 8.3 and Figure 8.8 show that both the refined approach and the closed-form equation provide relatively good estimates of the shear strength for SFRC beams, although their accuracy is slightly lower than when they are applied to simply supported beams subjected to point loading without steel fibres and without shear reinforcement. One of the main reasons for the larger coefficient of variation for SFRC beams is the larger scatter in the experimental results of statically determined SFRC structures in comparison with reinforced concrete structures without steel fibres [34]. The significance of this topic in future applications encourages further experimental investigations on the crack pattern, the load-deformation relationship, the dowelling action and the mechanisms of shear failure of SFRC beams.
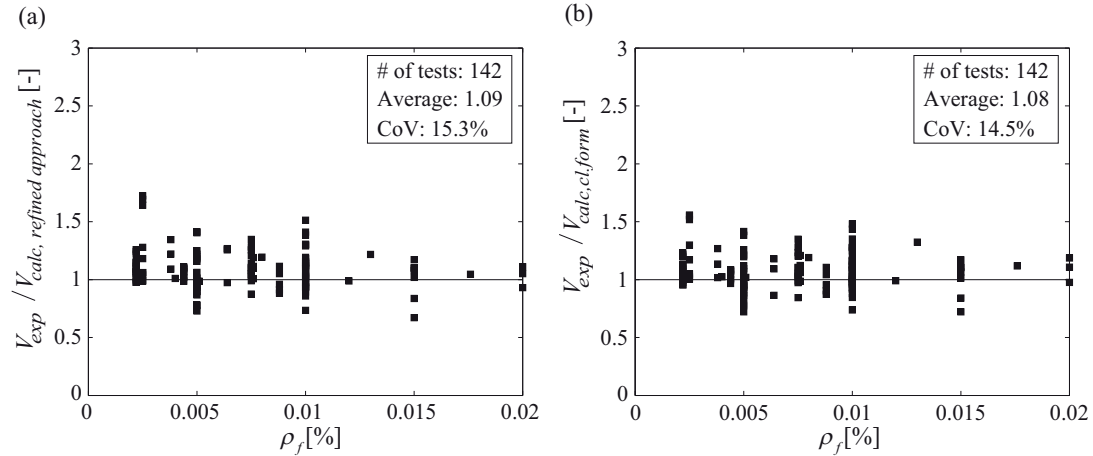
Figure 8.8 (a) Ratio V_{exp}/V_{calc} as a function of the volume of steel fibres: (a) V_{calc} calculated according to the refined appraoch (Eq. (6.5) and Eq. (8.17)); (b) V_{calc} calculated according to the closed-form equation (Eq. (8.24))

	V_{exp} / V_{calc} [-]	CoV [-]
Refined approach Eq. (6.5).+ Eq. (8.17), assuming $x_A = 0.5a$	1.09	0.153
Closed-form equation (Eq. (8.24)), assuming $x_F = a-d$	1.08	0.145

Table 8.3 Comparison of calculated and experimental shear strengths of simply supported SFRC beams subjected to point load: average value V_{exp} / V_{calc} and coefficient of variation (CoV)

8.2 Development of simplified design equations

This section presents some simplifications that can be introduced in order to enhance the use of the closed-form equation developed within the frame of the mechanical model presented in this thesis. As stated in Section 7.8, Eq. (7.18) is a general formulation that allows calculating in a simple manner the shear strength. In particular, Eq. (7.18) accounts for the influence of the location of the control section with respect to the axis of load introduction, through the coefficient k_c, and for the influence of the inclination of the critical shear crack, through the coefficient k_a. Eq. (7.18) is recalled hereafter:

$$V_c = k_c \cdot k_a \cdot \left(100 \cdot \rho \cdot f_c \cdot \frac{d_{dg}}{a_{cs}}\right)^{1/3} \cdot b \cdot d = \frac{1}{1 - 0.15 \cdot \dfrac{d}{r_F}} \cdot \left(0.5 + 0.2 \cdot \left(\frac{a_{cs}}{d}\right)^{1/3}\right)\left(100 \cdot \rho \cdot f_c \cdot \frac{d_{dg}}{a_{cs}}\right)^{1/3} \cdot b \cdot d$$

The coefficient k_c, defined in Eq. (7.12), is related to the geometrical parameters h_F and r_F, where h_F is the thickness of the compression zone above the tip of the critical shear crack and r_F is the horizontal distance between the tip of the crack and the axis of load introduction (see Figure 7.2b). The value of k_c is plotted in Figure 8.9a as a function of the reinforcement ratio ρ for different values of r_F (see black curves): it can be noted that k_c increases for larger reinforcement ratios, whereas its values decreases for larger distances of the investigated crack from the point of load application (larger values of r_F). In Section 7.3, in order to simplify the calculation, the coefficient h_F was assumed constant and equal to $0.3d$, leading to Eq. (7.17). As shown in Figure 7.5, the horizontal distance r_F of the theoretical governing control section varies between d and $2\,d$ for simply supported beams subjected to point loading, whereas its value is larger for simply supported beams subjected to distributed loading. However, r_F cannot be easily quantified when more complex load combinations are applied. Therefore, for design purposes, in the following, k_c is assumed constant and equal to approximately 1.1 for all cases (red curve in Figure 8.9a).

Concerning the coefficient k_a, Eq. (7.16) can be eventually approximated by a simple power-law equation of degree 1/6 (red curve in Figure 8.9b):

$$k_a = \frac{2}{3} \cdot \left(\frac{a_{cs}}{d}\right)^{1/6} \tag{8.25}$$

As shown in Figure 8.9b, Eq. (7.16) and Eq. (8.25) have a very similar shape; therefore, the considerations made in Section 7.3 for the coefficient k_a, calculated with Eq. (7.16), are still valid.
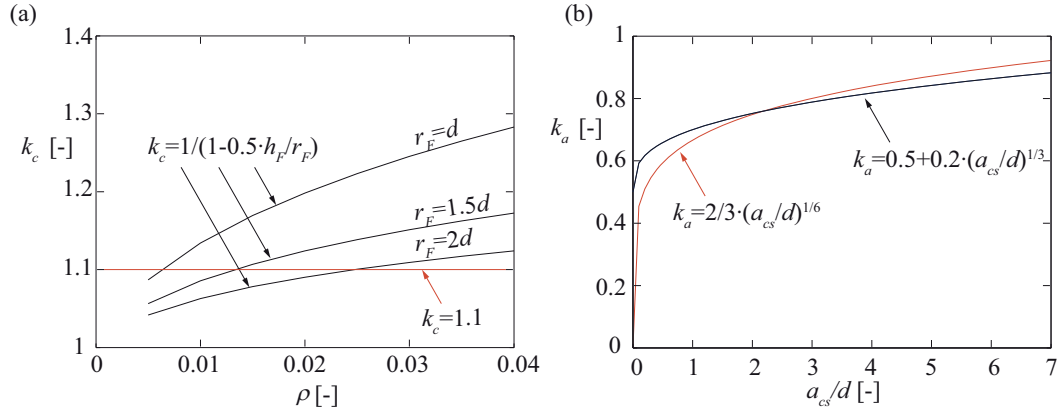
Figure 8.9 (a) Coefficient k_c calculated for a concrete f_c=30 MPa according to Eq. (7.12) as a function of the reinforcement ratio ρ for different values of r_F and assumed k_c in Eq. (8.26); (b) Coefficient k_a: comparison between Eq. (7.16) and Eq. (8.25)

Following the abovementioned assumptions, Eq. (7.17) results:

$$\kappa = k_c \cdot k_a = 1.1 \cdot 0.66 \cdot \left(\frac{a_{cs}}{d}\right)^{1/6} \approx 0.75 \cdot \left(\frac{a_{cs}}{d}\right)^{1/6} \tag{8.26}$$

By substituting Eq. (8.26) into Eq. (7.18), the closed form equation for shear design can be rewritten as:

$$V_c = 0.75 \cdot \left(\frac{a_{cs}}{d}\right)^{1/6} \cdot \left(100 \cdot \rho \cdot f_c \cdot \frac{d_{dg}}{a_{cs}}\right)^{1/3} \cdot b \cdot d = 0.75 \cdot \left(100 \cdot \rho \cdot f_c \cdot \frac{d_{dg}}{\sqrt{a_{cs} \cdot d}}\right)^{1/3} \cdot b \cdot d \tag{8.27}$$

where $a_{cs}=M_E/V_E$, M_E and V_E are respectively the acting bending moment and shear force at the control section, ρ is the reinforcement ratio, f_c is the compressive strength of concrete measured in cylinders and d_{dg} is a coefficient that takes into account the concrete type and its aggregates properties (refer to Eq. (6.17)). Note that the assumed equation for k_a (Eq. (8.25)) allows simplifying Eq. (7.18): the term $(a_{cs}/d)^{1/6}$ is included in the right part of Eq. (8.27).

Eq. (8.27) can thus be used to calculate the shear capacity at the governing control sections. The shear capacity has to be checked at each potential control section located at a distance d from a static discontinuity (edge of intermediate support or point load) or geometric discontinuity or from a section of zero bending moment (refer to Table 7.2 and to control sections in Figure 8.10), in agreement with the considerations on Eq. (7.18). Furthermore, the control section shear span a_{cs} is limited by the conditions $a_{cs} \geq d$, following the observations of Section 7.5.4. For members subjected to axial forces or prestressing, a_{cs} shall be assumed equal to $a_{cs,eff}$, defined according to Eq. (7.24) and Eq. (7.25). The shear resistance of members without shear reinforcement V_c, calculated with Eq. (8.27), has to be compared to the design shear force in the control section V_E and the following equation has to be verified:

$$V_c \geq V_E \tag{8.28}$$

In the presence of loads near intermediate supports or at cantilevers (loads acting on the tension face of the member), the reduction ΔV on the acting shear force V_E at the control section (refer to Eq. (7.35)) can be assumed equal to $V_E/5$, in agreement with the analyses shown in Figure 7.16a-d. However, note that, due to the assumption of a constant k_c, the shear capacity obtained with Eq. (8.27) for cantilevers subjected distributed loading is slightly lower than the shear capacity calculated according to Eq. (7.18). Therefore, the required reduction ΔV may be eventually increased. The shear strength shall thus verify:

$$V_c \geq V_E - \Delta V \tag{8.29}$$

In the regions where the shear resistance is exceeded ($V_E - (\Delta V) > V_c$), shear reinforcement has to be provided.
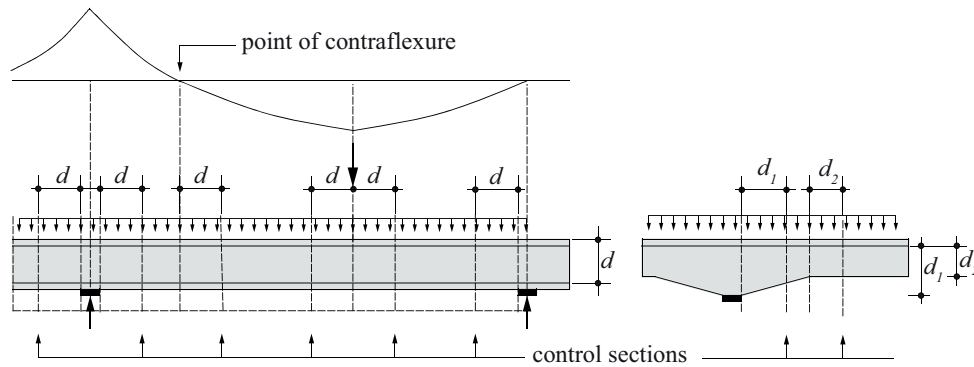
Figure 8.10 Location of the control sections

In Section 7.5.4, it was discussed that in case of variable loading conditions or variable positions of the applied loads, the coefficient k_a shall be calculated assuming a_{cs} equal to minimum moment-to-shear ratio at the control section obtained from the different load combinations, whereas in the right part of Eq. (7.18), a_{cs} shall be assumed equal to maximum moment-to-shear ratio at the control section obtained from the different load combinations. However, in Eq. (8.27), k_a is not explicitly expressed, as a_{cs}/d is introduced in the right part the equation, and thus the influence of the different load combinations on the shape of the critical shear crack and on the shear capacity cannot be directly considered. Therefore, in the case of a variable positions of the applied loads, it is proposed to assume ΔV equal to 0 and a_{cs} shall be taken equal to the maximum moment-to-shear ratio obtained at the control section from the different load combinations. This assumption is less physical, but it allows estimating the lower shear capacity due to the less favourable shape of the critical shear crack.

Further simplifications can be also introduced to use the design equation (Eq. (8.27)) for reinforced concrete beams with low amount of shear reinforcement and for steel fibre reinforced concrete beams without transverse reinforcement. As far as

members with low amount of shear reinforcement concern, Eq. (8.27) shall be modified in order to take into account the contribution of the shear reinforcement and the additional dowel capacity (refer to Eq. (8.15)). By assuming a constant value for k_c (refer to red line in Figure 8.9a) and k_{lin} equal to 0.75 (refer to Figure 8.4b), the additional contribution due to the stirrups and to the dowelling action in Eq. (8.15) can be rewritten as:

$$V_{stirrups} = k_c \cdot k_{lin} \cdot \left(V_{Dowel,cl.form} + V_{S,cl.form}\right) \approx 0.85 \cdot b \cdot d \cdot 5 \cdot f_{ct} \cdot \rho \cdot \left(k_{b,stirrups} - 0.25\right) + 0.85 \cdot b \cdot d \cdot \rho_w \cdot f_{yw} \tag{8.30}$$

where f_{ct} is the tensile strength of concrete, ρ is the longitudinal reinforcement ratio, $k_{b,stirrups}$ is defined in Eq. (8.5), ρ_w is the ratio of transverse reinforcement and f_{yw} is the yield strength of transverse reinforcement.

The shear capacity of a reinforced concrete beams with low amount of shear reinforcement ($\rho_w \leq 0.3\%$) can thus be calculated as:

$$V_{c,S} = V_c + V_{stirrups} = 0.75 \cdot \left(100 \cdot \rho \cdot f_c \cdot \frac{d_{dg}}{\sqrt{a_{cs} \cdot d}}\right)^{1/3} \cdot b \cdot d + 0.85 \cdot b \cdot d \cdot \left(5 \cdot f_{ct} \cdot \rho \cdot \left(k_{b,stirrups} - 0.25\right) + \rho_w \cdot f_{yw}\right) \tag{8.31}$$

with $k_{b,stirrups} - 0.25 \geq 0$.

Concerning SFRC beams without shear reinforcement, the post-cracking tensile strength of concrete due to fibres (refer to Eq. (8.24)) can be approximated, assuming a constant value for k_c and k_{lin} equal to 0.75, by the following equation:

$$V_{sfrc} = k_c \cdot k_{lin} \cdot V_{f,cl.fom} \approx 0.33 \cdot \alpha_f \cdot \rho_f \cdot \tau_b \cdot b \cdot d \tag{8.32}$$

where $\alpha_f = l_f/d_f$ is the aspect ratio of the fibre, ρ_f is the volumetric fraction of the fibres and τ_b is the bond stress between the fibres and the concrete matrix. The fibre-matrix interfacial bond stress can be estimated as $\tau_{bond} = k_{bond} \cdot \sqrt{fc}$, where k_{bond} is equal to 0.8 for end hooked fibres, 0.6 for crimped fibres and 0.4 for straight fibres [31].

The shear strength of SFRC beams without transverse reinforcement ($\rho_f \leq 2\%$) can thus be calculated as:

$$V_{c,f} = 0.75 \cdot \left(100 \cdot \rho \cdot f_c \cdot \frac{d_{dg}}{\sqrt{a_{cs} \cdot d}}\right)^{1/3} \cdot b \cdot d + 0.33 \cdot \alpha_f \cdot \rho_f \cdot \tau_b \cdot b \cdot d \tag{8.33}$$

Table 8.4 shows a detailed comparison of the results of the design equations (Eq. (8.27), Eq. (8.31) and Eq. (8.33) with $a_{cs} \geq d$) against the experimental results of 1179 tests on slender simply supported beams, slender cantilevers and slender continuous beams without transverse reinforcement subjected to point and distributed loading, slender simply supported beams with low amount of shear reinforcement subjected to point loading, and slender simply supported beams with steel fibres subjected to point loading. The average measured-to-calculated shear strength and the coefficient of variation are comparable to those resulting from the refined mechanical model and the closed-form equation presented in the previous Chapters.

Reinforced concrete beams without transverse reinforcement	No. of specimens	V_{exp} / V_c Eq. (8.27) [-]	CoV [-]
Simply supported beams or cantilevers subjected to point load	635	1.03	0.144
Simply supported beams or cantilevers subjected to point load (LWC)	50	1.08	0.110
Simply supported beams subjected to point load and axial compression or tension forces	95	1.04	0.132
Prestressed simply supported beams subjected to point load	27	1.26	0.133
Simply supported beams subjected to distributed load	63	0.99	0.131
Continuous beams subjected to distributed load (failure M⁻) ($\Delta V = V_E/5$)	26	1.20	0.125
Continuous beams subjected to distributed load (failure M⁺)	16	1.09	0.115
Cantilevers subjected to distributed load ($\Delta V = V_E/5$)	20	1.11	0.113
Reinforced concrete beams with low amount of shear reinforcement (ρ_w<0.3%)		$V_{exp} / V_{c,S}$ Eq. (8.31) [-]	CoV [-]
Simply supported beams or cantilevers subjected to point load	105	1.13	0.139
Reinforced concrete beams with steel fibres (ρ_f<2.0%)		$V_{exp} / V_{c,f}$ Eq. (8.33) [-]	CoV [-]
Simply supported beams or cantilevers subjected to point load	142	1.11	0.149

Table 8.4 Comparison of calculated and experimental shear strengths: average value $V_{exp} / V_{c,calc}$ and coefficient of variation (CoV)

8.3   Conclusions

This Chapter presents further applications of the mechanical model based on the development of the critical shear crack and the closed-form equation for lightweight reinforced concrete beams, reinforced concrete beams with low amount of shear reinforcement and steel fibre reinforced concrete members. In addition, a design formulation based on the mechanical model is proposed. The main conclusions are listed below:

1. The shear capacity of lightweight reinforced concrete beams can be satisfactorily estimated considering the aggregate size d_g equal to zero and reduced fracture properties of concrete due to the replacement of normal-weight aggregates with lightweight aggregates.

2. The shear strength of reinforced concrete beams with low amount of shear reinforcement can be calculated following the procedure described for beams without transverse reinforcement. The failure criterion is obtained accounting for the contribution of the beam shear-transfer actions (aggregate interlock, dowelling action, residual tensile strength of concrete, inclined compression chord) and, in addition, for the contribution of the shear reinforcement.

3. The shear strength of SFRC beams can also be investigated on the basis of the mechanical model. This can be done considering the contribution of the various beam shear-transfer actions and the additional post-cracking tensile strength due to the fibres.

4. Further simplifications of the closed-form equation, more suitable for shear design of reinforced concrete members with or without low amount of shear reinforcement or with steel fibres, are proposed. These simplified design equations are compared to the experimental results of 1179 tests reported in literature, leading to good estimates of the shear strength.

8.4   Appendix A

In this appendix, the test series on lightweight concrete beams, reinforced concrete beams with low amount of shear reinforcement and steel fibre reinforced concrete beams, used for validation of the mechanical model and the closed-form equations, are reported.

Table 8.5 Test series on lightweight reinforced concrete beams and comparison with Eq. (7.18)

Researchers	No. of specimens	f_c[MPa]	d [mm]	a/d [-]	ρ [%]	$V_{exp}/V_{closed-eq.}$ (COV)
Ivey et al. [35]	20	19.5 to 33.0	188 to 395	3.00 to 4.95	0.93 to 2.10	1.11 (0.094)
Taylor et al. [36]	24	26.0 to 39.8	221	3.80	1.21 to 1.88	0.98 (0.070)
Walraven [37]	6	27.8 to 31.4	125 to 720	3.00 to 3.11	0.74 to 1.58	1.11 (0.075)
	50					1.05 (0.104)

Table 8.6 Test series on simply supported beams with low amount of transverse reinforcement and comparison with Eq. (8.15)

Researchers	No. of specimens	f_c [MPa]	d [mm]	a/d [-]	ρ [%]	ρ_w [%]	$V_{exp}/V_{closed-eq.}$ (COV)
Angelakos et al. [38]	2	32 to 38	925	2.88	0.50 to 1.01	0.079	0.98 (0.102)
Bhal [39]	4	25.5 to 27.2	300 to 1200	2.70 to 2.88	1.26	0.147	1.08 (0.091)
Bresler et al [40]	2	24.1 to 29.6	464 to 466	3.76 to 3.78	1.80	0.098 to 0.195	1.27 (0.013)
Campana et al. [8]	4	41.5 to 57.2	346 to 354	3.45 to 3.53	1.06 to 1.52	0.062	1.05 (0.075)
Cladera et al. [41]	6	49.9 to 87	351 to 353	2.95 to 2.97	2.28 to 2.99	0.109 to 0.239	1.12 (0.058)
Huber et al. [9]	6	29.6 to 60.9	230 to 920	3.04	1.17 to 1.25	0.084 to 0.112	0.93 (0.119)
Johnson et al. [42]	3	36.4 to 55.9	539	3.10	2.49	0.078 to 0.156	0.96 (0.033)
Johnston et al. [43]	3	22 to 22.2	305	3.00	0.78 to 0.82	0.102	0.92 (0.077)
Kong et al. [12]	31	61.6 to 86.6	198 to 332	2.50 to 3.40	2.79 to 4.73	0.099 to 0.256	1.14 (0.113)
Krefeld et al. [44]	10	15.7 to 42.7	456	3.87	2.23	0.109 to 0.244	0.97 (0.104)
Ozcebe et al. [45]	5	61 to 82	310	3.00 to 5.00	2.59 to 4.43	0.209 to 0.279	1.10 (0.161)
Pansuk et al. [46]	1	35	300	3.50	4.50	0.343	1.15 (-)
Petersson [47]	1	38	322	3.57	1.07	0.215	1.02 (-)
Quast et al. [48]	1	47.3	355	3.27	1.33	0.091	0.91 (-)
Regan [49]	6	25.9 to 42.3	254 to 272	3.22 to 4.36	1.46 to 4.17	0.213	1.10 (0.099)
Roller et al. [50]	3	72.4 to 125.3	762	2.91	1.88 to 2.89	0.158 to 0.234	1.04 (0.133)
Rosenbusch et al. [33]	2	47.9 to 49.2	260	3.37	3.55	0.070 to 0.140	0.96 (0.107)
Sarsam et al. [51]	6	70.1 to 80.1	233	2.50 to 4.00	2.82 to 3.51	0.093 to 0.186	1.34 (0.168)
Yoon et al. [6]	9	36 to 87	655	3.28	2.86	0.081 to 0.236	1.12 (0.079)
	105						1.09 (0.137)

Table 8.7 Test series on simply supported beams with steel fibres and comparison with Eq. (8.24)

Researchers	No. of specimens	f_c [MPa]	d [mm]	a/d [-]	ρ [%]	ρ_f [%]	$V_{exp}/V_{closed-eq.}$ (COV)
Ashour et al. [52]	5	93.8 to 97.1	215	4.00 to 6.00	2.84 to 4.58	0.50 to 1.50	0.79 (0.114)
Barragan [53]	5	37.7 to 38.8	260 to 540	3.34 to 3.50	2.41 to 3.08	0.50	0.97 (0.132)
Batson et al. [54]	31	33.2 to.40.2	126	2.80 to 5.00	3.10	0.22 to 1.76	1.05 (0.079)
Casanova et al. [55]	1	90	225	2.90	3.57	1.30	1.32 (-)
Cucchiara et al. [56]	1	40.9	218	2.80	1.92	1.00	1.16 (-)
Dinh et al. [20]	6	29.6 to 49.2	381 to 610	3.44 to 3.50	1.56 to 2.67	0.75 to 1.50	1.11 (0.061)
Dupont et al. [57]	10	26.5 to 47.6	260	2.50 to 4.04	1.81 to 3.55	0.25 to 0.75	1.15 (0.121)
Jain et al. [58]	13	26.2 to 53.4	251	3.49	2.67	1.00	1.18 (0.114)
Li et al. [14]	11	50.2 to 62.6	102 to 204	2.50 to 3.00	1.10 to 3.30	1.00 to 2.00	1.09 (0.085)
Lim et al. [29]	5	34	221	2.50 to 3.50	1.19 to 2.39	0.50 to 1.00	0.90 (0.107)
Mansur et al. [15]	7	2.06 to 33.40	197	2.80 to.360	1.34 to 2.00	0.50 to 0.75	0.99 (0.127)
Minelli et al. [17]	7	24.4 to 61.1	435 to 910	2.50 to 2.51	0.99 to 1.04	0.25 to 0.64	1.32 (0.169)
Minelli et al. [59]	4	32.1 to 33	940 to 1440	3.00	1.01 to 1.07	0.64 to 1.00	0.95 (0.111)
Noghobai [60]	5	60.2 to 75.7	410 to 570	2.93 to 2.98	2.90 to 3.00	0.50 to 0.75	1.22 (0.130)
Parra-Montesinos et al. [61]	5	31 to 49.2	381	3.40 to 3.50	2.67	1.00 to 1.50	1.08 (0.047)
Rosenbusch et al. [33]	13	37.7 to 48.3	260 to 540	2.50 to 4.00	1.20 to 3.60	0.25 to 0.76	1.07 (0.093)
Schantz [62]	3	31.5 to 33.7	546	2.80	1.84	0.50 to 1.50	0.90 (0.055)
Shoaib et al. [18]	7	23 to 80	240 to 923	3.25 to 3.85	1.44 to 4.03	1.00	1.10 (0.184)
Swamy et al. [63]	3	35.5 to 39.8	210	4.50	4.00	0.40 to 1.20	1.07 (0.100)
	142						1.08 (0.145)

8.5   References

[1]   Cavagnis F, Fernández Ruiz M, Muttoni A. A mechanical model for failures in shear of members without transverse reinforcement based on development of a critical shear crack, submitted for publication in Engineering Structures. 2017.

[2]   Yang K-H, Sim J-I, Choi B-J, Lee E-T. Effect of Aggregate Size on Shear Behavior of Lightweight Concrete Continuous Slender Beams. *ACI Materials Journal* 2011; 108 (5):501–509.

[3]   Hordijk DA. Deformation controlled uniaxial tensile tests on concrete, TU Delft, Stevinreport 25.5.90-7 /VFA. 1990.

[4]   Muttoni A, Fernández Ruiz M. Shear strength of members without transverse reinforcement as function of critical shear crack width. *ACI Structural Journal* 2008; 105 (2):163–172.

[5]   Fédération Internationale du Béton (fib), fib Model Code for Concrete Structures 2010, Ernst & Sohn. 2013:434.

[6]   Yoon Y-S, Cook WD, Mitchell D. Minimum Shear Reinforcement in Normal, Medium and High- Strength Concrete Beams. *ACI Structural Journal* 1996; 93 (5):576–584.

[7]   Fernández Ruiz M, Muttoni A. On Development of Suitable Stress Fields for Structural Concrete. *ACI Structural Journal* 2007; 104 (4):495–502.

[8]   Campana S, Anastasi A, Fernández Ruiz M, Muttoni A. Analysis of shear-transfer actions on one-way RC members based on measured cracking pattern and failure kinematics. *Magazine of Concrete Research* 2013; 65 (6):386–404.

[9]   Huber P, Huber T, Kollegger J. Investigation of the shear behaviour of RC beams on the basis of measured crack kinematics. *Engineering Structures* 2016; 113:41–58.

[10]   Cavagnis F, Fernández Ruiz M, Muttoni A. An analysis of the shear transfer actions in reinforced concrete members without transverse reinforcement, accepted for publication in Structural Concrete. 2017.

[11]   Giurani E, Plizzari G, Schumm C. Role of Stirrups and Residual Tensile Strength of Cracked Concrete on Bond. *Journal of Structural Engineering* 1991; 117 (1):1–18.

[12]   Kong P, Rangan B. Reinforced High Strength Concrete (HSC) Beams in Shear. *Australian Civil Engineering Transactions* 1997; 39 (1):43–50.

[13]   Fernández Ruiz M, Plumey S, Muttoni A. Interaction between Bond and Deviation Forces in Spalling Failures of Arch-Shaped Members without Transverse Reinforcement. *ACI Structural Journal* 2010; 107 (3):346–354.

[14]   Li VC, Ward R, Hamza AM. Steel and Synthetic Fibers as Shear Reinforcement. *ACI Materials Journal* 1992; 89 (5):499–508.

[15]   Mansur MA, Ong KCG, Paramasivam P. Shear Strength of Fibrous Concrete Beams without Stirrups. *Journal of Structural Engineering* 1986; 112 (9):2066–2079.

[16]   Kwak Y, Eberhard MO, Kim W, Kim J. Shear Strength of Steel Fiber-Reinforced Concrete Beams without Stirrups. *ACI Structural Journal* 2002; 99 (4):530–538.

[17]   Minelli F, Plizzari GA. On the Effectiveness of Steel Fibers as Shear Reinforcement. *ACI Structural Journal* 2013; 110 (3):379–389.

[18]   Shoaib A, Lubell AS, Bindiganavile VS. Size Effect in Shear for Steel Fiber-Reinforced Concrete Members without Stirrups. *ACI Structural Journal* 2014; 111 (5):1081–1090.

[19]   Zarrinpour MR, Chao S-H. Shear Strength Enhancement Mechanisms of Steel FiberReinforced Concrete Slender Beams. *ACI Structural Journal* 2017; 114 (3):729–742.

[20]   Dinh HH, Parra-montesinos GJ, Wight JK. Shear Behavior of Steel Fiber-Reinforced Concrete Beams without Stirrup Reinforcement. *ACI Structural Journal* 2010; 107 (5):597–606.

[21]   Lim TY, Paramasivam P, Lee S. Analytical Model for Tensile Behavior of Steel-Fiber Concrete. *ACI Materials Journal* 1987; 84:286–298.

[22]   Naaman AE, Najm H. Bond-Slip Mechanisms of Steel Fibers in Concrete. *ACI Materials Journal* 1991; 88 (2):135–145.

[23]   Khuntia M, Stojadinovic B, Goel SC. Shear Strength of Normal and High-Strength Fiber Reinforced Concrete Beams without Stirrups. *ACI Structural Journal* 1999; 96 (2):282–289.

[24]   Voo YL, Poon WK, Foster SJ. Shear Strength of Steel Fiber-Reinforced Ultrahigh- Performance Concrete Beams without Stirrups. *Journal of Structural Engineering* 2010; 136 (11):1393–1400.

[25]   Rajagopalan K, Parameswaran VS, Ramaswamy GS. Strength of steel fibre reinforced concrete beams. *Indian Concrete Journal* 1974; 48 (1):17–25.

[26]   Parimi SR, Sridha K, Rao JK. Fracture Toughness of Fibre Concrete, International Symposium of Fibre Reinfroced Concrete, ACI Special Publication No. SP-44. 1973:80–92.

[27]   Swamy RN, Jones R, Chiam ATP. Influence of Steel Fibers on the Shear Resistance of Lightweight Concrete 1-Beams. *ACI Structural Journal* 1993; 90 (1):103–114.

[28]   Casanova P, Rossi P. Analysis and Design of Steel Fiber-Reinforced Concrete Beams. *ACI Materials Journal* 1997; 94 (5):595–602.

[29]   Lim TY, Paramsivam P, Lee SL. Shear and Moment Capacity of Reinforced Steel-Fiber-Concrete Beams. *Magazine of Concrete Research* 1987; 39 (140):148–160.

[30]   Sharma AK. Shear Strength of Steel Fiber Reinforced Concrete Beams. *ACI Journal* 1986; 83 (4):624–628.

[31]   Foster SJ. Design of FRC beams for shear using the VEM and the draft model code approach. In: FIB bulletin 57: shear and punching shear in RC and FRC elements. Lausanne (Switzerland); 2010:195–210.

[32]   Hordijk DA. Tensile and tensile fatigue behaviour of concrete; experiments, modelling and analysis. *Heron* 1992; 37 (1):3–79.

[33]   Rosenbusch, J., and Teutsch M. Trial Beams in Shear, Brite/Euram Project 97-4163, Final Report, Sub Task 4.2, Technical University of Braunschweig. 2003:105–117.

[34]   Di Prisco M, Martinelli P, Dozio D. The structural redistribution coefficient Krd: a numerical approach to its evaluation. *Structural Concrete* 2016; 17 (3):390–407.

[35]   Ivey DL, Buth E. Shear Capacity of Lightweight Concrete Beams. *ACI Journal Proceedings* 1969; 66 (6):634–643.

[36]   Taylor, R., Brewer RS. The Effect of the Type of Aggregate on the Diagonal Cracking of Reinforced Concrete Beams. *Magazine of Concrete Research* 1963; 15 (44):87–92.

[37]   Walraven JC. The Influence of Depth on the Shear Strength of Lightweight Concrete Beams without Shear Reinforcement, Report 5-78-4, Delft University of Technology, Faculty of Civil Engineering, Delft, the Netherlands. 1984:36.

[38]   Angelakos D, Bentz EC, Collins MP. Effect of Concrete Strength and Minimum Stirrups on Shear Strength of Large Members. *ACI Structural Journal* 2001; 98 (3):290–300.

[39]   Bhal NS. Über den Einfluß der Balkenhöhe auf die Schubtragfähigkeit von einfeldrigen Stahlbetonbalken mit und ohne Schubbewehrung. Otto-Graf-Institut, H.35, Stuttgart. 1968.

[40]   Bresler B, Scordelis AC. Shear strength of reinforced concrete beams. *ACI Journal* 1963; 60 (1):51–74.

[41]   Cladera A, Marí A. Experimental study on high-strength concrete beams failing in shear. *Engineering Structures* 2005; 27 (10):1519–1527.

[42]   Johnson MK, Ramirez JA. Minimum Shear Reinforcement in Beams with Higher Strength Concrete. *ACI Structural Journal* 1989; 86 (4):376–382.

[43] Johnston B, Cox KC. High Yield-Point Steel as Tension Reinforcement in Beams. *ACI Journal Proceedings* 1939; 36 (9):65–90.

[44] Krefeld WJ, Thurston CW. Studies of the shear and diagonal tension strength of simply supported R/C-beams. *ACI Journal* 1966; 63 (4):451–476.

[45] Ozcebe G, Ersoy U, Tankut T. Evaluation of minimum shear reinforcement requirements for higher strength concrete. *ACI Structural Journal* 1999; 96 (3):361–368.

[46] Pansuk W, Sato Y. Shear mechanism of reinforced concrete T-beams with stirrups. *Journal of Advanced Concrete Technology* 2007; 5 (3):395–408.

[47] Petersson T. Shear and Torsion in Reinforced Concrete Beams. 1972:276.

[48] Quast U, Los M. Zum Einfluß von Längszugspannungen auf das Schubtragverhalten von Stahlbetonbalken. *Bautechnik* 1999; 76 (8):646–650.

[49] Regan PE. Shear in Reinforced Concrete – an experimental study. CIRIA-Report, a report to the Construction Research and Information Association. Imperial College of Science and Technology, Dep. of Civil Engineering, Concrete Section. 1971.

[50] Roller JJ, Russel HG. Shear Strength of High-Strength Concrete Beams with Web Reinforcement. *ACI Structural Journal* 1990; 87 (2):191–198.

[51] Sarsam KF, Al-Musawi JM. Shear design of high-and normal strength concrete beams with web reinforcement. *ACI Structural Journal* 1992; 89 (6):658–664.

[52] Ashour SA, Hasanain GS, Wafa FF. Shear Behavior of High-Strength Fiber Reinforced Concrete Beams. *ACI Structural Journal* 1992; 89 (2):176–184.

[53] Barragan BE. Failure and Toughness of Steel Fiber Reinforced Concrete under Tension and Shear, PhD Thesis, Barcelona, Spain: Universitat Politecnica de Catalunya. 2002.

[54] Batson G, Jenkins E. Steel Fibers as Shear Reinforcement in Beams. *ACI Journal* 1972; 69 (10):640–644.

[55] Casanova P, Rossi P. High-Strength Concrete Beams Submitted to Shear: Steel Fibers Versus Stirrups, Structural Applications of Fiber Reinforced Concrete, SP-182, American Concrete Institute, Farmington Hills, MI. 1999:53–68.

[56] Cucchiara C, Mendola LL, Papia M. Effectiveness of Stirrups and Steel Fibres as Shear Reinforcement. *Cement and Concrete Composites* 2004; 26 (7):777–786.

[57] Dupont D, Vandewalle L. Shear capacity of concrete beams containing longitudinal reinforcement and steel fibers, Innovations in Fiber Reinforced Concrete for Value, SP-216, American Concrete Institute, Farmington Hills, MI. 2003:79–94.

[58] Jain K, Singh B. Deformed steel fibres as minimum shear reinforcement — An investigation. *Structures* 2016; 7:126–137.

[59] Minelli F, Conforti A, Cuenca E, Plizzari G. Are steel fibres able to mitigate or eliminate size effect in shear? *Materials and Structures* 2014; 47 (3):459–473.

[60] Noghabai K. Beams of Fibrous Concrete in Shear and Bending: Experiment and Model. *Journal of Structural Engineering* 2000; 126 (2):243–251.

[61] Parra-Montesinos BGJ. Shear Strength of Beams with Deformed Steel Fibers - Evaluating an alternative to minimum transverse reinforcement. *Concrete International* 2006; 28 (11):57–67.

[62] Schwanz BA. The Effect of Shear Stress on Full Scale Steel Fiber Reinforced Concrete Beams, Master of Science Thesis, Potsdam, NY, USA: Clarkson University. 1993:86.

[63] Swamy RN, Bahia HM. The Effectiveness of Steel Fibers as Shear Reinforcement. *Concrete International* 1985; 7 (3):35–40.

Chapter 9   Conclusions and Future Research

This thesis investigated the shear behaviour of slender reinforced concrete members without transverse reinforcement. This dissertation consists of two main parts: (a) an experimental investigation on reinforced concrete members subjected to different loading and support conditions: the experimental measurements allowed characterizing the development of the critical shear crack and identifying the shear-transfer actions governing for the shear-capacity; (b) the development of a mechanical model based on the new experimental evidences and the derivation of a closed-form equation for shear design.

The main results of the two parts are summarized in Section 9.1. Section 9.2 discusses several questions that are still open and may be addressed in future studies.

9.1   Conclusions

9.1.1   Experimental investigation

The experimental programme aimed at studying the influence of different loading and support conditions on the shear strength of reinforced concrete members without transverse reinforcement. Twenty-five experimental tests were performed on twenty reinforced concrete beams. The main conclusions of the experimental work are:

- Digital image correlation (DIC) is a very suitable tool that allows detailed tracking of the crack pattern and analyses of the crack kinematics during loading and during the process of failure.

- The experimental measurements show that the critical shear crack progresses to failure in different manners.

- The position, inclination and opening of the critical shear crack play a major role on the shear strength.

- There is a significant influence of the type of loading (point or distributed load) on the shear capacity of slender reinforced concrete members without transverse reinforcement. The shear resistance of slender cantilevers subjected to distributed load is higher than the one of cantilevers subjected to point load. However, this influence depends significantly on the location and shape of the critical shear crack. For instance, within the present testing programme, for non-slender members, the shear resistance decreased when distributed load was applied.

Regarding the crack pattern and the development of the critical shear crack in slender members, the most interesting findings are:

- Numerous bending cracks develop at the level of the longitudinal reinforcement, but only some flexural cracks (primary flexural cracks) propagate up to one-half of the effective depth of the member. Primary flexural cracks develop at a distance between each other that normally varies between $0.4d$-$0.8d$, with an average value of $0.56d$ for the investigated specimens. The angle of the primary flexural cracks β_{AB} is related to the acting bending moment and the shear force at the section at which the flexural crack develops.

- The shape of the critical shear crack can be idealized by a bilinear segment representing a quasi-vertical bending crack (primary flexural crack), which propagates up to the neutral axis, followed by a quasi-horizontal branch which develops from the quasi-vertical flexural crack within the compression zone.

- The development of the quasi-horizontal branch from a primary flexural crack can be explained and predicted by Kani's model (accounting for residual tensile strength of concrete). Such crack development is not directly associated to failure, as, in most cases, the load can still be significantly increased.

- After the development of a quasi-horizontal crack within the compression zone, combined crack opening and sliding may cause large concentration of aggregate interlock stresses in the steeper part of the flexural crack and failure may be triggered by the development of an aggregate interlock induced crack.

- The kinematics of the critical shear crack is characterized by the centre of rotation located close to the tip of the crack.

- The maximum opening of the critical shear crack develops approximately at mid-height of the specimen. When the opening of all secondary cracks developing within a length l_B is accounted for, the total crack opening follows a linear distribution over the beam depth.

- At peak load, the length that contributes to the opening of the critical crack l_B is roughly constant for the investigated specimens and it can be approximated by d-c, where d is the effective depth and c is the height of compression zone. The horizontal opening of the critical shear crack at the level of the longitudinal reinforcement can be assumed to be equal to the product between the longitudinal strain and the length l_B. With this assumption, the opening of the critical crack can be easily calculated as it is proportional to the acting bending moment at the section corresponding to the tip of the crack.

The laboratory measurements allow identifying different types of critical crack development and failure modes and their associated governing shear-transfer actions. The refined kinematical measurements of the relative displacements in the cracks in combination with suitable mechanical models allow calculating the contributions of the various potential shear-transfer actions (beam-shear transfer actions and arching action). The main conclusions of these analyses are:

- The relative significance of the various potential shear-transfer actions depends mainly on the shape, location and kinematics of the critical shear crack. During loading, as cracks progress, some shear-transfer actions become predominant while others lose on significance. Even in some cases, some specimens were reloaded after a first failure and were capable of developing alternative shear-transfer actions (particularly arching action and dowelling action of the compression reinforcement) with a strength comparable to the one of the first failure.

- The cantilever action is governing for load levels lower than the failure loads. This shear-transfer action is reduced by the development of a quasi-horizontal crack within the compression zone. Yet, the development of the quasi-horizontal crack does not imply failure of the specimen and the capacity to increase the applied load after this crack propagation is related to other beam shear-transfer actions (aggregate interlock, dowelling action and residual tensile strength of concrete).

- Dowelling action can be activated as flexural reinforcement follows a vertical displacement, which happens for an inclined primary flexural crack and when the quasi-horizontal crack progresses. The capacity of the dowelling action depends mainly on the location of the critical shear crack. Its contribution is generally limited, but not necessarily negligible. When distributed loads are applied on the tension side of the member, the contribution of the dowelling action is more significant.

- Aggregate interlock and residual tensile strength of concrete depend mainly on the shape and kinematics of the critical shear crack. After the propagation of the quasi-horizontal branch of the critical shear crack, only the upper part of the crack is subjected to pure opening and it is thus governed by the residual tensile strength of concrete. The quasi-vertical branch of the critical shear crack is subjected to combined opening and sliding and it is thus governed by aggregate interlock. When the critical shear crack develops below the load introduction plate and below the theoretical compression strut and it is almost straight, aggregate interlock is practically negligible.

- For slender members, beam shear-transfer actions are governing for the shear capacity, with aggregate interlock being the dominant shear-transfer action. The contribution of the inclined compression chord at maximum load is limited and in some cases almost negligible.

- For squat members, or when the critical shear crack develops below the load introduction plate and below the theoretical compression strut, the arching action becomes governing.

- Although the critical shear crack presents a variation of its shape and geometry through the width of the member, analyses of the shear-transfer actions do not reflect high sensitivity on this issue.

9.1.2   Theoretical investigation

A mechanical model for shear design of slender members without shear reinforcement is proposed. The mechanical model is consistent with the main assumptions of the CSCT [1]. The shear force transferred by the various shear-transfer actions is calculated assuming a realistic shape and kinematics of the critical shear crack (based on the experimental measurements) and integrating suitable constitutive laws for cracked concrete in mode I (residual tensile strength), and mode I-II (aggregate interlock), for dowelling action and for uncracked concrete (compression zone):

- A failure criterion can be obtained by summing the contribution of the different shear-transfer actions. The failure criterion can be used in combination with a load-crack opening (load-deformation) relationship to calculate the shear capacity, the role of the various shear-transfer actions at failure and the deformation capacity.

- The mechanical model allows determining the theoretical governing location of the critical shear crack, as the section where the shear strength curve is tangent to the shear force curve.

- The shear strength is shown to be dependent on the location, shape, opening and roughness of the critical shear crack.

- The mechanical model is suitable for shear design of one-way slabs and slender beams without transverse reinforcement subjected to different loading and support conditions: simply supported beams, continuous beams, cantilevers subjected to point load (with and without axial forces) or distributed load.

- The failure criteria obtained by integration of stresses at the crack surface can be approximated by power-law equations. These power law failure criteria in combination with the load-deformation relationship allow deriving a closed-form equation for shear design.

- The closed-form equation provides almost identical results to the general approach that accounts for the contribution of the various shear-transfer actions for each possible location of the control section.

- The derived closed-form equation allows calculating the shear capacity and understanding the role of the main mechanical parameters governing the shear strength (the reinforcement ratio ρ, the compressive strength f_c, the aggregate type and size d_g, the shear slenderness at the control section a_{cs}, the effective depth d, the location of the critical shear crack with respect to the load introduction plate (k_c) and the inclination of the critical shear crack (k_a).)

- For shear design, the closed-form equation can be applied to slender members subjected to different loading and support conditions by checking the shear strength at a control section located at a distance d either from a static discontinuity (concentrated load or intermediate support) or from a section with zero acting bending moment (end support or points of contraflexure in continuous beams). The control section shear span a_{cs} (calculated as the moment-to-shear ratio at the control section) needs to be limited by the condition $a_{cs} \geq d$. In the presence of distributed loads acting on the tension face of the members in the proximity of the intermediate supports of continuous beams or at fixed supports of cantilevers, a fraction of the loads $\Delta V = V/5$ shall be subtracted from the shear force at the control section.

- The mechanical model and the closed-form equation can be applied also to members with low amount of shear reinforcement and with steel fibres, failing due to localization of strains at the critical shear crack. The failure criteria can be calculated by accounting for the contribution of the various beam shear-transfer actions and respectively the contribution of the shear reinforcement for members with low amount of shear reinforcement or the contribution of the post-cracking tensile strength due to fibres for SFRC members.

- The mechanical model and the closed-form equations show a good agreement when compared to the experimental results of 1179 tests on slender reinforced concrete members subjected to different loading and support conditions.

9.2   Future Work

This section presents the principal issues that may be addressed in further investigations.

At the experimental level:

- The value l_B has been assumed equal to d-c and validated in this thesis for two amounts of flexural reinforcement ratio ρ (0.54% and 0.89%). Consistent results have also been obtained for slender members with a reinforcement ratio equal to 1.32% [2]. More experimental tests on slender reinforced concrete members with different amounts of

reinforcement ratio investigated by means of the digital image correlation technique are required: it is recommended to investigate sufficiently slender members in order to guarantee that the critical shear crack does not develop below the theoretical compression strut.

- A recent experimental investigation on the influence of the width-to-effective depth (b/d) ratio has shown that for members with a shear span-to-effective depth ration equal to 2.5, an increase of the ratio b/d from 1 to 3 leads to an enhancement of the shear capacity of approximately 25% [3]. According to Conforti et al. [3], the parameter b/d influences the crack development through the width of the specimen, leading to shear cracks with significant deviation and bifurcation that guarantee a larger aggregate-interlock capacity for higher values of b/d. This effect may eventually be more pronounced for members with larger a/d where aggregate interlock plays a more significant role. However, a good agreement with no noticeable trend with respect to the parameter b/d can be observed when comparing the proposed mechanical models with the available experimental results of 872 beams without shear reinforcement (see Figure 7.23f). The enhanced shear capacity measured by Conforti et al. [3] may be thus related to the low shear span-to-effective depth ratio (a/d=2.5), to the shape and location of the critical shear crack whose development allowed the activation of the theoretical compression strut above the critical shear crack for some specimens, leading to a large scatter in the experimental results. An experimental campaign of sufficiently slender members may provide additional knowledge on this issue.

- In the present experimental investigation, it has been observed that the shape of the critical shear crack is influenced by the moment-to-shear ratio at the section where the primary flexural crack develops. All investigated specimens in the databases have been tested keeping constant the static scheme, and thus the moment-to-shear ratio along the span of the member remained constant during the entire test. Recently, Tung et al. [4] carried out an experimental campaign on continuous members, where the static scheme was varied during loading: close to failure the distance of the point of contraflexure from the fixed support was increased from approximately 1.5d to 2.5d, leading to an increase of the moment-to-shear ratio at the critical shear crack location. For these members, the shear capacity can be correctly predicted if the angle β_{AB} of the critical shear crack is defined prior to the load adjustment, whereas, if the angle of the critical shear crack is calculated based on the moment-to-shear ratio at failure, the theoretical models presented in this thesis overestimate the shear-capacity. The significance of this topic encourages further experimental investigations on the influence of variable loads on the shape of the critical shear crack and on the shear capacity.

- Further experimental tests on continuous members subjected to distributed load and axial compression forces are needed: the existing database is insufficient.

- More experimental tests on slender reinforced concrete members with low amount of transverse reinforcement investigated by means of the digital correlation technique shall be performed, with the aim to validate the load-deformation relationship and to characterize the shape of the critical shear crack at failure. The existing database is also insufficient to extract valid conclusions on the transverse reinforcement ratio that avoids failure to occur by development of a single crack localizing strains and, of the flexural strength of the stirrups. Moreover, the influence of spacing between stirrups, flexural strength of stirrups and diameter of longitudinal bars shall be investigated.

- More experimental tests on slender reinforced concrete members with steel fibres investigated by means of the digital correlation technique shall be performed in order to understand the failure mechanisms and the shape and kinematics of the critical shear crack. For these members it is recommended to investigate sufficiently slender members (for instance with a/d>4) in order to guarantee that the critical shear crack does not develop below the theoretical compression strut.

At the theoretical level:

- Aggregate interlock is acknowledged as one of the most significant shear-transfer actions in cracked concrete members without shear reinforcement. A consistent physical approach that allows calculating the interface stresses shall be developed. The approach shall clarify the role of roughness due to aggregates (micro-roughness) and due to the shape (meso-roughness) of the critical shear crack. Moreover, the influence of the strengths of the aggregates with respect to the one of the concrete matrix shall be investigated. In addition, different histories of kinematics (different initial openings and tangent mixed mode angles γ_T, refer to Figure 6.4a) shall be studied. The final aim shall be to provide a consistent methodology for the calculation of aggregate interlock stresses on the basis of the crack shape and kinematics (opening w and sliding δ) of normal-strength, high-strength, recycled and lightweight reinforced concrete and to develop new simple formulations for shear design. Finally, the development of aggregate interlock induced crack shall be monitored and investigated in detail.

- For simply supported beams subjected to point load, the role of the dowelling action has been observed to be limited, but not negligible. The contribution of the dowelling action is more significant for cantilevers or continuous members subjected to distributed loading. A systematic investigation on the influence of the longitudinal strains on the dowel capacity shall be performed and a physical approach that accounts for the reduced capacity due to flexural strains shall be developed. In addition, the dowelling action shall be investigated in detail for members with low amount of transverse reinforcement and with steel fibres.

- As presented in Chapter 4, the length l_B contributing to the opening of the critical shear crack is roughly constant and equal to $0.67z$ when the quasi-horizontal branch of the critical shear crack starts developing. Moreover, it has been shown that the shear force that causes the development of the quasi-horizontal segment can be calculated in accordance with the simple Kani's tooth model [5], accounting for the residual tensile strength of concrete. On this basis, the mechanical model presented in this thesis may be improved, by assuming a more realistic history kinematics of the quasi-vertical segment of the critical shear crack (an initial opening followed by a mixed mode response) and by using a physical model for aggregate interlock that accounts for the different values of initial openings and mixed mode angles along the crack profile. By doing so, the length l_F of the quasi-horizontal branch shall not be fixed a priori, but it could be determined as the minimum length beyond which the sum of the contribution of the shear-transfer actions starts decreasing.

- The mechanical model and the closed-form equation can be applied to study the shear capacity of reinforced concrete T beams without shear reinforcement, by accounting for the beneficial effects of the compression flange on the shear strength. The contribution of the inclined compression chord shall be suitably evaluated taking into account for the flange-web interaction and the location of the control section shall be studied for these members.

- The mechanical model and the closed-form equation may be applied to cantilever slabs and simply supported slabs subjected to concentrated load near linear supports. For these members, the shear force is not constant along the control section and it may be averaged over a certain width. Additional studies on the location of the control section, internal force redistribution due to shear cracking and the effective width are required.

- The enhanced shear strength of prestressed beam requires additional studies, by further investigating the influence of the eccentricity of the post-tensioning tendons.

- The mechanical model shall be improved for reinforced concrete members with low amount of shear reinforcement, by quantifying the dowelling action in a more physical manner and eventually by refining the main assumptions on the shape of the critical shear crack and the load-crack opening relationship. The approach shall provide the minimum transverse reinforcement ratio that avoids strain localization.

- The mechanical model shall be improved for reinforced concrete members with fibres, by assuming a more realistic post-cracking softening law derived directly from experimental tensile tests, by investigating the dowelling action for these members and eventually by refining the assumed shape of the critical shear crack and the load-crack opening relationship.

9.3 References

[1]   Fernández Ruiz M, Muttoni A, Sagaseta J. Shear strength of concrete members without transverse reinforcement: a mechanical approach to consistently account for size and strain effects. *Engineering Structures* 2015; 99:360–372.

[2]   Tasevski D, Muttoni A. Shear tests under varying strain rate, Internal report IBETON, EPFL. 2017.

[3]   Conforti A, Minelli F, Plizzari GA. Influence of Width-to-Effective Depth Ratio on Shear Strength of Reinforced Concrete Elements without Web Reinforcement. *ACI Structural Journal* 2017; 114 (4):995–1006.

[4]   Tung ND, Tue NV. Effect of support condition and load arrangement on the shear response of reinforced concrete beams without transverse reinforcement. *Engineering Structures* 2016; 111:370–382.

[5]   Kani GNJ. The riddle of shear failure and its solution. *ACI Journal* 1964; 61 (4):441–467.

Appendix 1

In this Appendix, the photos of the specimens taken after failure are shown in Figure A1.1, Figure A1.3 and Figure A1.5. Moreover, the displacement profiles measured by means of DIC or NDI (or LVDT when no photogrammetry measurements were performed) at the top and bottom fibre at selected load steps are shown in Figure A1.2, Figure A1.4 and Figure A1.6. In the plotted deformed shapes, the rigid body rotation of the beam was corrected in order to have zero vertical displacement at the end support and at the intermediate support (refer to Figure 5.1 for the scheme of the test setup and loading conditions and to Figure 5.2 for the crack pattern at peak load).

Note that, in specimens SC52, SC55 and SC67, the development of a diagonal crack close to the right support was followed by a drop in the applied load of 5-10%. These specimens however could be reloaded. In specimen SC52a, a shear crack developed close to the left support. The specimen was repaired by means of external plates fixed with prestressed bolts and retested: a second failure crack developed close to the point of contraflexure (SC52b, see Figure A1.1). In specimens SC55a and SC67a, a direct strut action developed in the uncracked compression zone above the critical shear crack and failure occurred due to crushing of the compression zone (see respectively Figure A1.1 and Figure A1.5).
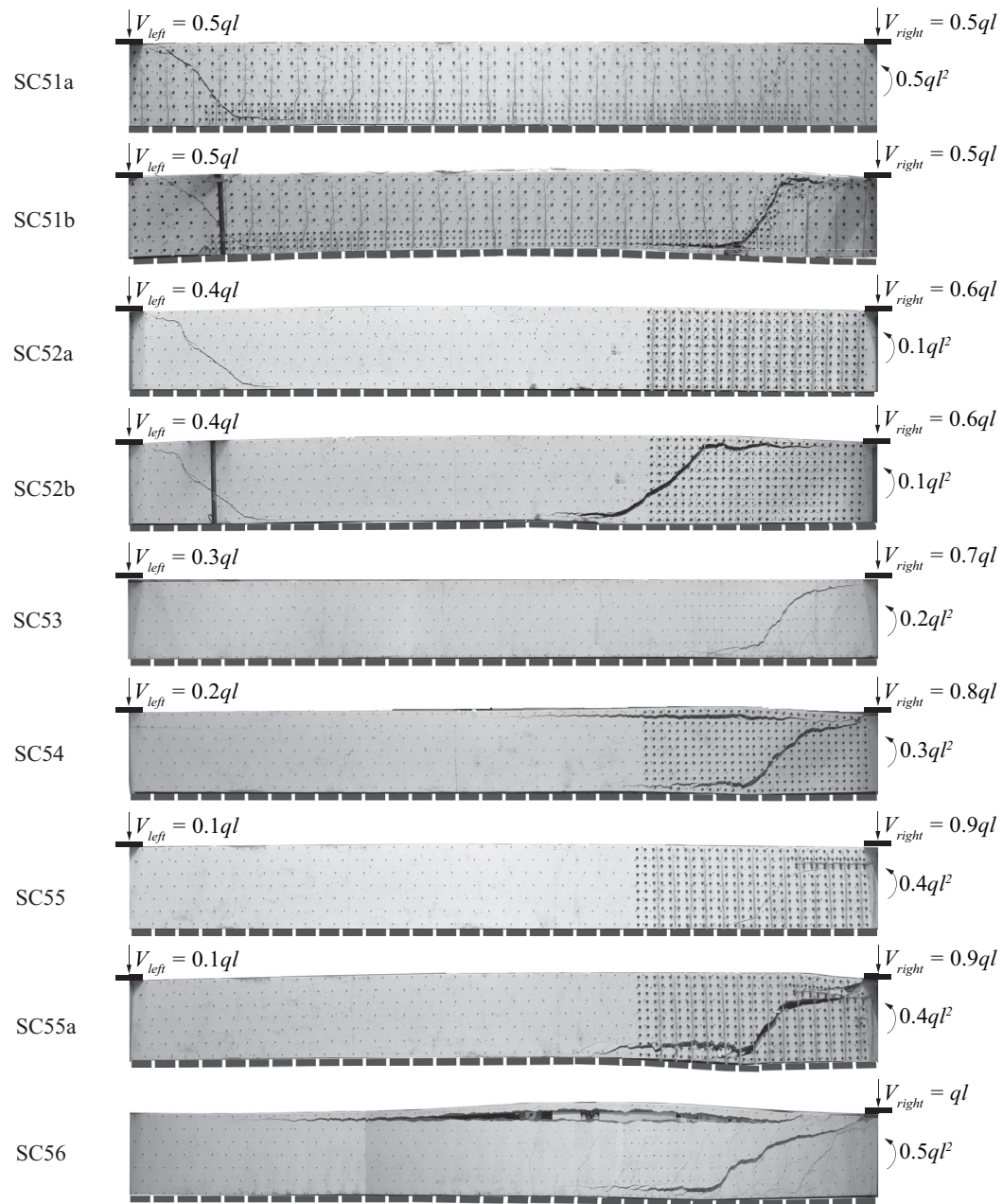
Figure A1.1 Photos of crack pattern after failure: members subjected to distributed loading.
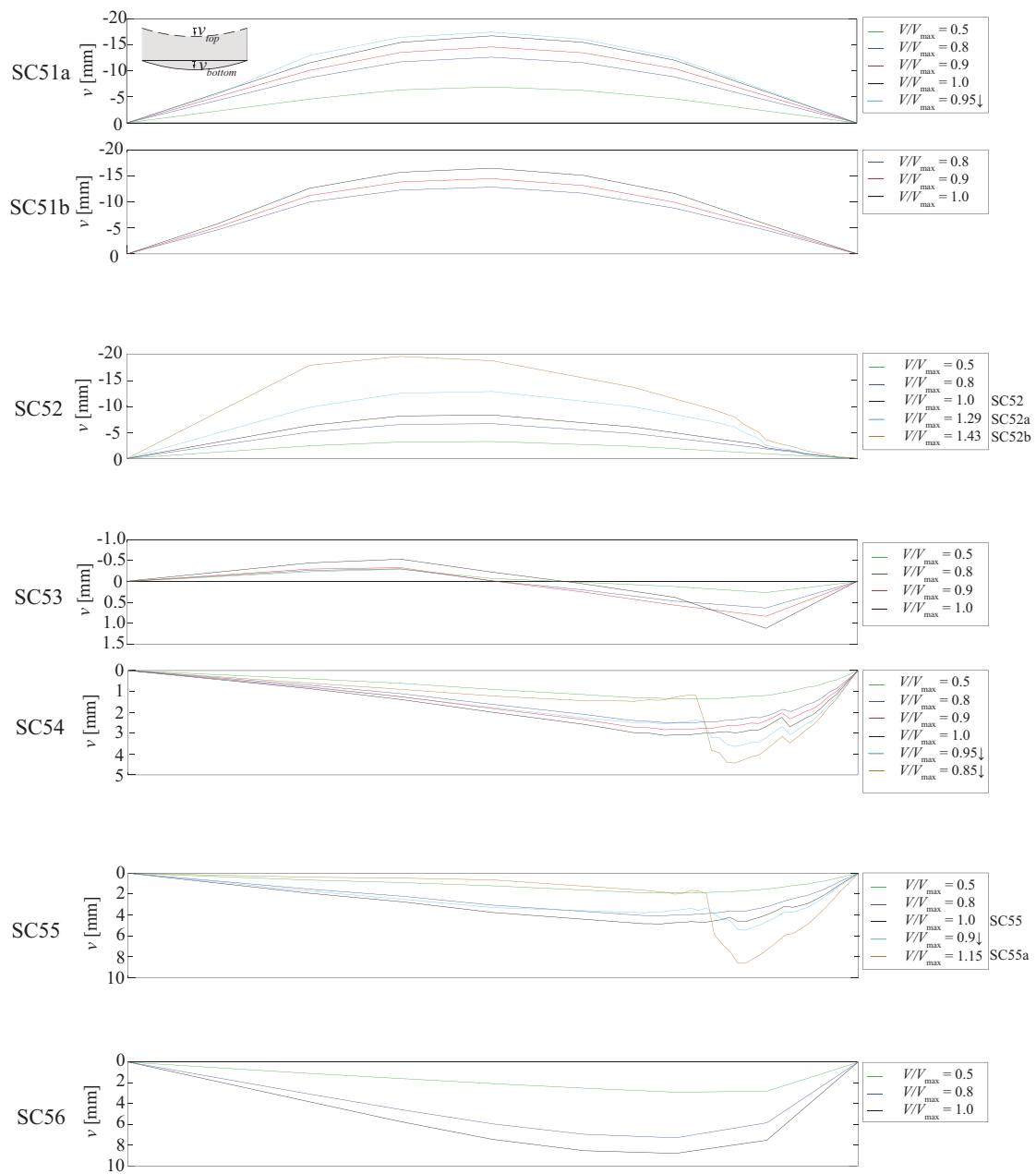
Figure A1.2 Members subjected to distributed loading: vertical displacement profile of bottom fibre at selected load steps (continuous lines).
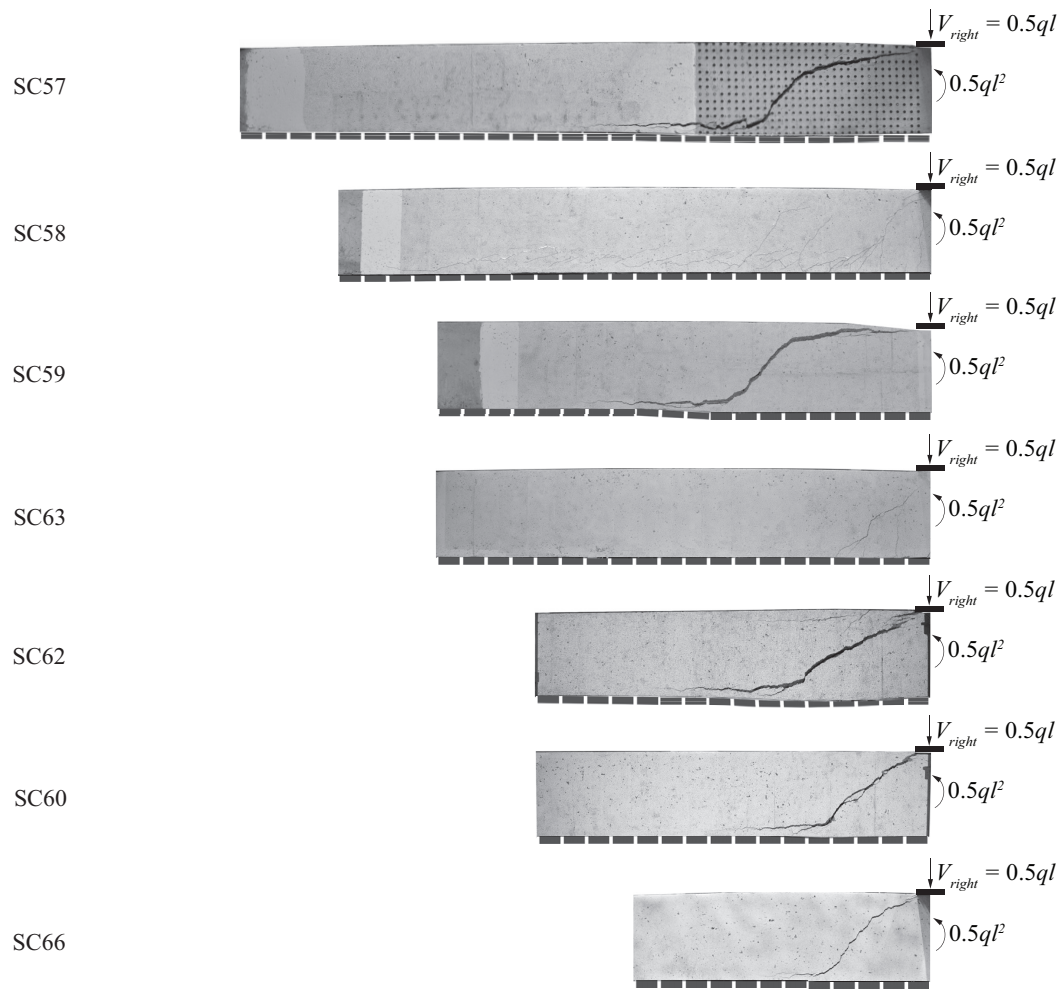
Figure A1.3 Photos of crack pattern after failure: cantilevers subjected to distributed loading
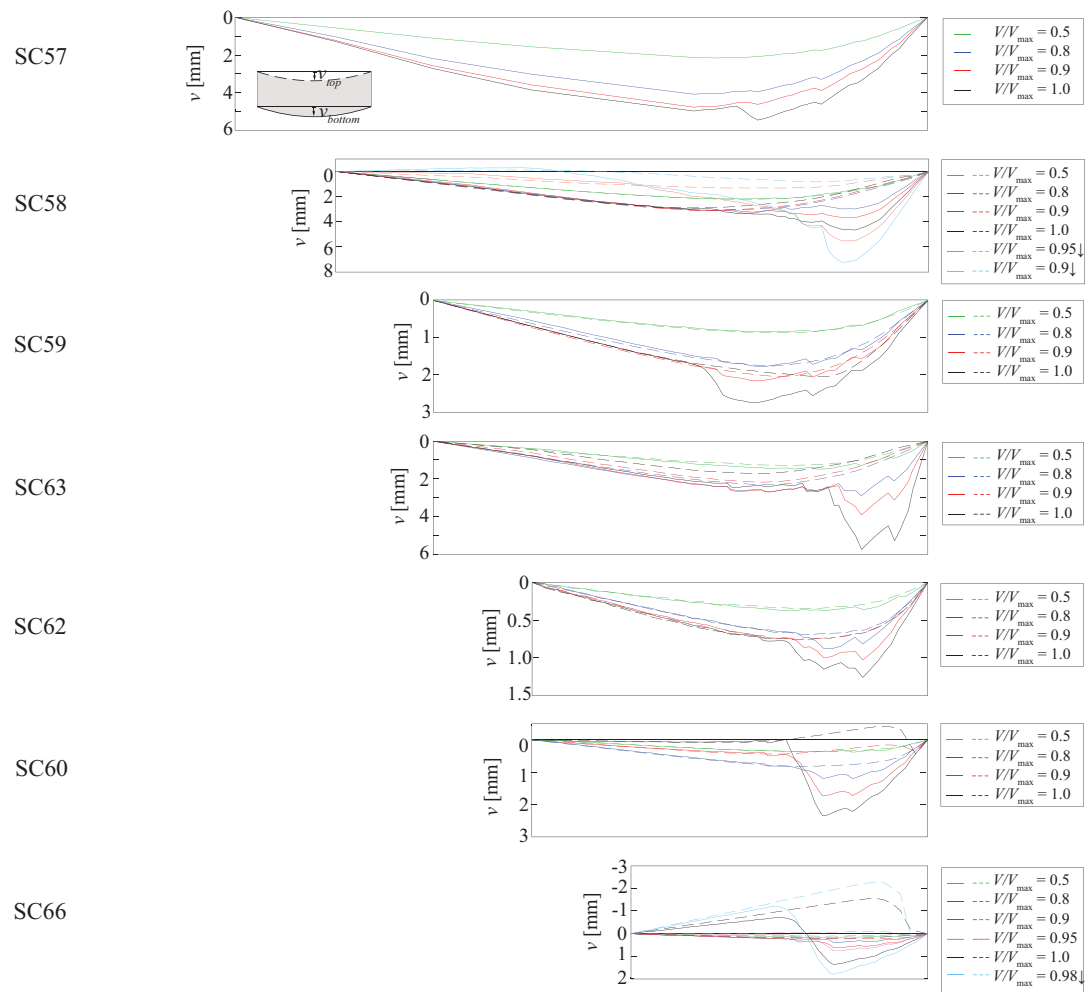
Figure A1.4 Cantilevers subjected to distributed loading: vertical displacement profile of top fibre (dashed lines) and vertical displacement profile of bottom fibre (continuous lines) at selected load steps.
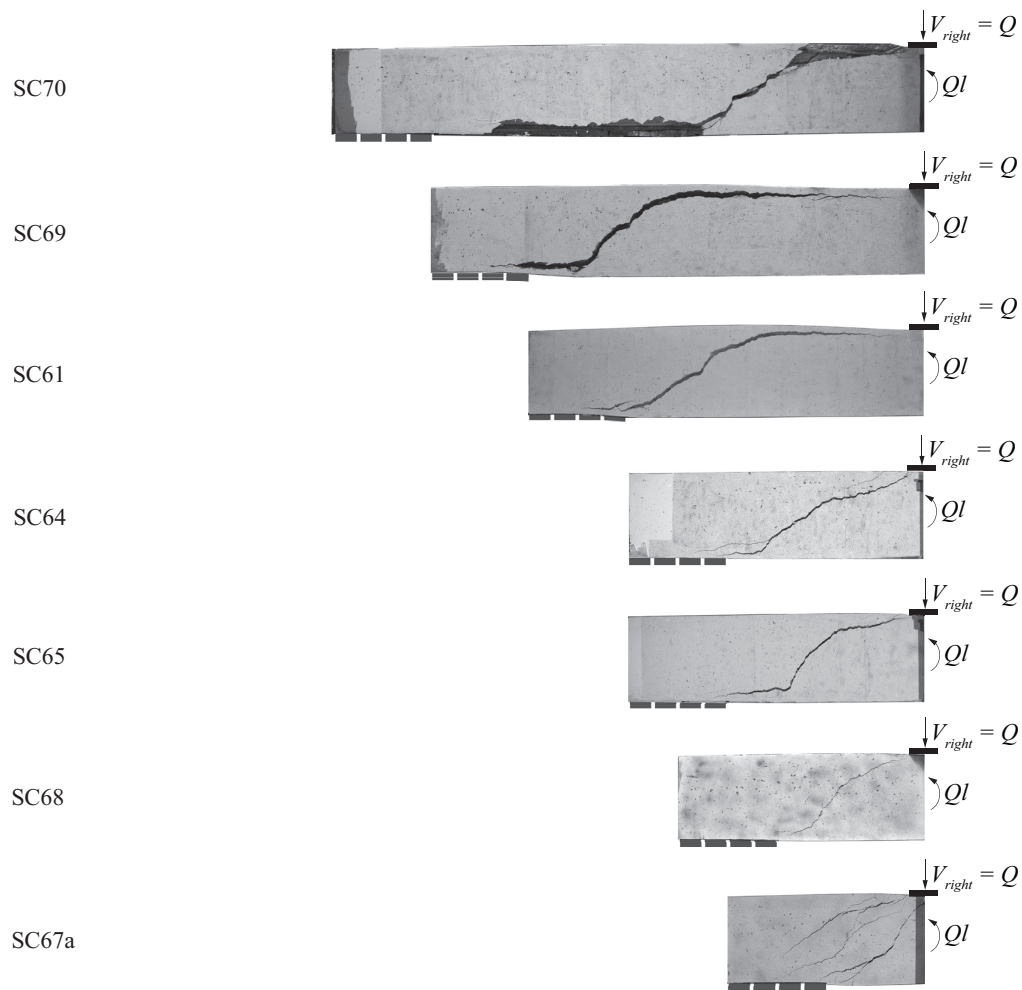
Figure A1.5 Photos of crack pattern after failure: cantilevers subjected to point loading.

SC70

SC69

SC61

SC64

SC65

SC68

SC67
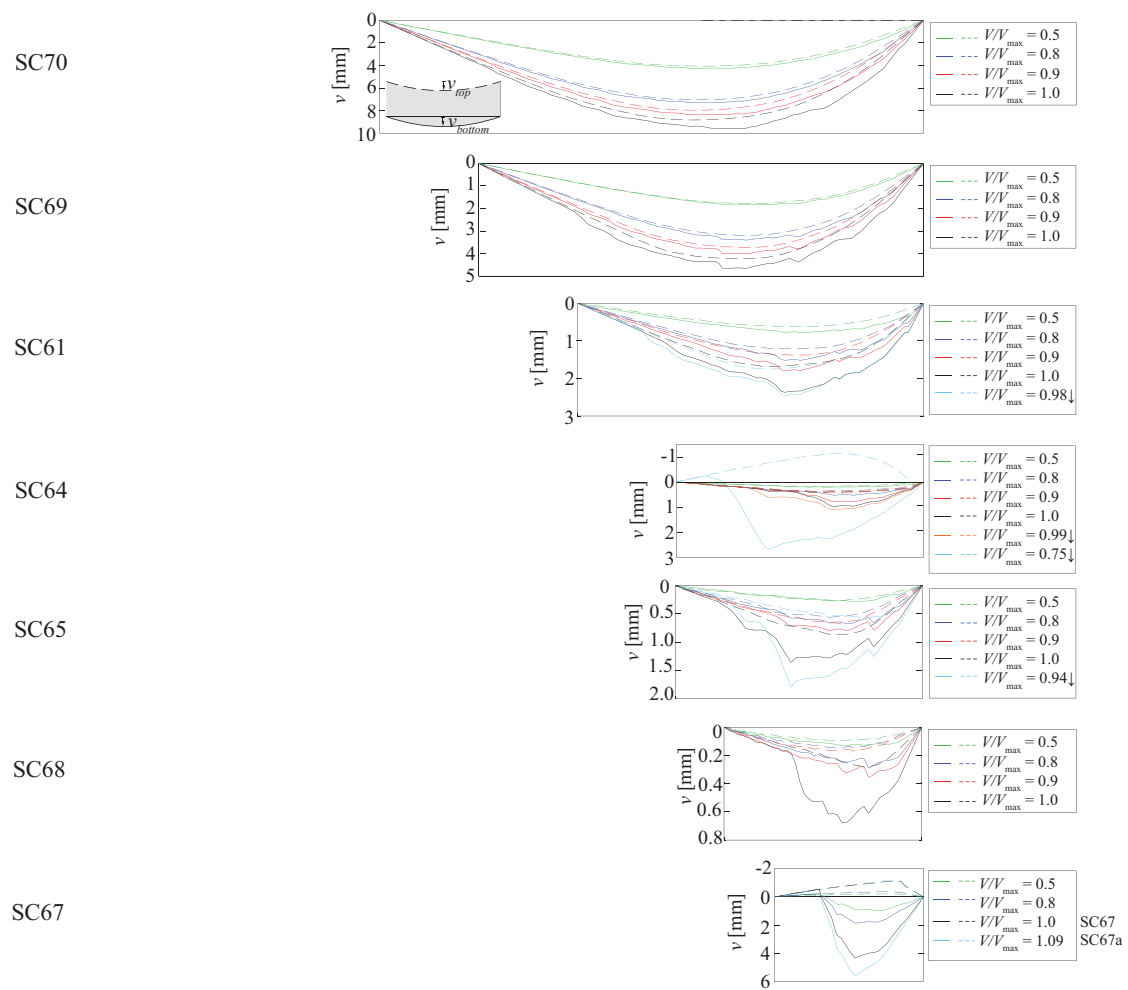
Figure A1.6 Specimens subjected to point loading: vertical displacement profile of top fibre (dashed lines) and vertical displacement profile of bottom fibre (continuous lines) at selected load steps.

Appendix 2

This Appendix includes several datasets on slender reinforced concrete beams subjected to different loading and support conditions. The experimental results included in the ACI-DAfStb databases on simply supported beams without and with shear reinforcement subjected to concentrated load [1, 2] are not listed in this Appendix, although they have been used to validate the theoretical approaches presented in this thesis. The reader should refer to reference [1, 2].

The databases comprise a total of 1179 tests of used for comparison. The datasets include also some tests that have been excluded from the analyses due to one of the following reasons: (i) non-slender members, (ii) unknown aggregate size, (iii) nonrectangular members, (iv) flexural failure, (v) shear compression failure with a direct strut developing above the critical shear crack allowing the plastic strength of the member to be partially reached, (vi) variable static scheme during testing.

Notation and definition of the main geometrical and mechanical properties are available in Chapter 6, 7 and 8 of this thesis.

The author acknowledges that the datasets might still contain errors.

Table A2.1 Simply supported beams without shear reinforcement subjected to point load

Reference	Specimen	f_c [MPa]	d_g [mm]	f_y [MPa]	d [mm]	h [mm]	b/d [-]	n_{bar} [-]	d_{bar} [mm]	ρ [-]	plate/d [-]	a/d [-]	V_{right} [kN]
Reineck et al. [1]	# 629 tests[a]	12.9 – 110.9	5 – 51	283 -1779	65 - 2000	80 - 2200	0.14-6.85	1 - 36	6 - 40	0.0014 – 0.0664	0-3.08	2.5 – 8.6	114
	SC70	33.3	16	713	556	600	0.450	2	28.0	0.0089	0.36	6.92	114
	SC69	32.9	16	713	556	600	0.450	2	28.0	0.0089	0.36	5.67	107
Cavagnis et al. [3]	SC61	35.3	16	713	556	600	0.450	2	28.0	0.0089	0.36	4.41	103
	SC64	35.6	16	713	556	600	0.450	2	28.0	0.0089	0.36	3.15	108
	SC68	32.6	16	713	556	600	0.450	2	28.0	0.0089	0.36	2.52	124
	SC65	35.5	16	760	556	600	0.447	2	22.0	0.0054	0.36	3.13	102

[a]Only the specimens respecting the following criteria were considered: (i) rectangular cross-section; (ii) $a/d \geq 2.5$; (iii) aggregate size specified. Two tests in the original database have been corrected: Cladera H50/5 V_{exp}=129.5 kN [4], Podgomiak BRH100 V_{exp}=357 kN [5]

Table A2.2 Simply supported beams without shear reinforcement subjected to point load and axial forces

Reference	Specimen	f_c [MPa]	d_g [mm]	f_y [MPa]	b [mm]	d [mm]	h [mm]	ρ [-]	plate [mm]	a [mm]	a/d [-]	N [kN]	V_{right} [kN]	Remarks[a]
	B1	26.0	25	458	152	252	304	0.0101	304	660	2.6	-89.0	66.0	$a_{eff}/d<2.5$
	B2	28.5	25	458	152	252	304	0.0101	304	914	3.6	-89.0	52.0	
	B3	26.3	25	393	152	252	304	0.0101	304	1168	4.6	-89.0	45.8	
	B4	28.2	25	458	152	252	304	0.0101	304	1422	5.6	-89.0	42.0	
Diaz de Cossio et al. [6]	B11	25.2	25	331	152	252	304	0.0337	304	660	2.6	-89.0	84.0	$a_{eff}/d<2.5$
	B12	27.0	25	391	152	252	304	0.0337	304	914	3.6	-89.0	65.5	
	B13	27.9	25	354	152	252	304	0.0337	304	1168	4.6	-89.0	58.5	
	B14	29.3	25	362	152	252	304	0.0337	304	1422	5.6	-89.0	52.5	
	B15	28.3	25	326	152	252	304	0.0337	304	1676	6.7	-89.0	46.9	
	ST-1	24.8	16	1027	200	165	200	0.0107	50	500	3.0	426.9	39.5	
	ST-2	26.1	16	1027	200	165	200	0.0107	50	500	3.0	96.8	43.5	
	ST-3	26.1	16	1027	200	165	200	0.0107	50	500	3.0	200.0	45.4	
	ST-6	26.8	16	1027	200	165	200	0.0107	50	500	3.0	300.0	43.0	
	ST-7	27.4	16	1027	200	165	200	0.0107	50	500	3.0	400.0	40.8	
	ST-8	27.4	16	1027	200	165	200	0.0107	50	500	3.0	500.0	39.8	
	ST-9	27.4	16	1027	200	165	200	0.0107	50	500	3.0	300.0	45.4	
	ST-10	28.1	16	1027	200	165	200	0.0107	50	500	3.0	400.0	36.9	
	ST-12	28.1	16	1027	200	165	200	0.0107	50	500	3.0	200.0	44.0	
Jorgensen et al. [7]	ST-13	28.8	16	1027	200	165	200	0.0107	50	600	3.6	100.0	33.9	
	ST-14	28.8	16	1027	200	165	200	0.0107	50	600	3.6	200.0	40.7	
	ST-15	28.8	16	1027	200	165	200	0.0107	50	600	3.6	300.0	44.6	
	ST-17	29.5	16	1027	200	165	200	0.0107	50	600	3.6	100.0	39.9	
	ST-18	29.5	16	1027	200	165	200	0.0107	50	600	3.6	200.0	32.8	
	ST-19	29.5	16	1027	200	165	200	0.0107	50	600	3.6	300.0	32.0	
	ST-20	29.5	16	1027	200	165	200	0.0107	50	600	3.6	500.0	30.2	
	ST-22	30.2	16	1027	200	165	200	0.0107	50	500	3.0	500.0	37.5	
	ST-23	30.2	16	1027	200	165	200	0.0107	50	500	3.0	600.0	34.5	
	ST-24	30.2	16	1027	200	165	200	0.0107	50	575	3.5	600.0	35.2	

Table A2.2 Simply supported beams without shear reinforcement subjected to point load and axial forces

Reference	Specimen	f_c [MPa]	d_g [mm]	f_y [MPa]	b [mm]	h [mm]	d [mm]	ρ [-]	plate [mm]	a [mm]	a/d [-]	N [kN]	V_{right} [kN]	Remarks[a]
	B2-2	45.9	16	558	400	300	260	0.0185	70	1250	4.8	200.0	122.5	
	B3-1	46.0	16	558	400	300	260	0.0185	70	750	2.9	400.0	164.4	
	B3-2	46.0	16	558	400	300	260	0.0185	70	1250	4.8	400.0	132.7	
	B4-1	46.2	16	558	400	300	260	0.0185	70	750	2.9	600.0	109.8	
	B4-2	46.2	16	558	400	300	260	0.0185	70	1250	4.8	600.0	125.2	
	B5-1	47.5	16	558	400	300	260	0.0185	70	750	2.9	800.0	139.4	
	B5-2	47.5	16	558	400	300	260	0.0185	70	1250	4.8	800.0	113.3	
	B6-1	45.8	16	572	400	300	260	0.0097	70	750	2.9	200.0	137.3	
	B7-1	43.8	16	546	400	300	260	0.0151	70	750	2.9	200.0	144.6	
	B7-2	43.8	16	546	400	300	260	0.0151	70	1250	4.8	200.0	109.0	
	B8-1	45.3	16	570	400	300	260	0.0236	70	750	2.9	200.0	150.2	
	B9-1	45.1	16	567	400	300	260	0.0260	70	750	2.9	200.0	150.8	
	B9-2	45.1	16	567	400	300	260	0.0260	70	1250	4.8	200.0	143.6	
	B10-1	47.5	16	572	400	300	260	0.0097	70	750	2.9	600.0	94.1	
	B11-1	47.2	16	546	400	300	260	0.0151	70	750	2.9	600.0	160.1	
Khulmann et al. [8]	B11-2	47.2	16	546	400	300	260	0.0151	70	1250	4.8	600.0	126.3	
	B12-1	46.8	16	570	400	300	260	0.0236	70	750	2.9	600.0	174.0	
	B12-2	46.8	16	570	400	300	260	0.0236	70	1250	4.8	600.0	140.7	
	C4-1	43.6	16	559	400	300	260	0.0151	70	1000	3.8	150.0	153.2	
	C4-2	43.6	16	559	400	300	260	0.0151	70	1000	3.8	150.0	144.2	
	C5-2	43.7	16	559	400	300	260	0.0151	70	1000	3.8	340.0	136.1	
	C7-1	44.4	16	559	400	300	260	0.0151	70	1000	3.8	150.0	129.8	
	C7-2	44.4	16	559	400	300	260	0.0151	70	1000	3.8	150.0	125.1	
	C8-1	44.5	16	559	400	300	260	0.0151	70	1000	3.8	340.0	127.6	
	C8-2	44.5	16	559	400	300	260	0.0151	70	1000	3.8	340.0	116.7	
	C9-1	27.1	16	559	400	300	260	0.0185	70	750	2.9	500.0	105.2	
	C10-1	51.5	16	559	400	300	260	0.0185	70	750	2.9	500.0	146.0	
	C11-1	45.0	16	559	400	300	260	0.0236	70	750	2.9	340.0	146.5	
	C12-1	45.1	16	559	400	300	260	0.0236	70	750	2.9	600.0	151.2	
	C12-2	45.1	16	559	400	300	260	0.0236	70	1250	4.8	600.0	144.0	
	C13-1	45.5	16	559	400	300	260	0.0185	70	750	2.9	600.0	111.2	
	C13-2	45.5	16	559	400	300	260	0.0185	70	1250	4.8	600.0	134.5	
	A1	19.1	16	625	150	200	175	0.0374	50	625	3.6	-219.8	49.0	$a_{eff}/d<2.5$
	B2	23.6	16	625	150	200	175	0.0374	50	625	3.6	-92.8	51.7	
	C1	24.2	16	625	150	200	175	0.0374	50	625	3.6	-186.9	50.3	$a_{eff}/d<2.5$
	D1	18.0	16	625	150	200	175	0.0374	50	625	3.6	-407.0	53.9	$a_{eff}/d<2.5$
	D2	18.0	16	625	150	200	175	0.0374	50	625	3.6	-464.3	51.9	$a_{eff}/d<2.5$
Madsen et al. [9]	E1	20.2	16	625	150	200	175	0.0374	50	625	3.6	-231.0	46.2	$a_{eff}/d<2.5$
	F1	20.2	16	625	150	200	175	0.0374	50	625	3.6	-346.2	50.6	$a_{eff}/d<2.5$
	F2	20.2	16	625	150	200	175	0.0374	50	625	3.6	-346.6	52.3	$a_{eff}/d<2.5$
	G2	22.1	16	625	150	200	175	0.0374	50	625	3.6	-84.7	52.4	
	H2	21.5	16	625	150	200	175	0.0374	50	625	3.6	-164.8	50.9	$a_{eff}/d<2.5$
	I1	21.4	16	625	150	200	175	0.0374	50	625	3.6	-40.9	39.6	
	I2	21.5	16	625	150	200	175	0.0374	50	625	3.6	-40.9	38.3	

Table A2.2 Simply supported beams without shear reinforcement subjected to point load and axial forces

Reference	Specimen	f_c [MPa]	d_g [mm]	f_y [MPa]	b [mm]	d [mm]	h [mm]	plate [mm]	ρ [-]	a [mm]	a/d [-]	N [kN]	V_{right} [kN]	Remarks[a]
	J1	19.5	16	625	150	175	200	50	0.0374	625	3.6	-70.2	35.3	
	J2	19.5	16	625	150	175	200	50	0.0374	625	3.6	-149.0	50.2	
	K1	19.5	16	625	150	175	200	50	0.0374	625	3.6	-182.4	45.7	$a_{eff}/d<2.5$
	K2	19.5	16	625	150	175	200	50	0.0374	625	3.6	-240.3	48.6	$a_{eff}/d<2.5$
	L1	23.2	16	625	150	175	200	50	0.0374	625	3.6	-223.6	46.9	$a_{eff}/d<2.5$
	L2	23.2	16	625	150	175	200	50	0.0374	625	3.6	-224.1	50.4	$a_{eff}/d<2.5$
Mattock et al. [10]	4	47.1	19	408	152	254	305	132	0.0102	762	3.0	29.4	45.4	
	5	16.4	19	408	152	254	305	132	0.0205	762	3.0	29.4	34.0	
	11	15.5	19	408	152	254	305	132	0.0307	762	3.0	62.1	43.1	
	16	30.9	19	408	152	254	305	132	0.0102	1372	5.4	49.0	28.6	
	19	18.8	19	408	152	254	305	132	0.0205	1372	5.4	29.4	40.8	
	20	49.2	19	408	152	254	305	132	0.0205	1372	5.4	29.4	59.0	
	21	51.5	19	408	152	254	305	132	0.0205	1372	5.4	62.1	58.1	
	23	18.8	19	408	152	254	305	132	0.0307	1372	5.4	29.4	43.1	
	25	28.1	19	408	152	254	305	132	0.0307	1372	5.4	49.0	52.2	
	26	29.4	19	408	152	254	305	132	0.0307	1372	5.4	81.6	43.1	
	29	54.3	19	408	152	254	305	132	0.0307	1372	5.4	29.4	68.0	
	2	15.8	19	408	152	254	305	132	0.0102	762	3.0	-62.1	41.7	$a_{eff}/d<2.5$
	6	18.7	19	408	152	254	305	132	0.0205	762	3.0	-62.1	54.9	
	7	17.8	19	408	152	254	305	132	0.0205	762	3.0	-130.6	61.2	$a_{eff}/d<2.5$
	8	44.6	19	408	152	254	305	132	0.0205	762	3.0	-62.1	94.3	
	9	48.9	19	408	152	254	305	132	0.0205	762	3.0	-130.6	107.5	$a_{eff}/d<2.5$
	12	16.5	19	408	152	254	305	132	0.0307	762	3.0	-62.1	63.1	
	13	50.8	19	408	152	254	305	132	0.0307	762	3.0	-62.1	90.7	
	17	28.3	19	408	152	254	305	132	0.0102	1372	5.4	-130.6	38.6	
	27	31.1	19	408	152	254	305	132	0.0307	1372	5.4	-65.3	54.4	
	28	24.7	19	408	152	254	305	132	0.0307	1372	5.4	-130.6	53.5	
	30	56.2	19	408	152	254	305	132	0.0307	1372	5.4	-62.1	68.0	
	31	53.7	19	408	152	254	305	132	0.0307	1372	5.4	-130.6	68.0	
Morrow et al. [11]	F38B2	12.7	25	381	305	362	406	177	0.0192	995	2.8	-115.5	115.5	$a_{eff}/d<2.5$
	F38E2	14.4	25	396	305	368	406	177	0.0051	991	2.7	-93.7	93.7	$a_{eff}/d<2.5$
	F38B4	32.0	25	393	305	375	406	177	0.0186	989	2.6	-176.4	176.4	$a_{eff}/d<2.5$
	F38D4	27.4	25	375	308	381	406	177	0.0133	991	2.6	-172.6	172.6	$a_{eff}/d<2.5$
	F38E4	32.8	25	375	305	378	406	177	0.0092	988	2.6	-150.7	150.7	$a_{eff}/d<2.5$
	F38A6	46.5	25	371	305	356	406	177	0.0294	989	2.8	-240.6	240.6	$a_{eff}/d<2.5$
	F38B6	42.4	25	386	305	381	406	177	0.0183	988	2.6	-202.1	202.1	$a_{eff}/d<2.5$
	F55B2	12.1	25	382	305	368	406	177	0.0189	1425	3.9	-96.2	96.2	
	F55A4	26.9	25	413	308	372	406	177	0.0201	1422	3.8	-154.0	154.0	
	F55B4	30.1	25	392	305	381	406	177	0.0183	1419	3.7	-128.3	128.3	
	F55D4	26.1	25	441	308	381	406	177	0.0148	1420	3.7	-128.3	128.3	
	F55E4	28.9	25	434	308	387	406	177	0.0096	1420	3.7	-132.8	132.8	
	F55A6	42.9	25	387	305	349	406	177	0.0336	1420	4.1	-192.4	192.4	
	F55B6	44.6	25	383	305	368	406	177	0.0189	1418	3.8	-144.3	144.3	
	F70B2	14.7	25	390	305	362	406	177	0.0192	1788	4.9	-93.0	93.0	

Table A2.2 Simply supported beams without shear reinforcement subjected to point load and axial forces

Reference	Specimen	f_c [MPa]	d_g [mm]	f_y [MPa]	b [mm]	d [mm]	h [mm]	ρ [-]	plate [mm]	a [mm]	a/d [-]	N [kN]	V_right [kN]	Remarks[a]
	F70A4	29.6	25	383	305	362	406	0.0220	177	1786	4.9	-144.3	144.3	
	F70A6	39.4	25	361	305	368	406	0.0343	177	1785	4.8	-176.4	176.4	
	F84B4	30.2	25	389	305	375	406	0.0186	177	2141	5.7	-133.1	133.1	

[a] Specimens with a_{eff}/d <2.5 are not considered for comparison with the models presented in the thesis

Table A2.3 Simply supported beams without shear reinforcement and with prestressed tendons subjected to point load

Reference	Specimen	f_c [MPa]	d_g [mm]	f_y [MPa]	b [mm]	d [mm]	h [mm]	ρ [-]	e_p [mm]	a [mm]	a/d [-]	P [kN]	V_right [kN]
	A1	35.9	19	1386	127	178	254	0.0045	51	889	5.0	80.1	27.1
	A6	28.0	19	1476	127	178	254	0.0069	51	711	4.1	48.9	38.9
	B4	32.0	19	1476	102	152	203	0.0100	51	610	4.1	48.3	29.3
Kar [12]	B5	28.0	19	1476	102	152	203	0.0100	51	686	4.6	41.2	25.8
	B6	30.2	19	1476	102	152	203	0.0125	51	711	4.7	59.6	27.3
	B9	33.3	19	1476	102	152	203	0.0100	51	762	5.1	65.5	26.3
	B10	35.4	19	1476	102	152	203	0.0100	51	762	5.1	82.7	33.7
	A1143	42.9	38	1434	152	209	305	0.0089	57	1321	6.3	227.0	54.8
	A1151	20.0	38	1503	152	214	305	0.0049	62	1321	6.2	126.3	31.6
	A1153	30.1	38	1503	152	204	305	0.0078	51	1321	6.5	206.6	42.2
	A2129	23.1	38	1503	152	215	305	0.0031	62	1321	6.2	42.4	18.6
	A2139	21.6	38	1503	152	227	305	0.0041	75	1321	5.8	57.1	24.9
	A2151	38.8	38	1503	152	206	305	0.0096	54	1321	6.4	122.8	38.9
	A2220	36.9	38	1434	152	215	305	0.0035	62	914	4.3	47.9	33.2
	A2224	23.9	38	1434	152	224	305	0.0028	71	914	4.1	38.5	32.2
	A2227	26.6	38	1434	152	213	305	0.0035	60	914	4.3	47.0	31.8
	A2228	24.0	38	1434	155	222	305	0.0033	70	914	4.1	38.6	29.7
Sozen et al. [13]	A2231	24.3	38	1434	152	205	305	0.0036	52	914	4.5	70.0	34.2
	A2234	28.6	38	1434	152	212	305	0.0047	59	914	4.3	61.4	31.6
	A2236	19.9	38	1434	152	212	305	0.0035	60	914	4.3	68.9	33.7
	A2239	17.8	38	1434	152	224	305	0.0033	71	914	4.1	28.3	24.8
	A2240	39.9	38	1434	152	208	305	0.0077	56	914	4.4	122.0	59.7
	A2249	32.8	38	1434	152	208	305	0.0077	56	914	4.4	96.3	52.0
	A3222	29.6	38	1434	152	238	305	0.0031	86	914	3.8	18.8	32.2
	A3227	19.3	38	1434	152	233	305	0.0032	80	914	3.9	7.8	28.8
	A3237	42.2	38	1434	152	208	305	0.0077	56	914	4.4	8.5	40.0
	A3249	32.8	38	1434	152	208	305	0.0077	56	914	4.4	57.6	47.5

[a] Only specimens with a_{eff}/d ≥2.5 are included in the database and considered for comparison with the models presented in the thesis (data from Reineck and Dunkelberg)

Table A2.4 Simply supported beams without shear reinforcement subjected to distributed load[a]

Reference	Specimen	f_c [MPa]	d_g [mm]	f_y [MPa]	b [mm]	d [mm]	h [mm]	ρ [-]	plate [mm]	l [mm]	l/d [-]	q [kN/m]	V_{right} [kN]	Remarks[b]
Acevedo et al. [14]	SB2	32.4	10	636	332	205	256	0.0172	38	2667	13.0	95.0	126.7	
Aoyagi et al.	BL	36.0	25	370	150	250	300	0.0405	120	3000	12.0	86.3	129.5	(F/SC)
Cavagnis et al. [15]	SC51a	33.6	16	713	250	556	600	0.0089	200	5600	10.1	60.4	169.1	
	SC51b	33.6	16	713	250	556	600	0.0089	200	5600	10.1	57.8	161.8	
Dassow [16]	LD2	28.1	25	478	914	541	610	0.0102	305	5486	10.1	197.6	542.0	
	LD3	24.3	25	478	914	541	610	0.0102	305	5486	10.1	198.3	544.0	
	LD4	25.6	25	470	914	541	610	0.0102	305	5486	10.1	231.6	635.4	
	D13	19.0	25	464	152	252	305	0.0099	152	2794	11.1	36.3	50.7	
	D17	41.0	25	586	152	252	305	0.0099	152	2794	11.1	39.3	54.9	
Diaz de Cossio et al. [6]	D4	35.1	25	305	152	252	305	0.0222	152	2235.2	8.9	104.7	117.0	$l/d<10$
	D14	32.7	25	462	152	252	305	0.0101	152	2235.2	8.9	80.8	90.3	$l/d<10$
	D15	27.1	25	461	152	252	305	0.0101	152	2235.2	8.9	77.2	86.3	$l/d<10$
	D16	40.3	25	586	152	252	305	0.0101	152	2235.2	8.9	95.2	106.4	$l/d<10$
	D1	30.8	25	295	152	252	305	0.0336	152	2794	11.1	66.4	92.7	
Feldman et al. [17]	D2	38.6	25	307	152	252	305	0.0336	152	2794	11.1	79.0	110.3	
	D3	33.2	25	314	152	252	305	0.0336	152	2794	11.1	67.3	94.1	
	D6	23.8	25	310	152	252	305	0.0336	152	2794	11.1	74.5	104.1	
Klein [18]	LD5	33.1	25	495	533	541	610	0.0105	305	6502	12.0	81.3	264.2	
	LD8	29.4	25	447	533	1151	1219	0.0098	305	13818	12.0	60.6	419.0	
	2CU	20.8	25	394	152	254	305	0.0131	178	3048	12.0	35.6	54.3	
	3CU	20.5	25	379	152	256	305	0.0199	178	3048	11.9	47.0	71.6	
	4CU	20.6	25	394	152	254	305	0.0262	178	3048	12.0	52.2	79.6	
	5CU	20.4	25	370	152	252	305	0.0335	178	3048	12.1	54.3	82.7	
	6CU	20.6	25	400	152	250	305	0.0428	178	3048	12.2	51.1	77.8	
	3EU	17.6	25	379	152	256	305	0.0199	178	3658	14.3	33.8	61.8	
	4EU	20.2	25	394	152	254	305	0.0262	178	3658	14.4	39.9	72.9	
	5EU	19.3	25	370	152	252	305	0.0336	178	3658	14.5	42.3	77.4	
	6EU	20.1	25	400	152	250	305	0.0430	178	3658	14.6	37.5	68.6	
	3GU	22.6	25	379	152	256	305	0.0199	178	4267	16.7	27.7	59.2	
	4GU	22.1	25	394	152	254	305	0.0262	178	4267	16.8	33.1	70.6	
	5GU	21.3	25	370	152	252	305	0.0335	178	4267	16.9	30.9	65.8	
	6GU	21.2	25	379	152	256	305	0.0430	178	4267	17.1	35.2	75.1	
	3JU	22.2	25	400	152	256	305	0.0199	178	4877	19.1	19.9	48.5	F
	4JU	22.2	25	394	152	254	305	0.0262	178	4877	19.2	23.4	57.1	
	5JU	21.5	25	370	152	252	305	0.0337	178	4877	19.4	27.2	66.3	
	6JU	21.0	25	400	152	250	305	0.0430	178	4877	19.5	23.5	57.3	
Krefeld et al. [19]	4CUa	32.3	25	394	152	254	305	0.0262	178	3048	12.0	63.9	97.4	
	5CUa	32.3	25	370	152	252	305	0.0335	178	3048	12.1	62.5	95.2	
	6CUa	36.8	25	400	152	251	305	0.0428	178	3048	12.2	70.6	107.6	
	3CUb	12.2	25	379	152	255	305	0.0199	178	3048	12.0	38.8	59.1	
	4CUb	17.1	25	394	152	254	305	0.0262	178	3048	12.0	46.4	70.7	
	5CUb	14.7	25	370	152	253	305	0.0336	178	3048	12.0	52.8	80.5	
	6CUb	13.7	25	400	152	250	305	0.0430	178	3048	12.2	47.0	71.6	

Table A2.4 Simply supported beams without shear reinforcement subjected to distributed load[a]

Referemce	Specimen	f_c [MPa]	d_g [mm]	f_y [MPa]	b [mm]	d [mm]	h [mm]	ρ [-]	plate [mm]	l [mm]	l/d [-]	q [kN/m]	V_{right} [kN]	Remarks[b]
	4EUa	14.3	25	394	152	254	305	0.0262	178	3658	14.4	27.5	50.3	
	5EUa	15.1	25	370	152	253	305	0.0336	178	3658	14.5	35.0	64.0	
	6EUa	12.8	25	400	152	251	305	0.0430	178	3658	14.6	33.8	61.8	
	3GUa	13.5	25	379	152	256	305	0.0199	178	4267	16.7	22.3	47.6	
	4GUa	11.6	25	394	152	254	305	0.0262	178	4267	16.8	20.7	44.1	
	5GUa	11.2	25	370	152	252	305	0.0338	178	4267	16.9	22.7	48.5	
	11A1	27	25	400	152	314	381	0.0343	178	1828.8	5.8	292.4	267.4	l/d<10
	12A1	30.6	25	400	152	238	305	0.0453	178	1828.8	7.7	197.5	180.6	l/d<10
	13A1	20.2	25	400	152	319	381	0.0080	178	1828.8	5.7	129.5	118.4	l/d<10 F
	14A1	22.8	25	400	152	243	305	0.0105	178	1828.8	7.5	97.8	89.4	l/d<10
	15A1	19.2	25	400	152	316	381	0.0134	178	1828.8	5.8	169.3	154.8	l/d<10
	16A1	21	25	400	152	240	305	0.0177	178	1828.8	7.6	115.3	105.4	l/d<10
	3AAU	34.6	25	400	152	255	305	0.0200	178	1828.8	7.2	167.4	153.1	l/d<10
	4AAU	36.4	25	400	152	254	305	0.0264	178	1828.8	7.2	200.5	183.3	l/d<10
	5AAU	29	25	400	152	252	305	0.0337	178	1828.8	7.3	219.4	200.6	l/d<10
	6AAU	34.4	25	400	152	251	305	0.0429	178	1828.8	7.3	235.0	214.9	l/d<10
	4AU	31.7	25	400	152	254	305	0.0264	178	2438.4	9.6	96.3	117.4	l/d<10
	5AU	31.7	25	400	152	252	305	0.0337	178	2438.4	9.7	108.8	132.6	l/d<10
	6AU	34.1	25	400	152	251	305	0.0429	178	2438.4	9.7	127.0	154.8	l/d<10
Leonhardt et al. [20]	14-1	31.8	16	465	190	273	320	0.0205	100	3000	11.0	71.3	107.0	
	14-2	31.8	16	465	190	273	320	0.0205	100	3000	11.0	71.6	107.4	
	15-1	33.6	16	465	190	272	320	0.0205	100	4000	14.7	47.7	95.4	
	15-2	33.6	16	465	189	273	320	0.0206	100	4000	14.7	50.8	101.6	
	16-1	33.1	16	465	190	273	320	0.0205	100	5000	18.3	38.5	96.3	
	16-2	33.1	16	465	189	274	320	0.0205	100	5000	18.2	38.3	95.8	
	17-1	31.1	16	465	189	273	320	0.0206	100	6000	22.0	29.0	87.0	
	17-2	31.1	16	465	190	274	320	0.0205	100	6000	21.9	29.0	87.0	F
	12-1	32.2	30	465	190	273	323	0.0204	100	2000	7.3	202.5	202.5	l/d<10
	12-2	32.2	30	465	189	272	322	0.0206	100	2000	7.3	160.5	160.5	l/d<10
	13-1	32.7	30	465	190	273	323	0.0204	100	2500	9.2	111.2	139.0	l/d<10
	13-2	32.7	30	465	189	272	322	0.0205	100	2500	9.2	111.2	139.0	l/d<10
Rusch et al. [21]	B01	22.4	15	400	100	200	240	0.0385	100	1440	7.2	117.8	84.8	l/d<10
	B02	22.4	15	400	100	200	240	0.0385	100	1440	7.2	108.3	78.0	l/d<10
	B03	22.4	15	400	100	200	240	0.0385	100	1440	7.2	117.8	84.8	l/d<10
	B04	22.2	15	400	100	200	240	0.0385	100	1440	7.2	107.8	77.6	l/d<10
	B05	22.2	15	400	100	200	240	0.0385	100	1440	7.2	101.1	72.8	l/d<10
	B06	22.2	15	400	100	200	240	0.0385	100	1440	7.2	103.9	74.8	l/d<10
Shioya et al. [22]	1	20.6	10	440	158	100	120	0.0036	20	1200	12.0	29.4	17.6	F [23]
	2	19.7	10	440	158	200	220	0.0036	40	2400	12.0	29.5	35.5	F [23]
	3	21.1	10	440	300	600	655	0.0038	120	7200	12.0	30.9	111.2	
	4	27.2	10	370	500	1000	1200	0.0044	200	12000	12.0	39.5	237.0	
	5	21.9	25	370	500	1000	1200	0.0044	200	12000	12.0	44.0	264.0	
	6	28.5	25	370	1000	2000	2100	0.0040	400	24000	12.0	77.0	924.0	
	7	24.3	25	360	1500	3000	3140	0.0039	600	36000	12.0	105.0	1890.0	

Table A2.4 Simply supported beams without shear reinforcement subjected to distributed load[a]

Reference	Specimen	f_c [MPa]	d_g [mm]	f_y [MPa]	b [mm]	h [mm]	d [mm]	ρ [-]	l [mm]	plate [mm]	l/d [-]	q [kN/m]	V_{right} [kN]	Remarks[b]
	1	20.6	10	440	158	120	100	0.0036	1200	20	12.0	25.6	15.4	ADT [23]
	2	28.5	1	440	158	220	200	0.0036	2400	40	12.0	28.3	33.9	ADT [23]
	3	21.6	25	440	158	220	200	0.0036	2400	40	12.0	29.4	35.3	F [23]
	4	27.3	3	440	300	655	600	0.0038	7200	120	12.0	25.5	91.8	
	5	21.2	25	440	300	655	600	0.0038	7200	120	12.0	38.7	139.3	
	6	28.2	5	370	500	1200	1000	0.0044	12000	200	12.0	33.0	198.0	
Smith [24]	8/0	28.0	19	500	150	230	200	0.0201	2440	100	12.2	48.4	59.0	
	10/0	34.5	19	500	150	230	200	0.0201	3052	100	15.3	33.1	50.5	
	12/0	36.2	19	500	150	230	200	0.0201	3660	100	18.3	28.4	52.0	
Tung et al. [25][c]	SV-2.R	33.8	18	670	170	450	407	0.0074	5000	200	12.3	70.6	70.6	
	SV-2.L	33.8	18	670	170	450	407	0.0074	5000	200	12.3	75.7	75.7	
Uzel et al. [26]	AP1	35.8	6	505	113	250	230	0.0116	1000	150	4.3	284.0	142.0	$l/d<10$
	AP2	35.8	6	505	113	250	230	0.0116	1500	150	6.5	86.0	64.5	$l/d<10$

[a] Only specimens with $l/d \geq 10$ are included in the database; [b] F/SC: flexural failure or shear compression failure. ADT: abnormal diagonal tension. Specimens labelled with F or ADT are not considered for comparison with the models presented in the thesis; [c] the distributed load q was applied at a distance of 400 mm from the edge of the support plates and not on the entire length of the specimen

Table A2.5 Cantilever and continuous beams without shear reinforcement subjected to distributed load

Reference	Specimen	f_c [MPa]	d_g [mm]	f_y [MPa]	b [mm]	h [mm]	d [mm]	ρ [-]	l [mm]	plate [mm]	l_c [mm]	l_c/d [mm]	l_{ss} [mm]	V_{right}/ql [kN]	q [kN/m]	V_{right} [kN]	V_{left} [kN]	Remarks[a]
Acevedo et al. [14]	S1	31.8	10	636	333	258	216	0.0109	2286	75	1429	6.6	1715	0.62	92.0	131.4	78.9	
	S3b	55.2	10	634	331	252	216	0.0097	1524	75	953	4.4	1143	0.63	306.0	291.5	174.9	F/SC
	S5	30.9	10	561	332	256	211	0.0044	1050	75	657	3.1	787	0.63	422.0	277.0	166.1	Failure M+
Aoyagi et al. [27]	DM1d	36.0	25	370	150	300	250	0.0405	2000	120	1125	4.5	1750	0.56	114.0	128.3	99.8	Failure M+
	DM2d	36.0	25	370	150	300	250	0.0405	2000	120	1250	5.0	1500	0.63	120.0	150.0	90.0	
	DM3d	36.0	25	370	150	300	250	0.0405	2125	120	1375	5.5	1500	0.65	123.2	169.4	92.4	
	DM4d	36.0	25	370	150	300	250	0.0405	2125	120	1500	6.0	1250	0.71	82.0	123.0	51.3	
	CM0.5d	36.0	25	370	150	300	250	0.0405	1875	120	1000	4.0	1750	0.53	152.0	152.0	133.0	Failure M+
	CM1d	36.0	25	370	150	300	250	0.0405	1750	120	1000	4.0	1500	0.57	168.0	168.0	126.0	Failure M+
	CM1.5d	36.0	25	370	150	300	250	0.0405	1625	120	1000	4.0	1250	0.62	178.0	178.0	111.3	
	CM2d	36.0	25	370	150	300	250	0.0405	1500	120	1000	4.0	1000	0.67	192.0	192.0	96.0	
	CM3d	36.0	25	370	150	300	250	0.0405	1250	120	1000	4.0	500	0.80	208.0	208.0	52.0	(F/SC)
	CM4d	36.0	25	370	150	300	250	0.0405	1000	120	1000	4.0	0	1.00	166.0	166.0	0.0	
Bryant et al. [28]	C5N	20.0	25	325	152	368	330	0.0258	2591	76	1619	4.9	1944	0.62	101.0	163.5	98.2	
	E5N	27.0	25	325	152	368	330	0.0258	2591	76	1619	4.9	1944	0.62	90.0	145.7	87.5	
	C11N	25.0	25	326	152	368	330	0.0258	2591	76	1619	4.9	1944	0.62	74.0	119.8	71.9	
	E11N	22.0	25	326	152	368	330	0.0258	2591	76	1619	4.9	1944	0.62	73.0	118.2	71.0	
	C11-0	25.0	25	283	203	368	330	0.0245	2591	76	1619	4.9	1944	0.62	126.0	204.0	122.5	
Cavagnis et al. [15]	SC52	36.8	16	713	250	600	556	0.0089	5600	200	3360	6.0	4480	0.60	59.5	199.8	133.2	
	SC52a	36.8	16	713	250	600	556	0.0089	5600	200	3360	6.0	4480	0.60	77.0	258.7	172.5	Failure M+

Table A2.5 Cantilever and continuous beams without shear reinforcement subjected to distributed load

Reference	Specimen	f_c [MPa]	d_g [mm]	f_y [MPa]	b [mm]	d [mm]	h [mm]	ρ [-]	plate [mm]	l [mm]	l_c [mm]	l_c/d [mm]	l_ss [mm]	V_right/ql [kN]	q [kN/m]	V_right [kN]	V_left [kN]	Remarks[a]
	SC52b	36.8	16	713	250	556	600	0.0089	200	5600	3360	6.0	4480	0.60	85.0	285.6	190.4	Failure M+
	SC53	33.2	16	713	250	556	600	0.0089	200	5600	3920	7.1	3360	0.70	40.2	157.7	67.6	
	SC54	36.5	16	713	250	556	600	0.0089	200	5600	4480	8.1	2240	0.80	40.6	182.1	45.5	
	SC55	33.7	16	713	250	556	600	0.0089	200	5600	5040	9.1	1120	0.90	33.4	168.2	18.7	
	SC56	35.3	16	713	250	556	600	0.0089	200	5600	5600	10.1	0	1.00	28.2	157.8	0.0	
	SC57	33.2	16	713	250	556	600	0.0089	200	4900	4900	8.8	0	1.00	30.0	147.1	0.0	
	SC58	36.1	16	713	250	556	600	0.0089	200	4200	4200	7.6	0	1.00	50.6	212.5	0.0	F/SC
	SC59	35.5	16	713	250	556	600	0.0089	200	3500	3500	6.3	0	1.00	52.3	183.2	0.0	
	SC62	35.8	16	713	250	556	600	0.0089	200	2800	2800	5.0	0	1.00	62.1	173.7	0.0	
	SC66	31.2	16	713	250	556	600	0.0089	200	2100	2100	3.8	0	1.00	91.4	191.9	0.0	
	SC63	33.6	16	760	250	559	600	0.0054	200	3500	3500	6.3	0	1.00	60.8	212.8	0.0	F/SC
	SC60	36.9	16	760	250	559	600	0.0054	200	2800	2800	5.0	0	1.00	58.9	164.8	0.0	
Klaus [29]	TCA1	36.4	20	683	610	159	203	0.0051	0	1827	1015	6.4	1623	0.56	239.4	243.0	194.3	
	TCA2	52.4	20	683	610	159	203	0.0051	0	1827	1015	6.4	1623	0.56	209.8	212.9	170.3	
	TCA3	60.7	20	683	610	159	203	0.0051	0	1827	1015	6.4	1623	0.56	225.5	228.9	183.0	
	TCA4	38.6	20	468	610	151	203	0.0139	0	1827	1015	6.7	1623	0.56	285.5	289.8	231.7	
	TCA5	44.7	20	468	610	151	203	0.0139	0	1827	1015	6.7	1623	0.56	302.3	306.8	245.3	
	TCA6	61.2	20	468	610	151	203	0.0139	0	1827	1015	6.7	1623	0.56	307.8	312.4	249.8	
	TCF1	68.1	20	624	610	109	152	0.0053	0	1357	762	7.0	1189	0.56	239.0	182.1	142.1	
	TCF4R	59.5	20	624	610	260	305	0.0045	0	2608	1524	5.9	2168	0.58	167.1	254.7	181.1	(F/SC)
	TCS2R	64.0	20	468	610	151	203	0.0139	0	1828	1016	6.7	1623	0.56	258.0	262.1	209.4	Failure M+
	TCS4	58.4	20	624	610	245	305	0.0144	0	2902	1525	6.2	2754	0.53	253.8	387.0	349.5	Failure M+
Pérez Caldentey et al. [30]	CR1	31.1	20	835	250	562	600	0.0079	210	3300	3300	5.9	0	1.00	52.7	174.0	0.0	
	CR2	33.6	20	835	250	562	600	0.0079	210	3300	3300	5.9	0	1.00	57.8	190.7	0.0	
Richart [31]	502A	24.3	25	420	1828	406	450	0.0054	305	1372	1372	3.4	0	1.00	898.7	1232.7	0.0	l/d<3.5 F/SC
	502B	22.7	25	420	1828	406	450	0.0054	305	1372	1372	3.4	0	1.00	937.6	1286.1	0.0	l/d<3.5 F/SC
	503A	24.4	25	420	1828	406	450	0.0054	305	1372	1372	3.4	0	1.00	950.6	1303.9	0.0	l/d<3.5 F/SC
	503B	24.0	25	420	1828	406	450	0.0054	305	1372	1372	3.4	0	1.00	892.2	1223.8	0.0	l/d<3.5 F/SC
	505A	25.4	25	420	1524	406	450	0.0068	305	1525	1525	3.8	0	1.00	799.3	1219.0	0.0	F/SC
	505B	25.7	25	420	1524	406	450	0.0068	305	1525	1525	3.8	0	1.00	765.6	1167.5	0.0	F/SC
	506A	23.1	25	420	1524	406	450	0.0068	305	1525	1525	3.8	0	1.00	729.2	1112.0	0.0	F/SC
	506B	26.3	25	420	1524	406	450	0.0068	305	1525	1525	3.8	0	1.00	729.2	1112.0	0.0	F/SC
Tung et al. [25][b]	SV3.1	32.5	18	670	170	407	450	0.0074	200	2500	2500	6.1	0	1.00		77.4	0.0	
	SV3.2	32.4	18	670	170	407	450	0.0074	200	2500	2500	6.1	0	1.00		87.7	0.0	
	SV4.1	33.2	18	670	170	403	450	0.0143	200	2500	2500	6.2	0	1.00		100.5	0.0	
	SV4.2	33.0	18	670	170	403	450	0.0143	200	2500	2500	6.2	0	1.00		94.1	0.0	
	SV5.1	33.2	18	670	170	403	450	0.0143	200	2900	2900	7.2	0	1.00		120.0	0.0	
	SV5.2	33.1	18	670	170	403	450	0.0155	200	2900	2900	7.2	0	1.00		110.8	0.0	
	SV6.1	33.8	18	670	170	405	450	0.0091	200	5000	2877	7.1	4186	0.58		128.8	88.0	Failure M+
	SV6.2	33.3	18	670	170	407	450	0.0074	200	5000	2797	6.9	4349	0.56		104.0	77.1	Failure M+
	SV7.1	33.3	18	670	170	407	450	0.0074	200	5000	2953	7.3	4031	0.59		64.1	40.4	VL
	SV7.2	33.2	18	670	170	407	450	0.0074	200	5000	2975	7.3	3987	0.60		50.0	30.8	VL

Table A2.5 Cantilever and continuous beams without shear reinforcement subjected to distributed load

Reference	Specimen	f_c [MPa]	d_g [mm]	f_y [MPa]	b [mm]	d [mm]	h [mm]	ρ [-]	plate [mm]	l [mm]	l_c [mm]	l_c/d	l_{ss} [mm]	V_{right}/ql	q [kN/m]	V_{right} [kN]	V_{left} [kN]	Remarks[a]
	SV8	33.3	18	670	170	407	450	0.0074	200	5000	2829	7.0	4284	0.57		88.1	63.2	VL
	AP3	35.8	6	505	113	230	250	0.0116	150	500	500	2.2	0	1.00	294.0	147.0	0.0	l/d<3.5 F/SC
	AP4	35.8	6	505	113	230	250	0.0116	150	750	750	3.3	0	1.00	94.7	71.0	0.0	l/d<3.5
Uzel et al. [26]	AF1	43.0	10	550	300	925	1000	0.0076	150	2997	2997	3.2	0	1.00	197.9	593.0	0.0	l/d<3.5 F/SC
	AF3	27.3	19	475	300	617	670	0.0076	150	2997	2997	4.9	0	1.00	90.3	270.5	0.0	
	AF11	36.2	19	562	300	925	1000	0.0076	150	2000	2000	2.2	0	1.00	661.3	1322.6	0.0	l/d<3.5 F/SC
	AF13	35.7	19	475	300	865	1000	0.0216	150	3000	3000	3.5	0	1.00	309.5	928.5	0.0	l/d<3.5 F/SC
	AF6	32.2	19	562	300	617	670	0.0076	150	1890	1890	3.1	0	1.00	216.3	408.8	0.0	l/d<3.5 F/SC
	A1L	19.6	8	500	150	150	180	0.0205	0	450	450	3.0	0	1.00	219.6	98.8	0.0	l/d<3.5 F/SC
	A1R	19.6	8	500	150	150	180	0.0205	0	450	450	3.0	0	1.00	288.4	129.8	0.0	l/d<3.5 F/SC
	A2L	21.7	8	500	150	150	180	0.0205	0	675	450	3.0	450	0.67	211.1	95.0	47.5	l_c/d<3.5 F/SC
	A2R	21.7	8	500	150	150	180	0.0205	0	675	450	3.0	450	0.67	233.1	104.9	52.5	l_c/d<3.5 F/SC
	A3L	21.0	8	500	150	150	180	0.0205	0	768	450	3.0	636	0.59	189.6	85.3	60.3	l_c/d<3.5 F/SC
	A3R	21.0	8	500	150	150	180	0.0205	0	768	450	3.0	636	0.59	173.1	77.9	55.1	l_c/d<3.5 F/SC
	A4L	23.1	8	500	150	150	180	0.0205	0	840	450	3.0	779	0.54	129.1	58.1	50.3	Failure M+
	A4R	23.1	8	500	150	150	180	0.0205	0	840	450	3.0	779	0.54	172.4	77.6	67.2	Failure M+
	B1L	19.8	8	500	150	150	180	0.0205	0	675	675	4.5	0	1.00	83.7	56.5	0.0	
	B1R	19.8	8	500	150	150	180	0.0205	0	675	675	4.5	0	1.00	83.7	56.5	0.0	
	B2L	20.3	8	500	150	150	180	0.0205	0	1013	675	4.5	675	0.67	116.0	78.3	39.2	
TNO [32]	B2R	20.3	8	500	150	150	180	0.0205	0	1013	675	4.5	675	0.67	98.4	66.4	33.2	
	B3L	22.2	8	500	150	150	180	0.0205	0	1152	675	4.5	955	0.59	99.0	66.8	47.2	Failure M+
	B3R	22.2	8	500	150	150	180	0.0205	0	1152	675	4.5	955	0.59	91.4	61.7	43.6	Failure M+
	B4L	23.3	8	500	150	150	180	0.0205	0	1260	675	4.5	1169	0.54	77.0	52.0	45.0	Failure M+
	B4R	23.3	8	500	150	150	180	0.0205	0	1260	675	4.5	1169	0.54	77.0	52.0	45.0	Failure M+
	C1L	22.7	8	500	150	150	180	0.0205	0	900	900	6.0	0	1.00	47.2	42.5	0.0	
	C1R	22.7	8	500	150	150	180	0.0205	0	900	900	6.0	0	1.00	45.6	41.0	0.0	
	C2L	19.0	8	500	150	150	180	0.0205	0	1350	900	6.0	900	0.67	57.0	51.3	25.7	
	C2R	19.0	8	500	150	150	180	0.0205	0	1350	900	6.0	900	0.67	67.0	60.3	30.2	
	C3R	26.0	8	500	150	150	180	0.0205	0	1536	900	6.0	1273	0.59	77.6	69.8	49.4	Failure M+
	C4L	23.7	8	500	150	150	180	0.0205	0	1679	900	6.0	1559	0.54	59.6	53.6	46.4	Failure M+
	A10L	23.7	8	500	150	150	180	0.0205	0	450	450	3.0	0	1.00	207.1	93.2	0.0	l_c/d<3.5 F/SC
	A10R	23.7	8	500	150	150	180	0.0205	0	450	450	3.0	0	1.00	203.6	91.6	0.0	l_c/d<3.5 F/SC

a Failure M+: failure within the region of positive bending moment; F/SC: flexural failure or shear compression failure with the crack not disturbing the development of the theoretical direct strut yielding an increase of the shear capacity; VL: Variable Load: position of the point of contraflexure was varied during testing. Specimens with l/d or l_c/d <3.5 failing within the region of negative bending moment and labelled with F/SC or VL are not considered for comparison with the models presented in the thesis; b the distributed load q was applied at a distance of 400 mm from the edge of the support plates and not on the entire length of the specimen

Table A2.6 Simply supported beams without shear reinforcement subjected to point load (LWC)

Reference	Specimen	f_c [MPa]	d_g [mm]	f_y [MPa]	d [mm]	h [mm]	b [mm]	ρ [-]	plate [mm]	a [mm]	a/d [-]	V_{right} [kN]
Walraven [33]	B1	30.1		540	125	150	200	0.0083	31	375	3.00	29.8
	B2	30.1		440	420	450	200	0.0074	84	1260	3.00	60.5
	B3	27.8		440	720	750	200	0.0079	144	2160	3.00	79.2
	C1	31.4		440	125	150	200	0.0152	31	375	3.00	35.0
	C2	31.4		440	405	450	200	0.0156	84	1260	3.11	86.7
	C3	28.9		440	700	750	200	0.0158	144	2160	3.09	106.4
Tylor et al. [34]	B1	26.2		420	221	254	191	0.0188	51	838	3.80	39.3
	B2	26.0		420	221	254	191	0.0188	51	838	3.80	39.1
	B3	26.2		420	221	254	191	0.0188	51	838	3.80	38.1
	B4	29.5		420	221	254	191	0.0188	51	838	3.80	40.9
	B5	37.3		420	221	254	191	0.0188	51	838	3.80	44.0
	B6	35.0		420	221	254	191	0.0188	51	838	3.80	48.9
	B7	35.0		420	221	254	191	0.0188	51	838	3.80	39.3
	B8	39.4		420	221	254	191	0.0188	51	838	3.80	41.4
	B9	29.5		420	221	254	191	0.0121	51	838	3.80	35.2
	B10	26.0		420	221	254	191	0.0121	51	838	3.80	36.6
	B11	37.3		420	221	254	191	0.0121	51	838	3.80	36.1
	B12	39.4		420	221	254	191	0.0121	51	838	3.80	39.3
	C1	27.5		420	221	254	191	0.0188	51	838	3.80	38.7
	C2	28.2		420	221	254	191	0.0188	51	838	3.80	43.4
	C3	27.5		420	221	254	191	0.0188	51	838	3.80	43.8
	C4	29.0		420	221	254	191	0.0188	51	838	3.80	43.4
	C5	34.4		420	221	254	191	0.0188	51	838	3.80	48.5
	C6	39.8		420	221	254	191	0.0188	51	838	3.80	53.2
	C7	39.8		420	221	254	191	0.0188	51	838	3.80	48.2
	C8	35.6		420	221	254	191	0.0188	51	838	3.80	47.5
	C9	29.0		420	221	254	191	0.0121	51	838	3.80	38.4
	C10	28.2		420	221	254	191	0.0121	51	838	3.80	37.2
	C11	34.4		420	221	254	191	0.0121	51	838	3.80	40.2
	C12	35.6		420	221	254	191	0.0121	51	838	3.80	42.9
Ivey et al. [35]	1.2	31.6		420	267	305	152	0.0125		889	3.33	39.9
	1.3	33.0		420	267	305	152	0.0125		1321	4.95	34.0
	23.1	28.4		420	267	305	152	0.0093		889	3.33	36.7
	23.2	29.3		420	267	305	152	0.0125		889	3.33	38.1
	23.3	29.2		420	267	305	152	0.0146		889	3.33	41.7
	23.1s	26.2		420	267	305	152	0.0093		889	3.33	34.8
	23.2s	27.2		420	267	305	152	0.0125		889	3.33	40.4
	23.3s	28.5		420	267	305	152	0.0146		889	3.33	40.4
	27.2	26.1		420	267	305	152	0.0125		889	3.33	39.9
	27.3	24.0		420	267	305	152	0.0125		1321	4.95	28.1
	23.4	25.0		420	188	229	108	0.0125		627	3.33	17.3
	23.5	30.2		420	267	305	152	0.0125		889	3.33	37.2
	23.6	26.9		420	333	381	191	0.0125		1110	3.34	59.9
	23.7	26.4		420	395	451	225	0.0128		1318	3.34	77.1

Table A2.6 Simply supported beams without shear reinforcement subjected to point load (LWC)

Reference	Specimen	f_c [MPa]	d_g [mm]	f_y [MPa]	d [mm]	h [mm]	b [mm]	plate [mm]	ρ [-]	a [mm]	a/d [-]	V_right [kN]
	23.12	23.0		420	267	305	152		0.0210	800	3.00	55.4
	23.13	22.5		420	267	305	152		0.0210	1067	4.00	39.1
	23.14	19.5		420	267	305	152		0.0210	1321	4.95	40.6
	23.15	22.0		420	267	305	152		0.0093	889	3.33	34.2
	23.16	19.5		420	267	305	152		0.0125	889	3.33	40.0
	23.17	27.1		420	267	305	152		0.0146	889	3.33	40.6

Table A2.7 Simply supported beams with low amount of transverse reinforcement subjected to point load

Reference	Specimen	f_c [MPa]	d_g [mm]	f_y [MPa]	b [mm]	d [mm]	h [mm]	ρ [-]	plate [mm]	a [mm]	a/d [-]	s_w	ρ_w [%]	f_yw [MPa]	V_right [kN]
Reineck et al. [2]	# 86 tests[a]	15.7–125.3	7–30	271–977	150–457	198–1200	270–1250	0.005–0.047			2.50–5.0	60–300	0.07–0.34	237–820	
Campana et al. [36]	SC12	41.5	16	580	302	354	405	0.0149	80	1220	3.4	150	0.062	497	179.0
	SC13	43.1	16	580	303	354	403	0.0106	80	1220	3.4	150	0.062	497	150.0
	SC16	56.0	16	580	302	346	402	0.0152	80	1220	3.5	150	0.062	497	199.0
	SC17	57.2	16	580	304	350	404	0.0107	80	1220	3.5	150	0.062	497	153.0
Huber et al. [37]	R250m35	35.9	22	550	75	230	250	0.0117	50	700	3.0	150	0.112	653	29.6
	R500m60	51.2	16	550	150	460	500	0.0117	100	1400	3.0	200	0.094	569	83.0
	R500m351	37.9	22	550	150	460	500	0.0117	100	1400	3.0	200	0.094	569	105.9
	R500m352	35.9	22	550	150	460	500	0.0117	100	1400	3.0	200	0.084	653	109.2
	R1000m60	60.9	16	550	300	920	1000	0.0125	200	2800	3.0	400	0.094	552	402.1
	R1000m35	29.6	22	550	300	920	1000	0.0125	200	2800	3.0	200	0.094	569	383.8
Yoon et al. [38]	N1-n	36.0	20	430	375	655	750	0.0286	150	2150	3.3	325	0.082	430	457.0
	N2-s	36.0	20	430	375	655	750	0.0286	150	2150	3.3	465	0.081	430	363.0
	N2-n	36.0	20	430	375	655	750	0.0286	150	2150	3.3	325	0.116	430	483.0
	M1-n	67.0	10	430	375	655	750	0.0286	150	2150	3.3	325	0.082	430	405.0
	M2-s	67.0	10	430	375	655	750	0.0286	150	2150	3.3	325	0.116	430	552.0
	M2-n	67.0	10	430	375	655	750	0.0286	150	2150	3.3	230	0.164	430	689.0
	H1-n	87.0	10	430	375	655	750	0.0286	150	2150	3.3	325	0.082	430	483.0
	H2-s	87.0	10	430	375	655	750	0.0286	150	2150	3.3	270	0.140	430	598.0
	H2-N	87.0	10	430	375	655	750	0.0286	150	2150	3.3	160	0.236	430	721.0

aOnly the specimens respecting the following criteria were considered: (i) rectangular cross-section; (ii) a/d $\geq$2.5; (iii) aggregate size specified.

Table A2.8 Simply supported beams without shear reinforcement and with steel fibres subjected to point load

Reference	Specimen	f_c [MPa]	d_g [mm]	f_y [MPa]	b [mm]	d [mm]	h [mm]	ρ [-]	plate [mm]	a [mm]	a/d [-]	FT	ρ_f [-]	l_f [mm]	α_f [-]	V_{right} [kN]	Remarks[a]
Ashour et al. [39]	B-4-0.5-A	95.4	10	460	125	215	250	0.0284		860	4.00	H	0.50	60	75	57.9	
	B-6-0.5-A	95.8	10	460	125	215	250	0.0284		1290	6.00	H	0.50	60	75	49.7	
	B-4-1.0-A	97.5	10	460	125	215	250	0.0284		860	4.00	H	1.00	60	75	80.8	F/SC
	B-4-1.5-A	97.1	10	460	125	215	250	0.0284		860	4.00	H	1.50	60	75	89.5	
	B-4-1.0-M	93.8	10	470	125	215	250	0.0458		860	4.00	H	1.00	60	75	97.5	
	B-6-1.0-M	95.0	10	470	125	215	250	0.0458		1290	6.00	H	1.00	60	75	73.6	
Barragan [40]	20-30-SFRC1	37.7	25		200	260	300	0.0283		910	3.50	H	0.50	60	67	111.0	
	20-30-SFRC2	38.8	25		200	260	300	0.0283		910	3.50	H	0.50	60	67	132.0	
	20-45-SFRC1	37.7	25		200	410	450	0.0308		1370	3.34	H	0.50	60	67	146.0	
	20-50-SFRC2	38.8	25		200	460	500	0.0241		1550	3.37	H	0.50	60	67	148.0	
	20-60-SFRC2	38.8	25		200	540	600	0.0273		1890	3.50	H	0.50	60	67	222.0	
Batson et al. [41]	A2	33.2	16		102	126	150	0.0310		605	4.80	P	0.22	25	100	26.7	
	B3	33.2	16		102	126	150	0.0310		554	4.40	P	0.22	25	100	31.6	
	C1	33.2	16		102	126	150	0.0310		529	4.20	P	0.22	25	100	31.5	
	C2	33.2	16		102	126	150	0.0310		529	4.20	P	0.22	25	100	28.0	
	C3	33.2	16		102	126	150	0.0310		529	4.20	P	0.22	25	100	25.2	
	D2	33.2	16		102	126	150	0.0310		542	4.30	P	0.22	25	100	29.6	
	D3	33.2	16		102	126	150	0.0310		542	4.30	P	0.22	25	100	28.0	
	E3	40.2	16		102	126	150	0.0310		529	4.20	P	0.44	25	100	33.0	
	F1	40.2	16		102	126	150	0.0310		504	4.00	P	0.44	25	100	33.2	
	F2	40.2	16		102	126	150	0.0310		504	4.00	P	0.44	25	100	31.2	
	F3	40.2	16		102	126	150	0.0310		504	4.00	P	0.44	25	100	33.2	
	G1	33.2	16		102	126	150	0.0310		554	4.40	P	0.22	25	100	28.4	
	G3	33.2	16		102	126	150	0.0310		554	4.40	P	0.22	25	100	27.0	
	L1	33.2	16		102	126	150	0.0310		504	4.00	C	0.22	25	75	30.1	
	L2	33.2	16		102	126	150	0.0310		504	4.00	C	0.22	25	75	30.2	
	L3	33.2	16		102	126	150	0.0310		504	4.00	C	0.22	25	75	33.2	
	M1	33.2	16		102	126	150	0.0310		580	4.60	C	0.22	25	75	25.9	
	M2	33.2	16		102	126	150	0.0310		554	4.40	C	0.22	25	75	27.1	
	M3	33.2	16		102	126	150	0.0310		554	4.40	C	0.22	25	75	25.7	
	N1	33.2	16		102	126	150	0.0310		630	5.00	C	0.22	25	75	24.4	
	N2	33.2	16		102	126	150	0.0310		605	4.80	C	0.22	25	75	26.9	
	O1	40.2	16		102	126	150	0.0310		504	4.00	C	0.44	25	75	31.5	
	P1	40.2	16		102	126	150	0.0310		529	4.20	C	0.44	25	75	33.8	
	P2	40.2	16		102	126	150	0.0310		529	4.20	C	0.44	25	75	30.1	
	P3	40.2	16		102	126	150	0.0310		529	4.20	C	0.44	25	75	32.5	
	R1	39.7	16		102	126	150	0.0310		403	3.20	C	0.88	25	75	36.7	
	R2	39.7	16		102	126	150	0.0310		428	3.40	C	0.88	25	75	34.3	
	S1	39.7	16		102	126	150	0.0310		428	3.40	C	0.88	25	75	33.1	
	S2	39.7	16		102	126	150	0.0310		428	3.40	C	0.88	25	75	41.9	
	S3	39.7	16		102	126	150	0.0310		428	3.40	C	0.88	25	75	39.5	
	U1	39.7	16		102	126	150	0.0310		353	2.80	C	1.76	25	75	56.3	
Casanova et al. [42]	HSFRC1	90.0	10		125	225	250	0.0357		653	2.90	H	1.30	30	60	154.4	
	HSFRC2	90.0	10		125	225	250	0.0357		653	2.90	H	1.30	30	60	153.3	F/SC

Table A2.8 Simply supported beams without shear reinforcement and with steel fibres subjected to point load

Reference	Specimen	f_c [MPa]	d_g [mm]	f_y [MPa]	b [mm]	d [mm]	h [mm]	ρ [-]	plate [mm]	a [mm]	a/d [-]	FT	ρ_f [-]	l_f [mm]	α_f [-]	V_{right} [kN]	Remarks[a]
	HSFRC3	90.0	10		125	225	250	0.0221		653	2.90	H	1.30	30	60	98.4	F/SC
Cucchiara et al. [43]	A10	40.9	10	435	150	218	249	0.0192		610	2.80	H	1.00	30	60	95.8	
	A20	43.2	10	435	150	218	249	0.0192		610	2.80	H	2.00	30	60	102.7	F/SC
Minelli et al. [44]	H500FRC	32.1	16		250	440	500	0.0112		1320	3.00	H	0.64	50	63	240.0	F/SC
	H500FRC	33.0	16		250	440	500	0.0112		1320	3.00	H	1.00	50	63	235.0	F/SC
	H1000FRC	32.1	16		250	940	1000	0.0107		2820	3.00	H	0.64	50	63	272.0	F/SC
	H1000FRC	33.0	16		250	940	1000	0.0107		2820	3.00	H	1.00	50	63	351.0	
	H1500FRC	32.1	16		250	1440	1500	0.0101		4320	3.00	H	0.64	50	63	484.0	
	H1500FRC	33.0	16		250	1440	1500	0.0101		4320	3.00	H	1.00	50	63	554.0	
	18-1a	44.8	10	455	152	381	455	0.0196	152	1310	3.44	H	0.75	30	55	170.6	F/SC
	18-1b	44.8	10	455	152	381	455	0.0196	152	1310	3.44	H	0.75	30	55	158.9	F/SC
	18-2a	38.1	10	455	152	381	455	0.0196	152	1310	3.44	H	1.00	30	55	175.2	F/SC
	18-2b	38.1	10	455	152	381	455	0.0196	152	1310	3.44	H	1.00	30	55	178.7	F/SC
	18-2c	38.1	10	455	152	381	455	0.0267	152	1310	3.44	H	1.00	30	55	200.2	F/SC
	18-2d	38.1	10	455	152	381	455	0.0267	152	1310	3.44	H	1.00	30	55	146.6	
	18-3a	31.0	10	455	152	381	455	0.0267	152	1310	3.44	H	1.50	30	55	148.3	
	18-3b	31.0	10	455	152	381	455	0.0267	152	1310	3.44	H	1.50	30	55	196.7	F/SC
	18-3c	44.9	10	455	152	381	455	0.0267	152	1310	3.44	H	1.50	30	55	190.1	
	18-3d	44.9	10	455	152	381	455	0.0267	152	1310	3.44	H	1.50	30	55	190.1	
	18-5a	49.2	10	455	152	381	455	0.0267	152	1310	3.44	H	1.00	60	80	170.6	
	18-5b	49.2	10	455	152	381	455	0.0196	152	1310	3.44	H	1.00	60	80	219.4	F/SC
Dinh et al. [45]	18-7a	43.3	10	455	152	381	455	0.0196	152	1310	3.44	H	0.75	30	79	190.5	F/SC
	18-7b	43.3	10	455	152	381	455	0.0196	152	1310	3.44	H	0.75	30	79	186.7	F/SC
	27-1a	50.8	10	455	203	610	685	0.0200	203	2135	3.50	H	0.75	30	55	361.9	F/SC
	27-1b	50.8	10	455	203	610	685	0.0200	203	2135	3.50	H	0.75	30	55	335.4	F/SC
	27-2a	28.7	10	455	203	610	685	0.0200	203	2135	3.50	H	0.75	60	80	345.0	F/SC
	27-2b	28.7	10	455	203	610	685	0.0200	203	2135	3.50	H	0.75	60	80	338.3	F/SC
	27-3a	42.3	10	455	203	610	685	0.0156	203	2135	3.50	H	0.75	30	55	338.3	F/SC
	27-3b	42.3	10	455	203	610	685	0.0156	203	2135	3.50	H	0.75	60	80	346.3	F/SC
	27-4a	29.6	10	455	203	610	685	0.0156	203	2135	3.50	H	0.75	60	80	269.5	F/SC
	27-4b	29.6	10	455	203	610	685	0.0156	203	2135	3.50	H	0.75	60	80	222.3	
	27-5a	44.4	10	455	203	610	685	0.0210	203	2135	3.50	H	1.50	30	55	429.1	F/SC
	27-6a	42.8	10	455	203	610	685	0.0210	203	2135	3.50	H	1.50	60	80	421.3	F/SC
Dupont et al. [46]	20	39.1	14	560	200	260	300	0.0181		650	2.50	H	0.25	60	65	108.2	
	29	26.5	14	560	200	260	300	0.0181		650	2.50	H	0.25	50	45	99.8	
	30	27.2	14	560	200	260	300	0.0181		650	2.50	H	0.75	50	45	120.1	
	21	38.6	14	560	200	260	300	0.0181		650	2.50	H	0.75	60	65	144.0	
	32	46.8	14	560	200	260	300	0.0181		650	2.50	H	0.50	60	65	157.6	
	2	46.4	14	560	200	260	300	0.0355		900	3.46	H	0.25	60	65	110.2	
	3	43.2	14	560	200	260	300	0.0355		900	3.46	H	0.50	60	65	120.1	
	4	47.6	14	560	200	260	300	0.0355		900	3.46	H	0.75	60	65	155.0	
	23	40.7	14	560	200	260	300	0.0181		1050	4.04	H	0.25	60	65	82.7	
	24	42.4	14	560	200	260	300	0.0181		1050	4.04	H	0.75	60	65	117.0	

Table A2.8 Simply supported beams without shear reinforcement and with steel fibres subjected to point load

Reference	Specimen	f_c [MPa]	d_g [mm]	f_y [MPa]	b [mm]	d [mm]	h [mm]	ρ [-]	plate [mm]	a [mm]	a/d [-]	FT	ρ_f [-]	l_f [mm]	α_f [-]	V_{right} [kN]	Remarks[a]
	NH35	27.9	13	550	150	251	300	0.0267	100	875	3.49	H	1.00	35	65	109.2	
	NH35	26.2	13	550	150	251	300	0.0267	100	875	3.49	H	1.00	35	65	123.5	
	NH60	26.3	13	550	150	251	300	0.0267	100	875	3.49	H	1.00	60	80	116.0	
	NH60	27.1	13	550	150	251	300	0.0267	100	875	3.49	H	1.00	60	80	104.7	
	NC30	27.8	13	550	150	251	300	0.0267	100	875	3.49	C	1.00	30	50	78.7	
	NC30	27.2	13	550	150	251	300	0.0267	100	875	3.49	C	1.00	30	50	77.9	
	NC60	27.6	13	550	150	251	300	0.0267	100	875	3.49	C	1.00	60	85	98.6	
Jain et al. [47]	NC60	27.9	13	550	150	251	300	0.0267	100	875	3.49	C	1.00	60	85	81.3	
	MH35	53.2	13	550	150	251	300	0.0267	100	875	3.49	H	1.00	35	65	144.2	F/SC
	MH35	55.3	13	550	150	251	300	0.0267	100	875	3.49	H	1.00	35	65	165.7	F/SC
	MH60	53.4	13	550	150	251	300	0.0267	100	875	3.49	H	1.00	60	80	128.0	
	MH60	51.0	13	550	150	251	300	0.0267	100	875	3.49	H	1.00	60	80	157.0	F/SC
	MC30	34.7	13	550	150	251	300	0.0267	100	875	3.49	C	1.00	30	50	99.4	
	MC30	36.2	13	550	150	251	300	0.0267	100	875	3.49	C	1.00	30	50	100.1	
	MC60	37.0	13	550	150	251	300	0.0267	100	875	3.49	C	1.00	60	85	110.3	
	MC60	38.3	13	550	150	251	300	0.0267	100	875	3.49	C	1.00	60	85	103.9	
		22.7	38	440	64	102	127	0.0220		306	3.00	H	1.00	30	60	20.5	F/SC
		22.7	38	440	64	102	127	0.0110		306	3.00	H	1.00	30	60	15.7	F/SC
		26.0	38	440	64	102	127	0.0220		306	3.00	H	1.00	50	100	23.0	F/SC
		53.0	2	440	64	102	127	0.0220		306	3.00	C	1.00	25	29	16.5	
		53.0	2	440	127	204	228	0.0220		612	3.00	C	1.00	25	29	50.5	
		50.2	2	440	64	102	127	0.0220		306	3.00	C	2.00	25	29	20.8	
Li et al. [48]		62.6	2	440	127	204	228	0.0220		612	3.00	C	2.00	25	29	66.3	
		57.0	2	440	64	102	127	0.0220		306	3.00	C	1.00	25	29	17.7	
		57.0	2	440	127	204	228	0.0220		612	3.00	C	2.00	25	29	61.4	
		62.6	2	440	64	102	127	0.0220		255	2.50	C	1.00	25	29	20.5	
		62.6	2	440	64	102	127	0.0220		281	2.75	C	1.00	25	29	17.8	
		57.0	2	440	64	102	127	0.0110		306	3.00	C	1.00	25	29	12.8	
		57.0	2	440	64	102	127	0.0330		306	3.00	C	1.00	25	29	17.8	
		57.0	2	440	64	102	127	0.0330		306	3.00	C	1.00	50	57	25.3	
	2/0.5/2.5	34.0	10	404	152	221	254	0.0119		553	2.50	H	0.50	30	60	58.8	F/SC
	2/0.5/3.5	34.0	10	404	152	221	254	0.0119		774	3.50	H	0.50	30	60	45.1	F/SC
	2/1/2.5	34.0	10	404	152	221	254	0.0119		553	2.50	H	1.00	30	60	60.7	F/SC
Lim et al. [49]	2/1/3.5	34.0	10	404	152	221	254	0.0119		774	3.50	H	1.00	30	60	47.0	F/SC
	4/0.5/2.5	34.0	10	404	152	221	254	0.0239		553	2.50	H	0.50	30	60	62.7	
	4/0.5/3.5	34.0	10	404	152	221	254	0.0239		774	3.50	H	0.50	30	60	49.0	
	4/1/2.5	34.0	10	404	152	221	254	0.0239		553	2.50	H	1.00	30	60	82.3	
	4/1/3.5	34.0	10	404	152	221	254	0.0239		774	3.50	H	1.00	30	60	66.6	
	B2	29.1	20		152	197	229	0.0134		552	2.80	H	0.50	30	60	52.5	
	B3	29.1	20		152	197	229	0.0134		709	3.60	H	0.50	30	60	45.0	
Mansur et al. [50]	C2	29.9	20		152	197	229	0.0134		552	2.80	H	0.75	30	60	60.6	
	C6	29.9	20		152	197	229	0.0200		552	2.80	H	0.75	30	60	65.0	
	E2	20.6	20		152	197	229	0.0134		552	2.80	H	0.75	30	60	44.8	
	E3	20.6	20		152	197	229	0.0200		552	2.80	H	0.75	30	60	59.8	

Table A2.8 Simply supported beams without shear reinforcement and with steel fibres subjected to point load

Reference	Specimen	f_c [MPa]	d_g [mm]	f_y [MPa]	b [mm]	d [mm]	h [mm]	ρ [-]	plate [mm]	a [mm]	a/d [-]	FT	ρ_f [-]	l_f [mm]	α_f [-]	V_{right} [kN]	Remarks[a]
	F3	33.4	20		152	197	229	0.0200		552	2.80		0.75	30	60	86.5	
Minelli et al. [51]	NSC1_SFRC1	24.8	20	512	200	435	480	0.0104		1090	2.51	H	0.38	30	50	134.0	
	NSC2_SFRC1	33.5	20	512	200	435	480	0.0104		1090	2.51	H	0.38	50	50	120.1	
	NSC3_SFRC1	38.6	20	512	200	435	480	0.0104		1090	2.51	H	0.38	30	50	140.9	
	HSC1_SFRC1	61.1	15	512	200	435	480	0.0104		1090	2.51		0.64	30	48	191.4	
	HSC1_SFRC2	58.3	15	512	200	435	480	0.0104		1090	2.51	H	0.64	30	79	222.7	F/SC
	NSC4_SFRC500_1	24.4	20	512	200	455	500	0.0099		1140	2.51	H	0.25	50	50	193.8	F/SC
	NSC4_SFRC500_1	24.4	20	512	200	455	500	0.0099		1140	2.51	H	0.25	50	50	153.8	
	NSC4_SFRC1000	24.4	20	512	200	910	1000	0.0103		2275	2.50	H	0.25	50	50	258.4	
	HSC2_SFRC1000	55.0	20	512	200	910	1000	0.0103		2275	2.50	H	0.25	50	50	338.5	
Noghabai [52]	7C	69.3	18		200	410	500	0.0300	200	1200	2.93	H	0.50	60	86	264.0	
	8C	69.3	18		200	410	500	0.0300	200	1200	2.93	H	0.50	60	86	312.0	
	9C	60.2	18		200	410	500	0.0300	200	1200	2.93	H	0.75	60	86	339.0	
	10C	75.7	18		200	410	500	0.0300	200	1200	2.93	H	0.75	60	86	292.0	
	4D	60.2	18		300	570	700	0.0290	200	1700	2.98	H	0.75	60	86	509.0	
Parra-Montesinos et al. [53]	11	49.2	10	410	152	381	457	0.0267		1295	3.40	H	1.00	60	80	172.0	
	7	31.0	10	410	152	381	457	0.0267		1295	3.40	H	1.50	30	60	148.3	
	10	44.9	10	410	152	381	457	0.0267		1295	3.40	H	1.50	30	60	188.8	
	9	44.9	10	410	152	381	457	0.0267		1295	3.40	H	1.50	30	60	190.0	
	12	49.2	10	410	152	381	457	0.0267		1295	3.40	H	1.00	60	80	217.7	F/SC
	8	31.0	10	410	152	381	457	0.0267		1295	3.40	H	1.50	30	60	195.2	F/SC
	4	38.1	10	410	152	381	457	0.0267		1334	3.50	H	1.00	30	60	146.5	
	3	38.1	10	410	152	381	457	0.0267		1334	3.50	H	1.00	30	60	200.4	F/SC
	1	38.1	10	410	152	381	457	0.0196		1334	3.50	H	1.00	30	60	175.5	F/SC
	2	38.1	10	410	152	381	457	0.0196		1334	3.50	H	1.00	30	60	178.9	F/SC
Rosenbusch et al. [54]	1.2/21.2	46.9	10	500	200	260	300	0.0360		910	3.50	H	0.25	60	67	110.4	
	1.2/31.2/3	43.7	10	500	200	260	300	0.0360		910	3.50	H	0.51	60	67	120.3	
	1.2/41.2/4	48.3	10	500	200	260	300	0.0360		910	3.50	H	0.76	60	67	155.4	
	2.3/22.3/1	40.0	10	500	200	262	300	0.0120		655	2.50	H	0.25	60	67	82.9	
	2.3/32.3/3	38.7	10	500	200	262	300	0.0120		655	2.50	H	0.76	60	67	107.6	
	2.4/32.4/3	38.7	10	500	200	260	300	0.0180		650	2.50	H	0.76	60	67	142.3	
	2.6/22.6/1	41.2	10	500	200	260	300	0.0180		1040	4.00	H	0.25	60	67	83.4	F/SC
	2.6/32.6/3	40.3	10	500	200	260	300	0.0180		1040	4.00	H	0.76	60	67	115.5	
	120×30-SFRC-1	37.7	10	500	200	260	300	0.0280		910	3.50	H	0.50	60	67	111.7	
	120×45-SFRC-1	37.7	10	500	200	410	450	0.0310		1353	3.30	H	0.50	60	67	146.0	
	220×30-SFRC-2	38.8	10	500	200	260	300	0.0280		910	3.50	H	0.50	60	67	132.8	
	220×50-SFRC-2	38.8	10	500	200	460	500	0.0240		1564	3.40	H	0.50	60	67	149.0	
	220×60-SFRC-2	38.8	10	500	200	540	600	0.0270		1890	3.50	H	0.50	60	67	222.0	
Sahoo [55]	M20-075	32.9	20	415	150	261	300	0.0195		900	3.45	H	0.75	60	80	108.5	F/SC
	M20-1	23.8	20	415	150	261	300	0.0195		900	3.45	H	1.00	60	80	93.2	F/SC
	M20_1.25	24.1	20	415	150	261	300	0.0195		900	3.45	H	1.25	60	80	113.6	F/SC
Schantz [56]	2	33.7	10		305	546	610	0.0184		1529	2.80	C	0.50	76	80	232.0	
	3	31.5	10		305	546	610	0.0184		1529	2.80	C	1.00	76	80	289.7	

Table A2.8 Simply supported beams without shear reinforcement and with steel fibres subjected to point load

Reference	Specimen	f_c [MPa]	d_g [mm]	f_y [MPa]	b [mm]	d [mm]	h [mm]	ρ [-]	plate [mm]	a [mm]	a/d [-]	F/T	ρ_f [-]	l_f [mm]	α_f [-]	V_{right} [kN]	Remarks[a]
	4	32.8	10		305	546	610	0.0184		1529	2.80	C	1.50	76	80	333.8	
Shoaib et al. [57]	N31	23.0	10	404	310	258	308	0.025	150	924	3.58	H	1.00	30	55	211.0	F/SC
	N61	23.0	10	404	300	531	600	0.0188	150	1800	3.39	H	1.00	30	55	252.0	
	N62	23.0	10	404	300	523	600	0.0255	150	1800	3.44	H	1.00	30	55	242.0	
	H31	41.0	10	404	310	258	308	0.025	150	924	3.58	H	1.00	30	55	278.0	F/SC
	N32	41.0	10	404	310	240	308	0.0403	150	924	3.85	H	1.00	30	55	281.0	
	H62	41.0	10	404	300	523	600	0.0255	150	1800	3.44	H	1.00	30	55	444.0	
	N10-1	41.0	10	404	300	923	1000	0.0144	150	3000	3.25	H	1.00	30	55	492.0	
	N10-2	41.0	10	404	300	920	1000	0.0203	150	3000	3.26	H	1.00	30	55	497.0	
	H32	80.0	10	404	310	240	308	0.0403	150	924	3.85	H	1.00	30	55	458.0	F/SC
	H10-1	80.0	10	404	300	923	1000	0.0144	150	3000	3.25	H	1.00	30	55	646.0	F/SC
	H10-2	80.0	10	404	300	920	1000	0.0203	150	3000	3.26	H	1.00	30	55	644.0	
Swamy et al. [58]	B52	35.5	10	460	175	210	250	0.0400		945	4.50	C	0.40	50	100	78.8	
	B53	37.4	10	460	175	210	250	0.0400		945	4.50	C	0.80	50	100	114.6	
	B54	39.8	10	460	175	210	250	0.0400		945	4.50	C	1.20	50	100	115.9	
	B55	38.2	10	460	175	210	250	0.0305		945	4.50	C	0.80	50	100	118.1	F/SC

[a] F/SC: flexural failure or shear compression failure with the crack not disturbing (or partially disturbing) the development of the theoretical direct strut. Specimens labelled with F/SC are not considered for comparison with the models presented in the thesis

[1]   Reineck K, Bentz EC, Fitik B, Kuchma DA, Bayrak O. ACI-DAfStb Database of Shear Tests on Slender Reinforced Concrete Beams without Stirrups. *ACI Structural Journal* 2013; 110 (5):867–876.

[2]   Reineck K, Bentz E, Fitik B, Kuchma DA, Bayrak O. ACI-DAfStb Databases for Shear Tests on Slender Reinforced Concrete Beams with Stirrups. *ACI Structural Journal* 2014; 111 (5):1147–1156.

[3]   Cavagnis F, Fernández Ruiz M, Muttoni A. An analysis of the shear transfer actions in reinforced concrete members without transverse reinforcement, accepted for publication in Structural Concrete. 2017.

[4]   Cladera A, Marí A. Experimental study on high-strength concrete beams failing in shear. *Engineering Structures* 2005; 27 (10):1519–1527.

[5]   Podgorniak-Stanik BA. he influence of concrete strength, distribution of longitudinal reinforcement, amount of transverse reinforcement and member size on shear strength of reinforced concrete members. PhD Thesis, Toronto, Canada: University of Toronto. 1998.

[6]   Diaz de Cossio R, Siess CP. Behavior and strength in shear of beams and frames without web reinforcement. *ACI Journal* 1960; 31 (8):695–735.

[7]   Joergensen HB, Hoang LC, Fabrin LS, Malgaard J. Influence of High Axial Tension on the Shear Strength of non-shear RC Beams Influence of High Axial Tension on the Shear Strength of non-shear RC Beams, Proceedings of the International IABSE conference: Assessment, Upgrading, Refurbishment of Infrastruct. 2013:7.

[8]   Kuhlmann U, Zilch K, Ehmann J, Jähring A, Spitra F. Querkraftabtragung in Verbundträgern mit schlaff bewehrter und aus Zugbeanspruchung gerissener Stahlbetonplatte ohne Schubbewehrung- Mitteilungen. Institut für Konstruktion und Entwurf Stahl-, Holz-, und Verbundbau, Universität Stuttgart, Germany. 2002:109.

[9]   Madsen MB, Hansen S, Hoang LC, Maagard J. N-V Interaction in Reinforced Concrete Elements without Stirrups. The Twelth East Asia-Pacific Conference on Structural Engineering and Construction. *Procedia Engineering* 2011; 14:2511–2518.

[10]   Mattock AH. Diagonal tension cracking in concrete beams with axial forces. *Journal of Structural Division* 1969; 95 (9):1887–1900.

[11]   Morrow J, Viest IM. Shear Strength of Reinforced Concrete Frame Members Without Web Reinforcement. *ACI Journal* 1957; 53 (3):833–869.

[12]   Kar JN. Diagonal cracking in prestressed concrete beams. *Journal of Structural Division* 1968; 94 (1):83–110.

[13]   Sozen MA, Zwoyer EM, Siess CP. Investigation of Prestressed Concrete for Highway Bridges, Part I, Strength in Shear of Beams without Web Reinforcement, Engineering Experiment Station Bulletin No.452, University of Illinois, Urbana, USA. 1959:68.

[14]   Aoyagi Y, Endo T. Ultimate Shear Capacity of Continuous RC Beams Subjected to Distributed Loading, Proceedings, Fourth East Asia-Pacific Conference on Structural Engineering and Construction, Seoul, South Korea. 1993:727–732.

[15]   Cavagnis F, Fernández Ruiz M, Muttoni A. Shear failures in reinforced concrete members without transverse reinforcement: An analysis of the critical shear crack development on the basis of test results. *Engineering Structures* 2015; 103:157–173.

[16]   Dassow NA. Effect of Uniform Load on the Shear Strength of Slender Beams without Shear Reinforcement, Master of Science Thesis, University of Texas at Austin, USA. 2014:117.

[17]   Feldman A, Siess CP. Effect of Moment Shear Ratio on Diagonal Tension Cracking and Strength in Shear of Reinforced Concrete Beams. Univ. of Illinois Civil Eng. Studies, Struct. Research Series No. 107. 1955.

[18]   Klein JR. Behavior of Slender Beams without Stirrups: Effects of Load Distribution and Member Depth, Master of Science Thesis, University of Texas at Austin, USA. 2015:164.

[19]   Krefeld WJ, Thurston CW. Studies of the shear and diagonal tension strength of simply supported R/C-beams. *ACI Journal* 1966; 63 (4):451–476.

[20]   Leonhardt F, Walther R. Schubversuche an einfeldrigen Stahlbetonbalken mit und ohne Schubbewehrung. DAfStb H.151, Berlin. 1962.

[21]   Rüsch H, Haugli FR, Mayer H. Schubversuche an Stahlbeton Rechteckbalken mit Gleichmassig Verteilter Belastung, Deutscher Ausschuss fur Stahlbeton, Heft 145, W. Ernst und Sohn, West Berlin. 1962.

[22]   Shioya T, Iguro M, Nojiri Y, Akiayma H, Okada T. Shear Strength of Large Reinforced Concrete Beams. *Special Publication* 1989; 118:259–280.

[23]   Brown MD, Bayrak O, Jirsa JO. Design for shear based on loading conditions. *ACI Structural Journal* 2006; 103 (4):541–550.

[24]   Smith RBL. Shear Reinforcement of Reinforced Concrete Beams Subjected to Distributed Loading. *Magazine of Concrete Research* 1970; 22 (70):17–24.

[25]   Tung ND, Tue NV. Effect of support condition and load arrangement on the shear response of reinforced concrete beams without transverse reinforcement. *Engineering Structures* 2016; 111:370–382.

[26]   Uzel A, Podgorniak B, Bentz EC, Collins MP. Design of Large Footings for One-Way Shear. *ACI Structural Journal* 2011; 108 (2):131–138.

[27]   Acevedo AB, Bentz EC, Collins MP. Influence of Clamping Stresses on the Shear Strength of Concrete Slabs under Uniform Loads, Research Report No. ROSE-2008/0.5, Rose School, Pavia, Italy. 2008:227.

[28]   Bryant RH, Bianchini AC, Rodriguez JJ, Kesler CE. Shear Strength of Two-Span Continuous Reinforced Concrete Beams with Multiple Point Loading. *ACI Structural Journal* 1962; 59 (9):1143–1177.

[29]   Klaus T. Shear Behaviour of Reinforced Concrete Box Culverts, Master of Science Thesis, Univesity of Toronto, Canada. 2007:197.

[30]   Pérez Caldentey A, Padilla P, Muttoni A, Fernández Ruiz M. Effect of load distribution and variable depth on shear resistance of slender beams without stirrups. *ACI Structural Journal* 2012; 109 (5):595–603.

[31]   Richart FE. Reinforced concrete wall and column footings. *ACI Journal Proceedings* 1948; 45 (10):97–127.

[32]   van den Beukel A, Monnier T. Dwarskracht, Rapport B-84-522/62.5.0804 IBBC TNO Delft, Netherlands. 1985:48.

[33]   Walraven JC. The Influence of Depth on the Shear Strength of Lightweight Concrete Beams without Shear Reinforcement, Report 5-78-4, Delft University of Technology, Faculty of Civil Engineering, Delft, the Netherlands. 1984:36.

[34]   Taylor, R., Brewer RS. The Effect of the Type of Aggregate on the Diagonal Cracking of Reinforced Concrete Beams. *Magazine of Concrete Research* 1963; 15 (44):87–92.

[35]   Ivey DL, Buth E. Shear Capacity of Lightweight Concrete Beams. *ACI Journal Proceedings* 1969; 66 (6):634–643.

[36]   Campana S, Anastasi A, Fernández Ruiz M, Muttoni A. Analysis of shear-transfer actions on one-way RC members based on measured cracking pattern and failure kinematics. *Magazine of Concrete Research* 2013; 65 (6):386–404.

[37]   Huber P, Huber T, Kollegger J. Investigation of the shear behaviour of RC beams on the basis of measured crack kinematics. *Engineering Structures* 2016; 113:41–58.

[38]   Yoon Y-S, Cook WD, Mitchell D. Minimum Shear Reinforcement in Normal, Medium and High- Strength Concrete Beams. *ACI Structural Journal* 1996; 93 (5):576–584.

[39]   Ashour SA, Hasanain GS, Wafa FF. Shear Behavior of High-Strength Fiber Reinforced Concrete Beams. *ACI Structural Journal* 1992; 89 (2):176–184.

[40]   Barragan BE. Failure and Toughness of Steel Fiber Reinforced Concrete under Tension and Shear, PhD Thesis, Barcelona, Spain: Universitat Politecnica de Catalunya. 2002.

[41]   Batson G, Jenkins E. Steel Fibers as Shear Reinforcement in Beams. *ACI Journal* 1972; 69 (10):640–644.

[42]   Casanova P, Rossi P. High-Strength Concrete Beams Submitted to Shear: Steel Fibers Versus Stirrups, Structural Applications of Fiber Reinforced Concrete, SP-182, American Concrete Institute, Farmington Hills, MI. 1999:53–68.

[43]   Cucchiara C, Mendola LL, Papia M. Effectiveness of Stirrups and Steel Fibres as Shear Reinforcement. *Cement and Concrete Composites* 2004; 26 (7):777–786.

[44]   Minelli F, Conforti A, Cuenca E, Plizzari G. Are steel fibres able to mitigate or eliminate size effect in shear? *Materials and Structures* 2014; 47 (3):459–473.

[45]   Dinh HH, Parra-montesinos GJ, Wight JK. Shear Behavior of Steel Fiber-Reinforced Concrete Beams without Stirrup Reinforcement. *ACI Structural Journal* 2010; 107 (5):597–606.

[46]   Dupont D, Vandewalle L. Shear capacity of concrete beams containing longitudinal reinforcement and steel fibers, Innovations in Fiber Reinforced Concrete for Value, SP-216, American Concrete Institute, Farmington Hills, MI. 2003:79–94.

[47]   Jain K, Singh B. Deformed steel fibres as minimum shear reinforcement — An investigation. *Structures* 2016; 7:126–137.

[48]   Li VC, Ward R, Hamza AM. Steel and Synthetic Fibers as Shear Reinforcement. *ACI Materials Journal* 1992; 89 (5):499–508.

[49]   Lim TY, Paramsivam P, Lee SL. Shear and Moment Capacity of Reinforced Steel-Fiber-Concrete Beams. *Magazine of Concrete Research* 1987; 39 (140):148–160.

[50]   Mansur MA, Ong KCG, Paramasivam P. Shear Strength of Fibrous Concrete Beams without Stirrups. *Journal of Structural Engineering* 1986; 112 (9):2066–2079.

[51]   Minelli F, Plizzari GA. On the Effectiveness of Steel Fibers as Shear Reinforcement. *ACI Structural Journal* 2013; 110 (3):379–389.

[52]   Noghabai K. Beams of Fibrous Concrete in Shear and Bending: Experiment and Model. *Journal of Structural Engineering* 2000; 126 (2):243–251.

[53]   Parra-Montesinos BGJ. Shear Strength of Beams with Deformed Steel Fibers - Evaluating an alternative to minimum transverse reinforcement. *Concrete International* 2006; 28 (11):57–67.

[54]   Rosenbusch, J., and Teutsch M. Trial Beams in Shear, Brite/Euram Project 97-4163, Final Report, Sub Task 4.2, Technical University of Braunschweig. 2003:105–117.

[55]   Sahoo DR, Sharma A. Effect of Steel Fiber Content on Behavior of Concrete Beams with and without Stirrups. *ACI Structural Journal* 2014; 111 (5):1157–1166.

[56]   Schwanz BA. The Effect of Shear Stress on Full Scale Steel Fiber Reinforced Concrete Beams, Master of Science Thesis, Potsdam, NY, USA: Clarkson University. 1993:86.

[57]   Shoaib A, Lubell AS, Bindiganavile VS. Size Effect in Shear for Steel Fiber-Reinforced Concrete Members without Stirrups. *ACI Structural Journal* 2014; 111 (5):1081–1090.

[58]   Swamy RN, Bahia HM. The Effectiveness of Steel Fibers as Shear Reinforcement. *Concrete International* 1985; 7 (3):35–40.

Francesco Cavagnis

Born in Padova (Italy) on November 11, 1985
francesco.cavagnis@gmail.com, +41787353767
Rue des Terreaux 19, 1003 Lausanne, Switzerland

EDUCATION

08/2012 – Present	PhD Candidate
	Structural Concrete Laboratory (IBETON)
	École polytechnique fédérale de Lausanne (EPFL), Lausanne, Switzerland
10/2009 – 04/2012	Master of Science in Civil Engineering – Structural Engineering
	Final grade: *110/110 cum laude* (top 5%)
	Politecnico di Milano – Politecnico di Torino, Italy (double degree programme)
09/2010 – 02/2011	Exchange Programme at **Danmarks Tekniske University** (DTU), Lyngby, Denmark
08/2010	Workshop at **Tongji University**, Shanghai, China
10/2006 – 07/2009	Bachelor of Science in Civil Engineering
	Final grade: *107/110* (top 5%)
	Politecnico di Milano, Milano, Italy

PROFESSIONAL EXPERIENCE

08/2012 – Present	Research Assistant / Teaching Assistant
	Structural Concrete Laboratory (IBETON)
	École polytechnique fédérale de Lausanne (EPFL), Lausanne, Switzerland
	- Experience in designing and conducting large-scale tests
	- Research on the shear strength of reinforced concrete members
	- Teaching Assistant (Structures, Concrete Structures) and Tutor of Master projects
07/2007 – 09/2007	Volunteer Coordinator
	Vancouver Fringe Festival, Vancouver, British Columbia, Canada
02/2006 – 09/2006	Practice Administrator
	The Well Beacon Clinic, Dublin, Ireland

PERSONAL SKILLS

Languages:	Italian:	Mother tongue
	English:	Proficient User (Certificate in Advanced English (CAE), 2007)
	French:	Independent User
	German:	Basic User (Zertifikat Deutsch (ZD), 2002)
Computer skills:	Software: Matlab, Autocad, Illustrator, JConc, Abaqus, Tno Diana, Sap2000, Fortran	

AWARDS

10/2009 – 04/2012	**Alta Scuola Politecnica** (ASP)
	Top 150 students in the Master of Science in Engineering, Architecture and Design at Politecnico di Milano and Politecnico di Torino

PUBLICATIONS

- Cavagnis F., Fernández Ruiz M., Muttoni A., Shear failures in reinforced concrete members without transverse reinforcement: An analysis of the critical shear crack development on the basis of test results. *Engineering Structures*, 2015, 103: 157-173.
- Cavagnis F., Fernández Ruiz M., Muttoni A., Analysis of shear transfer actions in reinforced concrete members using refined measurement techniques, *fib Symposium*, 2016, Cape Town, South Africa.
- Muttoni A., Fernández Ruiz M., Cavagnis F., Shear in members without transverse reinforcement: from detailed test observations to a mechanical model and simple expressions for codes of practice. *fib International Workshop on Beam Shear*, 2016, Zurich, Switzerland.
- Cavagnis F., Fernández Ruiz M., Muttoni A., An analysis of the shear transfer actions in reinforced concrete members without transverse reinforcement based on refined experimental measurements, *Structural Concrete*, 2017, doi: 10.1002/suco.201700145.
- Cavagnis F., Fernández Ruiz M., Muttoni A., A mechanical model for failures in shear of members without transverse reinforcement based on development of a critical shear crack, *Engineering Structures*, 2018, in press.

INTERESTS AND ACTIVITIES

Hobbies and Sport:	Skiing, Tennis, Playing piano (Diploma in Music Theory and Solfeggio, 2000)
Charity work:	Hospital assistance: Lourdes, France (since 2010) and Milan, Italy (in 2011)